eman ta zabal zazu

Universidad del País Vasco

Euskal Herriko Unibertsitatea

A NEW UNDERSTANDING OF ENTANGLEMENTS IN POLYMERS

APPLICATIONS TO RHEOLOGY AND PROCESSING

PhD Thesis

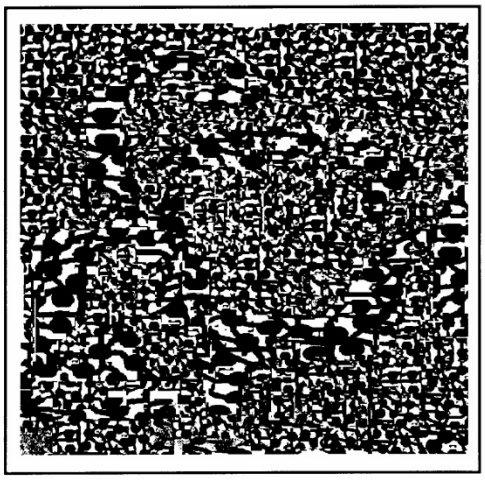

Jean Pierre Ibar

Donostia, 2017

DEPARTAMENTO DE CIENCIA Y TECNOLOGÍA DE POLIMEROS
Facultad de Química
UPV/EHU

A NEW UNDERSTANDING OF ENTANGLEMENTS IN POLYMERS APPLICATIONS TO RHEOLOGY AND PROCESSING

BY

JEAN PIERRE IBAR

A thesis submitted for the degree of Doctor of Philosophy
in Applied Chemistry and Polymeric Materials

SUPERVISOR: Prof. ANTXON SANTAMARIA

Donostia- San Sebastián June 2017

Universidad del País Vasco/Dto. Ciencia y Tecnología de Polímeros
Manuel de Lardizabal 3/20080 SAN SEBASTIAN (SPAIN).
Teléfono 943 01 81 84 . FAX 943 01 52 70 antxon.santamaria@ehu.es

Acknowledgments.

The author is thankful to the Fulbright Foundation and the Ikerbasque Foundation for sponsoring this research. This work has also been made possible by the award to the author of the IRG Marie-Curie Grant 200342 (European FP7 framework).

The following students have participated in the analysis of the experimental data and their dedication is gratefully acknowledged: Hannah Israel (Massachusetts Institute of Technology/ MIT), Ester Lomeli (MIT), Yassine Ezzyat (MIT), Zhengchi Zhang (University of Shichuan).

I am greatly honored and thankful that Prof. Alejandro J. Muller, Prof. Juan F. Vega Borrego and Dr. Peter Heidemeyer have accepted to serve as Members of the Examining Board.

Finally, the author would like to thank Prof. Antxon Santamaria who has been supportive of this research from the beginning and has helped setting it in motion.

I am dedicating this work to Christine, Manex, Titia, Oona, Maia, Katixa, Alaia, Emil (Gorka), Yola.

Jean Pierre IBAR
March 15 2017

A NEW UNDERSTANDING OF ENTANGLEMENTS IN POLYMERS: APPLICATIONS TO RHEOLOGY AND PROCESSING

Abstract

A primary motivation for my research is the interpretation of the phenomenon of "sustained-orientation" observed by submitting high molecular weight polymeric melts to Rheo-Fluidification processing conditions, which combine pressure flow, under cross-lateral vibrational shear flow, and expansional flow in an annular die. The phenomenon of "sustained orientation" appears to challenge the present understanding of strain induced deformation in polymer melts and its understanding may open up new avenues to clarify the concept of entanglement of polymer chain, the corner stone of polymer physics.

The chemical structure of macromolecules is well understood nowadays, and their syntheses are well monitored. This, I believe, is not fully true of their thermal and mechanical properties, i.e. of polymer physics in general. The whole subject of visco-elasticity, rubber elasticity, viscosity and glass formation has been the concern of extensive research for the last 60 years. For the most part, a consensus exists that our understanding of these properties of polymers is quite satisfactory. The current understanding of polymer physics is based on the description of the properties of a single chain embedded in a sea of average interaction from the other chains that disturbs its properties. For instance, in the case of rubber extensibility, one calculates the variation of the chain entropy with strain by determination of the average rms end to end distance characteristic of the equilibrium macromolecular coil assumed by the chain. The statistics at a molecular level is treated from a pure macromolecular perspective, for instance, entanglements are regarded as physical cross-links creating a network, defined by a molecular weight between entanglements, M_e. These classical concepts provide a roaster of satisfactory answers when dealing with the interpretation of "linear" phenomena, resulting from the deformation at low strain and low strain rates. Yet, problems and questions of polymer physics are still not fully answered, especially in the domain of non-linear visco-elasticity, which is the case when Rheo-Fluidification conditions apply and "sustained orientation" is observed.

In the type of research I propose, I look at polymer physics from a different angle: I consider the statistics of a system consisting of a set of interactive conformers belonging to all the chains put together at once. The statistical system is no longer a single macromolecule made

up of covalently interactive conformers, although this situation is also studied. The system is the global set of conformers belonging to all macromolecules. I no longer attribute to a mean field the influence generated by the other molecules on the configurational properties of a single chain (defining its entropy and enthalpy), I attribute a “grain-structure” to the field that describes the result of interactive coupling, i.e. I consider the existence of an inhomogeneous density of state due to local fluctuations of the interactions. The evolution with time of the state of interactions between the conformers, when the system is submitted to a mechanical force or to a temperature variation describes the change of the physical properties. This new statistics leads to the elaboration of a different understanding of visco-elasticity, rubber elasticity, and of the concept of entanglement of the macromolecules.

In order to tackle polymer physics from this new angle I first introduce a statistical model which can describe this concept of local grain structure of the interactions between all the conformers of all the macromolecules. This statistical model is called the Grain Field Statistics. I do not provide in this thesis the mathematics of the statistical model, I only present the results of the simulation (in the Preamble and in chapter 5) in a way which essentially renders simple and intuitive to grasp the concepts introduced.

I propose to understand “Sustained orientation” in polymers by application of the Grain-Field statistics to describe shear-thinning, strain-softening and the dynamic role played by the “free volume”.

Jean Pierre Ibar

August 17, 2016

TABLE OF CONTENTS

ABSTRACT & DESCRIPTION OF THE DIFFERENT CHAPTERS

Chapter 1: Preamble: Introduction to the Dual-Phase Model of Polymer Interactions and to the Cross-Dual-Phase Model of Entanglements.

We present in this preamble a short review of the concepts which led to the anticipation of the experimental results addressed in the following chapters.

In the classical views, the chain is particularized and its interaction with its surrounding is described in terms of a mean field of interactions. The entropy of a single chain is calculated from its intra-molecularly linked covalent bonds and the deformation (to express flow properties, for instance) is due to a modification of the entropy. The presence of the other chains is perceived as a restriction on the entropy, in particular by the confinement of the motion of the chain within a tube in which the chain can reptate ("the reptation model").

We summarize in this preamble our new way to describe the complexity of the interactions between polymer macromolecules, in particular a new way to determine the conformational state of its basic constituents, the conformers, which are covalently bound to each other along the chains, yet exert inter-molecular forces with adjacent conformers, belonging to the same or to other macromolecules.

A. I THE CLASSICAL VIEW OF POLYMER VISCO-ELASTICITY, SHEAR-THINNING AND ENTANGLEMENTS

A. II THE DUAL-SPLIT VIEW OF POLYMER VISCO-ELASTICITY, SHEAR-THINNING AND ENTANGLEMENTS

B. I A NEW MODEL OF POLYMER INTERACTIONS (SUMMARY).

B. I. 1 *Conformers: b and F type of conformers*

B. I. 2 *T he Dual-Split Statistics of the conformers [b/F ↔ (c,g,t)}*

B. I. 3 *The Crossed-Dual-Phase Statistics for long chains*

B. II A NEW UNDERSTANDING OF POLYMER MELT MOLECULAR MOTIONS AND FLOW PROPERTIES.

C. REFERENCES (Chapter 1).

Chapter 2: Trouble with Polymer Physics: "Sustained-Orientation". Ground Breaking Experimental Research Shakes the Current Understanding of the Liquid State of Polymers.

Recent research on the stability of entanglements of polymer melts and on the correlation between viscosity improvement during processing and entanglement stability are reported in this chapter. This research led to the discovery of a new property of the liquid state of polymers which may not be explained by the current models in polymer physics: it is called "sustained orientation".

In simple terms, by manipulation of the stability of entanglements, it is possible to create and maintain quasi-stable at high temperature in an amorphous polymeric melt (say 120 ^{o}C above T_g) a certain state of orientation that was induced by a mechanical deformation. The manipulation of entanglements was done by Rheo-Fluidification. In our experiments, the viscosity of a melt (e.g. PMMA) was measured at the exit of a Rheo-Fluidification treatment where the melt was submitted to a combination of shear-thinning and strain-softening via the use of cross-lateral shear vibration superposed on pressure flow (originated by an extruder feed). The exiting melt was frozen into pellets and the rheological properties of those pellets were studied. Under certain Rheo-Fluidification processing conditions, the viscosity reduction of the melt induced by the combination of shear-thinning and strain softening could be preserved in the pellets granulated at the exit of the disentangling processor. These "treated" pellets displayed sustained-orientation, i.e. a lower viscosity when they were reheated in a melt flow indexer, or in a dynamic rheometer after they had been compressed into disks. Yet, the molecular weight, M_w, was hardly changed (~3%) to justify the viscosity reduction, and it was also observed that the viscosity only gradually (sometimes over periods of hours) returned to the value it should have at the corresponding temperature (the Newtonian value), indicating that the changes were reversible.

These results suggest that the classical concept of M_e to describe entanglements is too simplistic and its usefulness is probably limited to the linear range of viscoelasticity. We suggest that these types of experimental results, recently presented, have resonance in our fundamental understanding of the interactions between the macromolecules, inviting us to redefine the nature of entanglements, the nature of molecular motions and flow, and reformulate the equations underlying rheology, crystallization, glass formation, and the stability of the interactions at different temperatures and under stress.

A. INTRODUCTION

B. EXPERIMENTAL DESCRIPTION

B-1 *The Rheo-Fluidification Processor*

B-2 *Sustained-Orientation: in-pellet retention of viscosity decrease*

C. RESULTS

D. DISCUSSION

E. SUMMARY AND CONCLUSIONS

F. NOTE

G. REFERENCES (Chapter 2)

Chapter 3: The Great Myths of Polymer Rheology, Part 1: Comparison of Theory with Experimental Data

This chapter examines the following issues in polymer rheology:

-Is the separation of temperature and molecular weight in the expression of viscosity an approximation (perhaps even a poor one) that theoretical models should not attempt to explain?

-Is the universality of the time-temperature superposition restricted to a narrow temperature range, so narrow, in fact, that most of the extrapolated data published as mastercurves in the literature were actually poised to be wrong?

-Is the concept of local friction coefficient (as related to relaxation time) misconceived to describe the change under stress of the state of interactions between the bonds, a phenomenon called flow?

-Is the reptation model reaching its limits in the non-linear range because it successfully describes formulas which are only approximations, even in the linear range, or because the network of entanglement must be understood by new concepts?

-Is there a liquid-liquid transition relaxation in the melt when the data are re-examined properly with the right regression tools? Is it time to consider new interpretations for its existence?

-Is there a need, in order to reconcile linear and non-linear experimental results, to reconsider the classical concepts of linear viscoelasticity: the terminal time, τ_d, the plateau modulus, G_{oN}, and the concept of Me, the molecular weight between entanglements? Are these concepts too simplistic and of limited value?

PREAMBLE FOR CHAPTER 3

A INTRODUCTION

B SHEAR-THINNING: NON-NEWTONIAN BEHAVIOR

C DESCRIPTION OF THE DATA SOURCES

D ANALYSIS PROTOCOLE

E ACCURACY CONSIDERATION

F CRITICAL ANALYSIS OF THE EQUATIONS OF RHEOLOGY

F-1 UNIVERSALITY OF WLF CONSTANTS AT T_g

F-2 VALIDITY OF THE 3.4 EXPONENT FOR $M > M_C$

F-3 FOR $M < M_C$ VISCOSITY IS NOT PROPORTIONAL TO M

F-4 ACCURACY IN THE DETERMINATION OF THE NEWTONIAN VISCOSITY

F-5 TIME-TEMPERATURE SUPERPOSITION

F-6 THE UPPER MELT TEMPERATURE DEPARTURE FROM SUPERPOSITION

F-7 THE LOWER MELT TEMPERATURE DEPARTURE FROM SUPERPOSITION

F-8 IS THE SUPERPOSITION EVER VALID?

G THE QUESTION OF UNDERSTANDING RHEOLOGY WITH A SPECTRUM OF RELAXATION

H CONCLUSIONS

I REFERENCES (chapter 3)

Chapter 4: The Great Myths of Polymer Rheology, Part 2: Transient and Steady State

One of the most difficult problems to solve in rheology is to predict the deformation of the melt during its "transient" conditions, i.e. before it reaches its steady state deformation. Most of our present understanding concerns the steady state when properties, such as viscosity or modulus, no longer depend on time and remain invariant. This paper is concerned with the transient states obtained under non-linear conditions and wonders why it sometimes takes a considerable length of time for the viscosity to reach a steady state value, when its terminal time, τ_o, calculated from the steady state viscosity at that temperature, or from the cross-over of G' and G" ($\tau_o = 1/\omega_x$) indicates that the melt should relax in much shorter times? In pure viscometry (at constant rate of shear), a transient behavior is expected before the melt reaches its steady state.

Questions regarding the origin of this transient are experimentally and theoretically investigated and debated for a LLDPE (M/M_e ~300). We show that the stability of the steady state is a function of the previous thermo-mechanical history of the melt. In order to study the instability of the melt under conditions that separate the effects of strain and strain rate, we investigate the triggering of time dependence of the moduli by strain in dynamic experiments performed in the non-linear range. We study, for linear PC and PS, the effects of various parameters affecting the stability of entanglements under dynamic non-linear conditions, that of frequency, strain amplitude and temperature. In all these experimental tests we observe the same phenomenon: as strain is increased beyond a certain critical value (which is a function of frequency and temperature), the melt starts to become transient, i.e., for instance, its viscosity changes with time until it reaches a steady state value. We review and rule out (for our results) the challenging interpretations based on melt edge fracture and melt surface decohesion. For transient and steady states obtained by pure viscometry or by dynamic shear oscillation, we compare the rheological properties (G' (ω) and G" (ω)) of the un-sheared melt, before the transient, and of the "sheared melt", after the transient, by performing a frequency sweep in the linear range. The results display large differences in G' (ω) and G" (ω) and in the value of the terminal time.

In the explanation we propose, we point to the limitation, as we enter the non-linear range, of the basic assumption of rheology regarding the scalability of the rheological parameters (stress and deformation tensors) in terms of viscosity, strain and strain rate to describe the effect of the gap thickness. The definition of viscosity (the ratio of stress and strain rate) and of strain rate (the gradient of the velocity profile across the gap) requires an homogeneous melt., or, as we further propose, an homogeneous, unstructured entanglement network, which is a valid

and justified concept only for certain conditions of deformation, for instance in the linear viscoelastic range. A melt can be brought out of equilibrium with respect to its entanglement state. The return to equilibrium explains the transient properties. New entanglement states can be made quasi-stable, even at high temperature in the melt, by coupling entropic and enthalpic effects produced under specific conditions of melt processing.

The currently accepted descriptions of rheology only apply to a stable entanglement state, which is not general enough and even becomes a severe limitation to explore new frontier research in the application of rheology to processing of polymer melts.

A. INTRODUCTION

-Transient and Steady State Behavior
-Step Strain Experiment in the non-linear Region
-Step Strain Rate Experiment under non-linear Condiitons.
-Strain Induced Transients under Oscillation Shear Mode
-Combining Rotation and Oscillation Shear Modes.
    -The work of Osaki et al.
    -Effect of combining rotation and oscillation in the non-linear regime: Shear-Refinement under Dynamic Conditions
- Combined Flow rates from Pressure Flow and Rotational Flow.
    - Combined Oscillation and Rotation.
    - Shear-Refinement: the Effect of Thermal-Mechanical History.
-Melt Fracture. Edge Fracture in Parallel Plate Experiments
- Objectives of this Article.

B. EXPERIMENTAL PROCEDURE, POLYMER CHARACTERIZATION, DEFINITION OF PARAMETERS.

1. Experimental Procedures

1A The simple time sweep at given T, w and strain %.
1B The simple time sweep at given T, w and strain % immediately followed by a cooling ramp test performed in the linear range.
2. The three Step Experiments of Type FTF (Frequency-Time-Frequency) in a Dynamic Rheometer.
3. The four Step Experiment of Type FT1-FT2-FT1-FT2 in a Dynamic Rheometer.
4. Pure Viscometry.
5. Pure Viscometry followed by a Frequency Sweep.
6. Viscosity Measurement under Extrusion Flow Conditions.
7. In-line viscosity Measurement at the end of a "treatment Processor".

2. Rheometers Used.

3. Materials.
    3.1 Polycarbonate
    3.2 Polystyrene
    3.3 LLDPE

4. Initial State and Sample Molding Procedure.
    4.1 PC
    4.2 LLDPE
    4.3 PS

5. Definition of the Rheological Parameters to Analyse the Stability of Melt.

C. RESULTS

1. Linear PC. Time Sweeps at various Temperatures, Frequencies, at 50% strain.

2. Viscometric Experiments on LLDPE
    2.1 Pure Rotation Experiment of Type 4.
    2.2 Pure Rotation followed by Frequency Sweep Experiment of Type 5
    2.3 Experiments of Type 4 on Melts with Prior Therm-Mechanical History.
    2.4 Transients created in Dynamic Conditions by Increase of Strain.

3. Dynamic Experiments of Type 2 (FS-TS-FS) on PC.

    3.1 Effect of Strain (γ) at low Frequency (0.1 Hz).
        - 3.1.1 5% strain
        - 3.1.2 20% strain
        - 3.1.3 500% strain
        - 3.1.4 5% strain using a disentangled melt obtained by controlled shear-refinement

    3.2 Effect of Frequency during Time Sweep (at constant strain of 5%).
        3.2.1 1 Hz
        3.2.2 10 Hz
        3.2.3 40 Hz

    3.3 Effect of Increasing Energy Input during Time Sweep: T=225 ^{o}C, Frequency= 5 Hz, and γ=20%

    3.4 Effect of Annealing the Melt after Treatment and Experiment of Type 3.

4. Long Term Entanglement Network Stability for a PMMA “disentangled” melt.

5. Entanglement Network Instability for a Polystyrene Melt.

-5.1 PS-1 (PS1070)

-5.2 PS-2: Thermal-Mechanical History to Create out-of-Equilibrium Melt Properties.

D. DISCUSSION

1- The Question of the Origin of the Time Dependency of the Visco-Elastic Parameters.

2- Challenging Interpretations:
- 2.1 -Viscous heating.
- 2.2 -Shear Degradation.
- 2.3 -Drooling of the Melt Outside of the Rheometer Plates.
- 2.4 -Plastification due to an increase of the monomer concentration by the shear process.
- 2.5 - Shear-Thinning.
- 2.6 - Edge Fracture Explanation:
  - -Melt Fracture Initiation. Vinogradov's criteria
  - -Simultaneous Dielectric and Dynamic Mechanical Measurements in the Molten State.

3- Effect of the Nature of the Surface Melt Contact.

4- Melt Flow Index of Disentangled Pellets and in-line Viscosity of Disentangled Melts.

5- Manifestation of Properties of Disentangled Polymers is not new.

6- The real problem is the understanding of the nature of entanglement and of the entropic character of polymer melt deformation.

E. SUMMARY

F. CONCLUSION

G. REFERENCES (Chapter 4)

Chapter 5: The Great Myths of Polymer Rheology, Part 3: Elasticity of the Network of Entanglements

In this chapter, we analyze dynamic data of polymer melts in a novel way presenting new correlations between the viscosity, G' and G" (the elastic and loss modulus), and strain rate and discussing the implications of the new formula to our understanding of melt entanglement network elasticity. In chapters 3 and 4, we showed that the existing models valid in the linear visco-elastic deformation range were not adequate to extrapolate to the non-linear regime, suggesting that the stability of the network of entanglement was at the center of the discrepancies. In this article, we introduce new tools for the analysis of the dynamic data and suggest new ideas for the understanding of melt deformation based on this different focus. In particular, we want to express classical concepts, such as shear-thinning, melt diffusion or melt elasticity and viscosity, in a different context, that of the existence of a Dual-Phase interaction, essential to our treatment of the statistics of interaction of the bonds responsible for the system coherence and cohesion. This is within that framework that visco-elasticity parameters emerge and a new view of the deformation of a polymer melt will result in a different definition of the entanglement network. The mathematical treatment serves as a way to support the concepts, but the reverse is also true, the concepts of dual-phase naturally lead to the search for these mathematical tools. Thus, the concepts are introduced early on, in a qualitative and intuitive way, and refined as the results emerge giving support or challenging the initial ideas. For instance, thermal diffusion in polymer melts is imaged by a continuous coherent sweeping wave of "the phase-lines", defining the boundaries between the dual phases, organized as a continuous network, constantly in motion, with natural frequency ω'_o, in order to insure melt isotropicity and homogeneity despite of the free volume difference between the dual-phases. At one stage of melt deformation, the orientation of the phase-lines occurs and creates anisotropicity which is compensated, at least partially, by an increase of the sweeping wave frequency to maintain the homogeneity of the cohesion between the interactive bonds: this is shear-thinning. We explicit this view mathematically in this article.

We consider a new parameter, $\omega_R = \omega /(G'/G^*)^2$, where ω is the radial frequency, G' is the elastic modulus and G* the amplitude of the complex modulus and study how it correlates to viscosity, suggesting that shear-thinning can be simply expressed in terms of ω and $(G'/G^*)^2$. We show that $(G'/G^*)^2$ can be split into two terms, χ_1 and χ_2 , i.e. $\chi=(G'/G^*)^2 = \chi_1 + \chi_2$, the variation of χ_1 and χ_2 with ω and temperature being fundamentally related to the mechanisms of deformation of the network of interactions (inter and intra molecular in nature, working coherently and defining the viscous cohesion). We show that the χ_2 term

is related to the energy stored by the network of phase-lines ("entanglements") by entropic modification of the orientation of the network (resulting in an increase of the sweep wave frequency), so χ_2 is a characteristic of the entropic nature of the network of interactions; and, by contrast, we show that the χ_1 term is related to the local conformational state of the bonds with respect to their equilibrium value, i.e. it has an enthalpic resonance. We define the rate of "dragged diffusion" of the entanglement network as $\omega' = \omega/\chi_2$ and show that ω' correlates simply with the total stress generated by the flow mechanism in the shear-thinning regime at low strain. At low ω, ω' converges to a finite value, ω'_o, that we associate, as already said, with the fundamental static diffusion of the network of entanglement, i.e. with the natural frequency of swing of the entanglement phase to interpenetrate the core phase, delimiting the contours of the boundaries between the dual-phases. We correlate ω'_o with the onset of non-Newtonian viscous flow behavior. Subtle differences of the variation of χ_1 and χ_2 emerge for various thermo-mechanical treatments of the melt or by varying temperature or the magnitude of the strain applied. The analysis of the split of $(G'/G^*)^2$ into χ_1 and χ_2 suggests to assign a physical dynamic attribute to the elastic entanglement network, whose deformation occurs by an activated mechanism of stretch-relax, and the need to characterize its stability under stress. We also define the elastic cohesive energy of the dynamic network, $\Delta_{\omega,\gamma}$, which varies with ω and γ, since it directly correlates with the number of activated strands of the dynamic network, χ_2 . We study the influence of $T_g(\omega,\gamma)$ on the visco-elastic behavior, showing that it plays a significant role in the mechanism of shear-thinning and strain softening, and propose a way to evaluate its impact on χ_1 and χ_2. Multiple examples are given comparing χ_1 and χ_2 for LLDPE, Polymethylmethacrylate (PMMA), Polycarbonate (PC), Polystyrene (PS), Polyethylene Terephtalate Glycol (PETG) and Polypropylene (PP) melts. The influence of temperature on the elasticity of the dynamic network of entanglements suggests a change of the characteristics of the elastic network in the melt above T_g, an observation already foreseen in chapter 3. The effect of strain is an important section of this paper. We show that strain participates in three different ways in the selection of the mechanism of deformation most appropriate to the rate of deformation imposed. It plays a role in defining the strain rate, $\omega\gamma$, and it plays a role in the calculation of the modulus, Stress/γ, which increases with ω, but decreases with strain softening, when this effect is triggered. In the discussion, we present a new understanding of "the network of entanglement" and show how its orientation and gradual instability gives rise to the mechanisms of deformation observed from very low ω to high ω, at various strains. We suggest that the network character of deformation is not due to topological considerations but, instead, due to the cooperative coupling nature of the interactions between the macromolecules conformers which organize according to a *Dual-Grain Field-Statistics*. In this model, the duality aspect comes twice: it comes at the local level of interactions between the conformers, and this

duality is dealt with by the introduction of the Grain-Field Statistics applicable to macro-coil systems. The equations of the Grain-Field Statistics predict the dynamic aspect of the interactions between conformers. But the interaction between macro-coils introduces a second level of duality, above a certain size for the macro-coils (which we consider to be the onset of entanglements), responsible for the molecular characteristics of the dynamic network. In summary, we introduce in this article new methods of analysis of the rheological results which appear to confirm an essential aspect of the cohesion of the interactions between the conformers and the existence of the “entanglements”, the existence of a Dual-Phase structure. The question of the stability of the network of interactions, which was an essential focus of experimental investigation in chapter 4 of this dissertation is reviewed here in terms of the Dual-Phase model.

Chapter 6: The Elastic Dissipative State of Polymeric Melts. Solid-Like Behavior in the Molten State

We report in this chapter the dynamic rheological properties of a Polycarbonate melt, Makrolon 2207, a typical amorphous polymer with no molecular particularities which would render the results unique to that polymer. We observed an increase of the viscosity at low ω, as $\omega \rightarrow 0$ (instead of a constant Newtonian viscosity) and a solid-like behavior for $G'(\omega)$ and $G''(\omega)$, which diverges from the classical rheological description accepted for a simple homopolymer melt. We show that these results are similar to observations reported by L. Noirez on other thermoplastics (PBD and polybutylacrylate). We offer an interpretation of this low ω "shear-thinning tail" in terms of the Dual-Phase visco-elastic model of entanglements proposed in the previous chapters which suggests that the phase-line diffusion mechanism (the sweep of the phase lines) occurring in the Newtonian region is influenced by "b-grain glassification" occurring above T_g. Thus the viscosity increase at low ω is essentially due to a "free volume" fluctuation decrease explaining the instability of the Newtonian state.

Chapter 7: Shear-Thinning of Polymeric Melts: the Failure of The Reptation Model.

A RHEO-SANS RESULTS OF WATANABE ET AL. (2007).

B RHEO-SANS RESULTS OF NOIREZ ET AL. (2009).

C DISCUSSION AND CONCLUSIONS

D REFERENCES (Chapter 7)

Chapter 8: THESIS CONCLUSIONS: Entanglements: A New Interpretation and Its Perspectives In Science and Technology.

A. The need for a New School of Polymer Physics?

B The development of plastic batteries from recycled plastics

C REFERENCES (Chapter 8)

PREFACE

40 YEARS OF PAINTING ON THE SAME CANVAS

It seems that my life for the last 40 years has been dedicated to the understanding of ideas I once conceived while student at the Massachusetts Institute of Technology (M.I.T.) [0]. These initial ideas were intuitive at first but evolved into a school of thoughts which are now grounded in me as the basis for a philosophy of life.

I realize in writing this preface for a new PhD dissertation how much the story of my life has been driven by this intense creative time spent while I was 22-25 years old, possibly triggered by my fortuitous presence at this prestigious institution and also inspired by the air of the time, the post hippie generation, which I had fully discovered and endorsed. This is also during this extraordinary focused time that I met the person who became my dear wife and the closest witness of my evolution and of its implications in our daily life.

My supervisor at M.I.T was at first Prof. E.W. Merrill, a true gentleman and a very good teacher, but Prof. Fred. McGarry had convinced me-by giving me a teaching assistantship- to become my supervisor and he also had opened up his contacts allowing me to meet and work with prestigious scientists such as R.F. Boyer and Turner Alfrey at the Dow Research Center (Midland, MI), or Profs. Bruce Maxwell and John Gillham at Princeton. He may also have had another agenda in mind when he introduced me to his family of six daughters, several of whom were approximately my age, students at Radcliff, beautiful and interesting young women who had just lost their mother of cancer, herself a classy and talented French and Spanish professor at Radcliff. In any case, history cannot be re-written and, at the end, my supervisor and father of these beautiful young women from Radcliff, refused to sign my thesis dissertation, although it was listed for graduation in May 1975. I can only blame myself: who plays with fire accepts the possibility to get burned! Yet, 40 years later, even after the negative impact and bitter consequences this event did have in the course of my career, I consider that not having my M.I.T thesis validated officially, whatever the true reasons, pushed me to improve it for all these years. Furthermore, to demonstrate that it had merits may have been the driving force leading to new discoveries which, in turn, resulted in improvements of the original concepts.

The research I started, just after MIT, on the use of vibration in molding processes, led to the "Rheomolding" and, more recently, to the "Rheo-Fluidification" technologies which are currently in use to help plastics processors and compounders. The TSC/RMA spectrometer which I developed under license from Prof. C. Lacabane and commercialized in the 90s stemmed from my interest in characterizing coupled and interactive molecular motions in terms of the new theory of polymer physics I had initiated at M.I.T.

From 1976 to 2006 I have had the chance and privilege to merge an interesting and challenging career as an entrepreneur developing projects and instruments directly resulting from and testing my new theoretical ideas in polymer physics, and the continuing theoretical research which demanded to improve and generalize those new ideas. Since 2007 I have turned my attention entirely to polymer physics from an academic stand point, first by catching up with and studying what the academic world had advanced since 1975, then by trying to combine theoretically what 15 years of experiments in solid state amorphous matter had taught me with another 15 years of experiments in melt flow dynamics (rheological experiments and processing manipulation). This is where I stand right now. In a certain sense, I have the clear impression that I have spent forty years re-thinking, modifying and re-writing my M.I.T. thesis, like a painter who would have spent his life re-touching over and over the same painting.

1. The M.I.T thesis: "**A THEORY FOR THE PROPERTIES AND THE BEHAVIOR OF POLYMERIC MATERIALS"**

My PhD dissertation at M.I.T (1975) presented the first version of what I now call "the Grain-Field-Statistics", the basis for my proposed new theory of polymer physics and the subject of this research. The conformational statistics of "bond-units ", which were defined along a single chain without intermolecular interactions, could be represented with a multi-conformational state model, similar to the type used by Volkenstein [1] or Robertson [2]. The effect of the inter-molecular interactions between the bond-units, belonging or not to the same macromolecule, was perceived as the influence on each other of randomly distributed bond-units assuming all types of conformations without any preference, creating nodules of bond-units called "bb-balls" (bonded-bonds). The bb-balls gathered into systems, "Energetic Kinetic

Systems", which were thermodynamically stable because of the formation of a few bonds of a special type, of lower conformation energy, i.e. of bond-units assuming the same and most stable conformation, trans or helicoidal for instance. This speculative interpretation of the Energetic Kinetic Network Theory resulted in the creation of "local order" in the morphology, which was presented as platelike bundles, small enough to be invisible to the microscopists (< 60A), and of nodules of randomly packed bonds surrounded at their interface by "free bonds". The size and shape of the bb nodules depended on the temperature and the amount of orientation. The macromolecules were wandering around, participating partially to the build up of the bb balls, and more scarcely to the bundles, at least in the case of true amorphous polymers (Figure 0-1).

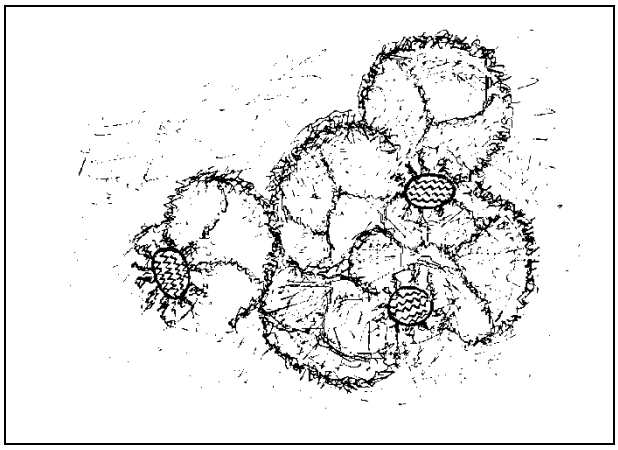

Figure 0-1

The Energetic Kinetic Systems were defined by the ensemble of bond-units in a group of nodules and their interface, stabilized by the presence of two adjacent bundles, so the stability of the systems was really the result of the existence of the bundles themselves. $T_{l,l}$ was the temperature of melting of the bundles, and the systems (EKS) ceased to exist at $T_{l,l}$ (66). Figure 0-1 is a reproduction of the 1975 thesis view on the morphology of amorphous polymers. The sketch represented the morphology which one could observe after etching the surface with a chemical reactant which would attack the interfaces (of lower density) first. The darker regions represent the interfaces.

At the present time (2016) the initial theory has been greatly modified and improved and, as a result, the presence of the bundles is not required to explain the stability of the EKS in terms of morphological structure, but the bb-balls and their interface made up of free bond-units are still present as discussed below.

2. The Search for a New Understanding of the b/F Coupling between Conformers: the Dual-Split Statistics.

It is probably Flory who was *indirectly* responsible for a new interpretation of what I called in my thesis "the Energetic Kinetic Network Theory (EKNET)". In a certain sense, the 1975 thesis contradicted Flory's views on the amorphous state [3], and he was leading the opposition over the raging controversy on the presence of "local order" in the amorphous state of polymers. R. F. Boyer was at the other end of the spectrum, claiming evidence for local order. Then Flory won the Nobel price, almost immediately after Benoit [4] had confirmed by small angle neutron scattering (SANS) the total randomness of the macromolecules in the bulk. In the 1975 dissertation a morphological interpretation of the Energetic Kinetic principles was not necessary but was presented for convenience since, in order to have stable systems, it was convenient to find a morphological reason for this stability. This was the reason for creating the bundle as a special bb-ball (Figure 0-1). But, after the work of Benoit [4], it became unclear how, if there was actually no local-order to stabilize the Energetic Kinetic Systems, the systems could become stable. **Could it be possible to have stable systems and no local-order after al**l?

The Dual-Split-Kinetic model, which provides the original set of equations for my understanding of the interactions between conformers to explain the presence of b and F conformers without local order, was conceived between 1976 and 1981. With this new proposed statistics of the conformers-see the next section- the local order concept was not needed to give life to the stability of the systems, and thus local order or "segment-segment melting", as it is now called [5], was not *required* to explain what I now see as a fundamental aspect of the interactive process between the conformers: the presence of the F and b dual-phase.

Hence, even if there are many similarities between the 1975 thesis version and the present presentation of polymer physics, there is also a fundamental difference which may be essential,

not only because, obviously, it may provide a new light in polymer science, but also because it could also be generalized to other systems in interaction in physics, and provide a new angle to deal with delocalization and entanglement in particle physics. The essential difference with my thesis's presentation derives from the introduction of a dissipative term in the dual-split statistics describing the coupled states of the interactive conformers. This will be explained in the 1st chapter, a PREAMBLE to this thesis. The dissipative character of entanglements in polymers, for instance, will be shown to be the consequence of the Dual-Split Statistics of the conformers, leading to the Cross-Dual-Phase-Statistics. Likewise, the stability of entanglements in a melt could easily be coined in terms of a rheological temperature of a melt, located at or similar to T_{LL}. It may be that Boyer was right in claiming strongly the existence of this upper transition but wrong in its interpretation as a local melting process. The confirmation of the existence of the T_{LL} transition might be a strong experimental evidence of the existence of dual-phases, but not of local order. This is *not* to say that local order never exists for some polymers, especially for those which have a tendency to crystallize, but this is not the reason for $T_{l,l.}$ although it can influence it. In this research strong evidence is offered suggesting that $T_{l,l}$ is associated with the stability of the Cross-Dual-Phase network, itself a function of the b/F dual-phase statistics.

3. The Search for a New Understanding of Flow Properties from the Conformers' Dual-Split Statistics (M<Me) and Crossed-Dual-Phase Statistics (M>Me).

This thesis is the compilation of several articles published in the J. Macromol. Sci. over the last few years dedicated to the subject of melt deformation and flow of polymers. The link between the chapters is the new model used to describe the source of molecular motions and flow, which is the Dual-Split Statistics of the conformers; this model provides a quantitative way to determine stress and strain from the variation of the conformational state of the conformers. The Grain-Field Statistics, which generalizes the application of the Dual-Split Statistics of conformers to "open dissipative systems", is responsible for the existence of "entanglements", i.e. the split of the system of interactions between conformers into two open dissipative systems, which we call Cross-Dual Phases. This is the main originality of this work.

The 6 chapters of the thesis concentrate in presenting the rheological results under this new view of the deformation of a network of interactive coupled dual-phase submitted to small or large deformations. Even without going into the mathematics of the Dual-Split Statistics or the Grain-Field Statistics, a separate subject on its own, the description of the linear and non-linear rheology of polymer melts from the perspective of a network of dual-phases at two interactive levels appears very simple and rich in potential applications. What is called "disentanglement", for instance, can be described in the context of the stability of the network of Cross-Dual-Phases (chapter 4). The industrial applications of "disentanglement" (and/or "shear-refinement") are readily commercialized or at the pilot stage: their large benefits are addressed in terms of energy savings during processing, throughput enhancement, mixing with thermally sensitive additives at low temperature, low degradation microinjection molding, and the manufacturing of new materials with enhanced physical properties (film permeability for the food packaging industry). Yet the lack of understanding of these achievements by the established models of flow (reptation) has impacted negatively the spread of this new technology, which has remained empirical and marginal, even looked down as "suspicious" by the reptation model followers…

The history of Science is full of these stories of rejection of new ideas which stem from explaining new experiments apparently contradicting previously established concepts. In this thesis, we have taken the time to expose at length the experimental procedure and analyze the possible artifacts which could explain the results (chapters 2-6). Yet one overwhelming convincing evidence stands out, in our opinion, it is from the discovery of "sustained-orientation", explained in chapter 2, and studied in chapter 4, that produces polymer granules with properties that completely challenge the existing views in polymers. Not a single paper from the reptation school has addressed the issue of "sustained-orientation" since its first publication more than 5 years ago.

We also present in Chapter 7 small angle neutron scattering (SANS) evidence that the established molecular dynamic models (e.g.reptation) misrepresent the deformation of a single macromolecular chain during shear-thinning, yet a basic fundamental phenomenon of linear rheology. In chapter 3, we carefully re-visit the basic concepts of linear rheology which have established dynamic molecular models as a trustworthy reference to study and explain flow in polymer melts. Our conclusions are somewhat at variance with those scientists who believe that

the current established understanding of linear viscoelasticity is the jewelry of polymer science. On the contrary, we suggest that the concepts of relaxation times, local friction coefficient, time-temperature superposition temperature and molecular weight between entanglement (Me), may be limitations to understand flow under conditions of deformation used by the industry, i.e. at fast throughput (strain rate) and large strain.

In short, we have initiated and propose to use another molecular approach to describe the deformation process in polymer melts which encompasses small and large deformation without the difficulty inherent to the established dynamic models of flow which are based on the description of the deformation of singular chains embedded in a mean field of interactions. In chapter 4 it is shown that the strain induced time dependency of the rheological parameters (G', G") cannot be explained by reference to the reptation time alone and yet that non-linear viscoelastic deformation results can be understood and extrapolated from their linear (low strain) state if we assume the instability of the network of interactions that modulates the kinetics. In chapter 5, we describe the physical parameters of the dual-phase rheology and the way to obtain them from experimental results. The important concept evolving from this new analysis is the existence and relative stability of the "network of entanglements", which is expressed by the dynamics of the Crossed-Dual-Phases, giving rise to the elastic dissipative wave character of the melt. The elasticity of the network is, in this view, responsible for shear-thinning, whereas, at rest, without shear-deformation, the network dissipative properties explain the Newtonian behavior and also the solid-like characteristics of the melt which are studied in chapter 6. The orientation of the entanglement network, generated by the anisotropicity of the blinking deformation process at large frequency (or amplitude) explains the rubbery plateau region in a totally different way than the established models.

We have designated the presentation of these new views about interactions in polymer chains and their entanglement "New School of Polymer Physics" and suggest that it may represent a paradigm shift which will inspire the development of new concepts in physics and new innovative products and processes in engineering.

REFERENCES FOR THIS PREFACE

[0] J.P. Ibar. M.I.T, PhD thesis (1975), unpublished : "*A New Theory For the Properties and the Behavior of Polymeric Materials*". https:// sites.google.com/a/eknetcampus.com/dual-split-statistics/).

[1] M. V. Volkenstein, *Doklady Akad. Nauk USSR*; 78, 879 (1951).

[2] R. E. Robertson, Annals of the New York Academy of Sciences, Vol. 371, J.M. O'Reilly and M. Goldstein Eds.; New York. Academy of Sciences (1981):"*Structure and Mobility in Molecular and Atomic Glasses"* ; R. E. Robertson: J. Chem. Phys. 44, 3950 (1966)

[3] A. D.Williams, P.J. Flory, *J. Polym. Sci.*; C16, 2981 (1968).

[4] H. Benoit. Polymer Preprints, 15, Vol. 2, 324 (1974).

[5] R.F. Boyer in "*Computational Modeling of Polymers*", J. Bicerano, Ed., Marcel Dekker, New York, pp 1-52 (1992).

Chapter 1

PREAMBLE: INTRODUCTION TO THE DUAL-PHASE MODEL OF POLYMER INTERACTIONS AND TO THE CROSS-DUAL-PHASE MODEL OF ENTANGLEMENTS.

Viscosity represents the resistance to flow. It describes how the constituents of a liquid interact to respond to a mechanical deformation, in this preamble a shear deformation imposed dynamically to polymer melts with radial frequency ω. At vanishing strain rate (or frequency ω—>0), the stress required to shear the melt vanishes to zero, but the ratio of stress to strain rate is finite: this is the Newtonian viscosity, a parameter that expresses the pure viscous character of the state of interactions between the macromolecules. Shear-thinning behavior (also called "pseudo-plasticity" behavior), describes the fact that viscosity decreases as the strain rate (or ω) increases. The melt is then designated as non-Newtonian. Fig. 1 illustrates the phenomenon of shear-thinning.

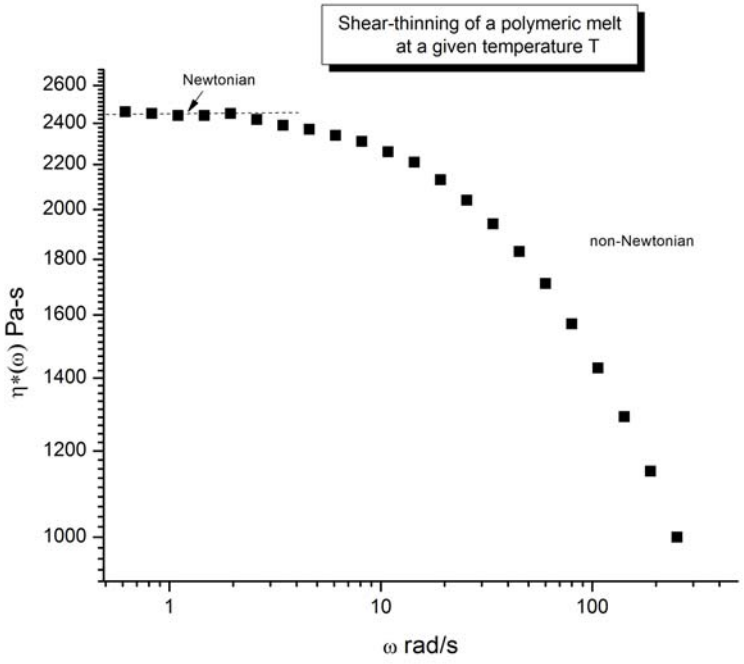

Fig.1

Viscosity vs Frequency (log-log) illustrating the concept of Newtonian and non-Newtonian viscosity (shear-thinning).

A. I The classical view of polymer visco-elasticity, shear-thinning and entanglements.

Classical visco-elasticity theory [2, 3] considers shear-thinning of a polymer melt as a disturbance by the flow rate of the pure liquid state -described by the Newtonian viscosity-due to the orientation of the chains by the stress field. "*This reduction of viscosity is due to molecular alignments and disentanglements of the long polymer chains*" claim Vlachopoulos and Strutt [4]. The well admitted Carreau' s formulation of the strain rate dependence of shear viscosity [5] correctly describes the relationship, from low to high ω, which translates this concept of a state variable, the Newtonian viscosity, continuously modified by a factor controlled by the degree of orientation of the singular macromolecular chains, which itself is a function of strain rate (ω). The concept of relaxation time, τ, and its correlation to the internal friction, thus to the viscosity, permits to transcribe the dynamic shear viscosity η* in molecular (effect of M) and topological (M/Me) terms, where M is the molecular weight of the chain and Me the critical molecular weight between entanglements. In the claimed molecular interpretations of shear-thinning [6-8], these parameters and the introduction of a characteristic relaxation time, called the reptation time, determine the dynamics of the melt, i.e. the effect of strain rate on viscosity and modulus. In the de Gennes's molecular interpretation of the viscosity results [6], the deformation of single chains is the focus of attention. The macromolecular chain is embedded in a field of interactions created by the other chains which confine its motion within a tube in which it can reptate; the process is governed by the reptation time. For polymer melts, a single relaxation time does not explain all the visco-elastic results in the linear regime (at low strain), yet a spectrum of relaxation times does, which can be derived from the properties of the reptation time and its dependence on temperature and molecular weight[2, 3, 6-8].

Doi and Edwards [8] attribute the departure from the non-Newtonian behavior to the reptation time, τ_d, of the de Gennes' theory, which they determine experimentally at the cross-over frequency, ω_x, of G'(ω) and G"(ω): $\tau d = 1/\omega_x$. When the melt is sheared in the terminal region, shear-thinning is due to the orientation of the macromolecules segments in the direction of the stress gradient. Shear-thinning occurs when the strain rate surpasses the reciprocal of the reptation time; the viscosity continues to decrease as strain rate increases until the rubbery plateau region is reached, which occurs at the minimum of tan δ, where δ is the phase difference between stress and strain, a characteristic of the visco-elastic nature of the melt. The phase difference is 90 ^{o} for a pure viscous liquid (Newtonian), 0 for a pure elastic solid and is minimum at the onset of the rubbery plateau, allowing to characterize the entanglement density and the rubbery plateau modulus $G_{o,N}$. For instance, for polycarbonate, Me=2,500 g/mole and $G_{o,N}$=1.5 MPa [9].

The Newtonian viscosity, η^*_o only depends on temperature, and has been correlated to the amount of free volume present in the melt. This was discovered for small liquids by Doolittle [10] and further applied to polymers by William, Landel and Ferry, authors of the famous WLF equation [3]. The molecular weight dependence of η^*_o is derived from the variation of the reptation time with M which scales like $M^{3.4}$.

In summary, classical visco-elasticity theory explains the melt deformation with one mechanism of deformation, the chains being stretched, their rms end to end distance increasing, and with the possibility of slips of the entanglement points which determine the network structure. Chapter 3 will provide an overview of the predictions, successes and shortcomings of the classical model of visco-elasticity. This can also be found in Ref. 11.

A. II The Dual-Split Statistics view of polymer visco-elasticity, shear-thinning and entanglements.

On the other hand, the Dual-Phase visco-elastic model, presented in Refs. 12-13, suggests a very different origin for shear-thinning, strain softening and entanglements. It actually projects the possibility to obtain various Newtonian viscosity values at a given temperature by bringing the melt out of equilibrium by processing it by Rheo-Fluidification [14, 15]. This model is briefly presented in the next section.

INTRODUCTION TO THE DUAL-PHASE MODEL OF POLYMER INTERACTIONS AND TO THE CROSS-DUAL-PHASE MODEL OF ENTANGLEMENTS.

For the sake of clarity in reading this dissertation it appears useful to present early on a short review of the concepts which led to the anticipation of the experimental results addressed below.

In the classical views, the chain is particularized and its interaction with its surrounding is described in terms of a mean field of interactions. The entropy of a single chain is calculated from its intra-molecularly linked covalent bonds and the deformation (to express flow properties, for instance) is due to a modification of the entropy. The presence of the other chains is perceived as a restriction on the entropy (in particular, in de Gennes's well praised model [6, 7] by the confinement of the motion of the chain within a tube in which the chain can reptate. The sophistication of the "reptation" model comes from the refinement of the definition of the tube itself [8,16-19].

In this preamble we summarize our new way to describe the complexity of the interactions

between polymer macromolecules, in particular a new way to determine the conformational state of its basic constituents, the conformers, which are covalently bound to each other along the chains, yet exert inter-molecular forces with adjacent conformers, belonging to the same or to other macromolecules.

B.I. A New model of Polymer Interactions (Summary).

A macromolecule can be viewed as a succession of real or virtual three-bond elements, which we call "conformers". For simple macromolecules (polyvinyl chloride, polyethylene, polytetrafluoroethylene, polystyrene, polyacrylates, etc., and most of the polyvinyls) the macromolecule can be described with a succession of three-bond elements, as presented in Fig. 2. For these simple systems the length of the conformer C_1C_2, C_2C_3, C_3C_4 corresponds to the length of 3 covalent bonds of the repeating unit.

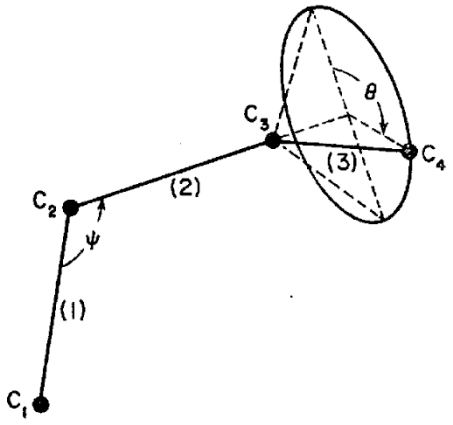

Fig. 2

Conformer.

For other systems the situation is slightly more complex and the length of the bonds of the repeating unit is not the length of C_1C_2, C_2C_3, C_3C_4 of the "virtual three-bond element". A good example is given in Figs. 3 and 4 for polycarbonate of bisphenol-A, the polymer studied in many chapters of this dissertation.

Champetier and Monnerie [20] and Lunn [21] reported the work of several authors [27] who studied the statistical shape of the random chain in dilute solution, i.e. the chain conformation less affected by intermolecular forces, and concluded that the carbonate group O-CO-O was planar (stabilized by

electron resonance over the three oxygen atoms) and that the "trans" form of the carbonate group was preferred over the "cis". See Figs. 3a and b. An infra-red spectroscopic study of polycarbonate [21] led to the conclusion that the planes of adjacent benzene rings in the polycarbonate chain lie nearly parallel to one another; steric hindrances prevent them from being completely parallel. From vibrational assignments of the principal bonds of O-CO-O, it was optically verified that the carbonate group is predominantly in the trans, trans conformation (Fig. 4) but some cis, trans conformations are also present [21]. The cis and trans conformers for polycarbonate are depicted in Fig. 4.

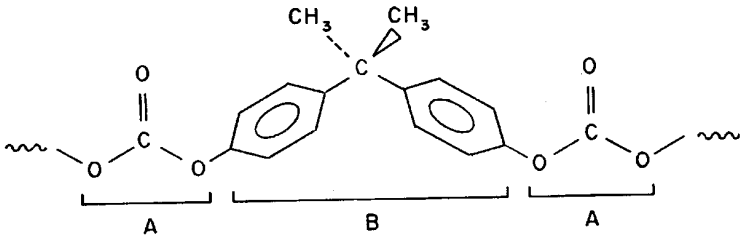

(a)

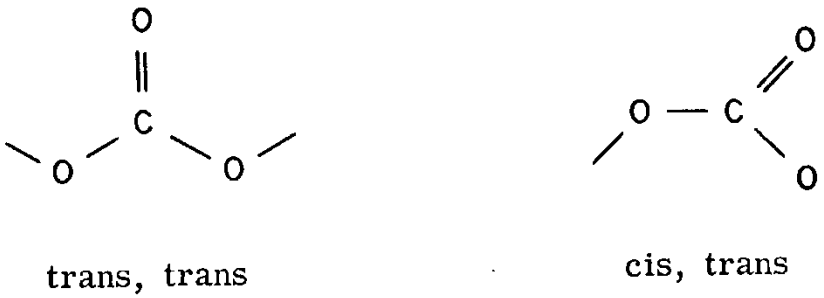

(b)

Fig. 3

(a) Configuration of the phenyl groups and the carbonate groups of polycarbonate. (b) Rotation about the carbonyl groups to define the cis/trans conformer isomeric states.

As already said, a macromolecule can be viewed as a succession of real or virtual "conformers", even in complex situations. The interest in "conformers" to describe the rotational isomeric state of macromolecules has resonance in the work of Lunn [21], Volkenstein [22], Robertson [23], Miller [24,

25], and Matsuoka [26].

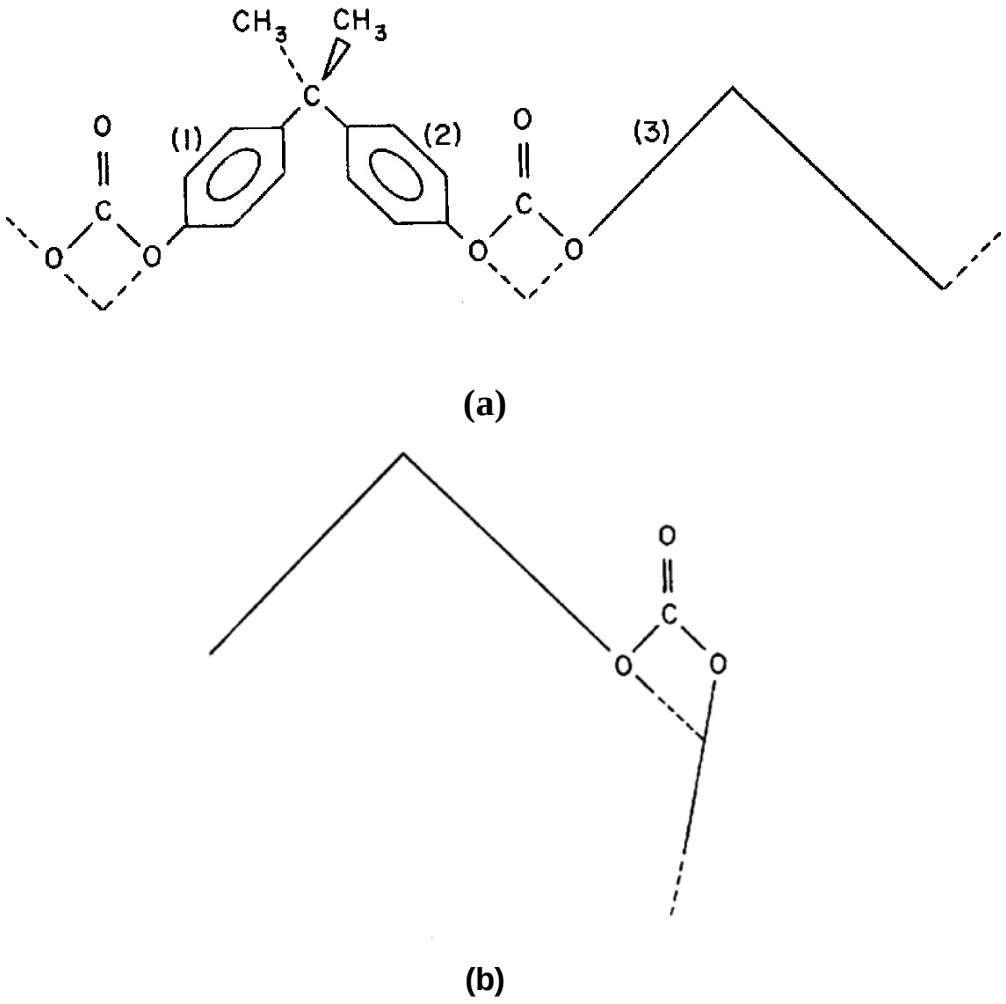

Fig. 4

Polycarbonate chain conformers. (a) The conformer is in the trans-conformation. (b) The conformer is in the cis-conformation.

B. I. 1 *Conformers:the b and F types of conformers.*

The "*conformation*" of a conformer can be described energetically just like the conformation of a small molecule, say, ethanol, CH_3 - CH_2OH. Like for ethanol, by rotation about the C-C bond of the hydroxyl-1 group-OH, a polymer conformer can assume different conformations, represented in Fig. 2 by the rotation of the angle □.

The internal rotation barrier energy of a "free" conformer, given a certain conformation, is the result of the electronic and steric interactions between adjacent atoms (or groups of atoms) of the same

conformer. The Pauling sinusoidal function is often used for the internal rotation barriers:

(1) $V_F = Vo\ (1 + \cos n\theta)$

n = 3 for all C-C bonds (but n = 2 for the CO-O bond of PMMA for instance). Vo represents the height of the barrier, and is approximately 2.7 kcal/mole for the C-C bonds, 8.7 kcal/mole for the CO-O bonds of PMMA [20, 28]. Other, more sophisticated, internal rotation potential energy profiles have also been described [27].

The potential energy of a bonded conformer accounts for the inter-molecular interactions, Van der Waals and electrostatic in nature, including hydrogen bonding type.

-Van der Waals interactions

The potential function for Van der Waals interactions between non-covalently bonded atoms can be approximated by a function of the form [29, 30]:

$V(r) = A\, r^{-D} * \exp(-B\, r) - C\, r^{-6}$ (kcal/2 atoms)

where r is the distance between two atoms i and k. A is a constant. D is zero for a Buckingham potential [29], whereas B = 0 and D = 12 for the more often used Lennard-Jones approach [30].

- Electrostatic Interactions

This term takes into account the possible dipole-dipole interactions which appear when some pendant or backbone atoms of the chain are polar. The well known dipole-dipole interaction equation is used to quantitatively express this type of interaction (e.g. hydrogen bonds). The potential energy between two point dipoles μ_i and μ_j is given by:

$$\varepsilon^{-1} * \left[\frac{\mu_i \mu_j}{a^3} - 3 * \frac{(\mu_i . a)(\mu_j . a)}{a^5} \right]$$

where a is the distance vector between the dipoles, and ε is the dielectric constant of the medium.

Consequently, the energy of a " bonded" conformer in a given conformation takes the theoretical form:

(2)

$$V_b(\theta) = \sum_h V_o/2(1+cosn\theta) + \sum_k A * r^{-D} * \exp(-Br) - C * r^{-6} +$$

$$\sum_l \varepsilon^{-1} * \left[\frac{\mu_i \mu_j}{a^3} - 3 * \frac{(\mu_i . a)(\mu_j . a)}{a^5} \right]$$

where h = summation over ALL non-covalently bonded pairs of atoms, k = summation over ALL adjacent pairs of atoms, l = summation over all pairs of dipoles. The value of V_b (Θ) can be theoretically computed from the above equation for any conformation of the conformer. This is practically done with the help of a computer and leads to the knowledge of the so-called "potential energy map" of a bonded conformer.

A bonded conformer has a different energy than a free conformer, according to Eqs. (1) and (2). A conformer can assume different "spatial conformations", correctly described by the value of the angle (θ) in Fig. 2. For each (θ), it is possible to compute the potential barriers $V_F(\theta)$, according to Eq. (1), and V_b (θ) according to Eq. (2). This last equation assumes that all bonds, from all other parts of the entire system, participate in the interactive stabilization of the conformer by inter-molecular coupling. Computer calculations show that the energy of a few conformers acting cooperatively converges quickly to the same energy as millions of conformers coupling as a whole.

Following this view, conformers can interact with one another according to formula (2), or they may be free of inter-molecular interactions and have a potential energy defined by Eq. (1). So, for a given spatial conformation of Fig. 2, there are two "energetic" states, depending on whether Eq. (1) or (2) is used. We call these two states “b” (bonded) and “F” (free). When conformers interact with one another, they do not necessarily require the whole set of bonds to interact with them, and, therefore, we conceive that nodules of bonded conformers, forming **b-grains** of coupled bonds, co-exist with free to move

conformers, located between the conformer nodules (i.e. at their interface). In that sense, the field of interactions described in Eq. (2) is not homogeneous, it is spatially and temporaly intermittent. As we developed extensively in the theoretical development of this model, the field is "granular", meaning it is not describable simply by Eqs 1 and 2, it also requires the definition of a fluctuation function.

We have formulated a long time ago [31], and improved over the years [1, 32, 33-35, 36], a statistical model, not explicitly shown here, which can quantitatively describe the split of the conformers between those which couple up in b-grains and those at their interface. All types of conformers are part of a grand ensemble statistics, and, therefore, coupling between all conformers occurs, whether they belong to grains or not, and across systems when several are defined. The statistics applies to a system (the number of conformers participating in the statistics), or to several coupled systems which are not all necessarily doing the same thing at all times, and the solution is obtained by following the minimization of the total free energy of the ensemble. For systems, the intrinsic energy, calculated from the conformational population of the conformers, varies with temperature, thermal history, pressure, etc. The number, size and activity of the systems vary with these variables.

B.I.2 *The Dual-Split Statistics of the conformers: [b/F <--> (c,g,t)].*

In the new statistics, the kinetic units (here conformers) are divided between the b and the F type (Fig. 5). There are N_b conformers of the b-type and N_F conformers of the F-type. As already stated, the definition of the F-conformers as free conformers from inter-conformer- interactions imposes that they gather at the interface between grains of b-conformers, and, therefore, a better cartoon than Fig. 5 is presented in Fig. 6, showing the b-grains and their in-between interface composing the F-conformers. For this reason the conformers are called the "grain-field conformers" to indicate that they are defined with respect to the statistical theory which provides their spatial conformation, c, g, F, and their b/F state. The spatial conformation assumed by the conformer can be either trans, cis, or gauche, irrespective of its b or F type. The energy of a conformer certainly depends on its type, b or F, according to Eqs. (1) or (2). Therefore, it is clear that several energy levels may correspond to a given spatial conformation.

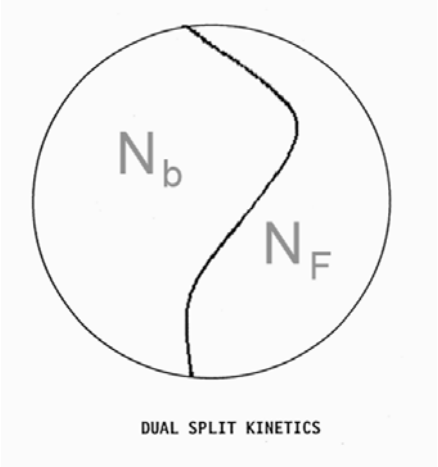

Fig. 5

Split between the b and F conformers. The size of each group, Nb and NF, varies with the dynamics of the interactions

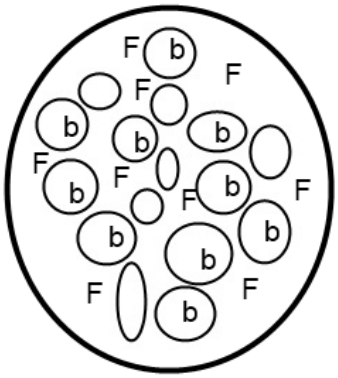

Fig. 6

"Grain structure" of the b/F Field. The b-conformers are dispersed in the F-field as b-grains to allow a local fluctuation of the interactions (b ↔ F).

Figure 7 describes a "certain" potential energy barrier profile. The shape of the curve in Fig. 7, and therefore the position of the minima, must be different for the b and the F conformers. As described in other publications [32, 36], the Grain-Field Statistics takes this into account, yet simplifies the problem by fluctuating the value of the field between the value given by Eqs. (1) and (2).

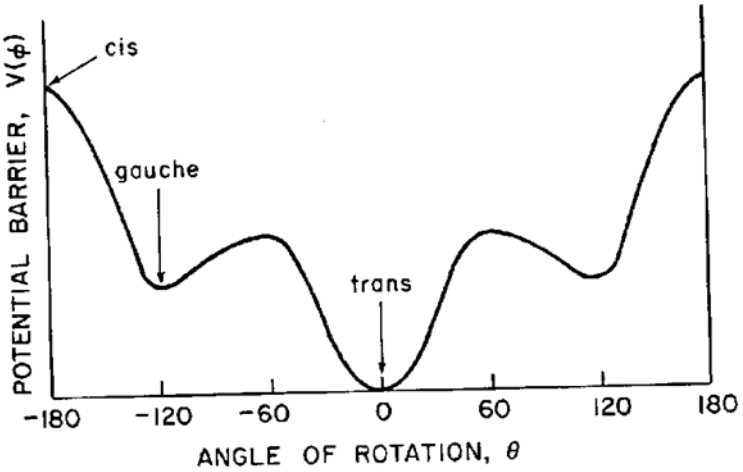

Fig. 7

Potential energy barrier for a conformer. The profile and values of minima are different for the b and F conformers.

In the following, all conformers with spatial conformations which do not correspond to trans are said to be in the "cis-gauche" (cg) conformation. Note that, contrary to what is depicted in Fig. 7, the trans energy level is not always, for all polymers, the most stable one, nor is the cis the less stable conformation. Figure 4 shows that the polycarbonate chain can assume the two spatial conformations, cis and trans, schematically presented. Without discussing here the details of the structure of the conformers of polycarbonate, it is already interesting to note that the spatial cis conformation presented in Fig. 4 is probably not the least stable of all possible conformations, since it corresponds to a stabilization of the O-CO-O group by resonance. Its cis conformation energy level is therefore expected to be the most stable of all cis-gauche conformations (yet still above the trans energy state). In cases where the helical form can be stabilized by electron resonance or other intramolecular energies (not to mention the hindrance effect due to bulky side groups), the more stable conformation will be the helical conformation and not the trans. However, in order to simplify, the corresponding energy level will still be called "trans" in the following.

Figure 8 schematically describes our assumptions at the level of local interactions. As already said, it is convenient to think of the F-conformers as distributed around the grains of b-conformers to which they are attached, thus creating an interfacial tissue of conformers. In many instances in this text, we will refer to the F-conformation tissue as the free-volume, and will consider the b-grains (also alternatively called the "bb-grains') a form of non-crystalline condensate which we associate with the process of

glassification when it occurs in very large quantity, thus the word "grain-glassification" in this work presentation.

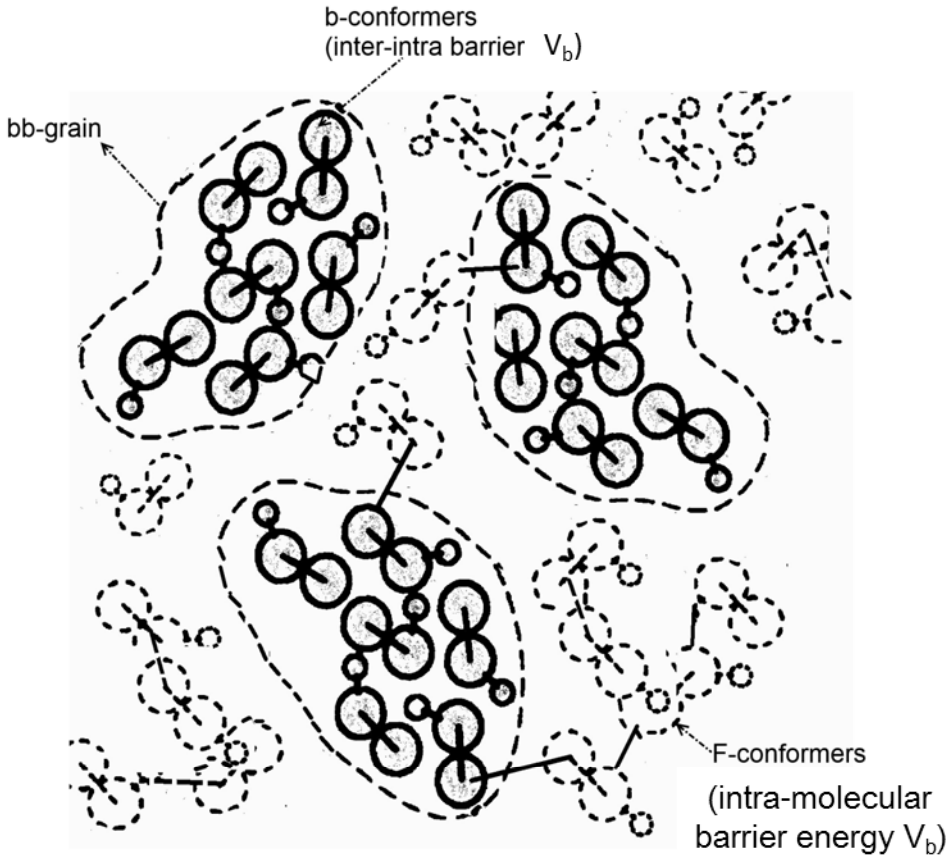

Fig. 8

Sketch of b-grains, F-conformers and b-conformers.

Figure 9 is a cartoon-sketch of the nanometric structure at an instant t, in accordance with this view of b-grains surrounded by the F-conformers tissue. Here the white zones are the F-conformers, the grey zones are the b-grains. Well above T_g, the boundaries between the b-grains are constantly being redefined, because of thermal motions, so it may be more difficult to localize the free volume around the b-grains and, under such conditions, a mean field might become a good approximation to describe the interactions. As we shall develop in the next section, this statement is valid for a polymer with a low molecular weight ($M < M_e$). Above this critical molecular weight there is a split of the N_b/ N_F solution in Fig. 5 into two groups $(N_b/ N_F)_1$ and $(N_b/ N_F)_2$ leading to two Dual-phases. A quantitative treatment of the statistics controlling the population of [b/F <--> (c,g,F)] shows that for a given split of N_b/ N_F in Fig. 5,

the size of the "b-grains" depends on temperature, non-equilibrium conditions (triggered by cooling and heating rate as well as mechanical deformation history), and the annealing time and temperature.

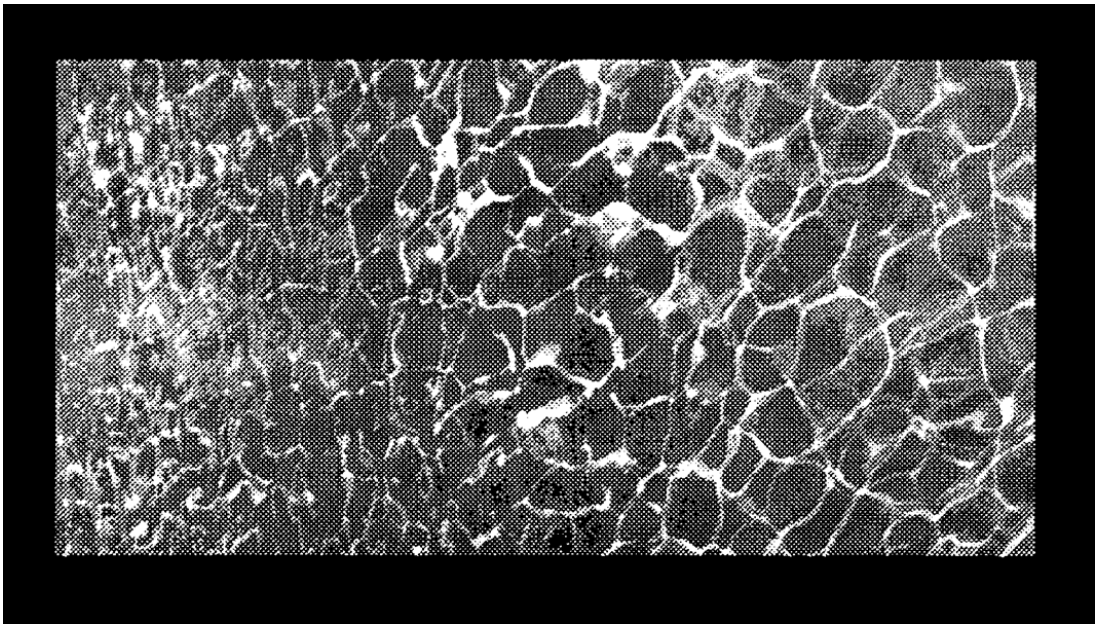

Fig. 9

Sketch of the dual-phase model [b/F <--> (c, g, t)]. The white regions represent the F-conformers. The gray areas represent the b-grains of Fig. 8. Conformers assume the conformation cis, gauche or trans, which have two energy states, b and F.

In a first mathematical modelization of the statistics [31], multiple coupled Eyring activated kinetic equations were used, which provided the variation of the concentration of the various conformers, the cis, gauche and trans conformers, either bonded or “Free to move”, which we express as: [(c,g,t) ↔ b/F]. The b and F conformers were generated by a fluctuation of the local inter-bonds interactions, which would either make the bonds inter-couple (b type) or not (F type). The case of crystalline type of bonds was also considered, when the inter-coupling occurred between conformers having the same conformation, say trans, providing the st-t conformational state (st-t standing for "stabilized" trans). Conformers packing inter-molecularly, while having different conformations, formed "bb-balls" which were not as stable as the st-t conformers which packed as nodular crystals (the nuclei). In this early stage of the creation of the theory, the whole conformer organization consisted of a mix of bb-balls, free conformers and some local crystal type st-t conformers packing as nuclei or folded crystals. However, this ensemble of conformers in interactions was not thermodynamically stable unless local order existed in the structure, even for amorphous polymers, a controversial notion which was disputed by SANS results [37].

In order to eliminate this problem, **a dissipative factor** was introduced in the kinetic equations which gave rise to the notion of dual-split kinetics [33-35]. The b / F statistics emerged from the asymmetric incidence on the conformational statistics caused by the dynamic split of the total population. The split was controlled by a minimum of the dissipative function.

The introduction of a dissipative factor gave birth to a novel kinetic formulation of dynamic systems. This dual-split statistics was first applied to a closed system formed by the conformers of a single macromolecule and it was found that the optimization of the b/F interactions resulted in the shaping of the macromolecule as a coil configuration, thus labeled a macro-coil [1]**.** We extensively studied the thermodynamics and the thermally or mechanically induced relaxational properties of macro-coils, showing that the new statistical model could explain well results obtained below (in the glass) and above the glass transition [1]. However the new model did not address the effect of molecular weight and entanglement, i.e. it applied to unentangled polymers ($M<M_e$).

B.I.3 *The Crossed Dual-Phase Statistics for long chains:*

$$[b/F\leftrightarrow(c,g,t)]_1 \;\leftrightarrow\; [b/F\leftrightarrow(c,g,t)]_2$$

The required improvement of the model came very recently [12, 13, 32] with the understanding of the influence of long chain length on the properties of the dual-split statistics. This advance became possible when it was realized that the fluctuation of the local density which made "granular" the inter-intra bonding between the conformers of a system **was equivalent** to a variation of the field that compensated with the size of the system to minimize the collective dissipative function [32]. In other words, the local fluctuation was due to the compensation between the system energy and the system size to make minimum the dissipative function [32].

This idea led us to apply the dual-split statistics to several interpenetrating macro-coils, keeping "open" the size of the systems to which the equations applied, and applying the dual-split equations individually to each open system defined by the interpenetration. The computer simulation, which was used to solve the system of equations, concentrated on the interpenetration of 3 macro-coils to create what was called a "2D interface" [1]. The question was to determine if the properties of the interpenetrating interface (the open system created by a split of the conformers in each of the 3 macro-

coils) would have different statistical properties than the rest of the conformers belonging to the un-penetrated macrocoils. Further, the question of the stability of the solution was crucial. The initial size of the macro-coils could be varied. The result of the simulation of the macro-coils penetration separated the case of small macro-coil systems ($M<M_c$) and large ones ($M>M_c$). See Fig.10.

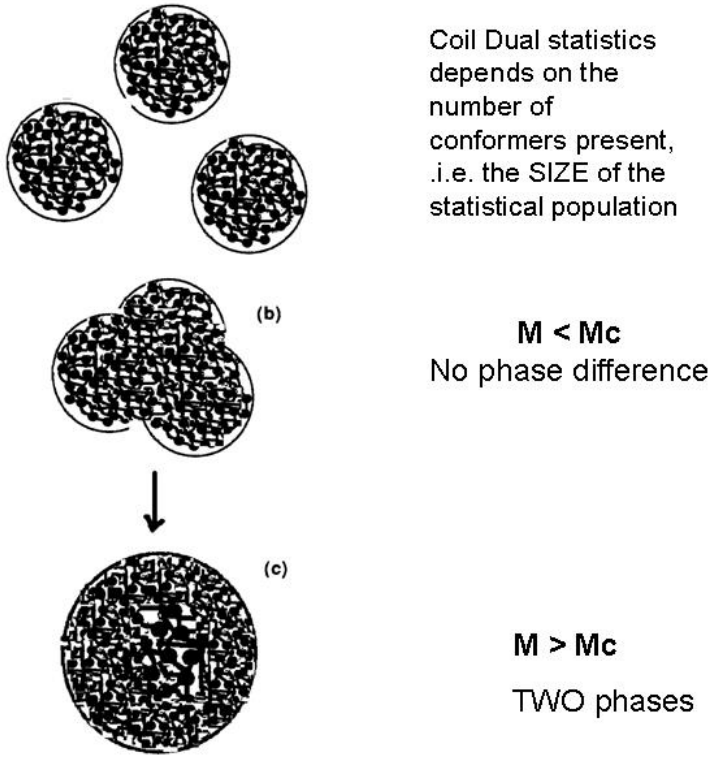

Fig. 10

Interpenetration of a set of 3 macro-coil systems. The equations of the Grain-Field-Statistics [36] are applied to solve this problem and result in an interesting result regarding the homogeneity of the [b/F <--> (c,g,t)] solution. When the number of conformers per macro-coil is smaller than a certain critical value, Mc, the interpenetration does not result in any distinction between the conformers of the intersection and the conformers from the original sets. The statistics [b/F <--> (c,g,t)] is modified by the interpenetration, but is everywhere identical. This is not the case for M>Mc, where a split of the statistics into 2 different groups occurs, creating two dual-phases $[b/F <--> (c,g,t)]_1$ and $[b/F <--> (c,g,t)]_2$. This is the heart of the new understanding of polymer entanglements and polymer physics.

For small systems, there was no difference in the phase plots for the interpenetrating system and the un-penetrated system (a phase plot is a plot of a rate of a conformer population change against its value). As M increased a difference appeared but was not stable in time: Fig. 10b. For large M, however, there were **two dual-phase statistics co-existing in the structure** (Fig.10c, bottom), and the

solution remained stable [12, 32]. This result, we have assumed, gives rise to entanglement effects [12-15].

The statistics leading to this model of entanglements is called the Crossed Dual-Phase Statistics [12, 13, 32]. There are now **two** coupled dual-phases to define the system. Fig. 11 is a cartoon sketch of the model. In Fig. 11 the existence of the two "phases" is represented by the light and dark regions, respectively (the boundaries constitute one of the phases). Both phases are of the same nature (representing local interactive coupling of conformers), but are visco-elastically different (e.g. their T_g is different by a few degrees) and their existence is due to the interpenetration of macromolecular coils. Each of the phases presented in Fig. 11 has, itself, another layer of duality due to the inter- and intra-molecular nature of the bonds interactions (Figs. 8 and 9). So, in fact, there are two interactive layers of duality, which is the reason why we use the expression Cross-Dual-Phase to describe the entanglement network. In other words the solution to the coupled dual-phase statistics of the interpenetrating macro-coils, which we call the Grain Field Statistics, does not define 4 phases but two dual-phases, like two types of crystallographic structures co-existing interactively. Melt cohesion implies a fluctuation of the channel/core phase contours, which is constantly in motion, like froth in an agitated sea near the shore (Fig. 11). The characteristics of this cross-dual-phase "entanglement network" are governed by the molecular weight of the macro-coils as well as the properties of the conformers ($b/F \leftrightarrow (c,g,t)$] described by the dual-phase statistics discussed earlier. The interpenetration of the macro-coils disturbs the dual-phase statistics which splits into two coherent and interactive phases, creating the river network sketched in Fig. 11. To simplify, we call the white fluctuating strands in Fig. 11 the "entanglement phase"; we also use the expression "phase-lines".

Fig. 11

Sketch of the Cross-Dual-Phase Entanglement Network model. The boundaries of the "white phase" are not static but fluctuating around with frequency □'$_o$ under no stress conditions. Stress increases the frequency of reorganization and, in the rubbery plateau region, preferentially orients the boundaries in the flow direction. This can be modeled by an activated process.

B.II A New Understanding of Polymer Melt Molecular Interactions and Flow Properties.

As a general statement, the problem of melt deformation consists in determining how the Cross-Dual-Phase network can produce strain coherently, from the local re-organization of the local conformers in one dual-phase or in each phase, to the orientation with the stress of the entanglement phase, resulting in the orientation of the network of entanglement. As described in details in another publication [12], this may occur, in each phase, by a stretch-relax mechanism that only involves the forced change of the isomeric state of the conformers during the stretch stage, the relaxation stage occurring by a diffusional mechanism permitting the re-localization of the conformers with respect to the deformation direction. We call this mechanism "blinking", which explains well the shear-thinning characteristics of polymeric melts. The frequency of blinking, ω', the number of times per second a part of the network channel, a strand system, is activated, i.e. stretch/relaxes, depends on the number of systems activated simultaneously, which is function of the frequency ω and the network strain elastic energy χ_2: $\omega' = \omega/\chi_2$. χ_2 can be determined from G*, the complex modulus, and from $\chi=(G'/G^*)^2$, the melt relative elasticity [12]. We showed that χ_2 was close to χ, under conditions of linear visco-elastic

deformation, but never equal to χ, so that: $\chi = \chi_1 + \chi_2$. Besides, χ_1 could assume positive or negative values, being mainly a function of the thermal history of the melt when LVE conditions applied. Yet, for non-linear visco-elastic conditions triggered by an increase of strain, it was shown that χ_1 could take large values, actually compensating with χ_2 to result in strain softening solutions [12, 13]. We concluded that at low stress, χ_1 was mainly a diffusional characteristic of the interactions between the conformers, transcribing the non-equilibrium state of the melt, i.e. the state of [b/F ↔ (c,g,t)] after the cross-dual-phase entanglement network had been deformed. Thus, the value of χ_1 as ω-->0 would be a strong indication of the amount of excess free-volume (excess of F-conformers) or excess bb-grains (b-conformers) resulting from a prior stretch history of the entanglement network going through a blinking process in a previous stage. This research led us to conclude that melts could remain stable (at least for very long times, so quasi-stable), yet be out of equilibrium with respect to their [b/F ↔ (c,g,t)] state.

Now, as is well known, the mechanism of shear-thinning, defined in our model by how ω' varies with G*, converges to the Newtonian regime at low stress of deformation (ω-->0), where the viscosity remains constant. Likewise, we can define ω'_o, the frequency of the undeformed entanglement network, which we can quantify from experimental plots of ω' vs G* extrapolated to G*=0 (see Fig. 9 of Ref. 12, reproduced below as Fig. 12).

We verified that the Newtonian viscosity, η^*_o (corresponding to G*=0), was, indeed, obtained by replacing the value of ω'_o in the expression of η*(ω) vs ω', which is linear on log-log axes (Fig. 7 of Ref. 12, reproduced below as Fig. 13).

Yet, this is an interesting issue: ω' is solely defined from χ_2, so the viscosity and G* are solely determined by the blinking parameters; thus, what is the role played by χ_1 at low ω, and how does it influence the value of the un-deformed entanglement network parameters, ω'_o and η^*_o? In particular, for a melt out of equilibrium (with respect to its entanglement state), should we not observe a variation of ω'_o and η^*_o with time, and with frequency?

One could easily understand any variation of ω'_o and η^*_o with time, as the melt would return to its equilibrium state, but why expect a variation with frequency? In essence, "blinking" establishes the link between the elasticity of the network, necessarily integrating the dynamics of the interactions between the local conformers in each phase, and the entropy of the dual-phase network, i.e. the

orientation of the phase-lines. One needs to return to Figs. 8, 9 and 11 to understand the meaning of ω'_o. For low molecular weight polymers ($M<M_c$ in Fig.10), it is Fig. 9 that applies: the b and F conformers are distributed along the shaded and white areas, in constant motion (in the melt) as a consequence of the thermal motion. The frequency is very high, ω_∞.

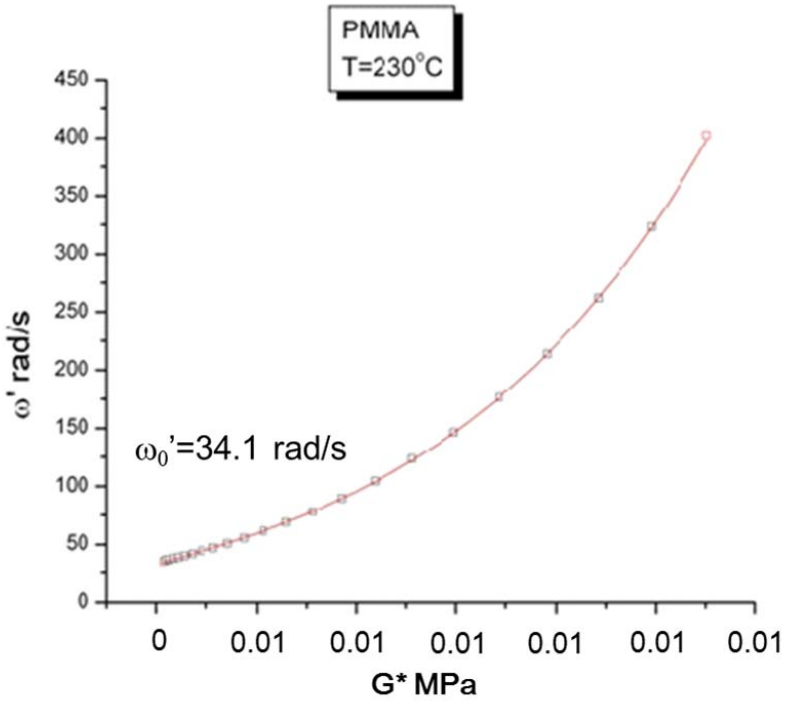

Fig. 12

Plot of ω' vs G* for PMMA. T=230 °C, 2% strain. ω'_o is found by extrapolation.

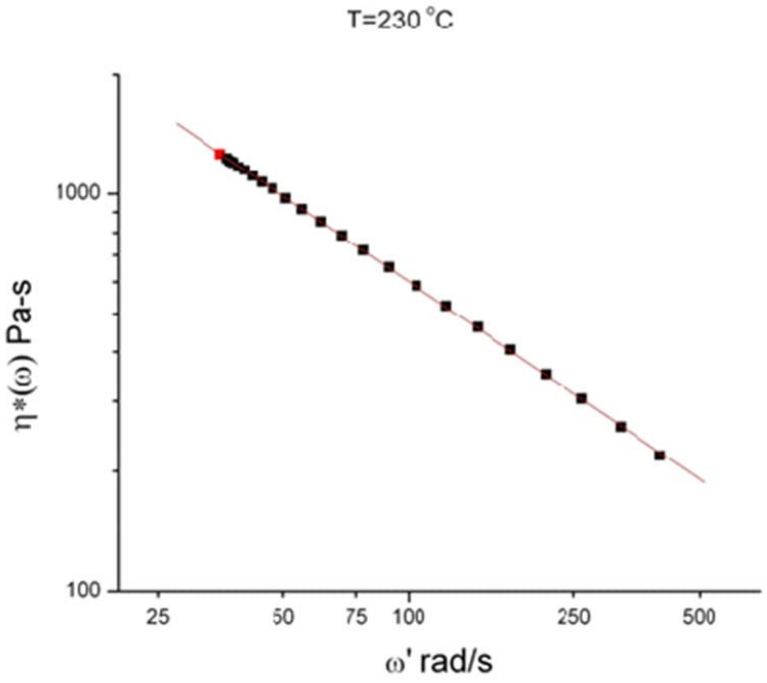

Fig. 13

log (η*(ω)) vs log(ω′) for PMMA T=230 °C 2% strain. The Newtonian viscosity η^*_o can be calculated from this graph by plugging the value of ω'_o obtained from Fig. 12 (ω'_o =34.1 rad/s) into the Eq. of the straight line. The first point of the frequency sweep, colored in red, here at the top left of the line, is always discarded in the regression to avoid possible measurement error.

But for cross-dual-phases, the motions of the bb-grains' interfaces with the F-conformers are now modulated by the existence of the two dual-phases which interactively compensate, defining a new stable equilibrium for the local motions, the [b/F↔(c,g,t)] statistics. The entropy defined by the fluctuations of the phase-lines in Fig. 11 is compensating for the thermal agitation of the b/F conformers, creating a fluctuating standing wave propagating constantly through the medium to homogeneize (average out) the differences between the phases. This is the equivalent of an elastic wave, which we call "phase-wave", sweeping through the entire network of conformers in interactions. In our model, this is the "sweeping" mode of deformation of a melt. This is the mode of deformation at low G*, occurring for a melt "at rest", i.e. in Newtonian conditions. ω'_o is the frequency for the sweeping wave. Since χ_2-->0 when G*-->0, and χ_1 depends on the state of equilibrium of the melt, we conclude that the diffusional sweeping wave must be, somehow, sensitive to the thermal history of the melt and, in particular, depend on the entropy of the phase-lines network, the result of a previous stage

mechanical deformation. When the previous history has yielded a different phase-line structure (a condition which we may or may not want to call "disentanglement"-see the discussion in Part III), the b/F state can readjust to compensate, i.e. the number of bb-grains evolves correspondingly and become different. The diffusional sweeping phase-wave will require more energy to diffuse through the melt if there are more bb-grains to carry through, which means, in rheological terms, that viscosity increases as the concentration of bb-grains increases (also equivalent to a decrease of free volume). This is a well known result, that the Newtonian viscosity can be described in terms of free volume (Doolittle, Ferry). In other words, the momentum of the sweeping phase-wave, its density times its speed of propagation, is expected to vary with the local density of the melt, i.e with the amount of bb-grains/free volume, and this is the reason we expect to see, for a melt out of equilibrium, and maintained out of equilibrium, a variation of ω'_o, η^*_o and χ_1 with frequency ω. Our question is to determine if our two regimes of deformation of the melt, the sweeping mode and the blinking mode can ever be separated out, perhaps by revealing situations where the non-equilibrium state creates a discontinuity at the junction, with a mismatch of ω'_o extrapolated from low ω values (sweeping) and high ω values (blinking).

As it turned out, the conditions to observe such effects were realized when studying polycarbonate. This will be the subject of Chapter 6.

In several chapters of this dissertation, we will describe the experimental work and procedure, focusing on determining whether the melt is chemically and thermally stable during the time of the dynamic frequency sweeps in the rheometer. Second, we will describe the rheological features observed using $\eta^*(\omega)$, then using $G'(\omega)$ and $G''(\omega)$ to compare with classical responses of polymeric melts. In the discussion of each chapter, we will examine all the possible artifacts or structural changes that could explain our results. Finally, we will analyze the data using the framework of the new dual-phase model of visco-elasticity, illustrating the concepts of dynamic free volume, shear-thinning by blinking, etc. and opening the debate to what lessons we can learn from using these new concepts. This will be the subject of the last chapter, chapter 7, which suggests a few perspectives-both theoretical and practical- for the new interpretation of entanglements.

REFERENCES (Chapter 1)

[1] Ibar, J. P., “Do we need a new theory in polymer physics?”, J. Macromol. Sci., Part C: Polym. Rev., 1997, 37, 389-458.

[2] Ferry, J. D. "Viscoelastic properties of polymers." John Wiley & Sons (1970). Ch. 11, 13.

[3] Williams, M. L., Landel, R. F., Ferry, J. D., “The temperature dependence of relaxation mechanisms in amorphous polymers and other glass-forming liquids.” J. Am. Chem. Soc., 1955, 77, 3701-3707.

[4] Vlachopoulos, J., Strutt, D., “The role of rheology in polymer extrusion”. In New Technology for Extrusion Conference. Milan, Italy. 2003, Nov (pp. 20-21).

[5] Carreau, P. J. Ph.D. Thesis, University of Wisconsin, 1968.

[6] de Gennes, P. G., “Scaling concepts in polymer physics”, Cornell University Press, 1979.

[7] de Gennes,P. G., “Reptation of a Polymer Chain in the Presence of Fixed Obstacles**”,** J. Chem. Phys., 1971, 55, 572–579.

[8] Edwards, S. F., Doi, M., “The theory of polymer dynamics”, Clarendon, Oxford, 1986.

[9] LeGrand, D. G., and Bendler, J. T., “Handbook of Polycarbonate Science and Technology”, Marcel Dekker Inc., NYC, 2000.

[10] Doolittle, A. K., Doolittle, D. B., “Studies in Newtonian Flow. V. Further Verification of the Free-Space Viscosity Equation.”, J. Appl. Phys., 1957, 28, 901-905.

[11] Ibar, J. P. The Great Myths of Polymer Melt Rheology, Part I: Comparison of Experiment and Current Theory. J. Macromol. Sci., Part B, Phys., 2009, 48, 1143-1189.

[12] Ibar, J. P. The Great Myths of Rheology Part III: Elasticity of the Network of Entanglements. J. Macromol. Sci., Part B, Phys., 2013, 52, 223-309.

[13] Ibar, J. P., “The Great Myths of Rheology, Part II: Transient and Steady-State Melt Deformation: The Question of Melt Entanglement Stability”, J. Macromol. Sci., Part B, Phys., 2010, 49, 1148-1258.

[14] Ibar, J. P., “Processing Polymer Melts under Rheo-Fluidification Flow Conditions, Part 1: Boosting Shear-Thinning by Adding Low Frequency Nonlinear Vibration to Induce Strain Softening”, J. Macromol. Sci., Part B, Phys. 2013, 52, 407-441.

[15] Ibar, J. P., “Processing Polymer Melts under Rheo-Fluidification Flow Conditions, Part 2: Simple Flow Simulations”, J. Macromol. Sci., Part B, Phys., 2013, 52, 442-461.

[16] Marrucci, G., “Dynamics of Entanglements: A nonlinear model consistent with the Cox-Merz rule”. J. Non-Newton. Fluid Mech., 1996, 62, 279-289.

[17] Marrucci, G., Ianniruberto, G., “Interchain pressure effect in extensional flows of entangled polymer melts”, Macromolecules, 2004, 37, 3934-3942.

[18] Wagner, M. H., Rubio, P., Bastian, H., “The molecular stress function model for polydisperse polymer melts with dissipative convective constraint release”, J. Rheol., 2001, 45, 1387-1412.

[19] McLeish, T. C. B., Larson, R. G., “Molecular constitutive equations for a class of branched polymers: The pom-pom polymer”, J. Rheol.,1998, 42, 81-110.

[20] Champetier G. Monnerie L., “Introduction à la Chimie Macromoléculaire”, Masson, 1969.

[21] Lunn, A. C. ,”The Molecular Basis of Homogeneous Deformation in Glassy Polycarbonate”. Doctoral dissertation, MIT, 1972.

[22] Volkenshtein, M. V.,” The linear polymer as mixture of rotation isomers”, Dokl. Akad. Nauk SSSR, 1951, 78, 879-882.

[23] Robertson R.E., “Theory for the plasticity of glassy polymers”, J. Chem. Phys. 44, 3950 (1966).

[24] Miller, A. A.,”A Molecular Interpretation of the Vogel Equation for Polymer Liquid Mobility”, Macromolecules, 1978, 11, 859-862.

[25] Miller, A. A., “Conformational Properties of Liquid Polyethylene”, Macromolecules, 1979, 12, 651-655.

[26] Matsuoka, S. Proceedings of the 18th NATAS Conference, San Diego, 1, 126 (1989).

[27] Flory, P. J., “Statistical mechanics of chain molecules”, 1969. Interscience Press, New York, 308, 1989
[28] Cereghetti P.M., Kind R., Higgins J.S., “Tacticity effects on the barriers to rotation of the ester methyl group in poly methyl methacrylate: A deuteron magnetic resonance study “, J. Chem. Phys., 2004,121, 8068-8078.

[29] Buckingham, R. A. ,”The classical equation of state of gaseous helium, neon and argon” Proc. Royal Soc. London, Series A, Math. Phys. Sci., 1938, 264-283.

[30] Lennard-Jones, J. E., “Cohesion”. Proc. Phys. Soc., 1931, 43, 461-482.

[31] Ibar, J. P. A New Theory For the Properties and the Behavior of Polymeric Materials. Ph-D thesis M.I.T, 1975. unpublished : “”. https:// sites.google.com/a/eknetcampus.com/dual-split-statistics/).

[32] Ibar, J. P., “Stability of the Entanglement Network of Polymers”. HDR Dissertation-Science Physique, Universite de Pau et Pays de l´Adour, 2010.

[33] Ibar, J. P., “A new theoretical approach to the kinetics of cooling of liquid like structures”, J. of Non-Crystal. Solids, 1985, 75, 215-221.

[34] Bernes, A., Boyer, R. F., Chatain, D., Lacabanne, C., Ibar J. P., Thermally stimulated current studies of transitions in amorphous polymers”. In Order in the Amorphous “State” of Polymers, S.E. Keinath, R.L. Miller and J. K. Rieke Eds. (pp. 305-326), Plenum Press, Springer US, New York, 1987.

[35] Ibar J. P., Proceedings of the 19th NATAS Conference; Vol. 2, 402, I. R. Harrison, Ed.: Boston (1990).

[36] Ibar, J. P., “Grain-Field Statistics Applied to Polymer Physics: the Network of Entanglements”, book in preparation.

Chapter 2

TROUBLE WITH POLYMER PHYSICS: "SUSTAINED-ORIENTATION" GROUND BREAKING EXPERIMENTAL RESEARCH SHAKES THE CURRENT UNDERSTANDING OF THE LIQUID STATE OF POLYMERS

A Introduction

Advances in rheology for the last 40 years have led to a better understanding of the influence of the chain configuration on its flow characteristics, such as viscosity [7-11]. The concept of entanglement has been debated all these years and led to many theoretical models as reviewed by Graessley [12]. The concept explains the change of slope (from 1 to 3.4) that characterizes the molecular weight dependence of the Newtonian viscosity, as well as the width of the rubbery plateau modulus [12] as M increases. More recently, modified versions by M. H. Wagner [11], G. Marrucci et al [10], of the original reptation models by de Gennes [8], Doi & Edwards [9] are admitted to describe fairly well the flow behavior of entangled chains. The reptation model of entanglement is in its full maturity stage. Yet, many questions remain for a full understanding of what an entanglement is, in particular to explain the challenging results obtained by submitting a melt to conditions of Rheo-Fluidification which combine shear, extensional flow and melt oscillation in order to compensate the effects of shear-thinning and strain softening in ways triggering "sustained-orientation". In this presentation we show that it is possible to create and maintain quasi-stable at high temperature in an amorphous polymeric melt (say 120 ^{o}C above T_g) a certain state of orientation that was induced by a mechanical deformation history. The melt is not branched nor cross-linked when this sustained-orientation occurs, it is simply brought out of equilibrium with respect to the thermodynamic state that represents the most stable configuration of the interactions between the bonds belonging to the macromolecules [2]. The relative stability of the non-equilibrium state is what makes this research very challenging to the admitted concepts of entanglement [12], including the reptation models [7-11]. We found that, under certain conditions, the sustained-orientation could be preserved for hours at high temperature before the entanglement state recovered its equilibrium value.

B Experimental Description

B-1 The Rheo-Fluidification Processor.

In a Rheo-Fluidification processor a melt extrudes continuously through treatment zones where it is submitted to a combination of shear-thinning and strain-softening via the use of cross-lateral shear vibration superposed to pressure flow (originated by an extruder feed). Fig. 1 shows 2 treatment stations (11) and (22) for a melt flowing from left to right to exit at the end of the processor, where its viscosity is measured continuously by an in-line rheometer and it is water cooled, granulated into pellets.

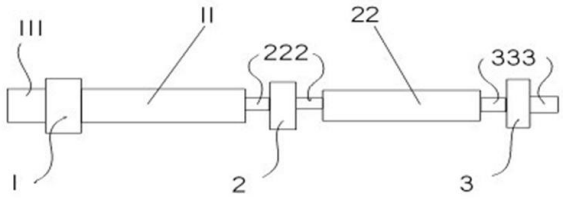

Fig.1
Schematic of a Rheo-Fluidizer with two stations.

The "treatment" in stations (11) and (22) is sketched in Fig.2: the melt flows through (from left to right) a gap "3" where the upper gap surface is static and the lower surface is rotated and (optionally) oscillated. Both surfaces contain small ribs, "12", detailed in Figs 3a and 3b, which create local vibrational extensional flow by squeezing and un-squeezing the melt as it is being swept forward helicoidally.

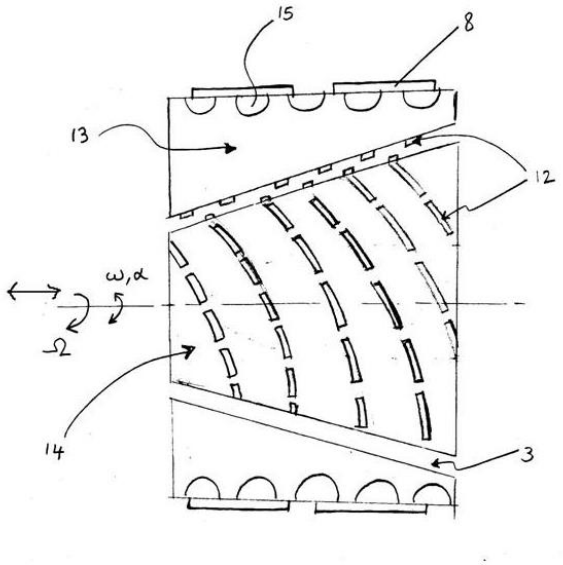

Fig.2
Details of the "inside" of one station in Fig. 1

Shear thinning is controlled by the shear rates, which add up vectorially from all types of flow (longitudinal and cross-lateral, vibratory or not), and strain softening is controlled by frequency and the strain amplitude of the cross-lateral shear component. The rotation of the rotor in station 1 and

station 2 were in opposite directions, a situation which we casually called “comb to the left-comb to the right”, referring to the sweeping induced by the ribs in relation to the rotation direction.

B-2 Sustained Orientation.

Figure 4 shows the viscosity of the exiting melt (PMMA) just after it has been “treated”, i.e. at the end of the second station of the two-station Rheo-Fluidizer shown in Fig. 1.

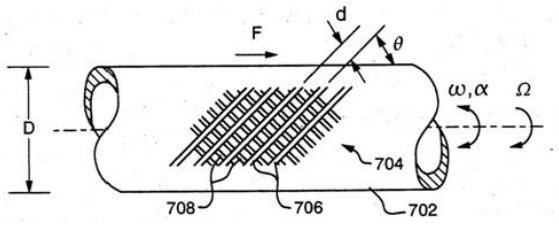

Fig. 3a
The surfaces touching the melt have a network of “ribs’ to induce vibration as the melt passes through.

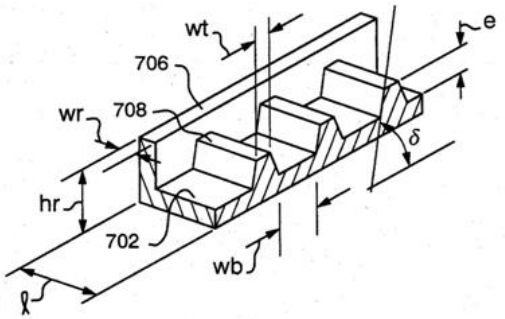

Fig. 3b
The design of the ribs determines the local vibrational profile both in shear and in extension (for ribs on divergent conic surfaces).

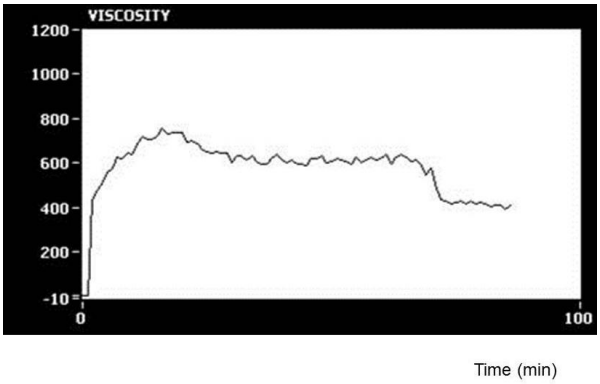

Fig.4
Trace of the viscosity of the melt at the exit die rheometer. Current theories predict no viscosity change (see text).

Temperature profiles are different in both stations. Rotation speeds and vibrational frequencies are also different in both treatment stations. The rheometer that measures the exiting melt viscosity is not far from the last treatment zone, but still, it takes the melt about 2 minutes to get there, and, at that temperature, which is 120 ^{o}C above the T_g of the polymer, the melt relaxation time is very small, of the order of 0.001 sec for that molecular weight. The x-axis in Fig. 4 is the extrusion time,

different parameters being tested until a "successful processing window" is apparently found, seen as the final value of viscosity, 500 Pa-s, which is 1/3 of the extrapolated "un-sheared" in-line viscosity 1,500 Pa-s. In Fig. 4, we observe a substantial drop of the melt viscosity at t= 20 min and another one at t=75 min, which is obtained by just changing the processing parameters of vibration in the treatment zones. Even if it is understood from theory that the melt viscosity could be decreased in the treatment zone under a different set of shear-thinning and strain softening conditions, the same theory predicts that the thermal-mechanical history should be erased totally in the 2 minutes times it takes to reach the rheometer, 2 minutes being 120,000 times greater than the longest relaxation time. One should not be able to observe any viscosity change at the exit of the Rheo-Fluidizer unless the orientation of the melt induced by shear-thinning and strain softening can be sustained 120 ^{o}C above T_g, an impossible proposition according to our current understanding of polymer physics!

C Results

Pellets were made of the treated melt by passing it through a strand die, and cooling the strands in water before pelletization. Two batches of 75 kg each of "treated" pellets were prepared by this procedure and sent for testing. By this comment we mean to say that the process was steady and could produce continuously "disentangled melts" that turned into "disentangled pellets" (the way we casually summarized the experiment).

The melt flow index (MFI) of these frozen-in treated pellets is plotted in Fig. 5 versus the in-line Rheometer viscosity value which varies as a function of the chosen processing parameters.

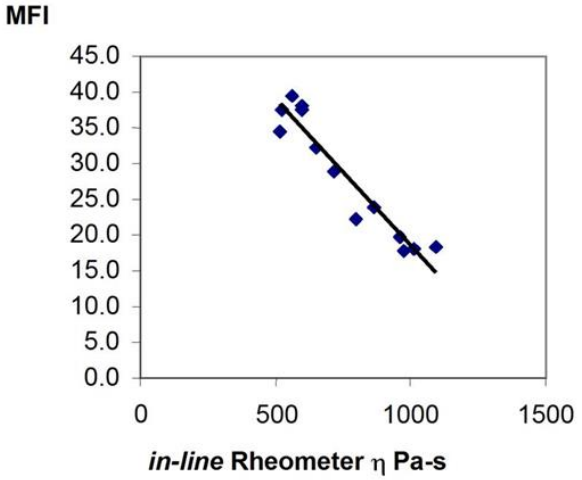

Fig. 5

MFI of treated pellets showing sustained-orientation vs in-line viscosity measured at the rheometer at the exit of the treatment.

The correspondence is remarkable and means that, indeed, it is possible to retain in the pellets a large portion of the viscosity reduction observed in the melt due to the Rheo-Fluidification process.

The orientation of the melt induced by shear-thinning and strain softening has been preserved and has survived reheating in the MFI barrel still maintaining a 100% lower viscosity than the reference (the melt with no treatment). Furthermore, the rheological properties of those pellets were studied, after the pellets were compressed into new samples as if they were a new polymer grade. Disks were molded to be studied by dynamic rheometry. Many of those results are given in Ref. 2 for polycarbonate. The viscosity reduction observed at the exit of the Rheo-fluidizer could survive a new heating in a molding press, and, additionally, a study of viscosity vs time in a rheometer at a high temperature. Yet, the molecular weight was hardly changed (~3%) to justify the viscosity reduction and it was also observed that the viscosity gradually returned to the value it should have at the corresponding temperature (the Newtonian value), indicating that the changes were reversible. Actually, it took 24 hours at 235 ^{o}C for the viscosity of the treated PMMA to return to its original value!. Again note that the sample in Figs 4 and 5 is a linear PMMA deformed 120 ^{o}C above its T_g, and thus, in terms of the conventional understanding of the rheology of polymer melts in the terminal zone, our results imply that the polymer has been retaining its orientation for a time 86.4 million times longer than its "longest relaxation time" (calculated from the cross-over point in a frequency sweep at the same temperature). **This appears to be totally incomprehensible in terms of our present understanding of "entanglement", the corner stone of long chain physics.**

These experiments could be interpreted by stating that the entanglement became unstable producing an increase of M_e, the molecular weight between entanglement (thus the wording which continues to be used: "disentanglement"). The instability of the entanglement lasted 24 hours! But there is no explanation to why M_e can vary independently of the relaxation time, and be increased (or decreased) by relatively low shear forces; **there is no explanation in the current theories for an unstable entanglement network resulting in an unstable liquid state for polymers, and for how it could be correlated to non-linear viscoelastic effects.**

Table 1 provides some MFI improvement results for polymers that were successfully "disentangled" by the Rheo-Fluidification processor of Fig. 1 with the viscosity reduction benefits preserved in the pellets. In these results the MFI found experimentally is corrected to account for the small molecular weight decrease (2-5%) that comes as a collateral consequence of the treatment that exposes the polymer to a high processing temperature where it can degrade by thermal degradation or oxidation etc. See details in Refs 2, 4. We discussed in another publication [2] the rheological properties of the polycarbonate and the PMMA pellets from this Table. The pseudo-plasticity of the treated resin can be varied by Rheo-Fluidification as well as the value of the

Newtonian viscosity (proportional to the inverse of the MFI). As the melt of the treated resin is annealed at high temperature, frequency sweep tests show a gradual return to a normal pseudo-plasticity and Newtonian viscosity.

Table 1
Flow Improvement for pellets showing sustained-orientation

	Virgin MFI	MFI after "Treatment" (and correction for Mw change)	Flow improvement
Polycarbonate	12	21	75%
PETG	8	12	50%
LLDPE	0.5	1.2	140%
Polystyrene	4	6	50%
PMMA	17	37	118%

D Discussion

Our research has two goals: a theoretical, fundamental understanding of the stability of the network of entanglement and a practical goal: how Rheo-Fluidification proceeds by way of "disentanglement of the chains", and how we can predict the processing parameters responsible for its triggering (temperature, strain, strain rate in both shear and extension) that will produce sustained-orientation. The theoretical objective raises fundamental questions regarding our present understanding of the interactions between the macromolecules which give rise to entanglements, these "physical cross-links". Our experiments at least suggest that the classical concept of M_e to describe entanglements is too simplistic and its usefulness is probably limited to the linear range of viscoelasticity.

The practical goal of this program will be fully achieved when we will be able to predict the processing parameters for a successful Rheo-Fluidification treatment, yielding any chosen value of sustained-orientation, given a polymer melt of known molecular weight characteristics, topology and chemical structure. In simple terms, for a given throughput of melt flow, what should be the Rheo-Fluidification processing temperatures in the stations, the value of combined strain rate (from pressure and drag flow, oscillatory and rotational), the value of extensional flow and strain rate, the value of pressure in the gap, and what will be the amount of sustained-orientation obtained?. Further, what will be the stability of the new entangled state (how fast will it re-entangle at any given temperature and pressure)? Therefore, the theoretical and fundamental part of this research is to provide a science base for molding processes under shear-thinning and strain-softening controls**,**

so that the process result can be achieved rationally based on scientific laws rather than only on experience.

All these operating questions can only be answered after entanglement, shear-thinning and strain softening are understood from a molecular base, i.e. after rheological and polymer dynamic studies have provided the correlations between the degree of "disentanglement" (melt degree of out-of-equilibriumness, the time of "re-entanglement" (equilibrium recovery), and relaxation times (reptation and tube renewal time τ_d and Rouse time τ_R). In attempting to do such a characterization of the entanglement instability from classical visco-elasticity parameters, we came to realize that the linear viscoelasticity theory itself may not be the correct base to extrapolate from to characterize the non-linear phenomena leading to entanglement instability. The "molecular dynamic" description of viscoelastic data in terms of a family of discrete relaxation times generated by a terminal time that varies with a local friction coefficient (thus providing the temperature dependence), and with topology (to explain the M or $M^{3.4}$ dependence) is an elegant and simple mathematical tool to compare the effect of structural and chemical parameters on melt properties, but, as we started to realize [1], perhaps too simplistic to have any value in terms of the physics of deformation of a set of long chains. The Rouse's or reptation models (de Gennes [7,8], Doi-Edwards [9]), based on such a spectrum of relaxation times, may not correctly describe the basic deformation process giving rise to viscoelastic effects (shear-thinning, normal stresses, extensional flow and the numerous other phenomena observed in non-linear deformation) at very high shear rate, or at high amplitude of strain, causing melt yielding, melt fracture and astonishing memory effects [1,2]. We suggested that the current models' shortcoming was probably deeply rooted in the misunderstanding of the concept of chain entanglement, and of the entropy of the melt deformation process [3]. A new physics of the interactions between the bonds of the macromolecules had to be found to explain viscoelasticity (linear and non-linear) and the spectroscopic behavior of polymers above and below the glass transition [13]. We propose a different model of understanding of the coupling between the bonds of polymer macromolecular chains, creating a novel statistics ("Grain-Field-Statistics") that does not singularize individual chains embedded in a sea of mean field interactions [14]. Instead, we consider the global set of chains of conformers with a re-definition of their conformational statistics to account for the coupling of their inter and intra molecular interactions. This new statistics provides a new understanding of entanglements, describes viscoelasticity and flow properties in a completely original way and suggests that the entanglement network can become unstable [2,3, 14].

E Summary and Conclusions

In this first Chapter we have described processing conditions triggering melts to behave in novel ways contradicting the currently admitted models of polymer rheology. For instance, the viscosity of a polymer melt could be greatly reduced and the reduction of viscosity maintained at high temperatures for times 100,000 to several million times greater than the longest relaxation time. The instability of the network of entanglement could be induced by coupling shear-thinning and strain softening in what we called a Rheo-Fluidification processor, which we used to "disentangle" polymers, subsequently "re-entangle" them in a different specific way, creating new exciting materials. We suggested that this research leads to re-visit our understanding of the concept of entanglement in polymer physics in order to clarify "sustained orientation", a condition which we have empirically observed in melts. In future work, the theoretical simulation of the stability of a network of conformers in collective interactions will be done using the equations of the Grain-Field Statistics to understand "sustained-orientation", in parallel to a series of experiments conducted to repeat conditions of sustained orientation in plastics, this time with a design dedicated to test the idea that plastics, perhaps recycled plastics, could be used as batteries to store energy [14].

F Note

This Chapter has been expanded into a full paper [15] with many more details of the Rheo-Fluidizer and the experimental procedure. In particular, the tests and results reported in this Chapter were conducted by this author from 1999 to 2001 at Eknet Research Lab.

G References (Chapter 2)

[1]. J.P Ibar, *J. of Macrom. Sci., Part B, Phys.* 48: 6, 1143-1189, 2009.

[2]. J.P. Ibar, *J. of Macrom. Sci., Part B, Phys.* 49, 1148 -1258 ,2010.

[3]. J.P. Ibar, *J. of Macrom. Sci., Part B, Phys.* 52:222-308, 2013.

[4]. J.P.Ibar, *J. of Macrom. Sci., Part B, Phys.* 52:411-445, 2013.

[5]. J.P. Ibar, *J. of Macrom. Sci., Part B, Phys.* 52:446-465, 2013.

[6]. J.P. Ibar, *Macromolecular Symposia*, Special Issue, 11th International European Symposium on Polymer Blends, 2012. Volume 321-322, Issue 1, p. 30-39

[7]. P.G. de Gennes, *J. Chem. Phys.55*, 572. 1971.

[8]. P.G. de Gennes, *Scaling Concept in Polymer Physics*; Cornell University Press: Ithaca, NY, 1979.

[9]. M. Doi, S.F. Edwards, *The Theory of Polymer Dynamics*; Oxford University Press: Oxford, 1986.

[10]. G Marrucci and G. Iannruberto, *Macromolecules*,36, 3934 ,2004.

[11]. M.H. Wagner, *J. Rheol*., 45, 1387 ,2001.

[12]. W.W. Graessley, Advances in Polymer Science, Vol. 16, "*The Entanglement Concept in Polymer Rheology*," Springer, 1974.

[13]. J.P. Ibar, *J. Macromol. Sci.-Rev. Macromol. Chem.Phys., C37*, 389, 1997.

[14]. https://sites.google.com/a/eknetcampus.com/mission-and-objectives/

[15]. J.P. Ibar, J. Macromol. Sci., Part B, Phys., 54,6,722-748,(2015).

Chapter 3

THE GREAT MYTHS OF POLYMER RHEOLOGY, PART 1: COMPARISON OF THEORY WITH EXPERIMENTAL DATA

Preamble

Viscosity of polymers is key to their behavior in the molten state and thus to their processing. The well known equations of rheology giving the temperature, strain rate, frequency and molecular weight dependence of viscosity are the basic equations that theories must explain. This is what de Gennes and other theorists before him have tried to explain. It is shown in this chapter that the admitted view that molecular weight and temperature separate in the expression of viscosity is only an approximation that theoretical models should not therefore succeed to explain. For instance, the classical 3.4 exponent for the variation of Newtonian viscosity with molecular weight is shown to be temperature sensitive in a systematic way, suggesting that this relationship is nothing more than another curve fitting approximation of the effect of entanglements on the viscosity.

"Shear-Thinning", the lowering of viscosity with an increase of shear rate, demarking the Newtonian regime, is a fundamental property of polymer melt. We review the use of scaling variable on log-log axes to describe shear-thinning, such as Vinogradov's plots, and show the limitations of such an approach, which often leads to very wrong extrapolated viscosity values when the results are compared to reality.

We also review, using statistical tools from regression analysis, the validity of the time temperature superposition principle, another fundamental concept of rheology, and demonstrate that the principle is not valid, even when a graphical fit " looks good".

The WLF equation (due to Williams Landel and Ferry) describes well the temperature dependence of the horizontal shift factor, log a_T. This well admitted

equation, the corner stone of free volume interpretations of the molecular friction coefficient, is also critically reviewed and shown to be molecular weight dependent, even at (T-Tg) constant. It is also shown that the interpretation of the shift factor in terms of the ratio of Newtonian viscosity is an approximation limited to a narrow temperature range. Same such approximation also applies to the ratio of the terminal times, calculated from plots of G'/ω *vs* ω in dynamic experiments. The vertical shift factor, log b_T , is not equal to ($T_1 \rho_1/T\rho$), as predicted by the temperature dependence of modulus, according to rubber elasticity. This is clearly coming out of accurate shifting done analytically, instead of graphically.

The concept of relaxation time and spectrum of relaxation times, another mammoth concept in rheology, is critically examined to show that it might be fundamentally limiting to apply it directly to polymer melt deformation (unless it is accepted as a curvefitting tool, on the same basis as polynomials or Fourier series that describe well any type of curves). In that context, it is shown that models that take roots in the spectrum of relaxation concept, such as the Rouse model, de Genne's, Doi & Edwards', and all their improved versions (for instance by Klein, Montfort, Graessley, Larson, Wagner, Marrucci, Allal, MacLeich), that describe well the molecular weight and temperature dependence of relaxation times, are necessarily limited in their description of melt deformation to the linear regime, where the curvefitting power of such mathematical tools is perhaps the reason for their success. The non-linear regime (high strain rates, high strain) is the only regime important to" real life", i.e. to processors of plastic melts. In particular, the present understanding of shear-thinning, normal stresses and strain-hardening of polymer melts in terms of "chain disentanglement" deserves critical attention.

Forty years ago, the polymer field was dominated by chemists and physical chemists who understood linear visco-elasticity in terms of networks of dashpots and springs, but were puzzled by large amplitude strain rates and strain behavior, especially by the effect of strain. Their interest and success in describing "*molecularly*" rubber elasticity and swelling (in equilibrium conditions only) by Gaussian chains whose length

could affinely be related to macroscopic strain, can be viewed as the birth mark of modern physics, a la de Gennes, but also, perhaps, the source of the mis-characterization and mis-understanding of what entanglements are, and how their existence affects melt deformation, in particular with respect to the entropic melt orientation. We critically review the present classical understanding of the influence of entanglements on melt deformation, and expose its limitations.

After critical discussion of the implications and limitations of the classical views, another model of melt deformation and of the influence of entanglements will be presented in part II. This model elaborates a profound different understanding of the source of visco-elastic behavior and of rubber elasticity.

A Introduction

The knowledge of viscoelastic properties and non-Newtonian flow of polymer melts is of paramount importance to the understanding of their processing behavior. The viscosity of polymeric melts has received considerable attention over the last sixty years [1], and is admitted to depend on the product of two parameters: a friction factor, which is controlled solely by local features *such as* the free volume, and a structure factor, which is controlled by the large scale structure and configuration of the chains [1,2].

The friction factor depends on temperature only and not on the molecular weight characteristics (M_w, M_n). It is best expressed as a function of (T-Tg), at least up to approximately Tg+100 ^oC. The structure factor, on the other hand, depends on the number of chains per unit volume and on their molecular weight and dimensions [1]. It is also admitted that the structure factor is largely the same regardless of the chemical nature of the repeating units, which form the macromolecules.

For polymers of low molecular weight (M_w <Mc), the viscosity[1] is quite reasonably well described by the Rouse model [1], with no adjustment for intermolecular interaction, which can be written:

[1] Note that viscosity is symbolized either by the parameter η or μ.

(1) $\eta o = K M_w$ $(M_w < Mc)$

where ηo is the Newtonian viscosity at temperature T, and K is a constant which varies with (T-Tg).

For longer chains ($M_w > Mc$), the well-known 3.4 power dependence reflects the strong influence of the entanglements on the viscosity:

(2) $\eta o = K' M_w^{3.4}$

The critical molecular weight Mc is obtained from intersecting the straight lines Log ηo vs Log M_w drawn in the two regions ($M_w < Mc$) and ($M_w > Mc$).

Formula (1) and (2) above simply state that molecular weight and temperature effects **separate** in the expression of viscosity of polymers. The temperature dependence of K or K' in Eqs (1) and (2) is often written with the WLF expression, Eq. 3, which, admittedly, describes well, between Tg and Tg+100, the typical curvature observed in Arrhenius plots of Log(ηo) v s 1/T:

(3)

$$\log \eta_o = \log \eta_{og} - \frac{C1g\,(T - Tg)}{(C2g + (T - Tg))}$$

where C_{1g} and C_{2g} are adjustable constants, often admitted to have the universal value of 17.44 and 51.6 respectively [16], η_{og} is the viscosity at Tg, generally considered to be close to 10^{13} poises. Note that (3) is sometimes re-written as a Vogel-Fulcher equation:

(3 bis): with $T_o = T_g - C_{2g}$

$$\log \eta_o = A + \frac{B}{T - T_o}$$

The 3.4 power dependence of molecular weight M_w has been extensively investigated and explained by several models of entanglements [3-5]. The friction theory of Bueche [3] determines a value 3.5, whereas the reptation model of de Gennes [4] and Edwards [5] predicts a value of 3.0, short of the experimental value of 3.4, but later modified, by way of tube length fluctuation, by de Gennes reptation model's protagonists to predict 3.4 [6].

Although it has been reported [7, 8] that in some polymers the 3.4 dependence increases at higher molecular weight, it is admitted, on the contrary, that the power exponent tends towards its uncorrected theoretical reptation value of 3 at high (M/Me) [9]. In general, there seems to be a good consensus, at present, that the 3.4 exponent is a universal characteristic of entanglements in macromolecular chains, and, furthermore, that this exponent is constant, independent of temperature, or molecular weight. This is, therefore, the expression that theorists try to understand.

B Shear-Thinning: non-Newtonian viscous behavior.

More than a decade ago, Hieber and Chiang [10] assessed the relative merits of the classical equations describing the shear-rate dependence of viscosity, a phenomenon described as "shear-thinning", based upon a compilation of steady-shear and dynamic-shear viscosity data from the literature for Polystyrene melts. Their analysis still holds the admitted understanding today. These authors generalize the popular models of Cross [11] and Carreau [12] and include an additional term to describe the second-Newtonian limit of polymer melt behavior at high strain rate and high frequency:

(4)

$$\mu = (1-s).\ \mu c + s.\ \mu o$$

where s is a constant, the ratio of the second-Newtonian viscosity at high rate to the low rate Newtonian viscosity (μo), and μc is the viscosity according to the generalized Cross-Carreau's formula:

(5)

$$\mu c = \mu o / [1+(a_1 . \mu o\ \omega)^{a2}]^{(1-a3)/a2}$$

with a_1, a_2, and a_3 temperature independent curvefitting parameters, ω, frequency for shear-dynamic data, or shear rate, $d\gamma/dt$, in the case of steady-shear flow. In particular, Eq. 5 reduces to the Cross model if $a_2 = (1-a_3)$, and to the Carreau model if $a_2 = 2$.

Equations 4 and 5 incorporate the admitted fundamental "universal" aspect of the rheology of polymer melts, stating both the principle of time-temperature superposition and the uniqueness of the viscosity - strain rate (or frequency) curves when the variables are rescaled as reduced viscosity, $\mu/\mu o$, plotted against a reduced time scale, $\mu o.\omega$, a so-called Vinogradov's plot [13].

The Cox-Merz 's rule [14] stipulates that curves of μ vs $d\gamma/dt$, at constant T, are *identical* to curves of μ^* vs ω obtained in dynamic shear conditions at the same temperature. μ^* is the dynamic viscosity, calculated from the dynamic modulus G* and the frequency of of oscillation of the melt, ω, expressed in rad/s. The Cox-Merz 's rule seems to still be a debatable proposition among scientists[15, 1]. Yet, very carefully conducted experiments on Polystyrene, both by capillarity and dynamic methods [17], seem to confirm the rule, which is generally admitted to be true for Polystyrene and Polycarbonate melts [16-18]. To study shear-thinning, capillary data are more difficult to handle and require careful corrections for the effect of pseudo-plasticity on the expression of shear rate (Rabinovitch's correction [19]), and for the end of die effect on the value of the stress (Bagley's correction [20]). In contrast, dynamic shear data do not require the application of any correction. The other main advantage of generating dynamic data at various frequency, various temperature, is that G', the storage modulus, and G", the loss modulus, are provided, from which μ^* is obtained, both calculated from the value of the phase angle θ between strain and stress:

(6)

$$G' / G^* = \cos \theta$$

$$G'' / G^* = \sin \theta$$

(7)

$$G^* = (G'^2 + G''^2)^{0.5}$$

$$\mu^* = G^* / \omega$$

The viscoelastic aspect of a melt is entirely characterized by the value of G'(ω,T) and G"(ω,T), at least in the linear viscoelastic region. The amount of elasticity in the melt increases with increasing frequency at constant T, as shown in Fig. 1 for a PE melt, and with decreasing temperature at constant frequency, as also shown in Fig. 1 by the relative position of the 4 curves obtained at 4 different temperatures.

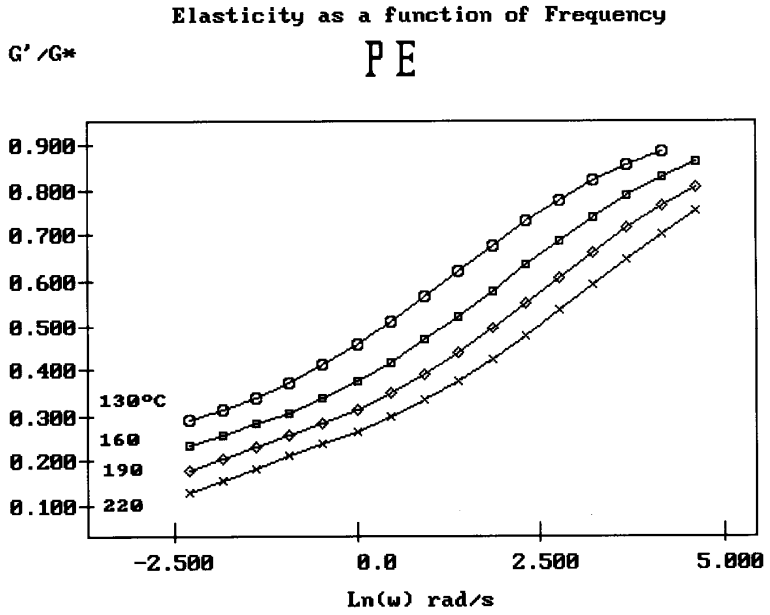

Fig. 1.
Stored elasticity (G_/G⋆) vs. ω for a linear low density Polyethylene (Engage 8180 from DuPont-Dow LLP) at 4 melt temperatures.

Theoretically, G'/ G* can take all values between 0 and 1. All existing theoretical models of viscoelasticity predict that G'/G* = 1 is the theoretical limit, corresponding to a totally elastic melt. For instance, for a generalized Voigt model, increasing frequency ω to infinity corresponds to such an elastic state [21]. This is also the prediction of the Leonov's model [22] and of the HN's model [23]. We must critically examine this proposition, as well as determine the origins of the second Newtonian regime obtained at high frequencies. We will show that the data do not display such a 2^{nd} Newtonian plateau when properly filtered for the influence of the transition relaxation terms, reflected by Tg (ω, γ, dγ/dt). We also examine the low frequency region, where the behavior becomes Newtonian, and determine the influence of extrapolating from higher frequencies, using various linearizing functions, such as Eq. (4) and (5), on the value of the Newtonian viscosity.

C Description of the Data Sources.

Newtonian viscosity data obtained at various temperatures from Tg to Tg+100 ^{o}C, for a series of monodispersed PS of various molecular weight M_w , are collected from the published thesis of Pierson [24] and Susuki [25]. We also examine dynamic results published by Marin and Graessley [34} and by Majeste [35]. The data, covering a very large molecular weight range (M_w = 800 to 1,200,000 g/mole), spread on both sides of the critical molecular weight (Mc=33,000 g/mole), and are tabulated as a function of temperature and molecular weight. Fig. 2 reproduces the Susuki's data [14].

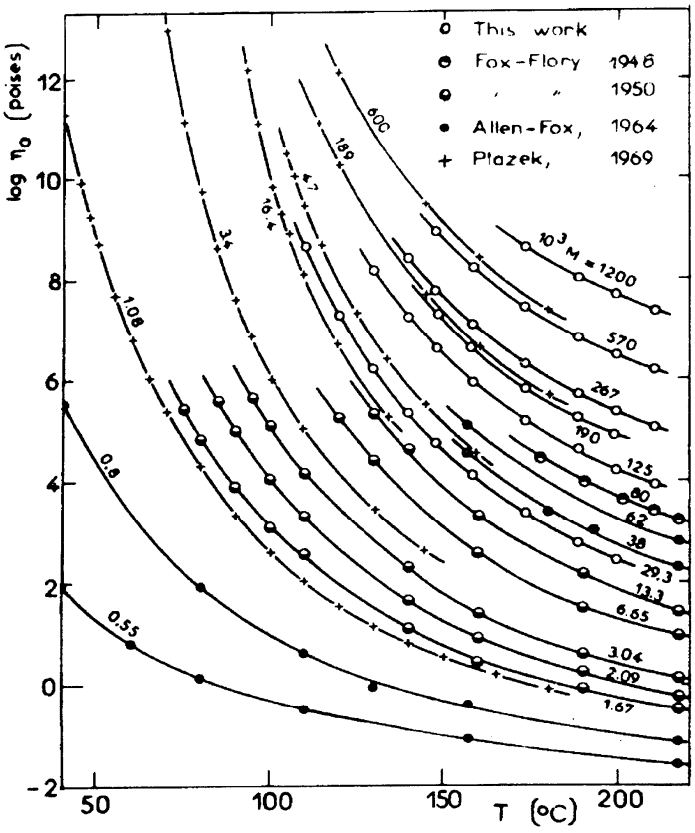

Fig. 2.

Log η_0 (Poises) vs. Temperature (°C) for a series of monodispersed PS according to Susuki.[25]

These studies [24, 25] regroup the work of several authors along with Pierson's and Susuki's own experimental data. Very good agreement with previously published work is claimed by both Pierson and Susuki. The dispersity ratio is close to 1.02 for all 23 molecular weight studied, so the PS chosen can be considered monodispersed..

Dynamic shear data on Polystyrene published by Pfandl et Al [17] are obtained between 124 °C and 290 °C, at 21 temperatures, for 16 frequency values ω between 0.00314 and 31.4 rad/sec. The molecular weight is M_w = 391,000 (obtained by GPC), and the dispersity ratio is 2.24. These data are used to analyze the non-Newtonian behavior (shear-thinning), and to determine the variation of Newtonian viscosity with temperature from dynamic data (the Newtonian value is obtained by extrapolation at low frequency

from curvefitted expressions).

We also analyze new dynamic data performed on three GE grades of Polycarbonate with various molecular weight characteristics. The melt flow rates for the three grades is respectively: 65 (g/ 10 min; 1. 2 Kg at 300 ^{o}C) for Grade 1, 10.5 for Grade 2, and 2.5 for Grade 3. Grade 1 and 2 are two linear polymers with T_g =136 ^{o}C and 145.4 ^{o}C respectively (measured from PVT data extrapolated to P=0). Grade 3 is a branched polymer, with T_g = 151 ^{o}C.

Both capillary and dynamic shear viscosity data are obtained at different temperature, strain rate and frequency. For both capillary and dynamic shear data, the Newtonian viscosity μo (or μo*) is obtained by curvefitting the non-Newtonian range, using several equations, including equations (4) and (5).

The capillary data are collected with a Goettfert Rheograph 2001, and corrected with Rabinowisch's formula [19]. Bagley's plots were obtained and the correction for end effects found negligible. Fig. 3 is a plot of log (μ) vs Log(strain rate) at 24 temperatures ranging from 195 ^{o}C to 305 ^{o}C, in 5 degree steps, across 2 decades of strain rates, for Grade 1, a high flow Polycarbonate resin with relatively few entanglements. The number of data points for each temperature is very large, as can be seen by the density of points in Fig. 3. Fig. 3 clearly demonstrates shear-thinning, e.g. the decrease of viscosity, at each temperature, as strain rate is increased.

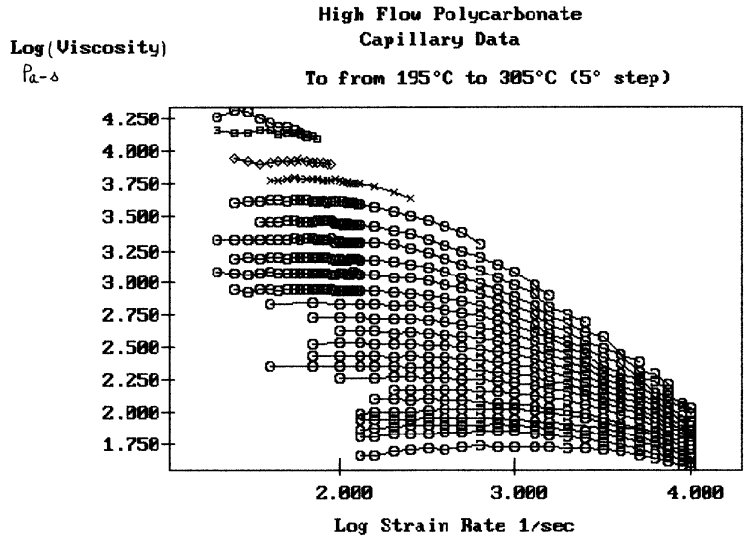

Fig. 3.

Viscosity vs. strain rate (log-log) for PC Grade 1 at various temperatures, every 5◦C from 195 to 305◦C.

The rheometer used to obtain the dynamic shear data for the 3 PC grades is a Rheometrics RDA-700, configured with a parallel plate cell, using 2" wide (in diameter), 2.0 mm thick specimens.

Fig. 4 shows the dynamic viscosity versus radial frequency for the Grade 1 of Fig.3 (a high flow grade PC resin used to inject mold compact disks), here analyzed under oscillatory shear conditions at 5% strain, between 168 ^{o}C and 283 ^{o}C, for 23 frequencies per isotherm (from 0.1 to 500 rad/s). Fig. 4 clearly demonstrates that applying a shear deformation at faster frequency causes the material to shear-thin, similarly to the effect of strain rate.

The dynamic data are obtained from Tg+25 ^{o}C to Tg+140 ^{o}C for the three grades, with a frequency varying between 0.1 and 500 rad/s. The viscosity data obtained on Polycarbonate are, we believe, of high reliability because they have been obtained by a unique operator, on a single instrument (Rheometrics RDA-700 or the Goettfert Rheograph 2001), using the same experimental set up and protocol for all samples, the

same method to mold them (by injection molding) and with an exceptionally wide range of frequency, temperature and step intervals.

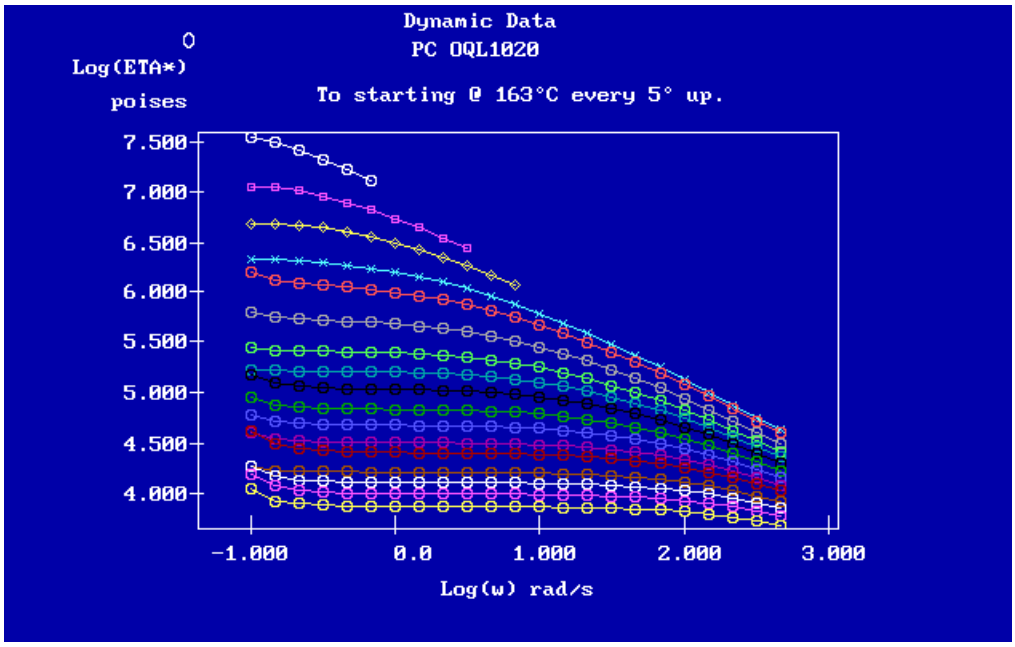

Fig. 4.
Dynamic viscosity log(μ^*) vs. log ω (in rad/s) for Grade 1 PC from 163◦C every 5◦C up.

D Analysis Protocole

For the purpose of this critical review of classical equations, we conform to the traditional procedure to analyse the data: the data are entered in a spreadsheet and analyzed in two ways:

At constant M_w, the temperature dependence of μo according to WLF formula is tested, Eq. 3, as well as the universal aspect of the free volume constants C_1, C_2 and μog.

Plots of Log(μo) vs Log(M_w), either at constant T or at constant (T-Tg), are constructed at each T to determine the constancy of the 3.4 exponent.

For Non-Newtonian behavior, the principle of superposition is tested in several

ways:

1. plots of (G'/G*) versus Log(ω) at different temperatures are superposed by horizontal shifting; no determination of the accuracy of the fit is done, except "visually".

2. plots of Log (μ) vs Log(ω) are superposed *analytically* to determine the best horizontal and vertical shift factors . One curve is chosen as reference and fitted with a mathematical expression which minimizes the rms deviation. The curvefitting constants found for the reference curve are then used to fit the other isotherms, only allowing the constants which correspond to a translation of the curve to vary. This technique [26] provides the horizontal and vertical shift factors by regression analysis and calculates the accuracy of the fit in terms of a r^2 and a standard deviation, thus allowing a *quantitative* evaluation of the validity of the procedure.

3. generalized Cross-Carreau equation, Eq. (5), is curvefitted by non-linear regression at each T. Other equations are also tested. The constancy of the exponents with temperature is checked to determine if these popular equations are merely good regressional fits or if they have any other merit. In particular, we address the issue of the accuracy in the determination of the Newtonian viscosity, μo, when it is obtained by extrapolation from the non-Newtonian range.

E Accuracy Consideration.

Hieber and Chiang [10] compile viscosity data on Polystyrene from a large variety of publications and claim apparent success in normalizing all these data into a single equation, Eq. (5), incorporating the classical formula (Eqs 2 and 3) for molecular weight and temperature dependence. However, upon re-examination of the accuracy of the fits found by these authors, it seems appropriate to investigate the kind of accuracy

which one should expect to get from viscous results. Hieber and Chiang produce a Vinogradov masterplot, i.e. a plot of reduced variables, Log (μ / μo) vs Log(μo . ω), for 67 data sets from the literature (1175 data points) and, based on Eq. (5) , find a rms deviation of 17.7% (Fig. 4 of ref. [10]). The WLF equation, Eq. (3), is said to be verified with a rms deviation of 14% (Table 3 of [10]), and Eq. (2), which predicts the effect of molecular weight, is also verified, for 102 data points, with a total rms deviation of 55%.

Are the rms deviations quoted by Hieber and Chiang so large that many types of formulation tested could be validated equally well? When the variables used to verify an equation or a fit are on the logarithm scale, there is a real contraction of the scale, compare to a linear representation (which is precisely the reason for its use), and one does not really visualize that a 17.7% rms deviation is, in fact, a very poor fit. Likewise, the predicting power of a formula, such as Eq. (2), which is shown to be correct with a 55% rms deviation, on a log scale basis, needs serious reconsideration. A slight variation of a few percents in the value of the exponent in Eq. (2) causes a drastic change in the value calculated for viscosity. If it is admitted that all the laws of rheology are correct within that accuracy, we need to verify that experimental results are, indeed, supporting such a poor performance.

For the viscous data obtained on Polycarbonate, for both the capillary and dynamic experiments, we conducted a series of tests to check the repeatability of the data and to determine the expected accuracy. Fig. 5 plots Viscosity (Pa-s) against Stress (Pa) for two independent capillary runs done at the same temperature, various strain rates, for Grade 1. The curves are not visually distinct.

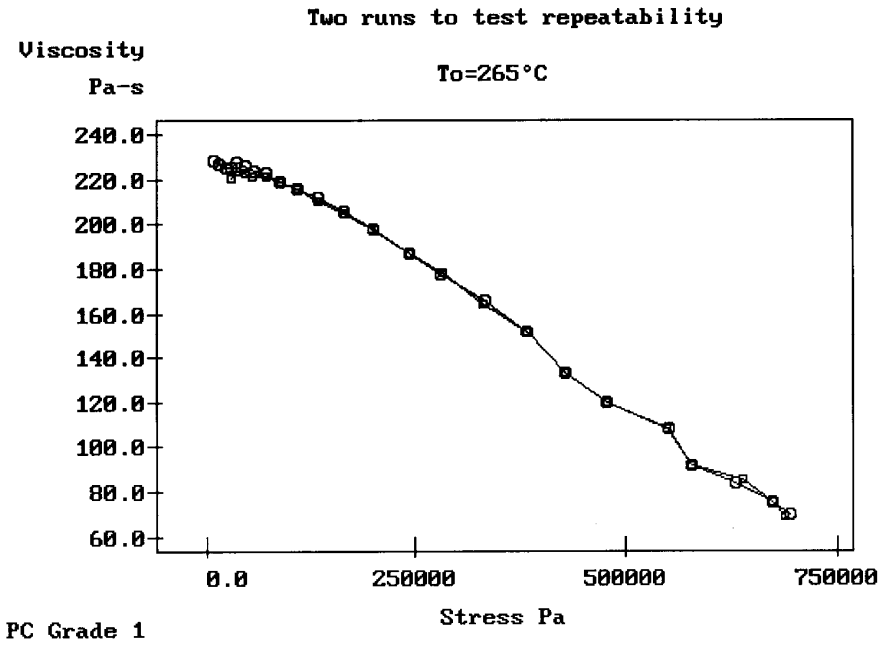

Fig. 5.

Viscosity vs. stress at T = 265◦C for Grade 1 PC. The points correspond to different apparent shear strain rates. Two different tests superpose almost perfectly showing high repeatability.

Fig. 6 shows that the difference between the two curves of Fig. 5 is random (except for the first points at low rates) and around 1-2%. The accuracy for the dynamic data is even better: for each temperature, three runs were systematically performed, each run with a new sample put in the cell. We could not distinguish between curves obtained at the same temperature, (except at the lowest frequency, which presented some particularity, as we shall explain, and the rms deviation between the curves was better than 0.5%. When we did observe some deviation, we could explain it and find what the reason was: either the temperature was not identical, or the preparation of the sample had been slightly different.

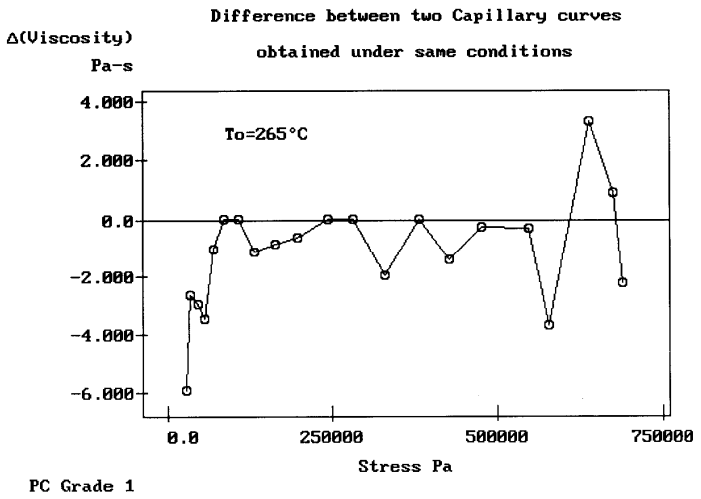

Fig. 6.

Difference in the value of the viscosity obtained for two different capillary runs under identical experimental conditions.

Take the curve of Fig. 7, for instance, which is a plot of μ* (Poises) vs G* (dyne/cm^2) obtained for Grade 1 at various frequency, constant temperature, 223 ^{o}C. If we rerun the same experiment 3 times, we obtain exactly the same curve, except for the portion at the beginning which is shown to drop from 38,394 to 26,753 Poises in this instance. In another run, the initial value was 31,440 and in still another run, 37,224, but it always dropped down to the same value 26,753 after the first 6 frequencies, and continued on with the same set of value of (μ*, G*) at the other frequencies.

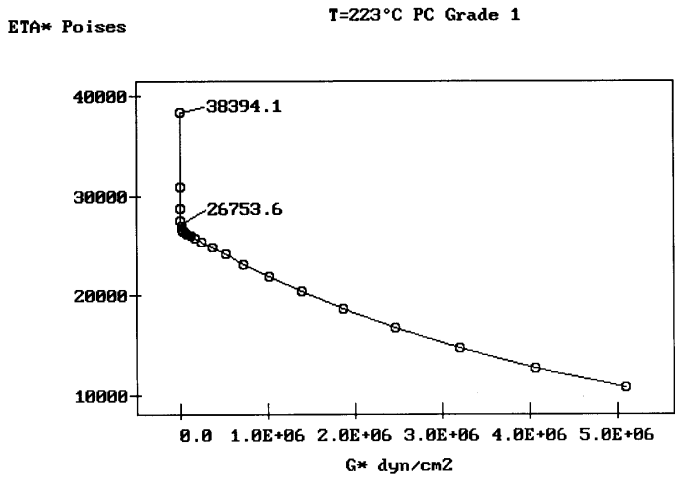

Fig. 7.

Plot of μ^* (Poises) vs. G^* (dyne/cm2) obtained for Grade 1 at various increasing frequencies, constant temperature, 223◦C. Viscosity drops sharply for the first 6 frequencies before reaching the value of 26,753 Poises. If we repeat the experiment with several samples, only the portion for the first 6 frequencies changes; the rest of the curve remains strictly identical.

Fig. 8 gives the cell temperature near the specimen tested at each measurement done. One sees that, indeed, there is a slight increase of temperature, here 1.85 ^{o}C (which was the worse case we observed), between the first measurement (obtained at the lowest frequency) and the sixth measurement, and that, perhaps, this error could account for the sharp drop of viscosity observed at the beginning of Fig. 7. However, for this Grade, the effect of temperature on the Newtonian viscosity (which is the case here since this is the low frequency range), can only justify 1/3 of the viscosity drop observed at the initiation of the curve. The rest can be related to the sample preparation technique which creates a thermal history on the specimen, slightly variable from specimen to specimen. The difference between specimens is quickly relaxed out at the beginning of the test, which takes place at the lowest frequencies. Once the small influence of thermal history has been erased, the viscosity curves become independent of any other parameter other than temperature, yielding excellent reproducibility and accuracy. In fact, it is probably significant to observe that the initial drop off observed at low frequency in Fig. 7 decreases in magnitude as temperature increases (because thermal history relaxes faster), and even disappears for temperatures higher than 260 ^{o}C.

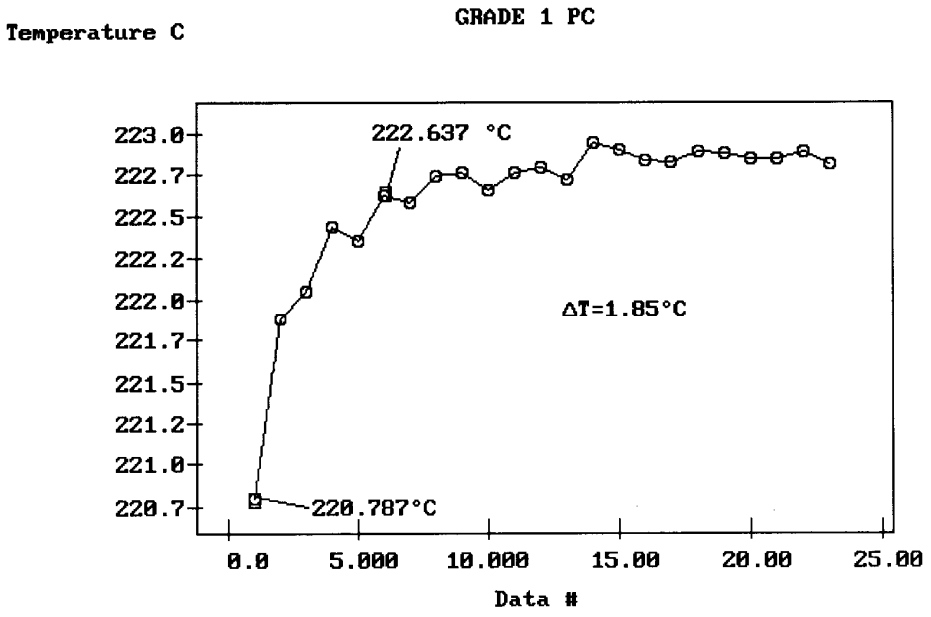

Fig. 8.
Stabilization of temperature in the rheometer oven as a function of the data point measurement (corresponding to a frequency increase).The increase of temperature of 1.85◦C corresponds to the 6th data point.

In summary, it seems in order to warn against the use of "uncontrolled" data from various sources to test the validity of sensitive equations. "Randomness" of the residuals for alleged good fits might be artificially created by mixing data from several workers, and mistaken with the effect of thermal history, which is known to create scatter and an unacceptable level of accuracy compare to experimental errors. As already said before, it seems more appropriate to generate the data carefully, using the same protocol of sample preparation, the same procedure to test the specimen, the same instrument to determine molecular weight characteristics, the same instrument to measure the viscoelastic data, by the same operator, and especially using the same lot for the resin.

F Critical Analysis of the Equations of Rheology

F-1 Universality of WLF constants at Tg.

The simplest myth to knock down, because it is already largely admitted, is the myth that universal constants C1g and C2g enter the WLF formulation of Newtonian viscosity, Eq (3).

Fig. 9 is a plot of Log(μo/μog) vs (T-Tg) for the three Polycarbonate grades. The value of Tg for the respective polymers is known from PVT analysis, by intercepting the rubbery and glassy volume-temperature behavior, at atmospheric pressure. The Newtonian viscosity μo at each temperature is obtained by fitting the non-linear behavior with the generalized Cross-Carreau equation, Eq. (5). For each grade, we verify that Log(μo) vs T can be fitted rather well (with r^2 better than 0.999) by an hyperbolic function, which can, indeed, be rewritten as a WLF equation, Eq. 3 [16], from which the two constants C_1g and C_2g are derived. The value of μog in Fig. 9 and Eq. 3 is computed by extrapolation from the hyperbolic fit, knowing the value of Tg. See Table 1.

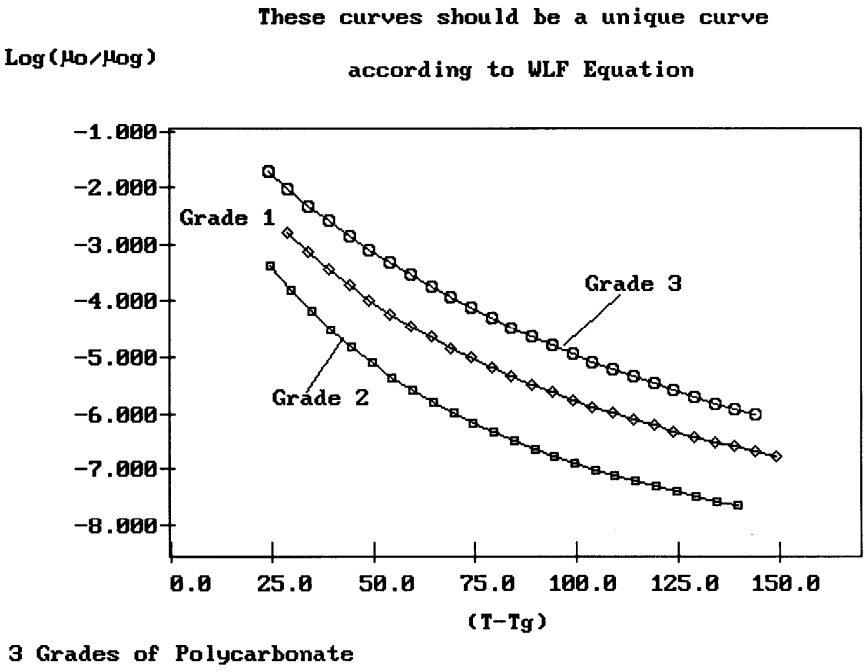

Fig. 9.

Log($\mu o/\mu og$) vs. ($T-T_g$) for PC. These 3 curves should be a single curve according to the WLF equation.

Table 1

Fitting Parameters in WLF Eq. (3) for the 3 PC grades of Fig. 9

	Tg^oC	Log(μog)	C_1g	C_2g
GRADE 1	136.0	9.842	10.22	76.70
GRADE 2	145.4	11.58	10.46	51.88
GRADE 3	151.0	12.06	11.87	84.16

Fig. 9 demonstrates that plots of Log(μo/μog) vs (T-Tg) for the 3 Polycarbonate grades do not resume to a single curve, as predicted if the WLF constants were universal [16]. The values obtained for C_1g and C_2g are convincingly different from the universal constants proposed by William, Landel and Ferry [16], respectively 17.44 and 51.6. Also, it is observed that Log(μog) for the 3 grades is not equal to 13, and does not stay constant with molecular weight, even for the two linear polymers Grade 1 and 2.

Fig. 10 is a similar Figure than Fig. 9, but for Polystyrene. Six monodispersed Polystyrene melts, of various Mw on both sides of Mc, seem to validate well the universality concept.

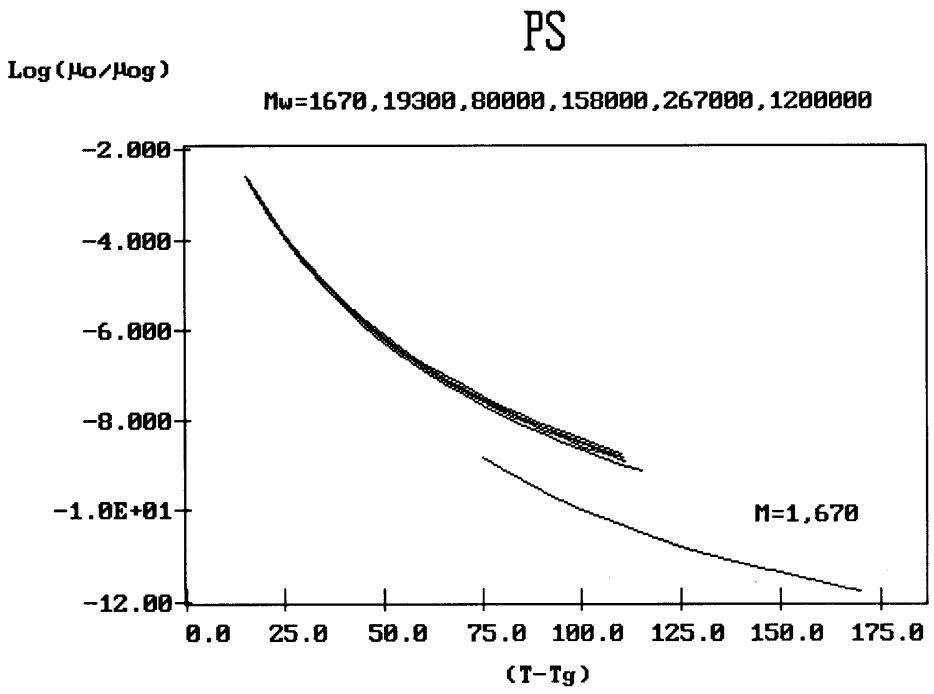

Fig. 10.
Same plot as in Fig. 9 to test the universality of the WLF equation. Data are from ref.[25] on monodispersed PS.

In Fig. 10, Tg is a function of molecular weight: Tg (M_w) is provided in Fig. 11, showing the leveling of Tg at high M_w. From a visual inspection of the data, Fig.10 seems to show that superposition of Log(μo/μog) vs (T-Tg) is quite good for PS, with the exception of the lowest molecular weight (M=1,670), which is singled out at the bottom of the graph. However, by changing the scale to examine the data better, as done in Fig. 12, a systematic deviation from a unique curve is clearly observed. For instance, if one compares the curves for M=19,300 and M=1.2 million at Log(μo/μog) = -8.5, a horizontal distance of about 8 ^oC exists between these 2 curves, which is quite significant rheologically speaking. The rms deviation between the curves in Fig. 10 is 12%, with systematically curved residuals, and the r^2 for the superposition is equal to 0.976, which indicates a poor correlation. In conclusion, although it is hardly visible when the whole curve is shown in Fig. 9, the curves actually do not superpose. This means that the "constants" K and K' of Eqs (1) and (2) are actually dependent on M_w, and are not simply

related to the monomeric friction coefficient, as classically admitted [1].

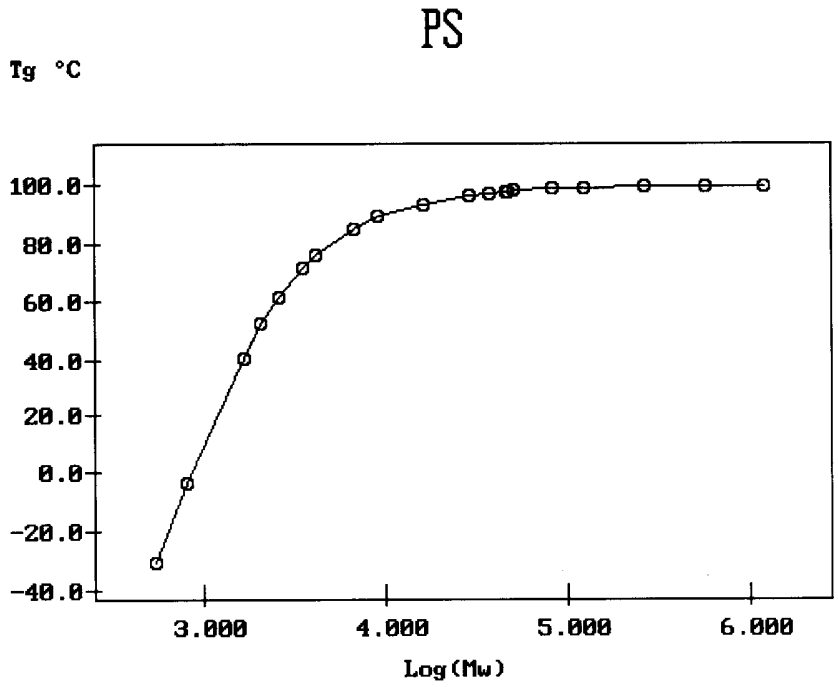

Fig. 11.

Plot of T_g as a function of molecular weight M_w for monodispersed PS (data from ref[25]).

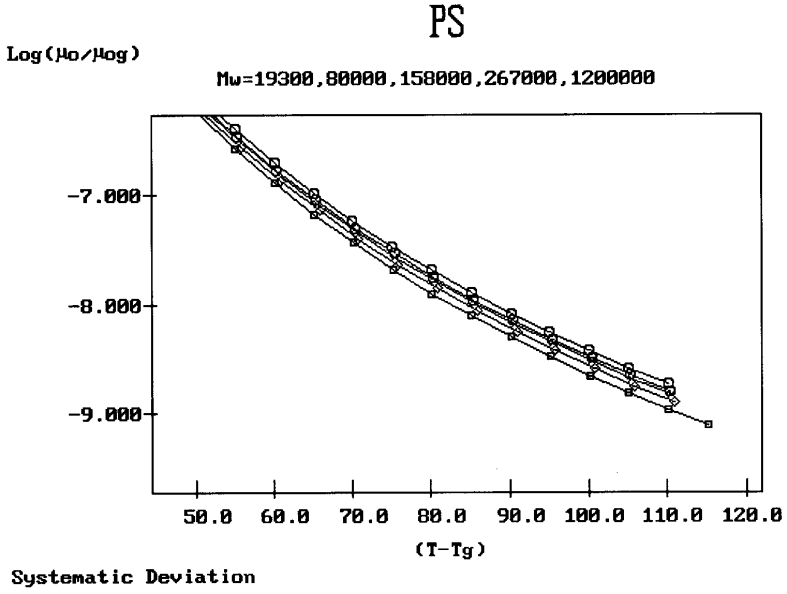

Fig. 12.

Detail of Fig. 11 showing the poor overlap of curves on close examination.

In summary, the universality of the WLF constants is, at best, a gross approximation. The Vogel-Fulcher equation, which translates the hyperbolic nature of the temperature dependence of Log(μo), is verified for all molecular weights, but, as shown in chapters 4 and 5, other equations, equally simple, linearize the data as well, or perhaps even better. In fact, it is quite possible that the *apparent* success of free volume expressions [16] to explain the curvature of Arrhenius plots, i.e. of Log(viscosity) - 1/T , has inhibited the search for other curve fitting expressions susceptible to bring a different perspective to the flow behavior.

In other words, temperature and molecular weight do not seem to accurately separate according to the classical formula of viscosity, Eqs 1, 2, 3. If so, the exponent 3.4 in equation (2) should itself be critically re-examined, as done in the next section.

F-2 Validity of the 3.4 power exponent for M > Mc.

Fig. 13a displays, for 4 temperatures, the log ETAo – Mw curves for all monodispersed Polystyrene melts across Mc ~33,000. The data are cross-plotted from the original data which were provided against temperature, for each M_w. The original data are first curvefitted with Eq. (3bis), which is in fact the Vogel-Fulcher formula, and re-tabulated every 10 degrees from 120 to 210 ^oC. Viscosity values, for different M_w, which correspond to the same T are then collected in a new file. Plots of Log(μo) vs Log(M_w) are analyzed with linear regression, for each T.

Let's concentrate first on the $M > M_c$ grades in Fig. 13a. In this region , the plot of Log(μo) versus Log (M_w), at each temperature, should be linear and the slope should equal 3.4.

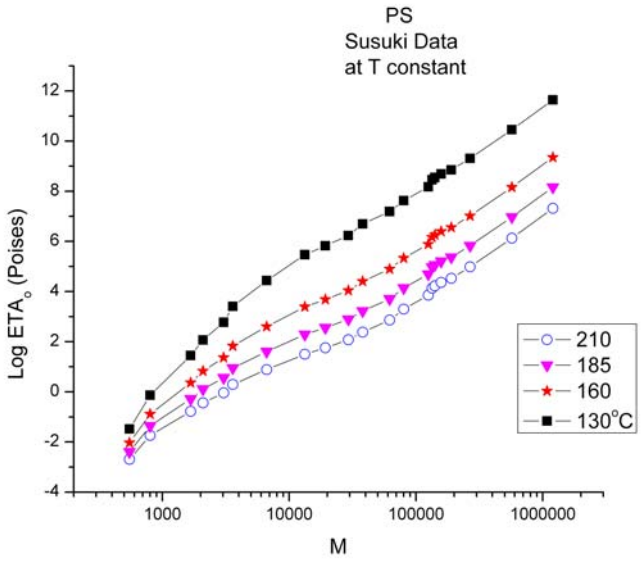

Fig. 13a.

Log η_0 vs. log M and b) Log (η_0/M$_{3.4}$) vs. M for monodispersed PS (data from ref[25]).

The first observation is that a straight line can, indeed, be drawn through the M > Mc data points, at each temperature, and, furthermore, that the slope of that line seems constant for all temperatures, from T=130 ^{o}C to T=210 ^{o}C, an apparent excellent validation of the classical views regarding the melt viscosity description. However, let's look at the results more closely (Fig. 13b).

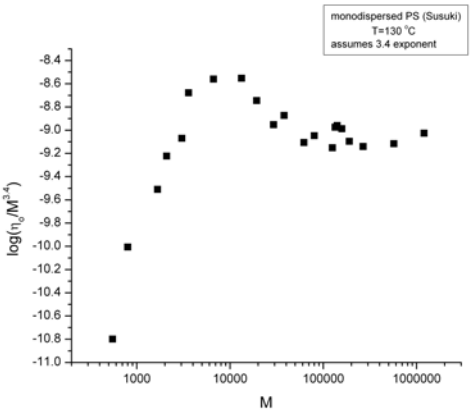

Fig. 13b

The 4 curves in Fig. 13a correspond to 4 temperatures that in b) are for T = 130◦C.

Fig. 13b clearly reveals a trend for curved residuals above M > Mc. Of course, one could also draw a short horizontal line to cover the points to the left. However, a fair assessment, based on residuals, would conclude that a better fit, above Mc (perhaps even starting at Me), is a curve, not a straight line, showing a systematic deviation from the behavior corresponding to a 3.4 exponent.

Fig. 14 is a plot of the slope of Log η_o vs Log M, for M > Mc, obtained by regression analysis, against temperature. One sees 1st that the best slope is not 3.4 but closer to 3.327, on average, and 2nd that the value of the slope is not temperature independent, the data indicating a systematic increase of the slope as temperature is decreased. The deviation is not large, but systematic, which is the point we want to make.

In conclusion, for M > Mc, PS monodispersed fractions, not only is the theoretical value of the exponent, 3.4, not validated, but the value of the best curvefit for the exponent is temperature dependent, not fixed.

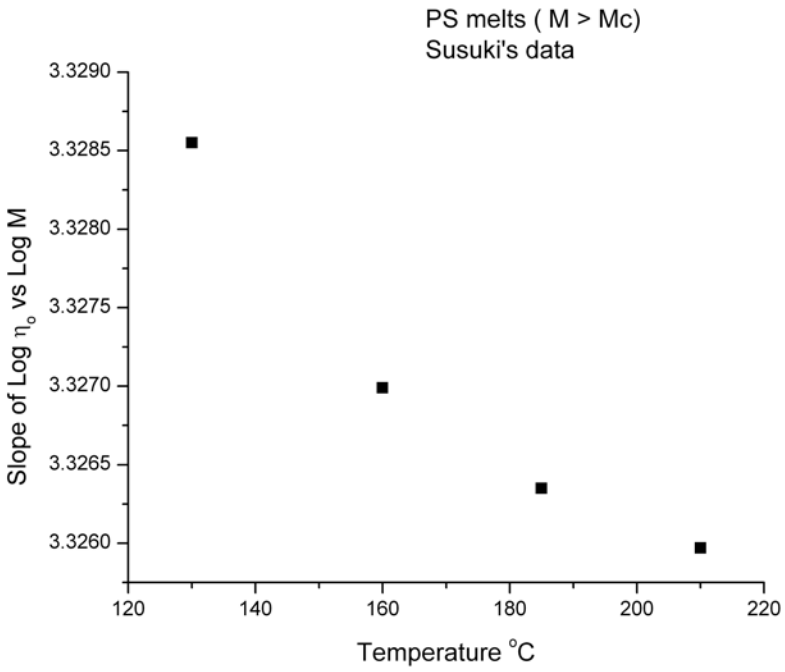

Fig. 14.
Systematic deviation with temperature of the "3.4" molecular weight power exponent for a series of M > Mc PS samples (data from ref. [25]). Also note that the value obtained within the range is always less than 3.4.

This demonstrates a result well known to regression analyst experts: starting from the wrong formula can lead to crude mathematical inconsistencies. One should not only test the coefficient of determination r^2 and the chi square κ^2 [28] of the regression, but analyze the randomness of the residuals before any claim to the validity of the fit is concluded. For the data of Fig. 13a above Mc, linearity seems admitted, not only based on visual inspection, but by regression analysis, with an acceptable r^2 of 0.996 and a κ^2 of 2.5%, but the residuals are badly curved, which is the reason for the pronounced curvature when the data are plotted a different way, such as in Fig. 13b. Also, Fig. 14 clearly demonstrates that the exponent is temperature dependent.

As already pointed out before, the reason for the small but systematic deviation is to be sought in the fact that T and M_w do not truly separate in the expression of viscosity, contrarily to what the admitted models assume, Eqs (1) and (2).

For Polycarbonate, the Log(μo) - T data for the two linear PC grades can be calculated with an accuracy better than 0.2 % over a temperature range between 165 and 280 ^oC. Knowing the average molecular weight M_w for these two grades at better than 5% [32], one can calculate, at each temperature, the ratio:

$$(\text{Log } \mu o_2 - \text{Log } \mu o_1) / (\text{Log } M_{w2} - \text{Log } M_{w1})$$

which should equal 3.4 and be independent of temperature. Fig. 15 reports the result using two molecular weights for Polycarbonate, grade 2 and grade 1. It is clear that the power exponent is not constant and systematically increases as T decreases; it becomes 5 at a temperature 30 ^oC above Tg in Fig 15. One might argue that using only two molecular weights to test a formula is not justified, even if the points are generated with great accuracy. Yet, these results for Polycarbonate are showing the same trend than those found for a series of 23 monodispersed Polystyrene (Fig. 14)..

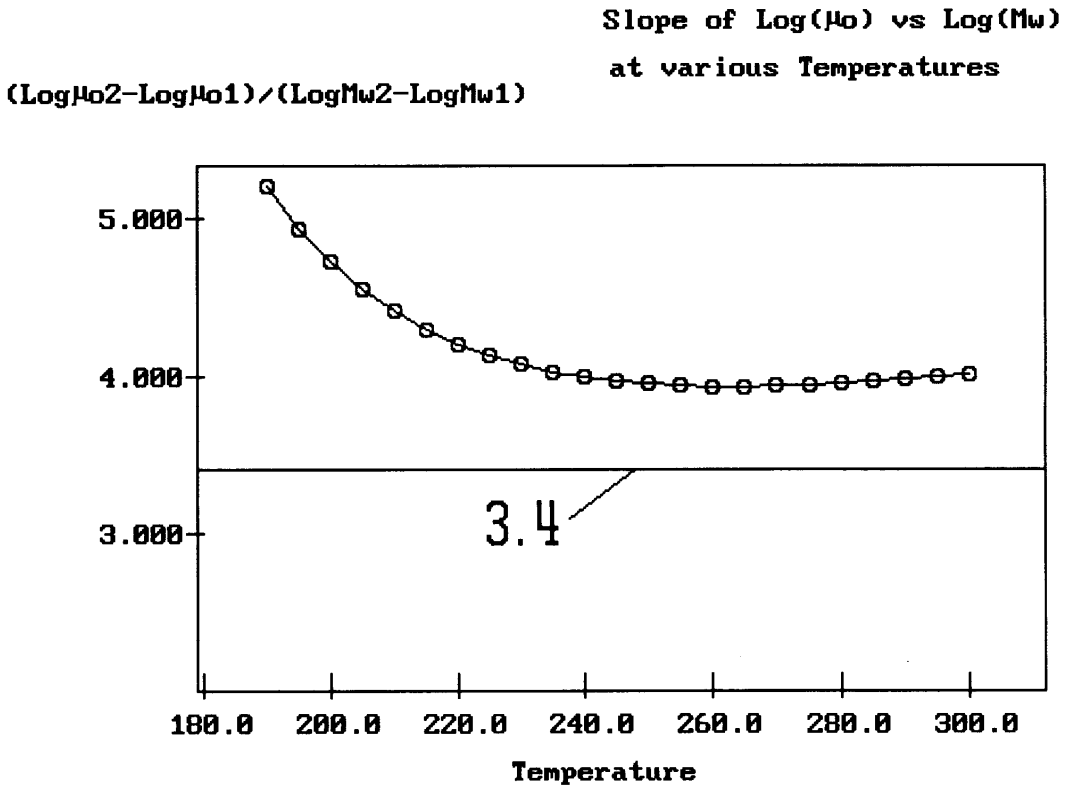

Fig. 15.

Variation with temperature of the viscosity-molecular weight power exponent for PC.

In summary, for both PC and PS, the criteria of constancy of the 3.4 exponent is shown to be a curvefitting approximation, which theoretical models should not try (nor succeed) to explain.

F-3 For M < Mc Viscosity is not proportional to M, contrary to Rouse's model.

Fig. 16 is a Log μo - Log M_w plot for M_w < Mc at T = 210 ^oC, showing that it is not linear. In other words, Newtonian viscosity is not proportional to M_w, at T constant, below Mc. This seems to contradict the Rouse's model known to apply well to unentangled melts[1].

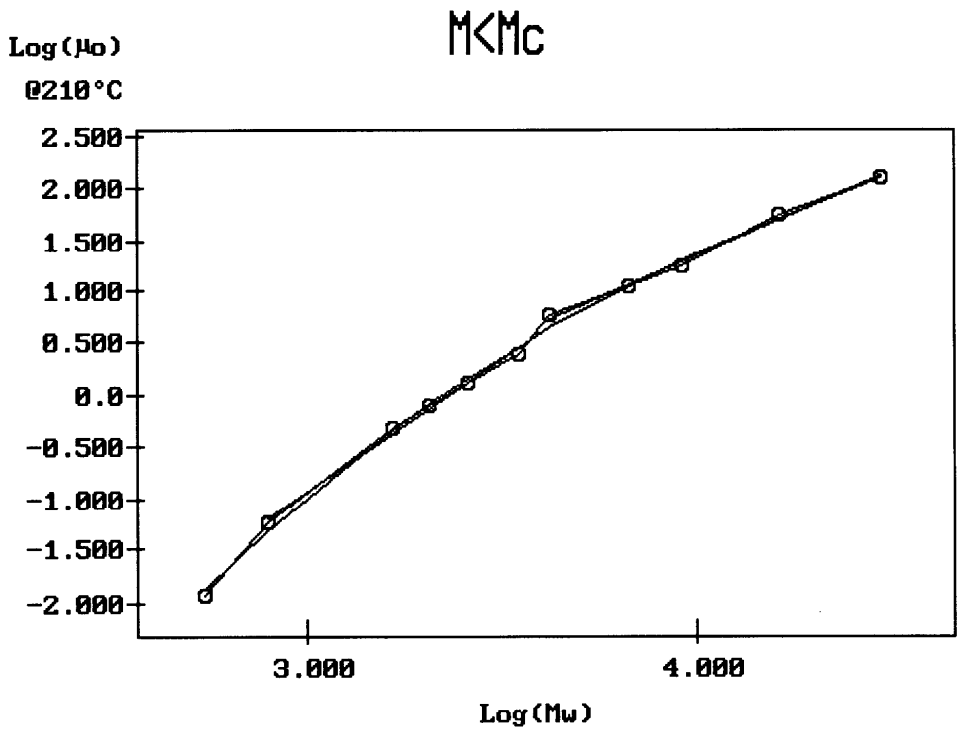

Fig. 16.

Log μ_o-log Mw plot for Mw < Mc at T = 210◦C for PS (data from ref. [25]).

It has been argued [1] that viscosity - M_w plots, below Mc, should be considered at constant friction factor, instead of constant temperature. Only under those conditions is viscosity proportional to M_w [1]. The requirement of a constant friction coefficient is met when the systems are compared at constant (T-Tg), which is assumed to correspond to constant free volume, hence constant friction factor conditions. This happens if one studies the molecular weight dependence, below Mc, at a "moving" temperature (Tg+X), where X is a constant, and Tg is function of molecular weight Mn ($M_w \sim$ Mn in monodispersed systems). We know the relationship between Tg and M_w in Fig. 11:

$$Tg\ (^oC) = -253.0 + 353.65\ .\ M_w / (M_w + 330.1)$$

Fig. 17 is a plot of Log(μo/ M_w) against Log(M_w) for a series of M_w selected across Mc, *at different temperatures*, all equal to (Tg+85) ^oC. A very good agreement

with theory is seen in this graph: not only the M>Mc behavior is well described by the expected 2.4 power exponent (the y-axis is Log(μo/ M_w)), but the M<Mc behavior is also correctly described by a horizontal line, as it should be if viscosity is proportional to M_w in this region. Furthermore, the intercept of the two lines in Fig. 17 provides the correct value for the critical molecular weight, Mc = 35,290, which agrees well with literature [1].

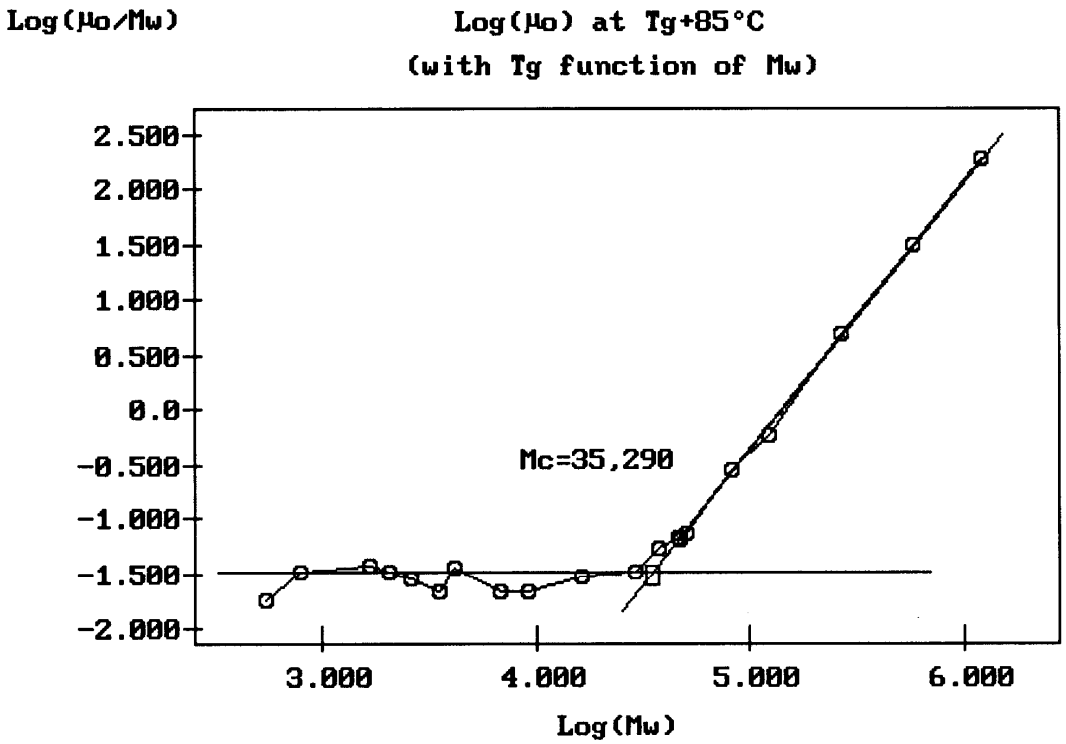

Fig. 17.
Log(μ_o/Mw) against log(Mw) of PS for a series of Mw selected across Mc at different temperatures, all equal to (T_g + 85)◦C. T_g varies with Mw.

However, plotting the data at variable temperature *and* variable M_w at the same time, which is what happens when plotting the data at constant (Tg+X), where Tg is M_w dependent, casts doubt to the simplicity of the real relationship, at T constant or M_w constant, between viscosity and molecular weight or viscosity and temperature. Eq. 1 is certainly not valid below Mc. Fig. 17 actually disproves the validity of the separation of

the variables, T and M_w, as originally stated in Eqs (1) and (2).

Furthermore, consider Fig. 18 which is the same as Fig. 17 but with different values of X, X=30 ^oC, 85 ^oC (same as in Fig. 17), and X=110 ^oC. It is clear, even without analysis of the residuals, that for M>Mc the behavior is more curved than straight. Also, for X=30, below Mc, the slope is definitely negative, a deviation which, seemingly, cannot be understood in terms of coefficient of friction.

In summary, Eqs (1) and (2), traditionally accepted to represent viscosity behavior, should be used with great caution. Molecular weight and temperature dependence on viscosity do not separate out. They do not separate out below Mc, because the data must be compared at constant (T-Tg), where Tg is molecular weight dependent. They do not separate out above Mc, because not only the temperature constant in Eqs (1) and (2) is shown to vary with molecular weight, as proven in Figs 9,10,12, but also because the 3.4 exponent varies with temperature, as clearly demonstrated in Figs 14 and 15.

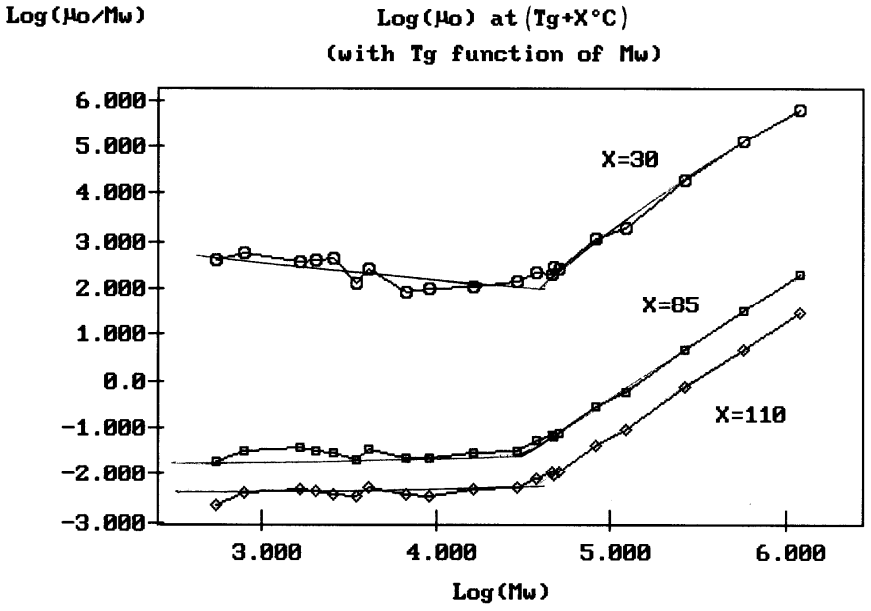

Fig. 18.

Log(μ_o/M) vs. log M at constant(T − T_g (M) = X for monodispersed PS (data from ref.[25]).

In conclusion, the well admitted view that the viscosity of polymer melts can be described by well known Eqs (1), (2), and (3) is far from satisfactory. At best, the well known equations should only be used if no other experimental data is available, as also admitted by Ferry [16]. For each material, one must specify the actual value of Log(μog), C_1g and C_2g in Eq. (3), and of the power exponent in Eq. (2). Furthermore, to be accurate, the temperature dependence of the power exponent should be known (Fig. 14). While this approach can arguably present some merit for prediction of the flow behavior at 20 to 50% accuracy [10], **theoretical models should not attempt to physically understand these formulas, simply because they are wrong and do not describe the data correctly.** Other formulations must be determined in order to find answers to the fundamental question of polymer melt rheology: what are entanglements and how do they influence viscosity and shear-thinning?

F-4 Accuracy in the Determination of the Newtonian Viscosity.

A possible explanation for the failure of traditional models and equations to describe well our data is a lack of accuracy in the determination of Newtonian viscosity. The quality of the experimental data and of the sample preparation has already been discussed in a previous section. But Newtonian viscosity values are essentially derived by extrapolation from the non-Newtonian range, and the method of extrapolation might be questioned. In particular, Newtonian viscosity calculated from different curvefitting formulas, either at vanishing strain rate (or ω) or vanishing stress, might be different. The common plot to present viscosity results, at constant temperature and variable frequency (or strain rate) uses a double logarithmic scale, Log(μ) vs Log(ω), which is shown in **Fig. 19** for Polycarbonate Grade 1 at T = 223^{o}C.

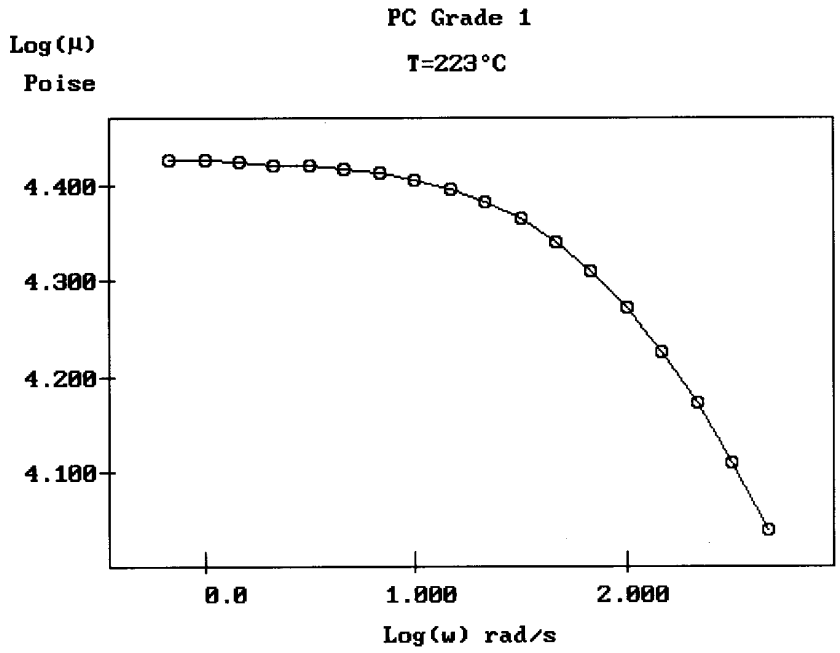

Fig. 19.

Curvefit of log μ^* vs. log ω with the Carreau's equation (line) for PC Grade 1 (T =223◦C).

The generalized Cross-Carreau equation, Eq. (5) curvefits such a plot almost perfectly, with r^2 better than 0.99995 and $\kappa^2 = 5.7\ 10^{-4}$. 4 curvefitting constants are determined from the fit, including the Newtonian viscosity corresponding to $\omega = 0$. The value of μo is 26,790 Poises. Fig. 20a is another representation of the same data, using a linear scale: μ versus G*. The Newtonian viscosity corresponds to G*=0, which is easily found if the curve is linearized. Fig. 20b shows a linear plot of μ against σ_N, where σ_N is a function of G*, with the dimension of a stress, such as the curve of Fig. 23a has become a linear function:

(8)

$$\sigma_N = (a3 + 10^5/G^*)^{-1}$$

$$\mu = \mu o + a1 \,.\, \sigma_N$$

a3 is a curvefitting constant, easily found by regression analysis. For Fig. 20b:

a3 = 0.01456 μo = 26,776 r^2 = 0.99994 and $\kappa^2 = 4.3\ 10^{-4}$.

Only 3 curvefitting constants are required.

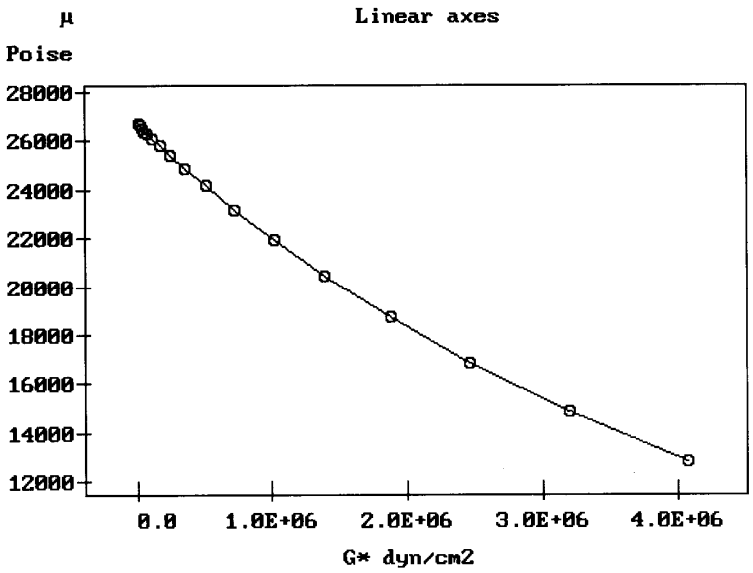

(a)

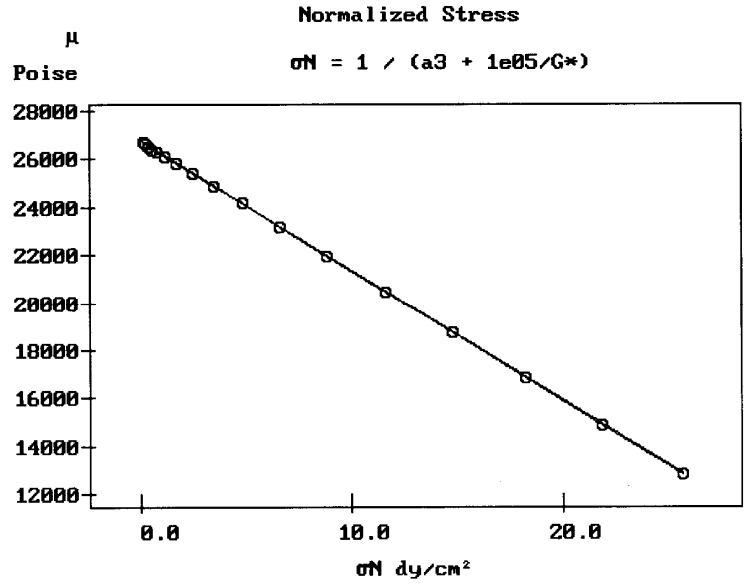

(b)

Fig. 20.

a) Different representation of the same data shown in Fig. 19. The dots correspond to various ω. Both axes are linear scales. b) Linearization of the curve in part a) by the introduction of the variable σ_N defined in Eq. (8). This allows an easy extrapolation to find the Newtonian viscosity μ_{*0}.

Finally, Newtonian viscosity is sometimes calculated from the extrapolation at G* = 0 of a Log(μ) vs Log(G*), shown in Fig. 21 for the same data at the same temperature. Such a plot is extremely well fitted by the following expression:

(9)

$$\text{Log } \mu = a1 + a2*\tanh(a3*\text{Log}G* + a4)$$

with a1, a2, a3 and a4 obtained by non-linear regression. Log μo corresponds to G*=0:

$$\text{Log}(\mu o) = (a1-a2).$$

For Fig. 21, Log(μo) = 4.419853, so μo = 26,294, and $r^2 = 0.99999$, $\kappa^2 = 3.5\ 10^{-4}$. Another excellent correlation with perfectly random residuals. The fit is shown as the line passing through the data points.

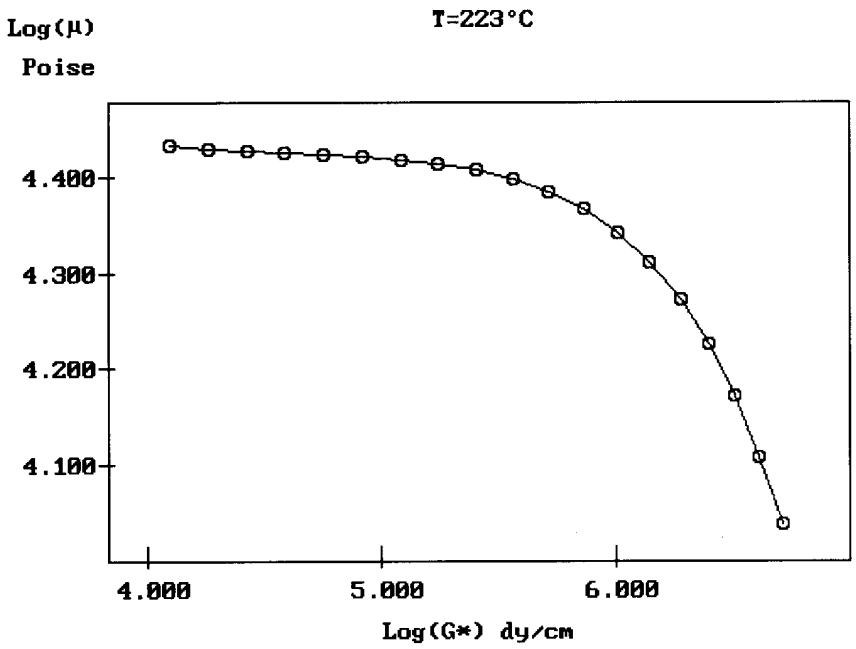

Fig. 21.

Same data as in Fig. 19, but with log G* for the x axis. The line in the figure is determined by Eq. (9).

One sees that the same value is found for the Newtonian viscosity, at 0.16% determination error, whether it is extrapolated from a Log-Log scale, from linear axes, from G*=0 or ω=0. But this was done at a single temperature: 223 ^{o}C. The same analysis

can be carried out at other temperatures, which allows the determination of Log μo (T) from several extrapolation techniques. The fits obtained at all temperatures are excellent, comparable to the results quoted for T=223°C. Fig. 22 gives the result for Polycarbonate Grade 2.

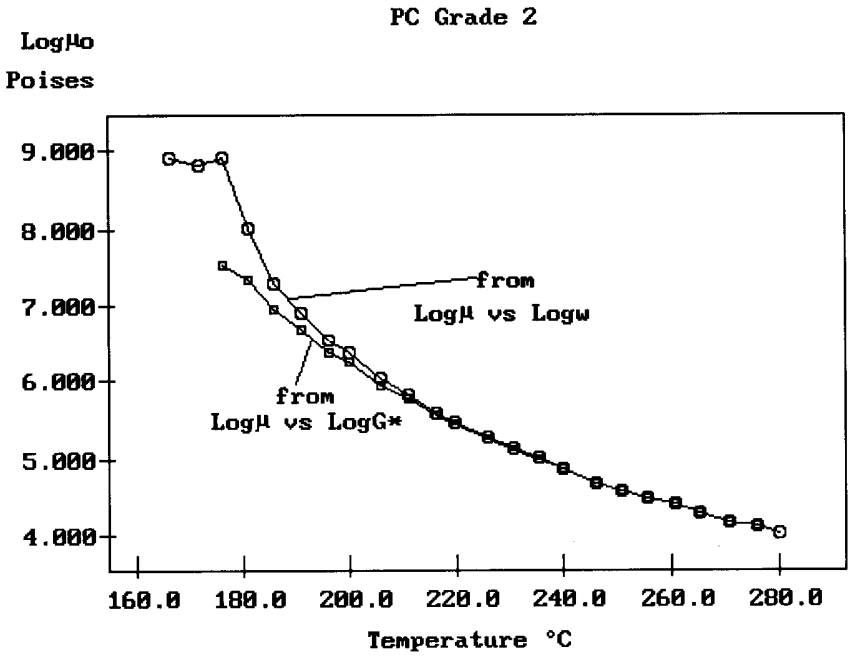

Fig. 22.

Variation with temperature of log μo calculated from either Eq. (5) (open circle) or Eq. (9) (squares).

In this figure, the two curves, obtained from extrapolating either Eq. (5) or Eq. (9), are identical from 280 °C to 210 °C, but separate out at lower temperatures, even showing a difference of more than a decade at 180 °C.

A Vogel- Fulcher or the WLF equation, Eq. (3), can be used to curvefit either the top or the bottom curve of Fig. 22, albeit with different C_{1g} , C_{2g} and Log(μ_{og}) constants. However, neither of these constants confirm the universal value provided by Ferry [16], and in any case, even if it seems impossible to conclude, at low temperature, which curve corresponds to the true Newtonian viscosity (in Fig. 9, it is assumed that it is the lower one), the behavior between 210 °C and 280 °C is unambiguous. Even in this temperature

range, where the extrapolated Newtonian values are not questioned, Fig. 9 clearly demonstrates a molecular weight dependence of the friction factor term in Eq.(2) which should only vary with temperature, should temperature and molecular weight truly separate. The next section confirms the distinct behavior one should expect below 190 ^{o}C for PC, and the reasons theoretical models should explain it.

F-5 Time-Temperature Superposition.

As time temperature superposition principle is applied in this section, for both dynamic and capillary data, many important issues of viscoelastic melts become apparent. As already pointed out before, for a Vinogradov's plot of Log($\mu/\mu o$) vs Log($\mu o.\omega$) all data points collect onto a single mastercurve. Eq. (5) predicts such a mastercurve, as long as the fitting parameters are truly independent of temperature. If Log($\mu*$) is plotted against Log(ω) at various T (Fig.2), the superposition principle stipulates that all curves superpose by horizontal and vertical shifting, both shift factors $Loga_T$ and $Logb_T$ being a function of temperature only.

The superposition can be performed by computer, as shown by Ibar [26]. The regression technique is described in Ref. [27]. Eq. (5) can first be applied to a reference curve, at temperature T_1 , to find the various fitting parameters:

$$\mu = b_1 / (1+ b_2 . \omega^{b3})^{b4}$$

and, at temperature T, the equation of the curve is the same, but shifted on both scales:

$$\mu . b_T = b_1 / (1+ b_2 . (\omega a_T)^{b3})^{b4}$$

with the same constants b_2 b_3 b_4. This can be rewritten:

$$\mu = b'_1 / (1+ b'_2 . \omega^{b3})^{b4}$$

with $a_T = \mu o/\mu o1$ and $b_T = 1/ a_T$ if Eq. (5) is correct, (the subscript 1 refers to the reference curve).

The r^2 and κ^2 of the regression fit, and analysis of the residuals, at each T, should tell us the quality of the superposition according to Eq. (5).

Fig. 23 clearly shows that, indeed, $b_T = 1/ a_T$, except in the lower T region (at the bottom right end side of the curve) for which a systematic deviation is visible. Fig. 24 also clearly demonstrates that $a_T = \mu o/\mu o1$, with perhaps a small deviation in the lower temperature region. T ref is equal to 225 ^oC.

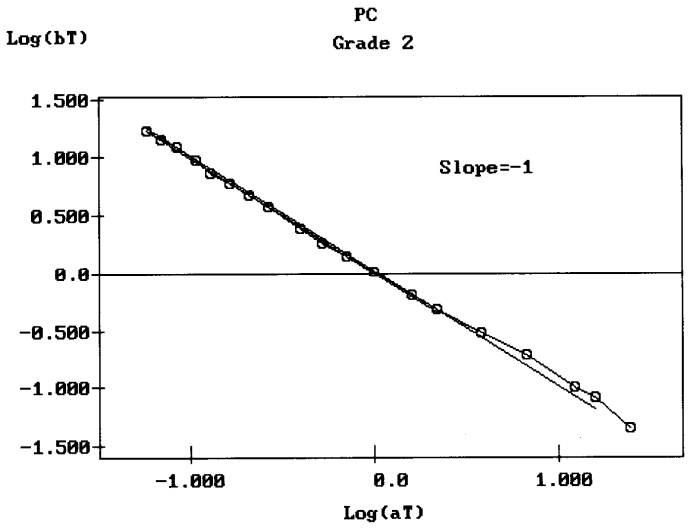

Fig. 23.
Log vertical shift factor vs. log horizontal shift factor, as determined by regression forPC Grade 2, T_{ref} = 225◦C. The straight line passing through the origin has slope −1.

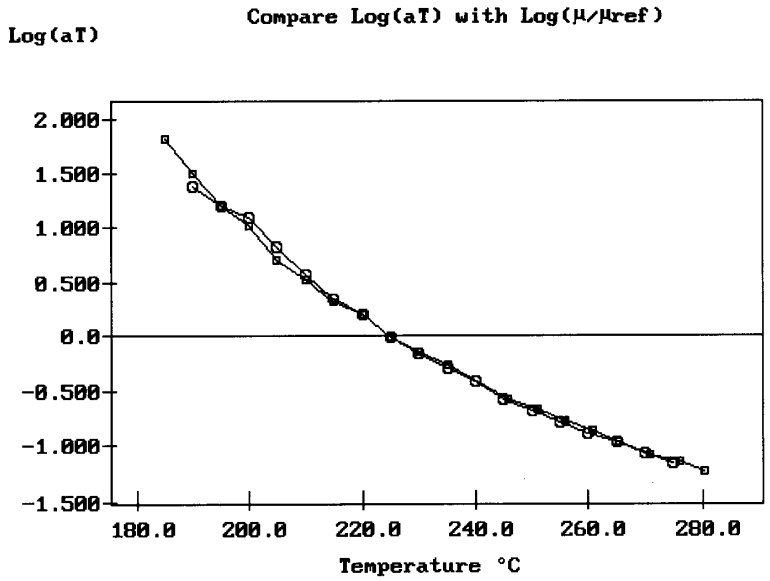

Fig. 24.

Variation with temperature of log a_T for the PC Grade 2 data of Fig. 23.

Notice that we do not see any apparent upper melt temperature discontinuity on neither Fig. 23 or 24: no $T_{l,l}$ transition in these two graphs. The classical views on melt flow are apparently forcefully validated here: the superposition principle is validated, Eq. (5) is validated, and there is absolutely no transition in the $T_{l,l}$ temperature region. This behavior is typically reported for polymer melts.

Figs. 25 and 26 plot the statistical results of the double-shifting procedure. Fig. 25 provides (r^2 -1) at each T and Fig. 26 displays κ^2.

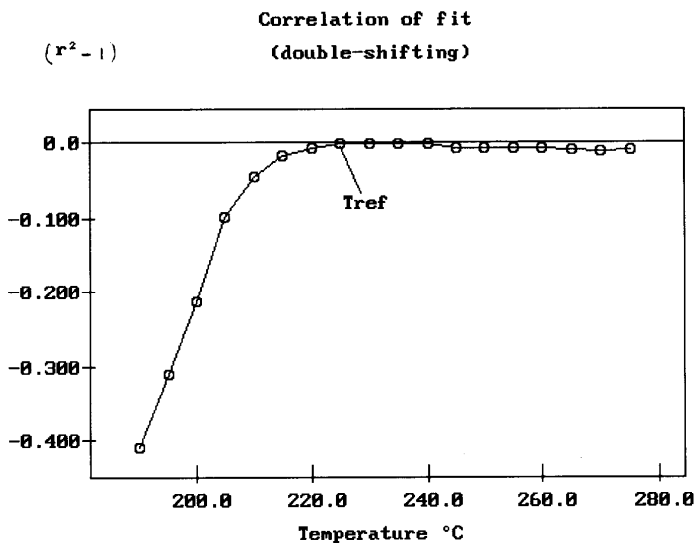

Fig. 25.

Variation of the correlation of fit, (r_2−1), with temperature for the data shifting procedure analyzed in Figs. 23 and 24.

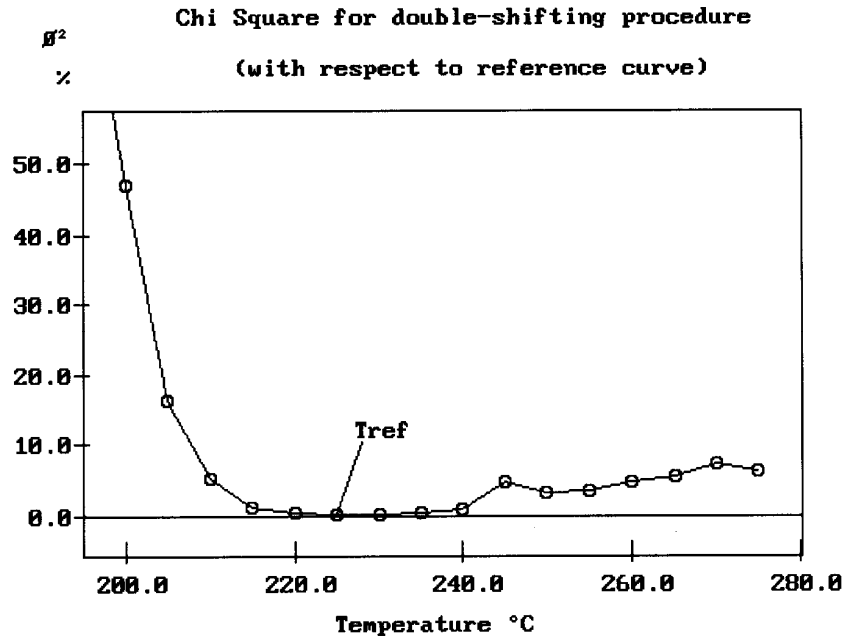

Fig. 26.

Variation of the chi-square, with temperature for the data shifting procedure analyzed in Figs. 23 and 24.

The superposition correlation is excellent for T values between 220 and 245 ^{o}C only. Below 220 ^{o}C, the superposition becomes worse and worse as T decreases, and, additionally, there seems to be a systematic deviation of the curve in Fig. 25 above 245^{o}C. This trend is unambiguously confirmed in Fig. 26 which clearly identifies a transitional behavior at 245 ^{o}C = (Tg + 100 ^{o}C). Furthermore, the regression of the superposition by double-shifting is totally inadequate below 215 ^{o}C as shown by the rapid rise of κ^2. The lower portion of the curve is purposely cut off below T = 200 ^{o}C in Fig. 26, in order to focus on the high temperature range, but κ^2 actually reaches 160% for T=185 ^{o}C, a temperature which is still 40 ^{o}C above Tg, right in the middle of the rubbery region [16]. Nothing in the classical theories predicts such a departure (remember, the superposition principle is supposed to work, and the WLF equation supposed to describe it, between Tg and Tg+100^{o}C)..

In other words, the same results which, plotted as Figs 23 and 24, apparently illustrate so powerfully the claims of classical views about the melt flow behavior, are, under close examination (Figs 25 and 26), revealing quite a different picture: **superposition is <u>not</u> validated** from Tg to Tg+100, Eq. (5) is wrong (the Carreau's "constants" are actually temperature dependent), and there is a transition temperature in the upper melt, located precisely where Boyer predicted it, at 245 ^{o}C [see later]. These same conclusions are found regardless of the equation used to curvefit the reference curve (onto which the other curves are superposed by computer shifting). For instance, in Fig. 27, a3 of Eq. (6) and of Fig. 20b, is plotted at different temperatures:

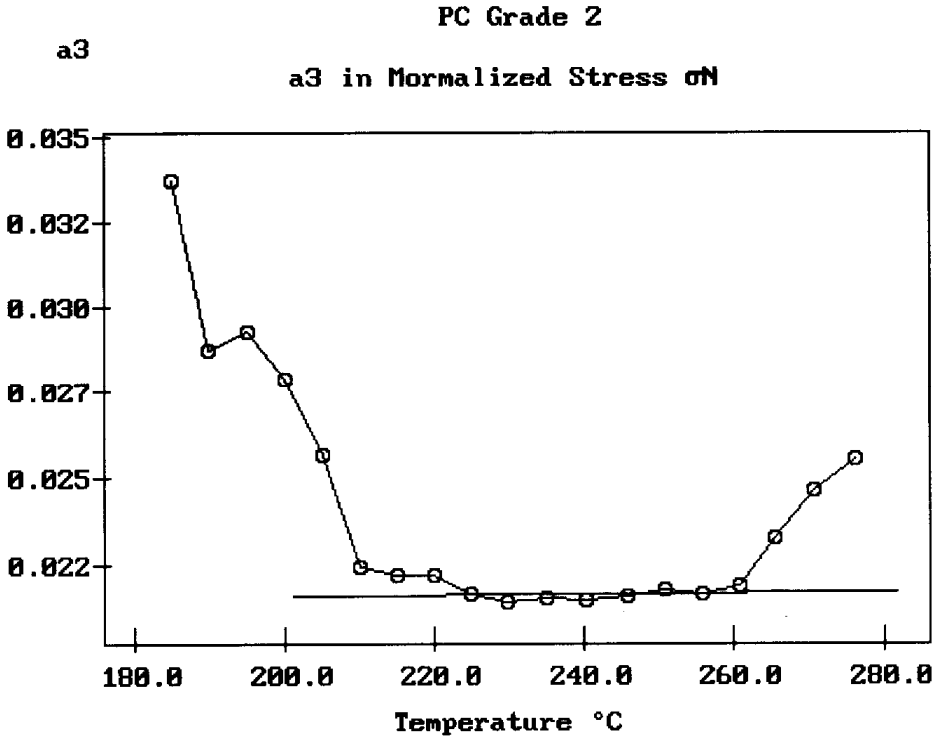

Fig. 27.
Variation of the fitting parameter a_3 of Eq. (6) and of Fig. 20b with temperature for PC Grade 2.

a3 remains constant on a small temperature range only, between 210 and 260 ^{o}C, and strongly deviates from a constant outside that range. The same behavior is observed for the other two Polycarbonate grades and for Polystyrene. The results for Polystyrene will be discussed later.

F-6 The Upper Melt Temperature Departure from Superposition.

Let's now study capillary viscosity data. The existence of the transitional behavior at around 245 ^{o}C for Polycarbonate is affirmed and well demonstrated when Stress is plotted against strain rate, instead of Viscosity. This is done in Fig. 28 for Grade 1 Polycarbonate. Temperature spans across 245 ^{o}C from 235 ^{o}C to 310 ^{o}C. Fig. 29 displays the mastercurve obtained by computer double-shifting, with Tref = 235 ^{o}C, demonstrating, once again, an excellent superposition of the curves, in the traditional

sense (b_T in Fig. 29 has a different meaning than in Fig. 23, since the variable used to superpose is different). However, the r^2 for the superposition fit, shown in Fig. 30, splits the temperature range into two clear regions, 1 and 2. In region 1, covering 235 ^oC to 260 ^oC, r^2 remains excellent (0.998) for all isotherms. R^2 sharply drops to 0.987 for the last 3 isotherms, 270 ^oC to 310 ^oC, which we designated region 2. The curves of region 2 do not superpose well with the curves of region 1, although they certainly do superpose between themselves. This confirms for Grade 1 what was found for Grade 2, e.g. the existence of a subtle transitional behavior in the upper melt.

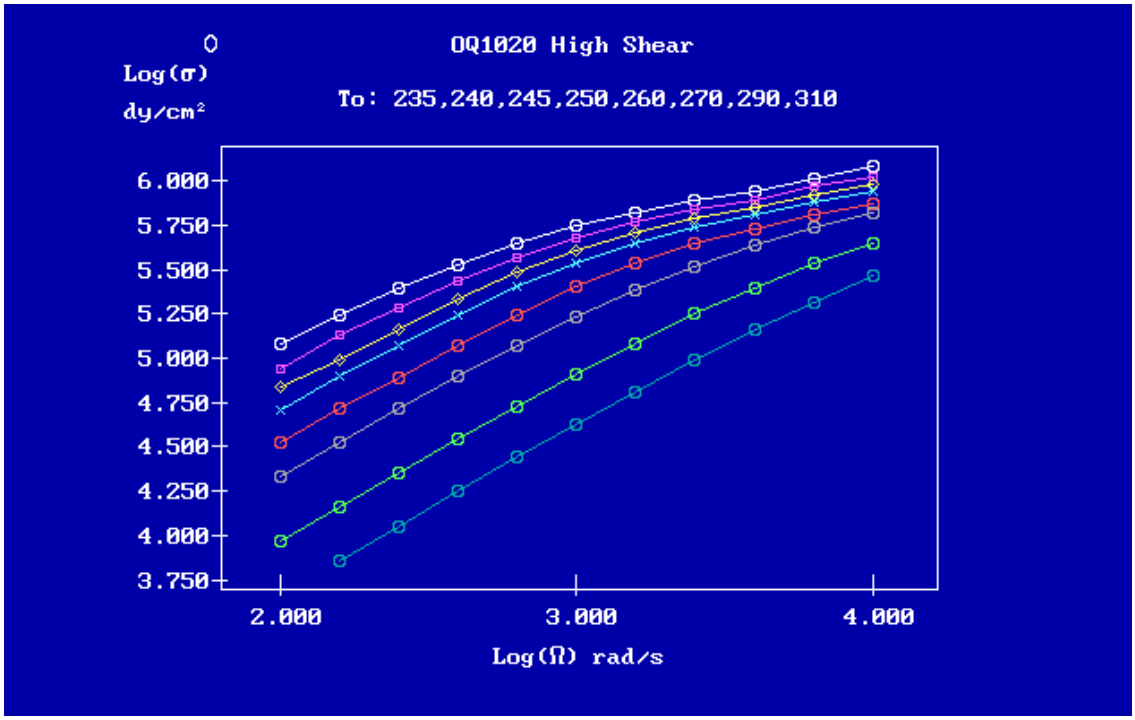

Fig. 28.
Stress vs. shear rate (log-log scale) at various temperatures for PC Grade 1. The data areobtained from a high shear capillary.

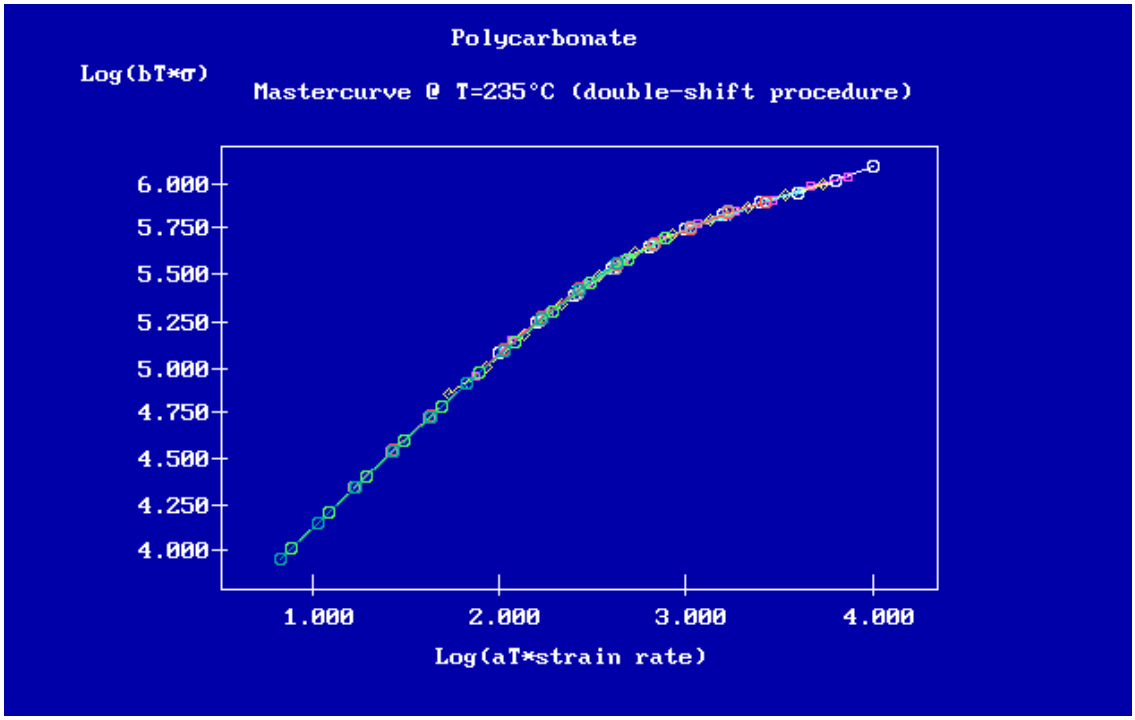

Fig. 29.
The mastercurve obtained by shifting on both vertical and horizontal axes. The procedurewas done by regression on a computer.

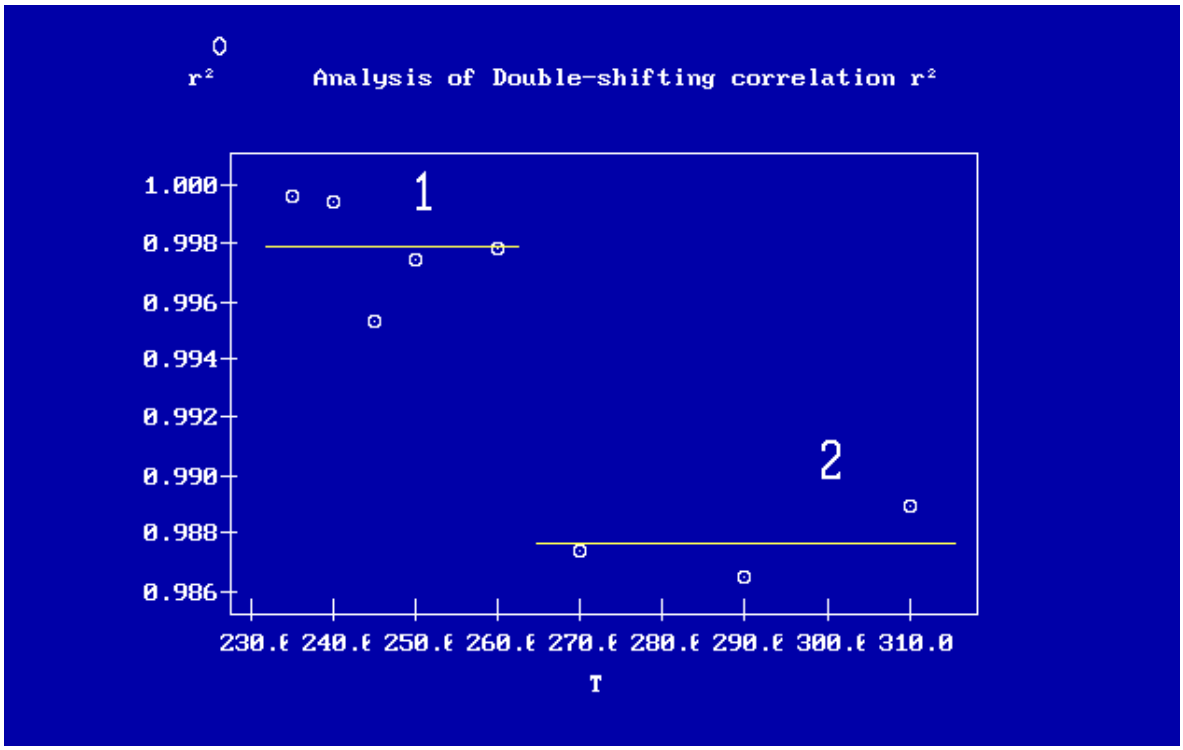

Fig. 30.
Double-shifting was done by computer. r_2 is plotted vs. temperature to determine the quality of the shifting process. The shift is justified in range 1, but not in range 2.

The use of an analytical superposition method, instead of a graphical one, is necessary to determine the existence of such a change of viscous mechanism, which, perhaps, explains its lack of recognition in the literature.

In 1981, Ibar [26] introduced such analytical shifting methods based on regression minimization algorithms [27], performing the shifting on both the vertical and horizontal axes. The temperature variation of the shift factors revealed the existence of the upper melt transition [26]. It was also shown that the vertical shift factor b_T , as determined from the optimized shifting of the curves, is not equal to $(T_1 \rho_1 / T \rho)$, as it should be according to classical views [1,8].

The distinct behavior across the two regions can further be analyzed by calculating what would be the stress in region 1 if we were to extrapolate results from

region 2. This is done by choosing T = 290 °C as new reference and finding the double-shifting factors to superpose the other two isotherms of region 2. Hyperbolic functions fit perfectly the temperature dependence of both log (shift factors), providing a way to calculate, by extrapolation from the high temperature region, what the stress would be, for a given temperature of region 1, and compare that to what the real stress is in this region. Fig. 31 compares the calculated curve from high T region extrapolation, to real data for T = 245 °C. It is clear that the real stress data are all located below the calculated stress, perhaps an indication that the change of flow mechanism across this (Tg+100) "transition" is similar to the effect of strain rate when the melt starts to shear-thin (see later). The behavior described in Fig. 31 seems to be general. It applies to all three Polycarbonate grades studied in this chapter, to Polystyrene, and to many other melts analyzed in the same way. In the case of Polystyrene, for instance, the authors of Ref. [17] fit the variation of the horizontal shift factor over the broad temperature range with **two** WLF hyperbolas, calling the transition in between "a network transition". Again, the stress (and therefore the viscosity) calculated for the lower temperature region, from extrapolation using the upper temperature WLF equation, gives too large stresses: something happens in the system of interactions between the bonds which makes it **easier to flow** at lower temperature. Notice that, contrary to common sense, flow ability increases when temperature goes down across that transition. This observation is quite important for theoretical reasons: the reptation model for entanglement [4-6, 9] does not predict the existence of such behavior, and is possibly not adequate to account for the characteristic melt behavior described here, i.e. a temperature-thinning effect. Another important observation is the location of that "melt transition", it occurs precisely where R.F. Boyer defined his Tll transition [see "Tll and Related Liquid State Transitions-Relaxations: A Review," Polymer Yearbook 2, Harwood Academic Publishers, Edited by Richard A. Pethrick, pp234-343 (1985)]. The existence of Tll has been denied by the polymer scientific community for decades. Flory denied it first with vehemence [ ]. Plazek followed, de Genne ignored it, probably did not know what to say. Boyer must be given the full credit, even if, as it turns out, his explanation for it was wrong, perhaps actually responsible for the controversy (non-believers associate Tll with local order, Boyer's explanation).

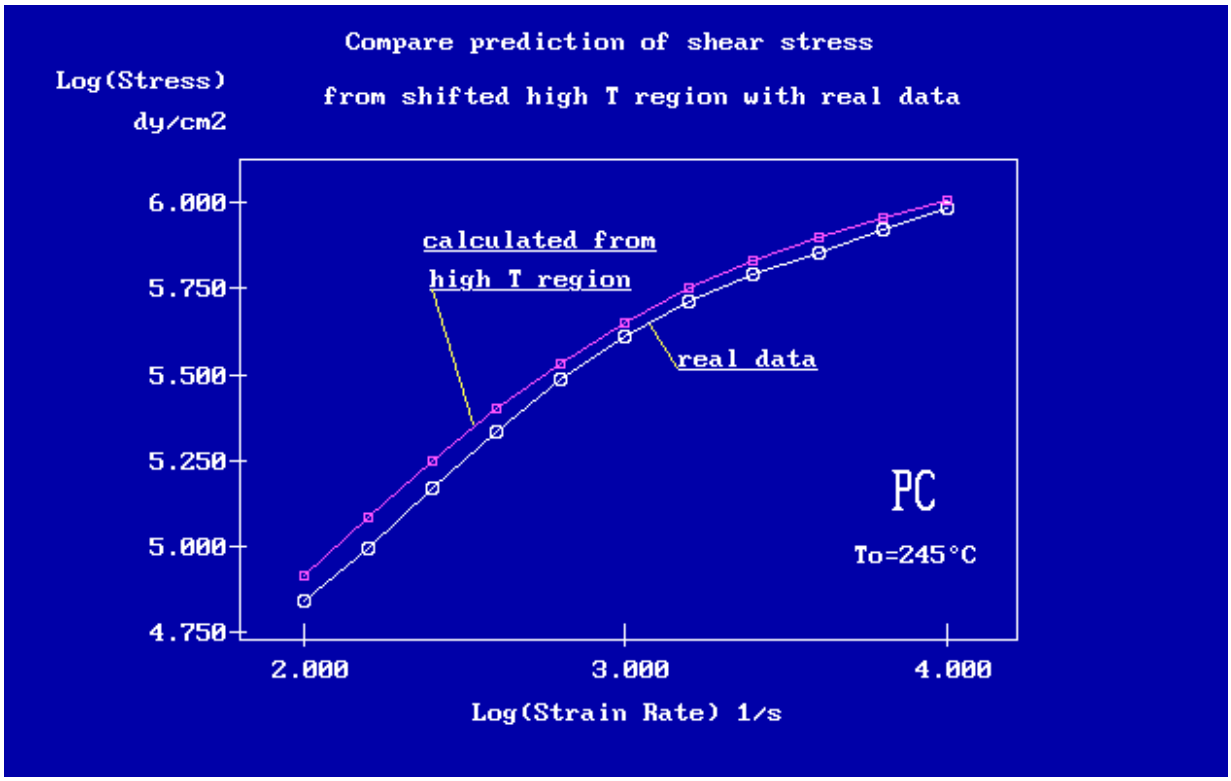

Fig. 31.
Comparison of the prediction of the value of the stress-strain rate in the low temperature region from using the fitting parameters obtained in the high temperature region.

The temperature dependence of viscosity beyond (Tg+100^{o}C), where WLF equation is known to fail [16], is described by an activated process, of the Eyring or Arrhenius type. Hence, it is well known and admitted that the WLF equation is valid between Tg and (Tg +100 ^{o}C) only, and resumes to an Arrhenius form, corresponding to an activated mechanism of flow, beyond that temperature range. If one can find a formulation for viscosity which does not seem to require a change from a free volume to an activated process mechanism in the middle of the temperature range, does it not make more sense to use such an expression? Viscosity is a parameter representative of the internal resistance to flow under stress, which has to do with the reorganization of the interactions between the bonds which form the macromolecules. Which thermodynamic quantities can be correlated with molecular parameters?

The reason for the failure of the free volume based WLF equation at high

temperature is left largely unexplained, ironically by the same scientists [29] who refute the existence of an upper transition in the melt, the Boyer's $T_{l,l}$ transition [30]. If there is such a transition in the upper melt, what causes it, and why are the accepted models of flow [4-6] not addressing such an important issue? What happens to the reptation tube below and above $T_{l,l}$?. Obviously, if one needs to change the form of the viscosity equation across a certain temperature in the melt, it seems very important to know why, not to mention the influence that such a complexity brings to the prediction of the flow viscosity when performing computer simulation of molding processes [31].

The issue of the existence of a transition in the upper melt must be re-addressed by rheologists and polymer scientists.

F-7 The Lower Melt Temperature Departure from Superposition.

Let's now turn to the departure from the superposition principle at the lower temperature end, as Tg is approached. The nature of the transitional behavior at around 190 ^{o}C -210 ^{o}C in Figs 25-28 can be better characterized by plotting the relative elasticity (G'/G*) against the strain rate (or frequency) at the various temperatures. Fig. 32 is actually a plot of the square of (G'/G*), for reasons which will be apparent later.

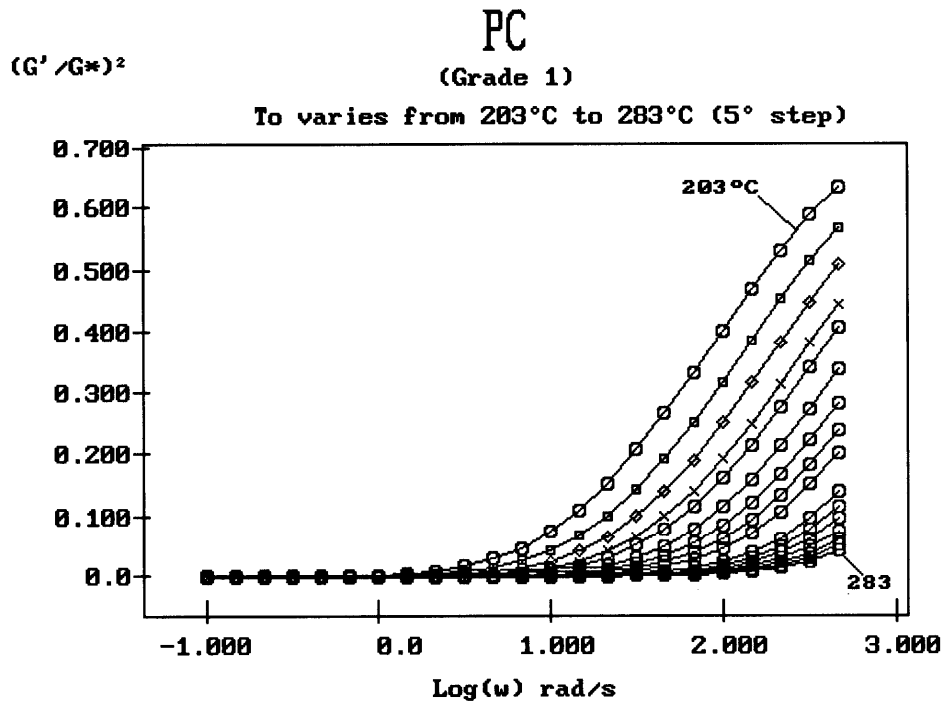

Fig. 32.

Variation with ω (rad/s) of the ratio of moduli $(G\_/G*)^2$ at various temperatures between 200–280 ◦C for PC Grade 1. G_ and G* are the elastic modulus and the complex modulus.

There is no doubt that superposition by horizontal shift is possible in Fig. 32, which covers the temperature range between 200 and 280 ^{o}C. However, the lower melt temperature range, shown in Fig. 33 from 163 to 200 ^{o}C, cannot be superposed with any reference curve of the previous graph, confirming the departure from superposition noticed earlier. This behavior is also true for the data on Polystyrene[17] re-plotted in Fig. 34. One distinctively observes, for both Polycarbonate in Fig. 33 and Polystyrene in Fig. 34, the presence of a maximum for the lower temperature isotherms. The frequency of the maximum increases with decreasing temperature. The traditional way for handling the superposition principle is to shift over the whole range of temperature above Tg, accepting somehow arbitrarily less precision for the lower temperature isotherms, for which the principle seems to deviate the most. The result is an "acceptable" mastercurve, as shown for Polystyrene in Fig. 35. However, to obtain superposition of the tails located after the maxima in Fig. 34, a sort of two-way shift is necessary, one shift for the lower

tail, another shift for the upper tail, casting doubt on to the validity of the superposition principle for these data points. In fact, if we eliminate the points located beyond the maximum, the superposition seems to be much more accurate, even for the low temperature isotherms. Furthermore, the points located on the high frequency tail, beyond the maximum, at different temperatures, superpose between themselves, with a different temperature dependence for the shift factor than the data localized on the lower frequency side of the maximum. This means that the mastercurve in Fig. 35, plotted against a single variable, $\mathrm{Log}(a_T\,\omega)$, is not representative of the real situation beyond the maximum. There is a change of the shift factor for the data below the maximum and for the data above the maximum: there is no single mastercurve for the whole temperature-frequency range. This result is also true for the 3 Polycarbonate grades studied.

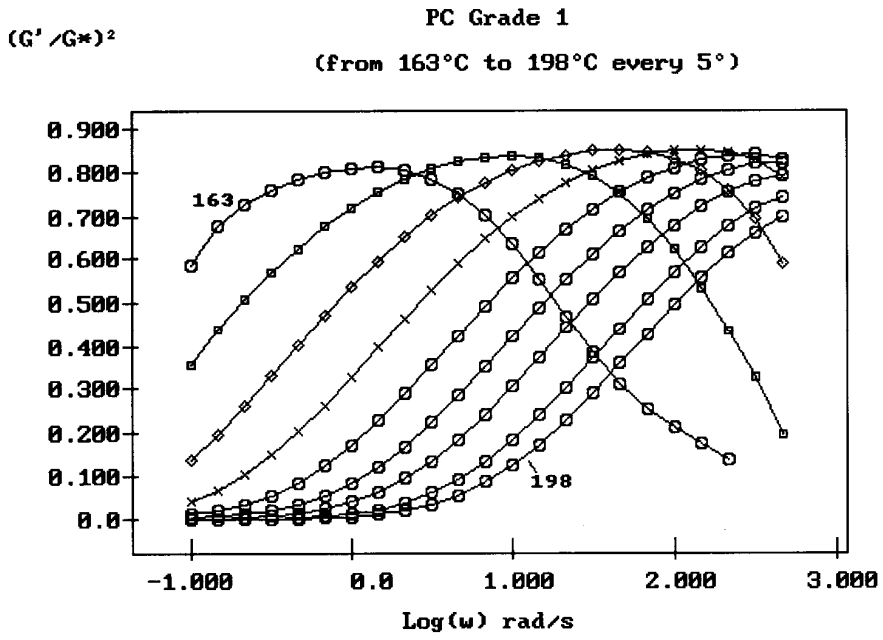

Fig. 33.

Variation with ω (rad/s) of the radio of moduli (G_/G⋆)2 at various temperatures between 163–198◦C for PC Grade 1. G_ and G⋆ are the elastic modulus and the complex modulus.

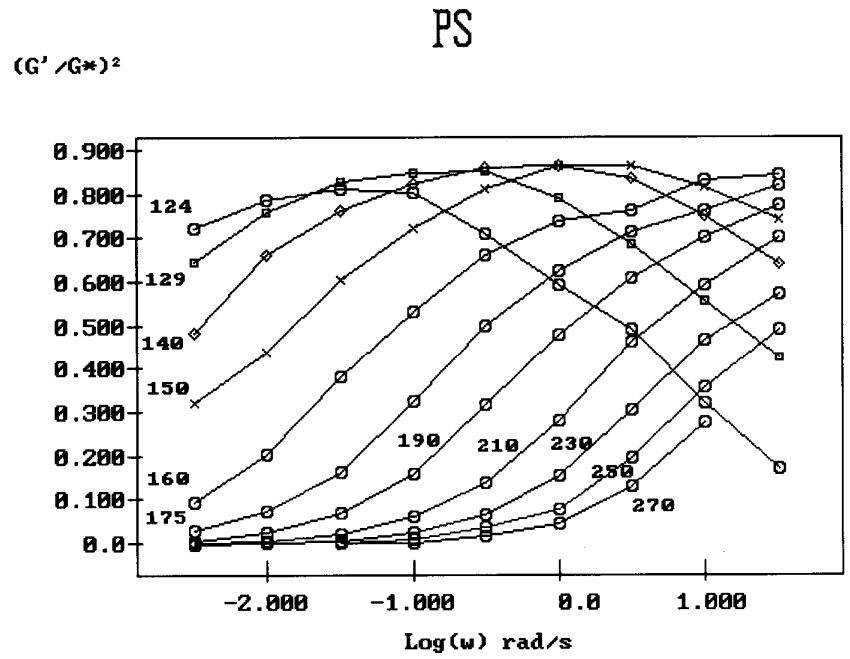

Fig. 34.

Variation with ω (rad/s) of the radio of moduli (G_/G∗)2 at various temperatures between 124–270 ◦C for PS. G_ and G∗ are the elastic modulus and the complex modulus.

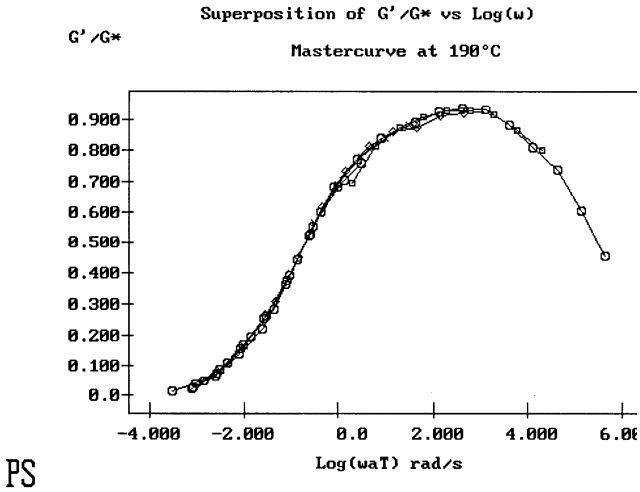

Fig. 35.

The superposition of all portions of the log ω curve, for all isotherms, can only be achieved if two superposition shifts are done, one with respect to the points located beyond the maximum, the other with respect to the points below the maximum.

In terms of traditional superposition of the data plotted as Log(μ) vs Log (ω), it appears, from the previous analysis, that those points which correspond to a frequency above the maximum in Fig. 34 should not superpose with the same shift factor, and should be eliminated from the regression analysis when superposing analytically, or from the pool of data points when curvefitting with the generalized Cross-Carreau equation, Eq. (5).

Fig. 36 shows that those points to eliminate, the high frequency data on the lower isotherms, are traditionally assigned to the existence of a second Newtonian regime, which Hieber and Chiang [10] try to incorporate into a new equation, Eq. 4. This approach has possibly little merit, from a physics point of view. By way of analogy, it amounts to put in the same bag, for analysis, data from the elastic state and from the plastic state of a stretched material, say a metal, or mixing data above and below Tg when fitting PVT results. In Fig. 35, the data from the left end side of the maximum correspond to one mechanism of deformation, an elastic deformation in our analogy; this mechanism is interrupted and triggers another deformation mechanism when frequency exceeds a certain value, corresponding to yielding of the melt, in our analogy. The data contributing to the second Newtonian regime, which is often perceived as a limitation to shear-thinning, should not be mixed with the data describing shear-thinning, because they "pollute" the regression coefficients obtained. Practically speaking, it seems difficult to determine which data should be eliminated, from a viscous -strain rate plot (Fig. 36). For instance, the last three high frequency points which look perfectly OK on isotherm 150 ^{o}C (the 4th curve from the top in Fig. 36) are actually located beyond the maximum in Fig. 34 and should be eliminated from the regression giving the parameters of Eq. 5. This might explain why the regression parameters for superposition always seem to diverge sharply at lower temperatures (Figs 25-27).

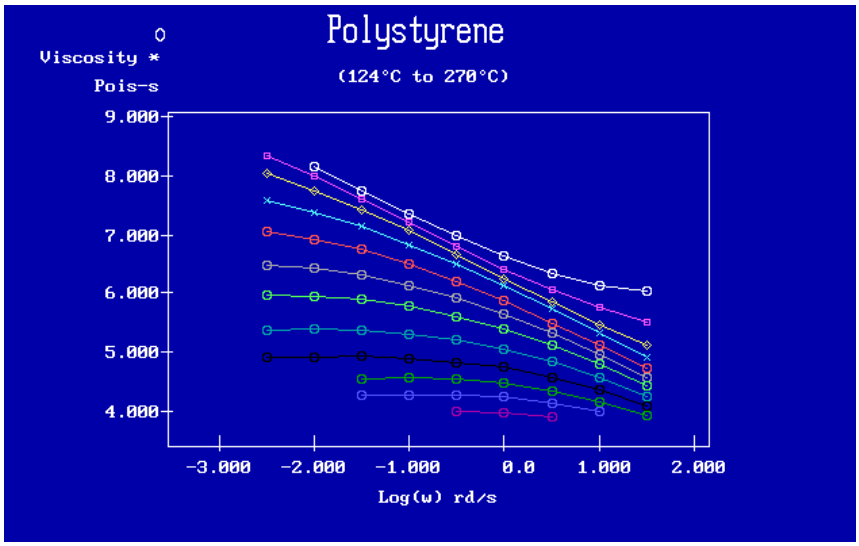

Fig. 36.

Classical representation of rheology results, log $\eta^*(\omega)$ vs. log ω at various temperatures. Notice the upturn at high frequency for the lower temperature curves This part of the curve corresponds to points located beyond the maximum in Fig. 34.

F-8 Is the Superposition Principle ever Valid?

The idea behind superposition is scaling, or the renormalization of the variables to describe temperature and strain rate effects. Over a 100 ^{o}C span above Tg+30, and within a 25%-50% error tolerance, the answer is yes, suffice it to quote all the papers which have tested its validity under those conditions, and routinely present their data after superposition has been performed. However, if the tolerated error is of the same order of magnitude than the experimental error, then the answer is no, even on a short temperature span of 30 ^{o}C , if the scaling variables to superpose have not been truly defined. Consider **Figs. 37** and **38** for a PS of Mw=250,000 (polydispersity 2.5). The temperature span is 30 ^{o}C, from 140 to 170 ^{o}C. The longest relaxation time (the terminal time) is determined from the maximum of $\eta'' = G'/\omega$ in Fig. 37. $\tau o = 1/\omega_o$ .. In theory, the scaling factor for the horizontal axis should be ω/ω_o and η / η_o for the vertical axis. These are the reducing variables, according to the traditional approach. It is, indeed, *almost* true. Fig. 38 is a close-up view of the masterplot and superposition is *almost* OK. Yet, if one is concerned

whether the curves truly superpose, a fair answer is that there is a systematic deviation visible for all curves, and that these curves, in fact, do not superpose. It should be noted the large number of points per decade to define the frequency sweeps at each temperature. Perhaps very significantly, if we filter out, starting from the same data set, the number of points down to 3 points per decade, a procedure followed in most routine sweeps, the superposition now *appears* quite satisfactory.

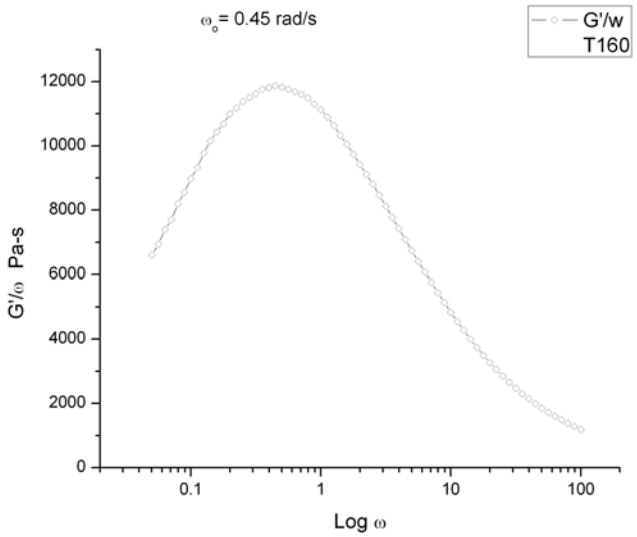

Fig. 37.
Determination of the location of the maximum of G'/ω vs. log ω to obtain the terminal relaxation time. PS 1960N from Total Petrochemicals. T = 160◦C.

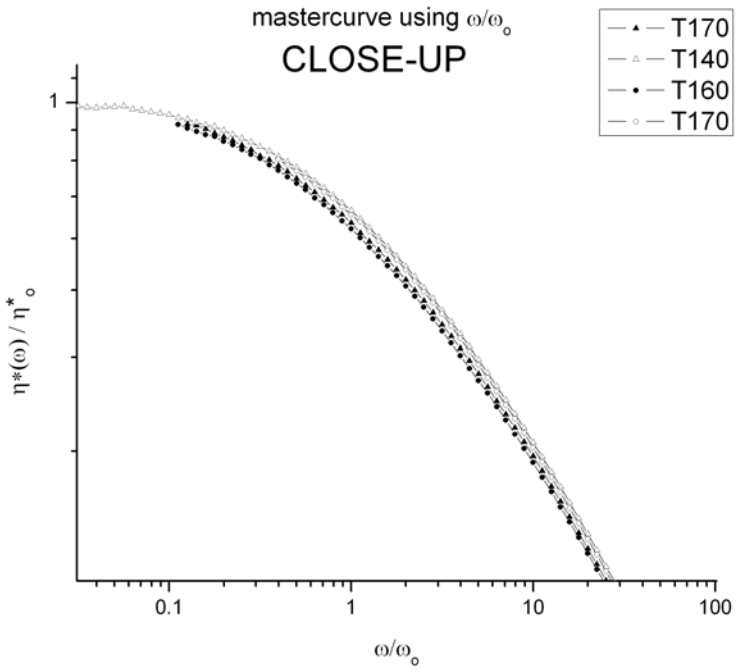

Fig. 38.

Masterplot of reduced variables log ($\eta^*(\omega)/\eta^*o$) vs. log ω for 4 temperatures covering a very short interval for PS.

The only way to make the superposition really work is to force it to work, by double-shifting, done analytically by regression. But, as explained by Ibar [26], when one analytically forces the data to fit an equation which includes fixed parameters, in order to accomplish a double-shift procedure, one invariably observes that the regression statistical parameters decline systematically on both sides of the reference temperature. This remains true even after the high frequency data corresponding to the second Newtonian regime have been eliminated. This observation is the proof that there is no validity of the time temperature superposition over the range of temperature suggested by Ferry [8], i.e Tg and Tg+100 ^oC. As shown earlier, it is possible to establish two ranges of strain rate and temperature, within which the time superposition does work, but if this is the case, one needs to admit the existence of a transition-relaxation above T_g, and theories should explain it: this is not the case at present, and, furthermore, the existence of such a transition is vehemently opposed by the current school of polymer physics. The ultimate test of validity for the time temperature superposition is to let all constants loose

in the curvefitting function and determine if there is any trend with temperature for those parameters which are supposed to remain constant. Does any break in the trend show up? This will be done in part II of this critical review.

G The Question of Understanding Rheology with a Spectrum of Relaxation.

Like with any concept that has shown extremely useful over the years, it is very tempting to explain new phenomena with the same concepts, by the same type of equations. The concept of relaxation time goes back to the explanation of resonance phenomena, in mechanics, in electrical circuits, in magnets orientation, in just about every single field of physics. When the time scale to observe is tuned to the time scale of what is changing, resonance occurs: $\omega\tau=1$. Mechanical and electrical analogs for resonant systems are taught in elementary physics classes. The simplicity of their equations is the elegant driver that makes us look for them. A resonant system can be defined by its relaxation time τ. When the experimental results are more complex than what can be described by a single resonant system, then a network of dashpots and springs or capacitors and resistors is defined, and "a spectrum of elementary relaxation times" relates to the complexity of the response. For dashpot and spring in series, the relaxation time is simply the ratio of the viscosity of the dashpot by the modulus of the spring (the spring constant).

In the case of understanding the visco-elastic properties of polymer melts, nothing seemed more appropriate than a network of dashpots and springs, a Maxwell network for stress relaxation experiments, a Voigt network for creep, and a set of fancy equations to coordinate one network to the other, in order to make it general.

The next step was to find what was moving and define it in molecular terms. Macromolecules are long chains of mers and their melt properties must be described by the constant motion of the bonds to re-organize within the restrictions imposed by other bonds, those on the same chain, and those located near-by on adjacent chains. The simplest well known theory to characterize statistically a set of atoms or molecules

submitted to thermal agitation is the statistical gas kinetic theory due to Maxwell. Pressure of the gas can be quantified from the average velocity of the molecules, so can diffusion in the gas. The link between macroscopic variables and molecularly defined entities is what makes Maxwell's description of the properties of a perfect gas a breakthrough. Of course, macromolecules are not as simple as simple molecules, because their mers are covalently linked to each other along a chain, which drastically reduces the degree of freedom of their motion. But the temptation seems natural to redefine the statistical units present in the theory of gases in terms of mers dimensions, and define a relaxation time (or a spectrum of those) that correlate to the local "spring and dashpot" properties of the mers. This is the successful Rouse's theory of diffusion in polymers [32bis]. Simply stated the relaxation time is the ratio of a spring constant, the same as for a statistical gas, $3kT/b^2$, and a viscosity, $N \xi o$, where N is the number of mers per chain, and ξo is the local friction coefficient per mer; b is the quadratic distance of two beads defining a chain segment (b= Rg, the radius of gyration).

(10)

$$\tau_R = \frac{1}{\pi^2} \frac{\xi_o N < R_g^2 >}{kT}$$

The diffusion constant is defined as the ratio of thermal energy to the total friction (from Stoke-Einstein):

(11)

$$D = \frac{kT}{N\xi_o}$$

and the shear modulus G(t) is:

(12)

$$G(t) = \frac{\rho RT}{M} \sum_p e^{-\frac{t}{\left(\frac{\tau_R}{p^2}\right)}}$$

where p=1,2,3…defining *a family* of *discrete* relaxation times:

(13)

$$\tau_p = \frac{\tau_R}{p^2}$$

The steady state viscosity is:

(14)

$$\eta_o = \frac{\pi^2}{6}\left(\frac{\rho RT}{M}\right)\tau_R$$

This formula gives an explanation to what was stated in Eq. (1). The Rouse time, in Eq. (10) varies with M^2 since Rg varies with $M^{0.5}$, so viscosity scales with M according to Eq. (14). We have shown that this was not true, at constant T (Fig.16) for M < Mc monodispersed PS, also confirmed by more recent results by Majeste et al [35], but could be be true (Fig. 17) at constant (T-Tg) where Tg is made a function of M (this could be defined as "a constant free volume" friction coefficient approach. See chapter 5).

In the frequency domain, Eq. (12) above can be transposed to give the Rouse complex modulus as a function of ω:

(15)

$$G^*_{Rouse}(\omega) = \frac{\rho RT}{M} \sum_1^N \frac{\omega^2 \tau_p^2 + j\,\omega\tau_p}{1 + \omega^2 \tau_p^2}$$

If one calls $G_o,^N = \rho\, RT/M$, and if, for the sake of illustration, one limits G* to the first term (p=1, terminal relaxation) of the series, then the above equations can be rewritten as:

(15bis)

$$G' = \frac{\omega^2 \tau_o^2}{(1 + \omega^2 \tau_o^2)} G_N^o$$

$$G'' = \frac{\omega \tau_o}{(1 + \omega^2 \tau_o^2)} G_N^o$$

$$\tan \delta = \frac{G''}{G'} = \frac{1}{\omega \tau_o}$$

(16)

$$\cos^2 \delta = \frac{1}{1 + \tan^2 \delta} = \left(\frac{G'}{G^*}\right)^2 = \frac{G'}{G_N^o}$$

(17)

$$\frac{G'}{\omega} = G_N^o \; \frac{\left(\frac{G'}{G^*}\right)^2}{\omega}$$

The reasons to write Eqs (16) and (17) will become apparent in the section below.

The Rouse model is admitted to describe well polymers with M < Mc (we saw earlier that it does only if data are re-tabulated at (T-Tg) constant), but is unable to explain the effect of entanglements on viscosity, or the existence of a molecular weight independent plateau modulus G_o^N = = ρ RT/Me for M > Mc melts (where Me is the weight of the strands between entanglement points). Rouse predicts that G_o^N decreases with M. Another problem, the contribution of the high frequency terms (the influence of the transitional relaxation terms), in addition to the Rouse term needs to be addressed. The following expression is due to A. Allal [36]:

(18)

$$G^*_{HF}(\omega) = G_\infty \left[1 - \frac{1}{\left(1 + j\omega\tau'_o\right)^{1/2}} \right]$$

$$\tau'_o = \frac{1}{\pi^2} \frac{\xi_o b'^2}{kT}$$

and now:

(19)

$$G^*(\omega) = G^*_{Rouse} + G^*_{HF}$$

For entangled polymers, the de Gennes [4] and Doi-Edwards's [5, 6] re-formulation of the motion of a chain embedded in a sea of topological obstacles created by the presence of other chains, resulted in the definition of a tube into which macromolecules could only move by reptation. The confined motion explained the viscosity increase. The tube could fluctuate in length, in proportion to $(M/Me)^{0.5}$, and could locally be renewed resulting in local constraint release from topological restrictions (Montfort, Des Cloizeaux, Klein, Graessley). The details are very sophisticated. For our purpose, the new model is merely a justification to refine Rouse's family of discrete relaxation times to make it fit to the increase of viscosity with M due to entanglements.

Thus, de Gennes' school redefines the terminal relaxation time τ_o, corresponding to p=1 in Eqs. 12, 15, with respect to the molecular weight, introducing the value of Me, proposes a different "structuring" of the relaxation time f*amily*, for instance with respect to the number of terms (p=1,3,5… only the odd terms relax), modifies the weight of each relaxation process ($G_p = G_o/p^2$ in the original Doi-Edwards's model), but keeps the same family description of the relaxation times τ_p as a function of p (Eq. 13, with τ_R replaced by τ_d). The whole exercise is driven by the need to explain the molecular weight dependence of viscosity, which is assumed to vary like $M^{3.4}$, with all the reservations made about this relationship in this chapter. Many authors gravitated around the reptation platform, modifying some aspects of it, debating about the improvements, creating a real school of thoughts about polymer flow based on reptation.

As an example of the new reptation ideas, the following formulas, given by Matsuoka [33], are claimed to describe well dynamic rheological data of monodispersed PS melts by Marin and Graesley[34]:

(20)

$$G' = \sum_{p\ odd} G_p \frac{\omega^2 \tau_p^2}{\left(1 + \omega^2 \tau_p^2\right)}$$

$$G'' = \sum_{p\ odd} G_p \frac{\omega \tau_p}{\left(1 + \omega^2 \tau_p^2\right)}$$

(21) with:

$$\tau_p = \frac{\tau_o}{p^{3.4}}$$

$$G_p = \frac{G_o}{p}$$

$$p = 1, 3, 5, ..., p_{\max}$$

$$p_{\max} = \frac{M}{M_e}$$

Matsuoka makes a variation in the definition of the Doi Edwards parameters in Eq. (20-21), but it should be pointed out that the Rouse's model and the reptation models have a common framework, only the definition of Gp and τp change.

In the following graphs, we apply formula (20) and (21) to the case of Marin's data on monodispersed Polystyrene, M= 110,000 (M/Me=6.47). The temperature is 140.9°C. The exercise is to learn how well a modified spectrum of relaxation, according to the reptation school, describes results obtained in dynamic shear. The terminal time τo is determined from the maximum of G'/ω vs logω and is equal to 13.15 sec at 140.9 °C. The elastic plateau modulus of Polystyrene is well known and equal to 0.2 MPa. Me is taken at 17,000 g/mole (consistent with Mc=34,000). The transition end of the entanglement plateau is determined by $\tau_T = \tau o * (Me/M)^{3.4} = 0.023$ sec, corresponding to a frequency ω_T of 43.48 sec^{-1}

The simulation is very straightforward: all parameters entering the terms of the series in Eq. (18) and (19) are defined as a function of the terminal time τ_o and, therefore, G'p and G"p can be tabulated for a range of ω values, as well as the sum G*, η*(ω), η*o, and the other functions included in Eq. (16) and (17). Figs 39-45 display the simulation results. The points colored in red are for $\omega > \omega_T$, i.e. beyond the transition frequency.

In Fig. 39 and 40, we learn how the elementary relaxation components combine, respectively for G" (Fig.39) and for G' (Fig.40), to add up to the blue curve, the simulated total loss and elastic moduli. The low ω behavior is totally dominated by the terminal time, and one sees the broadening of the G" peak by the addition of the secondary terms p=3, 5, 7. The influence of the secondary relaxations on G' is only visible above ωo, which also defines the sharp departure from the Newtonian viscosity value in Fig.41 (the Newtonian value is 2.65 Mpa-s.) This ω_o does correspond to the maximum of G'/ω in Fig. 42, which is the inverse of the terminal time τo.

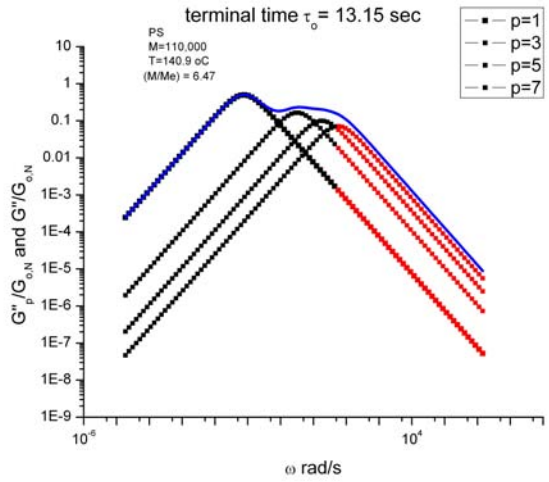

Fig. 39.

Simulation of a melt rheological response (normalized G”p) corresponding to a terminal time τ o = 13.15 sec according to Eqs. (20) and (21). The envelope curve corresponds to the sum of the elementary contributions (p = 1 to 7).

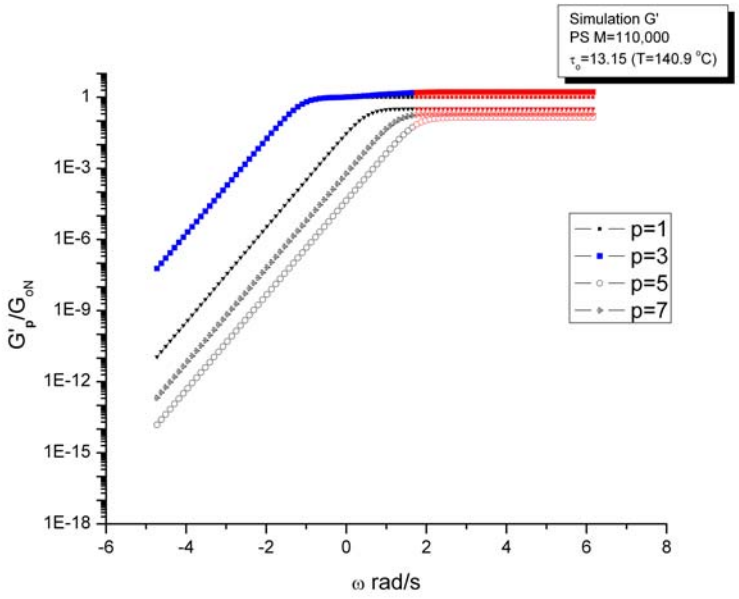

Fig. 40.

Simulation of a melt rheological response (normalized G’p) corresponding to a terminal time τ o = 13.15 sec according to Eqs. (20) and (21). The top curve corresponds to the sum of the elementary contributions (p = 1 to 7) and is largely dominated by p = 1.

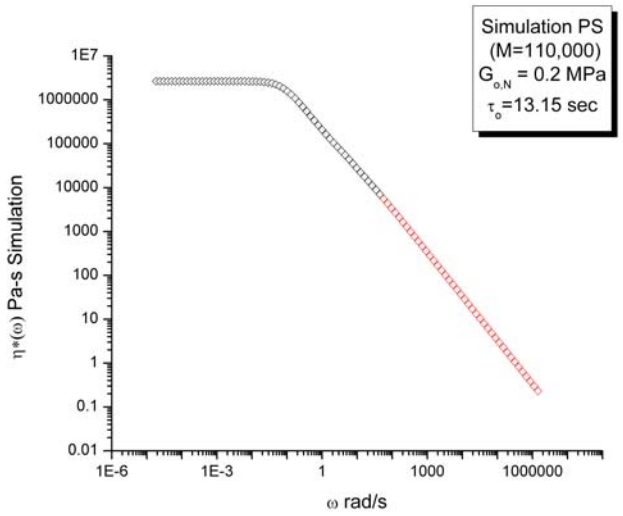

Fig. 41.

Simulation of viscosity vs. ω from the data of Figs. 39 and 40. The simulation stops to be valid beyond ωT = 43.43.

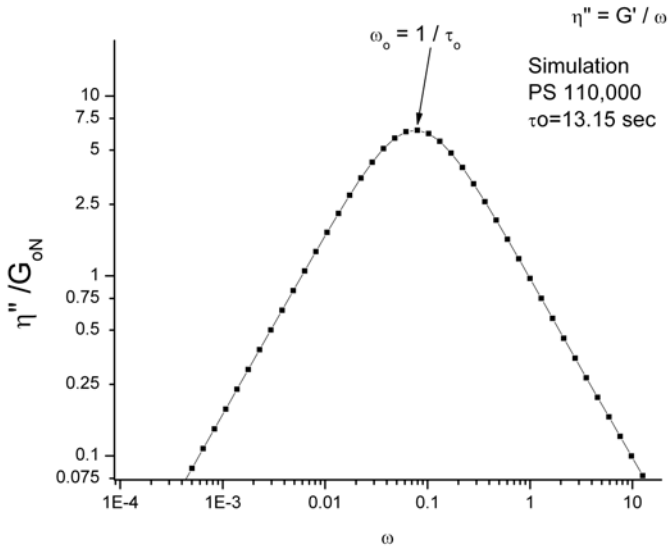

Fig. 42.

Simulation G'/ω vs. log ω to determine the terminal time $\tau_o = 1/\omega_o$.

In Fig. 43, a plot of normalized G" vs G' on a double-log axis, we determine that the slope is 0.5 for the low ω points, almost all the way up to the cross-over (G'=G"), but that the slope decreases as we get closer to the cross-over, to become zero at the cross-over. Additionally, at the cross-over $(G'/G^{o}_{N}) = 0.5$. From Eqs. (16) and (17), it should become apparent that the cross-over should be equivalent to the point of maximum of G'/ω to define ω_o

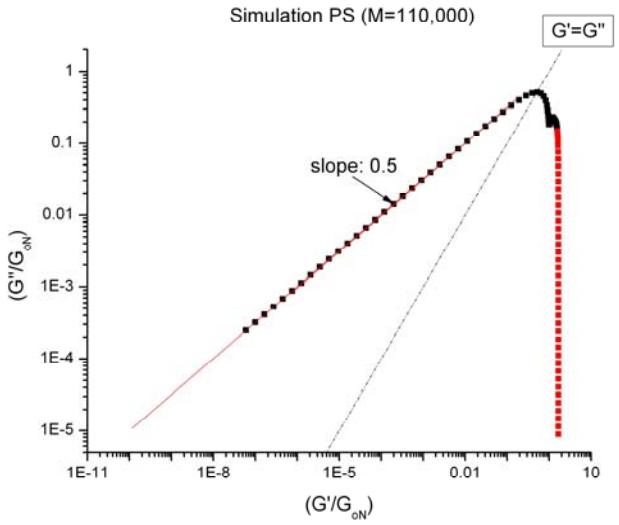

Fig. 43.
Log-log plot of normalized G" vs. normalized G' (by the plateau modulus G_{oN}) for simulated PS results corresponding to M = 110,000.

Fig. 44 is a plot of $(G'/G^*)^2$ vs (G^*/ G_{oN}). One sees that the upward curvature sharply reverses for $G^* = G_o^N$, and that $(G'/G^*)^2$ is very close to 1 at its maximum, 0.9684 to be precise. Also, another important feature of this plot is the good match between the values found on each axis corresponding to the cross-over point (G'=G"). It is equal to 0.5 on the y-axis and 0.707 on the x-axis (the square root of 0.5).

At this stage of the simulation, it must be admitted, many correlations seem to confirm and validate the feeling that classical concepts look very satisfactory. Additionally, their application seems quite simple and elegant: once the plateau modulus

and the terminal time are known, one can easily determine the family of discrete relaxation times. Furthermore, the time-temperature superposition is inherently included from the definition of the relaxation times that all scale with ξo, the local friction, that varies with temperature according to a molecular weight independent WLF equation.

However, let's have a closer comparison with the data of Marin (M=110,000 T=140.9oC). These data correspond to τo=13.15 sec, as confirmed by a plot of G'/ω vs logω.

Fig.45 is plot of $(G'/G^*)^2$ vs G^*/G_{oN} for real data, to be compared with Fig.44. The differences are simply staggering. Unlike for the simulation in Fig. 44, the real data curvature changes in the middle of the data range, showing an inflection point; the maximum is 0.839 compared to 0.968; the value of G^*/ G_{oN} corresponding to the cross-over-point on the y-axis, i.e. corresponding to $(G'/G^*)^2=0.5$, is 0.35 for the real curve and 0.707 for the simulation, and the y-value corresponding to the x-axis cross-over (G*/GoN = 0.707) is 0.8289 for the real data, almost the value of the maximum, and 0.5 for the simulation. The definition of the cross-over, from a spectrum of relaxation point of view, no longer works.

The discrepancy is confirmed when comparing Figs. 46 and 47, which are plots according to Eq. (17), established on the basis that G' and G" are proportional to G_{oN}, which is the case for the Rouse expressions (Eq. [15']), but remains valid for the reptation model of Matsuoka,[33], Eqs. (20) and (21), and thus for the simulation data (Fig. 46). The simulation data show two lines, one with slope -1 passing through the low ω data ($\omega < \omega_o$), and another line, with slope −0.92, which starts to separate from the low ω data line when the influence of the p = 3, 5, 7 terms become significant ($\omega>\omega_o$). Notice the small sharp angle between these two lines. Let us now compare in Fig. 47 these features for real data. One can pass a straight line (with slope equal to −1) through the first few points at the left of the graph, corresponding to $\omega < \omega_o$. One could also pass another line, but with slope −0.82, not −0.92, through several points for $\omega > \omega_o$. Also noticeable for the real data the upturn departure from that line at high ω that does not follow the −0.82 straight line behavior. All these features are significant and will be

discussed in subsequent chapters (4, 5 and 6) of this presentation. They cannot simply be explained by the equations derived from the Rouse or the Doi-Edwards models.

In appearance, one might find "good" fit between data and simulation: Newtonian viscosity is found to be "slightly" different, 1 MPa-s instead of 2.63 MPa-s, (+163% difference), and the slope of G''/G_{oN} vs G'/G_{oN} on a log-log plot (as in Fig. 44 for the simulation) is 0.514 instead of 0.5. One could also argue that the value of τ_o and G_{oN} in the simulation could be fine-tuned to obtain a better fit. Indeed, regression analysis on $G'(\omega)$ and $G''(\omega)$, using an even or uneven weighted modulus series matching Eq.(20), with all unknown parameters to be determined by regression will be successful.

The purpose here is to suggest from these selected observations our strong reservations regarding the interpretations of rheological data with the use of a spectrum of discrete relaxation. In other words, the classical approach itself, that claims to understand the physics of the visco-elastic phenomena in polymer melts, through the search of the dependence of the relaxation times with physical variables, such as molecular weight or temperature, is, in our views, approximate, limited, and theoretically wrong. One might argue that so many other good scientists have checked the relationships carefully before, and that it must only be coincidental that claims of failure would be advanced.

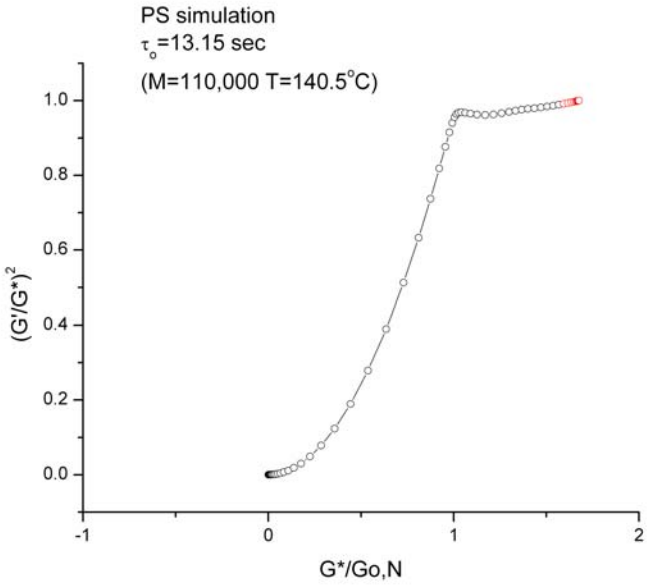

Fig. 44.

This plot of the simulated variables predicts that the crossover point (corresponding to G' = G"), that is (G_/G∗)^2 = 0.5, occurs for (G∗/G0N) = 0.707 and that the plateau modulus G0N is reached for (G'/G∗)2 = 1

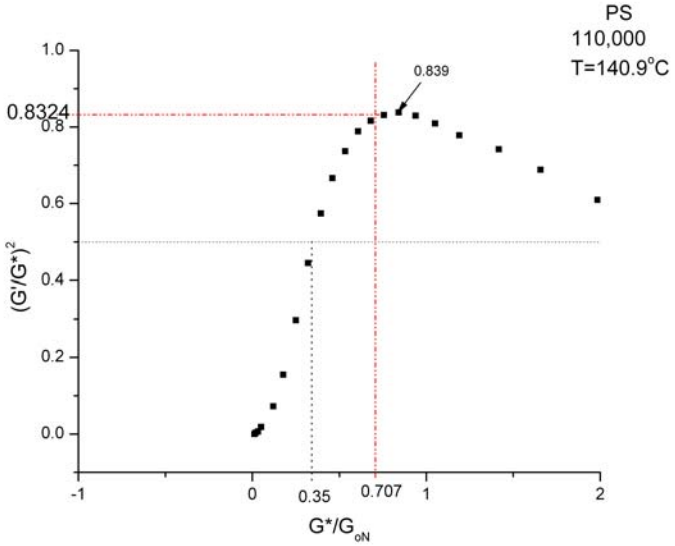

Fig. 45.

Same plot as Fig. 44 for the data of Marin and Graessley. The crossover point calculated from (G'/G∗)2 = 0.5 corresponds to G∗/GoN = 0.35 (half the value of the simulation) and for G∗/GoN = 0.707, (G_/G∗)2 reaches a maximum.

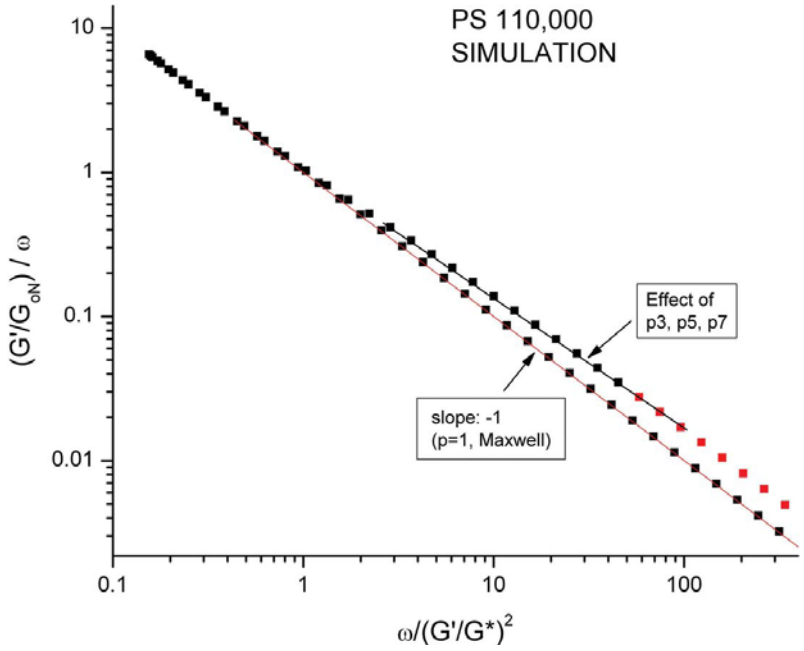

Fig. 46.

The lower straight line has slope −1 and intercept 0, according to Eq. (17). The validity for the simulated data is due to the assumption that G' and G" are still proportional to G_{oN} for the reptation model.

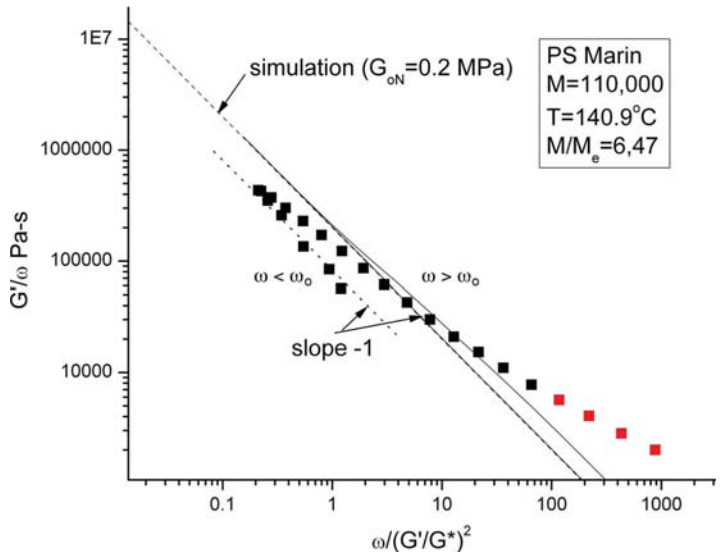

Fig. 47.

Variables are chosen to conform to Eq. (17). The simulated data correspond to the dotted line with slope −1 on this log-log scale. The sharp turn between slope −1 and −0.82 corresponds to ω_o. For $\omega < \omega_o$, the data line up on a straight line with slope −1, but with an intercept giving a lower value for G_{oN}.

In summary, the Rouse model is an application of Maxwell's statistics to beads and springs connected together, each bead having a friction force exerted on it created by the presence of the neighbors. The main idea behind the Rouse model is, in fact, the definition of the local friction coefficient ξo. Otherwise, this model is nothing more than a cartoon representation of a set of springs and dashpots, and the Rouse's relaxation time nothing less than the ratio of the viscosity of the dashpot by the modulus of the spring. This model assumes that chains are Gaussian, deformation is affine, and there are no excluded volume, in the Flory's sense, i.e. no perturbation to the local conformation of the bead-springs due to the presence of adjacent chains. It is rather intriguing, to say the least, to see such an enthusiasm for such a simplistic and crude model. The irony is that the popularity comes from the hidden foundation that the model is nothing more than a Maxwell spring and dashpot network, so popular by its own merits in the 60s and 70s. However, one realized immediately, then, the limitations of a network of dashpots and springs: it was clear to everyone that it had nothing to do with a real polymer systems of intra and inter molecular interactions. One might argue that Rouse's model introduced the motion of a *family* of relaxation times, which restricted the number of constants needed to define the network to the definition of the terminal time. True. But this simplification also amplified the error found when fitting equations to real data. Checking the success claimed by others [35] to the applicability of the Rouse's model to the dynamics of $M < Mc$ data, it is surprising how bad the fits actually work out to be, with residuals severely curved, and fitting r2 criteria hardly passing the 0.96 mark.

The Doi-Edwards-de Gennes model also assumes Gaussian chain, affine deformation and the existence of a family of discrete relaxation times generated by the terminal time. All these assumptions are severe limitations to the domain of applicability of the model, but, in the end, the apparent success comes from the fact that the melt behaves, within the restricted range, like a network of spring and dashpots, whose relaxation times have been forced to comply with the molecular weight 3.4 variation.

Yet again, upon checking the validity of the results, we are facing mediocre performance, and unsatisfactory projections and extrapolations.

The Myths of rheology start with the belief that linear visco-elasticity is well understood and under full control. We suggest otherwise.

H Conclusions (Chapter 3)

Let's summarize the great Myths of rheology. as reviewed in this chapter 3:

- In the expression of viscosity, the effect of temperature and molecular weight do not separate, whether M < Mc or M> Mc.
- The 3.4 exponent is not strictly temperature dependent, it increases as T decreases.
- For M < Mc, viscosity is not proportional to M, disproving the Rouse's model even for these low molecular weight fractions. Working at (T-Tg) constant seems to work within a restricted zone of temperature (T> Tg $+30^{o}C$).
- The WLF equation is just an hyperbolic curvefitting function. Expressing viscosity as a function of (T-Tg) does not make it molecular weight independent. There is not universality of the WLF constants for monodispersed PS fractions or well characterized linear grades of PC.
- The time-temperature superposition principle is not valid on the temperature range claimed by its present users. One requires at least two WLF equations to cover the range $Tg+100^{o}C$, and another Arrhenius fit beyong ~ 1.2 Tg. This diversity of response does not seem to receive an easy explanation from existing molecular dynamic models.
- There is a transition above Tg, as claimed by Boyer, called T_{ll} by Boyer. A careful analysis of data, when those same data do not show any transition according to the classical tools of analysis, reveals the existence of this transition-relaxation. "Thermal-thinning" occurs when crossing the T_{ll} transition, going downward: Newtonian viscosity is less

compared to extrapolations made from using data above T_{ll}.

- There is another time-temperature failure transition at higher frequency or lower temperature (around Tg+30oC or its frequency equivalent), corresponding to a different mode of melt deformation, where enthalpic forces interplay with entropic ones (see part II). Beyond this transition (corresponding to a maximum of $\cos^2\theta$, i.e. a minimum of $\tan\theta$), the time-temperature superposition applies with different shift factors than for the temperature on the other side (the melt side) of this transition.
- The time-temperature is only an approximation, a convenient tool for engineers. It should not be the foundation of existing theoretical interpretations of melt deformation. In fact, theoretical models should explain why it is only an approximation and correctly describe the true behavior.
- Rheology data in the literature should be presented in their "raw" state, without shifting, because the shifted data are probably wrong, providing the wrong experimental facts to theorists.
- The "molecular dynamic" description of visco-elastic data in terms of a family of discrete relaxations generated by a terminal time that varies with a local friction coefficient (thus providing the temperature dependence), and with topology (to explain the M or $M^{3.4}$ dependence) is an elegant and simple mathematical tool to compare the effect of structural and chemical parameters on melt properties, but, as we suggest, too simplistic to have any value in terms of the physics of deformation of a set of long chains.
- The Rouse's or reptation models (de Gennes, Doi-Edwards), based on a such spectrum of relaxation, are probably not describing <u>at all</u> the basic deformation process giving rise to visco-elastic effects, shear-thinning, normal stresses, extensional flow and the numerous other phenomena observed in non-linear deformation, at very high shear rate, at high amplitude of strain, causing melt yielding, melt fracture and astonishing memory effects. The models' shortcoming is probably deeply rooted in

the misunderstanding of the concept of chain entanglement , and of the entropy of the melt deformation process. Part II of this review intends to bring some light towards a new understanding of these concepts.

-

I REFERENCES (CHAPTER 3)

[1] W.W. Graessley, Advances in Polymer Science, Vol. 16, "*The Entanglement Concept in Polymer Rheology*", Springer (1974).

[1a] J.M. McKelvey, "Polymer Processing", John Wiley, New York (1962), Ch. 2, p. 32, Table 2-4.

[2] G.C. Berry and T.G. Fox, Adv. Polymer. Sci., 5, 261 (1968).

[3] F. Bueche et Al, J. Chem. Phys., 20, 1956 (1952).

[4] P.G. de Gennes, J.Chem. Phys., 55, 572 (1971).

[5] S.F. Edwards, J.W.V. Grant, J. Phys. A: Math.Nuclear.Gen, 6, 1169 (1973).

[6] M. Doi and S.F. Edwards, "*The Theory of Polymer Dynamics*", Oxford Univ. Press, Oxford, UK (1986)

[7] S. Onogi et Al, Kolloid-Z, Z Polymere, 222, 110 (1968).

[8] J.D. Ferry et Al, J. Phys. Chem., 67, 2297 (1963).

[9] P. G. de Gennes, *Scaling Concept in Polymer Physics*; Cornell University, Ithaca and London (1979).

[10] C.A. Hieber and H.H. Chiang, Rheologica Acta, 28, 231 (1989).

[11] M.M. Cross, Rheologica Acta, 18, 609 (1979).

[12] P.J. Carreau, Ph-D Thesis, University of Wisconsin (1968).

[13] G.V. Vinogradov and A.Y. Malkin, J. Polym. Sci., A-2, 4,135 (1965).

[14] W.P. Cox and E.H. Merz, J.Polym.Sci., 28, 619 (1958).

[15] L.A. Utracki, Polym.Eng.Sci., 23 (8), 446 (1983).

[16] J.D. Ferry, "*Viscoelastic Properties of Polymers*", J. Wiley (1970), Ch. 11, 13.

[17] W. Pfandl, G. Link, and F.R. Schwartzl, Rheol. Acta, 23, 277 (1984).

[18] C.A. Hieber and H.H. Chiang, Polym.Eng.Sci., 32, 931 (1992).

[19] B. Rabinowitsch, Z. Physik-Chemie, A145, 1(1929).

[20] E.B. Bagley, J. Appl. Phys., 28, 624 (1957).

[21] T. Alfrey, JR, in "*Mechanical Behavior of High Polymers*", Interscience Publishers, Inc, John Wiley, New York (1965).

[22] A.I. Leonov, Rheol. Acta, 15, 85 (1976).

[23] S. Havriliak and S. Negami, Polymer 8, 161 (1967).

[24] J.F. Pierson, Ph-D Thesis, CRM Strasbourg (1968). Numero d'ordre at Centre Documentation CNRS, Rue Boyer, Paris: AO 2106.

[25] R. Susuki, Ph-D Thesis, CRM Strasbourg (1970). Numero d'ordre at Centre Documentation CNRS, Rue Boyer, Paris: T 32307.

[26] J. P. Ibar, J. Macromol. Sci. Phys., B19 (2), 269 (1981): *Non-Newtonian Flow Behavior of Amorphous Polymers in the T > Tg Temperature Range: A New Analysis of the Data According to the "Double-Shift" Procedure*.

[27] Non linear regression routine is based on the Lenvenberg-Merquardt algorithm described in "*Numerical Recipes in C*", Press, Flennery, Teukolsdy and Vetterling, Cambridge University Press (1988)

[28] The Chi Square expression which is minimized during the routine is:

$$\chi^2 = \Sigma (Y_i - f(X_i))^2 \ / \ \sigma^2$$

where σ is the standard deviation.

[29] L.E. Nielsen, Polym. Eng. Sci,17, 713(1977). The general consensus in the polymer scientist community is that T_{ll} only existed in the imagination of R.F Boyer. A good review of the debate can be found in: R.F. Boyer's: "*Computational Modeling of Polymers*", J. Bicerano, Ed., Marcel Dekker, New York, pp 1-52 (1992).

[30] R.F. Boyer,"*Encyclopedia of Polymer Science and Technology", Vol.* 13, p.278, Wiley, New York (1970).

[31] H.H. Chiang, C.A. Hieber, and K.K. Wang, Part I and Part II, Polym.Eng.Sci., 31, 116 & 125 (1991).

[32] The molecular weight distribution for the two linear PC is Mw=16,300 for Grade 1 and 23,000 for Grade 2 (polydispersity 2.2 for both grades).

[32bis] P.E. Rouse Jr, J. Chem. Phys.,21,1272 (1953).

[33] S. Matsuoka, "*Relaxation Phenomena in Polymers*", Hanser (1992), p. 176. Also see the graph at p. 177.

[34] G. Marin and W.W. Graessley, Rheol. Acta, 16, 527 (1977).

[35] J-C Majeste, Ph-D thesis, Pau University, France (1998). Majeste quotes M < Mc Susuki's results (p.24) to be with an exponent of 1.49. His own results show an exponent of 1.25 (p. 69).

[36] A. Benallal, Ph-D thesis, Pau University, France (1991).

Chapter 4

THE GREAT MYTHS OF POLYMER RHEOLOGY, PART 2: TRANSIENT AND STEADY STATE. THE QUESTION OF MELT ENTANGLEMENT STABILITY.

A INTRODUCTION

Transient and Steady State Behavior.

The deformation of polymers melts has received considerable attention ever since macromolecules were identified by Staudinger [1] as being responsible for their behavior. The field of physics that concerns the deformation of liquids under stress is called rheology, and, in part I of this series [2], we presented the continuing challenges facing the rheology of polymers due to the complexity of the interaction between the macromolecules. One of the most difficult problems to solve is to predict the deformation of the melt during its "transient" conditions, i.e. before it reaches its steady state deformation. Most of our present understanding concerns the steady state when properties, such as viscosity or modulus, no longer depend on time and remain invariant. Understandably, transient states and steady states both result from the deformation of the macromolecules and to their interactions, but is it the same mechanism involved in both? Analytical solutions have been sought to express the fact that steady states derive from the transient states, at long time. In essence, when all transient relaxation has taken place, then the steady state solution is apparent and can be analytically described. Early models to qualitatively represent transient and steady state behavior were given by the Voigt or Maxwell models [3], often sophistically combined to be more realistic [4], and consist of deformed sets of springs and dashpots put in parallel or in series, or a combination of the two.

More recent non-linear models are described in textbooks; in particular, Table 4.4.2 of Macosko's book [5] compares the successes and shortcomings of popular constitutive equations that describe transient and steady state flow behavior. The author concludes "No single nonlinear constitutive equation is best for all purposes, and thus one's choice of an appropriate constitutive equation must be guided by the problem at hand, the accuracy by which one wishes to solve the problem, and the effort one is willing to expend to solve it". For an intuitive, first approach to the problem solution, a simple Maxwell element remains an excellent tool: for instance, in the case of a step strain experiment, the sudden deformation results in the "instantaneous" deformation of the spring, without any motion of the dashpot, so a stress is created, which is proportional to the strain, followed by a slow release of the stress in the spring as the dashpot expands at a rate that produces strain. When the dashpot has released, by its motion, all the strain that was initially produced by the deformation of the spring, the stress has relaxed to zero. The differential equation of motion of a Maxwell's element is straightforward and provides the solution for the time dependence of the stress, and of the individual strains in the spring and dashpot that add up to the imposed strain. In a step strain experiment, the strain rate is very high at start up, then is zero. The transient state is simply the description of the time dependence of the relaxation process, and the steady state value is zero. For polymers, the behavior is more complex than that described by mechanical equivalents, such as dashpots and springs; nevertheless, it is assumed that, as the melt is deformed "instantaneously", its modulus is raised to that of the glassy state and relaxes through the various regions representing the transition region, the rubber elastic plateau region and the terminal region. This relaxation takes place very fast above the glass transition temperature since the macromolecules, or parts of them, can rearrange their position at rates between 1 sec

at T_g to 10^{-5} sec 100 degrees above T_g, this time being dependent on molecular weight and temperature. Many of the sophisticated mathematical models of non-linear viscoelasticity described in Mascosko's textbook [5] are modifications of the differential equation of the Maxwell type, to account for a different stress tensor build up and/or a modified stress tensor relaxation rate. However, the physics behind the mathematics of the modifications, in terms of macromolecular deformation, becomes far less intuitive, and non-conclusive.

Step Strain Experiment in the non-linear region.

Figure 1 gives an example of step strain response for a PC melt sheared 55 ^{o}C above its T_g (137 ^{o}C) at a strain of 30%. The molecular characteristics of this PC were already described in Part I [2], the PC being labeled as Grade 1. The instrument to perform such a "stress relaxation" experiment was a classical equipment of rheology, a Rheometrics RDA-700 in this instance, utilizing a parallel plate geometry with a 2mm thick sample, 2.5 cm in diameter.

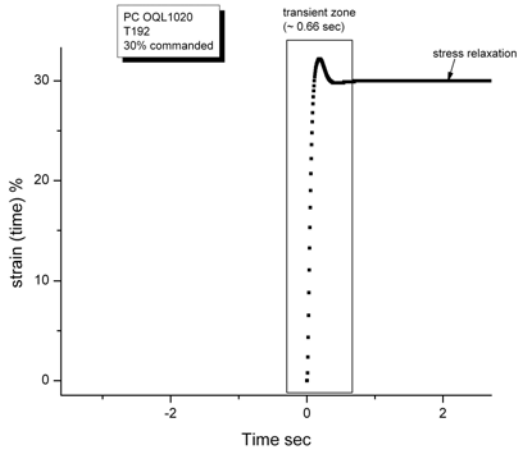

Fig. 1a

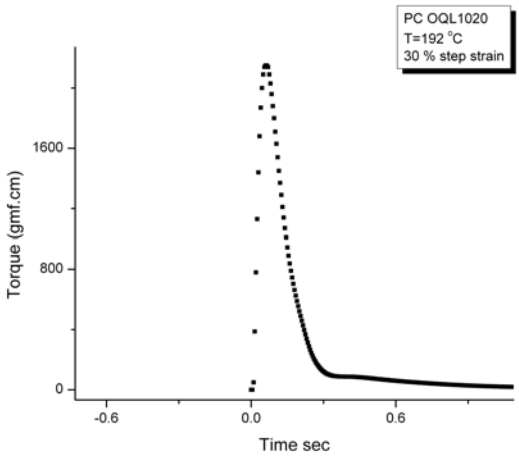

Fig. 1b

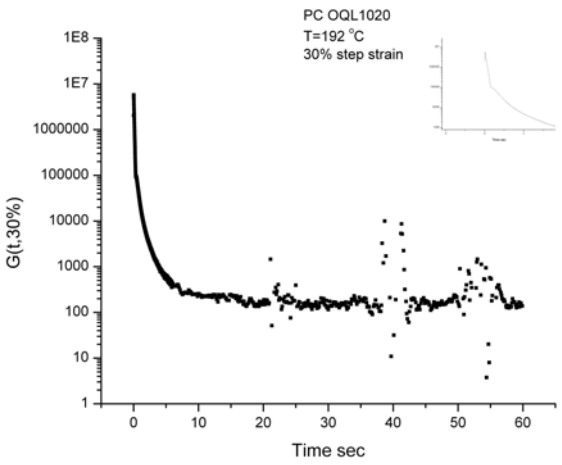

Fig. 1c

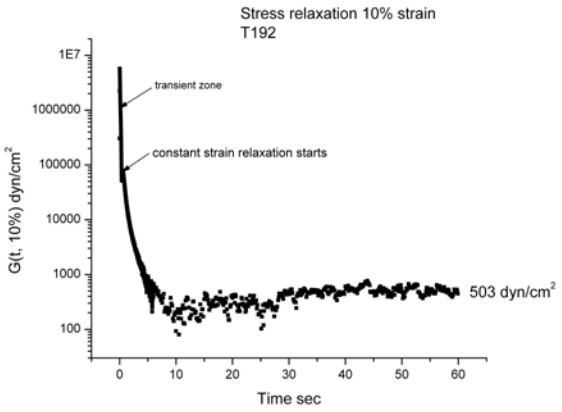

Fig. 1d

Fig. 1

Stress relaxation (G(t) vs time) at constant temperature (T=192 ^{o}C) and constant strain % (Figs. 1a, 1b, 1c: 30%, Fig. 1d: 10%) for PC-1.

Fig. 1a shows the strain plotted against time at start up. The step strain is not instantaneous, as one might have imagined, there is even a small overshoot followed by an even smaller undershoot, but the strain stabilizes to the commanded strain, 30%, in less than 0.66 sec. The strain rate, derivative of the strain, reaches a maximum (Figure not shown) of 4.55 sec^{-1} at time 30.22 ms, i.e. for a strain of 8.83%. The corresponding torque response is shown in Fig. 1b, which indicates that the stress build-up did not go as far as reaching the glassy region, far from it. The Torque reaches its maximum at time 62.5 ms, and the stress at the maximum corresponds to a modulus equal to only ~4% of G_{oN}, the plateau modulus for PC (1.5 MPa at 150 ^{o}C [6]). Most of the relaxation of the Torque takes place in the transient region and is very fast at this temperature of 192 ^{o}C. More than 95% of the build up Torque (at the maximum) has relaxed when the strain has stabilized to 30%, and only 5% is left to relax. Fig. 1c is a plot of G(t, 30%) vs Time, including the transient portion at the beginning (the insert graph zooms in on that zone). The shear modulus reaches an apparent steady value of 162 dyn/cm^2 (16.2 Pa)

which is stable for at least the 60 seconds of total recording. The relaxation at constant strain can best be fitted with two relaxation times, one 0.38 sec, the other 1.4 sec. (Note, in passing, that the apparent "plateau" observed for the modulus is also visible at other lower temperatures, at other strains (see next paragraph), but ceases to exist at temperatures above T= 200 ^{o}C.).

In summary, at this low temperature, the transient relaxation is phased-in with the relaxation of the stress: it follows the establishment of the commanded strain, and the value of the relaxation time is in line with what is calculated from dynamic viscosity measurements. Fig. 1d shows G(t, 10%) for the same PC, at the same temperature, just a different step strain value. The transient characteristics are different: the maximum strain rate is 1.31 sec^{-1}, it occurs at 37.2 ms, when the strain is 3.16%; the Torque reaches its maximum at 74.45 ms, the Torque max is 1/3 of that obtained for 30% strain. The apparent steady shear modulus is also different: 503 dyn/cm^2 (50.3 Pa), more than 3 times greater than that at 30%. The relaxation times in the constant strain region are 0.38 sec (same value as for 30%) and 1.28 sec. This example illustrates the kind of questions addressed in this paper: can different transient relaxation history induce different steady state values? Are strain and strain rate playing a similar or separate role in setting up transient mechanisms prior to the steady state melt? For instance, shear rate is known to shear-thin viscosity; comparing modulus under increasing strain is also known to reduce its value, not just in the example given in Figs 1c and d, but in general. The modulus in the non-linear visco-elastic region., G(t, γ), can be separated [Ref. 5, p. 160] into a time dependent term (given by linear viscoelasticity) and a strain dependent term, defining the damping function, h(γ) . In other words, shear strain also "shear-thins" the melt; the phenomenon is called "strain softening. Can we combine the shear-thinning effect of strain rate and strain softening in the non-linear regime to boost shear-thinning? This concept is at the origin of a treatment process of polymer melts described later in this introduction, but first let us study the effect of strain rate in high strain rate conditions.

Step Strain Rate Experiments under non-linear conditions.

In the more complex case of a constant strain rate imposed, for instance in a pure rotational viscometry experiment with the system being instantaneously deformed from a zero rate to a constant strain rate, the transient behavior corresponds to the build up of the stress at

initiation followed by the time it takes for the stress to relax to a constant value, which, when divided by the strain rate, becomes the steady state viscosity. Figure 2 gives an example of a step strain-rate experiment for a metallocene LLDPE melt (the Mw characteristics of which are given later), submitted to a viscosity measurement in a parallel plate viscometer at T= 190 ^{o}C with strain rate = 1 sec^{-1}. Figure 2a displays viscosity vs time, and Fig. 2b displays normal force vs time, the normal force being measured perpendicular to the direction of the flow by a sensitive probe positioned on the melt.

One sees, in the case of polyethylene in Fig. 2, that it takes a considerable length of time for the viscosity to reach a steady state value, if it ever does, (since its magnitude appears to be very low, almost 0, at this temperature), and one might wonder if this time is accounted for by the traditional explanation of relaxation times provided by classical rheology, in particular by the value of its terminal time, τ_o, calculated from the steady state viscosity at that temperature, or from the cross-over of G' and G" ($\tau_o = 1/\omega_x$). What could explain a transient time of over 30 minutes for a polyolefin without long branches? The cross-over frequency is 87 rad/s at that temperature (see later), which is 255 ^{o} above the T_g of PE, 153 ^{o}C above the melting temperature (37 ^{o}C) for this metallocene copolymer. There is no doubt that the melt should behave like a typical amorphous melt, subjected to the laws of rheology. M/ M_e is between 200 and 300 for this polymer (the uncertainty is due to the poor determination of M_e , the molecular weight between entanglements for PE, and the fact that it is a copolymer), so the entanglement density is fairly high. Nevertheless, the transient relaxation time (~600 sec) seems to be 43,500 times bigger than the terminal time (0.0115 sec), determined from the cross-over in the steady state regime. Since processing times in extrusion and injection molding machines and the like are of the order of seconds, perhaps a couple of hundreds of seconds in extrusion, it appears that the high viscosity encountered in processing plastic melts is due to transient flow. Needless to say, a great practical advantage would result if one could understand the transient regime and reduce it to non-existent, for instance by decreasing its relaxation time significantly; in the example of Fig. 2 say from 600 sec to 5 sec or so.

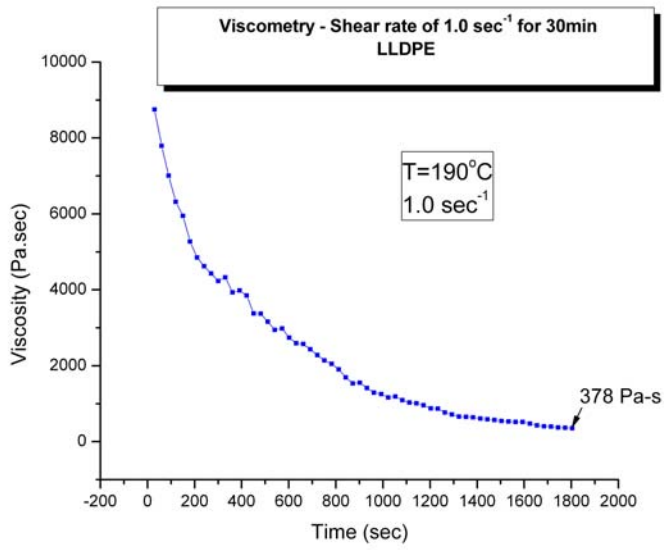

Fig. 2a

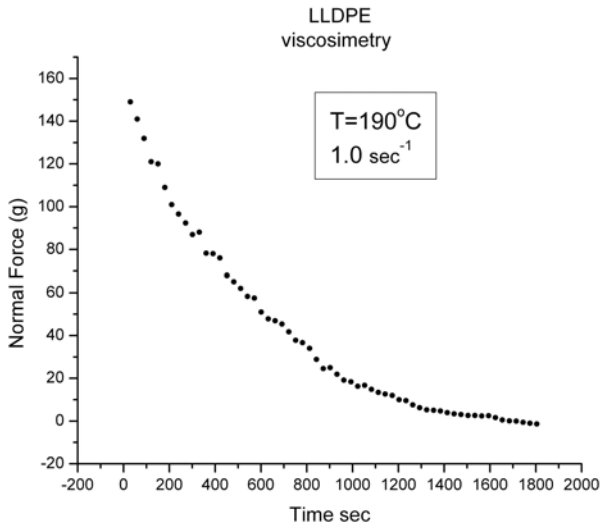

Fig. 2b

Fig. 2

Pure Viscometry test at constant strain rate 1 sec^{-1} for LLDPE at T=190°C. Fig. 2a: Viscosity vs time; Fig 2b: Normal Force vs time.

According to S.Q. Wang [7] who has recently carefully analyzed, with the special technique of particle velocity tracking (PVT), the behavior of melts during and after transients:

> *"an effective particle tracking velocimetric (PTV) method was developed to allow determination of the velocity profile across the gap in various shear*

apparatuses including cone-plate and linear sliding-plate set-ups for startup shear, large amplitude oscillatory shear (LAOS) and step strain experiments. Our PTV observations show an initial linear velocity variation across the gap and a nonlinear velocity profile beyond the stress overshoot [Phys. Rev. Lett. 2006,96,016001], growth of shear banding in LAOS [Phys. Rev. Lett. 2006, 97, 196001] and elastic breakup of several entangled solutions after step strain [Phys. Rev. Lett. 2006, 97, 187801]. These results present great challenges to both the prevailing theoretical description of entangled polymer flow that is based on tube models and the conventional rheometric protocols used to experimentally determine constitutive flow behavior."

Wang asserts that the inhomogeneous deformation is caused by "catastrophic disentanglement" occurring in the bulk of the polymer melt, not just at the surface. Wang [7-10] shows that the stress overshoot, widely observed in startup shear, has been wrongly explained by the accepted reptation models [8], since it assumes that the melt remains homogeneous across the stress maximum, a situation that his PTV measurements revealed to be false. A critical strain rate and strain are proposed by Wang [8-10] for the onset of the velocity profile breakup. The critical strain rate is the inverse of the "Rouse time" that Wang determines from the terminal time (obtained at the cross-over of G' and G") and (M_e/M): $\tau_R = \tau_o$ (M_e/M). In addition, strain must be equal to at least 5/4 to trigger macroscopic motions across the gap leading to inhomogeneous flow. For the polymer conditions of Fig. 2, the critical rate equals either 17,400 sec^{-1} or 26,100 sec^{-1}, depending on the value chosen for M_e (700 or 1000 for PE). In any case, the chosen strain rate of 1 sec^{-1} in Fig. 2 is much inferior to this critical value, so we do not expect inhomogeneous flow in our experiment. The reason why both viscosity and normal force appear to relax to zero (viscosity is 378 Pa-s in Fig.2a after 1800 sec, but still decreasing) must be explained by a different mechanism. As time increases, the rheometer continuously rotates the melt, and strain increases. It takes 125 sec to reach 125 % strain, another critical level that Wang claims corresponds to disentanglement in the melt [7-10], but the strain rate is far too low to meet both disentanglement criteria of Wang. The curves of Figs 2a and b can be fitted with two exponential terms, with the same relaxation times of 55 sec and 591 sec for both curves (assuming a steady state value of zero when the fit is done). The fast relaxation process (the 55 sec one) might be associated with the relaxation of the elastic energy pumped into the cohesive network of bonds by the initiation of the step strain rate jump, the second term (the 591 sec one) might be considered as a steady state of the first term that has become unstable and decays exponentially, perhaps as related to the kinetics of

disentanglement. If it is the case, in particular if M_e has increased due to disentanglement, the melt at the end of the 1800 sec must have rheological characteristics very different from the initial melt, before the transient relaxation took place. Hence a frequency sweep of the un-sheared melt and of the "sheared melt" should display large differences in G' (ω) and G" (ω) and in the value of the terminal time. We will study such results in this paper.

Strain Induced Transients under Oscillatory Shear.

Figures 3a and b concern a PS melt studied with a dynamic rheometer (AR 2000, TA Instruments) in the time-sweep mode. The temperature is 165 ^oC (65 ^{o} above the T_g of PS), the frequency is 20 Hz (125 rad/s), and the strain % varies from 5% to 23%, the strain being increased at the end of a time-sweep step to take the next successive value indicated in Fig. 3a. Fig. 3b provides the variation of G' and G" for the last step, corresponding to 23% of strain. It is apparent in Fig. 3a that a time dependent (transient) behavior is triggered by the increase of strain during time-sweep. For 5% and 10% strain, the viscosity is constant, but starting at 15.2% in Fig. 3a, viscosity starts to decay. The magnitude of the effect increases with strain, its kinetics does too. What transient relaxation does this time dependence of G' and G" describe? Could it be caused by "edge melt fracture"[60,61]? This question is discussed in a section below. Could it be related to the same disentanglement process, described for LLDPE in Fig. 2, triggered by a combination of strain rate and strain as suggested by Wang? The value of ω_x at T=165 ^oC for this PS melt is 0.1 rad/s, $M_w/ M_e = 19$, so the Wang's critical strain rate would be 1.9 sec^{-1} at this temperature. In a dynamic (sinusoidal strain) experiment, the maximum strain rate depends on both frequency and strain, it is equal to $\gamma\omega$, where γ is the strain, here 0.152 at the onset of viscosity transient behavior :(20 Hz * 6.28*0.152)= 19 sec^{-1}. This value is 10 times greater than the Wang's strain rate criteria. In Fig. 3, however, the strain is not 100%, but only 23% at maximum. This misses the strain criteria by Wang to produce inhomogeneous flow [7-10]. This paper addresses the following questions: is the transient decay observed in Figs. 3a and 3 of the same origin as what is observed in Fig. 2? Does it converge to a steady state? Is this steady state stable, and can it be destabilized trough a disentanglement process? Do we need different criteria to explain the transient states obtained in pure dynamic mode and in pure rotation mode?

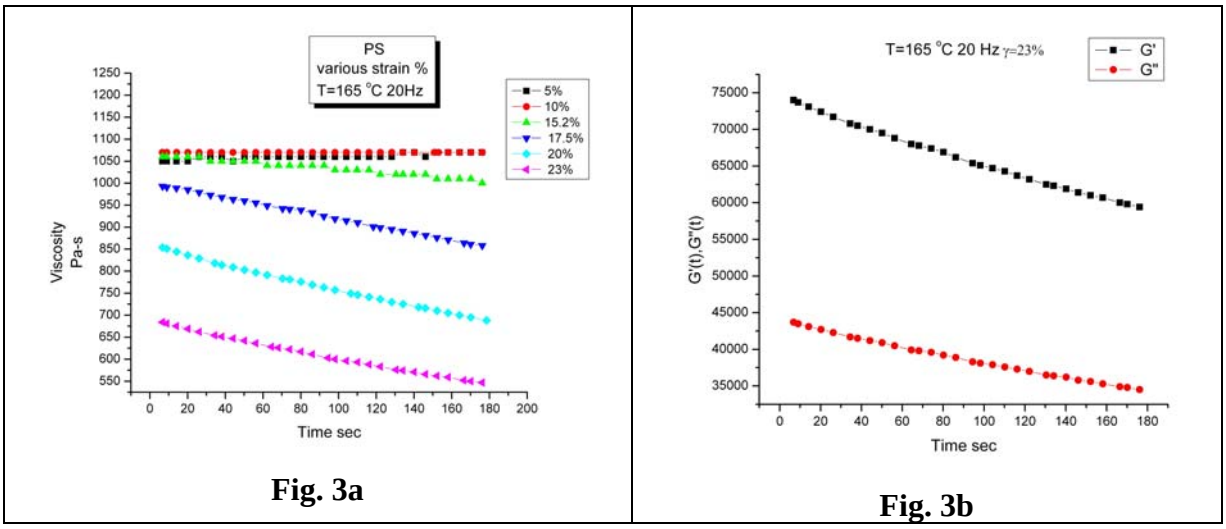

Fig. 3a **Fig. 3b**

Fig. 3

Time sweeps for PS-2 at 20 Hz T=165 °C. Fig 3a: effect of strain% on the dynamic Viscosity vs time; Fig. 3b: G' & G" vs time for 23% strain.

Combining Rotation and Oscillation Shear Modes.

The work of Osaki et al.

The combination of pure shear and dynamic shear in a rheometer, to determine how the superposed constant strain rate affects the value of G'(ω) and G"(ω), is not new and has been well described in the work of Osaki et al. for PS/ toluene concentrated solutions of different molecular weights to cover different regions of the relaxation spectrum [11]. These concentrated solutions behave like entangled melts that can be studied at or near room temperature. The authors use a Couette configuration with the outer cylinder submitted to independently-controlled superposed rotation and oscillation. The inner cylinder is concentrically suspended in the outer cylinder by a wire of known torsional stiffness. The gap is constant and equal to 1mm. The oscillation is performed at small amplitude to remain in the linear range and avoid disrupting the melt. Osaki's use of the oscillation is to reveal the state of the melt (via G'(ω) and G"(ω), converted into a spectrum of relaxation times) when it is deformed under constant strain rate steady state conditions . This objective is different from the use of oscillation to induce transient effects by strain increase (Fig. 3), and from the

combination of rotation and oscillation in the non-linear range, as described in the next section, to produce non-linear transients susceptible to altering the entanglement network. Osaki et al's objective was to prove that "the non-Newtonian effect in the steady shear viscosity may be explained as a result of a decrease in degree of entanglement with increasing rate of shear… Measurements of the complex modulus provide important information on the nature of segmental coupling". In other words, these authors suggest that shear-thinning is due to disentanglement. Figure 4 is taken from Osaki's paper [11], providing the G' and G" for a PS solution at 15% concentration of PS in toluene at 30 ^{o}C.

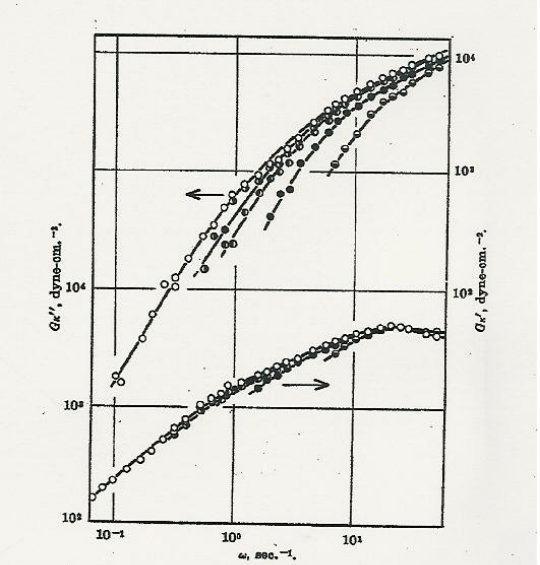

Figure 4. Real and imaginary parts of complex modulus in shear, $G\kappa'$ and $G\kappa''$, plotted against angular frequency, ω, for 15% solution of polystyrene B in toluene at 30°. Superimposed rate of shear in sec.$^{-1}$: ○, 0; ◑, 0.162; ◐, 0.505; ●, 1.62; ⊖, 5.13.

Fig. 4
(from Osaki et al [11]

The M_v of the PS in the concentrated solution is 2.51 10^6, and, at this concentration, M_c is 3 10^5, according to Osaki, so (M/M_c) is 8.33 , which corresponds to $M/M_e \sim 17$. The superimposed strain rate varies from 0 (purely dynamic frequency sweep) to 5.13 sec^{-1}. Fig. 4 demonstrates clearly the net reduction of G'(ω) and G"(ω) with the value of the superposed constant strain rate, giving the qualitative aspect that the melt behaves as if its molecular weight had been reduced, or, alternatively, since the molecular weight remained constant, as if its (M/M_e) ratio had been decreased by the increase of M_e, i.e. by disentanglement. Osaki

concludes “In a sense, the effect of the rate of shear resembles the effect of molecular weight depression as exemplified by the sharp cut of the long time end of the relaxation spectrum” In other words, these authors conclude that the terminal time τ_o is reduced by the shear rate: “The results are such that the relaxation spectrum H(Lnτ) as a function of logarithmic relaxation time is markedly cut off at the long time end and is heightened in the plateau region of shorter time scales” [11]. By extrapolation, a very strong strain rate would narrow the relaxation spectrum box to a single relaxation time: moving the melt faster would simplify its viscoelastic response.

Effect of combining rotation and oscillation in the non-linear regime: Shear-Refinement under Dynamic Conditions.

It appears conceivable that strain rates from pure rotation and oscillation deformations add up, increasing the amount of shear-thinning available for pseudo-plastic melts. Furthermore, one can foresee, from the work presented in Figs 2 to 4, that the combination of pure and oscillatory shear create both new transient and new steady states capable of altering the cohesion of the network of bonds that interact, and thus the entanglement density. Figures 5a and b reproduce the schematic of equipment capable of achieving the combination of rotation and oscillation that we have described previously [12-14]. This equipment is used to shear or pre-shear polymer melts under a combination of pure rotational shear (at given strain rate, governed by the RPM of the rotor) and dynamic shear (at given frequency and strain, controlled separately); details of the mode of operation can be found in references [12-16]. Several samples analyzed in this paper were produced by this method. It was claimed that experiments conducted by this set-up produced pellets that were totally unique in terms of viscoelastic properties, and challenging to the existing theories of melt deformation. A large section of this chapter is dedicated to presenting the controversial findings. In particular, disks ready for dynamic analysis were pressed from “treated” pellets, produced by the apparatus of Figs 5a and b, and analyzed in the linear viscoelastic region. The results, presented below, are not merely difficult to understand within the currently accepted framework of melt theory, but, in our opinion, impossible to understand within that context. Figure 5a describes the elements

composing one “shear refinement station”, and Fig. 5b shows the set-up for two stations put head to tail, each station being operated with its own set of specific parameters (temperature, pressure, gap, RPM of rotor, frequency and strain of the oscillation). The single station of Fig. 5a is connected (220) to a melt feeder section (an extruder) , and its exit melt (270) can either go through a strand die (with a pelletizing unit attached), or it can be pumped into the second shear-refinement station for further treatment before its exit to the pelletizing unit or a capillary rheometer positioned at the end of the second station.

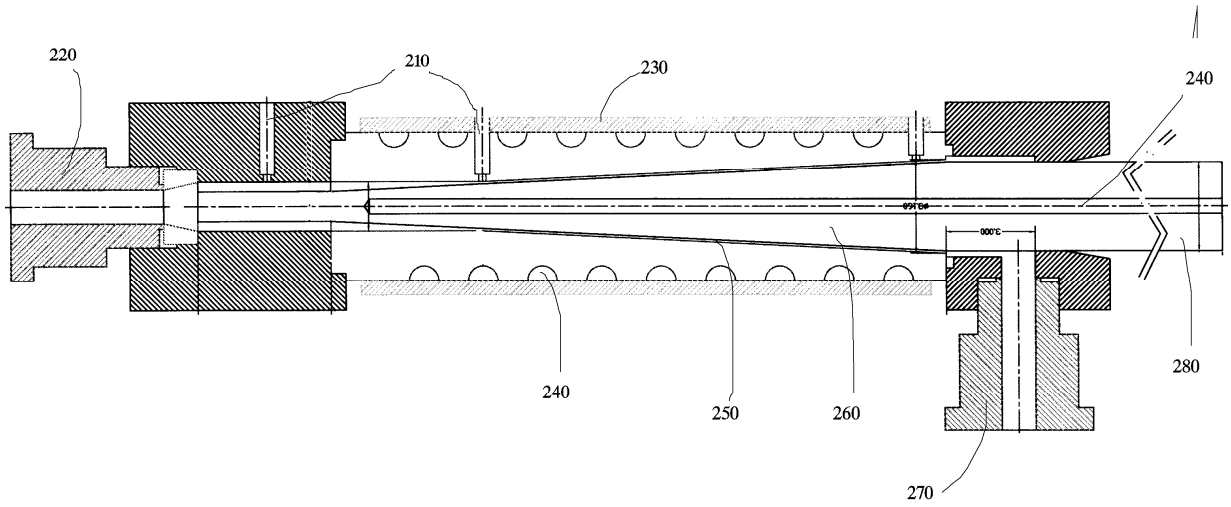

Fig. 5a

Apparatus described in Refs. 12-14 to submit a polymer melt to a combination of shear-flow and extensional flow. The shear-flow can be the superposition of a steady rotational component and a vibration component. This Fig. 5a provides the details for one treatment station. Fig. 5b below shows the combination of two treatment stations. See text.

Thermal Mechanical History is created by flowing through various PROCESS STATIONS, each combining **pressure flow** with **cross-shear flow** induced by **ROTATION** and **OSCILLATION** of the Couette's inner cylinder.

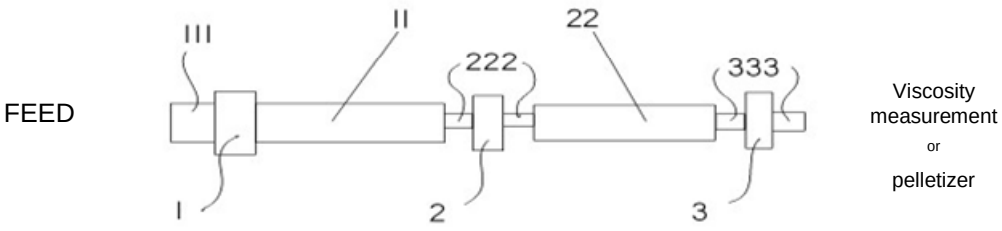

Fig. I

In each station, one can vary T, RPM, frequency, strain amplitude

Fig. 5b

Apparatus described in Refs. 12-14 to submit a polymer melt to a combination of shear-flow and extensional flow. The shear-flow can be the superposition of a steady rotational component and a vibration component. This Fig. 5b shows the combination of two treatment stations. See text.

A single treatment station (Fig. 5a) is essentially a Couette apparatus, with the rotor (260) capable of oscillation on top of rotation. An extruder, connected at (220), feeds the melt into the gap cavity (250). A motor assembly (not shown) rotates and oscillates the central shaft (280) connected to the treatment zone (cone area). In order to make the gap variable at will between 0.1 and 3 mm (as well as for other reasons [15]), the rotor is shaped as a cone, and the stator (230) designed so that the internal surface remains parallel to the rotor's surface, maintaining the gap constant. The melt temperature is measured by a probe touching the melt (210) and controlled despite of shear heating by the circulation of a cooling fluid through specifically designed channels (240). The extruder can be operated to just feed the "treatment zone" and stop, or it can be operated to extrude continuously, submitting the treated melt to an

additional strain rate from the extrusion. The continuous extrusion of the melt produces a pressure flow shear component that adds on top of the drag flow due to the cross-lateral rotational and oscillatory shear. In Fig. 5b, items 11 and 22 are the treatment stations of Fig. 5a, items 1, 2, 3 are gear pumps, items 111, 222 and 333 are zones with no drag flow. Details are provided in ref. 15.

Combined Flow rates from Pressure Flow and Rotational Flow.

The rheology of combining pressure flow and drag flow to decrease viscosity of melts has been developed by Cogswell [17], although this author did not include the oscillatory component which boosts the results [Ibar, Refs [12], [18]). The rheology is not as complex as it may first appear, and can be simulated in a rather simple manner [18], following the work of Cogswell, by applying the constitutive equations applicable to a Couette configuration with separate strain rates, respectively applicable to extrusion and rotational flow [19], and by calculating the total strain rate from the vectorial sum of the individual strain rates [17, 18]. For our purpose in this paper it is sufficient to say that the apparatus described in Figs. 5a and 5b allows the design of sophisticated strain rate histories that combine the effect of cross-lateral drag flow (in pure shear or shear superposed to an oscillation) with coaxial pressure flow. Figs. 6a and b give an example of such combined flow, replacing the cone in Fig. 5a by a cylindrical rotor, and not activating the oscillation, which simplifies the transcription of the process in terms of rheological parameters.

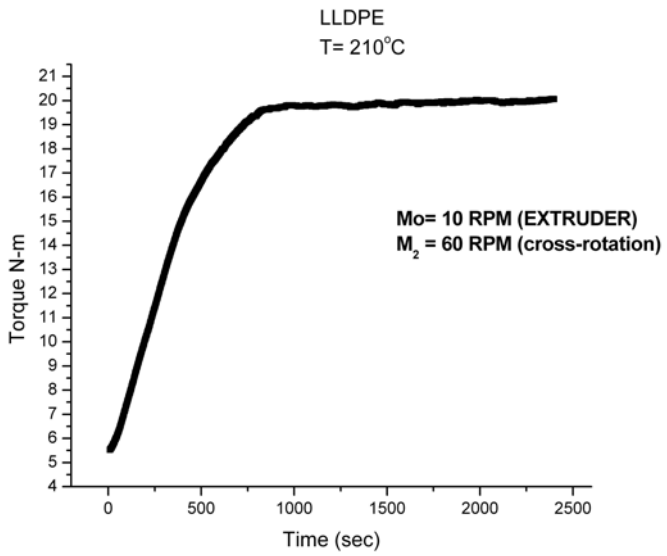

Fig. 6a

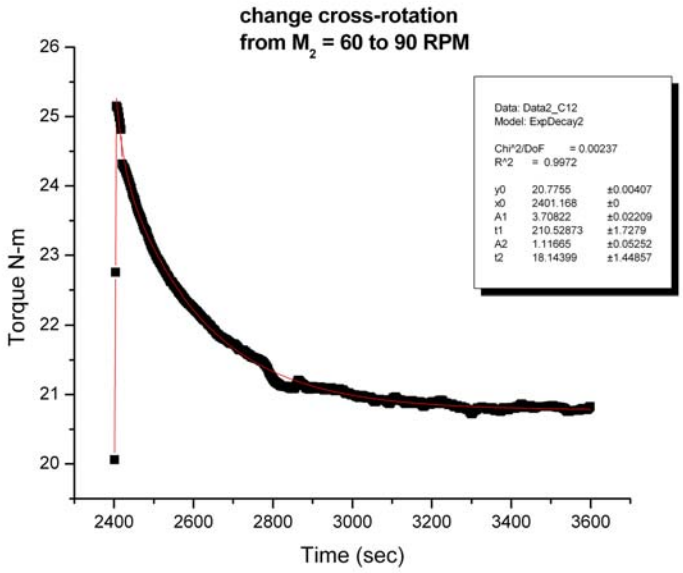

Fig. 6b

Fig.6

LLDPE at T=210 °C. Combination of pressure flow (from extrusion) and drag flow from the rotation of the inner shaft of a Couette attached to the end of the extruder. Fig. 6a shows the establishment of the torque at the start up of cross-rotation of the shaft (60 RPM). Fig. 6b shows the torque vs time for a change of speed of the cross-rotation from 60 to 90 RPM.

In Fig. 6a, the set up of Fig. 5a is used as a viscometer to measure the torque transient created by the onset of a sudden rotation of a melt extruded through the gap at given throughput, controlled by the extruder's RPM (Mo= 10 RPM, corresponding to 350 g/hour, i.e. 0.12 cc/s). The extrusion has reached steady state for 20 min at time t=0 in Fig. 6a, start up of the cross-rotation. The polymer is the same as in Fig. 2, LLDPE. Temperature is 210 ^{o}C. Fig. 6a applies to a step jump of the cross-rotation RPM of the rotor (called M_2 in the Figure) from 0 to 60, corresponding to a shear rate of 15.81 sec^{-1}. The longitudinal shear rate calculated from the extruder pressure flow is 1.36 sec^{-1}, already big enough to bring the melt in the non-Newtonian deformation range. Fig. 6b shows a subsequent step jump of M_2 from 60 RPM to 90 RPM, corresponding to a sudden change of the shear rate from 15.81 to 23.71 sec^{-1}.
One sees that the experiments of Figs. 6a and b describe the transient startup of a step strain rate experiment, as described in Figs. 2a and b. An important difference between Figs. 6a and b is clearly visible: there is no overshoot of the torque for the strain rate of 15.81 (Fig. 6a) and the transient consists of the torque rising rather slowly to a steady state value of 20 N-m. Contrasting with that, in Fig. 6b, a clear overshoot of 5.60 N-m is visible when the strain rate jumps to 23.71 sec^{-1}, followed by a decaying transient that can be fitted with two exponential terms, like in Fig. 2a. The fitting equation, given in the graph's inset (2 exponential decay terms $A_1 \exp(-(t-x_o)/t_1)$, $A_2 \exp(-(t-x_o)/t_2$ and a constant, y_o) shows that the transient relaxation times are a short one, t_2=18 sec and a long one, t_1=210 sec, a similar situation to that of Fig. 2a. (Note that x_o indicates the time at which the rotor's speed is increased). An important difference with Fig. 2a is the value of the steady state viscosity; it is finite in Fig. 6b and near zero in Fig. 2a. What makes the start up transient flow so different in Figs. 6a and b? Matsuoka ([20], p 193) explains that below a critical strain rate (=1/ τ_o), the melt behaves like a viscoelastic deformed body, which explains a gradual increase of the torque to its steady state value, as shown in Fig. 6a . When the strain rate exceeds the limit of viscoelasticity, the overshoot is due to viscoplasticity, according to Matsuoka, who suggests it is similar to melt yielding:

> *" The maximum stress level reached in stress overshoot is the yield stress in the true sense, since it reflects the mechanical strength of the structure, or in this case the limit at which the knots can reptate without tearing through the polymer melt. The steady state is reached when the relaxation time that is the*

characteristic of the new structure under the ongoing strain rate is equal to the reciprocal of the strain rate. If the rate of strain happens to be less than the reciprocal of the original relaxation time, the polymer can reptate without destroying the original structure, and viscoelastic relaxation ensues. In plasticity, steady state stress is determined by the ongoing rate of strain, whereas in viscoelasticity it is determined by the natural relaxation time. The virtual elastic strain ($\tau_o\, d\gamma/dt$) in plastic flow is thus 1…Stress overshoot means that the yield stress exceeds the steady state stress, hence it occurs when the plastic yield strain is greater than 1".

This argument qualitatively concurs with that of Wang quoted earlier [7-10] who also concluded that the transient relaxation, in particular the presence of the stress overshoot, was due to two criteria , one of a critical strain rate, and one of reaching a plasticity strain (125 % for Wang). Both Wang and Matsuoka agree that viscoplasticity, i.e. deformation of the melt at high strain rates, corresponds to the disentanglement of the structure of knots, as Matsuoka defines the entanglement network. In other words, shear-thinning is due to disentanglement. The stress overshoot is the onset of disentanglement and is due to plastic yielding. There are, indeed, some important differences between Wang's and Matsuoka's strain rate criteria, but these details are not important in this introduction, and left for the discussion section of the paper.

However, another possible interpretation of the results of Fig. 2a or of Figs. 6a and b must be examined, due to the particular experimental set up leading to Figs. 6a and b. The melt was already flowing in a steady state when it was submitted to the lateral step strain rate deformation. In Fig. 6a, the initial steady state (at t=0) was that obtained from the extrusion pushing the melt in the gap of the static Couette (static in the sense that it is not rotating). Macromolecules were deformed in flow layers sheared according to a parabolic velocity profile in the 3mm gap, corresponding to a maximum strain rate value of 1.36 sec^{-1}, that, to simplify the language, aligned them in the axial direction. The step strain rate of Fig 6a created a deformation in the cross direction, disrupting the steady state in the axial direction. It is conceivable that the transient response, which is the description of how the system re-organizes its molecular interactions before reaching a new steady state, is dependent on the orientation of the melt in its initial steady state, not just a question of rate, but a question of entropy as well. In Fig. 6b, however, the step strain rate was applied in the same cross flow direction after the

steady state of Fig. 6a had been reached. The difference of transient behavior observed in Figs. 6a and b might be primarily due to that. When starting from an already steady radial flow (the radial stress rate is more than 10 times the axial strain rate), the increased strain rate is acting like a jolt on the melt, which reacts elastically, creating a response more in line with a relaxation of stress under constant strain, as described in Figs. 1c and 1d. An "instantaneous" elastic strain, calculated from the ratio of the strain rates, (90-60)/60 = 50% here, was imposed in 50 ms or so, resulting in the application of a sudden start up strain rate of ~10 sec^{-1} and of the 5.6 N-m torque overshoot observed in Fig. 6b. The startup step strain rate experiment also resulted in a sudden increase of pressure in the gap, due to the normal stress, and a rise of the local temperature unless heat is actually removed from the treatment zone preventing the temperature to rise. In the apparatus of Fig. 5a , this is realized by circulating a cooling fluid in the orifices (240) of the stator jacket (230) The sudden increase of the strain rate is dissipated by reorganization of the network of interactive bonds, resulting in a new state of orientation of the macromolecules which adapt to the new strain rate gradient in the gap. In this explanation, there is no need to disentangle the melt to obtain the overshoot, the transient response is naturally due to the re-orientation of the entanglement network (not a decrease of the knots density) which initiates with an increase of the strain energy, like in the Maxwell spring and dashpot model in the first section of this Introduction. Concepts that must be elucidated are "the orientation of macromolecules or parts thereof that induces shear-thinning", and what is "the entanglement network of interactive bonds ". We will propose an interpretation of these concepts in this paper. We will also address the question of the stability of the entanglement network, and re-consider issues of disentanglement as formulated by Wang [7-10], Matsuoka [20] and by the present author [21-24].

The influence of the orientation of the melt on the value of the steady state viscosity and on the relaxation spectrum has been studied and is assumed to be well known [4,5,11]. For instance, Osaki's paper discussed above can be considered such a study. Osaki concluded that disentanglement explained his results [11], but he might have confused disentanglement and shear-thinning (see the discussion). For most rheologists, however, shear-thinning as well as other non-linear viscoelastic effects, such as the stress overshoot, are not due to disentanglement [25, 26].

In Fig. 6a, the experimental conditions suggest that it is more likely the influence of the original orientation of the melt in the axial direction, produced by the extrusion strain rate, that influences the transient characteristics so that no overshoot was observed, rather than a critical shear strain rate which, according to Wang's criteria or Matsuoka's criteria,.would preserve an homogeneous melt or linear viscoelastic behavior, for which no overshoot is predicted. This is the same polymer as in Fig. 2, but the temperature was 210 ^{o}C instead of 190 ^{o}C. This shifts the value of ω_x from 87 to 119 for this LLDPE (the activation energy for the Newtonian viscosity is 7.77 Kcal/mole). The critical Wang's shear rate for inhomogeneous flow would be increased by 36% due to the temperature increase. The initial steady state strain rate (from pressure flow) was 1.36 sec^{-1}, i.e. far below the critical strain rate for the onset of inhomogeneous flow proposed by Wang and, for the shear rate of 15.81 sec^{-1} produced by the rotation of the shaft in Fig. 6a, it was still below that critical strain rate criteria by several decades. In summary, we were operating under conditions of homogeneous laminar flow for which no disentanglement should be observed. In Fig. 2a we saw that the viscosity (and thus the torque) decreased towards a zero steady shear value (perhaps not zero exactly, but very small), which might be due to combined relaxation (orientation) and disentanglement of the melt, as we argued earlier. In Fig. 6a, the start-up melt had an initial torque value of 5.5 N-m, not zero (and incidentally it was the same value as the overshoot of Fig. 6b), which grows to 20 N-m Torque after 750 sec. Following Cogswell [17], the torque increase between the two steady states would simply be due to a shear rate increase from 1.36 sec-1 to 15.87 sec^{-1} (the combined vectorial shear rate $\dot{\gamma} = \sqrt{\dot{\gamma}_{ROT}^{2} + \dot{\gamma}_{EXT}^{2}}$). In the pseudo-plastic region, torque scales like the strain rate to the power n, where n is the melt power coefficient, around 0.2 for PE. In order to be more accurate, since the power law coefficient often varies with temperature and strain rate, which is the case for this LLDPE at 210 ^{o}C, a frequency sweep was done at that temperature to determine the effect of strain rate (or angular frequency ω) on the torque at ω = 1.36, 15.81 and 23.75 rad/s (the last value corresponding to the strain rate in Fig. 6b). For a jump between 1.36 and 15.81 sec^{-1}, the expected steady state torque increase is 4.13 times. For a jump from 15.81 to 23.75, this ratio is 1.1645. This should be compared with (20/5.5)=3.63 and (20.77/20)=1.03 respectively, which are the ratios of the steady state torques taken from Fig. 6a and 6b. In other words, the torque

predicted from the strain rate increase is too high by only a factor 1.135 in both figures. If there was disentanglement occurring in the steady states, it could only be due to this "extra 13% shear-thinning" observed. Perhaps this extra shear-thinning should be attributed to a kind of strain softening, as suggested by the damping factor $h(\gamma)$ discussed previously (actually, the amount of strain on the system in steady state could be determined that way, by applying Wagner's formula for $h(\gamma)$, for instance, $h(\gamma)=\exp(-c\gamma)$ [27] .For our present purpose, a 13% difference of viscosity is rather small, especially in view of the fact that the Cox-Merz's law was applied, and it is logical to conclude that the steady state results of Figs. 6a and 6 are consistent with the classical shear-thinning views, and that no disentanglement took place. This conclusion is, of course, based on the assumption that shear-thinning itself has nothing to do with disentanglement, an essential topic of discussion in this paper. As far as the Matsuoka's criteria for the presence of the overshoot is concerned, Fig. 6a passes the viscoelastic test since the strain rate was less than $1/\tau_o$, and no overshoot occurred, but Fig. 6b fails the strain rate criteria, because the critical strain rate was still not reached, yet the overshoot is clearly visible. In summary, the melt fails all criteria for disentanglement by Wang or Matsuoka, its steady state response confirms predictions made by Cogswell [17] that the combined strain rates simply increases shear-thinning, yet it displayed a strong transient behavior with relaxation times that seem to implicate disentanglement, and it showed an overshoot at start up under strain rates where none should be observed. The situation is not clear.

In the analysis above we saw that the magnitude of the combined strain rates from all sources determines the steady state viscosity, and nothing seems to indicate that there is an importance of the direction of flow, except in the vectorial calculation of the strain rate (the square root of the addition of the square of the strain rates). This might not be true for the transient response, as suggested in Fig. 6a by the very long time it took for the transient relaxation to vanish, as a change of the direction of flow took place from axial flow to almost entirely radial flow (the melt advances helicoidally around the rotor shaft with an angle equal to 85^o off the Couette axis of rotation). The effect of orientation of the melt on the transient kinetics seems an essential subject of investigation, as much important as the reverse effect, the influence of the transient kinetics on the new steady state of orientation, a subject discussed in the section on shear-refinement later on.

In our approach, the transient and the steady state are both the result of the same deformation and re-organization of the network of molecular interactions; they are inseparable and must be studied as interdependent on one another. The formula successfully describing shear-thinning, the Cross or the Carreau equations, for instance [see discussion of that formula in Ref. [2]), apply to the steady state, and do not describe the transient behavior. Additionally, they do not directly relate to either the orientation of the melt or to whether a disentanglement mechanism, if any, can be triggered at a given critical strain rate. These are serious shortcomings, revealing the present lack of understanding of the deformation mechanisms of the "entanglement network", at the molecular level, during transient and steady state response.

Combined Oscillation and Rotation.

We now consider experiments similar in nature to those described above, ones in which an oscillation is simultaneously added to the shear component produced by constant speed rotation. Figures 7a and b confirm the expectations that the added oscillation influences the transient and the steady states. The polymer melt was still the same LLDPE, operated at lower temperature, 130 ^{o}C, to enhance non-linear effects (ω_x is reduced). In these figures, the melt was extruded in the treatment station at a higher temperature, the extruder was stopped to confine the melt in the gap, rotation was started and temperature was decreased to 130 ^{o}C. The very high viscosity of the melt at T=130 ^{o}C was the reason why the RMP was started at a higher temperature; shearing the melt would not be possible otherwise, requiring too much torque. In Figs.7a and b, the current (proportional to the total torque) is plotted against time to detect changes occurring to the melt as it was submitted to either a simple cross-lateral shear produced by rotation of the Couette's rotor, corresponding to the upper left portion of Fig. 7a, or the combination of the same rotational shear and added vibration (bottom right portion of Fig. 7a), or while "recovery" was done, such as shown in Fig. 7b, either by stopping the oscillation (at time = 0 in Fig. 7b) or by decreasing the rotational speed of the rotor (after Time = 1800 sec in Fig. 7b).

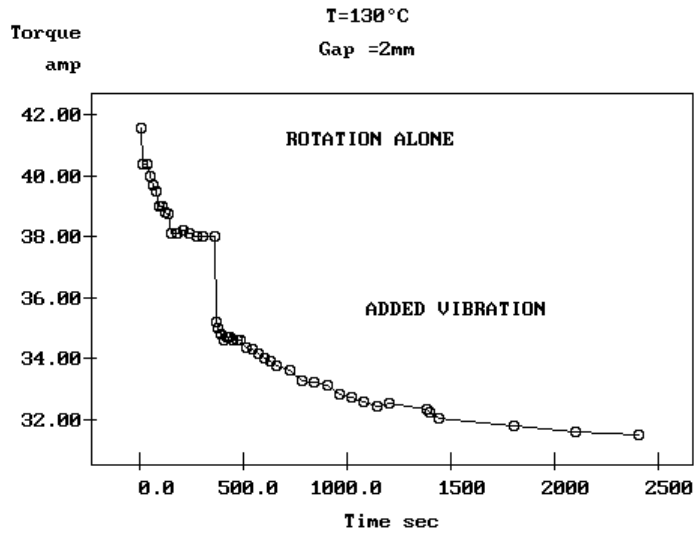

(a)

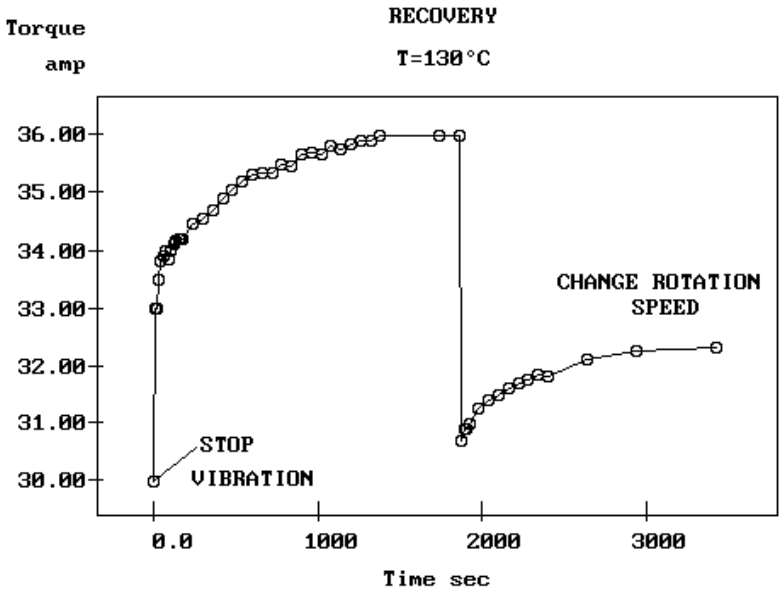

(b)

Fig. 7

Torque vs time for a melt confined in a gap with the inner surface rotating and oscillating (independently). In Fig. 7a the rotation is done without oscillation, then oscillation is added. In Fig. 7b, both rotation and oscillation are active at the start. Oscillation is first stopped, then the rotation RPM is reduced.

Rotation alone (Fig. 7a) was capable of producing a steady state shear-thinned torque value that was within the limit of the capability of the motor turning the shaft. The initial amperage needed was 42 Amp. Rotation of 90 RPM (for a gap of 2mm) decreased the torque to 38 Amp. The superposition of an oscillation (7 Hz, 40% strain) is most spectacular. The current drops down elastically to 35 Amp, followed by a slow transient relaxing to a new, low, steady state of 31 Amp. The melt could be extruded at T=130 ^{o}C under those lower torque requirements. An increase of the oscillation frequency (the maximum available for the equipment producing the results of Fig. 7 is 30 Hz) reduced the torque further (not shown). An increase of the strain amplitude (the maximum available was 80% at 7 Hz) had a drastic effect on the value of the steady state torque; this can be combined with the effect of frequency to decrease viscosity in the way described below. By increasing frequency and amplitude step by step, after letting the melt reach a new steady state at each step, we succeeded in reducing the torque to 8 Amp, which is 1 Amp above the value of the torque required to turn the shaft with no polymer melt filling the gap. In other words, by operating smoothly, increasing frequency and amplitude in steps of 15 min each, we were able to reduce the viscosity of this highly entangled LLDPE at T= 130 ^{o}C to almost nothing, a situation not very different from what was observed in Fig. 2 for the same polymer. Comparing the initial torque value, 35 Amp (42-7) to the final torque achievable (1 Amp), the viscosity appeared to be reduced 35 times, far exceeding the shear-thinning ratio observed at the same Cox-Merz's frequency/ strain rate in a frequency sweep done at T=130 ^{o}C. To be sure that the melt was indeed of lower viscosity when the torque reading was very low, we took advantage of the lower viscosity to reduce the temperature down, step by step, and repeated the same scenario of increasing the oscillation and rotation speed of the rotor, increasing the rate of inflow of the cooling fluid to maintain the melt at the desired temperature despite the intense release of heat generated by the shear process. Incredibly, this repeated operation allowed to cool the melt down to 42 ^{o}C (just about the value of the solidification temperature by crystallization), while it continued to be sheared at fast rotation and oscillation. The experiment was successfully repeated several times. Application of the Carreau's equation to the dynamic viscosity –angular frequency data generated at several temperatures (in a separate Rheometer, an ARES from Rheometrics) permits to extrapolate and calculate what the value of the viscosity would be at T= 42 ^{o}C, under the strain

rate conditions used, assuming that rotational and vibrational shear rates are additive, as mentioned before. The reduction of viscosity appears to be so extraordinarily large that our common sense in rheology raises the fundamental question: what is *really* happening to the melt? . Indeed, these experiments require answers and a careful analysis.
Figure 7b describes the reverse process of Fig. 7a., starting from a steady state obtained under conditions of pure rotation and oscillation combined, the oscillation was interrupted, and one sees the quick elastic jump followed by a transient torque build up corresponding to a viscosity increase. Then, on the same figure, the rotation speed was lowered, which showed up as a spontaneous torque reduction followed by another transient where torque continued to build up towards a new steady state. All these transient responses are the translation of changes occurring within the network of interactions between the bonds belonging to the macromolecules, undoubtedly related to the entanglement network. But again, is disentanglement involved, starting at what value of the strain rate, under what other conditions of temperature and strain, and can the disentangled melt be frozen-in into pellets that, on reheating, will preserve the viscosity reduction benefits? The question of the stability of the disentangled melt appears to be crucial to study. Much of the second part of this chapter is dedicated to this question.

Shear-Refinement: the Effect of Thermal-Mechanical History.

"Shear-Refinement" is the observed influence on subsequent viscoelastic behavior (e.g. viscosity) of a pre-shearing treatment of a polymeric melt. Cogswell mentions the influence of thermo-mechanical history on viscosity in his book [17, p.53]:

> *"Intense working, producing high shear, will usually lead to a reduction in viscosity and also a decrease in the elastic response".*

Note that the viscosity reduction discussed in this section is not due to a decrease of molecular weight, which is known to occur concomitantly, to a variable degree depending on the polymer and the experimental processing conditions. Most of the pioneering work was done 20 years ago by such authors as D. E. Hanson [28], M. Rokudai [29], B. Maxwell [30], J-F. Agassant [31], H. P. Schreiber [32] (who wrote a review of the subject up to 1966), G. Ritzau [33,34], who provides details of a shear-refinement apparatus, J.R. Leblans and Bastiaansen [35], Van Prooyen et al [36], Munstedt [37], who studied the effect of thermal

elongational history, and A. Ram and L. Izailov [38]. Hanson [28] showed that the Melt Flow Index of a branched PE (expressed in g/ 10 min) could be modified by shear-refinement from 0.28 to 0.66 and that the MFI returned to the initial value 0.27 after solution and re-precipitation of the pre-sheared sample. Cogswell [17] comments as follows on the results obtained by Hanson and others [28-30]:

> *"The change is seen to be reversible by solution treatment. Molecular weight characterization indicated that all these samples were identical…* [Shear-refinement effects] "*might at first appear to be the result of degrading the polymer, are frequently reversed by cooking the melt, though the time for which the melt may need to be cooked to achieve reversion may be much longer than the natural time of the material (viscosity/modulus at zero shear)".*

J-F. Agassant et al. [3**1**] show that the effects of shear-refinement are most obvious, and most commonly exploited, in the case of PVC which is known to have a morphology very sensitive to thermo-mechanical history. Recently interest is quickly re-emerging [**39-53]** as more data prove the value of the melt pre-treatment, and a large viscosity reduction ratio seems achievable for a variety of polymers, including linear polymers [31-53]. No clear explanation has been given to the origins of shear-refinement, except for the suggestion that disentanglement might be involved [31, 39-50].

Bourrigaud [**39**], and Berger [40] have recently investigated the shear-refinement of long-chain branched ("LCB") polyolefins in their thesis. Bourrigaud focused on several well characterized low density branched polyethylene grades and obtained proof of the influence of the strain amplitude of shear deformation on the degree of viscosity reduction during subsequent processing. Bourrigaud suggested that molecular topology is critical, and his results support the view that molecules with very long-chain branches are highly affected by shear refinement, whereas linear polyethylene seems to undergo much smaller changes (if any), under the experimental shear refinement conditions he used. Bourrigaud and co-workers [41] concluded that the degree of long chain branching or ramification qualifies or disqualifies, for the most part, the degree of viscosity reduction observed by shear refinement. In other words, controlled alteration by branching of the molecular weight distribution leads to the optimization of shear-refinement and of its benefits, according to these authors. Furthermore, Bourrigaud et al showed that refinement by elongation is more effective than refinement by shear for the same flow strength [39, 41]. Berger [40] and Berger et al. [42], worked with a

long chain branched polypropylene under very high shear strain rates and found similar results. Additionally, Berger and coworkers [42] confirmed that the MFI of branched PP, collected as pellets, could be increased by shear-refinement, and that solvent dissolution would reverse the effect; after evaporation of the solvent, the MFI returning to its original value. These authors concluded that disentanglement was responsible for the decrease of viscosity and die swell [42]:

> *The pre-treatment of the LCB-PP in the capillary rheometer at the highest shear stress applied causes a significant reduction of the tensile stress, which can be referred to the reduction of the mass-average molar mass. However, the significant decrease of the extrudate swell after the pre-treatment cannot be explained by the change of the molar mass, as the elastic behavior of polymer melts is known to be independent of the mass-average molar mass. Therefore, the reduction of the extrudate swell is an indication of a change of the entanglement network during the pre-treatment.*

We published a series of papers during the last decade related to the use of vibrational methods during melt extrusion to induce shear-refinement by shear strain energy coupled with extensional flow[12-14, 18, 43-54]. The emphasis of this "dynamic shear strain refinement" process was on the improved processability of **linear** high molecular weight polymer melts, such as Polycarbonate and Plexiglas (PMMA), i.e. polymers without branches. We showed [13, 14-16] that, to induce the shear refinement benefits, a combination of shear stress and superposed oscillation could raise the elasticity of the melt to a level identical or perhaps even superior to what branching could do. In other words, we proposed that, at least under dynamic conditions, both linear polymers and branched polymers could qualify for disentanglement by shear strain refinement. Furthermore, we drew attention to the requirement of rheological criteria to be fulfilled for shear refinement to occur [15,18, 46], and pointed out the importance of the shear strain amplitude of the oscillation to operate the melt in the non-linear viscoelastic range [43,45,48,49,51]. We suggested that "disentanglement" was only involved under certain conditions [47], and claimed that shear-thinning was a different mechanism of deformation, in many ways precursor to disentanglement, but not equivalent [14, 15, 18, 66].

Shear-refinement work has remained largely empirical. The viscosity reduction is temporary and rheological properties can be restored, which can occur in various ways not very well understood. Most of the comprehension necessary for its generalization and

extrapolation to all macromolecules is still needed. For instance, for linear polymers, the relaxation times calculated from the standard models (reptation), seem to be much shorter than those involved in shear refinement of the viscosity, sometimes by a factor 1000 or even 10 times that. The comprehension of shear-refinement in terms of transient kinetics is lacking in the literature, its positioning with respect to disentanglement confusing and debated. Properties of melts brought out of equilibrium are largely ignored. Yet, many plastic industries are directly concerned and will benefit from the fundamental understanding of what causes shear refinement viscosity drops, and how this can be applied to processing of polymer resins. The ability to process plastic melt at much lower temperature (50-80 ^{o}C below normal), because of reduced viscosity due to shear-refinement, opens up new boundaries not just in processing but also in blending, such as in nanoparticule dispersion, or for the processing of high temperature sensitive additives (wood flour, instable additives such as peroxides, etc.).

Part I of this "Great Myths in Rheology" series, ref. [2], challenged the accepted views [**25**] that advances in rheology for the last 40 years have led to a better understanding of the influence of the chain configuration on its flow characteristics, such as viscosity. It was argued [2] that the de Gennes' reptation model [55, 56] had reached its full maturity stage and showed signs of clear limitations, a view clearly shared by Wang [7-10]. More recently, modified versions by Marrucci et al [57], Wagner [58], and others, of the original reptation models by de Gennes [55], perfected by Doi and Edwards [**25**], have been claimed to provide a fairly good understanding of the flow behavior of entangled chains. Yet, many essential questions remain unanswered and/or are discarded by the present reptation school, such as the experiments by Wang [7-10], or how to explain the challenging results obtained by "shear-refinement" [28-42], or by shear induced, strain amplified, melt disentanglement under oscillation [43-54]. Bourrigaud [39] modified the McLeish and Larson's pom-pom model [59] to account for the increase, due to branching, of the value of the tube renewal relaxation time and explained, at least partially, some of the shear-refinement results, but <u>linear, disentangled polymers present a real challenge to existing models of flow.</u>

Melt Fracture. Edge Fracture in Parallel Plate Experiments.

In the deformation of a melt, studied either in a Couette or in a parallel plate (or cone and plate) apparatus, the motion imparted to the melt is driven by one surface in contact with the melt, the other surface remaining static. The question of the adhesion between the moving surface and the melt is essential to resolve. Another problem, regarding the formation of a "crack", or indentation, at a critical shear rate on the free surface at the edge of the liquid, has been raised and analyzed by several authors [60-65]. According to this interpretation, large amplitude oscillatory shear studied with a parallel plate configuration is plagued with artifacts caused by the propagation of these edge cracks [60]. In an article published recently [61], Friedrich and coworkers follow up on their initial edge fracture work [60], and mention similar melt fracture instabilities investigated by McKinley et al. [62] , Oztekin et al. [63], Byars et al. [64], and Larson [65]. All these authors have assumed that the occurrence of sample instabilities during rheological experiments at high shear rates and/or large deformation strains was due to the formation and propagation of edge cracks-indentations. In essence, Friedrich et al. [60, 61] provide an edge fracture interpretation for results performed under similar conditions that were published by us in a series of communications starting in 1997 [43-51, 66, 67], apparently unknown to Friedrich [68], and interpreted very differently. In these publications we reported results conducted since 1995 on Polycarbonate and LLDPE [1999] using a parallel plate rheometer under dynamic conditions, applying sufficient strain deformation to bring the melt into the non-linear range [15,44,45,47]. These are the same experiments as shown in Figs. 3a and b for Polystyrene. The observed decay of G'(t) and G"(t), and thus of viscosity, obtained under *certain* conditions of frequency and strain, which Friedrich et al. consider to be the signature of a surface fracture process, were described by us [12-18, 43-51,54, 66,67] as the orientation of the entanglement network, as defined in the Dual-Phase model [22-24], a situation very similar to what causes shear-thinning under strain softening conditions and/or shear-refinement, as described in the previous sections. We [43, 44] assigned the time dependence of the rheological parameters to the stability of the entanglement network, which can either elastically deform, to allow orientation of the dual-

phase, or plastically deform, creating a new entanglement network. To quote the 1999 paper [44]:

> "…*the decrease of viscosity is not the result of a mechanism of slippage at the surface of the rheometer, nor a mechanical degradation of the chain macromolecules, but rather is due to the destruction of the EKNET network of interaction by a vibration induced dual mechanism of first stiffening (by shear-thinning) and tearing (by a fatigue mechanism (induced) by the normal stresses) of the interpenetrating coils.*

All these concepts will be thoroughly developed in this chapter. We showed [47] that edge fracture can be avoided by slowly and step wisely increasing the strain amplitude, instead of jumping it to a large value, a procedure practiced by the edge fracture protagonists. By operating under the step-by-step-increase-of-strain conditions, and also by using smaller samples (12 mm in diameter vs 25 mm used by Friedrich et al. [60, 61], or thinner samples (less than 0.5 mm) and/or by using cups to confine the melt and serrated surfaces for the parallel plates, the artifacts caused by the non-linearity established too abruptly can be eliminated [47, 67]. This procedure and the validation of the assumptions that melt fracture is not involved in the results observed will be further discussed below.

Objectives of this Chapter.

In conclusion, all the above results (Figs 1-7) seem to indicate that the stability of the network of entanglement should be a major subject of investigation; in particular, it would be practically very important to know whether entanglements can be manipulated (increased or decreased at will) to facilitate processing. This chapter addresses the following issues:
- How can we distinguish between a transient melt that is decaying towards its steady state from a disentangling melt? Under what conditions is the steady state a disentangled state, as suggested by Osaki et al. [11]? What is the difference, if any, between shear-thinning and disentanglement?
Finally, the chapter examines the following proposition: a polymer melt can be disentangled if, and only if, it goes through a specific process of "melt yielding". How can a liquid yield, which is a phenomenon characteristic of solids (it is the transition between an elastic and a

plastic state). What is melt yielding? It is mentioned by several authors: Ibar [21-24], Matsuoka [20], and Wang [8,9]. How does it affect the homogeneity of the melt [7-10], and the rheology results? Are the results in Figs. 2 and 3 due to or affected by a laminar structuration of the gap created by local yielding, or disentanglement? Is disentanglement confined to a thin layer that becomes a surface of lower viscosity (a lubricating layer), preventing the penetration of further disentanglement towards the other surface? Is there a critical gap for full penetration of disentanglement, and how can it be controlled?

It is well known that the steady state viscosity varies with the strain rate, for high molecular weight polymers, as well as with molecular weight and temperature, and these experimental facts were reviewed in chapter 3 of this dissertation and also in Ref. [2]. It is expected that the transient behavior also varies with the same variables. An important issue addressed in this chapter is to examine how the transient states and the steady states are related, whether they can simply be derived from one another or require specific separate treatments. In particular, the effect of strain and strain rate on the transient behavior is addressed, both in pure rotational viscometry, in dynamic experiments, and in experiments which involve the combination of oscillation and pure rotation.

Can the combination of strain, strain rate and oscillation result in melt transients which relax to different steady states, and are those steady states stable? Is the melt capable of "yielding" in steady state or is it a property of the transient behavior? What are the macromolecules doing when deformed in steady state rotation? Is the concept of strain still valid when the melt has reached its steady state, under constant strain rate conditions? If strain is still a valid concept, what is the mechanism that makes strain grow to infinity in steady state? Is a steady state melt stretching and relaxing, orienting while stretching, orienting while relaxing, or both?
Some would consider all these questions to be trivial, and the answers well understood by rheologists. Yet, as the next section will demonstrate, the question of a melt out of equilibrium is not a naïve question and bears to the fundamental issue of what entanglements are. If a melt can be brought out of equilibrium and stabilized in that state, at least for a long period of time, say for 1,000 to 10,000 times the value of its terminal time, what does it say about the nature of entanglements? What kind of topological change could make this happen, in terms of the

reptation interpretation of entanglements? Additionally, if melts are capable of being metastable, like glasses, new processing techniques can be used to either decrease or increase their viscosity and affect many physical properties.

In the discussion section of this chapter, we distinguish the mechanisms of deformation that lead to simple transient behavior, with a full return of the melt to its initial equilibrium after cessation of the cause that created the melt transient, from those specific mechanisms capable of producing a modification of the entanglement network, with interesting processing consequences. Can we produce by induced mechanical treatments, through a combination of stress, strain rate and strain history, melts which are maintained out of equilibrium and present new steady states characteristic of a lower viscosity melt, at the same temperature? Are these melts disentangled in the classic sense (M_e is increased)?

B EXPERIMENTAL PROCEDURE, POLYMER CHARACTERIZATION, DEFINITION OF PARAMETERS.

1. Experimental Procedures

In this section we describe several types of experiments that we classify and label by names that will be used throughout.

1A. The simple time sweep at given T, ω and strain %. This is a classical test in rheology. The same tests were conducted by Friedrich et al. [60,61]. The only interest here is to explore the non-linear region, by choosing values of the rheological parameters where G' and G" are observed to become time dependent. A new sample is used for every single set of conditions chosen for the time sweep. Variables studied were: frequency, temperature, and time under oscillation. Strain was kept constant at 50%.

1B. The simple time sweep at given T, ω and strain % immediately followed by a cooling ramp test performed in the linear range.

An experiment of Type 1A is followed by another step, a cooling ramp test, at 1 ^{o}C/min, 1 Hz, 5% strain. As temperature cools down, the measurement of G'(T) and G"(T) is done until the torque exceeds its maximal permitted value, the apparatus automatically terminating the test. The second step, the cooling test, is always done under the same conditions, regardless of the parameters used during time sweep. In operating this way, the cooling curves obtained can be compared to reveal the changes, if any occurred, that resulted from the time sweep "treatment".

2. The three step experiment of type FTF (Frequency-Time-Frequency) in a dynamic rheometer.

Step 1 consists of a first frequency sweep (0.1 Hz to 40 Hz, at a given strain%, usually 5%) at a given temperature T (referred to as "1st Frequency Sweep" in some of the figures). Step 2 is a time sweep conducted for a given time, usually 20 min, chosen frequency and strain %. The temperature is either the same as for Step 1 (the type of the experiment is then called **2A**) or different (Type **2B**). Step 3 is a repeat of Step 1 done right at the end of the time sweep, also referred to as "2nd Frequency sweep" in some of the figures. Comparing the frequency sweeps at Steps 1 and 3 provide useful information regarding the changes occurring, if any, due to the time sweep "treatment", as Step 2 is sometimes referred to in the figures.

3. The four step experiment of type FT1-FT2-FT1-FT2 in a dynamic rheometer.

Step 1 consists of a first frequency sweep (0.1 Hz to 40 Hz, at a given strain%, usually 5%) at a given temperature T_1. Step 2 , referred to as "annealing" in some of the figures, is a frequency sweep performed at a temperature T_2 located 50 ^{o}C above T_1.. The "annealing" time of Step 2 is the time it takes to run the frequency sweep, usually 5 min, including the equilibrium times. Step 3 is a repeat of Step 1 done after the sample is cooled back down to T_1.

Step 4 is a repeat of Step 2 after the sample is re-heated to T_2. One can compare Step 1 and Step 3, Step 2 and Step 4. These tests can be considered an original melt frequency sweep and a rerun after annealing for 5 minutes at a higher temperature.

4. Pure viscometry.

These tests are the most basic in rheology. They provide the value of viscosity and of the normal force for a given strain rate, at a constant temperature. Figs. 2a and b are typical examples. In a simple variant of this type of deformation, the same melt can be submitted to successive steps of various strain rates, or no strain rate ("annealing step"). The sequence creates a strain rate history. In order to compare the effect of various strain rate histories, the final step can be done at low Newtonian rate, revealing any change, if any, due to thermal-mechanical history.

5. Pure viscometry followed by a frequency sweep.

This type of experiment is identical to Type 4, except that, at the end, a frequency sweep is performed in the linear viscoelastic range, to "reveal" the state of the melt.

6. Viscosity measurement under extrusion flow conditions.

These experiments are illustrated in Figs. 6a and b. An apparatus was built with a Killion lab extruder attached to a house-made Couette, positioned perpendicular to the extruder's axis. The rotor of the Couette was a cylindrical shaft. The dimensions are given in the section of the introduction above called "Combined Flow rates from Pressure Flow and Rotational Flow". Both the extruder flow rate, determining the longitudinal shear rate and the residence time in the Couette section, and the cross-shear rate, calculated from the gap dimension, the rotor's speed and the melt index, could be varied.

7. In-line viscosity measurement at the end of a "treatment processor".

For some experiments reported in this chapter an in-line capillary viscometer, that was also house-built, was used to reveal the state of the melt after its passage through a treatment station (see Figs. 5a and b). A small hole drilled on the side of the exit melt pipe directed a small portion of the melt through a miniature gear pump to a set of capillary tubes. Two capillary tubes, one short, one long, were positioned periodically in alignment with the flow, allowing pressure measurement to be made, from which viscosity was calculated. Viscosity was directly plotted as a function of time on a computer screen every minute or so (Fig. 8).

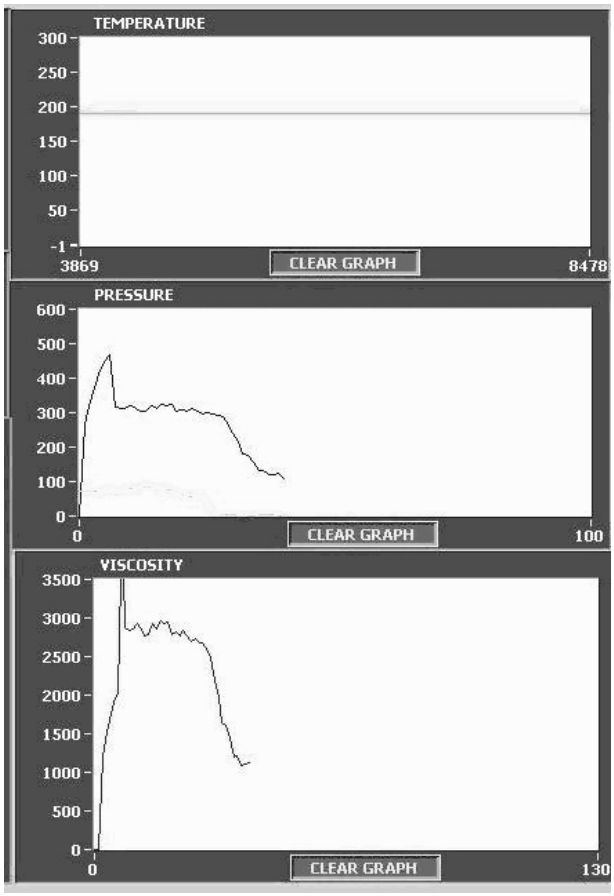

Fig 8

These 3 graphs, continuously updated, read the temperature (top), the pressure drop difference (between short and long capillary), and the viscosity (bottom) of the melt passing through a capillary viscometer after it has been "treated" (see Figs 5a and b). The operator "sees" the result of changing the rheological parameters in the treatment stations. Here the viscosity of the exiting melt has changed from 3,000 to 1,000 Pa-s. The melt is EVOH.

The interest in such an in-line viscosity measurement was two fold: first, and most obviously, it provided a quick and continuous quantitative assessment of the rheological state of the melt, as we built new thermal-mechanical history to modify it. Second, the viscosity read-outs from the "just exited melt" could be compared with viscosity measurements performed on the pellets, also extruded at the same time (Fig 5 b), which were melted subsequently in a Melt Flow Indexer.(Dynesco), as shown in Fig. 9.

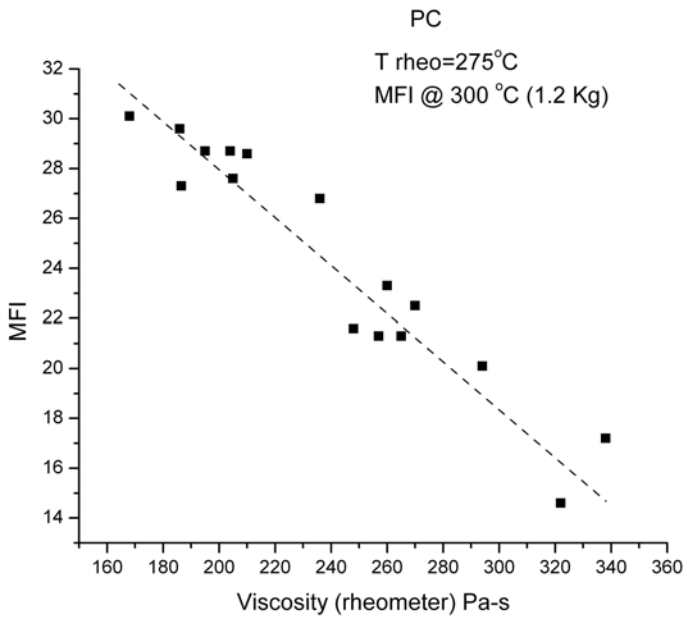

Fig. 9

This figure applies to a linear PC grade. One compares the MFI value found for pellets made out of a melt prepared by the treatment stations of Figs 5a and 5b with the value of viscosity measured by the in-line viscometer (shown in Fig. 8). Although the two temperatures are different (300°C for the MFI measurement, 275 °C for the in-line measurement), the correlation is validated: when the in-line viscosity drops, the melt has a higher MFI than the reference melt (11.3). In other words, the viscosity benefits obtained from the manipulation of the melt stability can be frozen into a state that will survive subsequent heating periods, about 20,000 times its terminal relaxation time value at 150 °C above its T_g.

2. Rheometers used.

Several types of dynamic rheometers were used for Type 1, 2 and 3 experiments: RDAII from Rheometrics, ARES from Rheometrics (TA Instruments), CVO from Bohlin

Instruments (Malvern), and AR 2000 from TA Instruments. Which instrument was used for which type of experiment will be specified in each section.. The viscometry experiments (Type 4 and 5) were conducted with the AR 2000 and the Bohlin.

3. Materials.

Results given in this chapter concern experiments with different types of resins.

3.1 Polycarbonate:

- PC-1: GE Lexan 141 (Mw=27,000 Mn=9,700 MFI= 9.7 g/ 10 min)
- PC-2: Bayer Makrolon 3208 (Mw=32000, Mn=11000 , MFI= 4.3)
- PC-3: Bayer Makrolon 2608 (Mw=26000, Mn=8800, MFI= 11.3)

3.2 Polystyrene:

- PS-1: Total Petrochemicals PS 1450N (Mw=190,000, Mn=80,000),MFI= 6.5 M/Me=11
- PS-2: Total Petrochemicals PS 1070 (Mw=300,000, Mn= 120,000). MFI=1.5 M/Me=17

3.3 LLDPE

- Dupont Dow Elastomers LLP Engage 8180 (Mw=173,000, Mn=(90,000 MFI=0.5). M/Me ~ 170

LLDPE is an octyl ethylene copolymer (metallocene technology) with a Tm of 38 ^{o}C, totally amorphous at T= 190-220 ^{o}C , the temperature range spanned in this chapter (Figs 14-28) .

.

4. Initial State and Sample Molding Procedure.

4.1 PC samples. All polymer resins studied came as pellets. PC pellets were systematically dried 4 hours at 120 ^{o}C before being processed in a Carver Press into 25mm diameter disks. The molding conditions were as follows: 10 ton platen force was applied onto 16 circular cavities of 2mm depth each, equally spaced in a 4*4 in plaque, each containing 1.57

g of dried pellets. Pre-heating time under no pressure :8 min; Heating time under pressure: 3 min; Cooling time 4 min; Number of disks prepared:16; Molding Temperature: 275^{o}C. The disks were dried 17h under vacuum at 70^{o}C prior to placing in the rheometer (the reason for this extra step and the low temperature of drying was that some samples were possibly heat sensitive (those which were "disentangled" prior to the viscosity measurements), and the drying at low temperature under vacuum was an extra caution to prevent any possible heat induced return to equilibrium state during drying too close to Tg). Test conditions were as follows:

1) Parallel plates with serrated surfaces (microscopic pyramidal indents) were used for all experiments.
2) Tests conducted under N_2
3) Start heating to 275 ^{o}C . Takes approximately 10 min.
4) Press to make gap of 1.5 mm. Trim.
The sample is then ready for the specific testing program type described in the section "1. experimental procedures". For instance, for a type 2 (FTF) program conducted at T=225^{o}C, the following sequence would apply:

5) Lower temp to 225 ^{o}C. Wait for temperature to stabilize.
6) Step 1: 1st frequency sweep from 0.1 to 40 Hz, 5% strain.
7) Step 2: conduct a time sweep at 10Hz-5% Strain for 20min at T=225 ^{o}C (as an example)
8) Step 3: 2nd frequency sweep under the same conditions as the 1st frequency sweep.

4.2: LLDPE

Same procedure and methodology as described above for PC, except that drying was not necessary, and the molding temperature in the Carver Press was 225 ^{o}C. The test procedure for the type 4 (viscometry) experiments (Figs. 2a, 2b, and 14) was as follows:
Serrated plates were used. Disk's initial.thickness was ~2 mm. Tests were run under N_2
- Start heating to the initial temperature (e.g. 190^{o}C) and hold for 3 min,
- Make gap of 1.6 mm. Trim the excess melt around the rim.
- Re-heat to 190^{o}C, wait for temperature to stabilize (approx.1min)

- Start viscometry test with a shear rate of 1.0 sec-1, record for 30min

.

4.3: PS

The same procedure and methodology as described above for PC was used, except that drying was not necessary, and the molding temperature in the Carver Press was 200 ^{o}C. A single cavity mold was used; 3 min pre-molding time at 200 ^{o}C, 3 min under 4 Ton force during molding, 2 min cooling time by pressure contact with cold Aluminum plates. Specimens of thickness varying between 1200 and 200 microns were used. Tests were conducted under N_2 to avoid degradation (proven to exist by separate tests conducted under air atmosphere).

5. Definition of the Rheological Parameters to Analyze the Stability of the Melt.

In the following, we present the dynamic rheology data in a way that, we believe, is most appropriate to reveal the difference between melt states. The classical presentation of the data is the use of log-log scales to display G' and G" vs ω at a given temperature, and the display of a cross-over point, defined by G'=G", found at a frequency ω_x, the cross-over frequency, usually associated with the terminal time (τ_o=1/ ω_x). It is well known that increasing temperature or decreasing molecular weight shifts the value of ω_x towards larger numbers. ω_x also increases with M_e, the molecular weight between entanglements, i.e. when "disentanglement" occurs, since the terminal time scales with $(M_e/M)^{\alpha}$. Note that, according to classical views, as discussed in ref. [2), G'(ω) and G"(ω) are the product of $G_{o,N}$, the plateau modulus ($G_{o,N} = \rho RT / M_e$, where T is absolute temperature and ρ the melt density), and a function of ω and τ_i , where τ_i are the relaxation times. . Hence a complementary way to compare two melt states, besides the comparison of the ω_x, as explained above, is to plot G" vs G' on a log-log scale for both melts and see whether they are shifted horizontally and/or vertically, and by what respective amount. The value of G' at the cross-over, defined as G'$_x$

(also equal to G"$_x$), can also easily be found from such a plot at the intercept of the curve G" vs G' and of the straight line G"=G'. At equal T and ρ, the value of G'$_x$ should be compared for the two melts.

A convenient way to find the cross-over [2] is to plot $(G'/G^*)^2$ vs log ω, as shown in Fig. 10

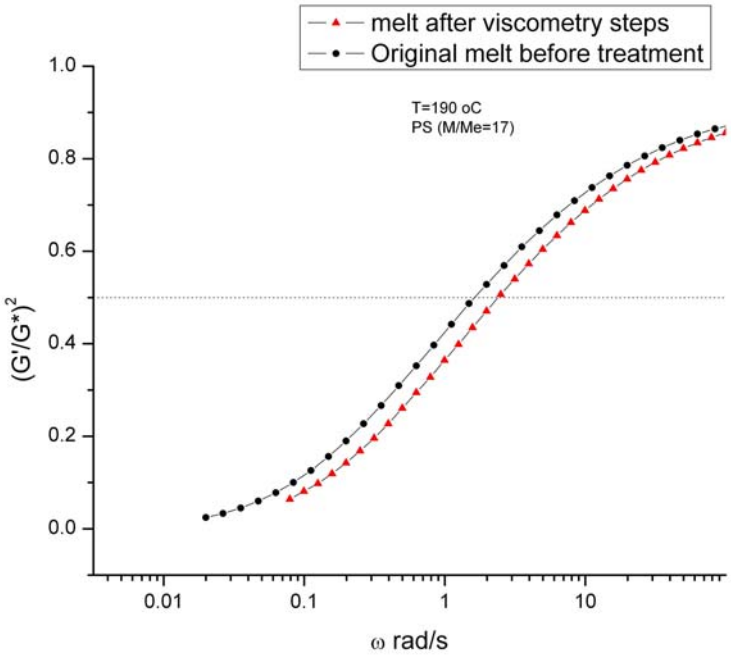

Fig. 10

Comparison of two states of a PS melt at the same temperature 190 ^oC. The un-sheared "original melt before treatment" (dots) has a lower ω_x. The "treated" melt (triangles) will be described later on. It has a higher frequency at the cross-over point.

ω_x is found for $(G'/G^*)^2 = 0.5$, so the comparison of the ω_x for two frequency sweeps is straightforward. The use of the ratio (G'/G*) offers other advantages. First, it is the stored energy per cycle, so it is a representation of the state of the bonds and of their interaction to bear stress (assuming that a totally relaxed system will not bear any stress). A second benefit for using the ratio of two moduli as a rheological parameter is to provide, at least partially, a response to certain scientists, such as Freidrich and coworkers [60,61], who assume that the decrease of modulus or viscosity with time is always due to the decrease of the area of contact at the surface between the polymer melt and the plate. While it is correct to state that pealing off the surface would decrease the area of contact being sheared and would, therefore, decrease

the modulus proportionally, it should be added that G', G" and G* would be affected in exactly the same way , which would translate mathematically to $\Delta G"(t) = \Delta G'(t)$, and the ratio (G'/G*) would remain strictly constant. This is a test that is easy to do, as illustrated in Figs 11a and 11b .

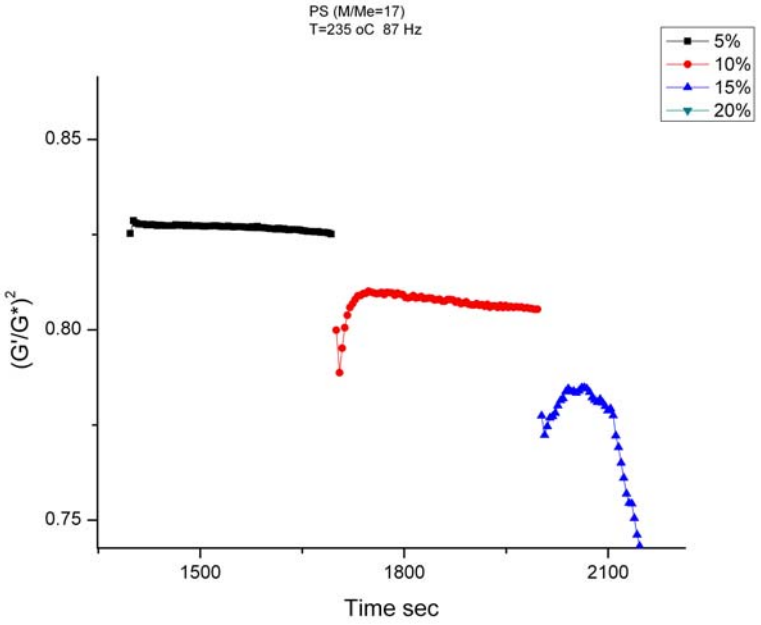

Fig. 11a

This is the same PS as in Fig. 10. The ratio (G'/G*)2 is plotted against time, as the melt is strained at various larger amplitudes 5%, 10%, 15%, 20% (the curve corresponding to 20% is not shown. The frequency of oscillation is 87 Hz. One sees that $(G'/G^*)^2$ is not constant, it can decrease or increase, following the same pattern as viscosity changes . This observation appears to contradict the argument that time dependence of moduli or viscosity is created by a surface effect [60,61].

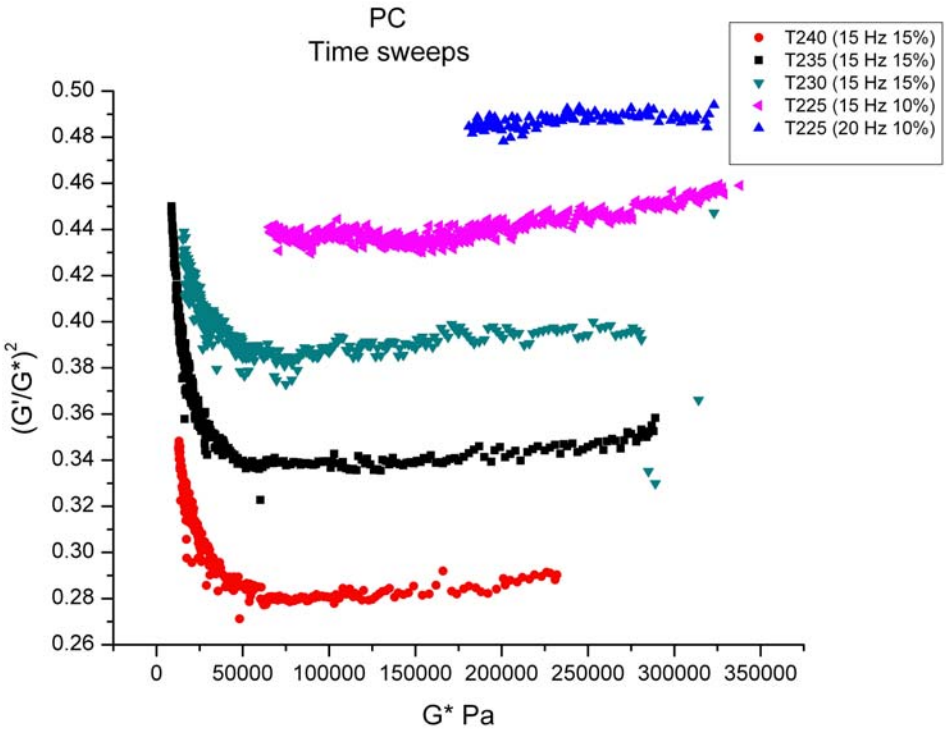

Fig. 11b

The x-axis is the complex modulus. The melt is a linear PC (M_w=32,000) submitted to time sweeps at given frequency and strain %, as indicated in the insert box. This results in the decrease of G* which becomes time dependent (in the Figure, the starting point for each temperature is the point located at the extreme right, then follow the curve leftward). One sees that $(G'/G^*)^2$ decreases a small amount as G* decreases, then increases sharply at the end of the time sweep. This is in contradiction with an interpretation based on a surface fracture to explain the time dependence of G* (and therefore of viscosity). Freidrich et al [60,61] mention the possible increase of tan δ (corresponding to a decrease of $(G'/G^*)^2$ in their experiments (on PS only), due to a bifurcation of the propagating crack inside the material, but how could such an interpretation explain an increase of the elasticity after the melt has presumably released the energy input from the oscillation?

It is true that for some polymers, e.g. PS, under certain conditions of frequency and strain during time sweeps, $(G'/G^*)^2$ remains constant, or quasi constant as G'(t) and G"(t) vary, as reported by Freidrich et al. [60,61]. This is the case for PS in Figs 3a and b. But this might be a viscoelastic property of melts, totally un-related to a surface effect; for instance, describing the re-organization of the bonds' interaction occurring internally, not at the surface, making

both G' and G" vary in a way that makes the ratio (G'/G*) constant, or appear relatively constant. We favor this interpretation and will argue why it is so later in this chapter.

Finally, the usefulness of the ratio $(G'/G^*)^2$ as a rheological parameter to characterize the state of a melt stems from its simple relationship to $\tan \delta = G''/G'$, since $\cos \delta = (G'/G^*)$ and $\cos^2 \delta = 1/(1+\tan^2 \delta)$. A plot of $\tan \delta$ vs $\log \omega$ displays a minimum, for a certain value of ω, classically viewed as the onset of the plateau of rubber elasticity, starting from the viscous end. In fact, as an empirical rule, the value of $G_{o,N}$ is taken as the value of G' at the minimum of $\tan \delta$. Because of the relationship between $\cos \delta$ and $\tan \delta$, a plot of $(G'/G^*)^2$ vs $\log \omega$ displays a maximum. The value of $(G'/G^*)^2$ at the maximum scales like $(M/M_e)^{0.8}$ according to the Marvin-Oser theory of entanglements [69]. While this relationship is empirical and applies to mono-dispersed melts, it is nevertheless another useful parameter to characterize the entanglement state of a melt, and can easily be found from plots of $(G'/G^*)^2$ vs $\log \omega$ to compare melts, in particular to know whether disentanglement occurred or not, as illustrated in Fig. 12.

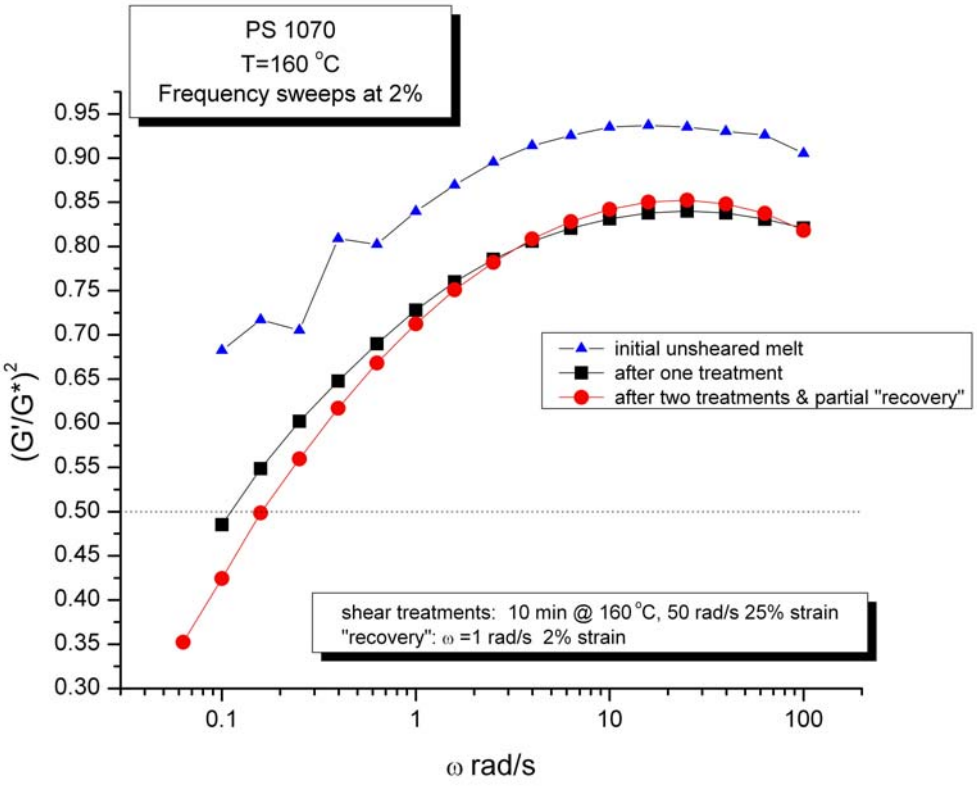

Fig. 12

Same PS as in Figs 10 and 11a. T is 160 °C. The curve at the top (triangles) corresponds to the un-sheared melt and is the Reference. The curve with squares applies to the state of the melt after it has been through a first" treatment", a time sweep of 10 min at 50 rad/s, 25% strain (the strain % is increased gradually by steps of 5% every 3 min) . The lower curve (dots) corresponds to the state of the melt after it has gone through TWO treatments and one "recovery" (time sweep at ω= 1 rad/s, 2% strain, one hour). Note the large increase of ω_x between the original curve (obtained by extrapolation) and the other two. Also, the value of ω for the maximum of $(G'/G^*)^2$ is approximately the same for all the curves, but the height at the maximum value is clearly different for the original and treated melts.

C RESULTS

1. Linear PC (Lexan 141). Time sweeps at various temperatures, frequencies, 50% strain.

The types of experiments performed correspond to Type 1A and 1B, as defined in the section on Procedure. The results were first reported in refs. [16, 43, 45]. The RDA 700 from Rheometrics was used.

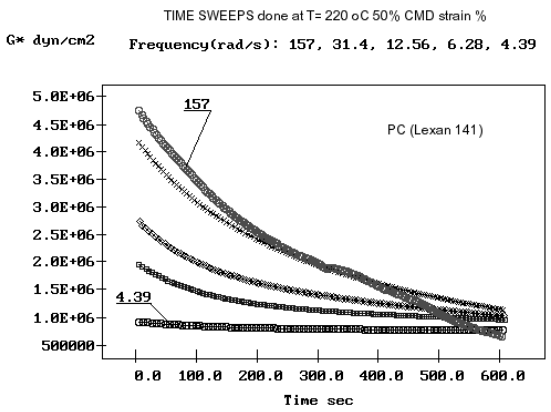

Fig. 13a

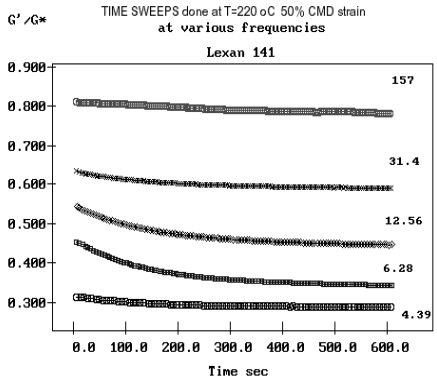

Fig. 13b

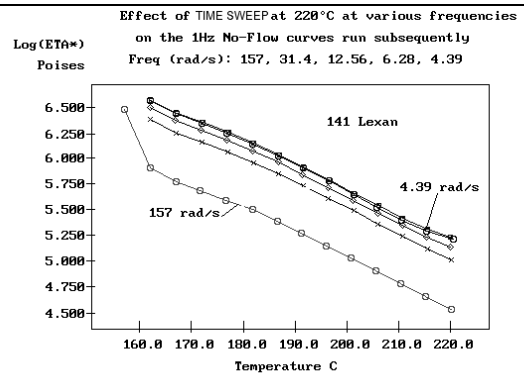

Fig. 13c

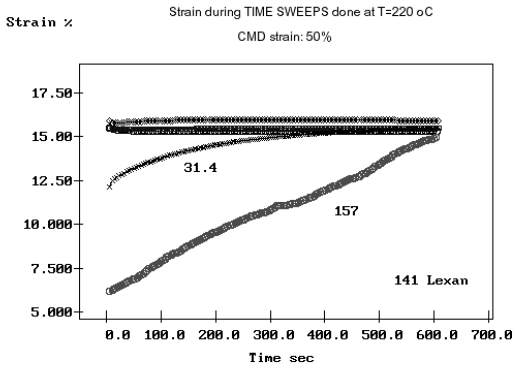

Fig. 13d

Fig. 13

Time sweeps for PC-1 at T=220 ^{o}C under various frequencies (157, 31.4, 12.56, 6.28, 3.39 rad/s) and 50% commanded strain (Figs. 13a, b, d). Fig. 13c shows the effect of time sweeps under those conditions on the No-Flow curve (temperature cooling sweep) performed afterwards (at 1 Hz, 5% strain).

Fig. 13a shows that as soon as the time sweep started, at a given temperature (here T=220 ^{o}C), frequency (157, 31.4, 12.56, 6.28 or 4.39 rad/s) and 50% strain, a transient behavior was observed, the complex modulus G* (and thus viscosity, G*/ω) decaying in time from an initial value (increasing with frequency) towards a value that looks like a steady state value, that is function of strain and temperature. The transient kinetics is a strong function of ω, the steady state being reached faster at higher frequency. The dynamic modulus G* is "pumped-up" by

the sudden application of an oscillation at 50% amplitude, more so as ω is increased. For example, in Fig. 13a, the start up G* varies from 0.01 MPa to 0.05 MPa (a 5 fold increase) when ω varies from 4.39 rad/s to 157 rad/s. The initial value of G* divided by frequency is the initial dynamic viscosity that decreases as ω increases, illustrating that the initial state is controlled by shear-thinning.

Figure 13b is a plot of (G'/G*) vs time for the same various frequencies during the time sweep. One sees that the stored energy increases as frequency increases, but slowly decreases as G*(t) decays. The apparently stronger relative decrease of (G'/G*) for ω=12.56 and ω=6.28 rad/s is actually due to the inability of the RDA700 temperature controller to maintain temperature strictly constant at the high strain amplitude applied (50%). Once the effect on the modulus of the small temperature rise is taken into account, the corrected variation of (G'/G*) becomes minimal at lower frequencies. The reason why the high frequency ω= 157 rad/s does not seem to show an even stronger effect of temperature rise due to forced oscillation at high amplitude is explained by Fig. 13d. The RDA700 is unable to keep the strain equal to the value of the commanded strain, 50%, even at the lower frequencies where 15.7% strain is reached and remains constant. At higher frequency, see ω=31.4 rad/s and worse ω=157 rad/s in Fig. 13d, the strain is not constant and continues to gradually ramp up during time sweep, from 5% to 15.7% at T=220 ^{o}C. This is due to limitations imposed by the maximum torque permitted by the RDA700. Because of the strain ramp up, the temperature rise was non-existent, explaining the result. In the case of ω=157 rad/s the decay of (G'/G*) is clearly visible and not due to temperature rise. Modern instruments are not plagued by the same problems as the RDA700, and are capable of maintaining temperature strictly constant (by better convective cooling inside the rheological chamber). Much higher torques are also provided in the new versions of rheological instruments now commercially available.

Figure 13b shows that the modulus increased with frequency at the start-up of Fig.13a is in accord with an increase of the stored elastic energy, G'/G*, from 0.3 to 0.8 (a 2.7 times . increase), which explains shear-thinning [66, 70]. Also notice that for T=220 ^{o}C and ω =157, the value of (G'/G*) is above the value of the cross-over (0.707), and, noticeably, this is for this frequency that we observe the strongest decay of G*(t) in Fig. 13a and the strongest departure of the No-Flow curve in Fig. 13c, which is discussed in the next paragraph.

Despite the experimental difficulties of keeping temperature and strain constant, which required careful corrections during analysis, the RDA700 was capable of providing evidence for the first time that time sweep treatments, operated under dynamic conditions that rendered the moduli transient, could give rise to new states of a melt; in other words that melts could be made rheologically unstable (in the same sense that a glass can be brought out of equilibrium). This is shown in Fig. 13c. This graph corresponds to a Type 1B experiment described earlier. It plots the complex viscosity against temperature for a temperature ramp down (at cooling rate -1 ^{o}C/min) under oscillation at 1 Hz (6.28 rad/s), 5% strain, done right after the 10 min of time sweep "treatment" (such a procedure is called "a no-flow curve" and is routinely done by scientists performing Mold-Flow simulations) . The purpose was to reveal the state of the melt after its treatment by comparing the No-Flow curves between a Reference melt, not submitted to any time sweep treatment, and a treated melt, submitted to a time sweep at given temperature, frequency and 50% commanded strain. It is clear from Fig. 13c that the No-Flow curves are different, depending on the frequency chosen during time sweep. The top No-Flow curves of Fig. 13c, obtained for the lowest ω during time sweep, are identical to the Reference, but the No-Flow curve obtained for a treatment at ω=157 rad/s is definitely lower, indicating a lower viscosity melt [16, 43, 66]. Many tests were conducted to study the effect of temperature of the time sweeps, their duration, the grade of the polymer, the gap thickness, and the strain %. Each of these variables play a significant role in determining the success of modifying the state of the melt, as indicated by the No-Flow curves that revealed the difference. The details of these experiments are reviewed elsewhere [45].

2. Viscosimetric experiments on LLDPE

2,1 Pure Rotation. Experiment of Type 4.

The rheometer used was an ARES, operated with a parallel plate geometry according to the Type 4 experiment described in the Procedure section. The sample was LLDPE. Temperature was measured during a run to check that it remained constant. N_2 was flowing in the rheometer, and a separate TGA showed that the sample was totally chemically stable at

these temperatures for more than 1 hour, i.e. the observations made in the figures to follow were not due to, or influenced by, degradation. In Fig. 14, a given strain rate (given in the graph insert) was "instantaneously" imposed on the melt and held constant for about 30 min. The strain rate was chosen to be in the vicinity of the reptation time calculated from the cross-over time ($1/\omega_x$) times the ratio of (M/Me), which turned out to be between 2 to 3 sec. The melt jumped to a certain stress (left box) and normal force (right box) level, and these started to decay in time towards a steady state value which was barely a function of the strain rate imposed. The initial value of the stress and normal force, as well as the relaxation times, strongly depended on the strain rate, as can be seen in Fig. 14. The top curve, corresponding to a strain rate of 1 sec^{-1}, was already presented in Figs. 2a and b.

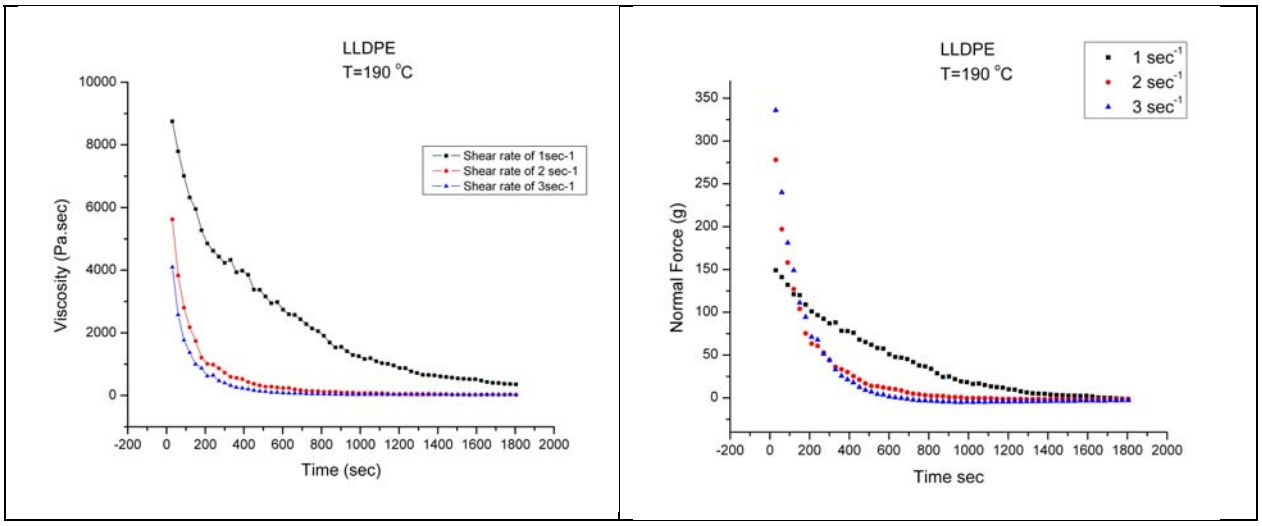

Fig. 14

Viscosity vs time (left) and Normal Force vs time (right) for pure viscometry at constant strain rate. The melt is LLDPE at T=190 °C. The rates are indicated in the inserts.

Notice the presence of a little hump at ~400 sec in the viscosity/stress-time curve corresponding to 1 sec^{-1}(this hump does not exist on the normal force decay curve). It is also visible for the 2 sec curve, but not for the 3 sec^{-1} strain rate. This feature, which we hardly notice in the case of Fig. 14 but is more visible for other conditions presented later, is almost always visible for melts for a certain range of strain rates. It might reveal the influence of the stress on the relaxation times, at least the first relaxation time, initially accelerating the

relaxation decay, and, thereafter, slowing it down (even to the point of a local reversal, see later) as the total stress itself decreases and no longer accelerates the decay of the first exponential term (in a mathematical sense, the potential barrier is lowered by stress which itself decays with time). The relationship between stress and normal force is analyzed in Fig. 15 , expanding further on the influence of stress on the relaxation time.

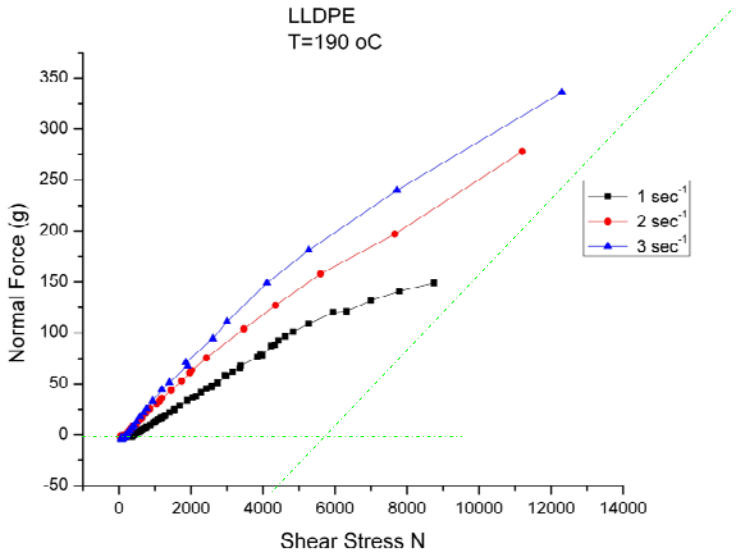

Fig. 15
Normal Force vs Shear Stress for the data of Fig. 14

Figure 15 eliminates time and cross-plots normal force vs shear stress measured during the transient stage that consists of a continuous decay of both shear stress and normal force. The 3 curves were obtained at 3 strain rates, 1, 2 and 3 sec^{-1}. The starting point to follow the evolution is on the upper right of each curve, the uppermost point corresponding to the shortest time. . One can extrapolate the curves of Fig. 14 to obtain the initial value of the viscosity, and thus of the stress, at t = 0. One can draw a line, shown as the tilted dotted line in Fig. 15, passing through these t = 0 points extrapolated for the 3 strain rates shown in Fig. 14. This line cuts the zero normal force x-axis at a stress of ~5,700 N. For any strain rate below 1 sec^{-1} , which is the lowest curve in Fig. 15, the t=0 point would be moving down on the dotted line; eventually we would reach the Newtonian value (corresponding to strain rate→0), and, in such

a case, there would be no normal force, and no time dependence, so the shear stress should vary along the horizontal dashed line in the Newtonian regime. In other words, the cross-over-point between the two dash-lines is the beginning of non-linearity, the start of non-Newtonian flow for higher stress. This is the point where the elastic contributions from the deformed melt start to come into play. Figure 15 suggests a shear stress criteria for the onset of transient behavior, rather than a strain rate criteria as advocated by others [8, 9].

Notice the initial pronounced curvature in Fig. 15 for plots of normal force vs shear stress, followed by subsequent apparent linearity between these two parameters. In the initial stage (upper right), the curve is "flatter", i.e., after the establishment of the rotation the shear stress variation was larger than the normal force change, whereas in a subsequent stage it appears to vary more linearly with normal force. This behavior is clearly seen for the lowest curve of Fig. 15, but also for the other two curves, although linearity is confined to the lower region and a log-log plot (not shown) would be more appropriate. The point raised by these observations regards the influence of stress on the relaxation times, as already mentioned for Fig. 14. Stress decay and normal force decay do not appear to decay in phase in the non-linear region, at the initiation of the deformation, the decay of normal force being simpler (one relaxation exponential decay instead of two, for instance). It could be that the transient stress decay starts to phase-in with the normal stress decay (where the two parameters would be linearly related) only after an extra relaxation term, only present in the decay of stress, has relaxed (its relaxation time being a function of stress), in a recursive way. In terms of an activated process to describe deformation, one term for the stress is created by a *pro-active* change of the conformation statistics of the conformers as a response to deformation; this defines the potential energy of isomeric rotation, which is plasticized by the *total* stress, creating the recursive process. As the stress rises, at the onset of the transient relaxation, the relaxation time is as small as it will ever be, since the stress is at its maximum. When the *total* stress relaxes, due to an orientation mechanism, the pro-active stress decay is slowed down, providing the hump seen in Fig. 14, already mentioned, and the strong non-linearity between stress and normal force at the beginning of the transient stage in Fig. 15. This interpretation also explains the effect of strain rate on the viscosity transient kinetics (Fig. 14), since a faster strain rate produces a larger stress, decreasing the relaxation times. The normal force does not

have this pro-active term, because the mechanism that generates it is the same as that which produces the *second* term of the total stress, the orientation of the conformers allowing relaxation of the deformed conformers statistics by diffusion. When the pro-active term of the stress has decayed, stress and normal force are in-phase and their time dependence is described by the same relaxation times. This corresponds to the linear (lower left) portion of Fig. 15.

Figures 16 (a) and (b) are similar to Fig. 14, but add two more strain rates, 0.1 sec^{-1} and 3.58 sec^{-1}, two of the other curves being reproduced as references. There are two interesting pieces of information:

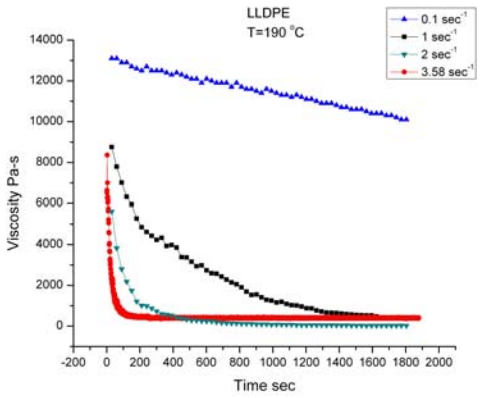

(a)

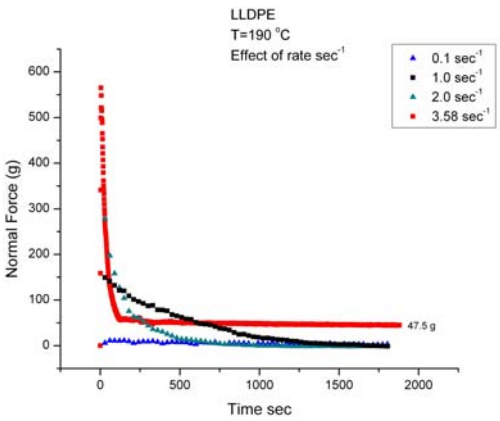

(b)

Fig. 16

Viscosity (a) and Normal Force (b) vs time for pure viscometry at constant strain rate (indicated in inserts) at T= 190 °C. LLDPE.

First, transient behavior is observed at all shear rates, even for 0.1 sec^{-1}, for which the normal force remains close to zero. This plot confirms the decrease of relaxation time with increasing imposed strain rate discussed previously. The steady state would be reached after an extremely long time for the 0.1 sec^{-1} strain rate and in less than 50 sec for the 3.58 sec^{-1} rate. Second, the value of the steady state viscosity and of the steady state normal force seem to be raised for the largest strain rate, 3.58 sec^{-1}. Such a behavior corresponds to shear-thickening of

the melt and is unexpected in pure shear. Note in Fig. 16b that normal force is also raised to a steady value of 47.5 g (4.75 N) corresponding to a normal pressure of 9,677 Pa.

Figures 17 to 28 expose well, in our opinion, the remaining challenges of rheology, in particular with respect to melt entanglement stability, and the nature of entanglements. The following examples apply to LLDPE, but similar results were obtained (not shown) with a (M/M_e=17) PS grade, and the results are thought to be general.

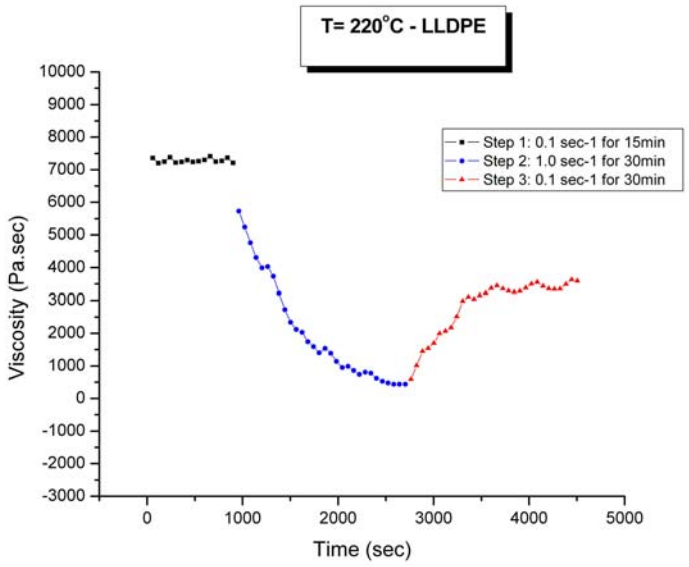

Fig. 17

Viscosity vs time for 3 successive Type 4 experiments conducted with the same melt. The successive strain rates and their time of application are written in the inset. The melt was LLDPE at T=220 ^{o}C.

Figure 17 shows the results of 3 successive type 4 experiments for LLDPE. The LLDPE melt was here at 220 ^{o}C. Initial viscosity, measured at strain rate 0.1 sec^{-1} , was quite stable for at least 15 min, a sign that it was the steady state value: 7,400 Pa-s. The viscosity became time dependent for a strain rate change from 0.1 to 1 (also note that, after extrapolation, viscosities match at the transition between the 2 rates). The viscosity decrease corresponds to a transient behavior that lasted 30 min. As the melt was reaching its new steady state value for the new strain rate (the step 2 curve shows that it had not fully stabilized, but that it was very close), the strain rate was then reversed back to 0.1 sec^{-1}, where one would expect the melt viscosity to

return to the initial viscosity of 7,400 Pa-s. Instead, it evolved, through a transient recovery behavior, to only 3,500 Pa-s.

The question is: was the initial viscosity of 7,400 Pa-s a steady state value or was steady state, instead, the value given by the plateau on the step 3 curve? If the initial viscosity at 0.1 sec^{-1} was a non-equilibrium viscosity, what makes it so stable for 15 min that one has the impression that it was a steady state viscosity? When does one know if viscosity is the steady state one or not? After all, at a lower temperature, 190 ^{o}C in Fig. 16, it was shown that a strain rate of 0.1 sec^{-1} resulted in a transient decay. Should we not expect a faster decay at a higher temperature? What is the origin of the transient decay?

The polymer melt was polyethylene; it was linear, without long branches, its entanglement density was 170 (M/Me), it had no polarity, it was at a temperature 216 ^{o}C above its solidification temperature (37 ^{o}C; crystals are unlikely to be present). It is one of the most simple polymer macromolecules that one could think of, and yet, a simple experiment such as the one presented here, and in the following figures, seems to be a challenge to traditional views regarding the understanding of what causes this behavior. If entanglements are responsible for the transient behavior, what do these results teach us about the meaning of what entanglements really are? The following figures deepens the level of our questioning of classical rheology.

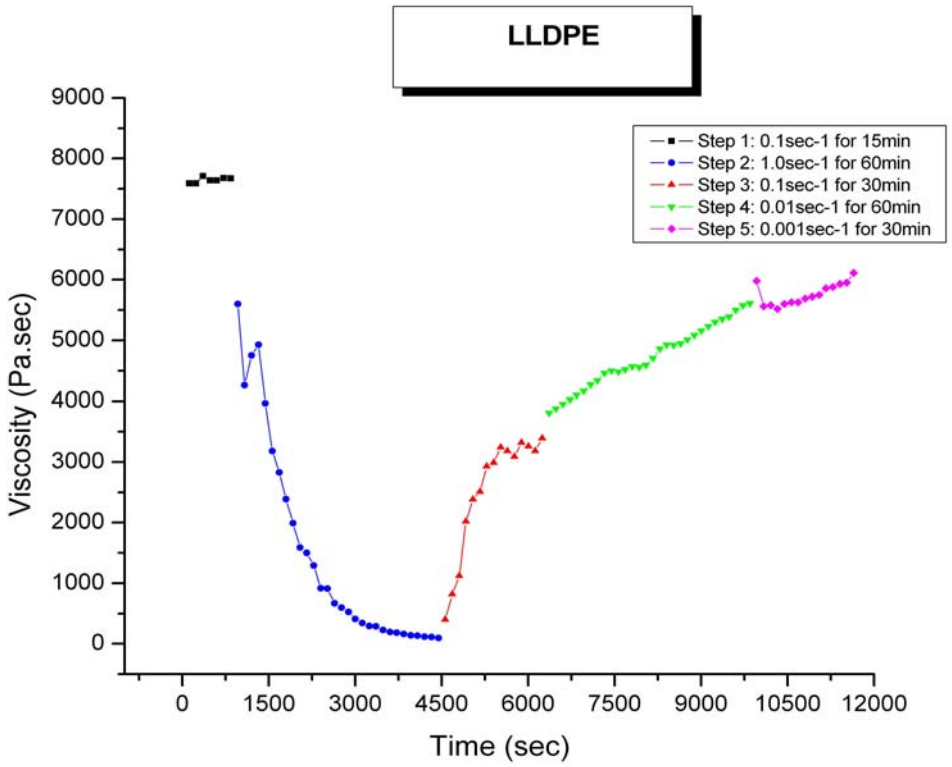

Fig. 18

Viscosity vs time for a series of constant strain rate segments performed sequentially (the rate is indicated in the insert).

The insert in Fig. 18 describes the sequence of strain rate jumps. Notice that, contrary to Fig. 17, the "junctions" of viscosity at the various shear rate jumps are not perfect. (This point, though, once said, is considered insignificant in comparison to the other comments to follow). Also notice the presence of the little hump in the step 2 curve (for 1 sec^{-1}), even more pronounced than in Fig. 14. Finally, and most importantly, the step 3 (0.1 sec^{-1}), step 4 (0.01 sec^{-1}) and step 5 (0.001 sec^{-1}) curves created a continuous tendency towards a return to the initial value of 7,400 Pa-s, the starting value for the 0.1 sec^{-1} strain rate. Since strain rate continued to decrease from step to step in each recovery section, the final extrapolated value of viscosity must correspond to the Newtonian value at that temperature.

Now there are two assumptions one can make:

1. the value of 3,500 Pa-s, observed for the plateau on recovery at rate 0.1 sec^{-1}, in Fig. 17 must be a shear-thinned value for that strain rate at that temperature. The fact that

initially, in Fig. 17, the initial melt responded to a strain rate of 0.1 sec^{-1} by providing the Newtonian value and not the shear-thinned value for that rate indicates metastability of the initial state, i.e. a phenomenon reminiscent of glasses in a state of thermodynamic instability with respect to their phase transition, such as water which can be frozen below the freezing temperature to become metastable, in a frozen glassy state with no crystals, or glassy polymer produced by quenching through Tg (see Kovacs's work in Ref. [71}).

2. A second conclusion would challenge the first one. Suppose that the initial viscosity at the rate 0.1 sec^{-1} *is* the real Newtonian value, but that, as the melt has been deformed at a rate faster than the reptation time for a duration long enough, a DIFFERENT MELT is produced, with different bond-interaction characteristics (let's call it a different entanglement state), then the application of the 0.1 sec^{-1} shear strain rate to THAT new melt would result in a new steady state viscosity value (3,500 Pa-s).

Thus, based on the second conclusion, a melt can have several steady states at the same temperature and strain rate, depending on its state of entanglement, and it appears that shear can modify the entanglement state at will: this is the basis of “shear-refinement”. If entanglements can be kept in an unstable state long enough, it is possible to produce "disentangled polymers" that, in terms of viscosity decrease are attractive commercial “grades”. The challenging question is how to retain in a metastable state (that we could control) the lower viscosity melt produced at the end of a transient "treatment' and then recover the original properties after processing.

Another conclusion seems to emerge from these experiments: shear-thinning might just become time dependent, under certain strain rate conditions. In other words, what ever causes shear-thinning produces a melt state that is not stable under certain conditions. The transient behavior observed would be the reflection of that time dependence of shear-thinning, and the molecular motions involved in shear-thinning and in the transient decay might be closely related, if not identical.

Figure 19, shows the effect of annealing the melt in the middle of a transient decay to see if the melt would reconstruct its internal structure to provide the original viscosity after

annealing. The shear rate history shown in the box of Fig. 19a was applied to the melt (the temperature was 215 ^{o}C). The difference with Fig. 17 is that the melt was rested (un-sheared) for 30 minutes, at the end of the transient decay induced by shear rate 1 sec^{-1}. Then the melt was sheared with rate 0.1 sec^{-1}. Figure 19b shows the variation of viscosity with time, Fig. 19c shows the variation of normal force, and Fig. 19d presents details of (c) around the zero normal force line. It is clear (Fig. 19b) that the melt nearly re-gained its original viscosity after the time of rest when no mechanical deformation was applied. This is evidence that the equilibrium state for strain rate 0.1 sec^{-1} was the original viscosity. The normal force was almost zero for the initial strain rate (Fig. 19c, left curve), went up and decayed when the strain rate was changed to 1 sec^{-1}, and was zero for the second application of 0.1 sec^{-1} strain rate. Zooming on the zero line region of box (c) shows that normal force decay during transient behavior actually converged to a small negative value (step 2 curve), but that after annealing (step 4 curve), the normal force had returned to zero

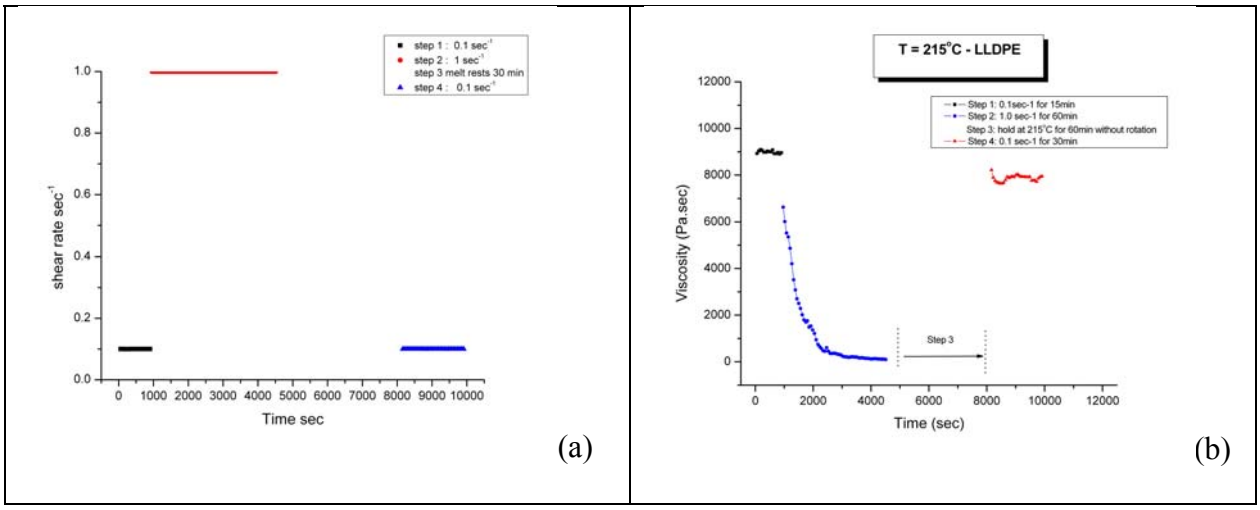

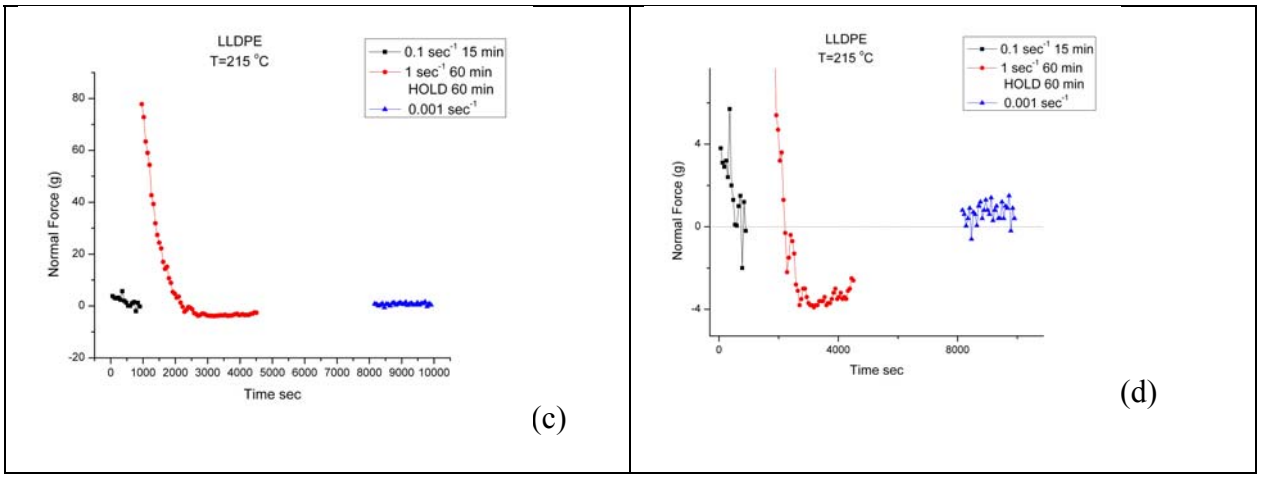

Fig. 19

Same type of experiments as in Fig. 18 but with a different mechanical history. T is here 215 °C. See text for details

To check whether the small tensile force on the melt in steady state conditions (Fig. 19d step 2 curve) was also observed for the strain rates of Fig. 18, Fig. 20 shows the variation of the normal force with time, confirming that the steady state melt obtained after application of the 1 sec^{-1} strain rate was, indeed, under a small tension. Switching the strain rate to a lower value released the tension towards zero. The phenomenon seems real, repeatable and requires an explanation (see discussion).

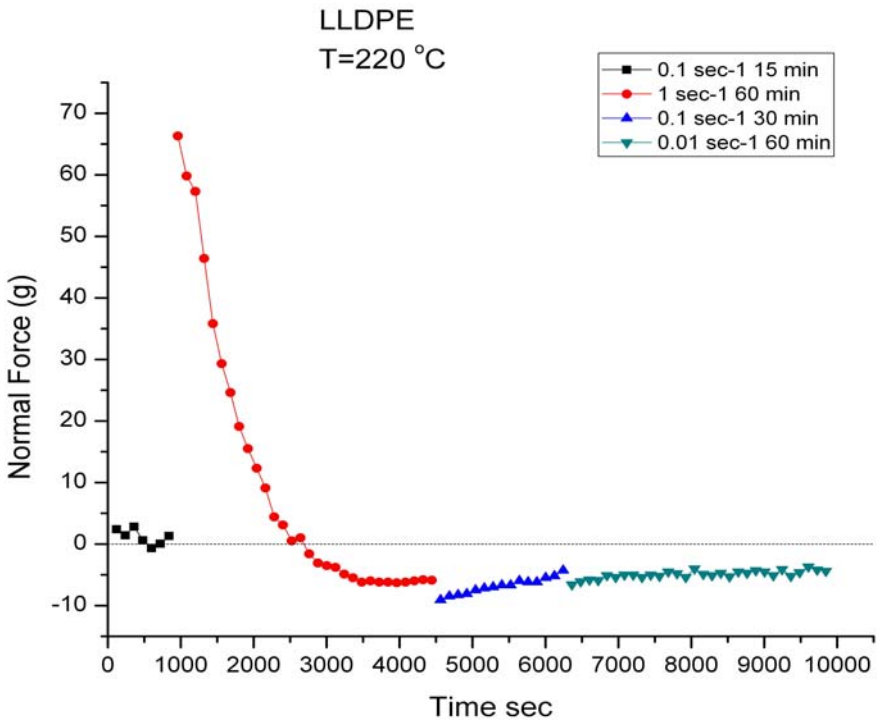

Fig. 20

This normal force vs time history applies to the deformation described in Fig. 18.A close-up view shows a small attractive normal force in the melt (~ - 5g) obtained in the steady state for the 1 sec^{-1} strain rate (step 2 curve). At each "instantaneous" step strain rate decrease (step 3 and 4 curves) a small initial negative jump of the normal force occured before normal force relaxed back towards zero. Each change of strain rate resulted in another small elastic tension of the melt.

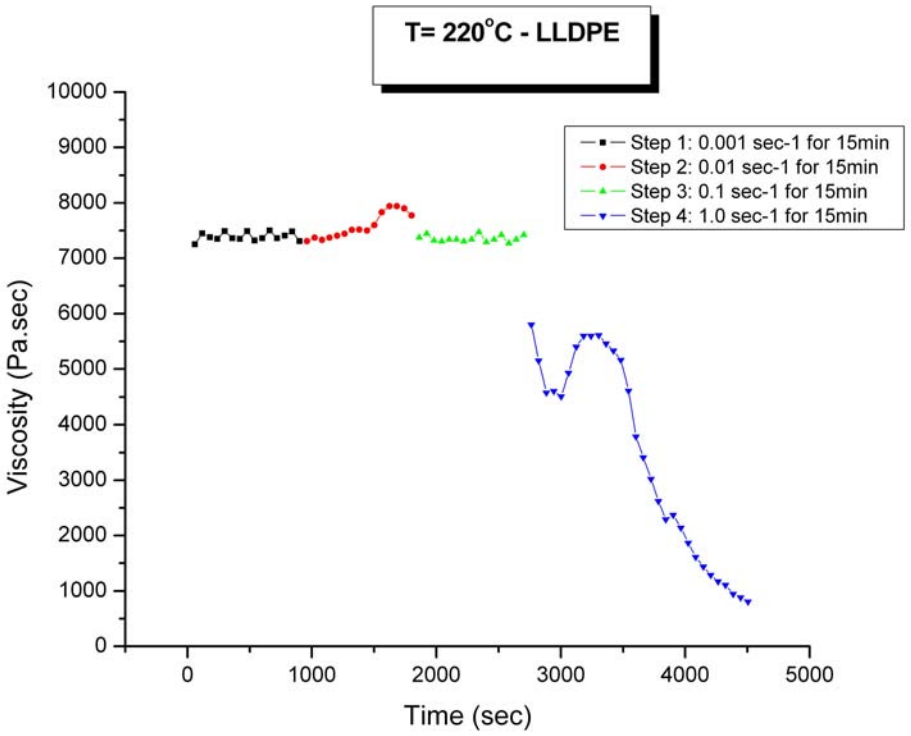

Fig. 21

Same type of experiments as in Fig. 18. The successive strain rates are indicated in the insert. T = 220 ^{o}C

Figure 21 is another exhibition of the difficulty of using classical rheological tools (and the classical understanding of the concept of entanglements) to characterize simple rheological experiments. In this set of conditions, very similar to those of Fig. 17, the melt was deformed first at very low strain rate, at 0.001 sec^{-1}, and then at 0.01 sec^{-1}, both for 15 min, before the initial conditions set in Fig. 17 were reached (0.1 sec^{-1} for 15 min followed by 1 sec^{-1}). The longer stay at 220 ^{o}C at very low shear rate magnifies the hump discussed earlier to the extent that it now looks like a true partial recovery of the viscosity at one point. After the instantaneous drop of viscosity due to shear-thinning, at the switch of rate between 0.1 and 1, the melt viscosity droped sharply at first, then hesitated between increasing or decreasing, with decreasing finally prevailing. The hump was no longer barely visible, it was a full feature of the melt's rheological behavior (incidentally, another small hump is also visible in step 2).

2,2 Pure Rotation followed by Frequency Sweep. Experiments of Type 5.

Figure 22 shows the result of an experiment of type 5, a viscometry at two shear rates followed by a frequency sweep to characterize the state of the melt at the end. The strain rate at 0.1 sec^{-1} was performed as a first step to establish a baseline for "the un-sheared melt" and compare with the viscosity obtained from the frequency sweep under similar conditions. Figure 22a shows the viscosity vs time history, including the viscosity during the frequency sweep. The viscosity was slightly transient in step 1, but the transient decay was much more pronounced for step 2. Notice that we waited 4,500 sec before triggering the frequency sweep, i.e. we waited for steady state to be well established under these strain rate and temperature conditions (215 ^{o}C and 1 sec^{-1}). Figures 22 b,c and d compare frequency sweeps for the "un-sheared melt" (the melt *before* it was submitted to viscometry at 1 sec^{-1} strain rate), and the melt *after* it had reached steady state, which we call "sheared" in these graphs. Frequency sweeps were done for both melts in the linear viscoelastic range (2% strain). Graph 22b compares the complex moduli. Graph 22c plots G' and G" vs ω for both the un-sheared (top) and sheared melts. Graph 22d refers to $(G'/G^*)^2$ vs log ω, showing identical stored elasticity up to the cross-over point $(G'/G^*)^2=0.5$), but a more elastic sheared-melt at higher frequencies, which might be surprising in view of the fact that both moduli G'(ω) and G"(ω) (Fig. 22c) were substantially reduced for the sheared melt.

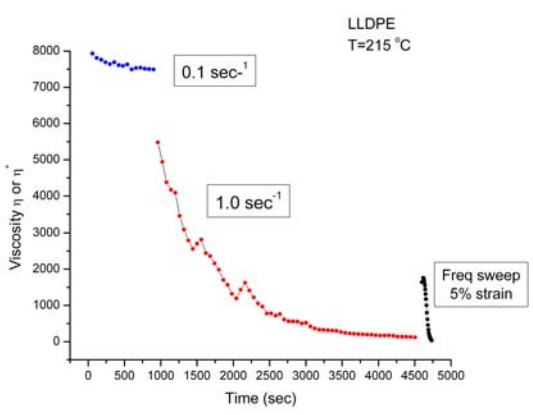

(a)

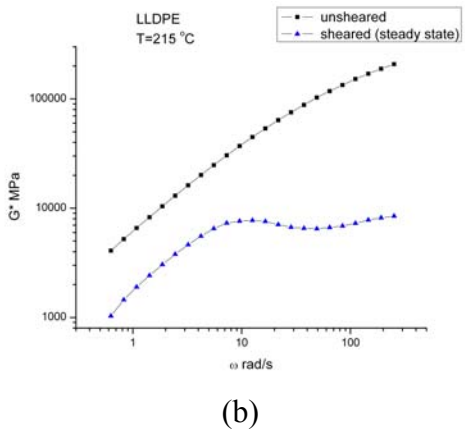

(b)

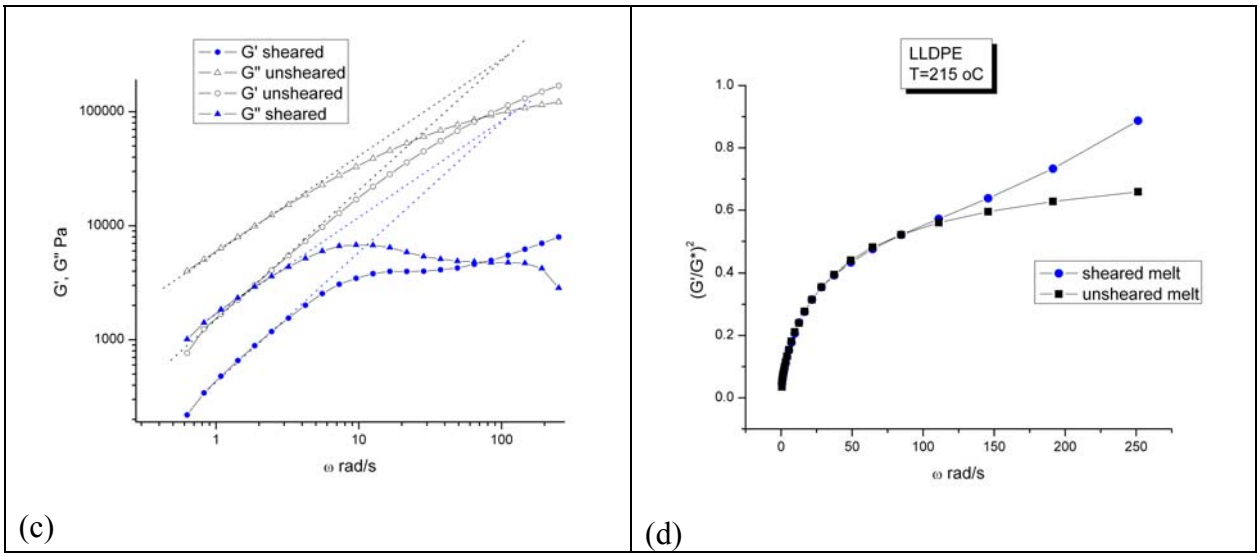

Fig. 22

The graphs apply to an experiment of type 5, pure viscometry at constant rate immediately followed by a frequency sweep in the linear viscoelastic range. See text for details

In Fig. 22b, for the un-sheared melt, the extrapolated value of G* was 800 Pa for ω = 0.1 rad/s giving a complex viscosity of 8,000 Pa-s, agreeing with what we obtained in pure viscometry (top left in Fig. 22a). However, for ω= 1 rad/s the value of G* was 6,000 Pa (giving a viscosity of 6,000 Pa-s), which was the initial value obtained for strain rate 1 sec^{-1} in pure viscometry (explaining the initial instantaneous decrease of viscosity in Fig. 22a at the change of rate between 0.1 and 1 sec^{-1}). However, a big difference between pure viscometry and dynamic viscosity measurement is that there is no transient, no time dependence, created by the oscillation at this small strain (2%), and, therefore, we were unable to obtain the equivalent of the steady state viscosity value arrived at under strain rate 1 sec^{-1} (i.e. 354 Pa-s). We will show below (Figs. 27, 28), for this same polymer melt, that it waspossible to create a transient viscosity in pure oscillating conditions, by just increasing the strain % amplitude and the frequency at which we operated.

Figure 22c shows that the magnitude of the modulus at the cross-over was18 times smaller for the sheared melt; the shape of the G'(ω) and G"(ω) were also very different (Fig. 22c), yet the cross-over point seems to be the same, ~ 71 rad/s (Figs. 22c and d). In Fig. 22c we attempted to

determine the Maxwell's time ($1/\omega_o$) for both the sheared and un-sheared melts. It is not certain that this procedure makes any sense at all, since the respective slopes of G' vs ω and G" vs ω were not 2 and 1, as they should be according to the Maxwell's model. Nevertheless, it is seen that the extrapolated cross-over-points are the same for both the sheared and un-sheared melts and about 2 times the cross-over value ω_x. This result questions the use of the cross-over point to depict the melt characteristics. One might argue that artifacts, such as slip or surface fracture might have occurred in the case of the sheared melt during transient viscometry (Fig. 22a, step 2 curve). Figure 22d suggests otherwise. Although $(G'/G^*)^2$ remained the same for both sheared and un-sheared melt at low ω, which could go along with a surface effect explanation, the fact that at higher ω the ratio $(G'/G^*)^2$ was greater for the sheared melt (the round dots) is a remarkable proof that there was something rheological going on, and that it cannot be due to a surface or a slip effect (which would maintain the ratio $(G'/G^*)^2$ constant, not increase it). Actually, the upturn of $(G'/G^*)^2$ at high ω implies a more pseudo-plastic melt (it shear-thins more), which is also demonstrated in Fig. 22b by G* becoming nearly constant for the sheared-melt beyond ω ~ 10 ra/s whereas the modulus of the un-sheared melt continues to rise with ω (viscosity is G*/ω).

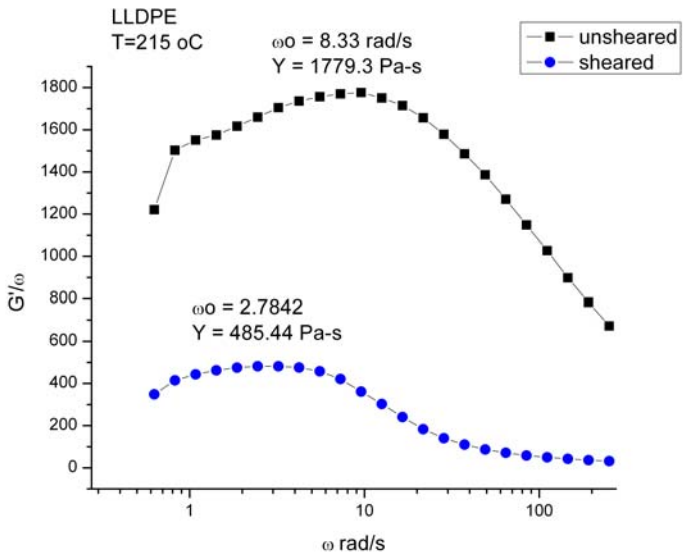

Fig. 23

G'/ω vs ω for the sheared and unsheared LLDPE melt at T=215 °C. The unsheared melt is the "normal" frequency sweep for a melt without prior shear history. The sheared melt is that described in Fig. 22a, prior to the subsequent frequency sweep.

Fig. 23 is a classical plot of (G'/ω) vs ω for the samples in Fig. 22. For a "normal" melt, i.e. responding at low ω according to the Maxwell's equations (see discussion on this subject in [2]) the value of ω at the maximum of G'/ω should be the inverse of the terminal time ($\omega_o=1/\tau_o$), the same as that which is found at the cross-over. It is expected that the sheared melt would have a higher ω_o (a smaller terminal time) than the un-sheared melt, since its viscosity is much lower, but we find the opposite, ω_o for the sheared melt is 3 times lower than that of the un-sheared one. Also, the value found for ω_o, from the maximum of G'/ω, does not agree with the value found from extrapolation of the slopes of G' and G" in Fig. 22c, nor with ω_x. The plot in Fig. 23 does not make any sense, or, perhaps, it illustrates the limitations of the traditional approach when analyzing melts which have been submitted to non-linear mechanical histories. Yet, one can hardly describe the sheared melt of Fig. 23 as a special non-linear melt, since it was just sheared at 1 sec^{-1} for a long time in order to reach its steady state. A GPC measurement conducted on the resin frozen from the steady state did not reveal any apparent difference in molecular weight or its distribution with the original melt. The conclusion seems to point towards the formation of a differently structured melt, presenting different rheological properties.

2,3 Experiments of Type 4 on Melts with Prior Mechanical History.

We have previously reported extensively that shear-refinement modifies the rheological properties of melts [28-54]. Obviously, when one has succeeded preserving in a pellet form the viscosity drop observed during shear-refinement processing, one can mold disks from the treated pellets and perform a type 4 (pure viscometry) experiment and compare the results obtained with those from a reference melt. This is done in Fig. 24. Alternatively, the treated melt (from compression-molded treated pellets), which we designate "mechanically disentangled" in the following figures, can be analyzed by a simple frequency sweep done in the linear region, so that there is no possibility of any artifact or rheological effect due to the application of larger strain. The frequency sweep of such a disentangled melt is compared with that of a virgin melt in Fig. 25, studied under identical conditions.

Figure 24 compares the transient behavior obtained in pure viscometry (T=190 ^oC 1 sec^{-1}) for an un-sheared melt (round dots) and a pre-sheared melt corresponding to a disentanglement treatment (squares). The resin is the same LLDPE as before. It is clear from

this figure that there was no transient decay for the disentangled sample. The viscosity "hesitated" between decaying and rising. This phenomenon of oscillation is the result of the recursive character of the effect of stress on the relaxation times, as discussed in previous sections. When stress decreases, activation energy increases, slowing down the process of decay. When a melt is successfully brought out of equilibrium, such as in the case of a disentangled melt made out of treated pellets, the relaxation time spectrum is modified (their stress dependence of the activation energies is not the same), the dynamics of deformation is disturbed, and, as in Fig. 24, melt viscosity appears to remain steady at its low value, as if the new entanglement state was quasi-stable. This quasi-stability of the melt is due to a balance between two opposite drives, one leading to a time dependent shear-thinning transient controlled by the melt elasticity, and the other by the kinetics of return to a thermodynamics equilibrium state of the interactions between the conformers. The treatment defines the out of equilibrium initial conditions that governs the kinetics of “re-entanglement”, as well as the rheological properties of the treated melt, under linear viscoelastic testing mode.

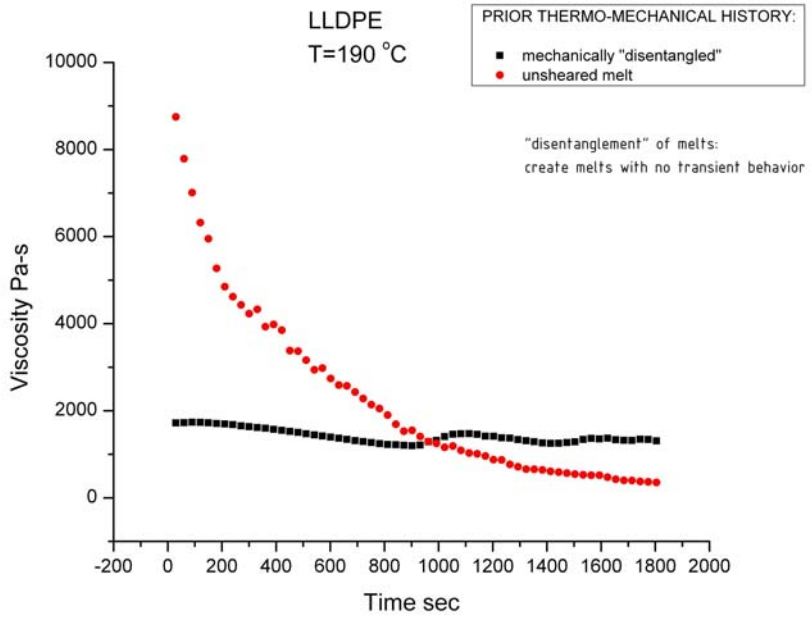

Fig. 24

Comparison of viscosity vs time for a mechanically disentangled melt (with the apparatus of Fig. 5b) and a virgin (unsheared) melt with no prior shear history. The same testing conditions (strain rate, temperature) are used for the two samples.

It is crucial to understand the stability of a disentangled melt from a theoretical point of view, not simply because it will reveal the true nature of entanglement, but also for commercial perspectives, in order to put shear-refinement benefits under control. The understanding of the stability of disentangled melt refers to the stress and temperature conditions that result in its return to equilibrium, and the prediction of its induction time, i.e. how long it can remain at a low viscosity before returning to equilibrium. An example of re-entanglement triggered by prolonged shear is given in Fig. 25:

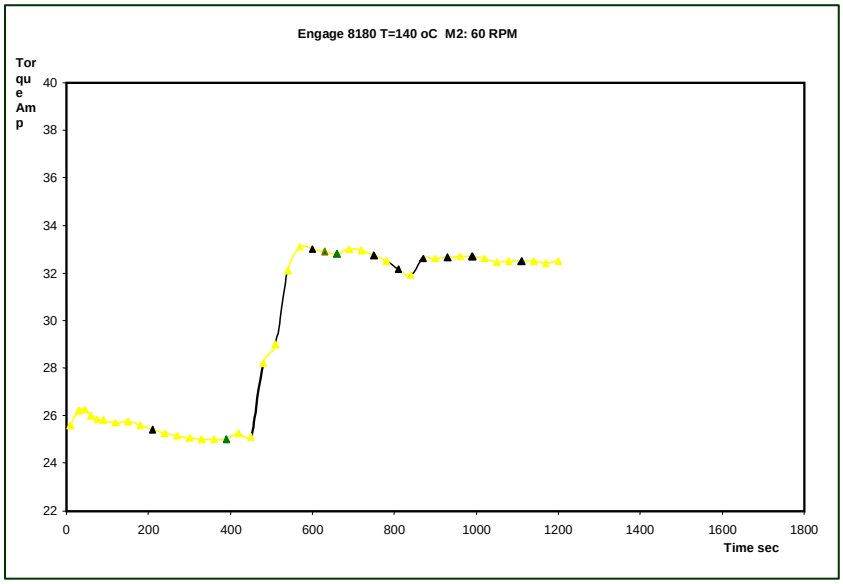

Fig. 25

A shear-refined LLDPE was sheared at 60 RPM, T=140°C. The torque (in Amp) was stable at the low initial value of 26-25 Amp for 500 sec, then, without any change of any input (RPM, temperature), it suddenly rose to another value, 34 Amp, which is the reference torque at that temperature. The shearing conditions (60 RPM, T= 140 °C) are associated with the induction time to trigger recovery of a more stable melt (other conditions would result in a different induction time).

The 4 times initial viscosity difference seen in Fig. 24 between reference and disentangled samples is not simply due to a change of the density of entanglements, but also due to some collateral damage to the chain molecular weight during the disentanglement treatment, as observed by GPC. We show in Fig. 26 the frequency sweep for both melts, after correction for the M_w change as decribed below. There still remains an important viscosity decrease, due to disentanglement.

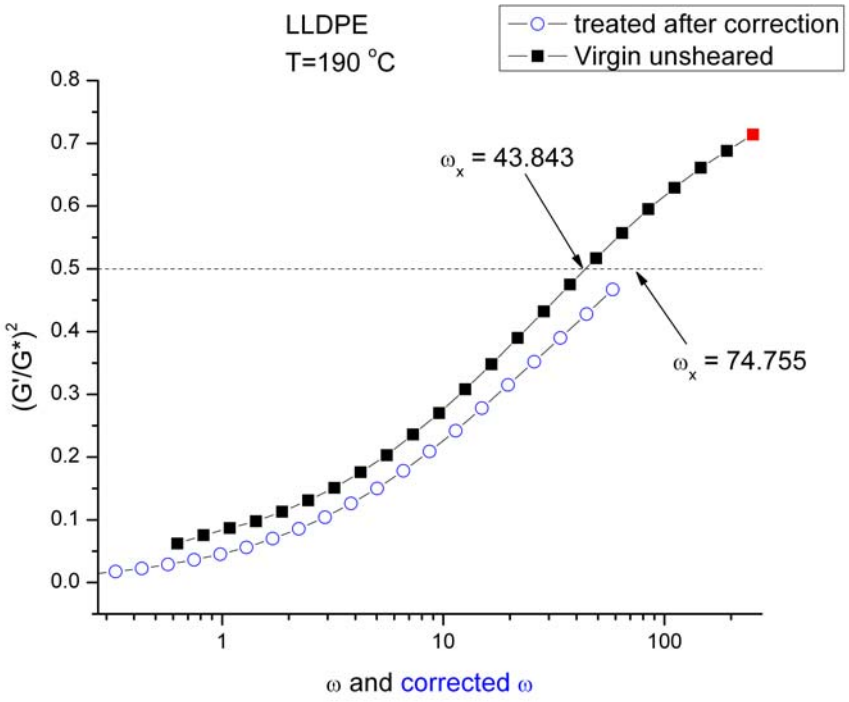

Fig. 26

Comparison of $(G'/G^*)^2$ vs ω for a Virgin/unsheared melt and a mechanically disentangled melt (the data have been corrected to account for the change of M_w. See text).

In the case of the treated LLDPE presented in Fig. 24, some collateral damage was due to the shear-refinement process, resulting in a decrease of M_w. The data must be corrected on both the horizontal and vertical scale to account for a change of M_w. The x-axis is corrected by multiplying ω by the ratio of $(M_w/M_{wref})^{3.4}$, assumed to be the amount of viscosity drop corresponding to a M_w change. A small correction on the y-axis is neglected. The net result of the correction on the x-axis (log scale) is the shifting of the raw data to the left. The resulting curves are shown in Fig. 26. It is clear that the shear-refinement process produced an important modification of the rheological behavior, even after correction for the M_w change. One sees, in particular, a substantial increase of ω_x. The situation is very similar to that depicted in Fig. 10 for a PS melt "treated" at high strain, high ω in a dynamic rheometer. The Melt Flow Index of the treated pellets can be determined and compared to the virgin reference pellets. After correction of the results for the M_w reduction, 55% MFI increase remained for the treated pellets. There is no possibility of attributing this lasting viscosity reduction to an artifact, surface slippage, or degradation. The analogy between Figure 10 and Fig. 26 is striking. Fig. 10 is for a melt submitted to a non-linear dynamic treatment in a dynamic rheometer, Fig. 26

relates to a resin submitted to a shear-refinement treatment. Other interpretations than those proposed by Freidrich et al [60, 61] must be found to explain the new results (see the Discussion section)

2,4 Transients created in dynamic conditions by increase of strain.

We saw in section 2.1 that step strain rate viscometry can cause transients resulting from the application of strain rates greater than certain values, yielding very large decreases of viscosity, from 8500 to 55 Pa-s in the case of LLDPE in Fig. 14. We also confirmed in section 2.2 (Fig. 22a and b) a common observation of rheology, the correspondence between viscosity values obtained from pure viscometry and dynamic viscosity measurements, except for the absence of transient behavior in the case of dynamic results. The difference was attributed to working at low strain, in the linear visco-elastic region.

Figures 27 and 28 summarize schematically the experimental procedure to create a transient with a dynamic rheometer, avoiding melt fracture. In the figures, a parallel plate configuration was used, but a cone and plate combination is also a valid option, providing essentially the same results. The resin was the same LLDPE, the temperature 155 ^{o}C, the rheometer, the ARES from Rheometrics. The gap was chosen between 1.2 and 2 mm.

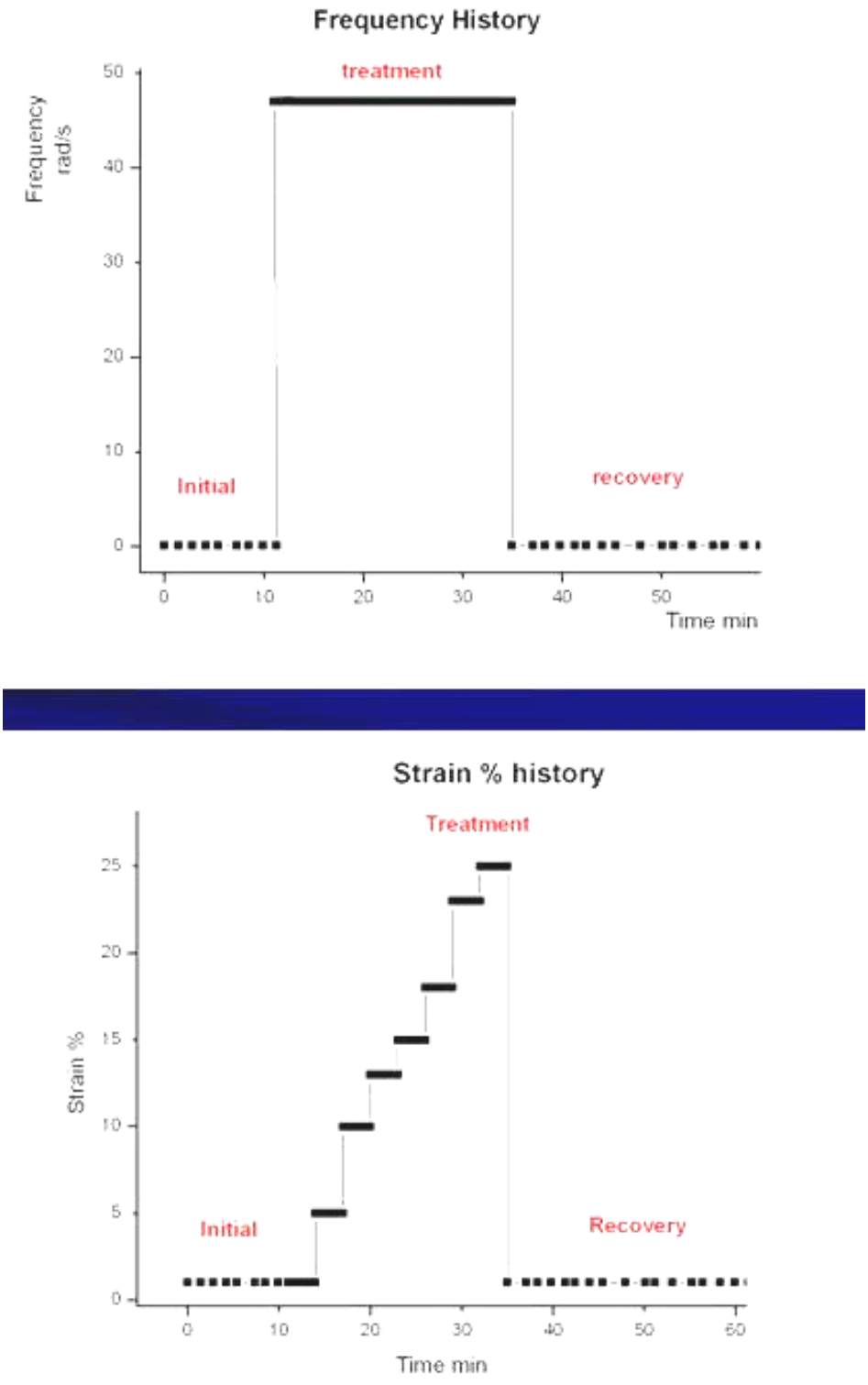

Fig. 27

Frequency and strain % history (plotted against time) for the data analyzed in Fig. 28

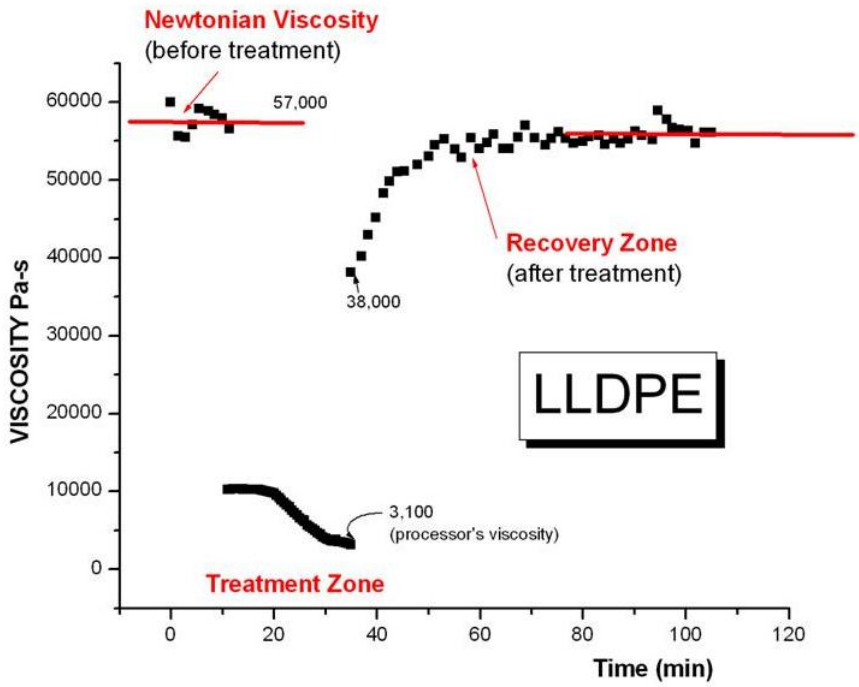

Fig. 28

Dynamic viscosity vs time for the 3 steps of Fig. 27a

Figures 27a and b describe the frequency and % strain history. Figure 28 plots dynamic viscosity against time. The first and last segment, called "initial" and "recovery" in Fig. 27 represent the baseline, the value of viscosity under linear viscoelastic conditions, i.e under very low frequency and amplitude (here 1 rad/s, 1% strain). The so-called « **treatment zone** » in Figs 27 and 28 was initiated by a jump of the frequency, from 1 to 47 rad/s, which created, in Fig. 28, an instantaneous drop of viscosity from 57,000 Pa-s to 10,000 Pa-s, due to shear-thinning. The jump was then followed by a gradual stepwise increase of the strain amplitude, from 1% to 25%. Figure 28 shows that for the first 2 steps of increase of strain, the viscosity held constant at 10,000 Pa-s, its shear-thinned value at that temperature and frequency, but that starting at strain = 13 %, the viscosity started to become transient declining from 10,000 to a steady state value of 3,100 Pa-s. This operation took about 25 min. Then the frequency and strain amplitude were changed back to their low values of the linear range (1%, 1 rad/s), and one observes an instantaneous partial loss of the effect of shear-thinning combined with strain softening, i.e. the viscosity jumped back to 38,000 Pa-s. Recovery of viscosity occured over the following 20 minutes, viscosity increasing slowly and finally regaining its original

Newtonian value, 57,000 Pa-s. In other words, the state of the melt produced by the transient treatment (let's call it disentanglement to simplify) was unstable when the energy that produced the transient behavior was released: this is why viscosity slowly increased in time and returned back to the original value for the melt. Nevertheless, it took 20 minutes for recovery, and this time is 60 times longer than the terminal time at that temperature, making it possible to exploit the benefits of a smaller viscosity during recovery if the melt were to be processed at that stage. One can define the viscosity benefit by comparing the initial Newtonian viscosity (57,000) and the Newtonian viscosity before recovery after the shear-thinning elastic loss (38,000), a ratio of 1.5 in this treatment **(« 50% disentanglement »).** Notice that a processor could still benefit from shear-thinning of the treated resin (Fig. 28), and work under much greater viscosity reduction (3,100 Pa-s versus 57,000 Pa-s, an improvement of over 1,700 % !).

The experimental procedure described in Fig. 27 has several variations: the time duration between strain amplitude step-ups can vary, the strain amplitude increment itself can be changed as can the temperature of the melt and the frequency of operation during treatment. The treatment could also be done differently, by increasing at low frequency the strain to 25%, say, and step wisely increase the frequency from 1 rad/s to 47 rad/s. All these changes contribute to the final % disentanglement, which can be as small as 20%, to as large as 3,000%. The wrong procedure can also produce artifacts or surface effects, as will be explained in the discussion section of this chapter.

In our interpretation of the results, strain softening, known to decrease the modulus at higher strain, combines with shear-thinning due to the effect of frequency to render the melt unstable in its original entanglement network configuration; thus the transient behavior occurs. In a step strain experiment conducted in the molten state, a softening factor is defined, h = G(strain)/ G(LVE), where G(strain) is the melt modulus for a given strain and G(LVE) refers to the strain independent Linear Viscoelastic Value (h <1). At low strain, the modulus is only time dependent, and an increase of strain produces an increase of stress proportionally. Pure viscometry experiments have demonstrated that above certain strain rates, corresponding to a certain stress level, a transient decay towards steady state released the elastic energy stored during initialization. It was suggested earlier in this chapter that the dynamics of this process

could be viewed as a recursive effect of the stress on relaxation times (also see the discussion).. As stress continues to grow, due to increased strain, strain softening is the first revealing sign of the modification of the structure due to the stress dependence of the relaxation time. Figure 28 reveals that under dynamic conditions, the softening factor h can become time dependent, which translates into a transient behavior. The advantage of producing transient behavior with a dynamic viscometer is that G' and G" become time dependent, so it is possible to analyze these curves individually and also follow how $(G'/G^*)^2$ varies during transient stress decay. The transient decay can be produced *in-situ* in the rheometer, and a frequency sweep performed before the transient and after it, allowing an easy way to analyze the differences due to the stay in the non-linear regime. This type of experiments, of type 2 in our definition (FTF), allows to analyze the influence of strain and frequency during time sweep ("the treatment").

3. Dynamic Experiments of Type 2 (FS-TS-FS) on PC

The resin was the Makrolon PC with M_w =32,000 described in section 3 "Materials", with the corresponding procedure to dry it and running the rheological tests. A typical experiment was as follows: Step1 was a frequency sweep from 0.1 to 40 Hz at 275 ^oC, with 5% strain. The test lasted about 120 sec (squares). In step 2, a time sweep done at the same temperature at ω=0.1 Hz, 5% strain was done for approximately 1,000 sec (dots curve). For step 3 (triangle curve), we repeated step 1, i.e. we reran a frequency sweep using the same conditions, from 0.1 Hz to 40 Hz, 5% strain T=275^oC. Fig. 29 is a plot of the complex viscosity in Pa-s versus "consolidated time", meaning the global time, starting from the beginning of the first frequency sweep, step1.

In this section, we vary the conditions of strain % and/or frequency during step2, and examine the difference between the frequency sweeps. We successively study the effect of strain % at constant low angular frequency (ω = 0.1 Hz), and of frequency at constant strain %. In the next section, we also vary the temperature at which the various steps are conducted.

3.1 Effect of strain at constant low frequency (0.1 Hz).

One of the purposes for using a low frequency for the oscillation was to avoid any possible artifact. The resin chosen was a "virgin" PC, provided by the manufacturer as presenting a "mild thermo-mechanical history" due to its extrusion conditions after the reactor's phase. We purposely chose this resin in this section of this chapter because of this particular feature. The reasons will become apparent as we study the effect of the various parameters. For the present purpose, let's categorize this melt as "mildly disentangled" due to its thermal-mechanical history.

We will present results of increasing strain during step 2, all other variables, including the time of time sweep, remaining the same.

3.1.1 5% strain

Fig. 29 is a consolidated plot of the 3 steps. For step 1 one sees that viscosity increased a little bit at the beginning (the low ω values of the frequency sweep), but that increasing frequency reversed the tendency, showing the classical display of shear-thinning: viscosity drops by about 400 Pa-s. In step 2, one sees that viscosity started at around 1,050 Pa-s- which is incidentally the extrapolated value for the very beginning of the black square curve, corresponding to the low ω range of the frequency sweep, then continued to rise to reach a plateau value of 1,200 Pa-s. Viscosity gained 275 Pa-s in step 2, i.e. 30% of its initial value. For step 3, shear-thinning started from the beginning of the frequency sweep, no longer did we observe a time dependent behavior at low ω; viscosity decreased as ω increased to reach approximately the same viscosity as for step1 for 40 Hz.

The conditions used during the time sweep were extremely "soft", in terms of energy input. This corresponds to letting the melt "anneal", and "taking pictures" of its evolution, as G' and G" are measured simultaneously. Since viscosity increased during step 2, no surface artifact was possible under those very soft conditions [60, 61]; thus we conclude that the true steady state value of viscosity, 1,200 Pa-s, was only obtained after 15 minutes of "annealing

time", i.e for a time 210,000 greater than the value of the terminal time responsible for molecular relaxation at this elevated temperature (τ_o=0.0055 sec). We speculate that the original melt was in a non-equilibrium state, not because the molecular motions do not have time to occur (like for a glass below T_g), but because "the entanglement network" had been brought out of equilibrium by a previous thermal-mechanical history that created the situation. Annealing the melt let the entanglement network parameters return to their thermodynamic value, re-adjusting along the "framework" of the molecular motions and instantaneously reaching a new steady state value (in time τ_o), as return to equilibrium of the network proceeded. All these concepts are used here without precise definition, as a way to introduce them, and with the knowledge that a quantitative description will be required.

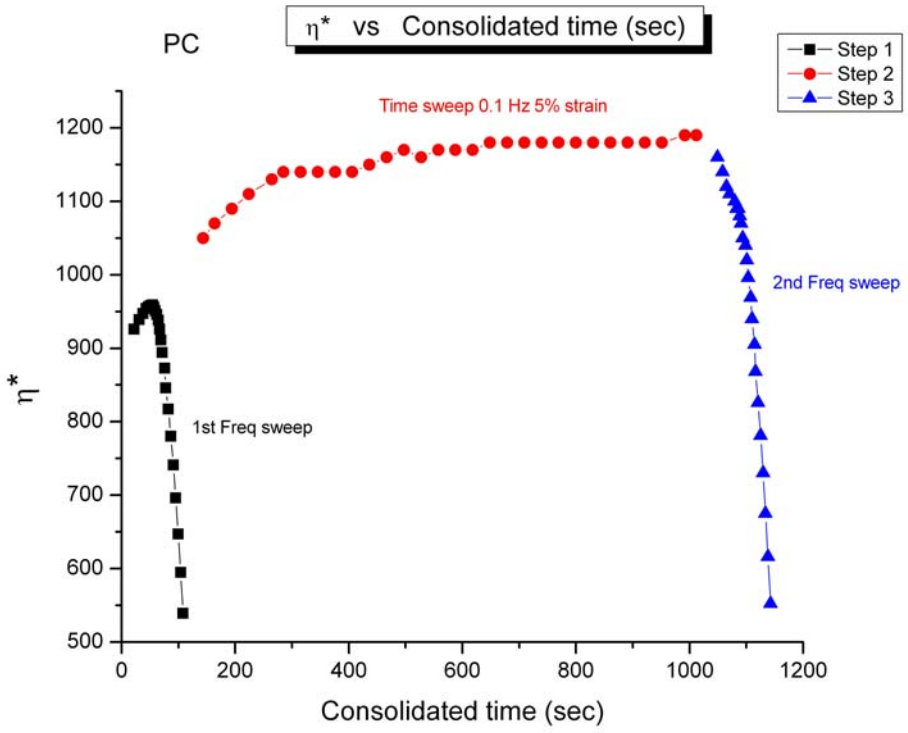

Fig. 29

Dynamic viscosity vs time. 3 steps: Frequency Sweep- Time sweep (0.1 Hz, 5% strain)-Frequency Sweep. PC-2. T=275 ^oC

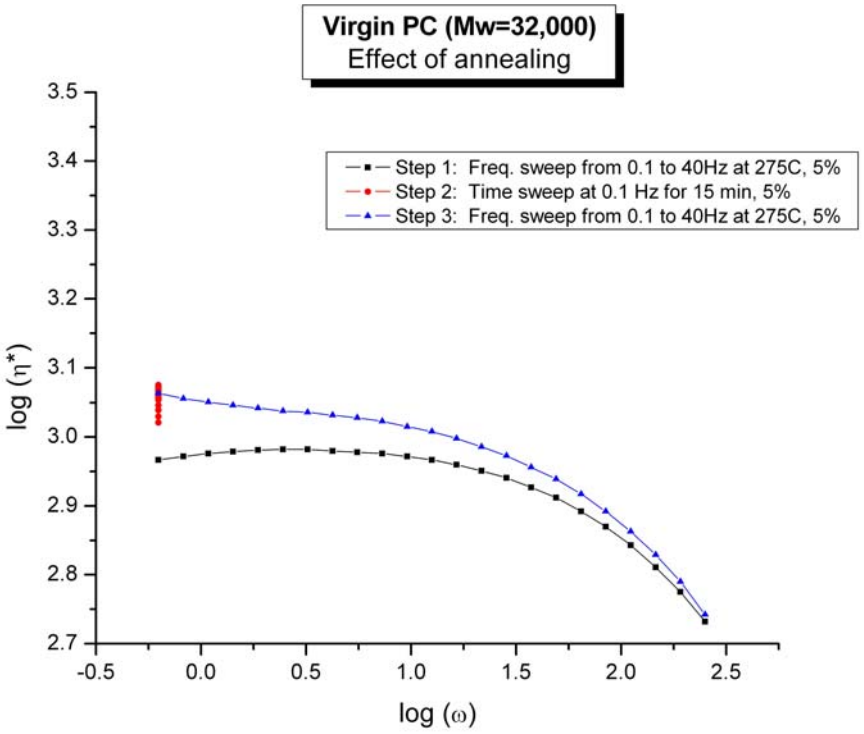

Fig. 30
Same data as in Fig. 29 but plotted against ω

Fig. 30 is a traditional log-log viscosity-ω graph for the same data presented in Fig. 29. The lower curve corresponds to step 1, the upper curve to step 3. Step 2 occured at constant ω=0.1 and is the short vertical segment. As already revealed in Fig. 29, the initial viscosity at the beginning of step 2 was higher than the original viscosity at the same frequency on the lower curve; this is because the initial melt had a "lower entanglement" level, due to a previous thermo-mechanical treatment, and that "re-entanglement" occurred during the step 1 frequency sweep. In other words, the melt entanglement network was initially in a disentangled state produced by a previous shear-refinement treatment, and some recovery already took place during step 1 resulting in a higher viscosity at the beginning of step 2. It is interesting to point out that, although higher ω values shear-thined the step 1 melt, as clearly evidenced for the square curve in Fig. 29 by a downturn of viscosity, some re-organization of the melt occurred, at the same time, to render its entanglement state closer to its thermodynamic equilibrium. This observation proves that one can obtain a frequency sweep curve but be uncertain that it

represents the true stable state of the melt. Classical views and equations describe a melt rheology as if it was in equilibrium. Figure 30 provides two different frequency sweeps of the same polymer, under the same rheological conditions, the same temperature, proving that the equations of rheology must incorporate the state of entanglement of the melt in its formulation. The next figure explores this issue.

Figure. 31 applies to the same data as those of Figs. 29 and 30. G”(ω) is plotted vs G’(ω) for the two frequency sweeps, step 1 (squares) and step 3 (dots).

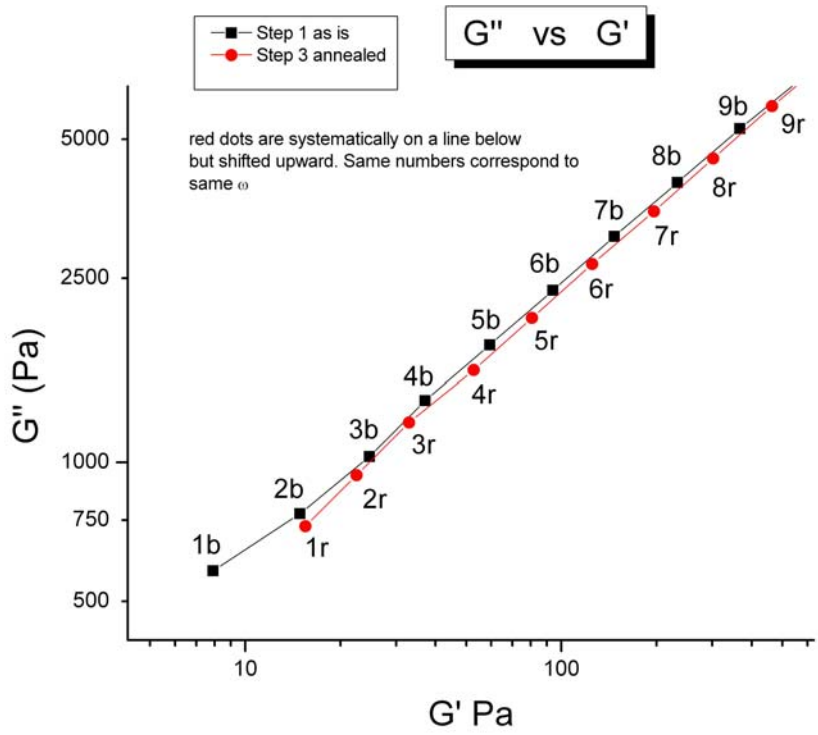

Fig. 31
G”(ω) vs G’(ω) for step 1 and step 3. Same data as in Fig. 29

As explained in part I of this series [2], in traditional visco-elastic theories that express G' and G" as a function of a spectrum of relaxation times, it is represented that G' and G" both scale with the plateau modulus G_{oN}, which itself can be expressed as a function of $\rho T/ M_e$ where M_e is the molecular weight between entanglements. As pointed out in the Introduction, if M_e increases (disentanglement) or decreases (re-entanglement) as a function of annealing, or as a function of the treatment conditions, and the spectrum of relaxation times remains unchanged, then a plot of G" vs G' on a log-log scale should show a shift of G’ and G” by the same

amount. In Fig. 31, the data points appear to be shifted so that they remain on the same line. The data points are numbered 1, 2, 3 etc. The same number applies to the same frequency, 1r and 1b, which should be compared, or 2r and 2b, etc. One sees that the squares and dots were shifted to almost stay on the same curve. The problem is that the slope of that curve is 0.57, not 1, so that the amount of shift on the horizontal and vertical axes are different, a significant departure from a classical change of M_e. What is also important to notice is the fact that the squares and dots curves superpose as a result of annealing, i.e. that the effect of re-equilibration of the network of entanglements resulted in the same horizontal and vertical shifting as the effect of frequency on G'(ω) and G"(ω). When this is the case (we will see later that it is not always true), the return to the equilibrium state of the entanglement network occurs without any modification of the network framework. This is the simplest kinetics to analyze, all changes being due to the re-orientation of the entanglement framework. Incidentally, as already mentioned, and shown in Fig. 31, the effect of this re-orientation on G' and G" seems to be similar to that described by shear-thinning as a result of changing frequency.

3.1.2 20% strain

In this section, we repeated the same type of experiments (FS=step 1, TS=step 2, FS=step 3) except that the "annealing treatment" occurred under a larger strain, 20% instead of 5% (at the same low frequency of 0.1 Hz and the same temperature 275 ^{o}C). The initial melt was the one produced at the end of step 3 in the previous section. The same overall behavior was observed, but the effect of increasing strain in the annealing step triggered interesting differences.

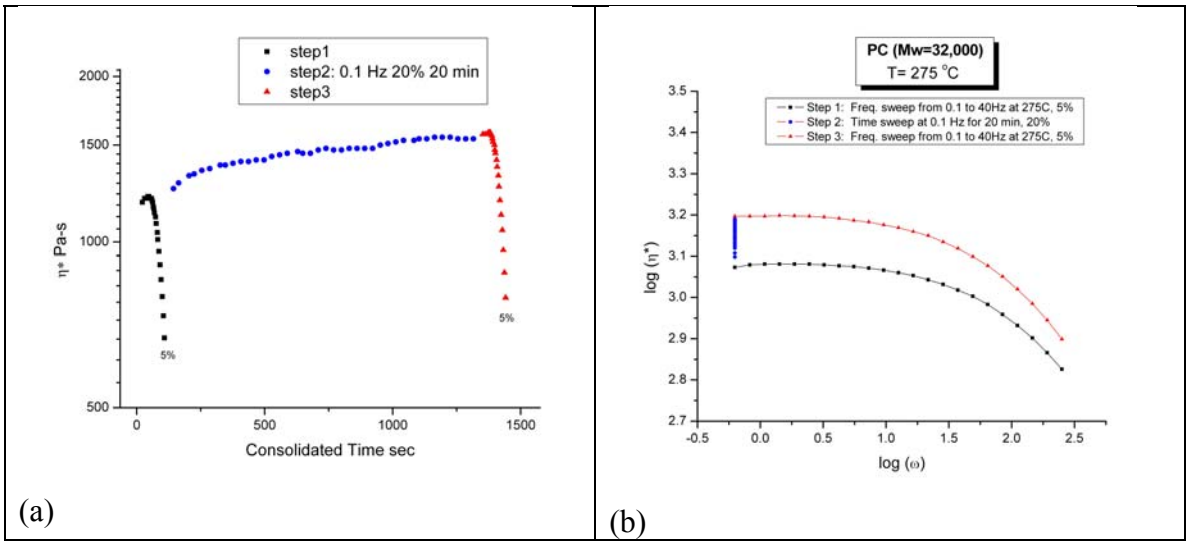

Fig. 32

Fig. 32a and 32b should be compared with Figs. 29 and 30, respectively. The initial state of the melt before the 1st frequency sweep (black square curves) corresponds to that obtained after step 3 of Fig. 29. The dots curve correspond to a time sweep under a strain amplitude of 20% . The triangles are for step3, the 2nd frequency sweep.

In Fig. 32a, viscosity at the beginning of step 2 started at almost the same value found for the same frequency (0.1 Hz, first data point) of the step1 curve, indicating that the frequency sweep producing shear-thinning did not occur simultaneously with a modification of the state of the entanglement network due to annealing. This is in line with the fact that the melt of Fig. 29 appeared stable at the end of step 2. Yet, in Fig. 32a, the 15 min time sweep at 20% strain did produce a new instability of the melt, visible by the viscosity which starts to rise again towards a new stable value of 1,575 Pa-s. Also notice in Fig. 32b that, contrary to what is observed in Fig. 30, for which the annealing treatment was done under 5% strain, the 20% annealing treatment produced a shift that seemed to affect equally the low frequency and high frequency regions (compare Figs. 30 and 32b in the high ω region).

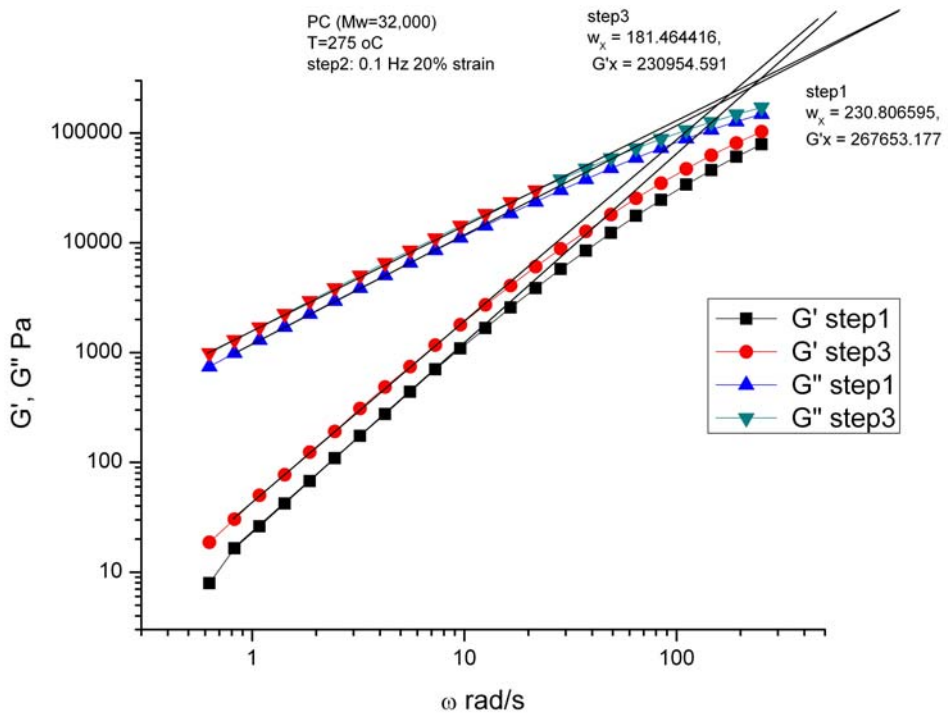

Fig. 33

Comparing the storage and loss modulus vs ω for step 1 (1st frequency sweep) and step 3, performed after 15 min of time sweep treatment at 0.1 Hz and 20% strain. The result of "annealing" under 20% strain was to shift the moduli upward. The amount of shift was different for G' and G" but remained constant as ω increased.

Figure 33 shows G' and G" versus the radial frequency on a log-log scale. This is a classical representation of the data, useful to determine the "cross-over" point, the value for which G'=G". All G'(ω) and G"(ω) for step 3 melt (after treatment) are in dots and up triangles, located above the G' and G" for step 1 melt. The cross-over frequency for the more viscous melt was lower (181 vs 231), which makes sense for a stiffer melt, but the modulus was lower (0.231 MPa vs 0.268 MPa), which does not make sense if one would assign the increase of viscosity to an increase of the entanglement density (M_e decreases). Traditional theories consider the cross-over point a characteristic parameter, the transitional change between a viscous and elastic behavior. The cross-over is considered the reciprocal of the terminal relaxation time. Figure 33 suggests that classical interpretations of melt behavior are too simplistic and not necessarily helpful to understand phenomena related to entanglement instability induced by mechanical treatment.

Figure 34 provides some preliminary insight of our new concepts proposed to understand visco-elastic deformation of polymer melts, in particular to separate out what relates to changes occurring to the entanglement network. In this approach [66, 67, 70, 72], the analysis of the variation of $(G'/G^*)^2$ versus ω (or G^*) is assumed to be related to the number of active strands (bearing stress by a mechanism of conformation statistics activation), whereas $(1-(G'/G^*)^2)$ would scale with the amount of relaxation-diffusion taking place simultaneously, and would require a stress computed from such diffusion mechanism. Polymers are assumed to have a dual-phase structure not only locally (to characterize the coupling between adjacent conformers), but also globally, induced by the interpenetration of the macro-coils [72], which produces the entanglement network phase. The mechanism(s) of activation and relaxation of strands is an interplay between the local dual structure due to the conformers interaction and the global dual structure due to the existence of the entanglement phase, which can itself be sketched as a channeling pipeline deformable network. More and more strands are activated as ω is increased. Depending on molecular weight, there is a maximum of active strands that can be activated. The deformation of the entanglement network is described by the number of strands that can be activated, and re-oriented towards the flow direction by relax-diffusion after activation has occurred. The deformation of the strands themselves involves a modification of the local dual structure of the conformer interaction, the more elongated trans-conformers being favored in the direction of flow. The viscous regime deformation is dominated by the variation of the number of active strands as a function of ω, strain rate, T and P, with the simultaneous orientation of the entanglement network dual phase in the direction of flow resulting from the concomitant stress relaxation-diffusion mechanism. Molecular weight affects the amount of entanglement phase available, and therefore increases the amount of orientation possible of the entanglement phase, which, in essence, explains the spreading of the width of the rubbery plateau modulus when molecular weight increases. When the orientation of the entanglement phase is completed (ending the "entropic character" of the strand network deformation), the local conformational changes become the dominant mechanism, visible as we approach the transition zone. These concepts will be elaborated in the discussion, but having been briefly presented here will allow their use in the description of the figures, as compared to a classical description.

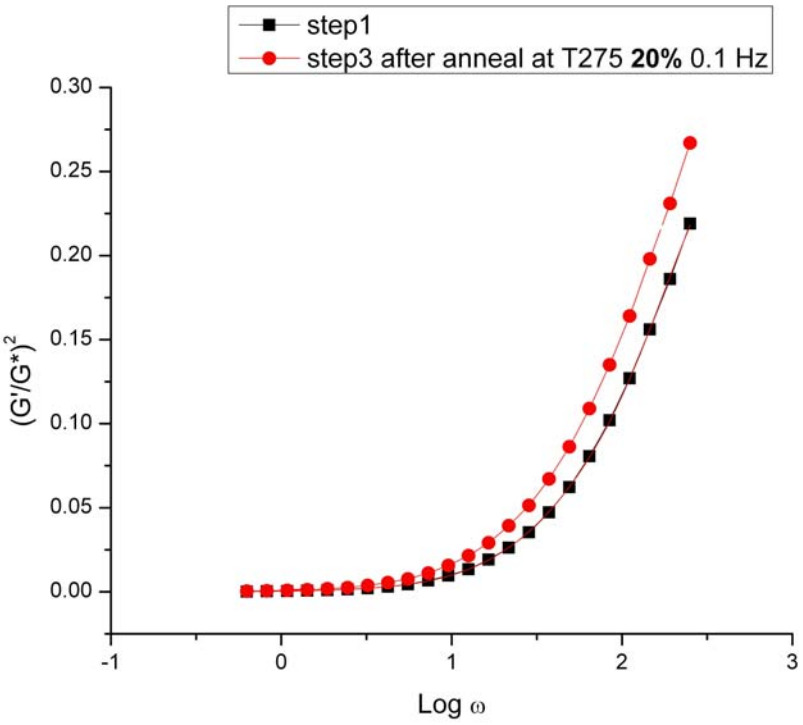

Fig.34

Comparison of $(G'/G^*)^2$ vs ω for step 1 and step 3 after time sweep at T=275°C with 0.1 Hz and 20% strain

In Fig. 34 one sees that the net result of the time sweep "treatment" was to increase, at each ω, the number of activated strands (the dots correspond to step 3). This is due to a re-orientation of the existing network of strands during the time sweep step because of the larger strain deformation demand (20 % instead of 5%). All of this occured at T= 275 °C, for which the terminal relaxation time was about 5 ms ($1/\omega_x$), but the molecular re-arrangements were 200,000 times faster than a re-alignment of the entanglement network responsible for the stability of the rheological parameters in time. We conclude that the original melt had an initial oriented entanglement network structure, corresponding to a metastable local conformer structure equivalent to a larger free volume content, thus a lower viscosity. As a thermodynamically more stable entanglement network was re-established-favored by an increase of strain % in step 2-the local dual conformer interaction structure lost some free volume, resulting in an increase of viscosity.

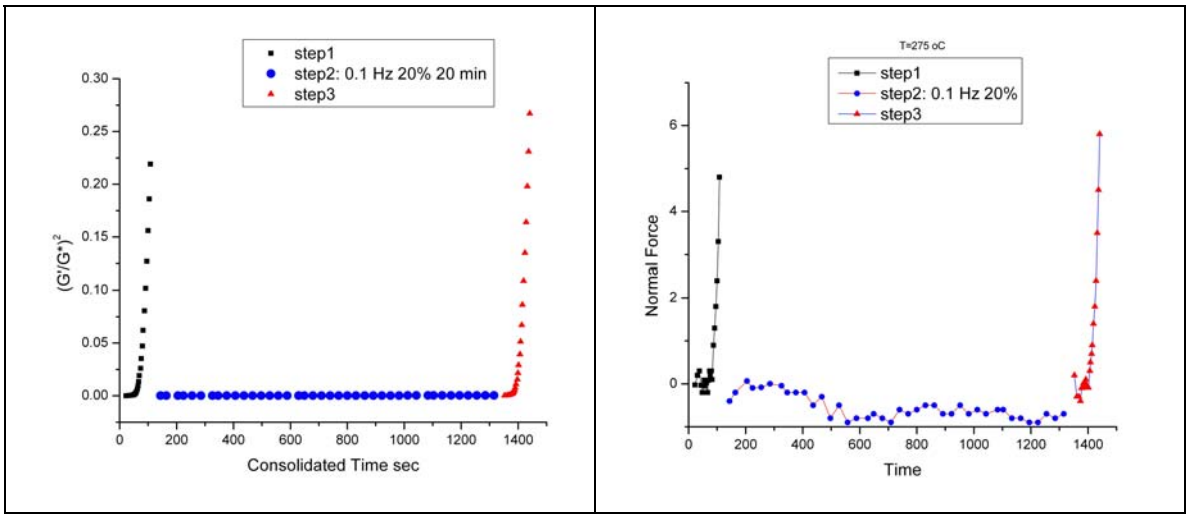

Fig. 35
$(G'/G^*)^2$ (a) and Normal Force (b) vs time for the data of Fig. 32

Figure 35 (a) shows that the number of activated strands $(G'/G^*)^2$ increased as ω increases in a frequency sweep. The annealing treatment was done under conditions of deformation (at 0.1 Hz, 20% strain) that do not activate the network of strands $(G'/G^*)^2$ was almost zero), yet, as we have seen in Fig. 34, there was a modification of the melt entanglement structure, yielding to a step 3 melt showing more activated strands during a new frequency sweep. This is due to the interactive character between the local structure of the conformers' interaction and the definition of the entanglement phase itself [72] In Fig. 35b the y-variable is now the normal force. The analogy with Fig. 35a is striking. Also notice that during step 2, there was a tendency for the normal force to decrease slightly, to become negative. This same observation was made for the sheared LLDPE melt after pure rotation at high strain (Figs 19d, 20).

In summary, shearing the melt at 0.1 Hz at T=275 oC under 20% strain does not involve enough energy input to activate the entanglement network, but it produces enough strain in the strands to modify the local conformational structure which interactively defines the orientation of the entanglement network. The best sign that this is the case appears to be the increase of the tensile force (negative normal force) acting perpendicular to the shearing

direction. This tendency will be even more visible in the next section, where the strain was increased to 500% during step 2.

3.1.3 500% strain

We now study the same melt (at the end of step 3 of the previous section) and perform the same type of successive step 1, step 2 and step 3 at T=275 ^{o}C, with a time sweep treatment under 500% strain, still at 0.1 Hz. A large strain amplitude forces the melt to be deformed faster, 100 times faster than it was when it was deformed at 5%. Figure 36 shows that under such conditions of large deformation, the melt viscosity decreased with time during the time sweep treatment.

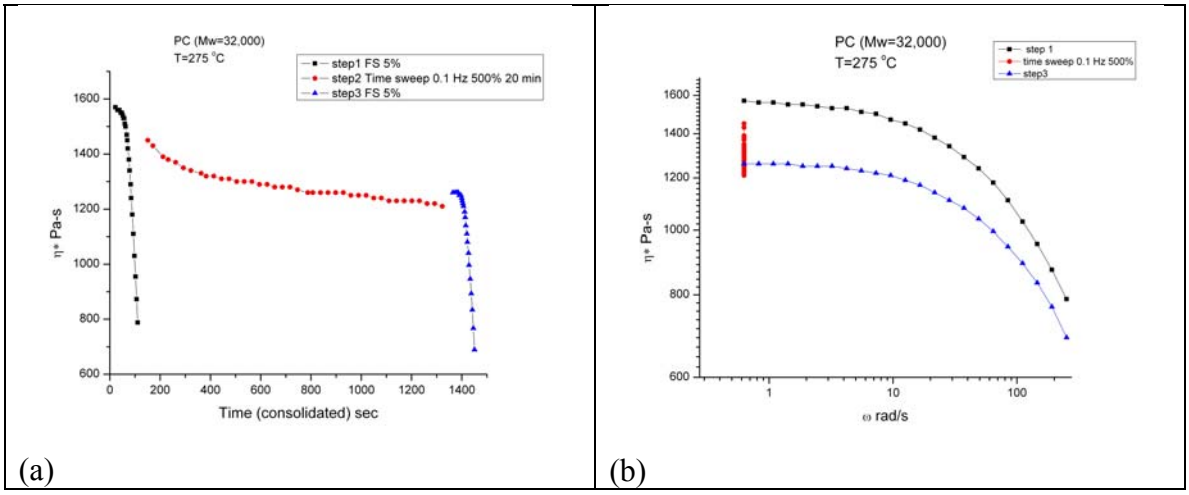

Fig. 36
Same conditions as in Fig. 32 but the time sweep (step 2) is done with 500% strain (0.1 Hz).

At the beginning of step 2 (dots), in Fig. 36, viscosity had a lower value than at the beginning of step 1 (squares). There was no frequency change between these two points, only a strain amplitude change between 5 % to 500%. This illustrates strain softening, as is well demonstrated and known in step strain experiments done at high strain. The reverse of strain softening triggered the small viscosity increase observed between the end of step 2 (dots) and the beginning of step 3 (triangles) in Fig. 36a. This small viscosity "jump" is like the spontaneous increase of viscosity observed upon suddenly decreasing frequency from a higher

value to a lower one. The drop of viscosity in step 2 is quite significant, from 1,575 Pa-s (beginning) to 864 Pa-s (steady state), these 2 values being extrapolated from a regression fit of the available data. This time dependence of viscosity is reminiscent of a transient behavior in a viscometry test at constant strain rate, here triggered by an increase of strain.

Figure 36b should be compared with Figs. 32b and 30. The increase of strain to 500% during the time sweep step produced a step 3 melt with lower viscosity, even in the Newtonian region, demonstrating that a new entanglement state was generated by the time sweep "treatment". Figure 36b shows that the new entangled melt had a lower viscosity at all frequencies. The frequency sweep shown as the lower curve in Fig. 36b (step 3) is, in fact, very similar to the frequency sweep for step 1 in Fig. 30, corresponding to the initial melt, which we characterized as a melt with a thermal-mechanical history. The 500% step 2 treatment in the rheometer induced similar modification to the entanglement network

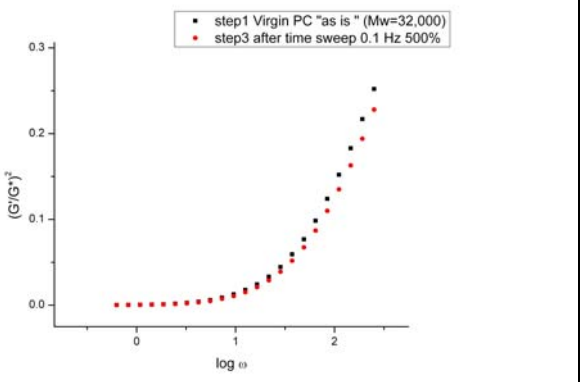

(a)

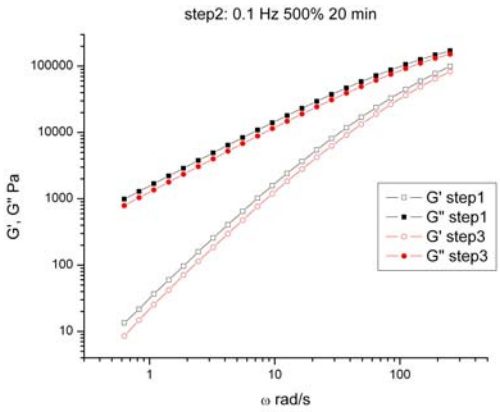

(b)

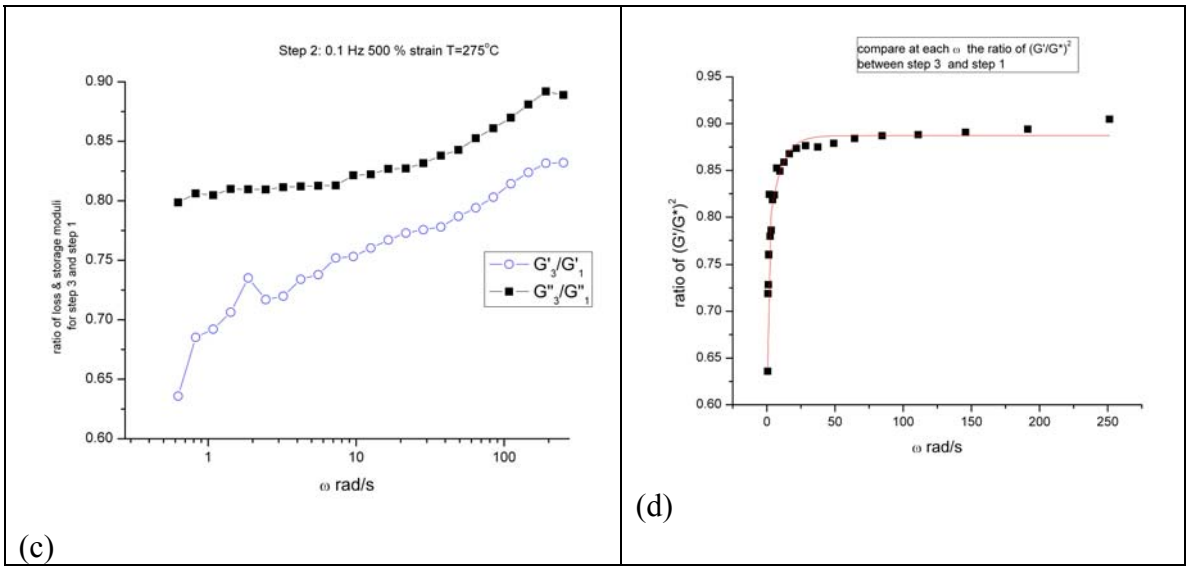

Fig. 37

Analysis of the results for the 3 step FS-TS-FS experiment with step 2 corresponding to 0.1 Hz 500 % strain. See text.

Figure 37a shows the data from Fig. 36, plotted as in Fig. 34. It is clear that Fig. 37a shows the reverse of that in Fig. 34, as expected from the reversal of the viscosity change during step 2. Using the language introduced in the previous section to interpret visco-elasticity, the number of activated strands of the entanglement network was less for melt 3 (the dots in Fig. 37a) than for melt 1 (the squares), at a given frequency. The time sweep treatment reduced the number of activated strands as a result of the re-structuration of the local dual conformer interactions. Figure 37b shows that both G' and G" were lowered for step 3, at each ω, the respective curves appearing shifted on the vertical axis. Fig. 37c denies the objectivity of such shifting attempt procedure (also see Ref. [2]). In this figure, we plot the ratio (G'_3/G'_1) and (G''_3/G''_1), each established at the same ω, versus ω. The subscript 3 and 1 refers to step 3 and step 1 data points.

There are two important conclusions from this plot:

- the time sweep treatment affects the storage modulus G' much more than the loss modulus, G"; this would contradict any explanation of the time sweep viscosity drop due to a surface effect [60, 61], for which G' and G" would be modified identically.

- the ratios are frequency dependent, being more pronounced in the Newtonian region. Besides, the ratio for the storage moduli varies faster with frequency than the ratio for the loss moduli. This is confirmed in Fig. 37d, a plot of the ratio of $(G'/G^*)^2$ with ω for step 3 and 1, where it is seen that the loss of the stored elasticity, as high as 35% at low ω, quickly plateaus to 12% beyond ω=25 rad/s. It is conceivable that the entanglement state induced by the time sweep treatment (step 2) is thermodynamically instable, and that the melt's return to a more stable state is accelerated by the increased stress generated by the increased ω during the step 3 frequency sweep. This decrease by the stress of the relaxation times of the entanglement network has already been mentioned earlier in the case of pure viscometry at constant strain rate (section 2.2 of RESULTS).

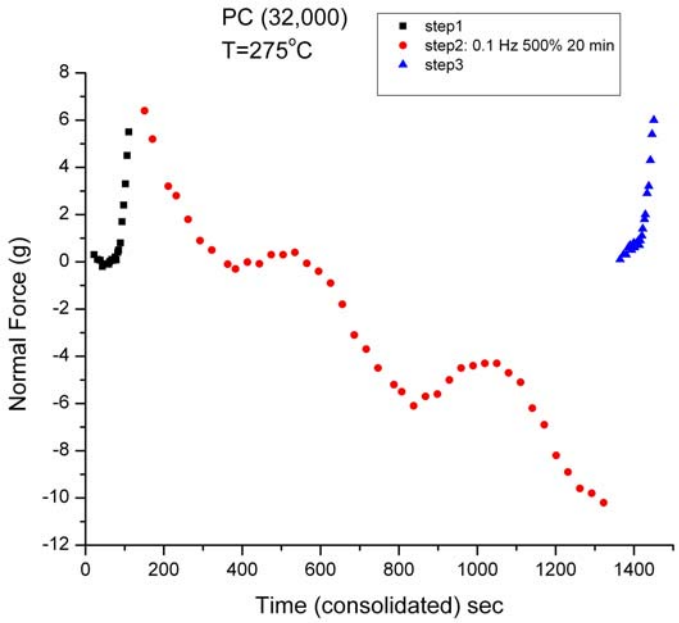

Fig. 38

Normal Force is plotted as a function of the cumulative time, showing their respective variation for step 1 (black squares), step 2 (red dots) and step 3 (blue triangles). Time sweep is done under the following conditions: T= 275 °C, 0.1 Hz 500% strain.

The graph of normal force vs time in Fig. 38 should be compared with the graph in Fig. 35b for which step 2 was done at 20% strain. The same behavior was observed for the frequency sweeps, but what is interesting is the oscillating decay of the normal force observed for step 2. We observed in Fig. 35b, during step 2 under 20%, a tendency of the normal force

to become negative, indicative of a pulling melt, but the magnitude of the effect is much more pronounced in Fig. 38, with a persistence of the oscillating character in the negative range. Also note in Fig. 38, at the end of the time sweep, the jump back of the normal force from -10 g to 0 corresponding to a release of the strain amplitude from 500% to 5%. Additionally, normal force at the beginning of step 2 was the same as that at the end of step 1. This might be strange, in view of the difference in frequency between the two points, 40 Hz for the last point of step 1 (with 5% of strain) and 0.1 Hz for the 1st point of step 2 (with 500% strain). But, as shown above, if a release of strain from 500% to 5%, at 0.1 Hz, results in a differential of normal force by 10 g, it is expected that such a build up of normal force would compensate for the decrease of frequency, when strain increases from 5% to 500% from step 1 to step 2: the odd behavior seems actually to be in line with the conclusion that strain softening, in many ways, behaves like shear-thinning, i.e. like the influence of shear rate on the stress and the normal force. Yet, the oscillating nature of the normal force decay, and the origin for becoming attractive (negative), must be addressed as a specific feature of time dependent strain softening and explained quantitatively.

3.1.4 0.1 Hz 5% strain using a "disentangled melt" obtained by controlled shear-refinement.

In the previous example of analysis of the melt entanglement instability of a PC, the initial entanglement state was unknown. All we knew was that some thermal-mechanical history produced a resin which required a certain degree of pre-annealing to stabilize. In the following example, a PC grade of smaller M_w/M_e (9.4 instead of 12.8 in the previous example) was mechanically disentangled in a disentangling machine (a two-stage processor, as described in Fig. 6), achieving a very large change in the entanglement state, as will be revealed in the following figures. The same 3 step procedure was used, corresponding to a first frequency sweep (at T=275 ^{o}C), followed by an annealing treatment for 20 min under "mild" oscillating conditions (0.1 Hz and 5% strain), followed by another frequency sweep (0.1 Hz to 40 Hz, 5% strain). Because the initial melt was disentangled mechanically to a very large degree (relatively speaking, i,e, compared to what can be produced in a lab rheometer), the changes

were most spectacular and significant, yet in line with what we have observed for lab induced "melt disentanglement".

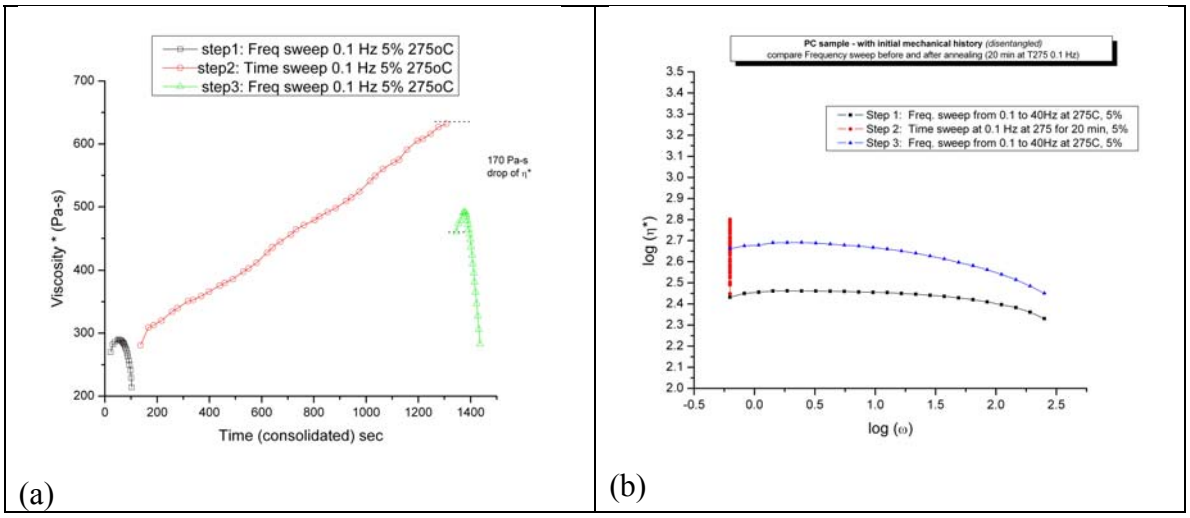

Fig. 39

Same type of experiments as in Figs. 29 and 30, with the same conditions for the 3 steps, but the polymer melt corresponds to a "disentangled polymer" processed by the apparatus in Figs. 5a and 5b

Figure 39 displays the two plots we have been using to describe the evolution of the entanglement state. The first frequency sweep (the squares) has the general features of a frequency sweep of a disentangled melt: first an increase of viscosity at low ω, the presence of a maximum at a certain frequency and a decrease of viscosity due to shear-thinning. Note in Fig. 39a the very low initial viscosity 300 Pa-s, and the short span of variation due to shear-thinning (a gain of about 100 Pa-s for ω between 0.1 to 40Hz), indicative of a melt with very little elasticity.

Step 2, annealing without any "strong" strain, displays a spectacular viscosity recovery in a short time: viscosity increased by a factor of 3, almost linearly.

Between step 2 and step 3, although frequency and strain remained the same, respectively 0.1 Hz and 5% strain, **one observes a drop of viscosity** by 170 Pa-s. This situation is extremely challenging to explain by the current theories which do not consider the thermodynamic stability of entanglements. The drop of viscosity was not induced by a change of strain or frequency, but by time alone, the time it took in the rheometer to switch from a

time sweep mode to a frequency mode, altogether about 30 sec. During that time, the entanglement network reorganized without any external stress on it.

Also notice that the 2nd frequency sweep (the triangles in Fig. 39a, and Fig. 39b) has a much "longer" length, due to increased shear-thinning: this is because the melt re-gained some elasticity during annealing, and this directly affected its number of active strands, thus the shear-thinning attributes.

Figure 39b plots the same data against frequency ω, showing the 3 steps. The use of the log-log scales changes the perspectives, but nevertheless shows the large change in the Newtonian viscosity obtained after "recovery" of entanglement produced by annealing. log η_o*= 2.65 instead of 2.45, a gain of 0.2 on the log scale. It is also interesting to note, in passing, that the use of the log scale minimizes the manifestation of shear-thinning at low frequency. In Fig. 39a, it is clear that viscosity continuously decreased with ω, even if for a short range, but in Fig. 39b the behavior looks Newtonian.

Fig. 40 is a plot of $(G'/G^*)^2$ vs time for the 3 steps.

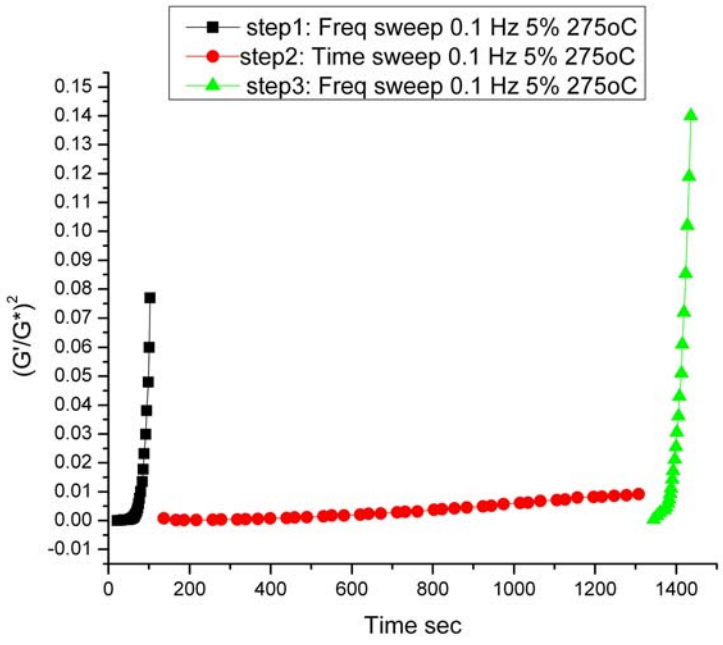

Fig. 40
$(G'/G^*)^2$ vs time for the data of Fig. 39

There are two important comments to be made for this figure:

1. It confirms the large increase of the number of activated strands for melt 3, after the recovery which occurred during annealing (step 2). The curve length for the triangles is twice as long as the squares one, for the same span of frequency. This increase of $(G'/G^*)^2$ is essentially the reason for the increased shear-thinning of the step 3 melt.

2. During annealing treatment (dots), a slight but visible increase of the number of active strands occurred, although the rheological variables (ω and strain) were very soft (0.1 Hz and 5%). This demonstrates a particular feature of a disentangled melt: an increased sensitivity to rheological parameters, such as strain and strain rate. Usually, for a stable virgin melt, there is no visible change of $(G'/G^*)^2$ during annealing at high temperature under soft treatment conditions. The drop of the stored elasticity between the end of step 2 and the beginning of step 3 is intriguing (it corresponds to the decrease of viscosity observed in Fig. 39a). The system probably overshot in trying to recover elasticity in step 2, and quickly re-adjusted in the short time between step 2 and step 3.

Figure 41 is a plot of G" vs G' on a log-log scale for step 1 and step 3. It is interesting in comparison to Fig. 31 obtained on a quasi-stable entangled melt strained under the exact same conditions.

Step 1 data correspond to the squares, numbered 1b, 2b, 3b etc, as ω increased. Step 3 data are the dots, shown as 1r, 2r, 3r etc. This plot also displays the G'=G" straight line, to determine the cross-over point by interception with the G" vs G' lines. The important aspect of this plot is the huge discrepancy in behavior between the shift on the G' or the G" axis. The difference between points 1b and 1 r, 2b and 2r, 3b and 3r etc. is clear: variations occurred with a much larger amplitude on the G' scale than on the G" scale. There is no longer a correspondence, as we observed in Fig. 31, between the effect of frequency and the effect of annealing on the value of G' and G". Time of annealing shifted G' much faster than G" (in comparison with the shift produced by ω on G' and G"). This observation is important, because it points to the deficiency of the traditional approach in its attempt to describe entanglement density by a single parameter M_e, which scales both the G' and G" in the same way. The reality is that the influence of entanglement on G' and G" seems different. Traditional incorporation of M_e in the expression of G' and G" via the introduction of G_{oN} (the plateau modulus) must be revisited since it does not describe experimental results.

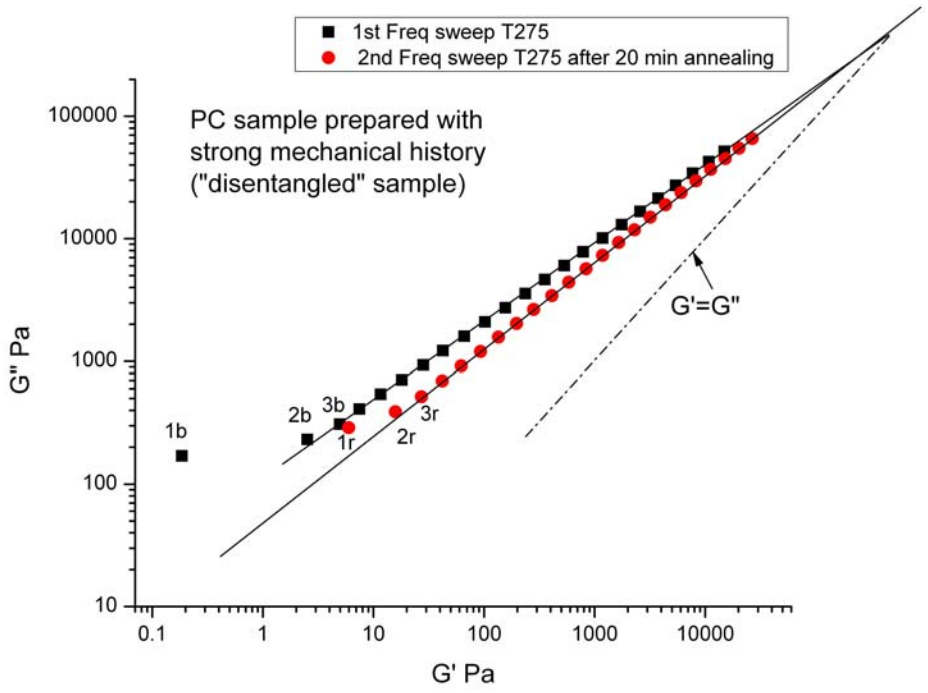

Fig. 41
G”(ω) vs G’(ω) for step 1 and step 3. Same data as in Fig. 39

Another point can be brought up from Figs. 41 and 42 regarding the value of the cross-over and its physical meaning. Identical G'_x were obtained for melt 1 and melt 3 (this is seen in Fig. 41 by the same value of the intercept of the straight line G”=G’ with the square and dot lines), but a lower ω_x characterized the annealed (re-entangled) melt, as clearly demonstrated in Fig. 42. Again, unless the cross-over must be determined differently, it appears that the classical understanding of the cross-over is defective.

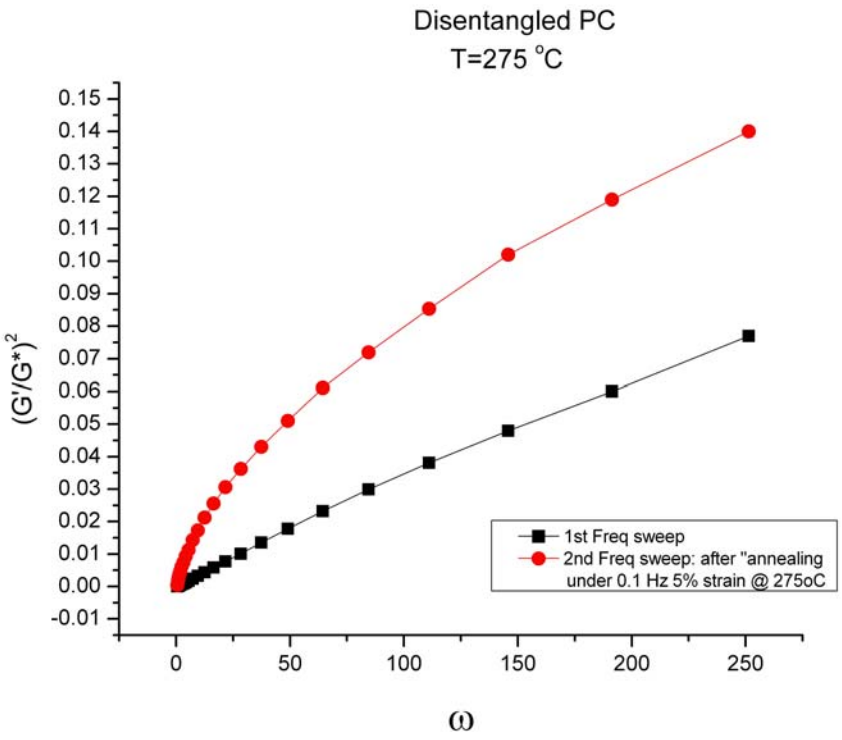

Fig. 42

The number of active strands $(G'/G^*)^2$, for a given frequency ω, was much larger for the re-entangled melt, after the annealing treatment, than for the original disentangled melt.
It can be predicted from this graph that ω_x for step 3 (the dots) is lower than ω_x for the squares (step 1). ω_x is obtained for $(G'/G^*)^2=0.5$.

3.2 Effect of Frequency during Time Sweep (at constant strain of 5%)

We study 1 Hz, 10 Hz and 40 Hz for PC (M_w=32,000) T=225 °C, all for strain of 5% (considered low, i.e. melt in the linear range).

3.2.1 - 1 Hz

Figures 43a-d show the results. Fig. 43a compares the dynamic viscosity vs ω curves before and after the time sweep. In Fig. 43a one observes a slight increase of viscosity at low ω but no change of the slope of the log-log curve (the "pseudo-plasticity index") beyond ω~20 rad/s. The dots apply to step 2 in both Figs 43a and b showing that there was a very small

increase of viscosity occurring during time sweep, but that it did not have a lasting effect since the value of viscosity at the beginning of time sweep (step 2 frequency is 1 Hz) was the same as the value found for 1 Hz (i.e. ω=6.28 rad/s) on the step 3 curve. The increase of the Newtonian viscosity was actually due to changes that occurred during step 1, the initial viscosity at 1 Hz at the beginning of step 2 being greater than the value found on step 1 for 1 Hz (Fig. 43a).

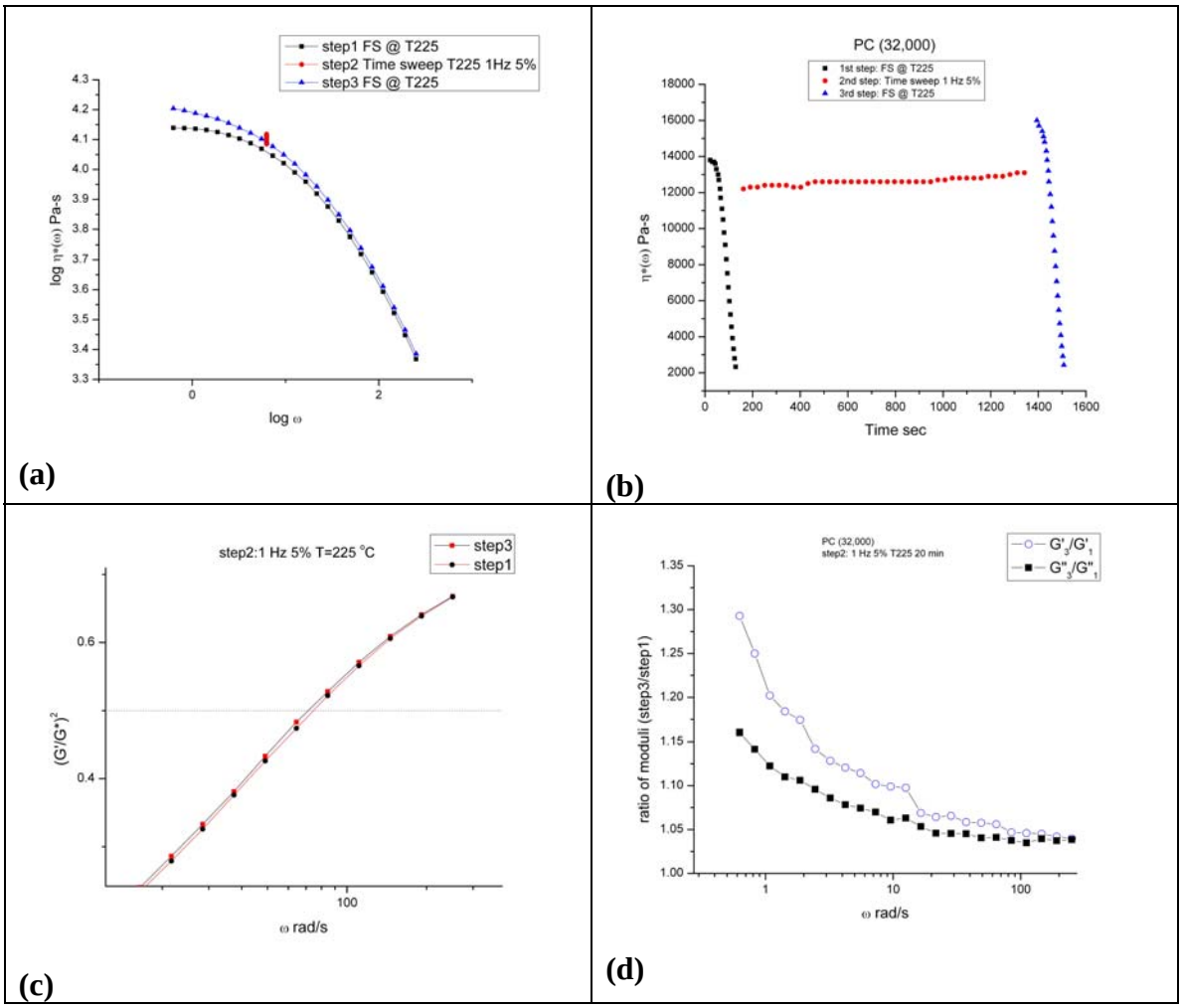

Fig. 43

Effect of a time sweep at 1 Hz 5% T= 225 °C for 20 min on the frequency sweep at T=225 °C , 5% 0.1-40 Hz. The figures compare a frequency sweep done before and after the time sweep step.

Figure 43c, a plot of $(G'/G^*)^2$ vs ω, confirms the absence of any *visible* significant effect on the value of the cross-over point (or on the number of activated strands) of the time sweep stage done under these "soft" oscillating conditions (1 Hz, 5% strain). However, Fig. 43d is interesting in that regard because some features due to annealing (which we said mostly

occurred during step 1) become apparent when different variables are used to analyze the dynamic data. The two curves in Fig. 43d correspond to linear scale plots, versus ω, of the ratio of G" for step 3 and step 1 (squares), and of the ratio of the G' (open dots), respectively. The fact that some recovery occurred after steps 1 and 2 is quite visible in Fig. 43d, which distinctively impacts G' and G"; it is clear that both G' and G" increased respectively (step 3 vs step 1) but that the elastic modulus increased to a larger extent. The increase of modulus was especially effective at low ω (+30% for G', +16% for G" at 0.1 Hz) and almost non-existent (+3% for both moduli) at higher ω . Fig. 43d is another demonstration that the interpretation of Friedrich and co-workers [60, 61], that the observed changes during time sweep are due to edge fracture or surface of contact effects, does not make sense. As already mentioned several times before, if Friedrich was correct, both moduli G' and G" would be modified by the same ratio; thus Fig. 43d would not consist of two distinct curves, but a single one.

3.2.2 - 10 Hz

The same experiments as those in section 3.2.1 were now done with a frequency of 10 Hz during step 2, every other parameter remaining the same. This is a 10 times increase of the frequency and should trigger important changes. The results are shown in Figs. 44 a-d.

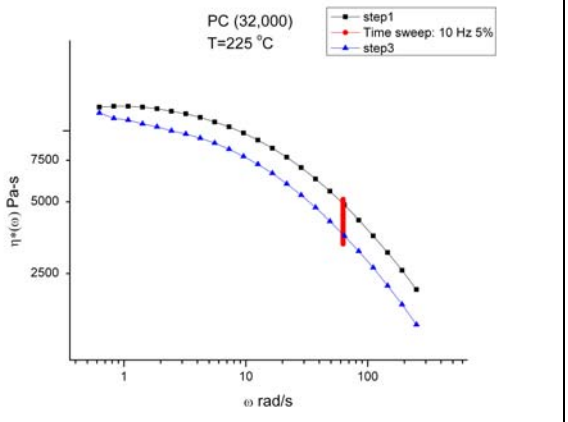

(a)

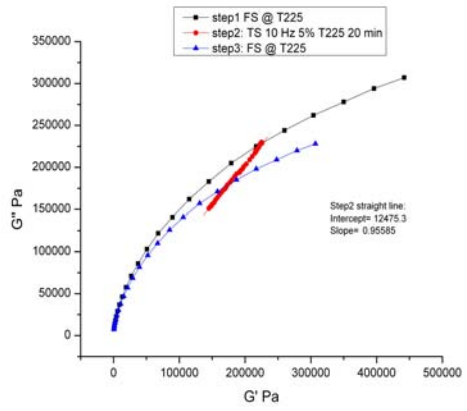

(b)

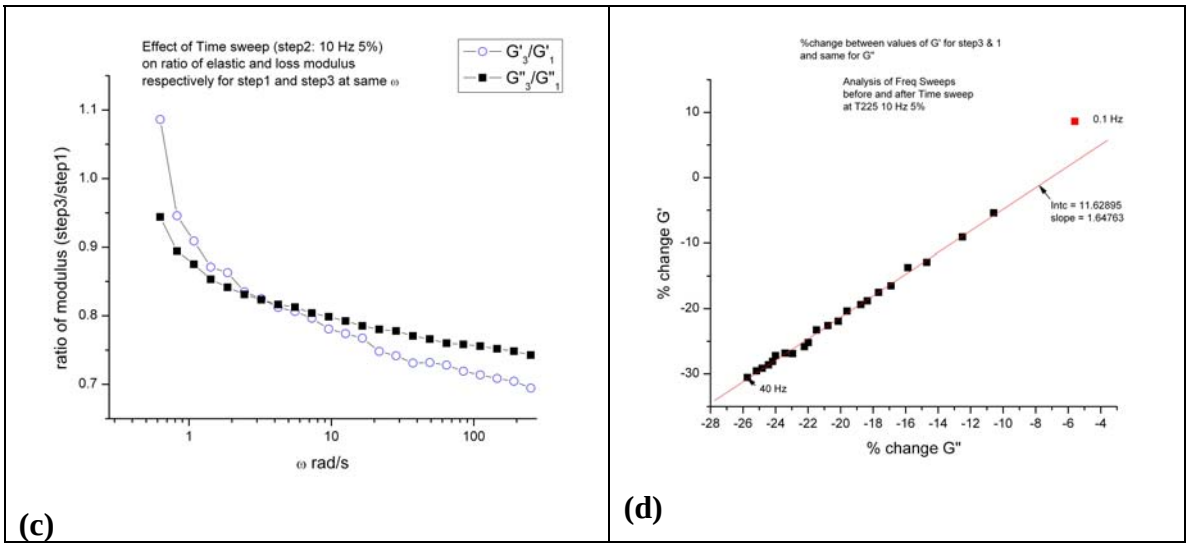

Fig. 44

Effect of a time sweep at 10 Hz 5% T= 225 ^{o}C for 20 min on the frequency sweep at T=225 ^{o}C , 5% 0.1-40 Hz. The figures compare a frequency sweep done before and after the time sweep step.

Figure 44a shows that the viscosity curve corresponding to step 1 (squares) is located above the one for step 3 (triangles) for all ω, and that the imparted viscosity decrease observed for step 3 is due, unlike in Fig. 43a, to the viscosity change occurring in step 2 (the dots), which was preserved.

Figure 44b shows G"(ω) vs G'(ω) for all the steps 1 to 3 (the scales are linear on both axes) demonstrating two aspects of the effect of the treatment:

- 1. G' and G" appear to have decreased more intensely as ω increased, meaning that the melt not only preserved its new viscosity attributes but even became more sensitive to frequency (or strain rate) than the original melt.
- 2. the time sweep treatment in Fig. 44b is shown as a straight line of G" vs G', (the dots) approximately passing through the origin. The regression of that line gives a slope of 0.96 and an intercept of 12,475 Pa. In other words tan δ = G"/G' was *almost* constant during the time sweep, a conclusion that Friedrich et al [60, 61] would attribute to a surface defect. In fact, the ratio G'/G' was not constant because the intercept is not zero, and Figs 44c and d also contradict Friedrich's proposal. Fig. 44c is the same type of plot as Fig. 43d, showing the ratio between step 3 and step 1 of the G" and the G', respectively. Fig. 44c clearly suggests that the effect of the time sweep treatment on G' and G" was much more complex than just a change of

the surface area of contact. Comparison between Figs. 43d and 44c also points to the same conclusion, favoring a modification of the viscoelastic properties of the melt due to a change of the melt entanglement state. The increase of frequency during step 2 not only reduced the value of (G''_3/G''_1) and (G'_3/G'_1), for a given ω of the frequency sweep, but the ratio for G' became smaller than 1 at higher ω, indicative of a softer melt (the ratio for G" is always smaller than 1). The percentage of change of G' (between step 3 and 1) is plotted against the percentage of change for G" in Fig. 44d. A straight line is drawn through the data (as frequency is increased , going downward on the line), and it is quite clear that, although a correlation existed between the changes occurring to the loss and elastic moduli, the slope was not 1 (it was 1.65), which would be the case if a surface defect was responsible for the viscosity decrease observed during step 2 (Fig. 44a). The apparent complexity of behavior seen in Fig. 44c, is simply explained by the straight line in Fig. 44d: the moduli ratio varied more for G' than for G", which means that the treated melt became more sensitive to frequency, i.e.it was a more pseudo-plastic melt.

Increasing frequency in the treatment stage, at constant strain, qualitatively yielded the same result as an increase of strain at constant frequency (compare Figs. 36b and 44a; also Figs. 37c and 44c): viscosity decreases and the changes are preserved for times long enough to be visible in subsequent frequency sweeps. Notice, however, the interesting differences between Figs. 37c and 44c, probably related to the difference in the operating temperature (Fig. 37 is at 275 ^{o}C, Fig. 44 at 225 ^{o}C): in Fig. 37c the ratios are increasing with ω, and in Fig. 44c they are decreasing. The stability of the treated (disentangled) melt is a function of the frequency, the strain and the temperature during the treatment. Like in the case of a glass brought out of equilibrium by an up-quench or a down-quench thermal treatment [71], showing an excess or a lack of free volume with respect to its equilibrium value, a melt can be brought out of its entanglement equilibrium value by a dynamic mechanical treatment, the frequency, strain and temperature determining the mechanical history. The melt properties are no longer uniquely determined, as current models would predict.

3.2.3 - 40 Hz

Figures 45 a to f show the results obtained when the frequency was 40 Hz (251 rad/s) during step 2. All other parameters remained identical to those in sections 3.2.1 and 3.2.2.

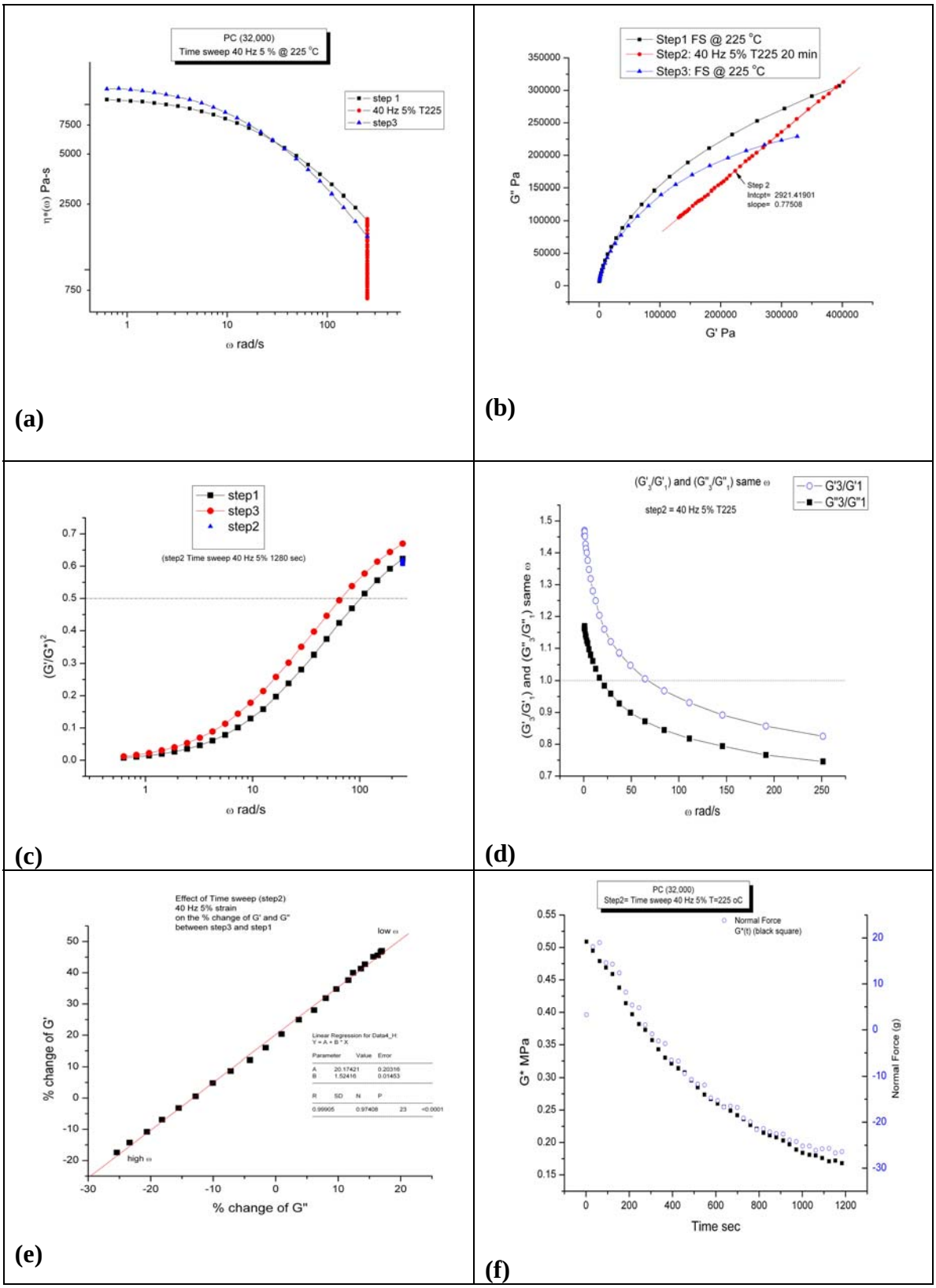
PC (32,000)
Time sweep 40 Hz 5 % @ 225 °C
step 1
40 Hz 5% T225
step3
η*(ω) Pa-s
ω rad/s
(a)
Step1 FS @ 225 °C
Step2: 40 Hz 5% T225 20 min
Step3: FS @ 225 °C
Step 2
Intcpt= 2921.41901
slope= 0.77508
G" Pa
G' Pa
(b)
step1
step3
step2
(step2 Time sweep 40 Hz 5% 1280 sec)
(G'/G")²
ω rad/s
(c)
(G'2/G'1) and (G"3/G"1) same ω
step2 = 40 Hz 5% T225
G'3/G'1
G"3/G"1
(G'3/G'1) and (G"3/G"1) same ω
ω rad/s
(d)
Effect of Time sweep (step2)
40 Hz 5% strain
on the % change of G' and G"
between step3 and step1
low ω
high ω
Linear Regression for Data4_H:
Y = A + B * X
Parameter Value Error
A 20.17421 0.20316
B 1.52416 0.01453
R SD N P
0.99905 0.97408 23 <0.0001
% change of G'
% change of G"
(e)
PC (32.000)
Step2= Time sweep 40 Hz 5% T=225 oC
Normal Force
G*(t) (black square)
G* MPa
Normal Force (g)
Time sec
(f)

Fig. 45

Fig. 45 caption: Effect of a time sweep at 40 Hz 5% T= 225 ^{o}C for 20 min on the frequency sweep at T=225 ^{o}C , 5% 0.1-40 Hz. The figures compare a frequency sweep done before and after the time sweep step.

Fig. 45a shows the viscosity-ω curves before (step 1) and after treatment at 40 Hz, to be compared with 44a (10 Hz) and 43a (1 Hz). The treatment (step 2) is shown at the right end side, corresponding to the dots. The Newtonian viscosity was higher for step 3 than for step 1 (13,100 vs 11,000 Pa-s) despite a very large decrease of viscosity occurring during step 2 (viscosity was equal to 750 Pa-s at the end of step 2). The viscosity decrease obtained during treatment does "not stick", it even reverted to an increase at low ω □□in a manner similar to what is observed in Fig. 43a. Yet, also visible in Fig. 45a, when ω was about 30 rad/s and beyond, a similar behavior to that observed in Fig. 44a characterized the flow properties: the step 3 melt was much more pseudo-plastic and its viscosity decreased much faster with an increase of ω. Extrapolation of the two curves in Fig. 45a, using equation (5) of ref. 2, predicts a 400% decrease of viscosity at ω = 1,000 rad/s, which would approximately correspond to the range of strain rate used in injection molding. In the case of Fig. 45a, the MFI of melt 3, the melt after treatment, would be smaller than the original melt, which could be interpreted as an unsuccessful attempt to decrease viscosity, but its fluidity at high rate of shear would be much improved. This shows that the impact of a history treatment on the final properties of the melt is not straightforward to elucidate. It is remarkable to point out that the only difference between Figs. 43a, 44a and 45a was a change of frequency during step 2. It suggests the important sensitivity of the entanglement state to frequency at T= 225 ^{o}C for this PC grade, even at low strain (5%).

Figure 45b is the equivalent of 44b; it shows the same trend, with noticeable differences though. The G" vs G' straight line (dots) corresponding to step 2, has a slope of 0.77 (vs 1.56 for 10 Hz) and an intercept of 2,921 (vs 12475 for 10 Hz), which is very close to zero, thus $(G'/G^*)^2$ remains constant during treatment (~ 0.62). It is also important to notice in Fig. 45b how the step 2 straight line crosses the step 3 line (for G'~ 275,000 Pa) and continues towards the left bottom corner as time proceeded during treatment (the values of G' and G" after 20 min treatment were 129,000 and 105,000 respectively). If the treatment had fully "stuck", like would be the case for a 100% plastic deformation, these values of G' and G" at the end of step 2 would be the ones found on a step 3 curve for ω= 40 Hz. The difference is

due to an elastic mechanism of retraction which we need to understand and control in order to optimize the technology developed from this type of work [46]. In Fig. 44b, for instance, the treatment seems to be more efficient, i.e. most of the changes of G' and G" induced by step 2 were preserved and recovered on step 3. One needs to understand why this is so.

Figure 45c shows the comparison for steps 1, 2 and 3 of $(G'/G^*)^2$ vs ω and the determination of the cross-over for $(G'/G^*)^2 = 0.5$. This graph confirms that $(G'/G^*)^2$ remained constant to 0.62 for step 2 (triangles), and reveals that the cross-over ω for step 3 ,ω_{x3}, was smaller than the one for step 1, ω_{x1} (67 vs 103 rad/s). The number of active strands was greater for the melt after treatment, for all ω. As we shall explain in the discussion, this means that cooperativity between conformers was increased, which is the reason for the increased shear-thinning ability, i.e. for the increased pseudo-plasticity. The treated melt behaved as if we had increased its entanglement density, not decreased it. A plot of G'/ω vs log ω (not shown) indicates for step 1 a maximum at ω_{x1}= 22.4 rad/s and for step 3 at ω_{x3} = 14.6 rad/s which would be consistent with that conclusion.

Figure 45d is the equivalent for this 40 Hz treatment frequency of Figs 44c (10 Hz) and 43d (1 Hz). In Fig. 45d the ratio for the G' varied between 1.47 down to 0.82 and extrapolated to 0.75 at infinite ω. The ratio for the G" varied between 1.17 and 0.75 and may have almost reached an asymptotic value for the largest ω value of the frequency sweep . The curves in Fig. 44c cross at ω~ 3 rad/s, but they never cross in Fig. 45d, which might be a key observation to understand the retention of the properties after treatment. The spread of % change of G' and G" was greater for the 40 Hz treatment than for the others at 1 Hz and 10 Hz. This is confirmed in Fig. 45e, which should be compared with Fig. 44d (the corresponding figure is not shown for the 1 Hz treatment). The slope was 1.524 and the intercept 20% in Fig. 45e, compared to 1.65 and 11.6 %, respectively, in Fig. 44d. The increase of the G' and G" changes was thus essentially due to a shift of the intercept, from 11.6% to 20%, which may be related to the increased stored elasticity of the strand network, as shown in Fig. 45c.

Figure 45f shows a plot of G* (left vertical axis) and of the normal force (right axis) versus time during step 2. Both parameters can be fitted with a double exponential function with a constant term. For instance, the normal force fit provides:
-32.5 -25.95 exp(-t /18.4) +58.87 exp(-t / 498.03) where t is time in sec. Fig. 45f is quite intriguing: why would the normal force become negative beyond t= 250 sec, and why would

this negative excursion continue to be in full agreement with the decay of G*? The asymptotic value found for the normal force was -32 g, which is an attractive normal force of magnitude 16,000 Pa.. For a "normal" melt, the induced elasticity by the torsional shear deformation creates a push against the plates of the rheometer, corresponding to positive normal force. In the case of Fig. 45f, it appears that the treatment reduced both the shear stress, G* and the corresponding normal force, and that the excursion into the negative normal force region is the mere continuation of the process that reduced G*(t). We do not see any discontinuity in the decay of these functions, nor in the ratio of $(G'/G^*)^2$ which remained equal to 0.62 beyond t=250 sec (not shown), nor in the variation of G"(t) vs G'(t) in Fig. 45b. We conclude that the occurrence of the "attractive" normal force was real and describes some real changes occurring in the melt. Such negative normal forces during transient behavior was already reported earlier, not only for pure rotational flow experiments (Type 4), see Figs. 19d and 20, but also for dynamic experiments (Figs. 35b and 38). The "structuring" of the melt into laminated layers might be responsible for these negative normal forces, as has already been mentioned when describing those figures. Incidentally, the structuring into layers might also be responsible for the partial lack of retention of the viscosity reduction, as we shall discuss later.

3.3 Effect of increased energy input during Time Sweep: T= 225 ^{o}C, Frequency=5 Hz and γ=20%.

In this section, the frequency was 5 Hz and the strain was raised to 20% during step 2, all other conditions remained the same as in section 3.2 The frequency sweeps were done with 5% strain. Figs. 46a to f show the results.

Figure 46a is the now familiar plot on linear scales of viscosity vs time across steps 1, 2 and 3. The comparison between step 1 and step 3 is very significant: there was a huge drop of the Newtonian viscosity from 12,000 to 3,500 Pa-s due to the step 2 treatment at 5 Hz, 20% strain for 20 min. The viscosity decrease is also visible at high ω, although Fig. 46b shows it better (the viscosity at 40 Hz on the step 3 curve was still 3 to 4 times smaller than the value found at 40 Hz on step 1).

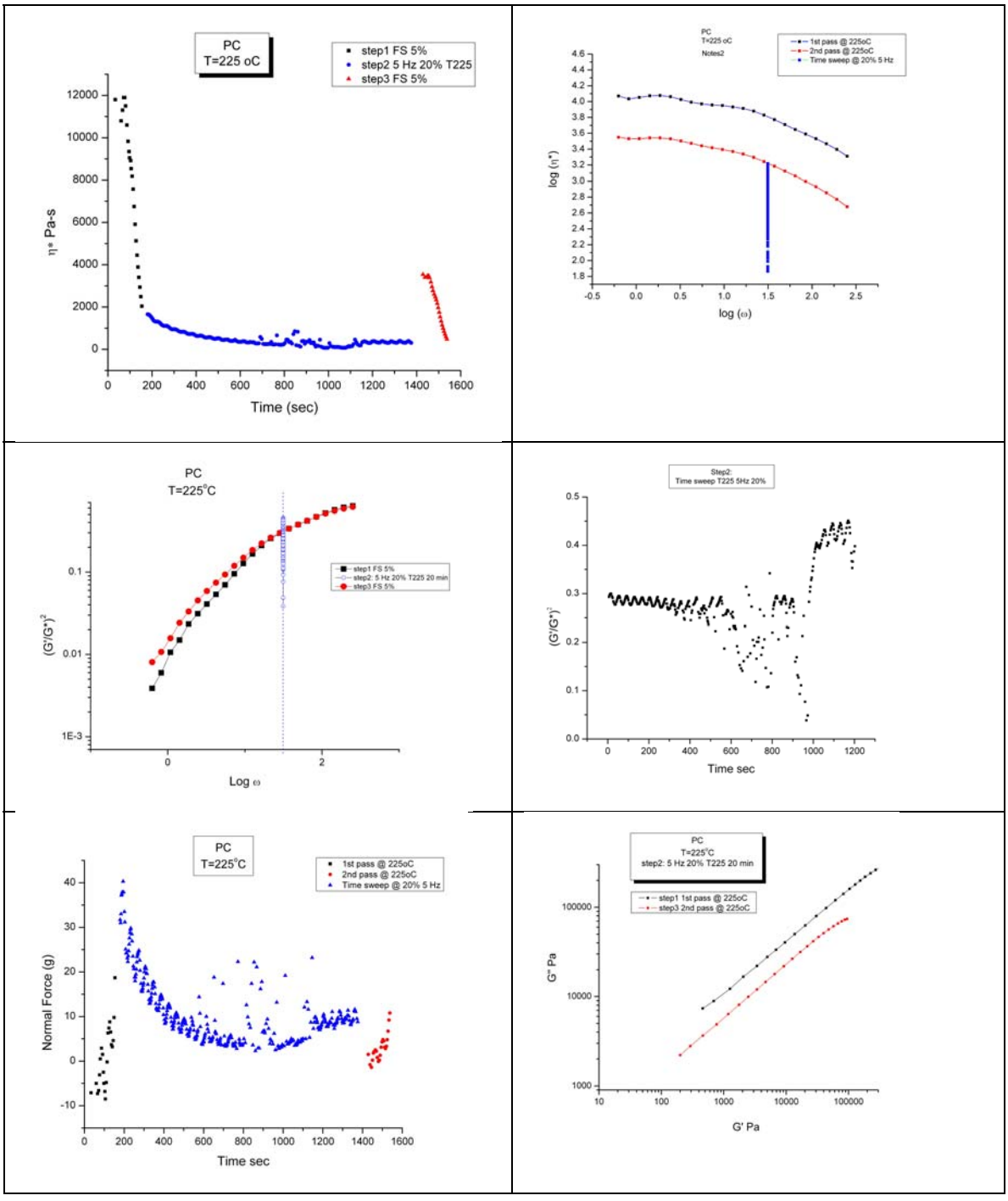

Fig. 46

Effect of a time sweep at 5 Hz 20% T= 225 ^{o}C for 20 min on the frequency sweep at T=225 ^{o}C , 5% 0.1-40 Hz. The figures compare a frequency sweep done before and after the time sweep step.

It is noticeable in Figs. 46a and b that the step 2 curve started at nearly the same viscosity level as at the end of the step 1 curve. Yet, frequency was 40 Hz at that point for the step 1 curve, and only 5 Hz for the step 2 curve. Viscosity should be higher than what was observed, based on shear-thinning due to strain rate effect. The lower viscosity observed at the beginning of step 2 is due to strain-softening obtained by the increase of strain, from 5% to 20% in this instance. It has been already noted that strain plays a thinning role, in many ways similar to the effect of strain rate. Actually, based on simple considerations, one can expect such a similarity: for a dynamic experiment, the strain rate is not ω, but $\omega\gamma$, where γ is the strain.

Figure 46b clarifies further the effect of changing the frequency and the strain at the end of step 1. The position on the ω axis of the step 2 vertical line indicates the frequency of work during the step 2 treatment. As already mentioned for Fig. 46a the step 2 curve initial viscosity approximately coincided with the value obtained at the end of the step 1 curve, i.e for 5 % 40Hz. This is a pure coincidence. The important observation is the difference between the step 1 curve (top) and the beginning of the step 2 curve on the vertical line corresponding to 5 Hz. That difference, due to strain softening at 5 Hz T=225 ^{o}C, was preserved in the step 3 melt. Notice that the two frequency sweep curves seem to remain parallel, in particular that they are shiftable on the log η^* axis. Notice also that the step 3 curve passes through the exact same point that originated the viscosity decay for step 2. In other words, the melt PRESERVED the same value of viscosity that was the result of coupling the effect of shear-thinning and strain softening at the beginning of step 2. There is apparently no incidence on the step 3 melt curve of the large decay of viscosity occurring during step 2 (the log η^* decreasing from 3.2 to 1.9!). All of the viscosity decrease in step 2 must have recovered in the lapse of time it took to switch from the experimental conditions of step 2 to those of step 3, about 20 sec.

Figure 46c compares the number of activated strands bearing stress (proportional to $(G'/G^*)^2$ for the original melt (step 1) and the treated melt (step 3), showing that this is not the parameter that was mainly modified by the treatment under those conditions. In Figure 46c the step 3 curve (dots) is located a little bit above the step 1 curve (squares) in the frequency region below the treatment frequency (5 Hz). However, there was no change observed above the treatment frequency. This lack of change of $(G'/G^*)^2$ is significant in view of the large decrease

of viscosity observed for melt 3. The vertical line in Fig. 46c corresponds to step 2 done at 5 Hz. One observes for step 2 a little portion of $(G'/G^*)^2$ values located *above* the step 1 and 3 curves. This is explained in Fig. 46d

Figure 46d is a plot of $(G'/G^*)^2$ vs time during step 2, showing the initial maintenance of the number of activated strands at approximately 0.3 for about 450 sec, followed by large fluctuations, an attempt to maintain the integrity and the cohesion of the initial entanglement network, followed by the construction of a new entanglement network of strands with a higher number of activated strands, approximately corresponding to $(G'/G^*)^2 = 0.42$. The final melt had a higher elasticity; this corresponds to the small tail, the portion of points for step 2 located above the step 1 and step 3 curves in Fig. 46c.

A small fluctuation of the signal is perceived in Fig. 46d; it is not related to the structural instability, it was due to a small temperature fluctuation imposed on the melt to allow a fine analysis of the mechanical deformation details [72].

A rheological criteria must be defined to account for the instability of the initial network under the excessive energy application induced by the parameters of deformation in step 2. Time obviously plays a crucial role, since it took 450 sec before the instability of the entanglement network created its re-structuring into a different network, with higher activated strands sustaining the deformation.

Figure 46e is a plot of normal force vs time across the three steps. The normal force value went up to 40 g in the first frequency sweep. That normal force decayed in step 2, in a way that mimics what happened to $(G'/G^*)^2$ in Fig. 46d, i.e. the decay was "normal" until about 450 sec when some large fluctuations appeared for the first time, seemed to stabilize somewhat, and then there was a slight rise of the normal force at the end, beyond 1200 sec. The step 3 melt had very little normal force, which only went up to 10 g, 1/4th the value found for step 1; the step 3 melt had lost 75% of its elasticity.

Figure 46f is a plot of G" vs G' on a log-log scale comparing melt 1 and melt 3. This plot should be compared with Figs. 31 and 41 for melts whose treatment during step 2 was done at higher temperature ($T=275^oC$) and lower frequency (0.1 Hz). In Fig. 46f the G' and G" values at each frequency was considerably higher for the untreated melt, the treated melt being located well below the initial melt, and the data collected onto parallel lines. Interestingly, the

amount of change on the G" axis was about twice as large as what is observed on the G' axis, and this ratio remained approximately constant as ω varied. This is different from what we observed for other treatment conditions, for which the changes were greater for the elastic modulus (Figs. 44d, 45e).

An important question arises from the results of Figs. 46a to f: what caused the viscosity decrease to "stick" ? Is it because the melt went into a new cohesive network of entanglement during step 2, which would be the equivalent of going through a plastic deformation (thus freezing the state –shear-thinning plus strain softening- that it had acquired before such freezing step)?

One observes in the middle of step 2 (Figs. 46d and e), a large scattering of data, as if the melt had lost its cohesion at one point. This is not melt fracture because there was no apparent modification of the MWD, as checked by GPC, and the stress was too low to produce melt fracture. We speculate that this feature corresponds to the renewal of the network of entanglement, a re-organization of the cohesive network of interactive conformers, the Dual-Phase "EKNET network" as we called it [73]. This is due to the amount of energy stored in the strained networked of strands reaching a critical value. In terms of the deformation of the dual-phases of the EKNET network, using the analogy of a pipeline network of branched rivers to represent the entanglement phase, this is as if new branches had to be created due to an overflow situation. The cohesion and stability of the entanglement network can be brought to their limit, to the equivalent of the onset of melt plastic yielding, beyond which new viscoelastic properties of the melt are expected. The decohesion and renewal of the entanglement network is essential to understand. It is quite possible that the success of preserving into a pellet form the viscosity changes induced by mechanical deformation will depend on whether the melt has crossed its plastic yielding criteria.

3. 4 Effect of Annealing the melt after treatment and experiments of Type 3

In this section we review published data [13, 14, 23, 50] obtained to characterize shear-refined (treated) PC by the technology described in Figs. 5a and b . This is the same PC grade

as in sections 3.1 and 3.2 above. The experimental procedure was described as a Type 3 experiment in section 1 “Experimental Procedures” and in section 4.1 of “Initial State and Sample Molding Procedure”. The difference with sections 3.1 and 3.2 is that the “disentanglement” treatment was not done inside the rheometer but through a disentangling processor and pellets of the treated melt was produced. We already studied in section 3.1.4 the properties of a melt produced out of such treated pellets.

The two graphs of Fig. 47 compare the complex viscosity – radial frequency ω curves at T= 275 ^{o}C (obtained in the linear viscoelastic range, with 5% strain) for a reference melt (prepared from the virgin pellets) and for a treated (disentangled) melt prepared from pellets obtained from the shear-refinement treatment. The symbols in Fig. 47 correspond to the frequency sweep data points, the continuous lines are fits with the Carreau’s equation [Eq. (5) of Ref. 2] and their extrapolation to ω = 1,000 rad.sec^{-1}. As mentioned before, this value corresponds to a strain rate in the range of what occurs in an injection molding machine. Figure 47 shows that the treated melt had a slightly lower Newtonian viscosity than the virgin melt. This was confirmed by an MFI test performed on both the virgin and treated pellets: the MFI of the treated pellets was only 20% higher than the virgin pellets. However, the situation was very different at high ω, due to a spectacular increase of the pseudo-plasticity of the treated melt. Fig. 47 indicates a 5 fold increase of fluidity at ω = 1,000 rad/s

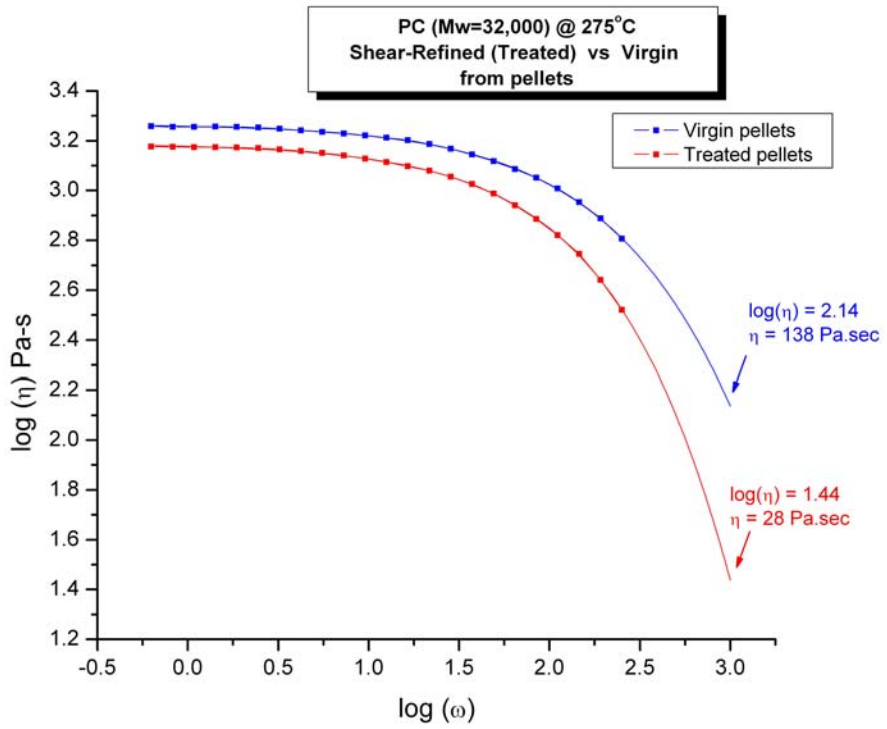

Fig. 47

Comparison of the frequency sweeps at T=275°C for the Virgin and the treated (disentangled) pellets made with apparatus in Figs. 5a and 5b.

Figure 48 compares the G' and G" between the reference and treated samples. It is clear that the difference between the respective moduli (treated vs virgin) was only significant and increasing at higher ω, confirming an increased shear-thinning ability at higher shear rates. Figure 49 compares the viscosity- ω curves of a treated melt before (1st pass), and after annealing it at T= 275 °C for 10 minutes (2nd pass) The frequency sweeps were conducted at T= 225 °C (the melt was cooled down to T=225 °C after its annealing period. The treated melt is represented by the dots (the lower curve). Annealing here was a true thermal treatment, with no mechanical deformation on the sample.

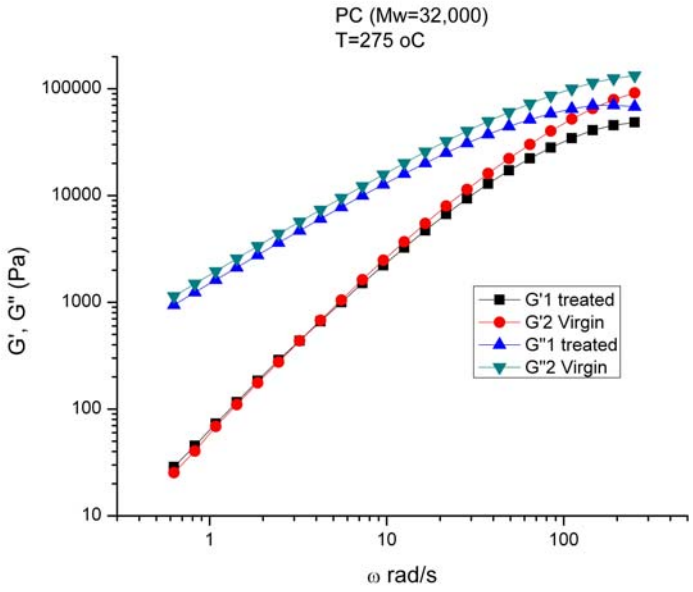

Fig. 48
G' and G" vs ω for the data of Fig. 47

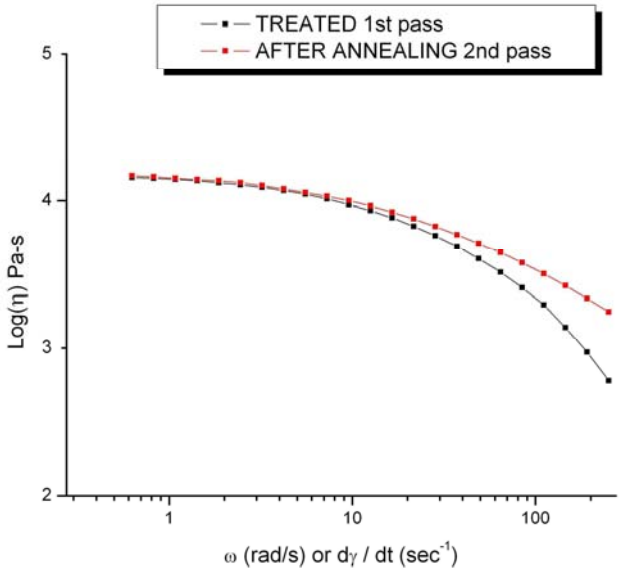

Fig. 49
Comparison of Dynamic viscosity vs w for a treated (dots) and a treated-annealed (square) melt. See text.

Figure 49 shows that the Newtonian behavior was unchanged by annealing. Both curves coincided at low ω. However, annealing converted the high frequency behavior back to its original virgin status: the extra-shear-thinning observed for the 1st pass, i.e the increase of pseudo-plasticity, was gone for the 2nd pass. The improvement of the pseudo-plasticity of the treated polymer melt appears to be temporary.

Figure 50 attempts to determine how fast the recovery takes place. For this test we operated at T= 275 °C for all steps, the 1st pass, the annealing step and the 2nd pass, in order to avoid the intermediary times of heating and cooling. Annealing was only for 5 minutes. Figure 50 shows the virgin melt, the 1st pass for the treated sample and pass 2 for the annealed sample. The instability of the treated melt is clearly evidenced: the melt had already started to revert back to its equilibrium (virgin) properties after only 5 minutes of annealing. Note, however, that the destruction of the benefits of an increased pseudo-plasticity by the 5 minute exposure at T=275 °C was far from complete. Considering that this temperature is 130 °C above the T_g, it is already remarkable that the melt could exhibit such "long" period of metastability (with respect to its terminal time). Yet this annealing test reveals another difficulty in producing treated disentangled melts, with regard to their time and temperature stability. If the time of exposure at a high temperature "re-entangles" the melt too fast, it will restrict the type of applications feasible with the use of such melts

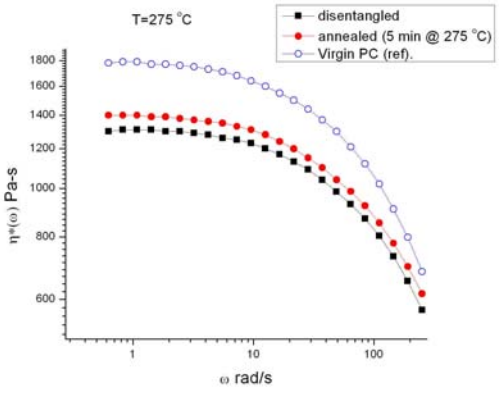

Fig. 50

Comparison of frequency sweeps (dynamic viscosity vs w) for a Virgin, a disentangled and an annealed disentangled melt. See text.

Figures 51a and b compare the respective ratio of elastic (G'_3/G'_1) and loss (G''_3/G''_1) moduli vs ω for a treated sample (step 1) and after annealing (step 3) on one hand (Fig. 51a) and for a reference virgin melt (Fig. 51b) that was annealed similarly. All steps were conducted at T= 275 ^oC including annealing. The annealing time was 10 min.

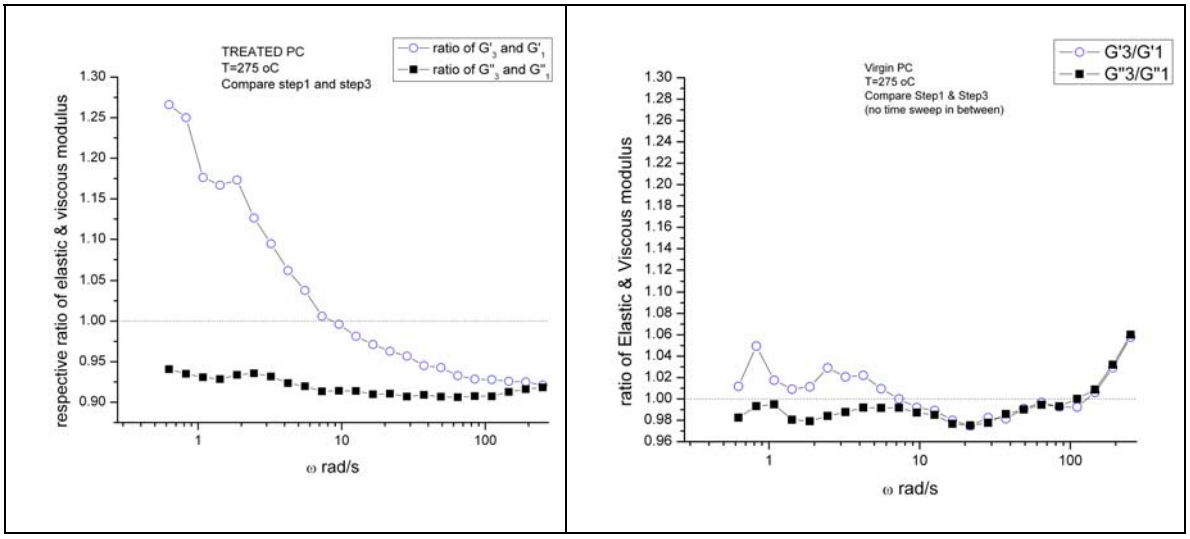

Fig. 51a **Fig. 51b**

Comparison of the respective ratio of elastic and loss moduli vs ω for a treated sample ("as is" and after annealing) and for a reference virgin melt. The frequency sweeps before and after annealing, and annealing were all done at T= 275 ^oC. Annealing time 10 min.

An horizontal line, corresponding to a ratio of 1, is also drawn on the graphs as a way to indicate the behavior expected for a melt that would not change before and after annealing. Figure 51b demonstrates that it was, indeed, the case for the virgin sample: the ratio for G' and for G" both remained the same and randomly equal to 1, respectively. Fig. 51a applies to the shear-refined (treated) sample and one can see that the ratio for G' and for G" were different. The ratio for G" remained quasi-constant at ~0.925 whereas the ratio for G' varied with ω, decaying from 1.27 to 0.925. This behavior resembles that of a boosted pseudo-plastic melt, as shown earlier for melt treatment of type 2 (Figs. 43d and 45d). This analogy of viscoelastic behavior between a disentangled melt processed by a disentanglement machine that produces pellets and by a time sweep treatment inside a lab dynamic rheometer may constitute a

convincing proof that no credit should be given to an edge fracture mechanism to explain the time dependence of viscosity in the case of the lab dynamic experiments [60.61].

For Fig. 52 we ran an experiment of Type 3 (specified in Section 1 "Experimental Procedures") on a shear-refined PC sample of M_w=35,000. The first frequency sweep ("1st pass") was done at T= 225 °C (dots), then the temperature was raised to 275 °C to run a frequency sweep at that temperature ("1st pass@275", triangles). The temperature was then lowered to 225 °C where a second frequency sweep was run at that temperature ("rt at 225", filled squares). Finally, the temperature was raised to 275 °C and a new frequency sweep ("rt @ 275°C", open squares) was done. All the frequency sweeps were done in the linear range (5% strain), so there is no question of a surface artifact whatsoever under such conditions. Figure 52 forcefully illustrates many features observed throughout this Section 3 about the rheological behavior of melts brought out of equilibrium. The comparison of the 1st and 2nd pass at T= 225 °C, after raising the melt temperature to 275 °C and running the 1st pass frequency sweep at 275 °C, is quite spectacular. The viscosity difference (decrease) at ω =250 rad/s between these two curves was 10 folds. "Annealing" at 275 °C did make the original treated melt lose a great deal of its pseudo-plasticity benefits, but not all of it, as can be deduced by comparing the 1st pass and the rerun at the higher temperature of T= 275°C. Only the rerun at T=275 °C was identical to the virgin at that temperature, meaning that there was still an important amount of boosted pseudo-plasticity remaining in the 1st pass at T=275 °C, and therefore in the 2nd pass at T=225 °C. In other words, the melt had only entirely recovered its entanglement equilibrium state after the 12 minutes it took to run the 1st pass at 225 °C, the 1st pass at 275 °C and the 2nd pass at 225 °C.

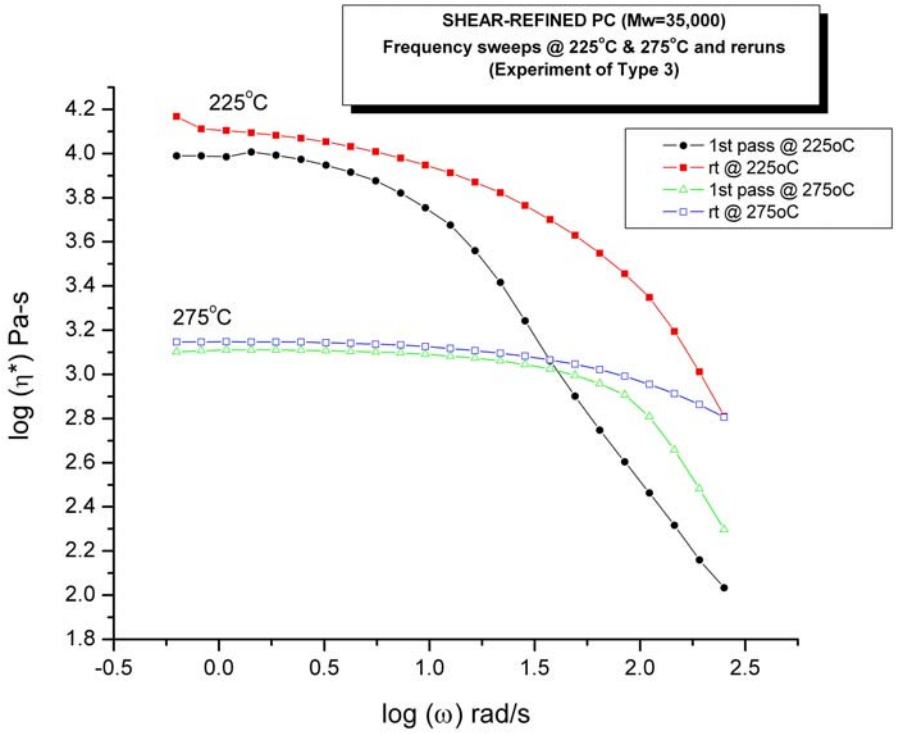

Fig. 52
Comparison of frequency sweeps for experiments of Type 3. The initial melt is disentangled by the apparatus in Figs. 5a and 5b. See text.

Figure 53a gives the variation of G'(ω) and G"(ω) for the two frequency sweeps done at T=225 °C, step 1 and step 3 (after "annealing" at T=275 °C). For the treated melt (step 1), both G' and G" go through a maximum for ω~20 rad/s. After "annealing" at 275 °C, the rerun shows that both G' and G" gained a decade in magnitude and that the value of the maximum of G' and G", still present, was shifted to ω~100 rad/s. This is a situation very similar to that depicted in Fig. 22c for another polymer, LLDPE, sheared in a type 4 experiment (pure viscometry) before running a frequency sweep. Figure 53b plots $(G'/G^*)^2$ vs ω for the initial (treated) melt (dots) and the melt after annealing (squares). It should be compared with Fig. 22d. For both the sheared LLDPE of Fig. 22d and the shear-refined treated PC sample in Fig. 53b, the higher ω behavior is matched by an increase of $(G'/G^*)^2$, which we attribute to an increase of the "internal stress" of the active strands, not to an increase of their number. This causes the pseudo-plasticity boost responsible for the excess viscosity decrease. As shown in

another paper [71] and in chapter 5, the degree of shear-thinning is directly correlated with $(G'/G^*)^2$, thus an increase of its value results in a decrease of viscosity. This represents one way to produce a decrease of viscosity and, as shown in Fig. 52, this method can be very effective.

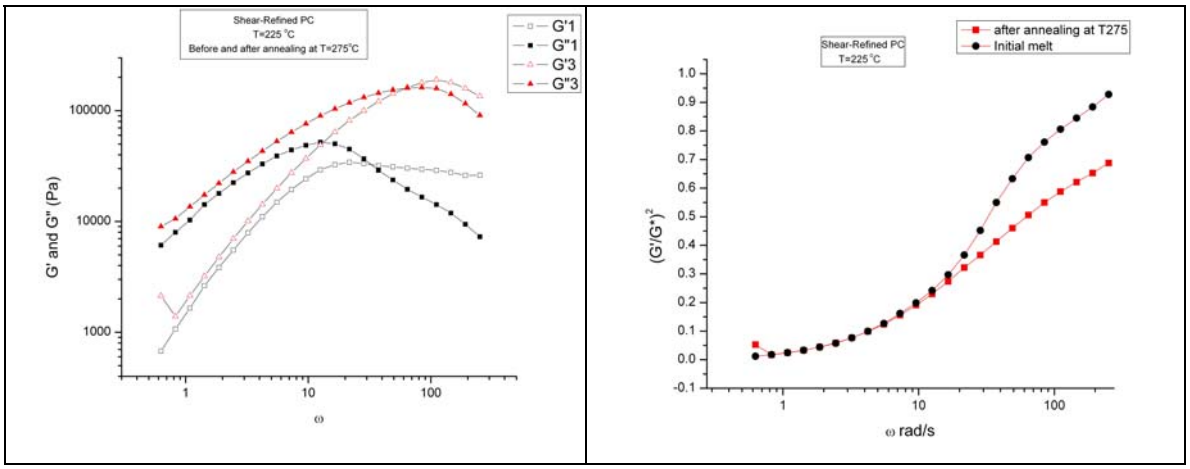

Fig. 53a **Fig.53b**

Analysis of a disentangled melt before and after annealing. (a): G' and G" vs ω; (b): $(G'/G^*)^2$ vs ω

However, as pointed out above, the relatively short term stability of the boosted melt might be a limitation for preserving its benefits. Long term stability arises when the shear-refinement process has focused (and succeeded) in modifying the number of active strands bearing stress: this is demonstrated by the lowering of the value of $(G'/G^*)^2$ at low ω. When this is the case, the Newtonian viscosity is substantially lowered as well (see below in Fig. 55 an example with PMMA). The goal is, of course, to find shear-refinement processing windows that combine a controlled modification of the number of active strands with the modification of the strand internal stress, resulting in "smart processing".

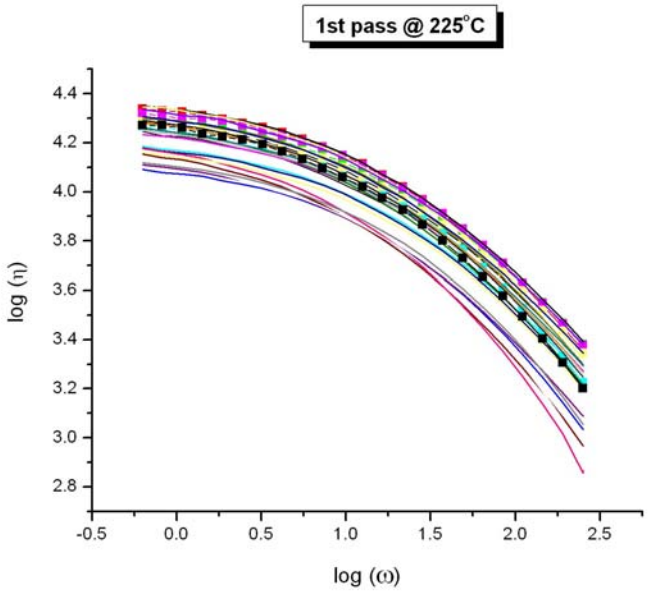

Fig. 54

Comparison of frequency sweeps (dynamic viscosity vs ω 1st pass) at the same temperature for a series of disentangled melts processed under different conditions.

Fig. 54 is a collection of 1st pass curves, such as the 1st pass curve in Fig. 52. They all correspond to shear-refined pellets molded into disks analyzed in the same rheometer, at the same temperature, following the same procedure, by the same operator. We showed in ref. 2 that such conditions yield a 0.5 % reproducibility between samples. Also eliminated from the collection in Fig. 54 were all samples which had a Mw different from the reference by more than 3% (as measured by GPC). According to traditional views of the molten state, all curves of Fig. 54 should be one single curve. The result is quite revealing: thermal-mechanical history, which is what differentiates these samples, can alter very significantly, by as much as 20 times, the value of the viscosity at any given point. In summary, the fundamental viscoelastic properties of a PC melt can be modified at will by entanglement manipulation. In Fig. 54 we demonstrate that we can create melt entanglement states which yield lower viscosity than the reference (the filled squares), presumably corresponding to thermodynamic conditions, but also greater viscosity than the reference (all curves located above the black squares). One of the melts of Fig. 54 was the starting melts (step 1) studied in section 3, which

could be heated and/or mechanically annealed in step 2 to induce viscosity recovery, back to the thermodynamic entanglement state. This is general. The melt entanglement state is like a glass state and can be brought out of equilibrium by thermal-mechanical means, such as pure viscosimetry or pure oscillation, or by a combination of those means.

4. Long Term Entanglement Network Instability for a PMMA melt

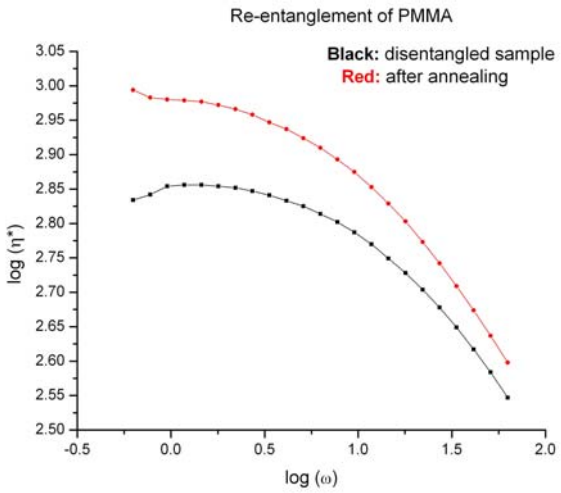

Fig. 55
Comparison of dynamic viscosity vs ω curves obtained for a disentangled PMMA sample before annealing (dots) and after annealing (squares). See text.

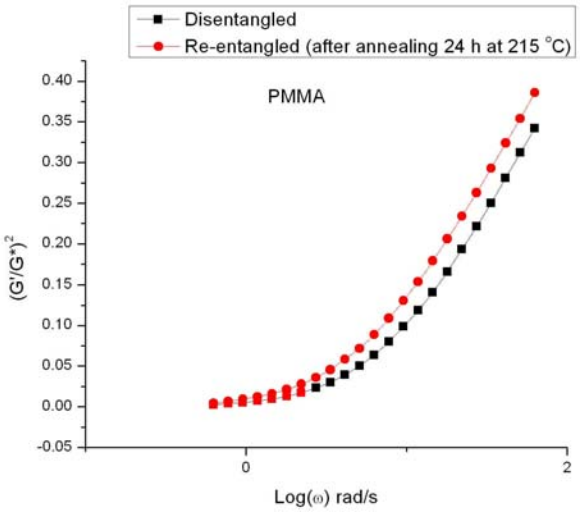

Fig. 56
$(G'/G^*)^2$ vs ω for the data of Fig. 55

Figures 55 and 56 apply to a PMMA random copolymer of 95% methyl methacrylate and 5% ethyl acrylate with M_w=78,000, M_n= 40,000 and Tg=104 ^oC. Figure 55 is a plot of complex viscosity vs ω on log-log scales, Fig. 56 is a plot of $(G'/G^*)^2$ vs log ω. The squares correspond to a frequency sweep performed at T = 215 ^oC (0.1 Hz to 40 Hz, 2% strain) on a melt made out of pressed, disentangled pellets. Shear-refinement was performed using the disentangling two-stage processor described in Fig. 5b, producing pellets showing a 70% decrease of its Newtonian viscosity (as measured by MFI).

This disentangled melt was very stable (compared to the PC melts of section 3, for instance). Annealing at T=215 ^oC for 1 hour under N_2 conditions did not produce any sign of recovery of the viscosity drop induced by the treatment. It took 24 hours of annealing time in the rheometer (under no stress) to finally obtain the dots curve in Figs. 55 and 56, which compares well with the initial untreated (virgin) melt frequency sweep.

Figure 55 clearly shows the decrease of the Newtonian viscosity for the treated sample as well as its lower viscosity at all frequencies. Fiure 56 compares the number of activated strands for the disentangled sample and the sample annealed for 24 hours, which we called "re-entangled". The disentangled melt had less activated strands than the re-entangled (and the virgin) melt. This is the reason, we suggest, why the Newtonian viscosity was lowered. This is perhaps also one of the reasons for the stability of the disentangled melt which required no less than 24 hours to recover its equilibrium entanglement network state. One may wonder why this disentangled melt became so stable. Could it be that for PMMA, under the conditions of operation of the two-station disentangler (Fig. 5b), a new entanglement network was created, in the sense of what we assumed to have occurred for the PC sample treated in step 2 at T=225 ^oC, 5 Hz 20% strain (section 3.3, Fig. 46d) This new entanglement network might be much more stable than just a disentangled melt produced by "orientation" of the entanglement network (note that this orientation is different but <u>driven</u> by the molecular orientation that is controlled by the terminal time). The type of entanglement network orientation and de-cohesion we are talking about is modulating the local interactions between the bonds which are occurring much faster, with rate $1/\tau_o$.

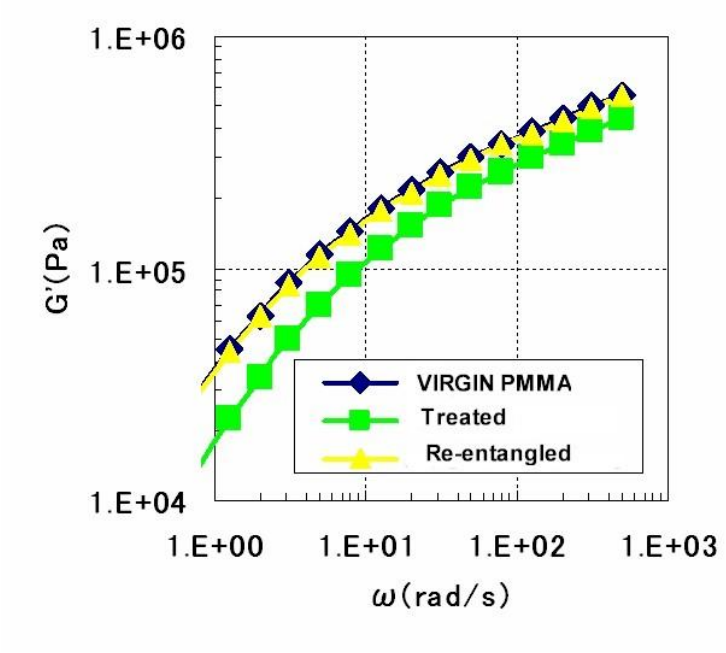

Fig. 57

Comparison of G' vs ω plots for a virgin sample, a treated (disentangled) sample and a re-entangled sample. See text.

In Fig. 57 G' is plotted against ω for 3 types of melt. The virgin PMMA (diamonds) corresponds to a melt prepared out of virgin PMMA pellets (the same PMMA as in Fig. 55), the squares correspond to pellets from a shear-refined (treated) melt, and the triangles apply to a "re-entangled" melt after disentangled pellets are dissolved in a solvent, the solvent evaporated, and new pellets produced to be melted and studied by frequency sweep. Figure 57 shows the shifted respective positions of the elastic moduli at all frequencies for the treated (disentangled) melt, and the return of G' to the reference curve, after re-entanglement through solvent dissolution had taken place. Fig. 57 is an excellent proof that disentanglement and re-entanglement are reversible phenomena that do not involve MWD changes. The same experiments were also reported by Hanson for PE [28] and by Stange et al. [42] for PP when those polymers were submitted to shear-refinement.

5. Entanglement Network Instability for a Polystyrene melt.

5.1 PS 1070

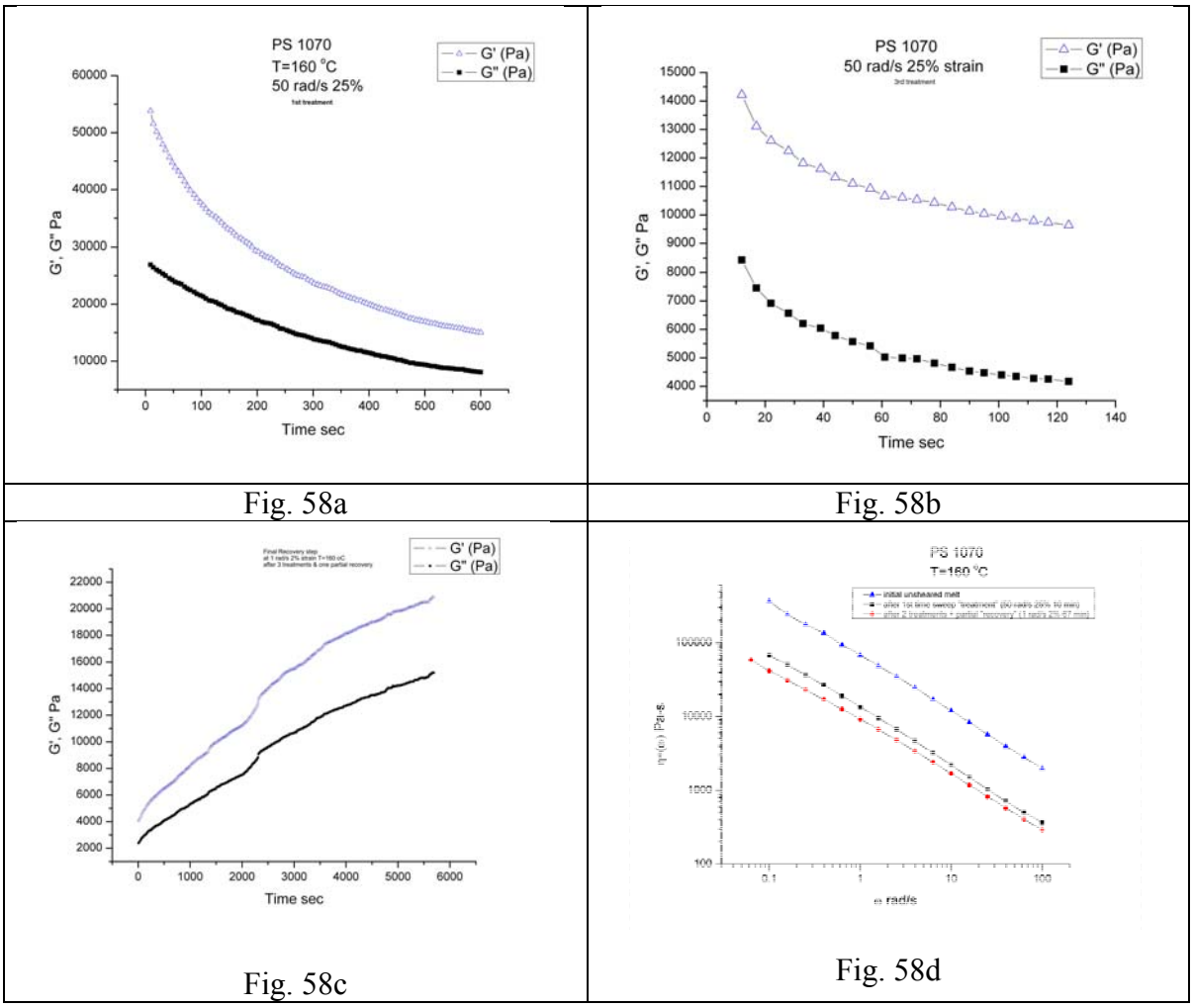

Fig. 58a

Fig. 58b

Fig. 58c

Fig. 58d

Fig. 58

Transient behavior observed in a dynamic rheometer with PS (Figs. 58a, b, c) for conditions given in the text. Fig. 58d compares frequency sweeps for different states of stability of the entanglement network, created by the previous time sweep "treatment" history.

Figure 58a to d relates to PS_1 from the section 3 "material" list. It is the same PS already described in Figs. 10, 11a and b and 12. Figure 58a displays G' and G" vs time during a time sweep done at 8 Hz (ω=50 rad/s), γ= 25%, T=160 °C to induce a transient decay. The strain was gradually raised to 22% by steps of 5% done every 3 minutes (as explained before, this ramp was to let the melt relax the amount of built-up elasticity at each step increase to avoid melt fracture). Fig. 58a is called "1st treatment". It lasted 10 minutes. Both G' and G" started to decay. The ratio (G'/G*) also decayed (not shown), a good indication that the transient was not due to a surface effect or slip. A second "treatment "of 10 min (a repeat of

step 1) was done just after the 1st one was finished, with an interruption of 2 min (rest) in between. Then a partial "recovery" was conducted (at ω=1 rad/s 2% strain) for 67 min. Neither of those two steps curves are shown. Fig. 58b corresponds to a 3rd treatment (using the same oscillation conditions ω= 50 rad/s γ=25%). The magnitude of the change of the modulus G' and G" should be compared with those in Fig. 58a: the initial value for both was decreased by ~25 times at the end of Fig. 58b.

Figure 58c shows a new recovery step conducted at the end of the thermal history, lasting 6,000 sec, with ω= 1 rad/s 2% strain, where it can be seen that G' and G" increased with time steadily but slowly, at a pace much slower than the decreases observed during the initial treatments. The difference of kinetics between treatment timescale and recovery may be related to the influence of frequency on the magnitude of the stress (by elasticity build up) which influences the barrier of the activated processes involved in the interactions between the conformers, as mentioned several times in this chapter. Interestingly, in Fig. 58c the recovery shows at t ~ 2,250 sec a sort of shift of the curve; this may be related to a memory effect for the transient network of strands, similar to what was observed by Kovacs [71] for a glass returning to equilibrium. The increase of the rate of recovery might very well reflect the incidence of either the 1st recovery step or the interruption of 2 minutes between the first two treatments, and demonstrate the kinetic aspect of the entanglement network. A melt behaves like a glass with respect to its entanglement network; it is capable of memory effects. This statement has profound consequences to understand what entanglements really are: static topological interpretations of entanglement cannot, in our view, account for the results presented here and throughout this dissertation.

Figure 58d provides the complex viscosity- ω curves (on a log-log scale) at various states of the melt evolution after the successive time sweep treatments. This plot should be analyzed along with the results of Fig. 12 which provide $(G'/G^*)^2$ vs ω for the same frequency sweeps (for the same polymer). The curve at the top of both Figs 58d and 12 (triangles) corresponds to the un-sheared melt, the Reference. The squares curve applies to the state of the melt after it was through the first 10 min treatment. The viscosity decrease incurred during the time sweep treatment was almost totally preserved ("the treatment stuck"). We saw in Fig. 12 that the extrapolated curve for the un-sheared melt cut the 0.5 horizontal line at a

ω_x~ 0.01. The cross-over for the 1st treatment curve was located at ω_x ~ 0.1, so 10 times bigger. This is the reason for the melt viscosity benefits "to stick": the number of entanglement strands were significantly reduced by the 1st 10 min treatment.

The dots curve in Fig. 58d (and in Fig. 12) corresponds to the state of the melt after it had gone through two treatments of 10 min each and the partial "recovery" (time sweep at ω= 1 rad/s 2% strain 67 min). One sees that the viscosity curve was no longer parallel to the reference, the recovery step affecting the higher frequency relaxation times faster than the slow ones. This observation relates to the complexity of the kinetics of the return to equilibrium of a metastable network of entanglements. Also, note the correspondence between the changes occurring to the viscosity and to the value of $(G'/G^*)^2$ after each step, the repositioning of these curves with respect to the reference curve being similar. As already mentioned for Fig. 12 the height at the maximum value of $(G'/G^*)^2$ was less for the treated melts. The maximum number of activated strands possible decreased for the sample that went through a transient decay.

5.2 PS2: Thermal-Mechanical History to Create Out-of-Equilibrium Melt Properties.

We present in this section another example of thermal-history to help understand the stability of the entanglement network and the various facets linked to its deformation. Figure 59 is a $(G'/G^*)^2$ vs ω plot for PS_2 (specified in section 3 of Experimental procedure). The frequency sweep was done at 2% strain, T=155 ^oC, i.e. in the linear range.

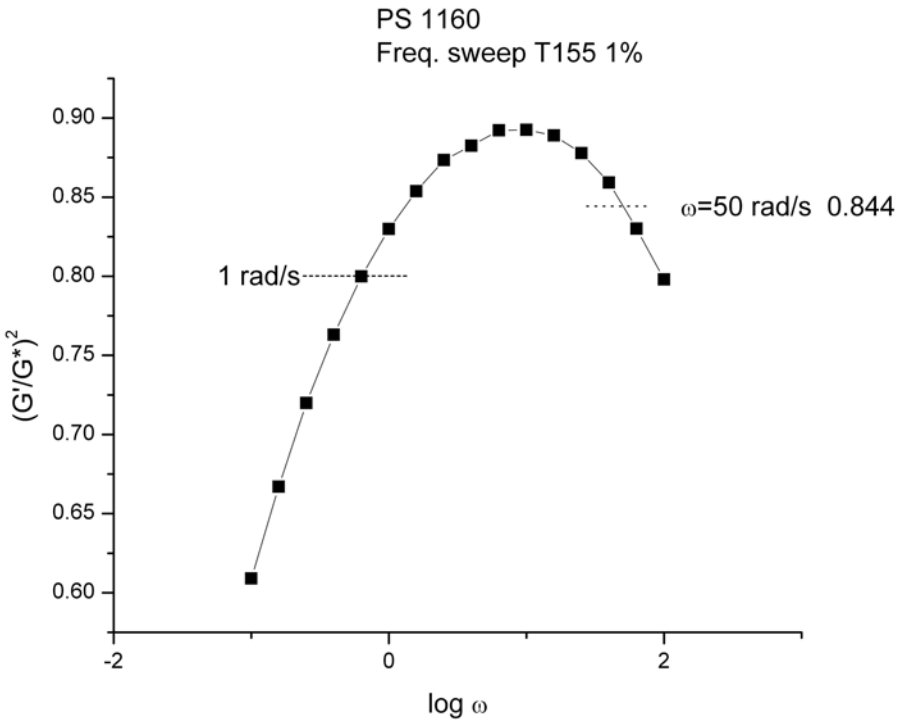

Fig. 59
$(G'/G^*)^2$ vs ω for PS-2 in the linear regime (1%) for T= 155 °C

One reads a value of 0.80 and 0.844 for ω = 1 rad/s and 50 rad/s respectively. For ω= 100 rad/s $(G'/G^*)^2$ was also equal to 0.8. Note that these three radial frequencies are located on two sides of the maximum, 50 and 100 rad/s being on the same side. A succession of steps, 1 to 8, corresponding to various time sweep "treatments" makes up what we called the "Thermal-Mechanical History". The objective was to follow the evolution of the network of entanglement and the "internal stress" build up of the activated strands, for instance by studying what happens to the curve in Fig. 59 after the melt has been submitted to step treatments in the non-linear range. This is explained in Fig. 60.

The strain history is shown in Fig. 60a. Steps 1, 2 and 3 were done at ω= 100 rad/s, The other steps were done at ω= 50 rad/s except step 8 for which ω= 1 rad/s. The strain for steps 6 and 8 was 1%. Fig. 60b displays the evolution of the complex modulus G*(t) and provides the frequencies used during the various steps. Figure 60c shows $(G'/G^*)^2$ vs time across all steps (this is the reason for the word "consolidated").

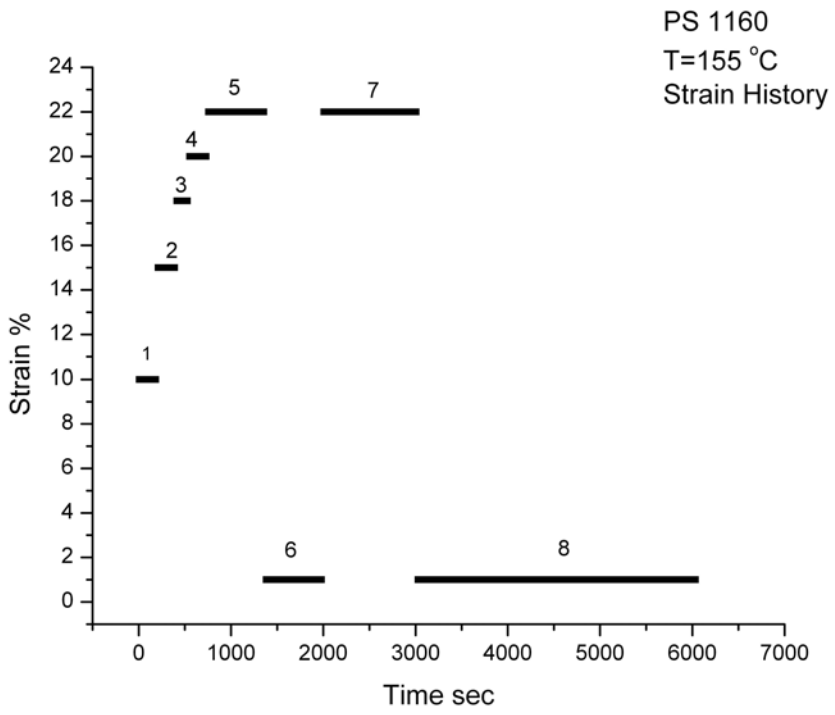

Fig. 60a

Strain% history for 8 steps 1 to 8. The insert of Fig. 60b indicates the frequency and strain % for each step.

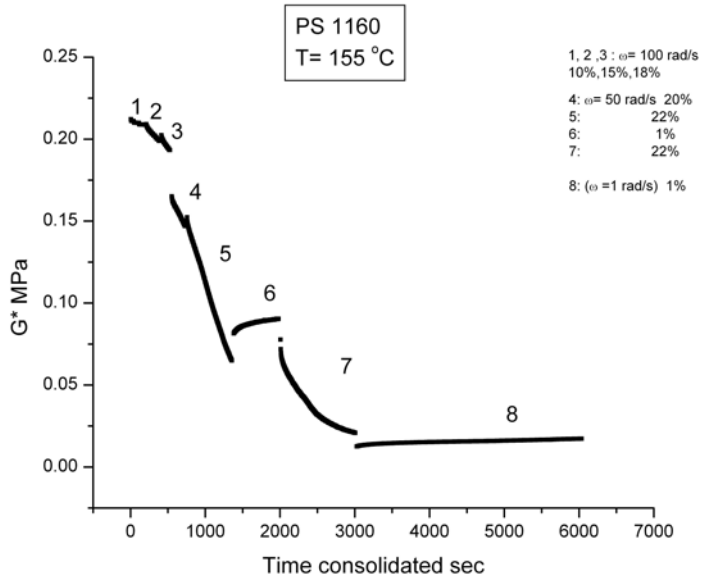

Fig. 60b

G*(t) for the various steps 1 to 8. The insert indicates the frequency and strain % for each step.

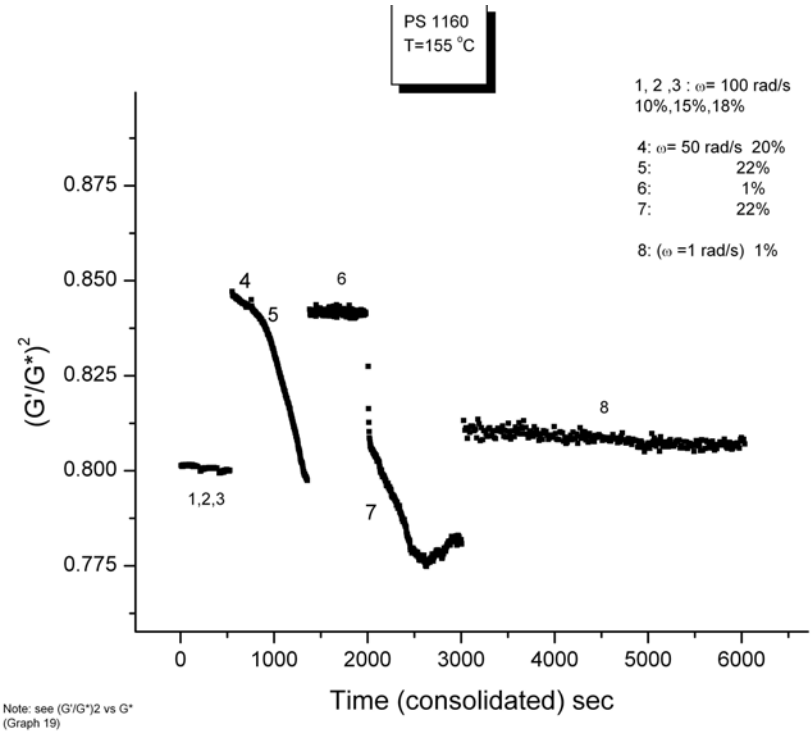

Fig. 60c

$(G'/G^*)^2$ vs time for the various steps 1 to 8. The insert indicates the frequency and strain % for each step.

The first observation is that $(G'/G^*)^2$ in Fig. 60c is a network parameter, as much as G*(t) is in Fig. 60b; it decreased, changed its rate of variation, reversed direction, increased. The changes occurring to these two parameters, $(G'/G^*)^2$ (t) and G*(t), must be correlated to understand which part of $(G'/G^*)^2$ describes a change of the number of activated strands bearing stress, and which part relates to a modification of "the internal stress" of the strands. Obviously, as mentioned for PC, their respective influence on the retention ability of the viscosity reduction benefit is crucial to understand. The boosting of the pseudo-plasticity of the melt, responsible for the high frequency behavior, is due to an increase of $(G'/G^*)^2$ caused by an increase of the strands' "internal stress". The low frequency behavior, i.e. the Newtonian viscosity changes, is correlated to the modification of the number of active strands of the entanglement network. Changing the treatment frequency from 16 Hz (ω=100 rad/s) in steps 1, 2, 3 to 8 Hz (steps 4,5,6,7), and at the same time changing strain % (Fig. 60a) produced different interplay between shear-thinning and strain softening effects. For instance, for steps

1, 2, and 3 $(G'/G^*)^2$ remained constant at the linear value of 0.8 found for w=100 rad/s (Fig. 59), The corresponding G*(t) in Fig. 60b declined with a faster rate as strain was increased from 10% to 18% (Fig. 60a). The situation between step 3 and step 4 is quite significant. The decrease of ω from 100 to 50 rad/s resulted in the expected increase of $(G'/G^*)^2$ seen in Fig. 59 (on the right end side of the maximum). However, the increase of strain, at the same time, from 18% to 20% in step 3 to 4, and to 22 % for step 5 resulted in increased strain-softening, which triggered a transient for both G*(t) and $(G'/G^*)^{2.}$ Step 6 was a strain step down recovery done under forced oscillation (ω stays at 50 rad/s). One sees that the value of $(G'/G^*)^2$ was only slightly lower than at the beginning of step 4 and remained constant. G*(t) increases, showing the time dependency of strain-softening. This step 6, which only lasted 10 min, had a spectacular effect on the subsequent decay of both G*(t) and $(G'/G^*)^2$ observed for step 7. At one point $(G'/G^*)^2$ had declined from 0.844 to 0.775 and the corresponding decrease of G*(t) was more than 10 times its initial value.

Figure 60d is a masterplot of "ELAS", equal to $G'/G^*)^2$, vs ETA*, the complex viscosity, across all steps, 1 to 8. The open dots correspond to the frequency sweep done in the linear region of viscoelasticity, for 2% strain.

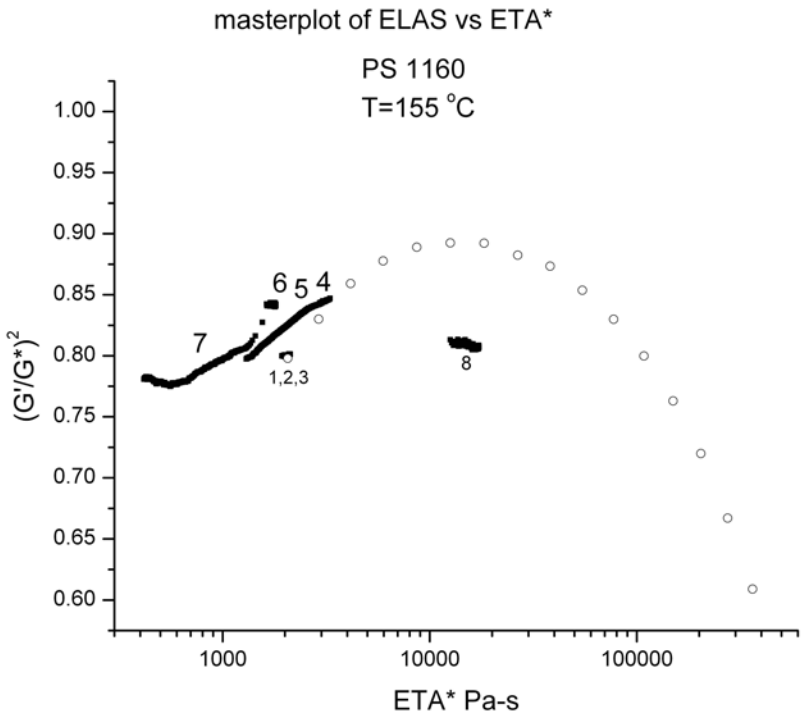

Fig. 60d
$(G'/G^*)^2$ vs dynamic viscosity (ETA*) for the 8 steps of the mechanical history

One sees that steps 1,2,3 were right on the linear region curve (the open dots), although the strain was increased to 18%. The deviation from the linear region curve occurred for viscosity values (steps 4 to 7) that became transient and inferior to their linear counterpart value for the same $(G'/G^*)^2$; this is why the curve for these steps is located above the linear range curve (dots). The viscosity at the beginning of step 8 (ω= 1 rad/s 1% strain) was equal to 12,000 Pa-s and should be equal to 100,000 Pa-s on the open dots curve.

We thus conclude that the effect of Thermal-Mechanical History on the entanglement network stability can conveniently be studied with a dynamic rheometer and applied to industrial shear-refinement practice to produce retainable viscosity reduction benefits. .

D DISCUSSION

1. The question of the origin of the time dependency of the visco-elastic parameters.

In pure viscometry (at constant rate of shear), a transient behavior is expected before the melt reaches its steady state. Questions regarding the origin of this transient are still experimentally and theoretically investigated and debated [7-9]. We showed in section 2.1 that the stability of the steady state could be a function of the previous thermo-mechanical history of the melt, which could be a sign that either "sustainable orientation" could be the result of a structured stratification of the network of entanglements inside the gap or the result of "disentanglement", or that, actually, "disentanglement" meant in reality "sustainable network orientation". Additionally, we suggested that the total stress could be split into an active stress and a relaxing stress, explaining some kinetic features obtained during transients (e.g. Fig. 21) and the negative normal force observed at the end of the transient behavior (e.g. Figs. 19d and 20). In order to study the instability of the melt under conditions that separate the effects of strain and strain rate, we proposed to investigate the triggering of time dependence of the moduli by strain in dynamic experiments performed in the non-linear range. Section 3 of the chapter presents the effects of various "treatment" parameters, that of frequency, strain amplitude and temperature. In all these experimental tests we observed the same phenomenon: as strain was increased beyond a certain critical value (which is a function of frequency and temperature), the melt starts to become transient, i.e., for instance, its viscosity changed with time. The time dependence of moduli in relaxation and creep experiments performed near T_g (~T_g +30 ^oC), are well known [e.g. Figs. 1a to 1d], but the relaxation times are extremely small (10^{-3} to 100 sec, depending on molecular weight) at these low temperatures; thus, far above T_g. (~T_g +150 ^oC), the melt is always considered to be in equilibrium after, say, 2 min of relaxation, even for the highest molecular weights. One could argue that in certain cases, for branched polymers in particular, the longest relaxation time could reach 10 minutes at T ~T_g +150 ^oC. Perhaps. But, what we are talking about in this work are linear polymers, with relatively low M/M_e (say 5 to 20), capable of transients which last 24 hours (see PMMA in Fig. 55). This is obviously not the same relaxation process involved as that in Figs 1a to 1c, or, if it is the same process (and we will suggest in sections of this discussion that it is), something is missing in the present

understanding of what entanglements are and how they actively determine the long term relaxation properties of melts.

The first thing we do in this discussion section is review the challenging interpretations of the time dependence of the moduli under non-linear dynamic conditions.

2. Challenging Interpretations.

In presenting the type of experimental data illustrated in Figs. 4 and 28 to the scientific community, a number of interpretations of the results emerged:

- The viscosity reduction is due to shear viscous heating.
- The viscosity reduction is due to shear degradation (M_w is decreased).
- The viscosity reduction is due to plasticization (T_g is decreased), caused by the production of monomers by shear degradation.
- The viscosity is reduced because drooling occurs at the edge.
- Slippage occurs. Viscosity reduction is due to a surface fracture effect and does not apply to the bulk of the specimen.
- The viscosity reduction is due to shear-thinning, which is a well known phenomenon.

These we explore in more detail below.

2.1 Viscous Heating: Shear generated heating is real and could explain some results (e.g. see the explanation regarding Fig. 13b) obtained with the use of first generation rheometers. If the heat generated is not controlled by cooling, the viscosity will decrease because of the temperature rise. However, the experimental procedure requires that one work at constant temperature. Early results using the RDA 700 were duplicated using more modern instruments, the ARES from Rheometrics, the Bohlin SVO200, and the AR 2000 from TA Instruments, which are known to have improved isothermal control of their furnace. Temperature does not rise more than 0.2 ^{o}C, as measured by a thermocouple placed right underneath the sample. Such a small temperature change is not capable of producing the large viscosity change observed during the transients triggered by non-linear shear oscillation. In the type of shear-refinement processor described in Figs. 5a and b, cooling conduits (element 240, in Fig. 5a) are

built in the static and rotor sections to dissipate out the heat generated by the shear oscillation at large amplitude. The temperature of the melt is directly measured by contact with the melt, and remains constant during the process. In conclusion, viscous heating is not responsible for the time dependency of viscosity, in particular for the decrease of viscosity.

2.2 Shear Degradation.

In the torsion experiments done in a lab rheometer (such as those of Figs. 27 and 28), the specimens did not show any sign of degradation after the time sweep "treatment". For all the dynamic results presented in this chapter, GPC tests were systematically conducted on samples extracted before and after the time sweep stage to ensure that the decrease of viscosity was not due to chain breakage or degradation. A GPC measures the molecular weight distribution, providing the various molecular weight averages: M_n, M_w, M_z and M_{z+1}. For all disentanglement experiments done in the lab rheometer, we did not observe shear degradation of the samples within 3% variance (which also equals the accuracy of GPC measurements). However, when shear-refinement processors were used to produce disentangled pellets, the level of degradation was visible and depended heavily on the treatment duration, the temperature, the amount of anti-oxidant present and mostly on the nature of the polymer. For PMMA, for instance, the degradation could be kept low, between 1 to 5% depending on the extent of disentanglement obtained. For polyolefins, the degradation could be as high as 25%. Despite these molecular weight changes, which could be accounted for by a correction factor, shear-refined pellets displayed an extra viscosity decrease that could be as high as 50% to 400%, measured by re-heating the pellets in a Melt Flow Indexer or by rheometry.

Figure 61 shows the Refractive Index (RI) measured by GPC as a function of molecular weight for 3 types of PC sample processing: one sample is the virgin pellet, another sample is a pellet after it had been disentangled by a disentanglement processor [Figs. 5a and b], and the third sample is the extruded virgin, i.e. the sample after the virgin pellets were extruded through the MFI process at 300 ^{o}C. The value for M_w and M_n are given in the figure for the 3 types of pellets (in g/mole). It is clear that the weight and number average molecular weights are practically the same for these 3 samples. The decrease of M_w for the treated PC is 5%, i.e. 2% more than the decrease corresponding to the virgin extrudate (3% degradation). A decrease of M_w by 5% corresponds to a viscosity drop of 16% (calculated from $(M_w/M_{wref})^{3.4} = 0.95^{3.4}$

= 0.84). This correction was applied to the MFI results which, after correction, still displayed an increase of 70% between the virgin pellet and the treated PC pellet. Note that we differentiate, in Fig. 61, the MFI results obtained for "dried" or "undried" pellets (whether they are treated or virgin): the undried treated pellets indicate an improvement of the MFI by +140% (with respect to the undried virgin), twice the value obtained for the dried treated pellets (dried at 110 ^{o}C for 4 hours under vacuum). All MFI results were compared after respective correction for the M_w small decrease. The difference between the MFI improvement when treated pellets were dried or not is perhaps indicative of the true reason for the viscosity changes. See below.

In any case, the decrease of viscosity due to the triggering of a transient state by increasing strain under shear-thinning conditions is not caused by shear-degradation.

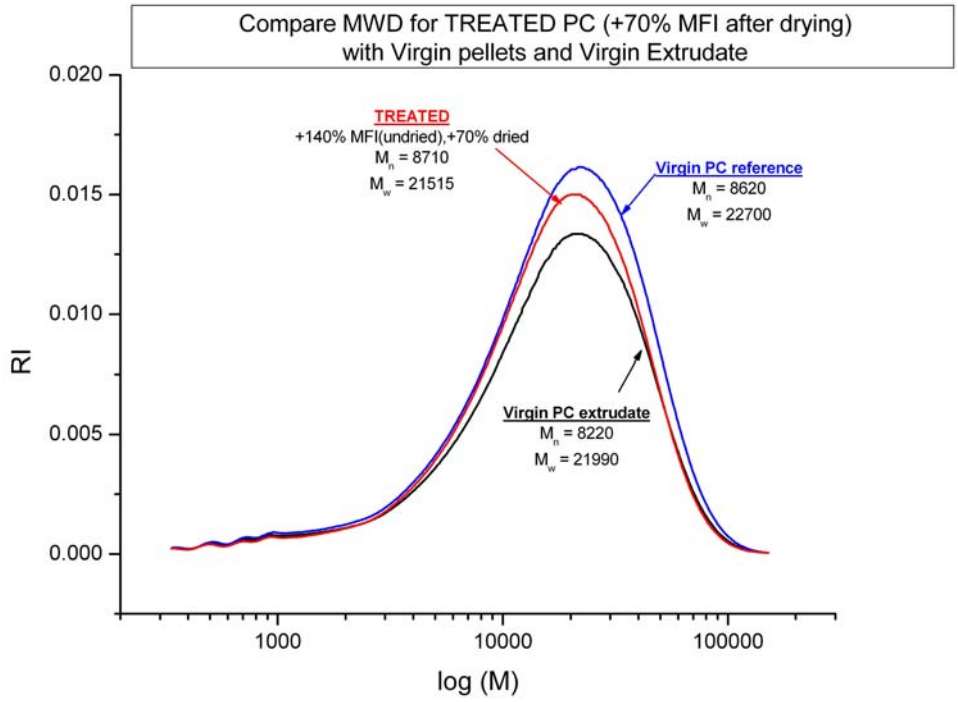

Fig.61

Refractive Index (RI) vs log M from GPC comparing the molecular weight distribution for a virgin pellet (top curve), a shear-refined ("treated") pellet displaying a +140% (undried) or +70% (dried) increase in MFI value after treatment (middle curve), and a virgin sample after it went through the extrusion process in a MFI measurement process (lower curve "Virgin PC extrudate"). The polymer is PC.

2.3 Drooling of the melt outside of the rheometer plates.

On certain occasions, drooling of the melt was visible by opening the door of the furnace right at the end of the time sweep step. We observed that drooling occurred for time sweeps done at high frequencies, high strains, and for thicker samples (2.5 to 3 mm thick). When drooling occurred, the results were discarded. Besides, an easy way to prevent drooling is to use a bottom plate shaped like a cup, preventing the melt from spilling out. Nevertheless it is interesting to briefly analyze how drooling could occur.

Let us consider the centrifugal force acting on a sliced ring located at distance r of thickness (δr). It is equal to $k*\delta m *V^2/r$ with δm = density*thickness*2π*r*δr and V is the local velocity. The constant k results from the integration over a period of the angular speed, which is not constant in a periodic deformation. The integration over the full specimen radius shows that total centrifuge force is proportional to the cube of the radius and to the square of the frequency. Additionally, the velocity V depends on the layer position in the gap since it is proportional to the strain rate times the gap between the moving layer and the static plate. We suggest that drooling is possible when the magnitude of the normal (lateral) force, proportional to γ^2 , due to the shear-deformation in the perpendicular direction, is overcome by the centrifugal force pulling the melt out of the parallel plates. When a transient occurs, the normal forces decrease (see examples in Figs. 38 and 45f for dynamic experiments and in Fig. 20 for pure viscometry), reducing the pull-in retractile force in the direction perpendicular to the shear deformation, permitting drooling to result. In other words, drooling is a sign that an imbalance of the forces maintaining the integrity of the melt in the gap occurred. This imbalance is due, we suggest, to gradients of velocity across the gap structuring the Dual phase layers differently (the strain rate is assumed to be constant across the gap in laminar shear flow defomation). The imbalance could also be due to gradients existing co-centrically. In summary, the shear vibration induces a great deal of extensional stress between concentric rings as well as a gradient of forces between the layers of the gap due to the dependence of the centrifugal forces with the position of the layers. The decrease of the magnitude of the normal forces results from this internal structuring, i.e. from the anisotropic distribution of the "entanglement phase"

which we called the orientation of entanglement network. Fig. 62 is a picture of an oriented dual-phase melt according to the Dual-phase model [73].

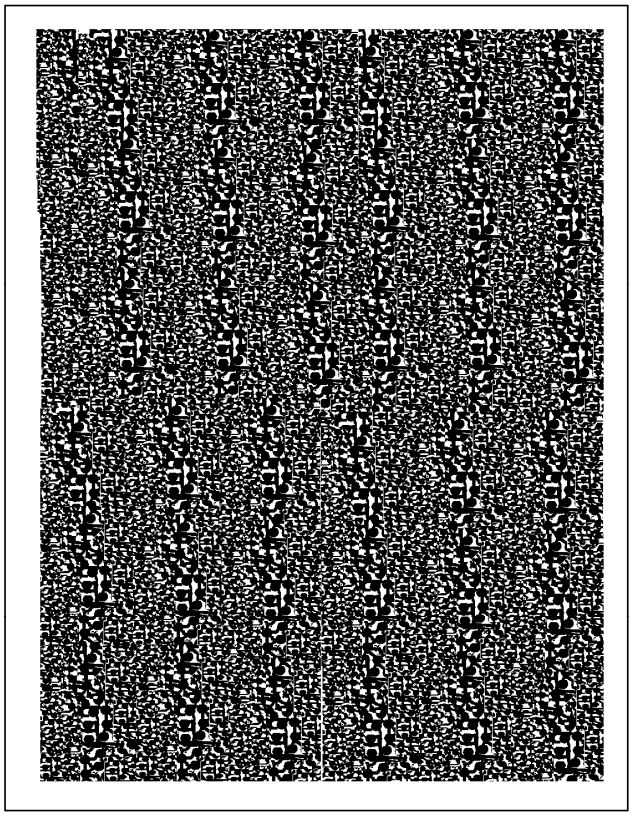

Fig. 62
In this cartoon sketch of the Dual-phase model [73] the "entanglement phase" is shown to align with the direction of flow (bottom-up direction) This figure represents one entanglement network layer of the gap (one virtual slice). For a circular motion, such as in a classical plate-plate rheometer, the entanglement phase line-up would form rings. The number of rings would be function of the radius r and of the layer position in the gap, creating an orientation pattern characteristic of the non-linear viscoelastic deformation, explaining the "sustained orientation" of the entanglement network. See later.

It is possible to eliminate drooling completely by working with thinner samples (~500 to 1000 μ thick) which might lessen the gradients across the gap. Furthermore, experiments repeated with samples using serrated plates, with the sample's gap adjusted at the high temperature, before lowering T to its treatment value, did not display any drooling at all, for frequencies up to 40 Hz. Additionally, a 1mm wide drooling ring would correspond to a

viscosity correction of the order of 10%, nothing of the order of magnitude of the viscosity reduction seen as a result of melt disentanglement (50% to 1300%). Finally, transients are still observed when the melt is confined to a closed chamber without the possibility to escape, such as in a dynamic disentanglement processor (Fig. 5a). The effect of combining strain and frequency on the viscosity decay appears to be very similar in a such a confined setting and in an open-edge plate plate rheometer.

In conclusion, drooling cannot explain the large viscosity changes observed in dynamic experiments triggered by an increase of strain at (high) frequency.

2.4 Plastification due to an increase of the monomer concentration by the shear process.

For PMMA, it was observed that the concentration of monomers increased from 1000 ppm (for the virgin pellet) to 2000 ppm (for the "disentangled" pellet) after shear-refinement. Could this increase result in the observed viscosity changes observed in Fig. 55?. It is well known that an increase of concentration of small molecules decreases the T_g, and that a decrease of T_g, at a given temperature, reduces the viscosity. So, the question is legitimate. The influence of the concentration of plasticizers on T_g is given in textbooks [79} and corresponds to a decrease of T_g by ~0.5 ^oC for the doubling of the concentration between 1000 ppm and 2000 ppm in PMMA. The WLF equation can be used to approximate the corresponding decrease of viscosity (see ref. [2], eq. (3)). For PMMA, we find that Log a_T is decreased by 0.03 when T_g is lowered by 0.5 ^oC. This corresponds to an increase of the Melt Flow Index by 7%, not the +70% reported for the "disentangled" PMMA pellet in Fig. 55.

Two other arguments against the plasticizing effect of monomers can be added. First, pellets were dried for a long time (17 hours) under vacuum at approximately T_g-40 ^oC before the MFI measurements are done. It can reasonably be assumed that the more volatile components, present in the pellets at ppm level, would not survive such a drying step. Second, the GPC lower tail, which focuses on the low molecular weight fractions, did not show any visible modifications for the samples reported in this work. This is evidenced, for instance, for the PC samples shown in Fig. 62.

In conclusion, the changes of viscosity observed by shear-refinement are not due to an increase of the monomer concentration

2.5 Shear-thinning.

"Shear-thinning" describes the reduction of viscosity induced by an increase of the strain rate, thus by frequency in a dynamic experiment. This is quite clear in Fig. 28, for instance. Shear-thinning occured as soon as the frequency of oscillation was increased from 1 to 47 rad/s: viscosity droped from 57,000 to 10,000 Pa-s . This means that the melt became less viscous when it was vibrated at 7.5 Hz frequency (47 rad/s). However, to induce this benefit, vibration must be applied to the melt and maintained. As soon as vibration was stopped, so did the shear-thinning effect on viscosity and the melt recovered instantaneously its original Newtonian viscosity. The value of shear-thinned viscosity was stable at low strain (up to 13% in Fig. 28). The viscosity became time dependent thereafter, the rate of viscosity change increasing with the strain (see, for instance, Fig. 60b). The triggering of the time dependent (transient) behavior and the holding of the melt in that state influences the post-treatment visco-elastic properties: in Fig. 28 the melt no longer sprang back to its initial Newtonian viscosity, it only sprang back to 38,000 Pa-s and not 57,000 Pa-s. The remaining viscosity difference was recovered over the next 20 to 30 minutes. This melt behavior is different from the classical shear-thinning characteristics. The longest relaxation time was apparently increased 60 times. We suggested that strain-softening coupled with shear-thinning was responsible for that situation. This, obviously, needs quantification. The point, however, is that the transient behavior triggered by non-linear strain displays marked differences with shear-thinning effect. What we called "disentanglement" corresponds to this "sustained" shear-thinning. Note that we previously introduced, relative to Fig. 20, the notion of "sustained orientation" to describe the orientation of the network of entanglement, .and its possible stability above T_g, as opposed to the orientation of local bonds .that relax very fast above T_g. Obviously, the local deformation inter-locks with the deformation of the network which still needs to be defined. The inter-lock must also be quantified.

2.6 Edge fracture explanation.

In this section we examine the proposal made by Friedrich et al. [60, 61] that the time dependency of viscosity triggered by an increase of strain in dynamic experiments is due to an edge fracture effect propagating inward. We have said many times in this presentation that, in our opinion, such an explanation was not correct. This conclusion was derived from the

analysis of several figures (Figs. 11a, 37c, 43d, 44c) which show that G'(t) and G"(t) did not vary in the way a surface contact decrease would affect the results. When the ratio G"/G' (equal to tan δ) was apparently constant (thus $(G'/G^*)^2$ was ~ constant), we suggested that the time dependence of G' and G" was due to the orientation of the network of strands, which occurs at constant total number of active strands. This is the same basic mechanism of deformation that controls shear-thinning and shear strain softening, with specific variants determined by the value of frequency, strain and temperature. What these time sweep experiments essentially teach us is the fact that the expression of G'(ω) and G"(ω) should also include a time dependent term which becomes noticeable under non-linear conditions of deformation. The "static" (time independent) expressions used in linear rheology (see for instance Eq. (15) of Ref. 2) have limitations, being only applicable to a small range of strain for which the entanglement network is stable in its current structure. For instance, shear-thinning at low strain corresponds to an increase of the number of activated strands with the increase of frequency. The transient behavior classically admitted to occur for constant shear rate viscometric experiments is the consequence of strain (which increases linearly with time) reaching a critical value that puts the network of strands in the time dependent (non-linear) visco-elastic region where it starts to deform, first, and then to structure. If the new network structure is relatively stable, one observes what we call "disentanglement". Like for pure viscometry, this situation can only be achieved in dynamic experiments above a certain strain (e.g. Fig. 28). Thus it does not seem unexpected (and we do not need a surface artifact explanation) to find for dynamic experiments, conducted beyond critical conditions of strain and frequency (Fig. 28), a similar transient behavior to that which we observe in fast shear rate viscometry (Fig. 2a).

In this chapter we have shown several examples of time dependence of G' and G" occurring at either increasing (Figs.11b, 40 (step 2), 46d, 60c (end of step 7)) or decreasing (Fig. 60c (steps 4, 5)). $(G'/G^*)^2$. When the transient occurs at constant $(G'/G^*)^2$, the network of strands deforms but does not structure. When structuring occurs, the network of activated strands orients and can assume new stable structures. The stability of the new network entanglement structure depends on the way it was established, thus on the thermal-mechanical history. An elaborate combination of strain softening and shear-thinning can be set up to create thermal

mechanical histories capable of defining at will, it seems, the future visco-elastic behavior of the melt. Examples are given in Figs. 60a to d. The sustainability of the new network describes the stability of the new inter-lock between the local bonds and their organization as a system, under stress. A new "terminal time" must be defined to account for the stability of the network. Based on our experience, it can be 100,000 times greater than the local τ_o that is supposed to define the longest relaxation time of the melt.

Figure 63a. below is the same as Fig. 11a. of the introduction section, with a full scale disclosure of the effect of the largest strain amplitudes (15% and 20%) on the time dependence of $(G'/G^*)^2$. Fig. 63b displays the decrease of viscosity occurring at the same time.

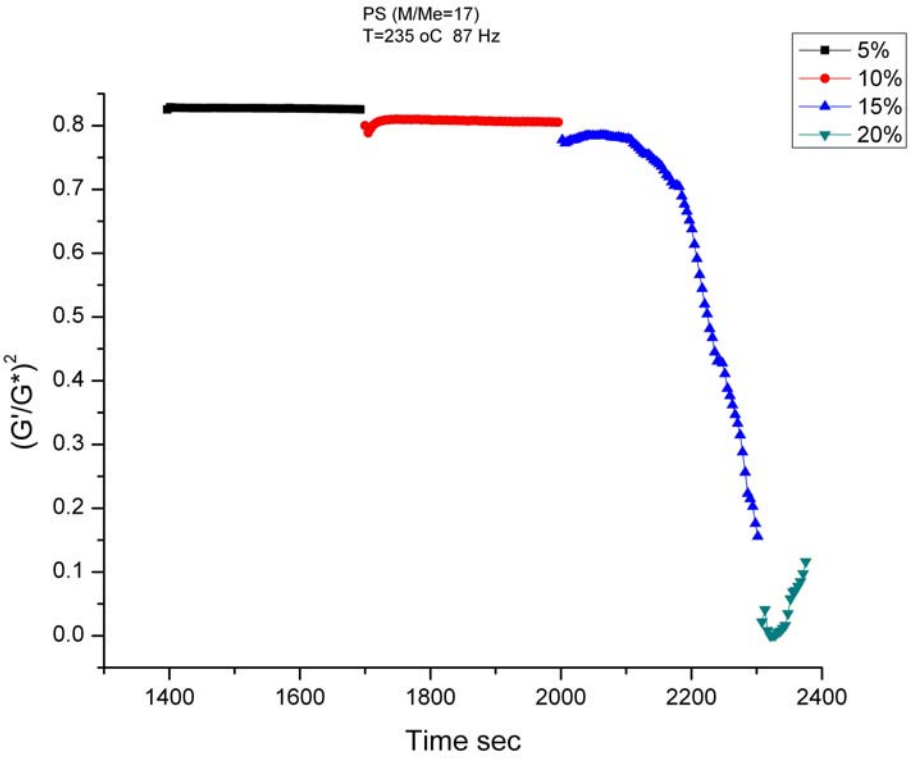

Fig. 63a

4 time-sweep steps done with increasing strain % at each step, triggering a transient of both $(G'/G^*)^2$ in this Figure and of dynamic viscosity in the next Figure.

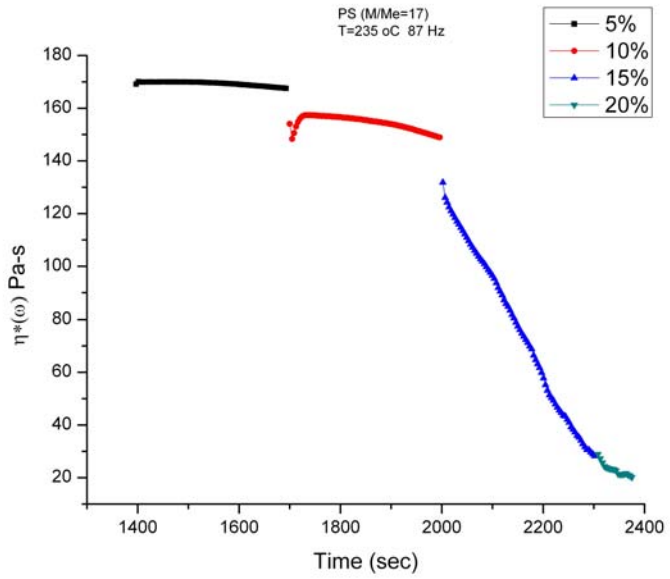

Fig. 63b

4 time-sweep steps done with increasing strain % at each step, triggering a transient of both $(G'/G^*)^2$ in the previous Figure 63a and of dynamic viscosity in this Figure. See text.

The sample in Figs. 11a, and 63a and b was a film of thickness 484 μ. The time sweep occurred at T=235 ^oC, under a relatively high frequency (87 Hz). The transient decay of both η* and $(G'/G^*)^2$ became very pronounced after the strain reached 15%. The dynamic viscosity (Fig. 63b) continued to decrease but leveled off at 20 Pa-s (a 750% decrease) for a strain of 20%, whereas the stored elasticity, which had dropped from 0.775 to 0.15 during the transient decay at strain =15%, showed an initial drop to approximately zero when the strain reached 20%, followed by an increase of its value afterwards (Fig. 63a).

Friedrich and collaborators [60, 61] acknowledge that tan δ increases at one time of the time sweep under strain but suggest that the fracture mechanism (which they say remains confined to the surface up to that point) has somehow started to penetrate inside the sample. They also report that the stress and/or strain signals become distorted as soon as tan δ starts to increase. Figure 64 shows the stress and strain signals (which are displayed continuously by the AR 2000 dynamic rheometer) at a point near $(G'/G^*)^2$ ~0. in Fig. 63a. These signals are not distorted. It is true that Friedrich uses thicker samples (2 to 3 mm) and that Fig. 64 applies to a film; the gap thickness makes a significant difference with respect to the question of integrity

of the gap, as clearly evidenced by Wang [8, 9]. As mentioned earlier, the structuring of the gap into an anisotropic entanglement network layers depends on the gap thickness. It is quite possible that Friedrich's experimental set up triggers effects described by Wang, which are in no way responsible for the transient behavior itself but interfere with it. The best proof is that for thinner samples, for which the integrity of the gap is more preserved, the transient behavior is more pronounced (Figs. 65a to c), for reasons that we explain below. This result appears to contradict Friedrich's conclusions regarding the effect of the gap thickness on the intensity of the transient behavior [61].

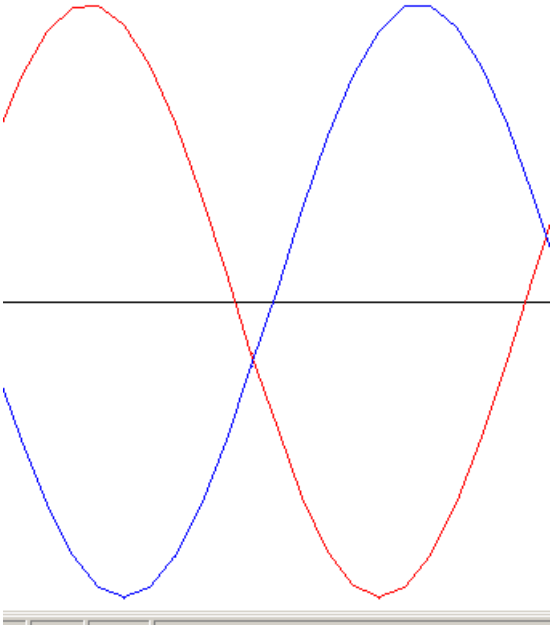

Fig. 64
Signals observed for strain and stress in the region where transients of $(G'/G^*)^2$ and G^* are visible.

Friedrich et al. mention that the thickness of the gap influences the onset of the increase of tan δ (corresponding to a decrease of $(G'/G^*)^2$), i.e., in their case, the beginning of the distorted signals. These authors did not explore the use of films (as in Fig. 64, showing no signal distortion) or the use of a cup bottom plate which eliminates the openness of the melt at the edge, and thus edge fracture, yet still showing a transient behavior triggered by higher strains..

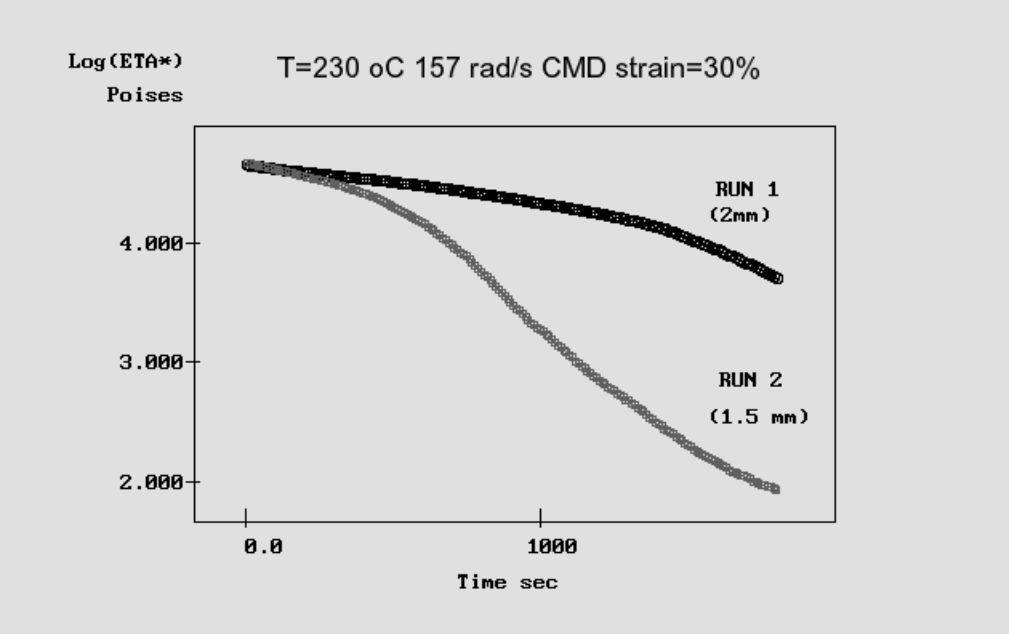

Fig. 65a

Compare the transient viscosity decay (Log η*(t) in Poises vs time) for two successive time sweeps done on the same melt, changing the value of the gap (from 2mm to 1.5 mm) after the first run. The sample is a branched PC; T=230 ^{o}C, ω=157 rad/s and the commanded strain is 30%.

Figure 65a shows the transient decay of the dynamic viscosity obtained for a branched PC from GE Plastics (PK 2870) triggered by the application of a commanded strain of 30% with a frequency of 25 Hz (157 rad/s) at a temperature of 230 ^{o}C. The rheometer was the RDA 700 already mentioned relative to Fig. 13. The gap was initially 2mm. (Run 1). At the end of run 1, we squeezed the gap to 1.5 mm, checked by opening the furnace door to determine whether there was a need to trim an expanded bulge from the edge (there was a little trimming necessary), and rerun a new time sweep using the same parameters, lasting another 1,800 sec (Run 2). This experiment is very interesting for several reasons. First, one observes that the viscosity at the start of run 2 was the same as the viscosity at the start of run 1. This could be interpreted as a clear demonstration that the transient decay of run 1 was an artifact. In other terms, if the viscosity remained unchanged, after squeezing the gap, it is because the transient behavior was due to a surface effect or drooling or some other artifact. This was the interpretation given for Fig. 65a by a majority of scientists and technicians, when these transient tests were first introduced by us in 1996. However, let us study the results more

closely. Although the viscosities for run 1 and run 2 at the beginning of the time sweeps are almost identical in Fig. 65a, the transient path lines look very different for the two gaps. The decay is much more pronounced for run 2. Figure 65b provides more insight to the reasons.

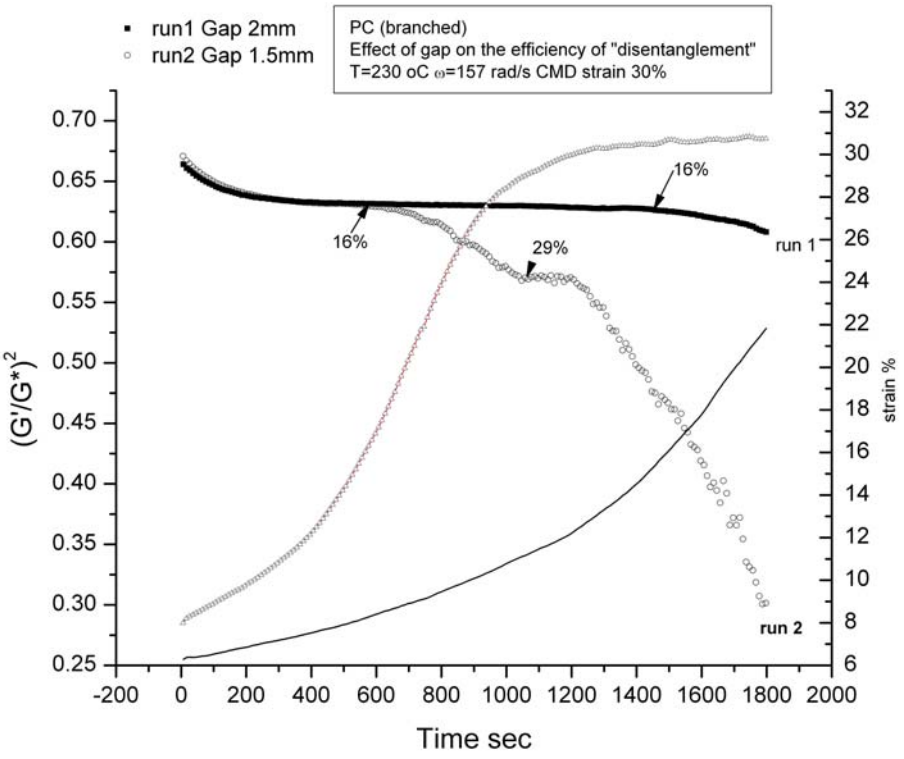

Fig. 65b
$(G'/G^*)^2$ vs time (left axis) and strain % vs time (right axis) for the data of Fig. 65a

In Fig. 65b we have two types of graphs corresponding to either the vertical axis on the left or on the right. The left vertical axis is $(G'/G^*)^2$ and the right vertical axis is the strain %. The data are extracted from the same time sweeps experiments of Fig. 65a for run 1 (gap=2 mm) and for run 2 (gap=1.5 mm). The x-axis is the time (in sec). One sees that, although the commanded strain was constant (and equal to 30%) for both runs 1 and 2, the actual strain was increasing with time and only reached 30% in the case of run 2. The value of $(G'/G^*)^2$ decreased slightly at the beginning of the time sweep, for about 200 sec, then stabilized and remained constant, starting to drop only when the strain reached 16% for both run 1 and 2. The final decrease of $(G'/G^*)^2$ is very small for run 1 since the strain only increased to 22 % before

the end of the 1800 sec time sweep. For run 2, the 16% strain, for which $(G'/G^*)^2$ started to decrease, was reached much sooner (for t~550 sec) compared to t~1,500 sec for run 1. The kinetics are totally different for these two gaps.

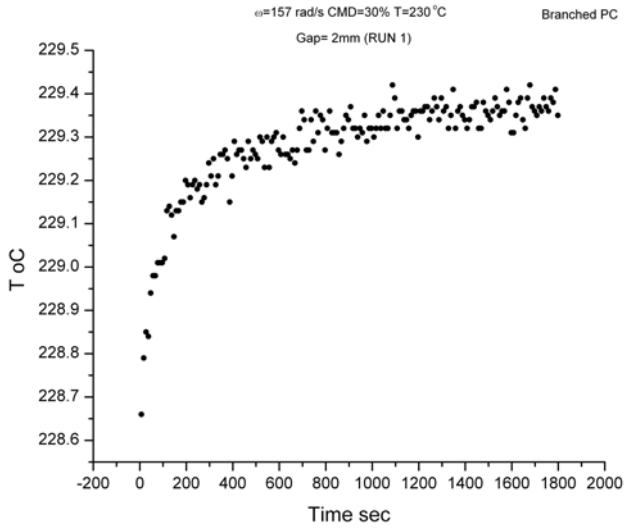

Fig. 65c

Variation of the melt temperature for run 1 in Figs 65a and b. The asymptotic temperature is 229.4 ^oC. The rheometer was a RDA 700, a first generation rheometer with limited cooling capabilities in the non-linear visco-elastic range**.**

Fig. 65c explains the reason for the initial decrease of $(G'/G^*)^2$ for the first 200 sec. It is a plot, for run 1 (the plot for run 2 is not shown), of the melt temperature against time during time sweep. The temperature rose by 0.5 ^oC (from 228.7 to 229.2 ^oC) in 200 sec, as a consequence of the application of the oscillation at 25Hz. As already mentioned, the RDA 700 used for the experiment was a first generation rheometer, quite satisfactory to work with in the linear visco-elastic range, but with insufficient cooling capabilities to maintain the temperature of the melt constant while working under non-linear conditions. Figure 65b shows that, after correction for the small increase of temperature at the beginning, $(G'/G^*)^2$ remains constant for both runs 1 and 2 until the strain reaches 16%. As mentioned in the previous section, when $(G'/G^*)^2$ remains constant, the network of strands is not even deformed. The transient response of G' and G" (and therefore of the viscosity) is elastically driven, due to the local re-organization of the bond interactions to accommodate the imposed strain. There is no structuring of the network of strands possible under such conditions, i.e. no possibility of

sustained orientation. Hence, it does not seem surprising that, as run 1 ended, the viscosity change did not "stick", i.e. the melt had the same entanglement state (with the same τ_o) as at the beginning of run 1. We can consider that run 1 did not create a thermal history for run 2 because strain was not above the critical value 16% long enough, and the squeezing of the gap (from 2mm to 1.5 mm) destroyed whatever small changes of the network of strands there were, from t =1,500 to 1,800 sec, visible by a slight decrease of $(G'/G^*)^2$ in that time range. Run 2 had a different transient dynamics than run 1 because the gap was thinner, not because it was a second run. The controlling parameter is the strain, γ, which varied towards the commanded strain γ_c much faster for run 2. In fact, a log-log plot of $\eta^*(t)$ vs $\gamma(t)/\gamma_c$,not shown, proves that melts 1 and 2 had the same transient behavior up to 16%, diverging beyond that strain, where strain alone was no longer the controlling parameter. One sees in Fig. 65b that $(G'/G^*)^2$ steadily decreased for a strain between 16% and 29%, reaching a value of 0.575 at which it leveled off for about 100 sec, then continued to significantly decrease at an even steeper rate to finally reach the value of 0.3 for a strain of 30%.

Following Friedrich's explanation (61) of the increase of tan δ (i.e. a decrease of $(G'/G^*)^2$), the propagation of the edge fracture inside the sample should be much faster in the case of the thinner sample (run 2). This appears to contradict Friedrich's own findings regarding the effect of gap thickness (61).

One could argue that the effect of the gap on the viscosity response is well known to rheologists studying wall slippage [78] and that run 2 has a lower viscosity in time due to an increase of the wall slippage velocity. This explanation is discussed later in the section dealing with the effect of the plate surface on the transient results, in particular the value of the steady state viscosity, but was unlikely in the present situation (Figs. 65a and b) because the initial value of the stress was much less than the critical stress for initiating the no-slip violation (~ 100,000 Pa). The stress was 41,192 Pa at t=0 for run 1 and 58,521 Pa for run 2.

In the explanation we propose to explain Figs. 65a and b, and all the other figures in this chapter, it is clear that we concur with Wang's results [7-9] pointing to the limitation, as we enter the non-linear range, of the basic assumption of rheology regarding the scalability of the rheological parameters (stress and deformation tensors) in terms of viscosity, strain and strain rate to describe the effect of the gap thickness. The definition of viscosity (the ratio of stress and strain rate) and of strain rate (the gradient of the velocity profile across the gap)

requires an homogeneous melt., or, as we further add, an homogeneous, unstructured entanglement network, which is a valid and justified concept only for certain conditions of deformation, for instance in the linear viscoelastic range. In the non-linear region, as strain increases, the network of entanglements first deforms without structuring (at constant $(G'/G^*)^2$, this is the only range for which the separation of the effect of time and strain is valid), followed by the orientation/structuration of the network of entanglements itself, finally yielding to its instability, and eventually its rupture and re-organization into a new network (Figs 46c and d). All these manifestations of "entanglement instability" must be well defined molecularly, and correlated with the macroscopic variables, torque and global strain. The assumptions regarding the affine correlation that exists between local deformation and global strain must be reviewed, refined and revised when working in the non-linear region.

Figs 65a and b are important because they show that the gap plays another role than just defining the strain ($\gamma = \alpha$ R/h, where α is the radial angle, R the radius and h the gap). Not just the velocity gradient across the gap is important in the non-linear deformation range, but also the velocity of the layers, leading to the structuring of a dynamic network of interactions for which the interplay between entropic and enthalpic forces account for the stability of the network in time and under stress.

Simple concepts borrowed from the linear range (Fig. 65a) can mislead the understanding of the physics behind non-linear effects (Fig. 65b). The gap plays another role, in the non-linear range, when no slip occurs, than what can be predicted from the concepts developed in the linear-range.

Melt Fracture Initiation: Vinogradov's criteria

Edge fracture is an instability of cone-plate and parallel plate flows reported for low molecular weight viscoelastic liquids and suspensions, characterized by the formation of a `crack' or indentation at a critical shear rate on the free surface of the liquid [76]. As mentioned in the Introduction section, certain authors [60,61] suggested that, at least for PS, an edge crack formed on the free surface of the bulge of the melt between the parallel plates which propagated inwards, concentrically, in effect gradually peeling off the melt from the surface of contact to cause the observed decay of viscosity. One needs to understand how an

edge fracture would initiate in the case of a highly viscous polymer, not a low molecular weight liquid or a grease, for which an inertia explanation has been advanced [76].

A possible answer might be provided by examining the Vinogradov's melt fracture criteria applicable to high molecular weight polymers [74] , as reported and modified by van Krevelen [75]. Van Krevelen uses Bueche's dimensionless strain rate number, Γ, and specifies the critical value for melt fracture to occur according to Vinogradov's experimental results. The equations below define the parameters:

$$\Gamma = \frac{12}{\pi^2}\,\dot{\gamma}\,\eta_o\,\frac{M}{\rho RT}$$

$$\eta^* = \frac{G^*}{\omega}$$

$$\dot{\gamma} = \omega\,\alpha$$

$$G_{o,N} = \frac{\rho RT}{M_e}$$

$$\Gamma = \frac{12}{\pi^2}\,\frac{\eta_o}{\eta^*}\,\frac{\sigma}{G_{o,N}}\,\frac{M}{M_e}$$

σ = Stress

Melt Fracture criteria: $\Gamma = 350$ and $\frac{\eta_o}{\eta^*} = 40$

where γ is the strain, ρ the melt density, ω the radial frequency, M the weight average molecular weight, M_e the molecular weight between entanglements, η_o the Newtonian viscosity at temperature T, R the perfect gas constant, α the maximum angular displacement per cycle, $G_{o,N}$ the plateau modulus defining the entanglements, σ the shear stress, and η^* the complex viscosity. For instance, for the PC of Fig. 46, by plugging both melt fracture criteria into the above equation of the dimensionless strain rate, and the known values for M_e and $G_{o,N}$, respectively 2,500 g/mole and 1.5 MPa [6], one can compute the stress causing the melt to fracture at that temperature: 0.987 MPa. Figure 46b shows that the stress at the beginning of the time sweep (at 5 Hz, 225 ^oC) was only 49,791 Pa, corresponding to a viscosity of $10^{3.2}$. The critical stress for melt fracture is 20 times greater than the actual stress at the onset of the time sweep showing transient behavior: why would an edge fracture occur, a fracture process nevertheless, under the present low stress conditions? Even if Vinogradov's fracture stress criterion was too large by a factor 2, which has been found by Archer [78] for some polymers,

one would need such a large stress concentration factor to reach the critical level (10 times), that the likelihood of its occurrence appears remote for high molecular weight liquids. Friedrich et al. [60, 61] show that once the edge fracture crack is initiated (for whatever unexplained reason), their results can be quantitatively explained by the propagation of the crack or indentation, using the same formula used by several authors studying edge fracture in low molecular weight viscoelastic liquids and suspensions, in particular grease and toothpaste [76]. According to Keentok and Xue, "the Tanner-Keentok theory of edge fracture in second-order liquids can be extended to cover the Criminale-Ericksen-Filbey (CEF) model" [76]. They used a finite volume method program to simulate the flow of a simple viscoelastic liquid, and obtained the velocity and stress distribution in parallel plate flow in three dimensions. The simulation, specifically applicable to lubricating grease and toothpaste, showed that edge fracture in viscoelastic liquids depends on the Reynolds number, and is broadly consistent with the CEF model, allowing to simulate its dependence on the physical dimensions of the flow (i.e. parallel plate gap or cone angle), on the surface tension coefficient, on the critical shear rate and on the critical second normal stress difference. The simulation [76}explains how stress concentrations of the second normal stress difference (N_2) can be found in the plane of the crack; how the velocity distribution could show a secondary flow tending to aid crack formation if N_2 was negative, and how a secondary flow could tend to suppress crack formation if N_2 was positive. In summary, the effect of inertia on edge fracture of these low molecular weight viscoelastic liquids was predicted by the simulation. Furthermore, a video camera was used [76] to record the inception and development of edge fracture in four viscoelastic liquids and two suspensions. All these findings on low viscosity liquids probably influenced the authors who believe [60-65] that a similar behavior could result for high molecular weight polymer melts. The extrapolation attempt to polymers was/is, indeed, a credible approach and could apply to certain processing conditions (as we have, indeed, observed ourselves at high frequency and high strain, for instance, using thick samples). However, the validation of this assumption fails badly, in our opinion, to explain the transient evidence within the conditions presented in this chapter; in particular we conclude that a surface contact deficiency is not compatible with the unequal transient variation of $\Delta G'(t)$ and $\Delta G''(t)$ observed in our work. Other criteria of the paper by Keentok and Xue [76] also do not seem to apply to the conditions of transient behavior observed for our polymer melts, such as

the value of the Reynolds number for the validation of the inertia criteria. Finally, the experimental evidence presented by Gonnet and collaborators [77], explained in the next section, gives further credibility to the suggestion that the integrity of the interface is not responsible for the transient decay of the moduli.

Simultaneous Dielectric and Dynamic Mechanical Measurements in the Molten State

If the protagonists of an edge artifact were correct regarding the inward propagation of a surface fracture initiated at the edge of the melt [60-65], a simultaneous measurement of the melt dielectric properties would reveal such a peeling of the polymer from the metallic surface of contact. In particular, space charges would be created and an increase of the noise level would be expected.

Gonnet et al. [77] published an article about the behavior of a polymer melt during large strain sweep experiments performed in a modified dynamic rheometer equipped with dielectric measurement means. The strain amplitude was increased to beyond the linear viscoelastic regime, in the domain where we would expect "disentanglement manifestations" to take place (a transient behavior). The decrease in the mechanical signals G' and G" corresponding to disentanglement activity was indeed observed by Gonnet et al. [77], yet the dielectric probe response proved that these changes were not surface artifacts but truly bulk property events, which could be characterized dielectrically. In particular, there is no mention in ref. 77 of an increase of noise due to space charges. The dielectric signal was coherent with the mechanical signal, although a transient decay was observed. The polymer studied by Gonnet (PVDF) was different from those studied by either Friedrich [60, 61] or by us in this chapter. Yet, the triggering of the transient decay by an increase of strain at low frequency provided a similar response to those shown in Figs. 37a to d for PC. There is no reason to believe that the nature of the polymer would require a different explanation when the rheological response to the same type of deformation yields the same result. We suggest Gonnet and collaborators' article provides an elegant and definitive answer to the question whether the effects observed with a dynamic rheometer are due to a bulk viscoelastic response or artifacts generated by some surface effect; they are, indeed, due to bulk properties.

3-Effect of the nature of the surface melt contact

Figures 66a and b suggest that the interaction of the melt with the surface of the dragging layer (the top parallel plate) influences the steady state viscosity, thus the melt structure that gives rise to that steady state. Figure 66a plots the viscosity (experiment of type 4) versus time for the LLDPE of Figs 14-23. Figure 66b plots the normal force vs time for the same data. Three different types of surface were used: serrated, smooth and rough. The material used for the disk plate was Aluminum. The smooth surface was polished to a very fine finish, the rough surface was sand-paper treated to leave some scratches across it, and the serrated disk surface was densely sparkled with a multitude of homogeneously distributed pyramid-shaped clits of height 150 μ. Both the stationary and moving surfaces had the same surface treatment, for a given test. The experiment with the rough surface was repeated twice using a different sample, to assess repeatability. Temperature was 190 ^{o}C, the strain rate was 3.0 sec^{-1}. The gap was the same for all tests, 1.6 mm. Repeatability was, indeed, excellent in Figs. 66a and b, shown by the perfect superposition of the viscosity and normal force curves for the rough sample and the rough repeat one.

We assumed that the serrated plates created a better contact, a better interfacial grip, due to the microscopic indents at the surface. It appears from Fig. 66a that the more the melt grips to the moving surface, the lower the steady state viscosity. The smooth surface gave the top curve with a steady state viscosity of 800 Pas-s. The second lowest steady state viscosity value was obtained for the rough surface (200 Pa-s), and the lowest steady state viscosity corresponds to the serrated surface (almost zero). The same order is seen for the normal force in Fig. 66b, 75, 10 and -15 g for the smooth, rough and serrated surfaces, respectively. The nature of the surface of the disk also influences the transient decay relaxation time, as is clearly shown in Figs 66a and b, the serrated plates providing the slowest decay.

The effect of the surface on the viscoelastic response is not new [81] and is usually considered to be caused by wall slippage [78, 80, 81]. It is commonly established that above a certain critical stress (~100,000 Pa for most melts) slippage occurs at the stationary wall, reducing the velocity of all layers all the way up to the dragging surface. Polymer viscosities measured in pressure-driven and drag flows have been reported to systematically decrease as the dimension of the flow channel is reduced [78, 80]. According to Larcher [78]:

> *"Work by several groups…clearly indicates that fundamental understanding of polymer adsorption and interactions between polymer chains near the polymer-solid interface are important for resolving the molecular scale processes responsible for slip violations."*

Hence, in Figs 66a and b, one could conclude that the results reflect the strength of adhesion between the mobile plate and the melt, the slip being more pronounced for the smooth surface. This explanation, however, is unlikely to be the correct one in view of the value of the stress at the initiation of the transient behavior with respect to the critical stress for slippage. The extrapolated viscosity is ~ 10,000 Pa-s for a strain rate of 3 sec^{-1}, giving a stress maximum of 30,000 Pa, three times less than the critical stress to initiate slip. The solution must be found somewhere else.

The established view considers that in planar Couette shear flow, driven by one mobile surface, the strain rate in the gap, alone, characterizes the rheology, and that, above a critical shear stress, some correction of the apparent strain rate is necessary to account for the effect of the gap thickness and the nature of the contact with the wall on the slip velocity. We suggest that this is a simplification which is only valid within certain conditions of laminar flow and that results such as those in Figs 66a and 66b are indications that the polymer melt organizes its structure across the gap in ways which are not simply predicted by macro-variables independent of the nature of the polymer or its state of entanglement. In the non-linear range that we talk about, such as in Figs 66a and b, the different moving layers across the gap are dragged at different speeds from top to bottom. The maximum stress is at the stationary surface and there is no slip. If and when the transient decay is due to orientation of the active strand network in the flow direction, the success of the orientation is not just a function of the strain rate (assumed constant in the gap), but also on the stress, which varies across the gap. Since we do not reach the critical stress criteria for slip in Figs. 66a and b, we suggest that smooth plates are not capable of creating an orientation pattern across the gap which penetrates deep enough, serrated plates appear to be the best, the rough surfaces being intermediary. In other words, "disentanglement" is not uniform across the gap.

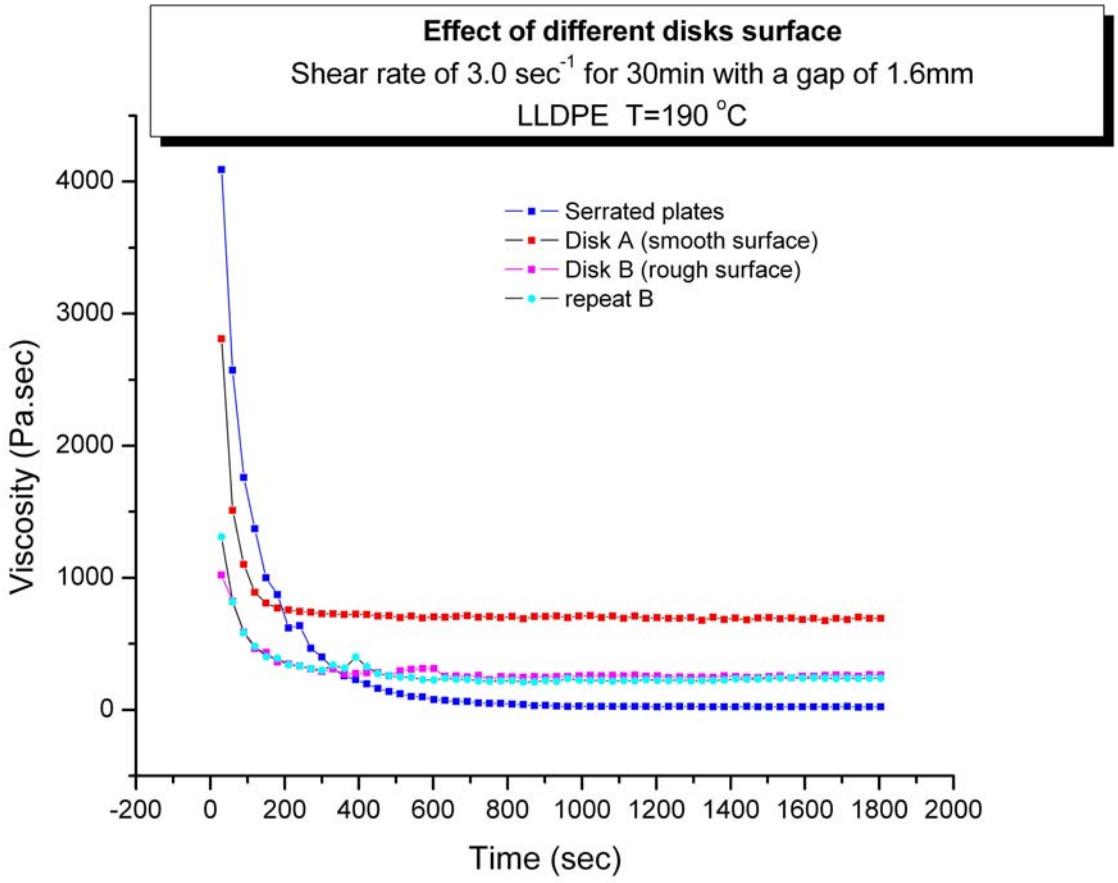

Fig. 66a
Viscosity vs time for different surfaces. The conditions are found in the inserts

The structuring of the entanglement network occurs both concentrically and across the gap, with the orientation of the entanglement phase in circular rings, the number of rings varying from layer to layer, and the structuring being influenced by the state of adhesion with the stationary and dragging surfaces.

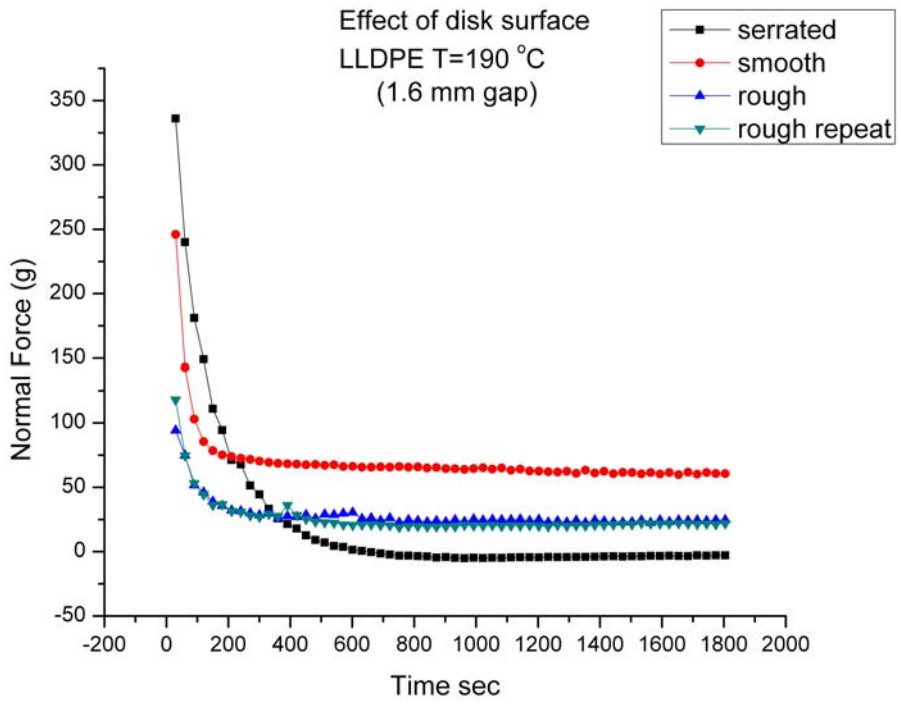

Fig. 66b
Normal Force vs time for different surfaces. The conditions are found in the inserts

In Fig. 66b, the serrated plates were the only ones capable of producing a steady state melt with negative force. All other plates had a positive remaining normal force (10 g for the rough surface, 75 g for the smooth surface). These are significant clues to what was happening during transient decay and could be interpreted by a layered orientation structure of an active strands network.

If the degree of disentanglement is not uniform across the gap, it is expected that squeezing of the gap after the transient stage (like was done in Figs. 65a to b between run 1 and run 2) will result in at least the partial destruction of the structure. This is particularly important when the benefits of the viscosity drop are sought to be preserved after shear-refinement into pellets.

4 Melt Flow Index of Disentangled Pellets and in-line Viscosity of Disentangled Melts.

To explain the transient decay of polymer melts and results such as those in Figs 3, 7a and b, 28, 58a to d, the most crucial and convincing evidence in favor of the "disentanglement hypothesis", is to measure the viscosity of the melt obtained by the disentanglement treatment after it has been treated and ensure that the decrease of viscosity was not due to chain breakage or degradation by measuring its molecular weight distribution with a GPC. There were two methods that we used to perform those convincing tests. They were both described in the introduction section of this chapter. One method (Fig. 8) consisted in measuring the viscosity of the melt at the exit of the disentanglement processor by side-dispatching a small amount of the treated melt into a capillary viscometer working in the linear range. This corresponds to an in-line viscosity measurement done between 2 to 5 min after the melt left the treatment section (depending on the throughput rate). Another method consisted in measuring the Melt Flow Index (MFI) of the pellets produced by passing the treated melt through a strand die and a pelletizer. MFI is, roughly speaking, the inverse of viscosity. We consistently compared the in-line viscosity with the MFI measurements (Fig. 9). Results of 1996 on PC were published in 1999 [16], and several papers followed suit in subsequent years covering a decade of experiments [12-14,18, 43-54]. In fact, the entire lab activity of the author (9 persons) was dedicated to the characterization by MFI and GPC of disentangled samples produced by the disentanglement processors described in Figs. 5a and b. Figures 67a and b provide another example of good correlation between the MFI of the disentangled pellets and the in-line viscosity measurement at the exit of the disentanglement processor.

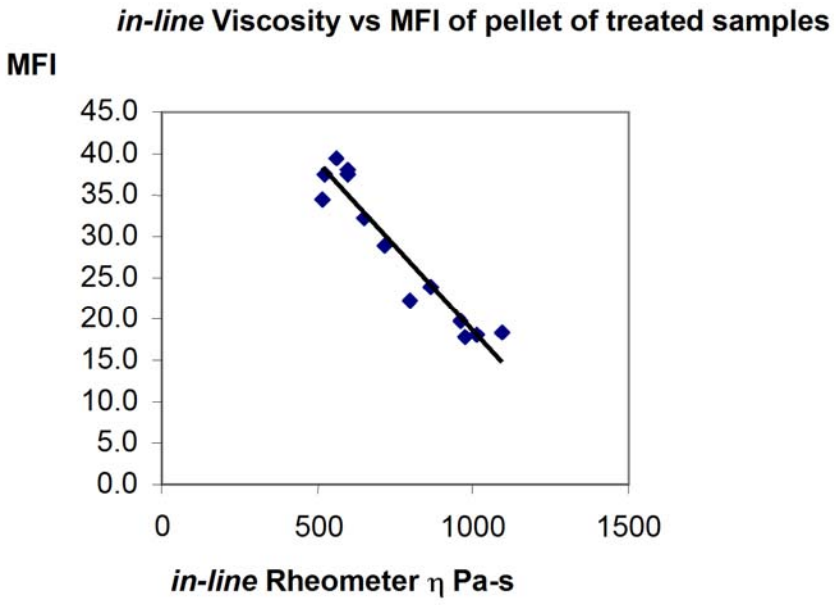

Fig. 67a

This plot is similar to the one in Fig. 9 except that it applies to a different polymer, PMMA, already described in Figs. 55-57. The reference MFI (for the virgin) was 16.3 g/ 10 min. The various points correspond to changing the processing conditions in the 2 stations of Fig. 5b. Degradation due to the treatment was between 1.5 and 4%. The MFI values given are corrected for the small M_w degradation and are expressed in g/10 min at T=230 ^oC under 3.8 Kg. Pellets were dried at 60 ^oC for 17h before performing the MFI test. For the in-line rheometer, temperature was 225 ^oC, strain rate was 36.5 sec-1 corresponding to a flow rate of 5.8 cc/min. A picture of the in-line rheometer screen for this PMMA treated melt is shown in Fig. 67b.

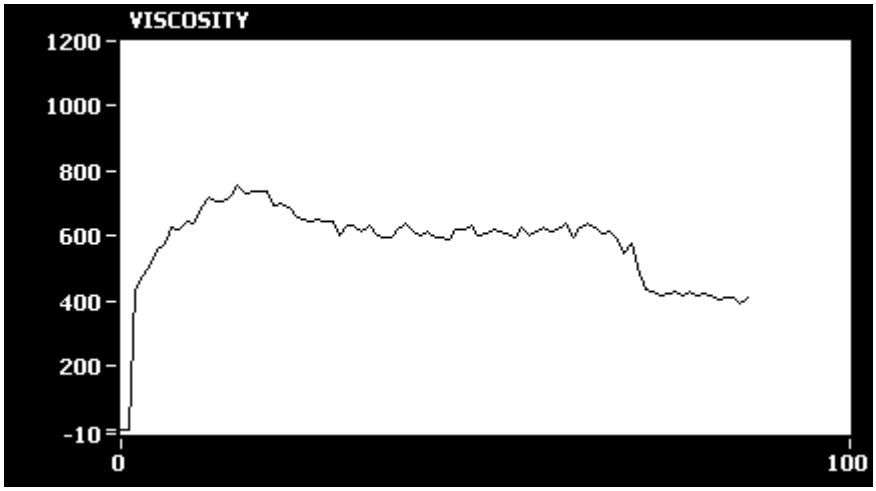

Fig. 67b

In-line viscosity measurement at the end of the disentanglement processor.

Thousands of experiments were conducted with samples sent to the testing laboratories of large resin manufacturers and to universities. To summarize, time sweep treatments done in "disentanglement processors" (Figs. 5a and b) under a combination of shear, shear oscillation and extensional flow appeared to produce what we call "disentanglement", that can be characterized by the % improvement of MFI of the pellets produced by the shear-refining flow after correction of the viscosity by the M_w change (which affects viscosity as $M_w^{3.4}$). The improvement of viscosity was also measured by the in-line viscometer which followed the state of the melt as we varied the treatment parameters.

We conclude that it is, indeed, possible to submit polymer melts (branched or linear) to specific thermal-mechanical treatments that not only favor (immensely) the "in-line" conditions of flow inside the disentangling processor but also permit to capture in pellet form at least a part of the viscosity benefits imparted during the in-line viscosity reduction. Such "in-pellets" sustained viscosity reduction improvement was reported by us for PC, PETG, LLDPE, PP, EVOH and PMMA [43-54]**.** Is this technology applicable to all resins? The limitation seems to be related to:

- the collateral degradation of M_w caused by the length of the treatment in the Shear-Refinement processor (from 3% to 25% depending on the type of polymer and the amount of antioxidant additives).
- the cost of the shear-refinement processor and the cost of the research to find the appropriate processing windows for each new resin.
- the issues related to the control of the re-entanglement kinetics (too fast for certain conditions and polymers, too slow for others), i.e. the stability of the new entanglement network.
- the apparent increase of the sensitivity to thermal degradation of the disentangled resin
- the lack of quantitative theoretical understanding of the results, and, as a consequence, the disbelief that such experiments can be integrated with the current established understanding of polymer science.

As already mentioned in the introduction, there is no apparent problem in combining the effect of strain softening and shear-thinning to boost the viscosity reduction of melts during the in-line disentanglement process to very large values (say +1500%) with very little degradation present (1-3%). However, the capture of, say, +100% viscosity reduction in the pellet appears to be a much more difficult task. It is true that the use of small concentrations of additives during the disentanglement processing, in combination with the thermal-mechanical treatment [82], has opened up new prospects of success that have rendered the in-pellet technology much more efficient (+300%). For instance, an extrusion grade (higher M_w) can be converted by this method into an injection molding grade (lower M_w) with boosted flow properties (+300%) compared to the same molecular weight untreated grade [82].

5. Manifestation of properties of disentangled polymers is not new

Prevorsek and De Bona [83] prepared, by a solution process, unentangled polymers to establish whether the effects of chain entanglement persisted also in the glassy state. The polymers investigated were prepared by a solution process which, in the purification step, involved precipitation from dilute solutions

> *In the course of this study, we discovered that the melt viscosity of highly entangled polymers isolated from dilute solutions exhibits behavior which suggests that with such polymers it takes considerable amount of time for the molecules to attain equilibrium interpenetration and entanglement. This phenomenon allowed the preparation of samples where the chain entanglement could be varied without changing the chemical composition. This, in turn, provides the possibility to study the role of chain entanglement on properties belowT_g without an interfering effect of chemical composition* [83].

Prevorsek and De Bona determined the melt viscosity of these precipitated polymers using a capillary rheometer. Their reported "unusual behavior" is reproduced below in Fig. 68**.**

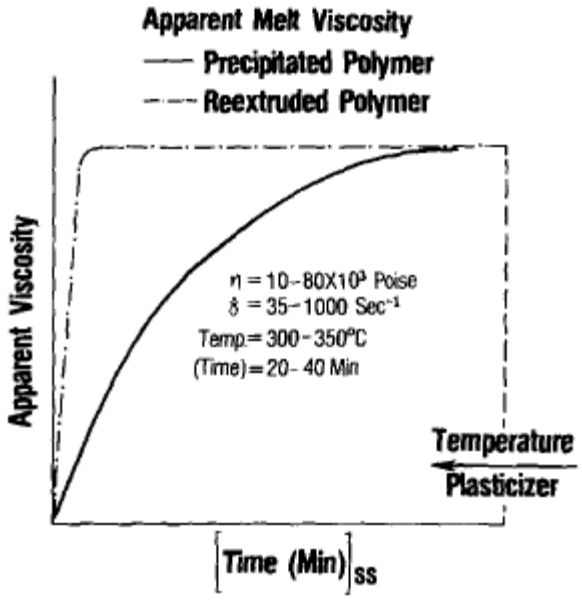

Fig. 68

Melt viscosity vs time for a precipitated PCT and comparaison with a re-extruded melt (after Prevorsek and De Bona [ref. 83, Fig.4]. Reproduced with permission. Compare the transient viscosity increase in this figure with that of Fig. 58c attributed to the re-entanglement of disentangled PS.

The melt viscosity of the polymers precipitated from solutions increased slowly towards their steady state level (the lower curve in Fig. 68). Depending on the temperature of the melt, the time to reach equilibrium could be between 10-100 min. When the polymer extruded from the steady state was re-extruded, the melt viscosity reached its steady state in a few minutes, as shown by the upper (dashed) curve in Fig. 68. Prevorsek and De Bona report [83] that chemical analyses and molecular weight determinations showed that no significant changes in composition **or** molecular weight occurred during the transient increase of viscosity for the melts produced from precipitation. . Furthermore, these authors characterized the extrudates by optical and electron microscopy and showed that no difference existed between the control and the transient melt. Prevorsek and De Bona showed that the transient response of the "precipitated melt"could be varied by changing the "solution history" and concluded:

> *In view of the results presented below on the effects of solution history on chain entanglement… it appears that only a systematic study could resolve the question whether the observed differences between predicted trend and experimental data should be attributed to inadequate theory or inaccurate experiments* [83].

S. Rastogi and collaborators [84-86] explored the role of entanglements in obtaining a homogeneous product of ultra high molecular weight polyethylene (UHMW-PE). In this original approach to produce stable disentangled polymers, "the disentangled state is obtained directly from the reactor by controlling the polymerization conditions or in the solid state when there is enhanced chain mobility along the c-axis of a unit cell" [84]. Rastogi et al. claim [85] that their novel approach to synthesize disentangled polymers is applicable to polymers in general as long as three criteria are met during polymerization:

- homogeneous polymerization, the catalyst sites being separated from each other as far as possible.

- low reaction temperature to work in the range in which the rate of crystallization is faster than their synthesis.

- living polymerization system to achieve a narrow molecular weight distribution.

Rastogi and collaborators show that the disentangled state can be maintained in the melt over a long period of time, "invoking implications in polymer rheology" [84]:

> *"Flow behavior of polymers through confined geometry is of fundamental and technological relevance having implications in fiber spinning or extrusion processes. Presence of entanglements and their realization in polymer melt is a basis of the flow behavior dunng polymer processing, crystallization and thus the mechanical properties. So far studies have been performed extensively on the entangled polymers in the thermodynamically stable melt state because of the non- availability of disentangled polymers. The availability of the disentangled polymers will provide an opportunity for the first time, to address the influence of disentangled (or partially entangled) melt state on chain orientation, relaxation time, viscosity and its implications on polymer crystallization*"[85].

Talebi [86} studied the kinetics of the re-entanglement process starting from well characterized disentangled UHMWPE synthesized by Rastogi's method [84]. Like we did for the mechanically disentangled LLDPE .(Fig. 28 (recovery zone), Talebi used a time sweep experiment at low strain (1%) and low frequency (10 rad/s) to follow the growth of the moduli G' and G" with time, slowing returning to the equilibrium entanglement value. The recovery curves presented by Talebi (Figs. 4.12 and 4.13 of ref. [86]) are very similar to what we observed for mechanically made disentangled melt, see Fig. 28 (recovery zone) for LLDPE or Fig. 58c, for PS. Talebi also found the same increase of the strain softening ability for

disentangled melts, showing that the critical strain to trigger time dependent effect (transient viscosity) is lower for disentangled melts [86].

In summary of what we learned from the work of Prevorsek et al. [83] and Rastogi et al. [84-86], one can say that one of the most demonstrative proofs that the effect of melt disentanglement by mechanical treatment is, indeed, to disentangle the macromolecules is evidenced in post-treatment thermally induced viscosity « recovery » experiments which look so much like what other authors find for their chemically synthesized or solvent precipitated disentangled polymers. One clearly sees in Fig. 28, for instance, that the viscosity of the initial specimen, which had been decreased by melt disentanglement treatment, was slowly and kinetically growing back to its initial viscosity value at the corresponding temperature, as the system was left alone in the rheometer chamber and the entanglements allowed to recombine to their stable thermodynamic level. The same behavior was observed when we operate the treatment at different temperatures. The thermally induced recovery behavior observed in Fig. 28 is kinetically driven and an activation energy can be determined for the process**.** These recovery experiments are most spectacular and convincing of what is taking place during the treatment: disentanglement. In Fig. 60b (step 6), for PS, the recovery experiment was triggered by just reducing the strain %, keeping frequency the same (50 rad/s). This is clearly a demonstration that the decrease of viscosity was not the result of a mechanism of slippage at the surface of the Rheometer, nor a mechanical degradation of the chain macromolecules, but rather due to a viscoelastic effect in the bulk, which manifests the thermo-kinetic nature of the network of interaction (dynamic entanglements), and the possibility to modify it by mechanical means. For instance, Figs. 14 to 24 show that transients caused by pure rotational shear at high shear rate and strain are the same manifestation of this re-organisation of the dynamic entanglement network. Viscosity recovery curves are clearly triggered by a decrease of the strain rate in Fig. 18, in a way similar to what causes the recovery step in Fig. 28.

We studied the inducement of non-equilibrium states for the entanglement network by dynamic solicitations (oscillatory) in the non-linear range (beyond a critical strain), separately analyzing the effect of increasing strain at given low frequency (Figs. 29-42), the effect of increasing frequency at given low strain amplitude (Figs. 43-45) or combining both (Figs. 46, 60a to c).

We showed that sophisticated disentanglement processors (Figs 5a to b) could induce a lasting modification of the network of entanglement to the point that pellets could be extruded with sustained viscosity decrease that could last for long times, say tens of minutes or even hours at elevated temperatures far above T_g, say 150 ^oC above it. These pellets could be pressed into samples that could be reheated in a rheometer and studied in the linear range (Figs 39-42, 47-57) or in the non-linear range (Fig.25).

We also explained that it was not straightforward to succeed in obtaining in-pellets a "sustained orientation (i.e. disentanglement)". When in-pellet disentanglement is ***not*** successful, it is either because the shear conditions are not strenuous enough to exhaust the cooperative mechanism responsible for shear-thinning (via the increase of the number of activated strands), or because the elasticity of the melt is too high, the shear stress at the wall is over the fracture stress, causing degradation, melt instability and possibly slippage. So, it is true that several experimental conditions could cause adverse effects, preventing disentanglement to take place. The art and science of disentanglement technology resides in obtaining the largest disentanglement possible, in the minimum amount of time, and with as little degradation and melt fracture as possible. After the disentanglement processing window has been found, the best re-entanglement method and conditions must also be found.

6. The real problem is the understanding of the nature of entanglement and of the entropic character of polymer melt deformation.

In this section, we present the results of an investigation carried out on disentangled pellets of PC. This study is quite revealing, in our opinion, of what causes "disentanglement", i.e. of the reasons why pellets of treated melts (processed by the disentanglement processors of Figs 5a and 5b) sustain viscosity changes at elevated temperature for much longer times than what is predicted by the value of their τ_o at that temperature.

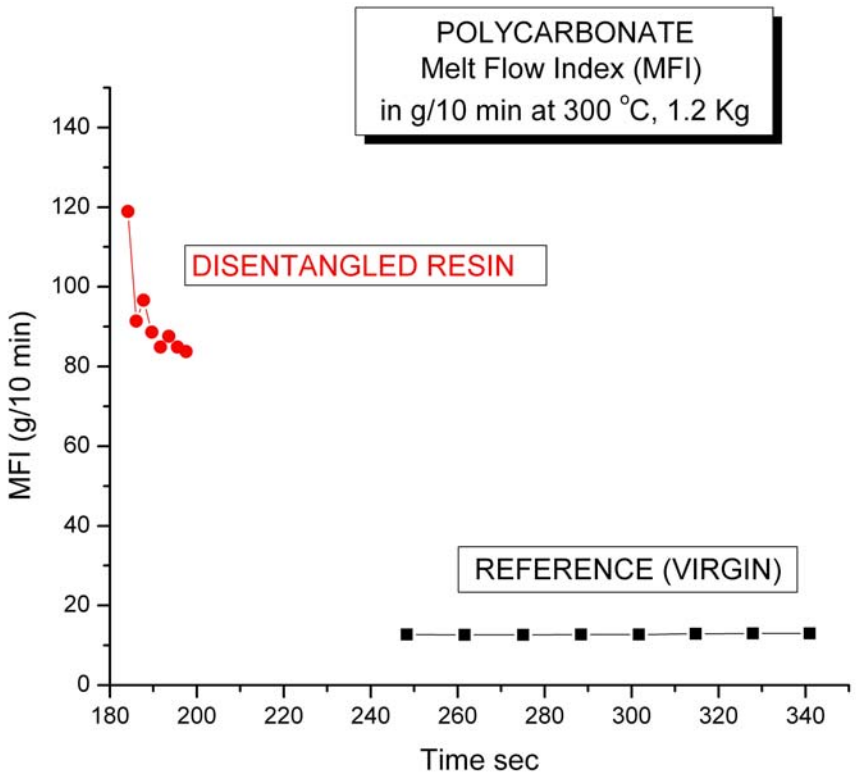

Fig. 69a

MFI (g/10 min) *vs* "flag" time for a virgin PC (Reference) and a disentangled pellet. T= 300 °C, 1.2 kg. The pellets were <u>not</u> dried before running the MFI test. The MFI testing equipment (from Dynisco) was fully automated and determined the starting time and the duration of the test, which were both dependent on the fluidity of the melt in the barrel. There were 8 measurements ("flags") done to provide a given average of the MFI value. A computer was attached to the output of the MFI tester so that all MFI values for all flags could be recorded, giving the data in this figure.

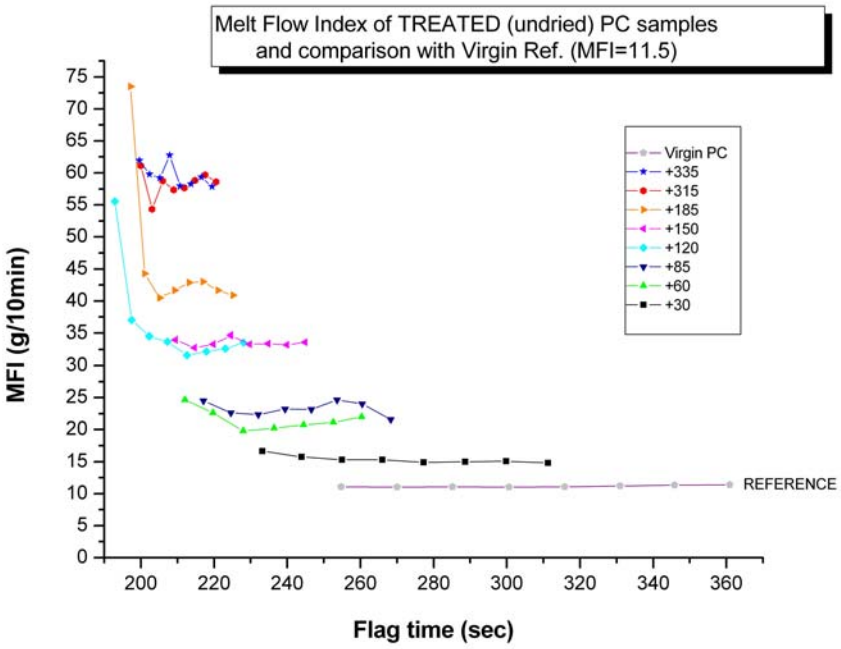

Fig. 69b

Same as in Fig. 69a but for different thermo-mechanical treatments in the disentanglement processor. The numbers in the insert give the % increase of MFI with respect to the reference MFI for the virgin (11.5). Different processing conditions yield different magnitudes of "improvement".

Figure 69a compares the MFI measurements for undried pellets of "disentangled" PC and the reference (the virgin pellets). The MFI remains constant during the time it takes the melt to pass through the capillary (the flags correspond to specific "indexed" measuring intervals). The MFI of the disentangled sample is 10 times greater than the reference at the beginning but drops steeply with time, from 120 to 85. The rate of passage through the capillary is so large for the disentangled sample that the 8 flags are accomplished in less than 15 seconds whereas it takes a minute and a half for the reference test. In Fig. 69b, several treatment conditions (changing the speed of rotation of the shaft, the frequency and amplitude of oscillation, the temperature profile of the zones, etc.) provided pellets with a variety of MFI response, but all show the same trend of a steep initial drop of the MFI followed by a stable plateau value. Figure 69b gives the impression that, given a certain grade (MFI=11.5), we can choose the MFI we want, from 120 (Fig. 69a) to 20. This may look like a very powerful asset to polymer processors. However, these results apply to undried pellets. Table 1 analyses the difference of the MFI obtained for undried and dried pellets (treated and virgin). The drying

conditions are described in the Table's caption. The 1st column identifies the pellets (2 lots are considered, with slightly different MFI as shown for Virgin PC1 and Virgin PC2, although it is the same grade from the same manufacturer), the next two columns give the absolute value for the plateau MFI for the undried and dried sample, the next two columns convert those results to % MFI increase (with respect to the respective virgin MFI for the same lot), and the last two columns compare the undried and dried pellets after the correction for the amount of M_w degradation has been accounted for, as explained before. One sees, for instance, that the Treated-1 sample, which showed a +106% increase of MFI when undried and uncorrected has only +3 % left after drying and correction for the Mw decrease. Likewise, Treated -5 sample, which showed +434 % improvement has only left +77% after drying and M_w correction. Is this behavior "normal"?

1	2	3	4	5	6	7
Sample ID	**MFI**	**MFI**	**% MFI Increase**	**% MFI Increase**	**% MFI Increase after Degradation correction**	
	undried	**DRIED**	**undried**	**DRIED**	**undried**	**DRIED**
Treated -1	23.00	12.39	+106	+22	+ 85	+3
Treated -2	33.89	20.15	+151	+59	+ 150	+57
Treated -3	41.52	25.98	+208	+105	+ 185	+91
Treated -4	25.02	18.23	+86	+44	+ 85	+44
Treated- 5	59.52	22.97	+434	+127	+ 315	+77
Treated- 6	61.57	26.89	+357	+112	+ 335	+103
Virgin PC1	13.48	12.69				
Virgin PC2	11.50	10.13				

Table 1

Column 2 and 3: MFI measurement (in g/10 min at 300 ^oC , 1.2 Kg) of "disentangled" PC pellets (M_w of virgin=23,000). The reference MFI is for the virgin pellets (2 lots are shown for the same grade). Pellets were **dried** (4h @ 120^oC and MFI done under dried N_2) or **undried** before the MFI test. Columns 4 and 5 display the result in % MFI increase with respect to the reference (virgin). The last two columns, 6 and 7, show the final % MFI increase (which we call "% disentanglement" for convenience) after the MFI have been corrected for the effect of the small % of degradation due to the treatment (the M_w of the treated and reference pellets were measured by GPC).

Sample ID	T_g °C	ΔC_p @ T_g	Pellet density g/cc	% moisture content
Treated -1	146.43	0.163	1.19851	0.198
Treated-2	145.87	0.272	1.19339	0.273
Treated-3	146.52	0.238	1.19684	0.206
Treated-5	147.08	0.244	1.19529	0.192
Treated-6	148.76	0.244	1.19318	0.116
virgin PC1	147.45	0.225	1.19712	0.265
virgin PC2	149.22	0.240	1.19855	0.183

Table 2

The moisture content % was measured with the Mark2 Moisture Analyzer from Omnimark Instrument Corp. The Tg data were obtained by DSC. The density of the pellets was according to ASTM D1238. C_p is in J/g-°C

The change of MFI between the undried and dried virgin pellets is what defines normality. One sees that the drying step does decrease the MFI of virgin PC1 by 6% and that of virgin PC2 by 13%. But this magnitude of change is 10 to 20 times **less** than what is observed for the undried vs dried treated pellets, from +434 % MFI increase to +127% only for Treated-5 sample, for instance. The difference is quite significant. This is particularly intriguing in view of the results of Table 2 which displays the moisture content, the density and the glass transition characteristics (T_g and the ΔC_p at T_g) for the undried samples. It was originally expected that a large increase of moisture content would be observed for the undried treated pellets, explaining the MFI increases of Figs. 69a and b due to degradation by hydrolysis. But this was not the case: as Table 2 clearly indicates, the moisture content (expressed in % of weight loss) of the treated pellets and of the virgin pellets do not differ significantly. The same can be said of the density, which we measured to be sure that the treated samples were not less dense. The T_g and the change of the heat capacity at T_g were also the same for the treated and the virgin undried samples.

.

One must conclude from Table 2 that the disentangled pellets and the virgin pellets have the same AVERAGE density and moisture content, although it should also be realized that any sample anisotropicity would not be revealed by such measuring techniques.
Since we have hypothesized that "disentanglement" (the viscosity decrease retention) could be due to the formation of a structured multi-level orientation of the entanglement network of active strands, showing significant anisotropicity, the results of Figs. 69a and b and of Tables 1 and 2 lead us to believe that it is not the average functions that might be responsible for the extraordinary different flow behavior of the undried treated and virgin pellets, but, precisely, their anisotropic character. In more specific terms, and as a way of illustration, let us talk about the distribution of free volume in a polymer melt. It is well known that the free volume content influences the viscosity of polymers [3], an increase of free volume decreasing viscosity. The free volume is considered to be a local property which is isotropically distributed across the bulk of the sample. Diffusion of small molecules, such as water molecules, into the free volume of the polymer would be isotropic. However, what would happen to that diffusion process if we had succeeded in creating structures where the free volume was heavily anisotropically localized?. The water molecule local concentration would actually follow the pathways created by the channels of free volume. This may be the situation for the undried PC pellets, explaining many features observed for the treated pellets in Figs. 69 a and b). In summary, the "sustained orientation" of disentangled pellets could be the result of a modification of the free volume distribution in the melt, not simply its amount but also its orientation. If the thermo-mechanical deformation history has resulted in an increase of the average free volume, one would expect a drop of the Newtonian viscosity because of the corresponding influence of the free volume on T_g. But one could also conceive cases where, say, for the same average free volume, a reorganization of free volume distribution would result in zones of layered concentration increase of excess free volume alternating with zones of lower than mean free volume. Such a vision could be describing Fig. 62. See later.

In the following figures, we use the technique of TMA (Thermal Mechanical Analysis) to test the hypothesis of high anisotropic sustained orientation in treated pellets of PC and PMMA. In a TMA experiment a thin sample slice is placed on a plate and a probe touches it connected to an LVDT (Linear Variable Differential Transformer), constantly measuring the increment of thickness due to a small force on the probe (1 to 5 g). A constant heating rate (+

10 ^{o}C/min) raises the temperature of the sample linearly in time. The temperature holds constant at the programmed maximum temperature for two minutes, and then the sample is cooled down at constant cooling rate. A pellet of polymer is made by cutting at regular intervals (with a pelletizer) a set of strands slowly pulled out of a strand die, at the exit of the extrusion process, after the strands have been cooled by immersion in a cooling bath. In Fig. 6b, the treated melt goes through a strand die and pellets of "disentangled" polymer are collected. The pellet is a short piece of the cooled strand, cut across by the pelletizer blade. To obtain a TMA sample we cut a small slice from the pellet itself. We can cut the pellet across the strand pull out direction or make a slice in the direction parallel to the strand flow direction. The final cut is about 1 to 1.5 mm thick flatly disposed on the lower plate of the TMA cell. For a virgin pellet, we also cut it in the cross-section ("cs" sample) or in the parallel direction ("parallel"), the pellet being a small cylinder longer in the direction of strand pull out. Figure 70a plots % L/Lo vs temperature for a PC virgin pellet.

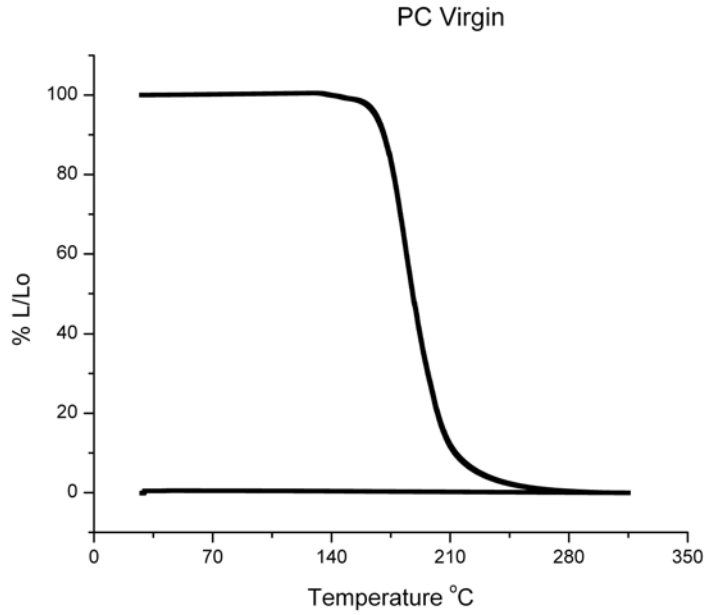

Fig. 70a

L_o is the initial thickness of the sample, at room temperature, L is the thickness calculated by the instrument as $L=L_o-\Delta L$, where ΔL is measured by an LVDT attached to the probe applying a small weight on top of the sample as temperature is linearly increased. The maximum temperature was 300 ^{o}C where the sample was held for 2 min, then was cooled down to room temperature at constant cooling rate.

Figure 70a is typical of what was observed for a virgin PC pellet. Either a "cs" or a "parallel" slice gave the same TMA response. The T_g of the PC sample was observed at a temperature of 143 ^oC, for which a very small deflection is visible. The steeper decrease of L started around T= 170 ^oC and continued until L collapsed to practically zero. The cooling curve looks like a straight line not very far above 0 (~1%).

Figures 70b and 70c are the TMA responses for two different treated PC samples, each figure showing the distinct response obtained for a "cs" section and a "parallel" section.

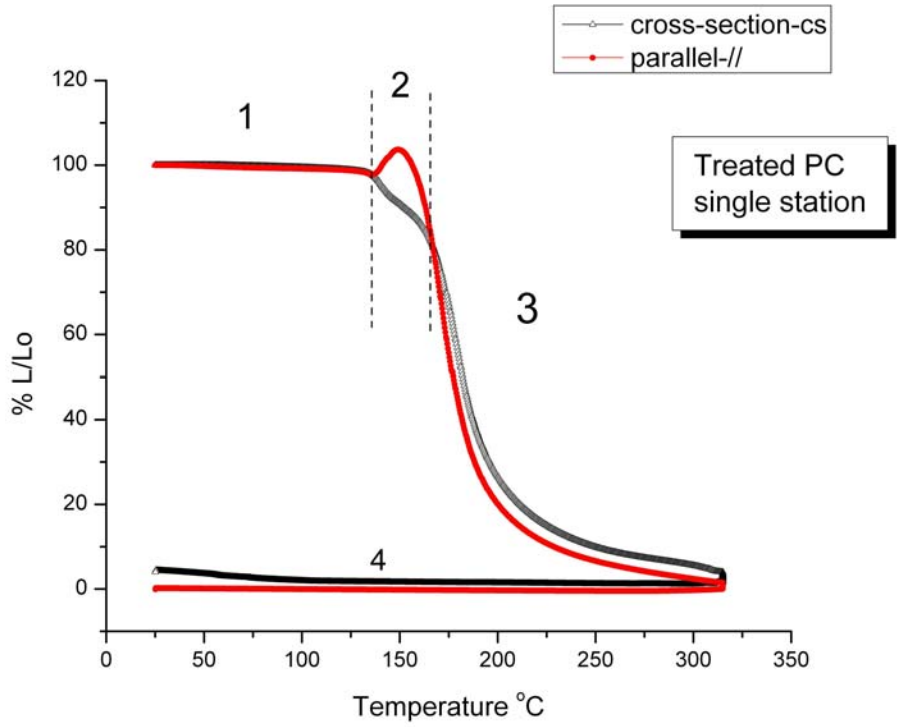

Fig. 70b

TMA curves for cs and parallel sections of PC disentangled pellets obtained after treatment by a single station in Fig. 5b (the melt exited after the first station and was pelletized).

Figure 70b applies to a treated PC after treatment through a single disentangling processor ("single" station), and Fig. 70c shows the result for a pellet from a melt that went through 2 successive stations, as described in Fig. 5b. Additionally, for the pellet of Fig. 70c, the rotation of the shafts in the first and the second stations were reversed in order to "comb" the melt in one direction in station 1 and in the other direction in station 2.

Let us examine the features of Fig. 70b first (the melt obtained with a single station). We have indicated 4 zones (1 to 4), and there are two curves, one for the cross-section sample (triangles) and the other for the parallel cut, which shows an up-turn just above T_g. Zone 1 corresponds to the glassy region, it is identical for both cs and // pellets. In zone 2, comparing with the virgin (Fig. 70a) and comparing the cs with the // sample, the // curve pushes upward and the cs curve downward. This is typical of the response of an oriented sample which retracts in one direction and contracts in the other, just above T_g. The steep decrease of the thickness (in zone 3) is slightly different for both cuts, and, likewise, the cooling curves (zone 4) display some differences, but not in a very significant way.

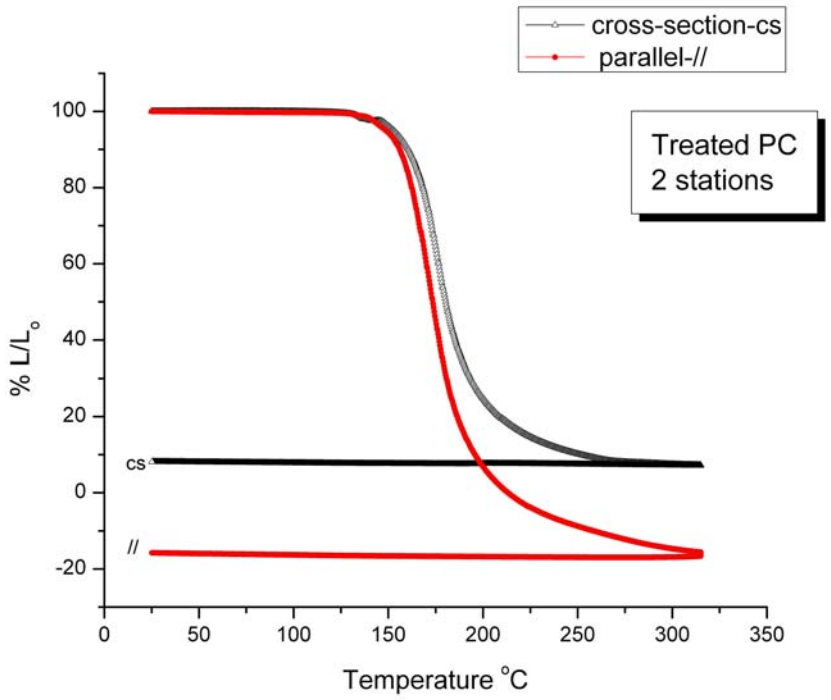

Fig. 70c
TMA curves for cs and parallel sections of PC disentangled pellets obtained after treatment by 2 successive stations as depicted in Fig. 5b (the melt exited after the 2nd station and was pelletized). Additionally, the shaft rotation was reversed for station 1 and 2.

The two TMA curves of Fig. 70c are strikingly different than those in Fig. 70b. First of all, zone 1 and 2 are the same for both the cs and // cuts: there is apparently no sign of orientation above T_g. However, a marked difference between the samples arise in zones 3 and 4. In zone 3, the cs sample appears to push upward, especially above T=200 ^oC, resulting in a slow down of

the decrease of L with temperature. The final value of the thickness ratio is not zero but +10%.in zone 4. In the case of the parallel sample (//), the opposite trend is visible, the sample appearing to pull L downward, which results in the further decrease of L towards negative values, the final thickness ratio being -15% in zone 4.

We suggest that Fig. 70b corresponds to a typical behavior of local entropic orientation, for which chain segments have been oriented and return to their random equilibrium position as soon as T_g is reached. However, Fig. 70c is not typical of a traditional orientation process and displays the relaxation of a sustained oriented entanglement network with a strong anisotropicity between the transverse and parallel flow directions, and a high temperature stability of the network resulting from the compensation (the coupling interlock) between entropic and enthalpic interactions between the conformers. When such a situation occurs, the pellet shows the ability to retain at high temperature, far above T_g , its new "state of entanglements" responsible for the viscosity improvements shown in Figs. 47-54. In Fig. 70a, the orientation is not sustained at high temperature and collapses as soon as T_g is reached. The ability to retain orientation is, therefore, due to 1. the orientation of the entanglement network and 2. its stabilization (lock-down) by enthalpic forces. This determines the success whether viscosity decrease benefits will "stick" and for how long.

In Fig. 70c, the final % L/L_o levels are +10% for the cs sample and to -15% for the // sample. How is that possible? As we said, the LVDT in the TMA instrument measures increments of thickness variation, not the absolute value (which is calculated). When the initial sample cut has frozen-in orientation below T_g, the initial thickness L_o does not correspond to the stable state; heating above T_g relaxes out the frozen strain, freeing up the internal motions to coordinate their interactions to obtain a stable state. The first motions to occur are those triggered by the presence of the available local free volume allowing a local re-organization of the conformal state of the bonds, showing entropic effects such as those observed in Fig. 70b. The small force on the TMA probe is sufficient to flatten-out the thickness to almost zero. When the network of active strands has been oriented and stabilized by an enthalpic-entropic compensation mechanism, the release of the internal orientation not only occurs at a higher temperature than Tg (Fig. 70c) but also induces structures which resist the further relaxation by the small weight on the probe (case of the cs sample), or, conversely, favor it in the transverse direction (parallel sample), depending on the contribution of the enthalpic forces in

establishing the distorted coil structure. In Fig. 70c the enthalpic contributions appear to have been less for the parallel sample since the final level of strain is 5% lower (in absolute value of % L/Lo), i.e -15% vs 10%.

Figures 71a to c, Figs. 72a to b relate to the PMMA sample already described in Figs. 55-57 and Figs. 67a and b. Figures 71a to c display the TMA response for a cross-section cut of three types of pellet, a virgin sample, a +70% (MFI increase) disentangled sample and a +100% disentangled pellet. The three figures focus on different temperature ranges, comparing the behavior of the virgin and the disentangled pellets in zones 1, 2 , 3 and 4. The first observation (in Fig. 71a) concerns the decrease of the T_g for the disentangled sample, especially for the +100% disentanglement. This ~10 ^oC difference in the T_g can be associated with an increase of free volume due to the treatment. The respective position of the curves in the $T > T_g$ region is, overall, controlled by this increase of free volume (Fig. 71a), but Fig. 71b shows an interesting feature of the treatment at temperatures above T=225 ^oC: the curve for the virgin (indicated by the label "3" on the graph), which was located above the other two curves for T< 255 ^oC, is now located underneath them (note that the +100% disentangled pellet is designated as "1"). This apparent greater stiffeness of the disentangled melts at higher temperature is maintained all the way through cooling, resulting in a higher value for the $\%L/L_o$ at the end of the experiment (Fig. 71c). This result is intriguing in view of the fact that if the free volume was the only parameter modified by the treatment, a shift along the temperature axis would be expected, for all temperatures, hence the disentangled melt should be less stiff, not stiffer. Here, it appears that the free volume increase is just one of the several features altered by the disentanglement treatment, and that there is, in addition to it, an effect of modulus stiffening in the rubbery and rubbery flow region, in other words, the signs of a weaker but more stable network of entanglement. This is the same situation as in Fig. 70c for PC. However, in Figs. 72a and b, the effect of free volume increase superimposes on top of the phenomenon of sustained orientation and thus of extended stability of the network of entanglements. Thus the viscosity decrease can be accounted for by the decrease of T_g and the stability of the shift of time scale is maintained at high temperature because of the lock down between enthalpic and entropic contributions permitting the sustained orientation to occur.

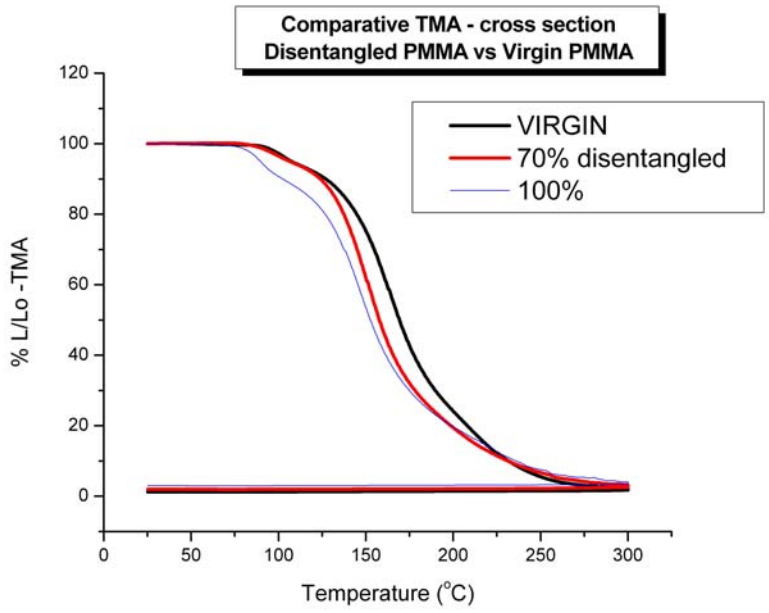

Fig. 71a

This is the same PMMA studied in Figs. 55-57 and Figs. 67a and b. The Virgin pellet is the curve on the top for T=175 ^{o}C, below it is the +70% disentangled pellet, and below it is the +100% disentangled pellet, showing a substantially lower T_g. These TMA curves correspond to cross-section cuts.

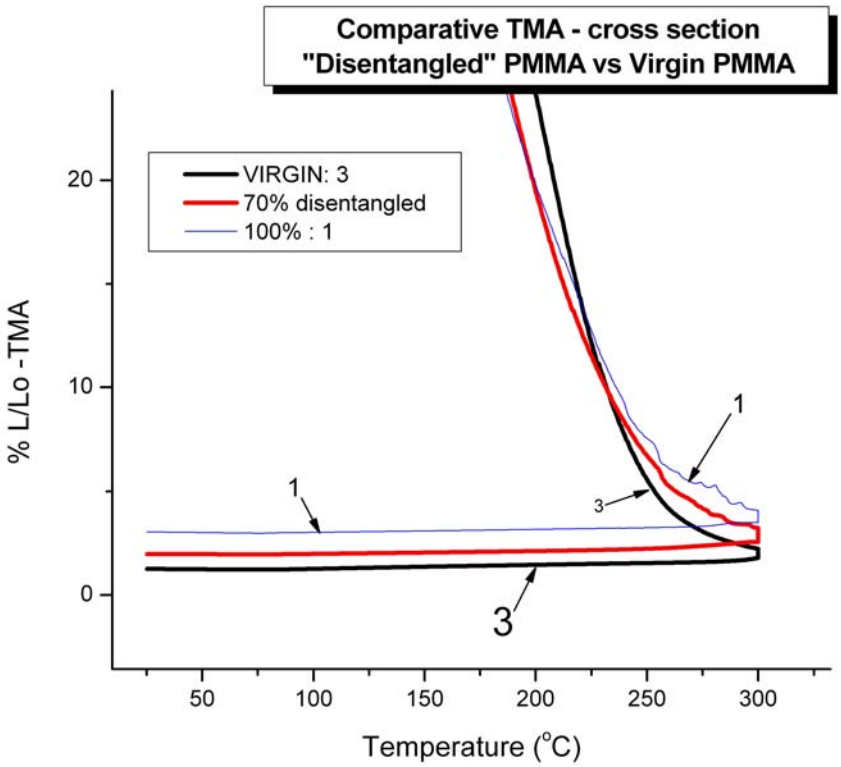

Fig. 71b

Detail of Fig. 71a focusing in the higher temperature region.

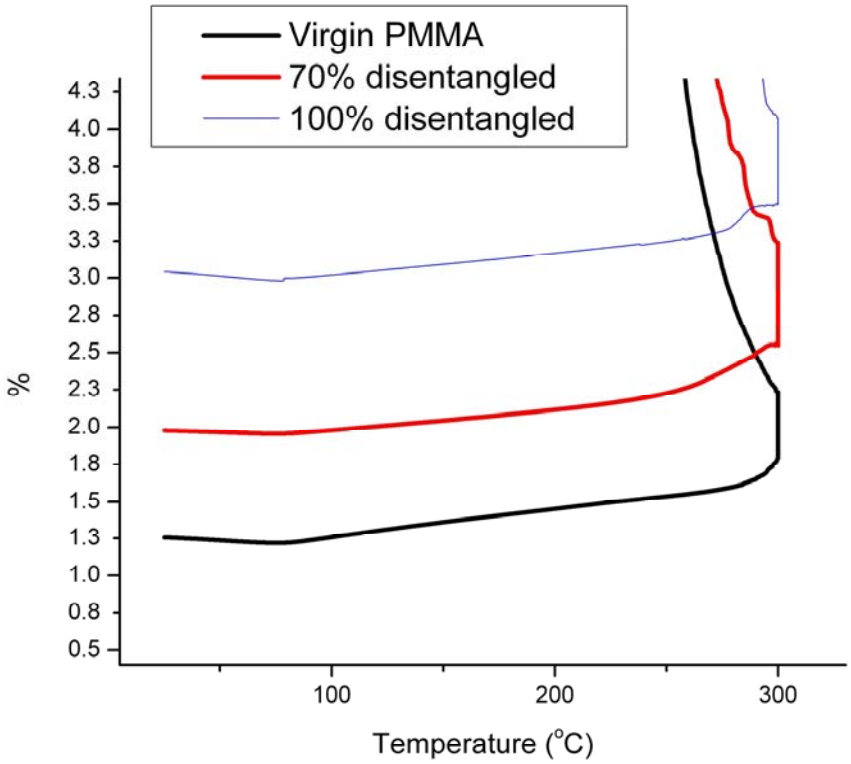

Fig. 71c

Detail of Fig. 71a in region 4 (cooling), showing the respective final level of % L/Lo present at the end of the heating-cooling cycle. The top curve corresponds to the +100% disentangled pellet, followed by the +70% disentangled pellet, the virgin pellet being the bottom one.

Figures 72a and 72b give the rate of change of the TMA signal as a function of temperature, obtained by differentiating the virgin and the +100% disentanglement curves in Fig. 71a. The study of the rate permits clarification of the respective role of free volume excess and of the increase of stability of the network of entanglement on the relaxation behavior. For the comparison we refer to the values given in the respective graphs which point to certain features of the relaxation process, such as the onset of the thickness decrease (associated with T_g) or the maximum of the rate, etc. The general features observed for both the virgin (Fig. 72a) and the disentangled (Fig. 72b) pellets are the presence of two peaks, one smaller at lower temperature, the other one of greater magnitude (their sign is negative because the thickness decreases), and of a plateau in the high temperature region of the melt before the rate goes to zero. These features are characteristics of how the changes due to processing affect the

relaxation due to the small force on the TMA probe. It is clear that the information in Figs. 72a and b are complementary to the rheological analyses of Figs. 55-56.

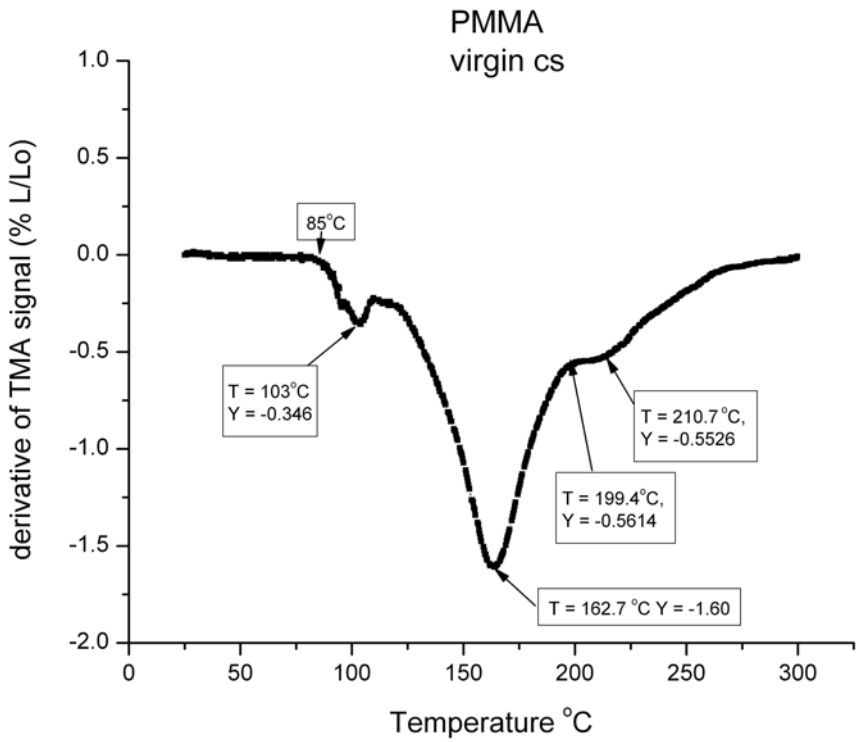

Fig. 72a
This graph corresponds to the rate of change of the TMA signal for the virgin pellet in Fig. 71a

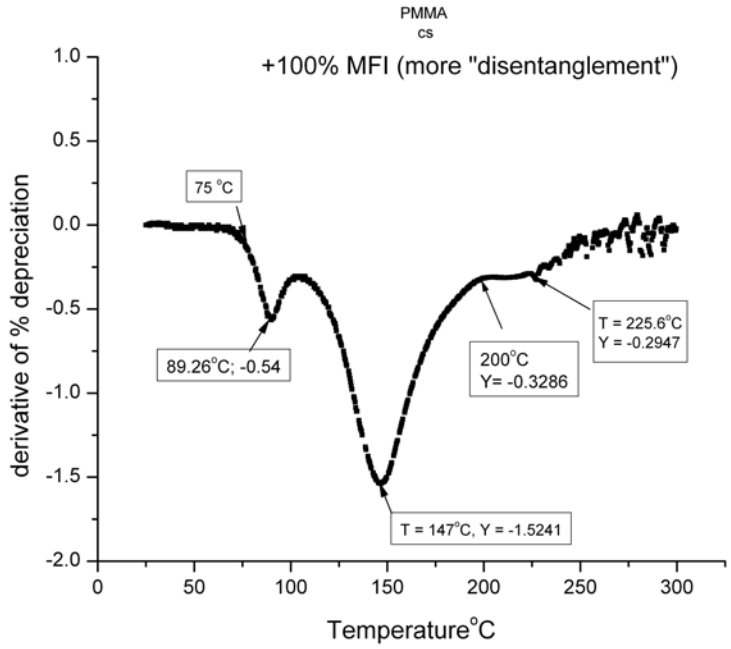

Fig. 72b
Rate of change of the TMA signal for the +100% disentangled pellet of Fig. 71a

A first observation is that the T_g onset, the temperature at the first minimum and the temperature at the second minimum are all shifted to lower temperature, by 10 ^oC, 14 ^oC, and 15.7 ^oC, respectively. This is the consequence of the free volume excess. The rate at the first minimum is 56% higher for the disentangled sample than for the reference (-0.54 vs -0.34), but is only 5% lower at the major peak (where the rate is maximum).

The second observation concerns the kinetics beyond the 2nd maximum, at T > 150 ^oC, comparing Figs. 72a and b. In this temperature range, the rate for the disentangled melt spreads towards the right, in a way which appears to slow down or even reverse the effect of the free volume (which shifts temperatures towards the left for the disentangled sample). This is quite visible when one looks at the temperature values for the "slow down" of the relaxation process, shown as a plateau in Figs. 72a and b. The onset of the plateau occurs at the same temperature of 200 ^oC for both the reference and the disentangled samples, although one would have expected a shift of -10 to -15 ^oC or so for the disentangled melt because of the free volume excess shifting T_g by this amount. Furthermore, one sees that the end of the slow down

occurs for a temperature 15 ^{o}C higher for the disentangled melt, 225.6 ^{o}C vs 210.7 ^{o}C. This is a +25 ^{o}C to +30 ^{o}C shift difference from the temperature value expected after the free volume excess is taken into consideration. The value of the rate at the plateau is -0.55 for the virgin and -0.31 (average) for the +100% disentangled sample. In other words, the melt remains stable for a longer time, to a higher temperature and varies at a slower rate for the disentangled pellet. This is quite a crucial observation which explains the stability of the disentangled network at high temperature. As we mentioned previously for Fig. 55, the viscosity frequency sweep of the disentangled PMMA melt took 24 hours at T=225 ^{o}C to recover its original shape (that of the reference).

The above result appeared as an extraordinary challenge to existing theories of molecular motions in polymer melts. The explanation of the results, we suggest, is related to a new understanding of the concept of entanglements of long chain molecules and of its impact on the mechanism of deformation in the rubbery and rubbery flow region. In this chapter we have shown that transients were triggered by the combination of strain rate and strain, whether it was in pure shear (rotational viscometry), in pure dynamic oscillatory shear, or in the combination of the two (Figs. 7a and b). Transient responses reveal how bond interactions evolve as a result of an imposed deformation. There are different mechanisms of response which are related to the initial state of interaction at the initiation of the deformation process. Depending on "the severity" of the deformation, i.e. on the magnitude of "the demands" (speed of deformation, magnitude of strain), chain segments are able to freely diffuse in 3 D (in the Newtonian region) or actively interactively cooperate to determine how many of them are stretched together as a strand unit, and for how long (before they relax by cooperative diffusion). When the deformation conditions have reached a level where all the strands are activated simultaneously (at the maximum of $(G'/G^*)^2$), then the network of entanglement starts to orient by a mechanism of cooperative interaction between enthalpic and entropic forces. This situation may result in the formation of **a** stable oriented network of activated strands and result in the long term viscosity retention behavior observed in this presentation. The anisotropicity of the network is probably linked to its stability, and vice-versa. Working in the proper range of frequency (or strain rate) and strain amplitude represents the first set of conditions specifically needed to create a new oriented network of entanglement, but the lock down of this entanglement network (resulting in the sustainability of orientation) is due to

another condition, only realized by the concomitant orientation of the laminar flow layers into a stratified structure where both entropic and enthalpic contributions "compensate". Both entropic (orientation) and enthalpic (changes of the conformation distribution along the chain) forces must influence one another to result in the lock-down of the entanglement structure. When this is realized, melts can behave rheologically in extraordinary new ways, and new applications can be derived, as further publications will reveal.

E SUMMARY

To summarize some of the findings and thoughts expressed in this chapter:

- Transients and steady states must be described by a unique theory of the deformation of interactive conformers. We suggest it is necessary to understand non-linear effects first and to have linear viscoelasticity derived by extrapolation to infinite time. In other words, time, frequency (or strain rate) and strain should be involved in the mathematical description of the deformation process (in the quantification of the moduli).
- A melt can be brought out of equilibrium with respect to its entanglement state. The return to equilibrium explains the transient properties. New entanglement states can be made quasi-stable, even at high temperature in the melt, by coupling entropic and enthalpic effects produced under specific conditions of melt processing.
- The currently accepted descriptions of rheology only apply to a stable entanglement state, which is not general enough. For instance, the WLF-Carreau equation of viscosity-strain rate does not correctly describe the rheology of an unstable entanglement network. The modelization of the influence of a network of entanglement on the melt deformation mechanism in terms of parameters introduced in linear viscoelasticity (τ, G_{oN}, M_e) provides the wrong answers when the entanglement network has become transient.
- The influence of strain on the rheological equations is currently not addressing the issue of its influence on the stability of the network of entanglement, and therefore is incomplete.
- The interpretation of the phase angle between stress and strain in terms of a dissipative and an elastic component represents an over-simplification of the mechanism of

deformation which, we believe, mischaracterizes the relative influence of a network of strands on the elasticity / relaxation process versus the influence of the local bond orientation (the conformer statistics). The difference between the two permits to define the amount of interactive coupling reorganization due to entropic vs enthalpic drives and under what conditions of strain rate and strain they occur. An entropic driven coupling mechanism of deformation can be viewed as an activation, then orientation process of the active network of strands. We have made the suggestion, in this presentation, that the active number of system strands (defining the EKNET network) is proportional to $(G'/G^*)^2$. In fact, the active number of strands is not exactly proportional to $(G'/G^*)^2$ but can be calculated from $(G''/G^*)^2$, and is almost exactly equal to $(G''/G^*)^2$ shifted by a constant when its value is approximately less than 80% of the maximum of $(G'/G^*)^2$ .The enthalpic contribution starts beyond that.point and corresponds to the orientation of the network. We suggest that only certain compensations of enthalpic and entropic contributions result in stable "sustained oriented entanglement states". This set of conditions would be the equivalent of "plastic yielding" and implies highly anisotropic samples.

- An increase or decrease of G* (t) and thus of viscosity can be produced when the network of strands is unchanged (Figs 1a to d) and local orientation/relaxation is responsible for the transient behavior, and the relaxation times relate to the properties of this network. In order to obtain a modification of the network, one needs to add energy to it until it yields. Strain rate or frequency are capable of reaching that point for any strain % deformation, but the value of the strain % allows to decrease the frequency or strain rate at which the network starts to deform.

F CONCLUSION

The deformation of a polymer melt in shear mode is the main subject of interest in the science of rheology of such materials. It is a crucial topic for successfully processing these materials. As illustrated in part I of this series [2] and in the above examples, it is a complex and rich subject which is far from being fully understood. In part I of this series [2], we

suggested that even the linear visco-elastic behavior of polymer melts (at low strain rate and low strain) was not satisfactorily described by the accepted theoretical models, when carefully comparing experiments and theoretical predictions. In the non-linear range, at high strain rate and strain, the subject of this part II, it is generally admitted that the current theoretical developments that successfully predict the main characteristics of polymer melts in the linear range come short but merely need improvements. The improvements proposed generally consist in tweaking certain assumptions of the linear viscoelastic model to be able to extrapolate to the non-linear behavior. There is no current theoretical challenge to the dominant reptation model of melt deformation in polymer physics. The aura this model has reached among polymer scientists makes it more difficult to search for other explanations for visco-elasticity and rubber elasticity. Yet, as we suggest, it is possible that the experiments described in this work challenge the reptation school to its limits, to the edge of usefulness. As already concluded in the previous chapters of this dissertation dedicated to flow, the theory seems to be fine in the linear range in ***appearance*** only. The "devil is in the details" says the old saying. The present understanding of the physics of macromolecules is based on an analysis of the properties of a single chain. The presence of the other chains is perceived as a mean field influence on the properties of that chain. The reptation school considers that this mean-field can be described as a topology, an homogeneous field of obstacles restricting the motion of the single chain and explaining the molecular weight dependence of viscosity. The mobility is constrained within an imaginary tube and the chain "reptates" within that tube. The shortcomings of the predictions of that model made the initial static tube evolve into a more dynamic tube, capable of evolution, in time and as a consequence of the various modes of deformation of the melt. The tube was therefore thought to have a stability of its own, it could fluctuate in length, and, to address some of the non-linear issues, it could get thinner and elongate in length. In other words, the tube itself had evolved into a "super macromolecule" capable of deformation very similar to what early polymer scientists would assign to macromolecular chains themselves. Perhaps, at the horizon of the reptation school, also lies the concept of entanglement of the tubes themselves!. We are not suggesting this idea totally ironically, because it illustrates another concept that we will develop in a follow up publication, that of the need to not only define the scale of the basic unit that participates in the deformation process, but also to determine the link and the modulation between cooperative

scales. In explaining several figures of this chapter, we made reference to a "network of strands" to describe the cooperative interactive process resulting from the macroscopic deformation. We obviously referred to a basic unit of deformation that involved the cooperative motion of a group of bonds responding as a set [87]. We must define what cooperation means, how many bonds cooperate in an active strand and where they are located, on a single chain or on several chains?. The physics of dealing with all the chains at once is the model that we have adopted to describe the deformation of polymer melts and solids, above T_g and below T_g, [72, 87]. The theory not only addresses the interaction between the conformers of a single chain to assume the shape of a macro-coil (which can be deformed), but also defines why entangled macro-coils exhibit the response of a network of active strands when all the chains participate cooperatively in the deformation process. The link between the deformation of a conformer, of a macro-coil and of a network of strands must be fully described

To be useful the new model should understand the influence of chain molecular weight to predict a change of behavior below and above a critical molecular weight, in other words the characteristics of "entanglements" and their influence on the dynamic melt properties G'(ω,T) and G"(ω,T). It must predict shear-thinning and strain-softening in shear mode, and strain-hardening in extensional mode. It should also successfully describe the transitional behavior at T_g, from a solid-like to a liquid-like behavior. Additionally, it must find a reason for the existence of "thermal-thinning" at a temperature below the Boyer's $T_{l,l}$. Finally, the theory should describe the stability of entanglements. We propose to address these issues in the next chapter, chapter 5, and in future publications such a model of macromolecular interactions [88].

G REFERENCES (CHAPTER 4)

[1] H. Staudinger, "Makromoleculare Chemie und Biologie", Bale, Wepf & Co, 1947].

[2] J.P. Ibar, "The Great Myths of Rheology", Part I, J.Macrom. Sci. Phys. (2009)

[3] J.D. Ferry, "*Viscoelastic Properties of Polymers*", J. Wiley (1970), Ch.1.

[4] T. Alfrey, Jr, in "*Mechanical Behavior of High Polymers*", Interscience Publishers, Inc, John Wiley, New York (1965).pp 103-220.

[5] C. W. Macosko, "*Rheology Principles, Measurements, and Applications*", John Wiley (1994), in Chapter 4 (by R.G. Larson, "Non-Linear Viscoelasticity").

[6] D. G. Legrand and J.T. Bendler, "*Handbook of Polycarbonate Science and Technology*", Marcel Dekker , Inc (2000).

[7] S.Q. Wang, " Macromol. Mater. Eng. 2007,292, 15-22 "*A Coherent Description of Nonlinear Flow Behavior of Entangled Polymers as Related to Processing and Numerical Simulations.*

[8] S-Q Wang et al, « *Nonquiescent Relaxation in Entangled Polymer Liquids after Step Shear* », Physical Review Letters, 97, 187801 (2006).

[9] P. Tapadia and S.Q. Wang, "*Direct visualization of continuous simple shear in non-Newtonian polymeric fluids*", Phys. Rev. Lett., 96, 016001 (2006).

[10] Y. Wang, S-Q Wang, P. Boukany, and X. Wang, "*Elastic breakup in uniaxial extension of entangled polymer melts*", (received by Phys. Rev. Lett.17th January 2007).

[11] K. Osaki, M. Tamura, M. Kurata, T. Kotaka, "*Complex Modulus of Concentrated Polymer Solutions in Steady Shear*", J. of Phys. Chem., 69(12), 4183 (1965)].

[12] J.P. Ibar, ANTEC Proceeding, paper 481 (2001) " *Extrusion of Polymer Melts under Intensive Shear-Thinning Inducing Lower Pressure and Temperature Requirements".*

[13] J.P. Ibar, Proceedings European Society of Rheology ESR, Grenoble (2005). "*Control of Pseudo-Plasticity of Polymer Melts by Disentanglement Methods*". Also:J.P Ibar, ANTEC Proceedings, paper 10370 (2005) "*Control of Thixotropicity of Polymer Melts by Disentanglement Processing*".

[14] J.P. Ibar, US2005/0267289A1 (2005) "*Process for the Control of Flow Properties of Polymers".*
[15] J.P. Ibar, US Patent 6,210,030. (2001). "*Method and Apparatus to control Viscosity of Molten Plastics prior to a Molding Operation*".

[16] J.P. Ibar US Patent 5,885,495.(1999). "*Viscosity Control for Molten Plastics Prior to Molding".*

[17] F.N. Cogswell, in "*Polymer Melt Rheology, a Guide for Industrial Practice*", Woodhead Publishing Ltd (1997), p. 57.

[18] J.P. Ibar, ANTEC Proceedings, paper 1071 (2004), "*Flow Simulation for Polymer Melt under Disentanglement Conditions*".

[19] J.M. McKelvey, "*Polymer Processing*", John Wiley, New York (1962), Ch.3
[20] S. Matsuoka, "*Relaxation Phenomena in Polymers*", Hanser (1992), p. 176. Also see the graph at p. 177.

[21] J.P. Ibar, J.P. et al, Bulletin of the American Physical Society, 42(1), 283 (1997). "*Viewing Entanglements as a Blended Phase in Polycarbonate".*

[22] J.P Ibar, ANTEC Proceedings, paper 225 (1999),"*Viewing Entanglements as a two-phase system in Polymeric Materials*"

[23] J.P. 22. Ibar, Proceedings of the Society of Rheology SOR 77th meeting Van Couver, Canada, paper PO59 (2005). "*Are Entanglements Stable? For How Long? What Entanglements are we Talking about?*".

[24] J.P. Ibar , Proceedings of the Society of Rheology SOR 77th meeting Van Couver, Canada, paper SM32 (2005). "*Non-Equilibrium Entanglement States for Polymer Melts*"

[25] M. Doi, and S.F. Edwards, "*The Theory of Polymer Dynamics*", Clarendon Press, Oxford (1986).

[26] D. Venerus, J. Rheol. **49**, 277 (2005)].

[27] M.H. Wagner, Rheol. Acta, 15, 136 (1976)].

[28] D.E. Hanson, Polym. Eng. & Sci., **9**, (6), 405-414 (1969) "*Shear Modification of Polyethylene*",

[29] M. Rokudai, J. Appl. Polym. Sci., 23(2), 463-471 (1979) "*Influence of shearing history on the rheological properties and processability of branched polymers*". Also
M. Rokudai, S. Mihara, and T. Fujiki., *J.Appl. Polym. Sci*., 23:3289, 1979, "*Influence of shearing history on the rheological properties and processability of branched polymers*."

[30] B. Maxwell, "*Controlled Shear Modification of Low Density Polyethylene*", paper presented at the 50th Anniversary Conference of the Society of Rheology, Boston (1979)].

[31] J.F. Agassant, P. Avenas, J-P. Sergent, B. Vergnes, and M. Vincent. *La mise en forme des matières plastique*s. Lavoisier Tec et Doc, 1996.

[32] H. P. Schreiber. *Polym. Eng. Sci*., pages 317–323, October 1966, "*Cause and effect in time dependent flow of thermoplastics melts -a review".*

[32bis] M. Gahleitner. *Prog. Polym. Sci*., pages 895–944, 2001, "*.Melt rheology of polyolefins".*

[33] G. Ritzau. Shear modification of polyolefins and its integration on polymer processing. *Int.Polymer Process*., 1(4):188–197, 1987.

[34] G. Ritzau, A. Ram, and L. Izrailov. Effect of shear modification on the rheological behaviour of two LDPE grades. *Polym. Eng. Sci*., 29(4):214, 1989.

[35] P. J. R. Leblans and C. Bastiaansen, *Macromolecule*s, 22(8):3312–3317, 1989. "*Shear modification of low density polyethylene: its origin and its effect on the basic rheological functions of the melt*".

[36] M. Van Prooyen, T. Bremner, and A. Rudin. Polym. Eng. Sci, 34(7):570–579, mid-April 1994."*Mechanism of shear modification of low density polyethylene".*

[37] H. Münstedt. *Colloid Polim. Sci*., 259:966–972, 1981, "*The influence of various deformation histories on elongational properties of LDPE*"..

[38] A. Ram and L. Izailov. *J. Appl. Polym. Sci*., 31:85–100, 1986. « *Shear modification of polyethylene".*

[39] S. Bourrigaud, "*Etude de la modification des propriétés rhéologiques induite par l'écoulement : application à l'extrusion-couchage* », Ph-D, Universite de Pau (2004).

[40] S. Berger,"Einfluss der Mechanischen Vorgeschichte aud das rheologische Verhalten von Langkettenierzweigtem Polypropylen", Ph_D Thesis, University of Erlanden (2005).

[41] S. Bourrigaud, G. Marin and A. Poitou, Macromolecules ,36, 1388-1394 (2003), "*Shear-Modification of Long-Chain branched Polymers: A Theoretical Approach using the Pom-Pom Model"*.

[42] J. Stange, S.Berger and H. Munsted, ESR AERC Grenoble (2005), " *Influence of flow history in the rheological properties of a long-chain branched Polypropylene*"

[43] J.P Ibar et al, 42(1), 106 (1997). Bulletin of the American Physical Society, "*Methods to Alter Entanglements prior to Processing*."

[44] J.P Ibar, ANTEC Proceedings, paper 226 (1999). "*Control of Viscosity of Polymer Melts Prior to Molding by Disentanglement Methods*"

[45] J.P. Ibar, ANTEC Proceedings, paper 480 (2001). "*Time Dependence of Shear-Thinning of Polymer Melts"*.

[46] J.P Ibar, ANTEC Proceedings, paper 482 (2001). *"Reduction of Viscosity of Polymer Melt by Shear-Thinning and Disentanglement: Rheological Criteria and Commercial Perspectives"*.

[46]. J.P. Ibar and S.Morneau, ANTEC Proceedings, paper 818 (2003), "*Characterization of Polymer Resins Produced by Melt Disentanglement"*.

[47] J.P Ibar, ANTEC Proceedings, paper 579 (2004). "*Disentanglement of Polymer Melts"*.

[48]. J.P Ibar, Proceedings of APS Division of Polymer Physics, N29-010, Abstract 22112, Montreal, March 22-26 (2004). "*Disentanglement of Polymer Melt to Produce Lower Viscosity Melts and Higher MFI for their Pellets upon Subsequent Processing*".

[49] J.P Ibar, Proceedings of APS Division of Polymer Physics, N29-017, Abstract 218110, Montreal, March 22-26 (2004). "*Disentanglement of Polymer Melts Using a Lab Dynamic Rheometer"*.

[50] J.P Ibar, Proceedings European Society of Rheology ESR, Grenoble (2005). "*Characterization of Polymer Resins Produced by Melt Disentanglement"*.

[51] J.P Ibar, Proceedings European Society of Rheology ESR, Grenoble (2005). *"Time Dependence of Viscosity of Polymer Melts"*.

[52] J.P Ibar, T Hicks. and S Morneau., Proceedings SPE, paper 101117 (2005). "*PET/PC, PC/PC Properties from Disentanglement Processing*".

[53] J.P Ibar, T Hicks., S. Morneau and R.Amba, Proceedings SPE, paper 101385 (2005). "*Flow and Mechanical Performance of Disentangled Polypropylene*".

[54] J.P. Ibar, ANTEC Proceedings, paper 101381 (2005), "*PC Flow and Mechanical Performance from Disentanglement Processing*".

[55] P.G. de Gennes, J.Chem. Phys., 55, 572 (1971), « Reptation of a Polymer Chain in the Presence of Fixed Obstacles ».

[56] P.G. de Gennes, *Scaling Concept in Polymer Physics*; Cornell University, Ithaca and London (1979).

[57] G. Marrucci and G. Iannruberto, Maromolecules, 36, 3934 (2004).

[58] M.H. Wagner, J. Rheol., 45, 1387 (2001).

[59] T.C. McLeish and R.G. Larson, J.Rheol., 42, 81 (1998).

[60} C. Friedrich, K. Mattes, D. Schulze, MACROIUPAC 2004, Paris, France "*Non-Linear Viscoelastic Properties of Polymer Melts as Analysed by LAOS-FT Experiments").*

[61] K.M. Mattes, R. Vogt, C. Friedrich, Rheol. Acta, 47, 929(2008) "*Analysis of the edge fracture process in oscillation for Polystyrene melts"*.

[62] G.H. McKinley, J.A. Byars, R.A. Brown, R.C. Amstrong, J. Non-Newton Fluid Mech., 40,201 (1991) "*Observations on the elastic instability in cone-and-plate and parallel plate flows of a polybutadiene Boger fluid*."

[63] A. Oztekin, R.A. Brown, G.H. Mckinley, J. Non-Newton Fluid Mech., 54, 351 (1994) " *Quantitative Prediction of the Viscoelastic Instability in Cone-and-plate flow of Boger fluid using a multi-mode Giiesekus model*".

[64] J.A. Byars, A. Oztekin, R.A. Brown, G.H. McKinley, J. Fluid Mech., 271, 173 (1994), "*Spiral instabilities in the flow of highly elastic fluids between rotating parallel disks"*

[65] R.G. Larson, ,Rheol. Acta, 31, 213 (1992), "*Instabilities in viscoelastic flow*"].
[66] J.P. Ibar, Bulletin of the American Physical Society, 42(1), 283 (1997), "*Manipulation of Dynamic Entanglements during Processing. A new Understanding of Shear-Thinning*".

[67] J.P. Ibar, Proceedings of the Society of Rheology, 78th meeting in Portland, Maine (2006), "*Effect of strain % on the viscosity-Frequency Curve of Polymeric Melts*".

[68] C. Freidrich, personal communication (2009).
[69] H. Oser and R.S Marvin, J. Res. Nat. Bur. Standards, 67B, 87 (1963).
[70 J.P. Ibar, ANTEC SPE Proceedings, paper 224 (1999),"*A New Formulation and Interpretation of Shear-Thinning of Polymeric Melts. Effect of Temperature, Strain Rate and Frequency*".

[71] A.J. Kovacs, J.J. Aklonis, J.M. Hutchinson, A.R. Ramos, J. Polym. Sci. Polyme. Phys. Ed., 17, 1097 (1979).

[72] J.P. Ibar, "*Do We Need a New Theory in Polymer Physics?"* J.M.S-Rev. Macromol. Chem. Phys., C37(3), 389-458 (1997),

[73] J.P. Ibar, *"Effect of Temperature Modulation during Time Sweeps"* in the International Rheology meeting proceedings, Monterey, USA (August 2008).

[74] G.V. Vinogradov et al, Akad. Nauk.154, 1421 (1964).

[75] D.W. Van Krevelen,"*Properties of Polymers*", Elsevier (1972).

[76] M. Keentok and S-C Xue, Rheologica Acta, Vol. 38, 4, 321-348 (1999) "*Edge fracture in cone-plate and parallel plate flows*",.

[77] J.-M. Gonnet, J. Guillet, I. Sirakov, R. Fulchiron and G. Seytre, J. Rheol. 47(3), 631 (2003). "*Simultaneous dielectric and dynamic mechanical measurements on PVDF in the molten state: study of the linear/non linear viscoelastic transition*"

[78] L.A. Archer in "*Polymer Processing Instabilities. Control and Understanding*" book edited by S.G. Hatzikiriekos and K.B. Higler, Marcel Dekker (2005), Ch. 4

[79] M.T. Shaw and W.J. MacKnight in "*Introduction to Polymer Viscoelasticity*", Third Edition, Wiley-Interscience (2005), p. 136, Eq. 5-8.

[80] S-Q Wang, Adv. Polym. Sci,138, 227-275 (1999) "*Molecular Transitions and dynamics at polymer/wall interfaces: origins of flow instabilities and wall slip*"

[81] V.R. Mhetar and L.A. Archer, Macromolecules,31,8617-8622 (1998),"*Slip in entangled polymer melts. 2. Effect of surface treatment.*"

[82] J.P. Ibar, US patent 2005/ 0182229 A1. "*Process for Incorporating Substances into Polymeric Materials in a Controllable Manner*".

[83] Prevorsek, D. C. and De Bona, B. T. Journal of Macromolecular Science, Part B, 19:4, 605 – 622 (1981) *'On chain entanglement in high-Tg amorphous polymers'*,

[84] S. Rastogi, L. Kurelec, J. Cuijpers, D. Lippits, M. Wimmer, and P. J. Lemstra, Macromolecular Materials and Engineering, Volume 288 Issue 12, Pages 964 – 970 (2003), "*Disentangled State in Polymer Melts; a Route to Ultimate Physical and Mechanical Properties"*.

[85] A. V. Pandey and S. Rastogi, "*Role of entanglements on the flow behaviour of polyolefins*", research announcement, Loughborough University. Project Duration: Dec2007- Dec2010.

[86] Saeid Talebi, Ph-D thesis Eindhoven University of Technology (2008),"*Disentangled Polyethylene with Sharp Molar Mass Distribution; Implications for Sintering*", ISBN: 978-90-386-1477-9.

[87] J.P. Ibar in "Order in the Amorphous "State" of Polymers", Edited by S. E. Kenath, R. L. Miller and J. J. Rieke, Plenum Press, New York-London (1987).

[88] J.P. Ibar "Grain-Field Statistics Applied to Polymers", book in preparation.

Chapter 5

THE GREAT MYTHS OF POLYMER RHEOLOGY, PART 3: ELASTICITY OF THE NETWORK OF ENTANGLEMENTS

Introduction Background

The mathematical treatment serves as a way to support the concepts, but the reverse is also true, the concepts of dual-phase naturally led to the search for these mathematical tools. Thus, the concepts are introduced early on, in a qualitative and intuitive way, and refined as the results emerge giving support or challenging the initial ideas. For instance, thermal diffusion in polymer melts is imaged, in our views, by a continuous coherent sweeping motion of "the phase-lines", defining the boundaries between the dual phases, organized as a continuous network. These phase-lines are constantly in motion, with natural frequency ω'_o, to insure melt isotropicity and homogeneity despite the free volume difference between the dual-phases. At one stage of melt deformation, the orientation of the phase-lines occurs and creates anisotropicity which is compensated, at least partially, by an increase of the sweeping wave frequency to maintain the homogeneity of the cohesion between the interactive bonds. We describe this mechanism (and other competing ones) mathematically in this article.

We consider a new parameter, $\omega_R = \omega /(G'/G^*)^2$, where ω is the radial frequency, G' is the elastic modulus and G* the amplitude of the complex modulus and study how it correlates to viscosity, suggesting that shear-thinning can be simply expressed in terms of ω and $(G'/G^*)^2$. We show that $(G'/G^*)^2$ can be split into two terms, κ_1 and κ_2 , i.e. $(G'/G^*)^2 = \kappa_1 + \kappa_2$, the variation of κ_1 and κ_2 with ω and temperature being fundamentally related to the mechanisms of deformation of the network of interactions (inter-and intra-molecular in nature, working coherently and defining the viscous cohesion). We show that the κ_2 term is related to the energy stored by the network of activated phase-lines ("entanglements") which may lead to its entropic modification (orientation) resulting in a further increase of the sweep wave frequency, so κ_2 is a characteristic of the deformation mechanism occurring in the "strand-channel-phase" of the two dual-phases. By contrast, we show that the κ_1 term is related to the core-phase, the other dual-phase, which participates in the response to deformation by way of compensation with κ_2, either

by diffusion (at low strain) or by a stretch-relax mechanism (at higher strain) similar to what is observed for the κ_2-phase when shear-thinning is active.

We define ω' as the dynamic frequency of the entanglement network, $\omega' = \omega/\kappa_2$, and show that ω' correlates simply with the total stress generated by the flow mechanism in the shear-thinning regime at low strain. At vanishing ω, ω' converges to a finite value, ω'_o, that we associate, as already said, with the fundamental static diffusion of the network of entanglements, i.e. with the natural sweeping wave frequency of the entanglement phase to interpenetrate the core phase, delimiting the contours of the boundaries between the dual-phases. We correlate ω'_o with the onset of non-Newtonian viscous flow behavior. Subtle differences of the variation of κ_1 and κ_2 emerge for various thermo-mechanical treatments of the melt or by varying temperature or the magnitude of the strain applied.

The analysis of the split of $(G'/G^*)^2$ into κ_1 and κ_2 suggests to assign a physical dynamic attribute to the elastic entanglement network, whose deformation occurs by an activated mechanism of stretch-relax, and the need to characterize its stability under stress. We also define the elastic cohesive energy of the dynamic network, $\Delta_{\omega,\gamma}$, which varies with both frequency, ω, and strain, γ, since it directly correlates with the number of activated strands of the dynamic network, κ_2 . We study the influence of the T_α transition, the mechanical manifestation of T_g, which varies with ω and γ ,and which we write $T_g(\omega,\gamma)$, on the visco-elastic behavior, showing that it plays a significant role in the mechanism of shear-thinning and strain softening, and propose a way to evaluate its impact on κ_1 and κ_2. Multiple examples are given comparing κ_1 and κ_2 for linear low density polyethylene (LLDPE), polymethylmethacrylate (PMMA), Polycarbonate (PC), Polystyrene (PS), polyethylene terephtalate glycol (PETG) and polypropylene (PP) melts. The influence of temperature on the elasticity of the dynamic network of entanglements suggests a change of the characteristics of the elastic network in the melt above T_g, an observation already foreseen in a previous communication [1].

The effect of strain is an important section of this paper. We show that the essential role of strain is to activate the κ_1-phase to participate *actively* (by shear-thinning) in the deformation process. In linear viscoelastic conditions, the conformers[1] in the κ_1 dual-phase do not deform, their motion is through diffusional reorganization, i.e. delocalization in the structure triggered by

[1] Conformers are defined in refs. 33-35. Also see Fig. 12a.

the stretch-relax deformation mechanism (shear-thinning) of the κ_2-phase conformers. When the κ_1-phase is activated by an increase of the strain, strain softening occurs. In the discussion, we present a new understanding of "the network of entanglement" and show how its orientation and gradual instability gives rise to the mechanisms of deformation observed from very low ω to high ω, at various strains. We suggest that the network character of deformation is not due to topological considerations but, instead, due to the cooperative coupling nature of the interactions between the macromolecules conformers which organize according to a *Dual-Grain Field-Statistics*. In this model, the duality aspect comes twice: it comes at the local level of interactions between the conformers, and this duality is dealt with by the introduction of the Grain-Field Statistics applicable to macro-coil systems. The equations of the Grain-Field Statistics predict the dynamic aspect of the interactions between conformers. But the interaction between macro-coils introduces a second level of duality, above a certain size for the macro-coils (which we consider to be the onset of entanglements), responsible for the molecular characteristics of the dynamic network.

In summary, we introduce in this article new methods of analysis of the rheological results which appear to confirm an essential aspect of the cohesion of the interactions between the conformers and the existence of the "entanglements", the existence of a Dual-Phase structure. The question of the stability of the network of interactions, which was an essential focus of experimental investigation in part II of this series [2] is reviewed here in terms of the Dual-Phase model.

INTRODUCTION

The viscosity of polymers is key to their behavior in the molten state and thus to their processing. Viscosity is a scalar equal to the stress divided by the strain rate, which, in the case of a dynamic deformation, can be rewritten as:

$$\eta^* = \frac{\tau}{\dot{\gamma}} = \frac{G^*.\gamma}{\omega.\gamma} = \frac{G^*}{\omega} \qquad (1)$$

where η^* is the dynamic viscosity, τ is the shear stress, and $\dot{\gamma}$ is the strain rate, the other parameters having been defined above. The viscosity is known to remain constant at low strain rate of flow, in the so called Newtonian region, and its value is the "Newtonian viscosity", η_o. Polymer melts are not as simple as Newtonian fluids, and, as the strain rate increases, the viscosity becomes strain rate dependent, a phenomenon described as "shear-thinning" if the viscosity decreases with increasing shear rate. It is important to realize that the stress continues to grow with strain rate, as shear-thinning occurs, it is simply not growing as fast as it would if the Newtonian stress still applied (in the Newtonian regime of deformation, stress is proportional to the shear rate).

The phenomenon of shear-thinning of polymeric melts has been analyzed and mathematically modeled "satisfactorily" for more than 60 years [1]. The power law equation was one of the first equations used to quantify the strain rate dependence of viscosity, and applies well, at high strain rate, over a short range of strain rate. The power law is useful when modeling flow in complex geometry at the strain rate usually applied in industrial processes. The power law equation is not applicable at low strain rate: it predicts much higher values for the viscosity than what is observed at low strain rate, and does not provide the Newtonian value. Shear-thinning is classically described by another equation, the Cross-Carreau equation, also called the Carreau-Yasuda equation, that has the advantage to converge to the power law formula at high strain rate, and to predict the Newtonian viscosity value at low strain rate. Critical issues related to the validity of the Cross-Carreau's formula are not discussed in this paper; they were presented in part I of this series [**1**].

The Cross-Carreau equation can be written as:

$$\eta = b_1.(1+ (b_2. \omega)^{b3})^{(n-1)/b3} \quad (2)$$

where b_1, b_2, b_3 and n are all curve-fitting constants. n is between 0 and 1, b_1 is the value for $\omega=0$, so it is the Newtonian viscosity η_o. For large ω, Eq. (2) simplifies to a power law, since the second term inside the parenthesis becomes much larger than 1:

(3) $$\eta = \eta_o \, (b_2 . \, \omega)^{(n-1)}$$

On a log-log plot of η vs ω , a straight line with slope (n-1) is observed for Eq. (3). Although Eq. (2) has been verified with great accuracy for many un-branched polymers, b_3 and n are often found to vary with temperature, even though slightly, and thus are not true constants. Another problem is the multiplicity of solutions found for the constants b_1, b_2, b_3 and n by regression, all providing an apparent excellent fit. Besides, for dynamic data which only vary over a small ω range (typically from 0.1 to 300 rad/s at low strain amplitude, ~2%), one needs to assume rheological simplicity for the melt to extend the ω range to larger spans by use of the frequency-temperature superposition principle. We showed in Chapter 3 that true superposition was not verified in most cases, even in those cases with "apparent" good curve overlap.

As explained in Chapter 3 and also in part I of this series [1], our interest in using (G'/G*) to analyze dynamic data originated from our review of the claims of the time-temperature superposition temperature. In order to avoid addressing the need, while performing superposition of the viscosity-ω curves, to know the melt density ρ, which enters the expression of the vertical shift factor, one can introduce the ratio of two moduli, say (G'/G*), which cancels out the correction for density and absolute temperature. The vertical shifting is thus eliminated. Furthermore, plots of $(G'/G^*)^2$ versus log ω seemed even more appropriate when such horizontal shifting was performed, because of the interest brought to the special case $(G'/G^*)^2 = 0.5$ corresponding to the "cross-over point" $G'_x = G''_x$, often considered as an important characteristic of the molecular weight of the chains. Figure 1 displays such a plot for PS data.

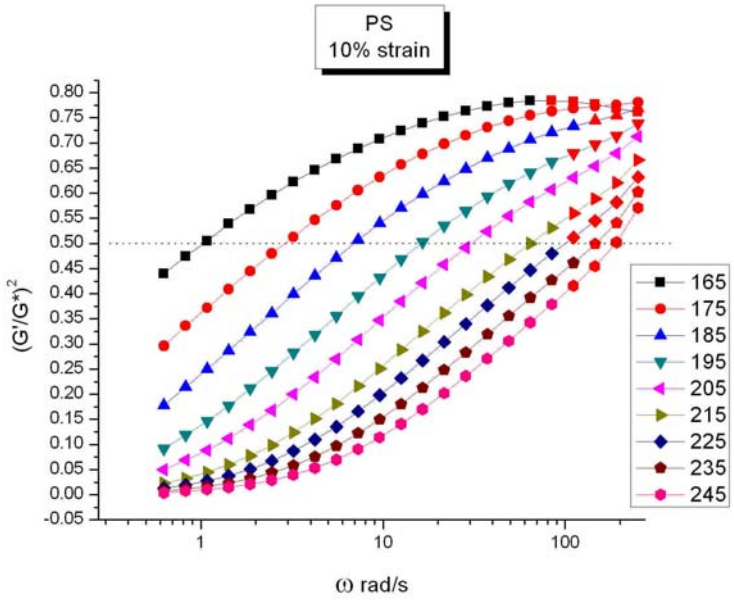

Fig. 1

$(G'/G^*)^2$ vs ω for Polystyrene at 10% strain for T 165 to 245 °C

This failure of the time-temperature principle drove our interest over the last few years to analyze, in detail, plots of $(G'/G^*)^2$ vs log(ω) and, as this chapter will show, more specifically plots of $(G'/G^*)^2$ vs G*. The latter pair of variables was found in part II of this series [2] to be most appropriate to characterize melts "treated"[2] to exhibit various states of disentanglement or re-entanglement. Related plots are shown in Figs 2a-d for PC.

In Figs 2a and b, a treated melt ("treatment$_1$", squares) is compared with a virgin melt (circles), and, similarly, a different disentanglement treatment ("treatment$_2$") provides the comparative plots found in Figs 2c and d. It is remarkable that the respective position of the treated melt with respect to the reference melt, on a plot of $(G'/G^*)^2$ vs G*, produces a corresponding viscosity curve, log(η∗(ω) vs log(ω), located either above (treatment$_1$) or below (treatment$_2$) the reference curve

[2] The treatment was mechanically done, mostly consisting of the superposition of pressure flow and cross-lateral drag flow (combining rotational and vibrational shear).

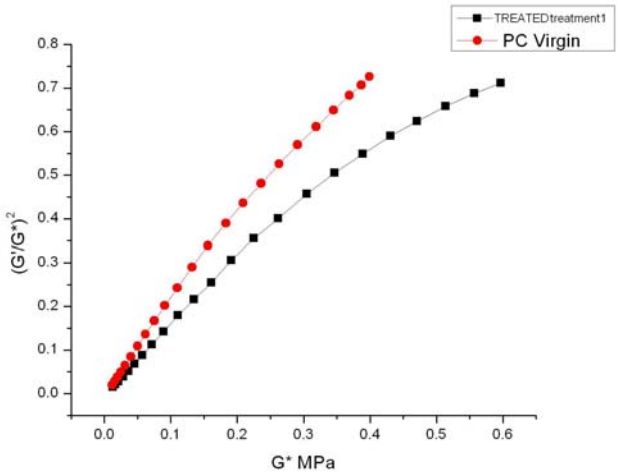

Fig 2a
$(G'/G^*)^2$ vs G* for Virgin and treated Polycarbonate ($treatment_1$).

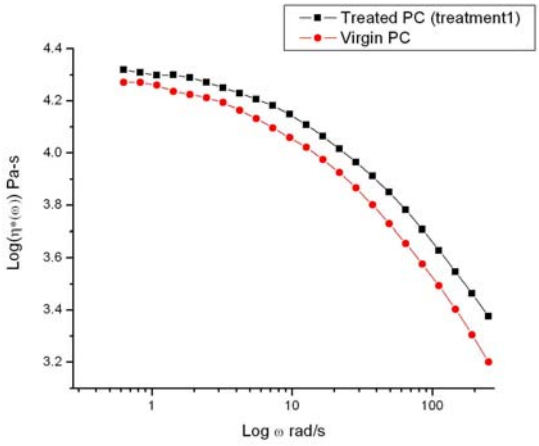

Fig. 2b
log(η∗(ω)) vs Log(ω) for Virgin and treated PC ($treatment_1$)

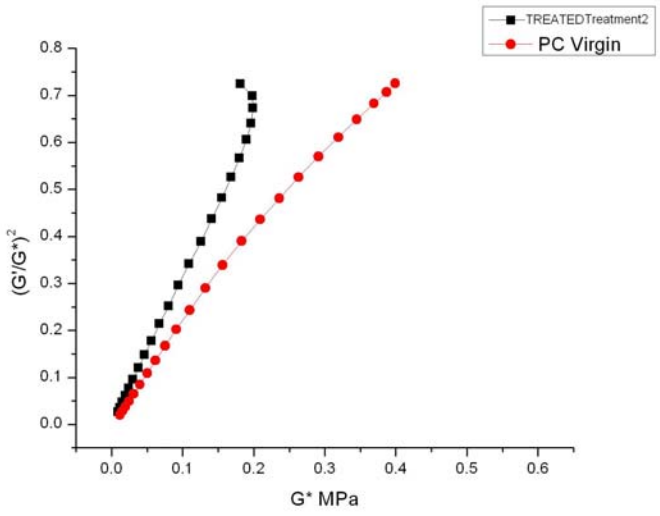

Fig 2c
$(G'/G^*)^2$ vs G* for Virgin and treated Polycarbonate ($treatment_2$).

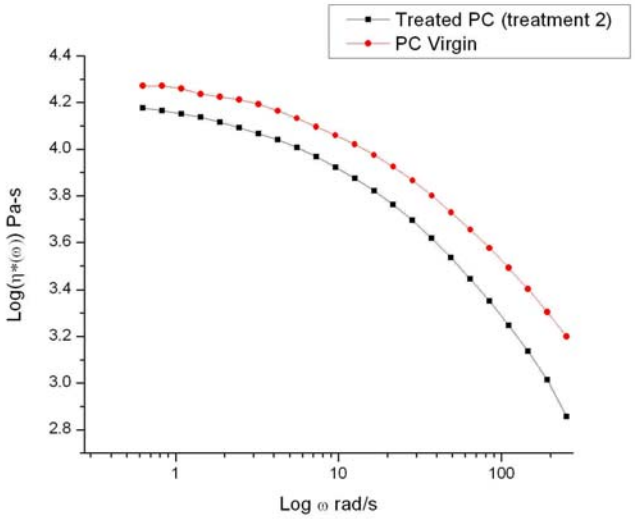

Fig 2d
log(η∗(ω)) vs Log(ω) for Virgin and treated PC ($treatment_2$)

In Fig. 2a, the treatment$_1$ curve is below the reference, and, correspondingly, in Fig. 2b, the viscosity of treatment$_1$ melt is located above the reference; an increase of G', at $(G'/G^*)^2$ constant, corresponds to a higher viscosity melt. This treatment corresponded to a "boosted entangled" melt, as if entanglement had been increased. Similarly, but reversing the role of the treated and reference samples, Figs. 2c and d demonstrate the case of a "disentangled melt", obtained by treatment$_2$, which displays a lower viscosity at all ω (Fig. 2d), while the $(G'/G^*)^2$ vs G* curve is located above the reference curve for this treated melt (Fig 2c). Also notice in Fig. 2c the backturn at high G* for the treated melt (squares), corresponding to a decrease of G* as $(G'/G^*)^2$ continues to increase. As we shall see in the section that analyzes the effect of strain amplitude on the structure of the entanglement network, such a feature is indicative of strain softening.

In the following we analyze quantitatively the relationship between $(G'/G^*)^2$ vs G*, and relate it to the behavior of viscosity versus ω. In doing so we develop a new, simple formulation between viscosity and the relative elasticity of the melt, which we attribute to the entanglement network. A plot of $(G'/G^*)^2$ vs G* for PMMA at T=230 ^oC, 2% strain, is shown in Fig. 3. This curve is typical of the behavior observed at low strain, in the linear viscoelastic region. One sees that all the points, except the last one, are on a fitted curve that passes through the data and extrapolates to a plateau value for the melt elasticity (Eq. (4), discussed below, was used to create the fitted curve of Fig. 3). The maximum melt elasticity is not 1 but less. Remember that $(G'/G^*)^2$ is equal to $\cos^2 \delta$, where δ is the phase shift between stress and strain. In our model of the nature of the network of entanglement (part II, [2]), the difference between the maximum of $(G'/G^*)^2$ and 1 relates to the structure of the network, in particular to the number of phase-lines unconnected to the network, thus not producing any active strands capable of bearing stress. (See later). The last point of Fig. 3 is above the extrapolated line, not because its elasticity is higher, but because the G* increase has started to slow down, a first sign of strain softening, even at this low strain of 2%. One sees that the increase of the stress magnitude, as ω increases, eventually resulted in strain softening effects. We will extensively develop this observation in the strain effect section of this paper.

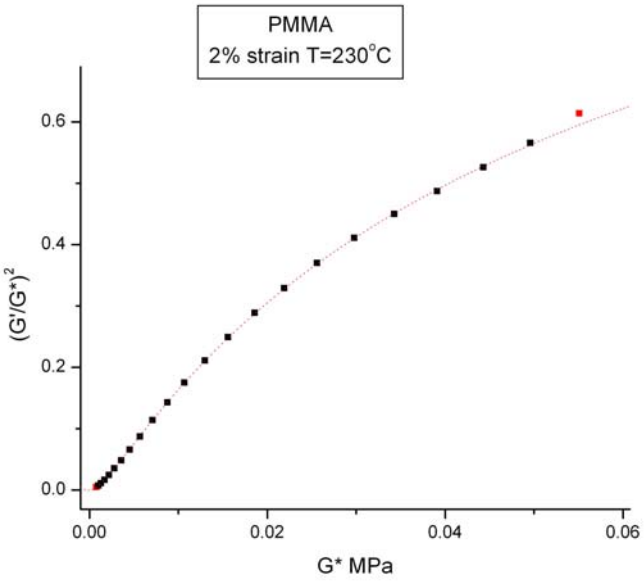

Fig. 3
$(G'/G^*)^2$ vs G* for PMMA T=230 °C 2% strain.
The continuous line is the result of the fit by Eq (4).

A. the Cross-Dual-Phase Network of Entanglement

In Chapter 1 we defined early on the meaning of "the network of entanglements". Much of the development in this Chapter expands on this concept and, therefore, we copy below in Fig.4 the sketch of a Cross-Dual-Phase network of entanglement already presented in Chapter 1 and summarize the essential difference between our model of an entanglement network and previous models.

Fig. 4
Sketch of the Dual-Phase Entanglement Network model.

The boundaries of the "white phase" are not static but fluctuating around with frequency ω'_o under no stress conditions. Stress orients preferentially the boundaries in a given direction and increases the frequency of reorganization. This can be modeled by an activated process.

The existence of the two "phases" is represented by the light and dark regions, respectively (the boundaries constitute one of the phases). Both phases are of the same nature (representing local interactive coupling of conformers), but are visco-elastically different (e.g. their T_g is different

by a few degrees) and their existence is due to the interpenetration of macromolecular coils. Each of the phases presented in Fig. 4 has itself another layer of duality due to the inter- and intra-molecular nature of the bonds interactions (see below). So, in fact, there are two interactive layers of duality, which is the reason why we use the expression Cross-Dual-Phase to describe the entanglement network. The characteristics of this Cross-Dual-Phase "entanglement network" are governed by the molecular weight of the macro-coils as well as the properties of the conformers (described by the Grain-Field-Statistics discussed in detail in refs. 35, 36). The interpenetration of the macro-coils disturbs the Grain-Field-Statistics which splits into two coherent and interactive phases, creating the river network sketched in Fig. 4. To simplify, we call the light gray fluctuating strands in Fig. 4 the "entanglement phase"; we also use the expression "phase-lines". The "deformation of the network of entanglement" can be sketched as the orientation with the stress of the entanglement phase, resulting from the local re-organization of the local conformers in each phase. This may occur, in each phase, by a stretch-relax mechanism that only involves the change of the isomeric state of the conformers during the stretch stage, the relaxation stage occurring by a diffusional mechanism permitting the re-localization of the conformers with respect to the deformation direction. We postulate that the elasticity of the network, necessarily integrating the dynamics of the interactions between the local conformers in each phase, can also be expressed in terms of the entropy of the dual-phase network, i.e. the orientation of the phase-lines, which simplifies the solution a great deal.

The rate of deformation of the entanglement network (defined above) is equal to the frequency of motion of the thermally activated "phase-wave", the network of fluctuating phase-lines. The first task is to define that frequency of thermal diffusion from the rheological data.

B. The Static and Dynamic Frequency of the Phase-Wave.

At first, we made the assumption that the cooperative fluctuation of the phase-wave scaled like $\omega_R = \omega/(G'/G^*)^2$ and were searching for a way to correlate it with the viscosity $\eta^*(\omega)$. One of the curves in Fig. 5, corresponding to the black squares, is a log-log plot of dynamic viscosity versus ω_R for frequency sweep data on PMMA at T=230 ^oC in the linear range (γ=2%). The point corresponding to the lowest ω is the highest black square on the curve. Another curve is also shown in Fig. 5, a straight line of open dots, but this will be discussed in

the next section. The value of ω_R first decreases as ω increases, while viscosity remains almost constant, and then, in a second region, ω_R increases as $\eta*(\omega)$ decreases, a straight line passing through the points.

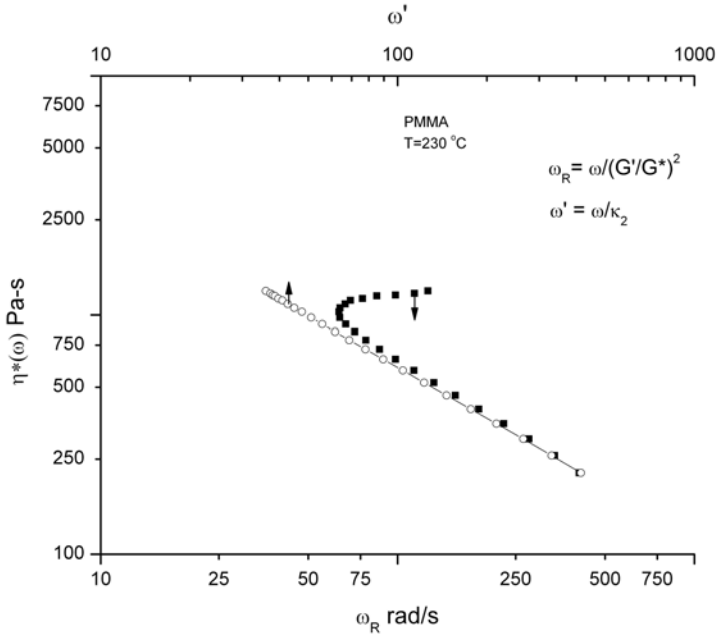

Fig. 5

Dynamic viscosity vs ω_R (black squares, bottom scale) or vs ω' (dots, axis-at the top). ω' is the Dynamic Frequency of the phase-wave (entanglement) network defined by Eq. (5).

In Fig. 3, $(G'/G^*)^2$ vs G* can be fitted by two exponential term functions, κ_1 and κ_2:

(4) $\quad (G'/G^*)^2 = \kappa_1 + \kappa_2$

where κ_2 is one of the exponential terms: $p_4 .(1-\exp(-G^*/p_5)$, with p_4 and p_5 curvefitting parameters, κ_1 is discussed below. This led to a modification of the definition of the network rate of deformation, ω_R to become ω' :

(5) $\quad \omega' = \omega / [(G'/G^*)^2 - \kappa_1] = \omega/ \kappa_2$

Plots of log(η∗(ω) vs log(ω') became linear, which is demonstrated in Fig. 5, by the open circles. In Fig. 5, the ω' scale is shown at the top. Obviously, a simple relationship exists between ω' and ω_R:

$$\omega_R = \omega' \left(1 - \frac{\kappa_1}{\left(\frac{G'}{G*}\right)^2}\right) \quad \text{(5a)}$$

and one sees that $\omega_R \sim \omega'$ when the second term in the parenthesis is small, explaining why the two curves converge in Fig. 5 at higher ω.

Figure 6 displays the split of $(G'/G^*)^2$ into its two terms κ_1 and κ_2 as a function of ω (note that we sometimes call κ_1 "$ELAS_1$", and κ_2 "$ELAS_2$" in the graphs).

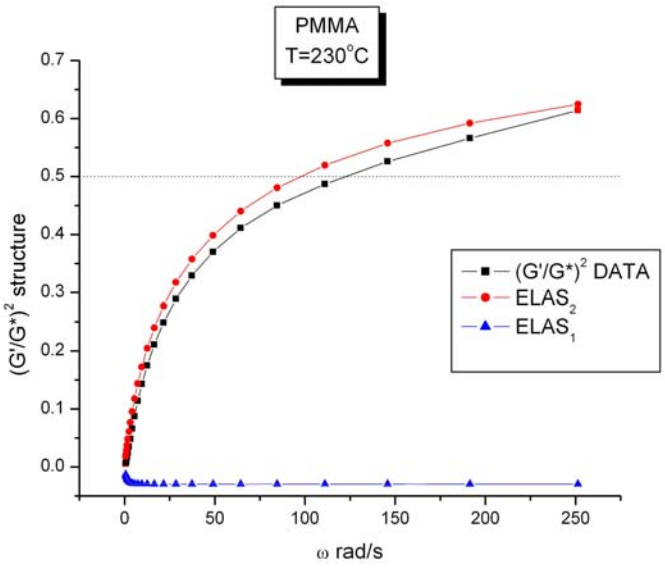

Fig 6

Split of $(G'/G^*)^2$ of Fig 3 into its resolved **κ_1= "$ELAS_1$"** and **κ_2= "$ELAS_2$"** terms

For PMMA, the κ_2 curve (circles) is located above the real data points (squares). The term κ_1 (triangles) remains small, only varies at low G* and can be fitted by a simple exponential function (see Eq. 6) that makes its value converge "rapidly" to a constant value p_1. For this PMMA, in the conditions of Fig. 6 (T=230 °C, 2% strain), p_1 is negative and κ_1 stabilizes to -0.0245 after a small and sharp decay. Recall that we attribute, at this stage of the paper, network

elastic properties to κ_2 and properties directly related to the conformers diffusion or isomeric state changes to κ_1. The meaning of the negative sign is that elasticity is produced by motion of the conformers under the action of the stress which counteracts the action of the *network* to store the external energy. After analyzing hundreds of dynamic frequency sweeps with the above method, we have found that p_1 varies with the type of polymer, temperature, strain % and thermal history. p_1 is positive for highly disentangled melts of PMMA (produced by a shear-refinement processor, see Part II of this series [2]) as well as for melts of semi-crystalline resins, such as LDPE and PP (see later). We found that a simple exponential term was a good fitting function for κ_1:

(6):

$$\kappa_1 = p_1 (1-p_2.\exp(-G^*/p_3))$$

where p_1, p_2, and p_3 are curve fitting constants. Thus, the frequency of the phase-wave network can be rewritten:

(7):

$$\omega' = \frac{\omega}{\left(\left(\frac{G'}{G^*}\right)^2 - p_1.(1 - p_2.e^{-\frac{G^*}{p_3}})\right)}$$

Note in Eq. (6) the possibility that κ_1 does not converge to zero at infinitely low G* (corresponding to $\omega \rightarrow 0$). For melt in equilibrium, p_2=1. For certain thermal-mechanical history, if we impose p_2= 1 in the regression, the fit becomes worse. This seems very intriguing, implying a solid-like behavior at low ω, but is not to be discarded, since an important aspect of our work is to produce and characterize melts which are brought out of equilibrium. As we already mentioned, we have found p_1 positive and p_2 different from 1 for heavily disentangled PMMA melts described in Part II [2]. In addition, the solid-like behavior of liquids at low ω may have recently found experimental justification in the work of Noirez et al. [3].

Figure 7 is a plot of $\log(\eta^*(\omega))$ vs $\log \omega'$ for PMMA showing a perfect linearity all the way from low ω to the maximum ω used in these dynamic rheometry tests (251 rad/s corresponding to 40 Hz).

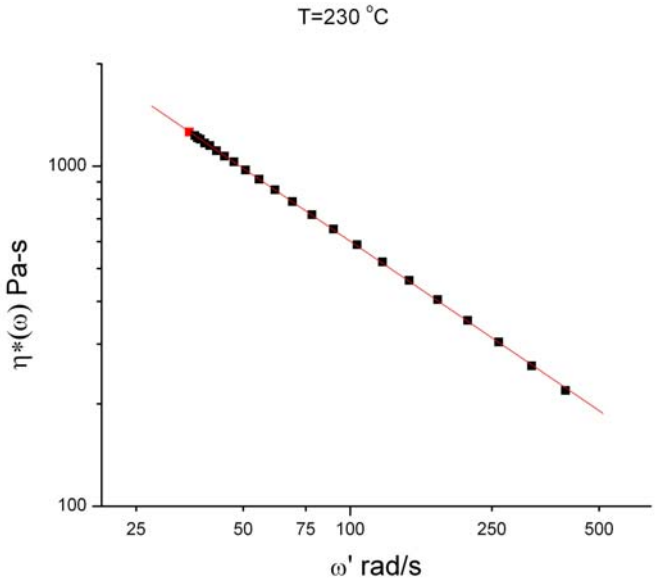

Fig 7

log(η∗(ω)) vs Log(ω') for PMMA T=230 °C 2% strain. α_o intercept α_1 slope. R^2=0.99998. This plot (same as the dots of Fig.4) expresses the dynamic shear viscosity results as a power law of the dynamic frequency of "the entanglement network", ω'.

Figure 7 permits determination of the slope and intercept α_1 and α_o, respectively:

(8) $$\text{Log}(\eta*(\omega)) = \alpha_0 + \alpha_1 \text{Log}(\omega')$$

with α_0 =4.20198 and α_1 = -0.7103 for T=230 °C, 2% strain.

Figure 8 shows the variation of ω' with ω, showing that as ω→0, ω' →34.66 rad/s = ω'_o at that temperature. This value (34.1) is confirmed by the intercept in a similar plot of ω' vs G* displayed in Fig. 9.

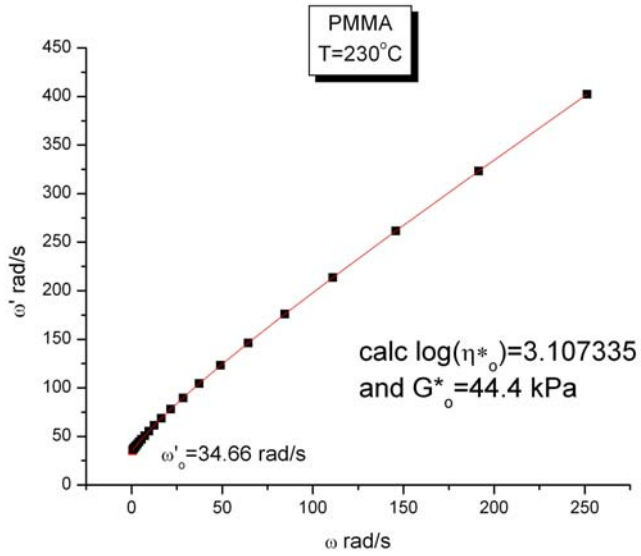

Fig 8

Plot of ω' vs ω for PMMA T=230 °C 2% strain. η^*_o is calculated from Eq. (9) and G^*_o is equal to $\eta^*_o.\omega'_o$

The conclusion is that the straight line in Fig.7 "starts" at ω'_o, for which we can compute a corresponding viscosity and compare it to η^*_o :

(9)

$$\text{Log}(\eta^*_o) = \text{Log}(\eta^*(\omega \text{ --->} 0)) = \alpha_0 + \alpha_1 \text{ Log}(\omega'_o)$$

From the value of α_0 , α_1 and ω'_o found for the PMMA melt of Fig. 7 at T=230 °C we calculate η^*_o = 1,280.4 Pa-s, which compares very well with the value extracted from a Carreau's fit (b_1 in Eq. 2) applied to the same data.

In general, for low strain (in the linear viscoelastic region), α_1 was found to be negative with magnitude between 0.5 and 1; it is 0.71 in Fig. 7. $(1+\alpha_1)$ is the equivalent of the power law index, when ω' substitutes for ω in the expression of viscosity. In the following, we investigate

the meaning of the magnitude of the exponent α_1 and how it varies with strain when strain softening occurs. In particular, we seek to describe the influence of strain on the stretch-relax mechanism occurring due to the deformation of the entanglement network. The value $G_o^* = (\eta^*_o * \omega'_o)$ can be calculated from the Newtonian viscosity and the static phase-wave frequency of the network. It has the dimension of a modulus and could be the spring of a Maxwell element descriptive of the diffusive motion; η^*_o would be the viscosity of the dashpot. G^*_o is 44.4 kPa for this PMMA melt at T=230 ^oC (see Fig. 8).

In Fig. 8 and Eq. (10) it is shown that ω_o' can be obtained by empirically fitting the function $\omega' = f(\omega)$:

(10) $\omega' = a_1 * \exp(-\omega/a_2) + a_3 * \exp(-\omega/a_4) + a_5 + a_6 * \omega$

with $a_1 = -9.465$; $a_2 = 14.712$; $a_3 = -35.28$; $a_4 = 81.9694$; $a_5 = 79.40$; $a_6 = 1.2912$ in the case of the PMMA of Fig. 8. ω'_o corresponds to $\omega = 0$. i.e. $\omega'_o = (a_1 + a_3 + a_5) = 34.66$ rad/sec. The continuous line in Fig. 8 is drawn from Eq. 10. We emphasize that Eq. (10)'s only purpose is to describe the data well enough to determine ω'_o accurately. There are other empirical functions, such as a Carreau's type of equation, Eq. (2), which could be applied to describe the relationship between ω' and ω equally well within the range of ω. Figure 9 demonstrates another way to find ω'_o that, in our opinion, has much more physical significance, as will be shown later. This figure shows that ω' can be expressed as a function of G^* and that it could be fitted (for small strain) by a simple exponential growth function:

(11)

$$\omega' = \omega'_o + A_1 * [\exp(G^*/G^*_1) - 1]$$

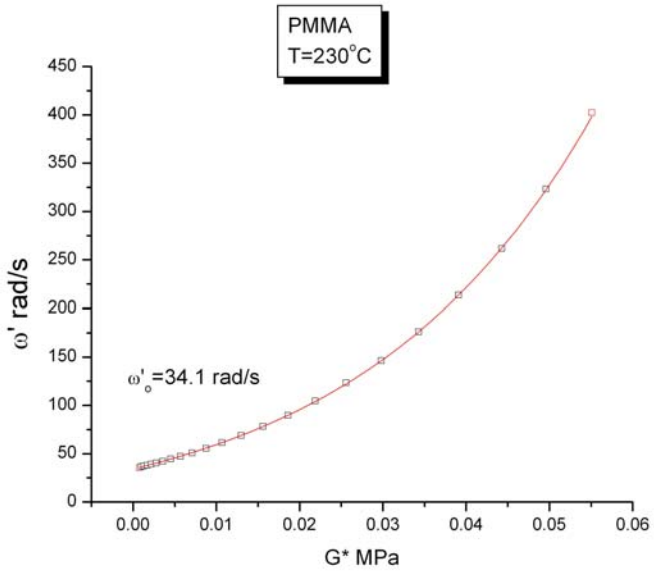

Fig 9

Plot of ω' vs G* for PMMA T=230 °C 2% strain. ω'_o is found by extrapolation to G*=0. The continuous line is a fit by Eq. (11).

Here, in Fig. 9, $\omega'_o = 34.1$; $A_1 = 58.733$; $G^*_1 = 0.0279$ MPa, . Eq. (11) can be rewritten as: (12)

$$Ln\left(\frac{k\,\omega' + (1-k)\,\omega'_o}{\omega'_o}\right) = \frac{G^*}{G^*_1}$$

$$\text{with } k = \frac{\omega'_o}{A_1}$$

In this form, a mixing formula between ω' and ω'_o appears in the numerator of the logarithm, with compounding factor k. One can define an average ω'_{av} equal to $(k\,\omega' + (1-k).\omega'_o)$, with k constant in the regime of deformation described in Fig. 9 (we will see later that k is a strong function of the strain γ). In the section dealing with the effect of strain, we identify k with the activated phase-lines coherence factor for a given ω', the (1-k) non-activated (or relaxed) ones having the static frequency ω'_o. This concept that the phase-lines of the entanglement network in Fig. 4 do not need to be strained all at once, nor all the time, implies a sequential stretch-relax mechanism, and in that sense, k can be regarded as the fraction of time an activated phase-line is stretched (with ω' a frequency defining the stretched state), while (1-k) is the fraction of time it

is in the static, unstressed state (characterized by ω'_o). A similar mixing rule formula will be described in a later section giving a description of shear-thinning from the point of view of the cohesive energy of the network.

When k=1 in Eq. (12), the formula simplifies to the classical Eyring modelization of flow, Eq. (13), in which stress "plasticizes" the activation energy of diffusion, which we find from the temperature variation of ω'_o (see next section):

(13)

$$\omega'_o = \omega'_{oo} \exp\left(-\frac{\Delta_{\omega'}}{RT}\right)$$

$$\omega' = \omega'_{oo} \exp\left(-\frac{\left(\Delta_{w'} - \left(\frac{RT}{G_1^*}\right) G^*\right)}{RT}\right)$$

where $\Delta_{\omega'}$ is the activation energy for the diffusion of the static phase-wave, T is absolute temperature, R is the gas constant, and ω'_{oo} is the frequency of fluctuation at absolute zero temperature (which should match the frequency of the conformer motions at T=0 ^oK). The ratio (RT/G^*_1) appearing in front of the modulus can be re-written by re-plotting the data in Fig. 9 as a function of stress, instead of modulus, to conform to what the Eyring formula stipulates. The modulus G* is equal to τ^*/γ where $\boldsymbol{\tau}^*$ is the shear stress amplitude; so, if we plug this expression into Eq. (12) we now obtain $(RT/G^*_1 \gamma)$ for the stress coefficient in Eq. (13). For instance, for the PMMA of Fig. 9, obtained from a frequency sweep done at 2% strain: ω'_o=34.1, k=0.5807, (T/G^*_1)= 0.01803 and thus $(T/G^*_1 \gamma) \sim 1$. This gives an order of magnitude for the stress coefficient in Eq. (12).

When k is different from 1, we can apply the same rewrite of Eq.(12) into the Eyring format, but using ω'_{av} instead of ω'. We obtain:

(14)

$$\omega'_o = \omega'_{oo} \exp\left(-\frac{\Delta_{\omega'}}{RT}\right)$$

$$\omega_{av}' = \omega'_{oo} \exp\left(-\frac{\left(\Delta_{\omega'} - \left(\frac{RT}{G_1^* \gamma}\right) \tau^*\right)}{RT}\right)$$

$$\omega_{av}' = k\,\omega' + (1-k)\,\omega'_o$$

a plot of Ln (ω'_{av}/ω'_{o}) *vs* τ^{*} / T would be linear with slope R, the gas constant. Note that ω'_{av} must be used, and not ω', to observe linearity, so the absence of linearity of a plot involving $\log(\omega'/\omega'_{o})$ does not indicate that the system cannot be described by an activated process, it simply indicates that $k \neq 1$ in Eq. (14).

We need to understand the physical significance of the parameters A_1, k and (RT/G^*_1), analyze how they evolve to eventually trigger new deformation mechanisms as stress increases, and how they vary with temperature, molecular weight and strain. We also need to compare these values between melts of different polymers and see the influence of processing conditions. An example of such a diversity of response is given in Fig. 10 which displays the melt stored elasticity, $(G'/G^*)^2$, *vs* complex modulus, G*, for various PC and for PMMA. The temperature was 225 ^{o}C. The PMMA is the same grade used for Figs. 5-9. The PC samples in Fig. 10 had different thermal-mechanical processing histories that modified the entanglement state of the polymer. The technology of melt disentanglement is described in part II of this series [2], in Figs. 5a and b. The disentanglement processor shears the melt under vibration, while pulling on it, so that transients are created which destabilize the entanglement network. The treated melt is then pelletized providing a type of new grade for this treated polymer. The melts of PC shown in Fig. 10 were based on such treated pellets, which were re-melted in a Carver press and shaped into disks ready for characterization by dynamic rheology (frequency sweep 0.1 to 40 Hz 5% strain at T= 225 ^{o}C). The curves of $(G'/G^*)^2$ vs G* were extracted from the analysis of the frequency sweeps. One curve in Fig. 10 (" PC REF") corresponds to a reference curve, since the pellets to mold the disks were taken from the untreated virgin PC provided by the resin manufacturer. The "PC elongated" melt was processed in the same disentanglement processor, but without rotational shear, at fast throughput rate through the two treatment stations (refer to [2] for more details). The "PC disentangled" was submitted to a combination of pressure flow, elongational flow, cross-lateral drag flow and shear oscillation at 40% strain. The cross-over point (where G'=G") is found at the intersection of the horizontal line corresponding to $(G'/G^*)^2 = 0.5$ and the curves of Fig. 10.

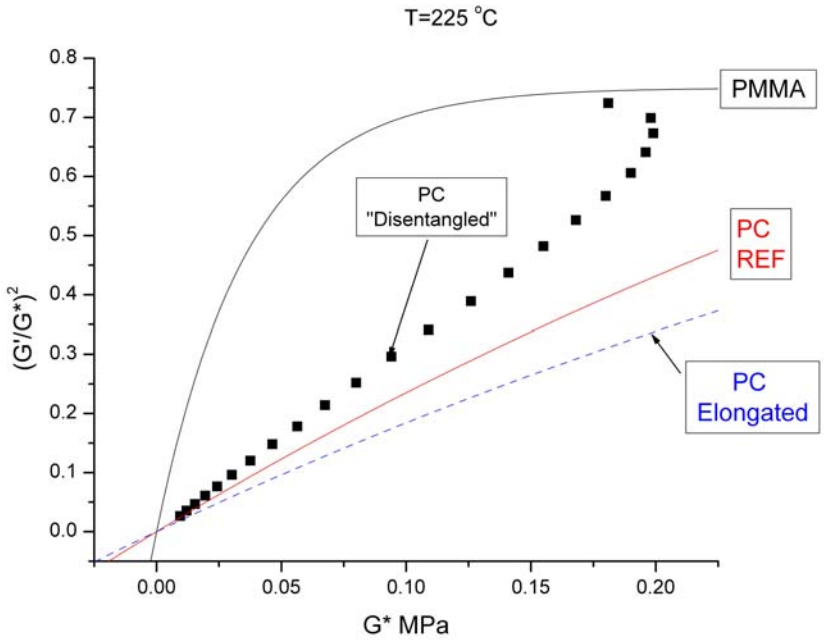

Fig. 10

Comparison of plots of $(G'/G^*)^2$ vs G* for PC and PMMA at T=225 °C, the PC melts assuming 3 different thermal-mechanical histories. See text.

One sees that the PMMA melt is much more elastic than the PC REF melt, requiring very little force to reach the cross-over point (0.05 MPa vs 0.15 MPa, respectively). Yet, the PMMA is at a temperature 120 °C above its T_g, whereas the PC is only 75 °C above its own T_g. Figure 10 also demonstrates for PC the strong influence of processing history on the melt elasticity and the entanglement stability. To understand the influence of these parameters, we need the new analysis framework presented above and discussed further below.

Equations. 11-14 demonstrate a very simple relationship between the dynamic frequency of the entanglement network ω' and G*. Note that ω' starts at ω'_o (thermal fluctuation of the phase-wave) and increases exponentially with stress, a situation that we expect will affect the stability of the elastic network and, for instance, result at high stress in non-linear responses and a change of the deformation mechanism to avoid fracture of the network. As we shall see later when studying the effect of the strain, it is under those stressful conditions for the network that the κ_1 term in the split of the elasticity (Eq. (4)) starts to play an important role in the

deformation process and that non-linear viscoelasticity manifests itself. When we mention "fracture of the network", it does not mean breaking of the chains, it means that a different network (pattern) of phase-lines is created. We suggested in part II of this series (Fig. 46 of Ref.[2]) that this re-structuration of the entanglement network happened as a result of intense synergy between the frequency of deformation and the strain in the case of a disentangled melt of PC.

To summarize, shear-thinning (at low strain) can be described by two simple equations in terms of ω', the dynamic frequency of the phase-wave entanglement network:

(15)

$$\eta^*(\omega)/\eta^*_o = (\omega'/\omega'_o)^{\alpha_1}$$

$$\text{Ln}\,(\omega'_{av}/\omega'_o) = (G^*/G^*_1)$$

$$\text{with} \quad \omega'_{av} = k\,\omega' + (1-k)\,\omega'_o$$

The elimination of ω' between these two equations and substituting $\eta^*(\omega)$ by G^*/ω provides the analytical expression between G* and ω in terms of ω'_o, k, G^*_1 and α_1. This exercise is straightforward and is useful for other purposes explored in other publications, yet it is not explicitly written down here because it is not important to our present discussion.

Notice in Eq. (15) that only κ_2 appears in the expression of shear-thinning, through $\omega'=\omega/\kappa_2$. We thus ask, what is the role played by κ_1 in the deformation mechanisms? The role played by κ_1 at low strain, γ, becomes apparent by examining Fig. 11.

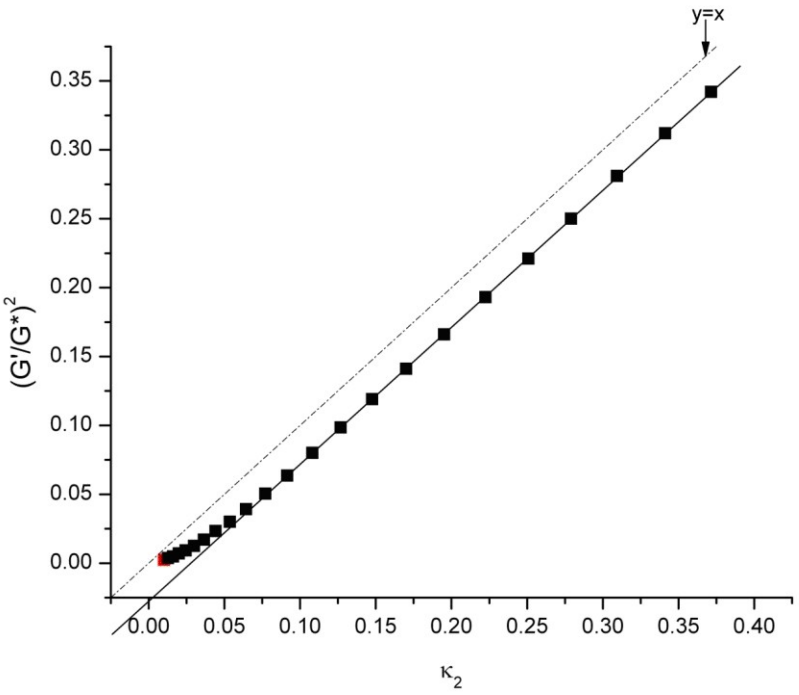

.

Fig. 11

Plot of melt (stored) elasticity, $(G'/G^*)^2$, *vs* "the network elasticity", $\kappa_2=\omega/\omega'$, where ω' is the phase-line frequency. In this Figure, which is for PMMA at T=225 ^oC, the strain is in the linear range (2%).

For a given value of κ_2 in Fig. 11, corresponding to a specific stress produced by the network of activated phase-lines, the melt (stored) elasticity, $(G'/G^*)^2$, is smaller than κ_2 (the dashed line in Fig. 11 corresponds to y=x, and the squares are located below the dashed line). This process of dissipation of strain energy starts at very low ω, and is completed for very low stress. In Fig. 6, for instance, the decay of κ_1 can be described by -0.0245*(1-exp(-G*/1430)) with G* in Pa. Accordingly, κ_1 reached its stable value for $\omega<4$ rad/s corresponding to a modulus equal to 1,430 Pa. This low value of stress is much smaller than that involved in the deformation of the entanglement network, which is a long range interactive process (compare the magnitude of the change of κ_1 and κ_2 in Fig. 6). We assume that the decay of κ_1 at the beginning for low ω is due to the effect of stress on the conformation of the "free-conformers" (F-conformers), which are disposed everywhere in the structure, in the phase-lines as much as in the core phase, and can be equated, to simplify, to the local free volume. Let us explain.

In our model of the local interaction of conformers, the Grain-Field Statistics [35], one distinguishes two types of conformers, the "b" and the "F" conformers, in addition to defining the conformational attributes of the conformers, cis, gauche or trans, depending on the value of ϕ in Fig. 12a. Additionally, for a molecular weight of the chain above a critical value, M_e, the Grain-Field-Statistics applies to *two* populations, the dual phases, not just a single one (occurring only for M<Me), defining the two regions of Fig. 4 and the network of phase-lines that we call the entanglement network. In this situation, which applies to all entangled polymer melts, such as the PMMA of Figs. 5-11, the degree of interaction between the bonds needs to be characterized by two types of b and F conformers that coexist in the ensemble, the b_2 and F_2 conformers of "the entanglement phase", and the b_1 and F_1 conformers of "the core phase". The F-conformers, however, are the ones free to rotate (Fig.12a) regardless of whether they are located in the entanglement or the core phase. If a free volume was to be assigned to the local motion of a conformer, the F-conformers would be the ones with a larger free volume; this is the reason for our statement that the F-conformers motions by ϕ rotation could be equated to the diffusion of free-volume in the system.

At low strain energy, the F-conformers from both dual phases modify their conformational isomeric state and assume a new equilibrium to favor the *trans* conformers, which are more elongated. This mode of local deformation competes with the deformation of the network which re-localizes the dual-phase boundary, by a change of ω'. Figures 12a and b give the deformation of a conformer by rotation of one of the covalent bond around the chain.

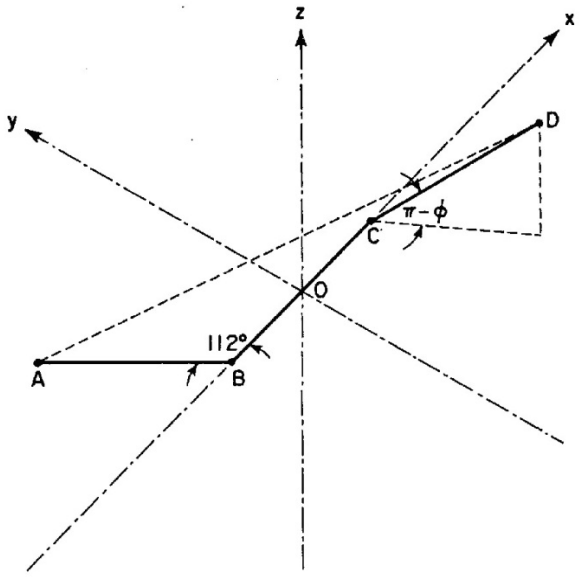

Fig. 12a

Schematic of a conformer in the system of axes (x,y,z). AD is the end-to-end distance of the conformer. A conformer's length can assume various degrees of extension depending on the value of the rotation angle ϕ.

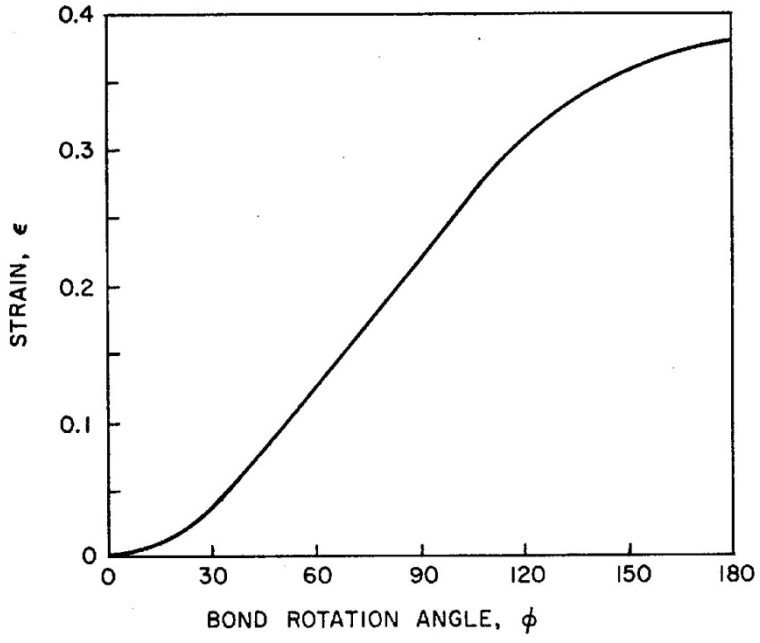

Fig. 12b

True strain $\varepsilon = \mathrm{Ln}(AD/AD_o)$ for the end-to-end distance AD of the conformer of Fig. 12a, as a function of rotation angle (after A.C. Lunn [4]).

One sees from Fig. 12b that the maximum strain a conformer can assume by isomeric rotation is 0.4 (40%). Assuming a given population of F-conformers for a given state of the bonds (see later for more details), and assuming that these conformers are well dispersed in the structure and free to rotate locally, one sees that this type of "stand-still" deformation results from a change of the statistical population, say to simplify, from a cis to a trans conformer, i.e. from $\Psi = 0$ to $\Psi = 180$ in Fig. 12b.This is what we believe creates the κ_1 decay at low stress.

There are cases where κ_1 is positive at vanishing stresses ($\omega \rightarrow 0$), as illustrated in Fig. 13 which applies to a PP melt (BP- 103463), which suggests that the melt was not "classical", in the sense that it was not a pure liquid ($\kappa_1 \neq 0$) at rest. This situation was recently reported by Noirez et al. [31,3b]. Figure 13 provides the split of the melt elasticity, $(G'/G^*)^2$, according to Eq. (4). Curve 1 is the raw data, curve 3 is κ_2, the entanglement network elasticity, and curve 4 is κ_1. Curve 2 was calculated by adding, at each ω, the value found for curves 3 and 4. Note that, similar to the case of PMMA (Fig. 6) for which κ_1 was found to vary negatively as ω increased (but from an initial $\kappa_1 = 0$ value), curve 4 shows a decay which can be described by Eq. (6). Curve 3, representing the variation of κ_2 according to the phase-wave shear-thinning solution, $p_4*(1-\exp(-G^*/p_5)$, is located below curve 1 for all ω, which is different from the situation with PMMA in Fig. 6. Also notice that the melt elasticity is different as the strain energy increased at high G*, i.e. the last 5 points of curve 1 are above the fitted curve obtained by adding the two components of the split, curves 3 and 4. The difference between curve 1 and curve 2 at high ω values can be explained either by "a stretch" of the entanglement network, the equation describing curve 2 requiring to be modified, or by an increase of κ_1 at high ω values, the difference between curves 1 and 2 being added to curve 4. This dilemma between the two solutions is not trivial and is discussed further in the section on the strain effect.

The starting of "non-linearity", shown here as the take off of curve 1 from the extrapolated line (curve 2) is strongly affected by the magnitude of the strain. In Fig. 13 the strain was 25%, which is large enough to trigger non-linear effects for the last 5 frequencies of the frequency sweep ($\omega \geq 85$ rad/s).

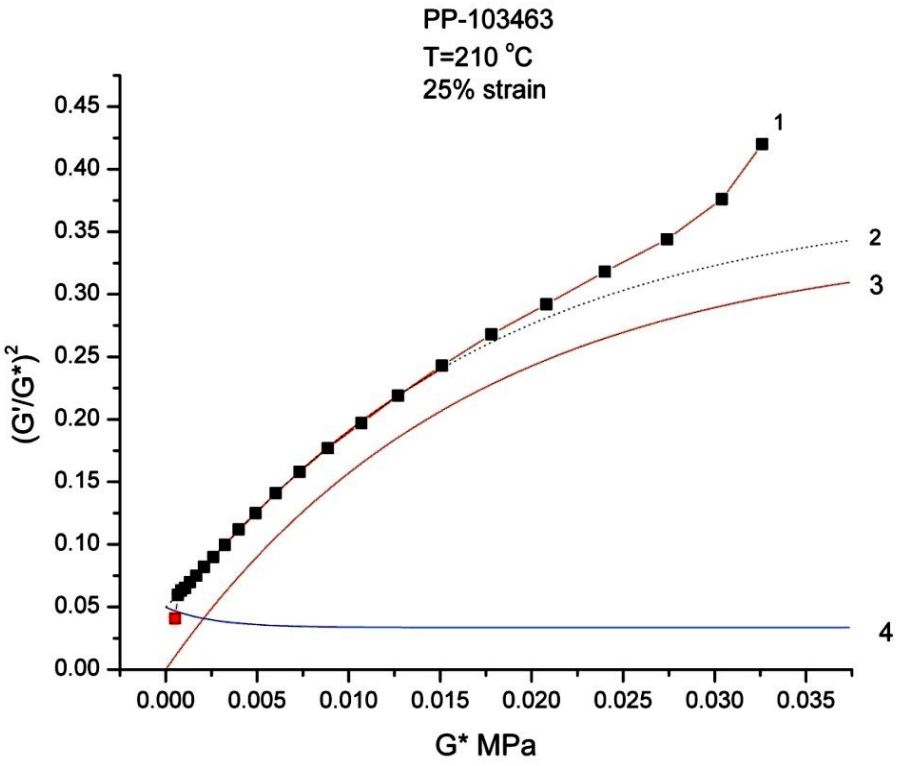

Fig. 13

Split of $(G'/G^*)^2$ vs G* according to Eq. (4) for a PP melt at 210 °C with γ=25%. κ_1 corresponds to curve 4, and κ_2 to curve 3. See text.

The upturn from the purely diffusional mechanism is either due to a decrease of the modulus G* by strain softening, or by an increase of the melt elasticity by isomeric rotation of the conformers in the core phase, leading to an increase of κ_1. In Fig. 13 the maximum value of κ_2 is low, 0.35, which indicates that the entanglement network will never reach its cross-over point at any frequency and, therefore, that it will always remain "liquid". Also, in a way remarkably different from what we observed for PMMA, the initial *positive* value (~0.05) of κ_1 at low ω, renders the viscosity calculated from ω'_o , in Eq. (9) a little bit too small compared to the Newtonian viscosity, η^*_o.at that temperature. This is a very significant observation if we want to be able to modify, for instance by shear-refinement, the Newtonian viscosity (i.e. the MFI) of plastic melts. The Newtonian viscosity calculated from Eq.(9) provides the network contribution to the viscosity. One needs to add the contribution from the κ_1 term (at vanishing ω), which

corresponds to the locked-in elasticity in the core-conformers, due to a mechanical history that creates quasi-equilibrium (metastable) states. In other words, to summarize a point that we will explain further in this paper, the initial state of the PP melt analyzed in Fig. 13 was not thermodynamically stable, and this was due to a successful synergy of interaction between the entropic (κ_2) and enthalpic (κ_1) deformation mechanisms during the processing conditions of the pellets in the extruder at the exit of the reactor. By "successful" we refer to the discussion in part II of this series [2] regarding the ability to preserve in the pellet, after cooling, the state of entanglement created by an intense non-linear deformation (shear-thinning coupled with strain softening in ref. [2], leading to *in-pellet disentanglement*). As it turned out for the PP melt of Fig. 13, the processing conditions used by the resin manufacturer- unknown to us- led to a frozen-in "boosted-entanglement state", the reverse situation of a disentangled melt that can preserve its low melt viscosity. The same situation ($\kappa_1>0$ at $\omega\rightarrow 0$) occurred for several other polyolefin polymers synthesized using metallocene catalysts (Dow Affinity 8500, for instance[3]). It seems logical to ask: since κ_1 can become *positive* through thermal-mechanical history, and this increases the Newtonian viscosity, could we not think of thermal-mechanical conditions specifically designed to make κ_1 *negative* at $\omega\rightarrow 0$, lowering the Newtonian viscosity? Being able to answer this question is to have the key to the art and science of disentanglement technology [2]. Obviously, one needs to understand what molecular or thermodynamic parameter controls the sign and the magnitude of κ_1.

C. The influence of $T_g(\omega, \gamma)$ on the rheology data.

In many ways, what we say about the unstable state of the entanglements due to processing resembles what was discussed forty years ago about the glassy state [5a, 5b], which, too, could be influenced by thermal-mechanical history and annealing [6]. The kinetics of the return of a glass to equilibrium have been expressed in terms of a structural parameter defining the thermodynamic state of the glass [7], and by its "fictive temperature", defined from the T_g manifestation upon heating or cooling, which can be varied by annealing, cooling rate, pressure and other thermal and mechanical variables applied during and after glass formation [8,9]. The temperature T_α of polymers is the mechanical equivalent of the T_g, usually observed in a

[3] The results will be presented in a separate article.

dynamic mechanical analyzer (DMA) operating under a small oscillation (<0.5% strain) at a fixed frequency (0.1 to 100 Hz). While T_g is considered the static temperature for the start-up of the long range mobility under no external stress, the α transition is often viewed as its mechanical representation, i.e. the value of T_g under stress.

Another characteristic temperature of the mobility in polymers is T_2, of the Vogel-Fulcher equation (see Eq.(16) below), which determines the temperature of the total collapse of free-volume, in the free volume theories, or the temperature of zero conformational entropy according to the Gibbs-DiMarzio model of flow [10].

(16)

$$\log \eta_o = A + \frac{\Delta_o}{T - T_2}$$

where η_o is the Newtonian viscosity, A and Δ_o are curve fitting constants. T_2 and T_g are simply related, as suggested by the WLF equation ($T_g = T_2 + C_{2g}$, with C_{2g} a universal constant), or by the similar variation they display with molecular weight. For instance, for monodispersed PS fractions ($M_n = M_w$) studied by viscometry and expressed as in Eq. (16) or by the WLF equation, both T_g and T_2 vary linearly with M^{-1} according to several authors quoted by Majeste [11], confirming the simple relationship existing between these two characteristics parameters.

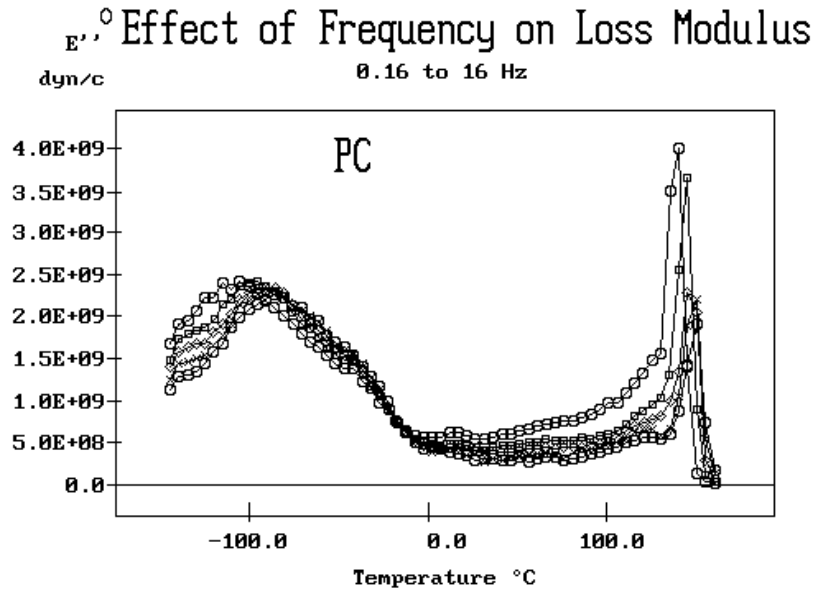

Fig. 14a

E" (dyne/cm^2) vs temperature for PC at 5 frequencies from 0.16 to 16 Hz. The α transition is seen as the loss peak at around 150 ^{o}C.

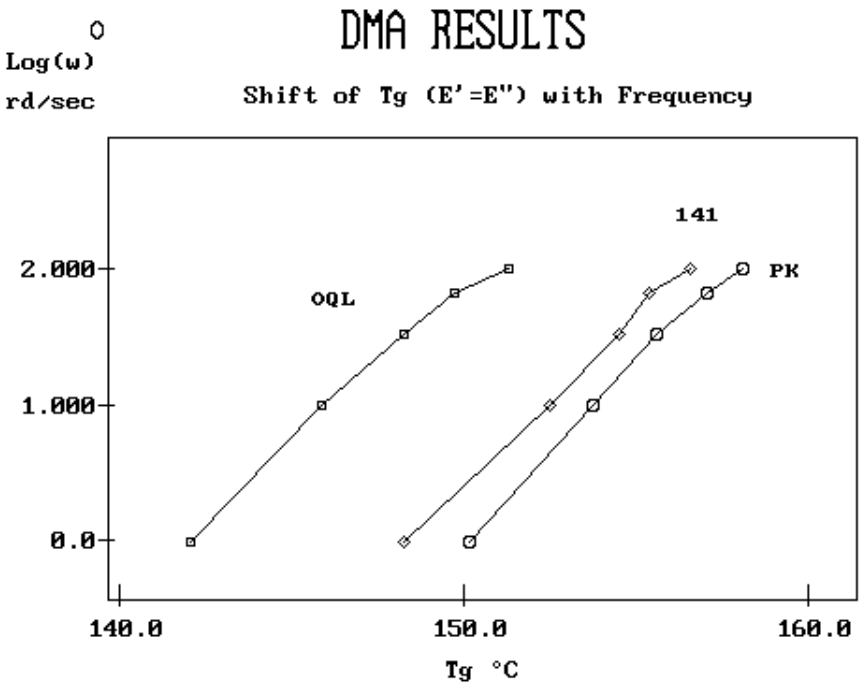

Fig. 14b

The T_g is determined at the cross-over point (E'=E"). T_g increases with the frequency used during the DMA test. Three grades of PC are shown, with an increase of M_w in the order OQL, 141, PK.

The reason for the present interest in T_α , which we call $T_g(\omega, \gamma)$ in the following, is two fold. First, we suggest that the term κ_1 and the value of T_α of a glass (such as in a sample molded out of pellets made from an unstable melt), are related. It is known, for instance, that the value of T_α can be varied by annealing the glass [12], or by erasing the thermal history of the melt before freezing the melt into a glass by holding it at high temperature for a sufficient amount of time. Secondly, a classical "frequency sweep" done at constant temperature in dynamic rheometry involves the step by step increase (or decrease for a down-sweep) of the frequency of the melt oscillation from a low value to a high value, say from 0.001 to 500 rad/s. It is clear from Fig. 14b that T_α, called T_g in the figure, is increasing as ω increases, and, therefore, when transposed to a frequency sweep test, $T_g(\omega)$ increases as ω increases while T remains

constant. In other words, $(T-T_g(\omega))$, representing the rheological state of the melt, is decreasing. In Fig. 14b, for instance, ω spans a range between 1 to 100 rad/s, only covering two decades, yet $T_g(\omega)$ increases by approximately 8 to10 ^oC for the 3 grades of PC. Extrapolating to the broader range of ω used in dynamic rheometry (say 3 to 5 decades), we find a variation of T_g by 23 to 33^oC. This is a significant amount on the temperature scale of polymers. To compare with the effect of pressure on $T_g(P)$, an increase of T_g by 23 ^oC for PC corresponds to applying a pressure of 442 bars (6,350 PSI) on the melt! For PS, it would correspond to a pressure increase of 719 bars. Such a pressure increase would result in a higher melt viscosity due to the decrease of free volume [37].

In summary, the frequency of oscillation plays two roles, it shear-thins the melt, as we studied before, so the viscosity decreases, but it also increases the value of $T_g(\omega,\gamma)$, which increases the viscosity at a given T. The relative magnitude of the two effects on viscosity must be elucidated. Fig. 15a, copied from Boyer [12], is a plot of log f (in Hz) vs 1/T for PS, a "Frequency Map" showing the two relaxations, T_α and T_β. The β relaxation corresponds to local motions of the polymer chain and is of no concern in this article. The α relaxation (T_g) has an activation energy of 84 Kcal/mole on an Arrhenius plot (left curve in Fig. 15a). This is an approximate value since, in fact, a slight curvature instead of a straight line could also be used to fit the α transition of PS on a frequency map, but this detail does not really matter here. The straight line of Fig.15a is a good approximation for our purpose. Fig. 15b is a re-plot of the α transition of Fig. 15a, making use of the radial frequency, ω, instead of frequency, f, in order to comply with what is commonly used in dynamic rheometry.

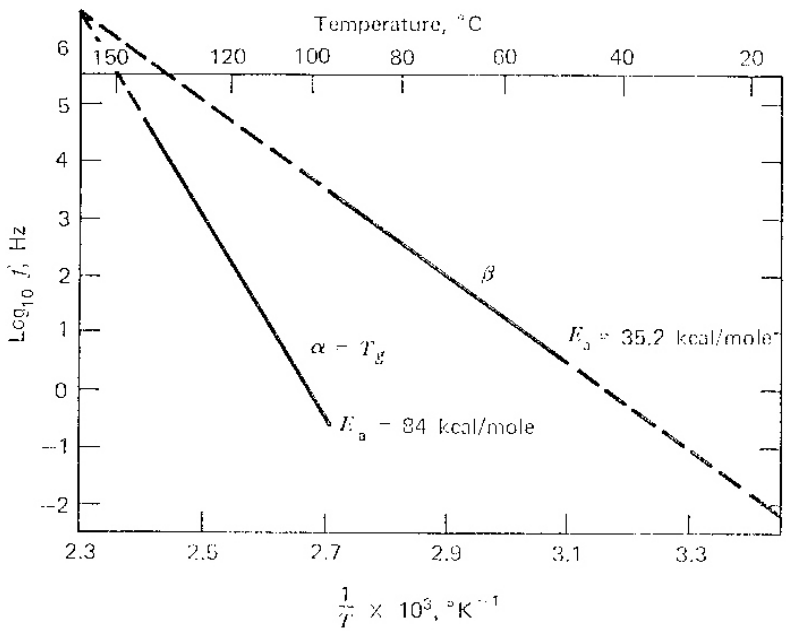

Fig. 15a

Frequency, f, dependence of T_g and T_β loss peaks based on dynamic mechanical and dielectric loss measurements compiled from the literature [12]. After Boyer.

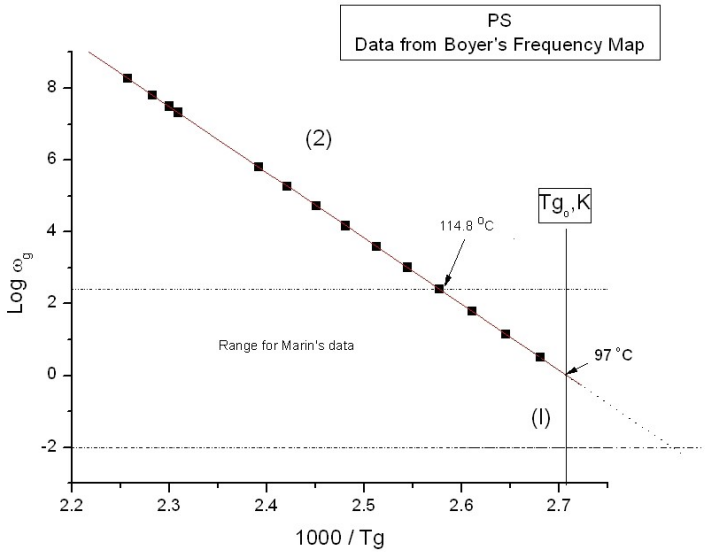

Fig. 15b

This plot is created from Fig. 15a (re the α-transition) for PS. ω_g is the frequency for which $T_g(\omega) = T$. The $T_{go,K}$ value (97 °C) corresponds to the "kinetic" T_g (with no stress, $\omega=0$)), obtained by DSC for instance. In dynamic rheometry, ω typically varies between 0.01 and 300 rad/s (the two horizontal dashed lines in Fig. 15b) for which $T_g(\omega)$ is 82.1 and 114.8 °C, respectively. $T_g(\omega)$ varies by 33 °C during a frequency sweep.

Dynamic "frequency sweep" data are obtained at constant temperature T by sweeping ω from, say, 0.01 to 300 rad/s. We obtain the value of G' (ω, T), G"(ω, T) and η*(ω, T) by repeating the sweeps at different temperatures. In our analysis in this section we propose to compare melts at the same ($T-T_g(M,\omega)$), not at the same temperature. The reason is that for a melt with a given molecular weight M (monodispersed), T_g is a function of M (see Fig.11 of [1]), and of the frequency ω. According to Fig. 15b:

(17)

$$T_g(\omega) = B / (\text{Log}\ \omega - C)$$

where B and C can be determined from the Arrhenius plot (if a Vogel-Fulcher function is used, an extra fitting parameter must be added to Eq.(17)).

Let us give a few examples for PS (Figs 16-19). The data are taken from Marin [13]. Figures 16 and 17 are for a monodispersed PS melt with M=110,000 (grade W11) and Figs. 18 and 19 apply to another grade, W39, with M=390,000. Both grades are entangled polymers, since their molecular weight is above the critical molecular weight for entanglement; for PS $M_c \sim$ 35,000 [14].

The "kinetic" T_g (with no stress, $\omega \rightarrow 0$)), obtained by DSC for instance, is called $T_{go,K}$ in this paper; its value is 97 °C for the PS of Fig. 15b. Since T_g is modified by ω, see Eq.(17), we need to find the value of G' and G" at a temperature $T_1 = T+(T_g(\omega)-T_{goK})$, to provide $G'(T_1)$ and $G"(T_1)$. One sees in Fig. 15b that, depending on the value of ω, $(T_g(\omega)-T_{goK})$ can be positive or negative, which makes T_1 greater or smaller than T, respectively. We can use the principle of time-temperature superposition to determine $G'(T_1)$ and $G"(T_1)$ from G'(T) and G"(T), respectively. Although we argued in part I of this series [1] that the time-temperature superposition was not valid over an extended temperature range, it is an extremely useful tool to perform the type of data manipulation needed here, especially valid since the temperature span (T_1-T) due to the $T_g(\omega)$ variation is rather small (33 °C max for PS in Fig. 15b). According to the time-temperature superposition the moduli at T_1, $G'(\omega,T_1)$ and $G"(\omega, T_1)$, can be determined from the moduli at temperature T provided one shifts the frequency from ω to ω_1: $G'(\omega,T_1) = G'(\omega_1,T)$ and $G"(\omega, T_1) = G"(\omega_1,T)$. ω_1 is calculated from ω in Eq. (18), derived from the Vogel-Fulcher Eq. (16):

(18)

$$\log\left(\frac{\omega_1}{\omega}\right) = \Delta_o\left(\frac{1}{T_1 - T_2} - \frac{1}{T - T_2}\right)$$

We see from Eq. (18) that $\omega_1 < \omega$ if $T_1 > T$, thus making the right hand side of the equation negative ($\Delta_o > 0$). The moduli G' and G" at T_1 are smaller than at T because G'(ω) and G"(ω) are monotonously increasing functions of ω and $\omega_1 < \omega$. In order to calculate G' and G" at ω_1, we perform, with polynomial functions, the fit of log G' vs log ω and log G" vs log ω, respectively. When $(T_g(\omega) - T_{goK}) > 0$ the moduli are over-estimated by working at constant T because the free volume is decreased by the increase of $T_g(\omega)$ with an increase of ω. If we consider that the effect of including $T_g(\omega)$ in the analysis amounts to working at constant free volume, then our new analysis provides the dynamic data G'(ω) and G"(ω) at constant free volume. Such a "free volume correction" must be applied to dynamic data for unentangled melts (M < Mc) if one wants to compare experimental data with theories of the terminal region, such as the Rouse model [15]. Our free volume correction proposed here for entangled melts (M > Mc) serves the same purpose, and we suggest that the correction must be applied to compare experimental data with the predictions of the reptation model [27, 29, 30]. The amount of correction is not trivial and its physical significance is very instructive, as demonstrated in Figs 16-19.

But first, before we explicitly describe these figures, let us go back to Fig. 15b because the $T_g(\omega)$ variation raises important issues at low ω. The Arrhenius straight line Log ω_g vs 1/T cuts the $T_{go,K}$ vertical line for a frequency approximately equal to 1 rad/s, which we call ω_c. We have called (2) the region of the Arrhenius line corresponding to a temperature higher than $T_{go,K}$. The question is what happens to $T_g(\omega)$ when $\omega < \omega_c$, for instance for $\omega = 10^{-2}$ rad/s, indicated by the lower horizontal dash line in Fig. 15b. The intercept of that dash line with the Arrhenius line provides a T_g of 82.1 °C, which is below the $T_{g,oK}$ determined by DSC. We have called this region (1) in the figure (corresponding to $\omega < \omega_c$). There are two possibilities we can consider. First, we can consider that the lower value of $T_g(\omega)$, i.e. T_α, is $T_{go,K}$. In other words, for all values of $\omega < \omega_c$ $(Tg(\omega) - T_{g,oK}) = 0$, there is no correction of the data below ω_c. This is explored in Figs. 16-17 and gives us information about the influence of the higher frequencies on the

rheological data. The second assumption is that $T_g(\omega)$ is not bottomed out by $T_{go,K}$ but by T_2 of Eq. (16), and that it continues to go down towards T_2, as ω becomes smaller and smaller. Both assumptions are backed by theoretical models of T_g, the kinetic school of Kovacs on one hand [16], and the thermodynamic school of Gibbs and DiMarzio [10], on the other hand. We explore both possibilities in Figs 16-17 and Figs 18-19, respectively.

Figure 16 is a plot of G' vs ω (on log scales) for PS with M =110,000 before and after the correction for the $T_g(\omega)$. We have assumed that $T_g(\omega)$ remains contant and equal to T_{goK} when $\omega < \omega_c$ which occurs when $T_g(\omega_c)=T_{goK}$, i.e for $\omega_c=1$. All the data corresponding to $\omega<1$ are not affected by the correction. Figures 17a and b provide, for the same data, the variation of viscosity $\eta*(\omega)$ and of the network elasticity, $(G'/G^*)^2$, against ω, either at constant T=150.4 ^oC, or at constant (T-Tg(ω))=53.4 ^oC.

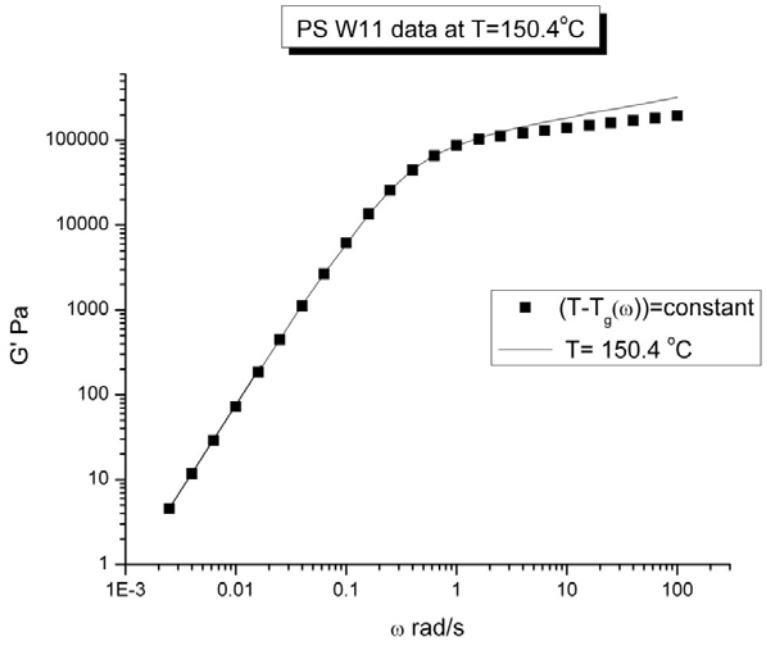

Fig. 16

Comparison of G' vs ω for PS ($M_n=M_w$=110,000) with (squares) or without the correction due to $T_g(\omega)$. The data are taken at T=150.4 ^oC.

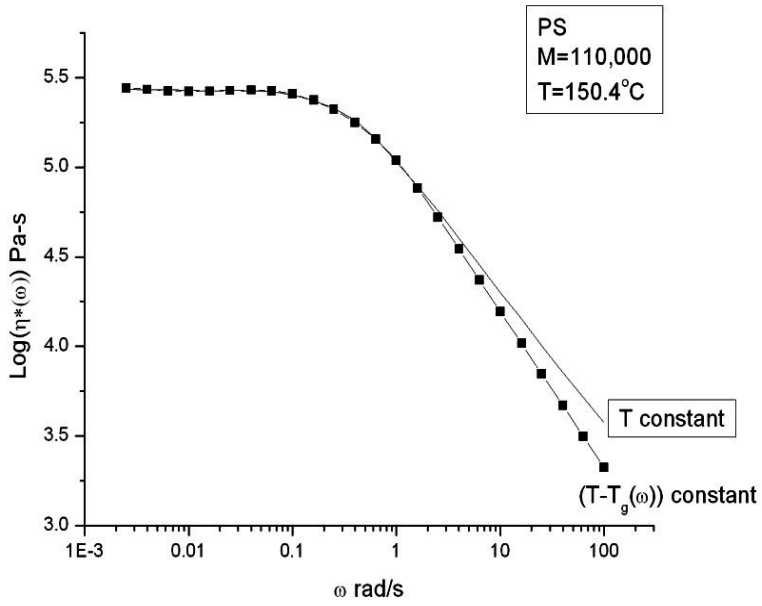

Fig. 17a

Same data as in Fig. 16. η*(ω) is plotted against ω at constant T and at constant free volume, i.e. (T-T$_g$(□)) constant.

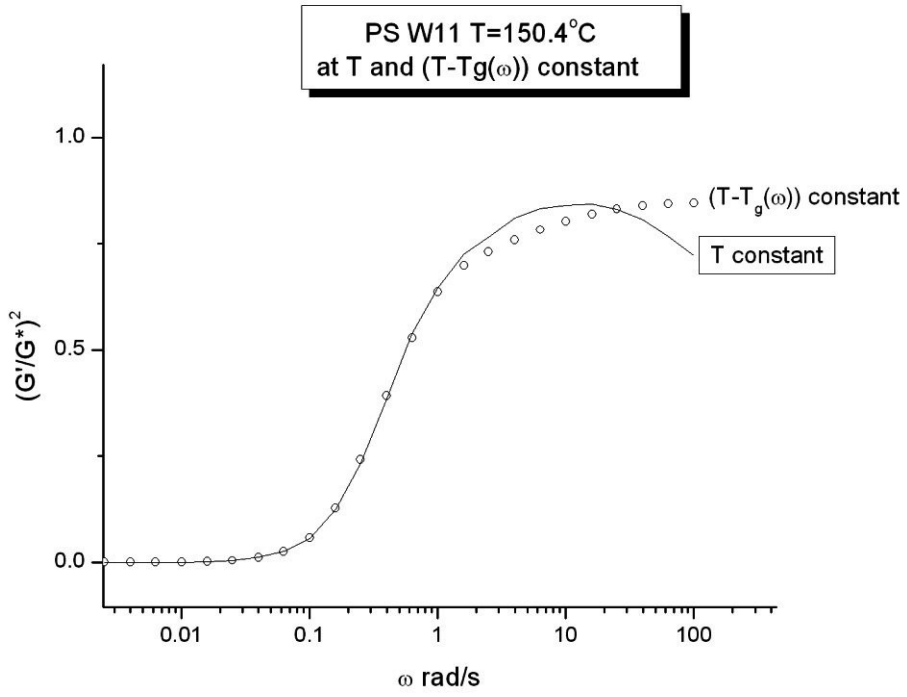

Fig. 17b

Same data as in Fig. 16. (G'/G*)^2 is plotted against ω at constant T and at constant free volume, i.e. (T-Tg(ω)) constant.

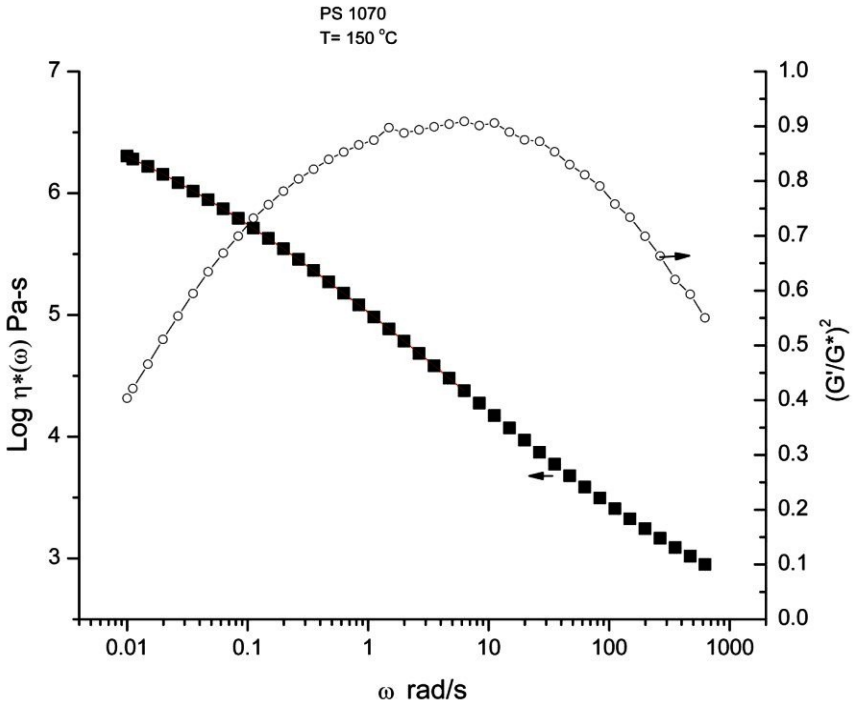

Fig. 17c

Same data as in Fig. 16. $\eta^*(\omega)$ is plotted against ω (left axis, squares), and $(G'/G^*)^2$ is simultaneously plotted *vs* ω (right axis, circles), at constant T. The inflection in the viscosity curve corresponds to the maximum in $(G'/G^*)^2$. If the data were continued at higher ω values, the viscosity would presumably eventually reach the "2nd Newtonian plateau" which we attribute to the effect of $T_g(\omega)$ on viscosity.

Figure 17a shows that viscosity shear-thinning is more pronounced for the corrected data. In essence, the effect of increasing frequency, which induces shear-thinning, is slowed down by its influence on $T_g(\omega)$, corresponding to a decrease of the overall free volume. In fact, a Carreau's equation, Eq. (2), can be used to curvefit equally well the two curves of Fig. 17a, but with very different curve fitting constants, showing the empirical nature of such a classical equation.

Another interesting observation arises from Fig. 17b, which shows the classical maximum of $(G'/G^*)^2$ vs logω , corresponding to a minimum of tan δ vs log ω, a plot used by rheologists to determine the value of the plateau modulus G_{oN} (they assume that G_{oN} is equal to the value of G' at the minimum of tan δ). When looking at the corrected data in Fig. 17b, it appears that there is no maximum in the frequency range of measurement, which means that

either the maximum would occur at a higher frequency if there was no $T_g(\omega)$ effect, or that there would be no decrease of the network elasticity at all in the absence of $T_g(\omega)$. Fig. 17a also explains the reason for the apparent occurrence of a "high frequency Newtonian viscosity plateau" observed especially at lower temperatures for higher molecular weight grades [17].

Fig. 17c is for a PS grade of M_w=300,000 (polydispersity ~2) at T=150 ^oC, showing simultaneously the variation with ω of $\eta^*(\omega)$ and $(G'/G^*)^2$. The inflection in the slope of the viscosity curve observed around ω~4 rad/s is, like in Fig. 17a, a consequence of $T_g(\omega)$, the effect of the free volume decrease compensating shear-thinning. Figure 17c suggests that the $T_g(\omega)$ effect on the rheological data starts earlier than the maximum, so that any regression of the data to determine the characteristics of the Carreau-Yamada equation, for instance, would require to eliminate from the regression range all the points affected by $T_g(\omega)$. Many authors do not pay attention to this corruption of the data by the high frequency relaxation component and obtain erroneous curvefitting constants for the Carreau's equation, which is often used to determine the Newtonian viscosity $\eta^*_o(T)$. At even higher frequency than the maximum in Fig. 17c, it is expected that shear-thinning will be fully compensated by the free volume decrease and that the viscosity should increase. So, instead of predicting a second Newtonian plateau, which is described by certain authors [17], we predict an upturn for the viscosity, shear-thickening. This counter effect of the influence of oscillation frequency on viscosity is amplified by an increase of the strain amplitude, as we will study in another section.

We now analyze the consequences on the rheological data of the second assumption regarding $T_g(\omega)$, and will no longer consider that it is bottomed out by $T_{go,K}$, but by T_2 instead. We call this situation in the figures "T_g loose". This means that in region (1) of Fig. 15b, the Arrhenius line continues to be valid until we reach T_2, which is about 60 ^oC for PS. As already mentioned, the $T_g(\omega)$ for ω=0.01 rad/s is 82.1 ^oC, which is above T_2.

Figure 18 applies to the PS W39 grade of Marin's data [13] for a temperature of 188.3 ^oC. The plot compares the viscosity vs ω (on log-log scales) at T constant (open square) and at $(T-T_g(\omega))$ constant (filled square).

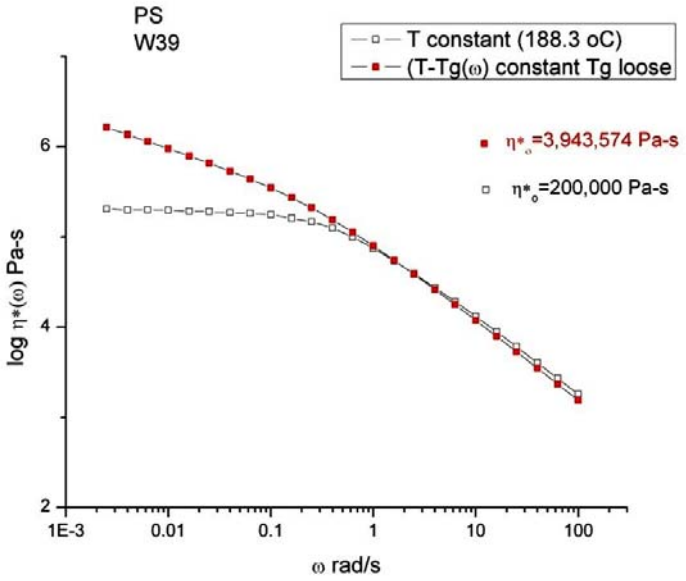

Fig. 18

Comparison of $\eta^*(\omega)$ vs ω for PS (M_n=M_w=390,000) at constant T (188.3 ^oC) and at constant free volume ($T-T_g(\omega)$ constant). We assume that T_g is "loose", i.e. it continues to decrease towards T_2 as ω decreases**.**

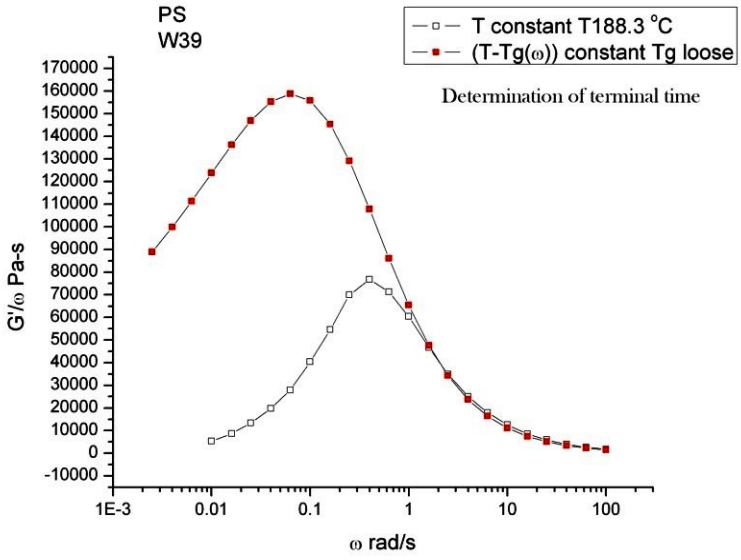

Fig. 19

For the data of Fig. 18, comparison of the terminal time at T constant and at free volume constant ($T-T_g(\omega)$) constant, where the terminal time is calculated from the maximum of G'/ω *vs* ω.

One sees in Fig. 18 that the corrected dated points (filled squares) correspond to a higher viscosity in the terminal zone, at low ω. The value of the Newtonian viscosity can be obtained from a fit of the curves by Eq.(2). We find 200,000 Pa-s for the original data (at T constant) and 3,943,574 Pa-s, almost 20 times higher, for the corrected data corresponding to a constant (T-$T_g(\omega)$). Figure 19 plots G'/ω vs log ω to determine the value of the terminal time ($1/\omega_{max}$) and compare it for T constant and (T-$T_g(\omega)$) constant. The terminal time increases by a factor 10 from 0.5^{-1} for T constant to 0.05^{-1} for free volume constant. The corrected curve is shifted with respect to the original data to the left and upward.

How do we make sense of these results?

Note in Figs. 18 and 19 that the value of $T_g(\omega)$ reference chosen to hold the (T-$T_g(\omega)$) constant was the value of T_g at ω=1, i.e. 97 ^oC. Since T was 188.4 ^oC, to maintain (T-$T_g(\omega)$) to (188.4-97)= 91.4 ^oC we need to find G'(T_1) and G"(T_1) where T_1 is above T in the ω>1 region, but below T in the ω<1 region (the value of 1 corresponds to the value of ω_g for the reference T_g, 97 ^oC). .This means that T_1 varies between 168.45 ^oC, for ω=0.0025, and 202.28 ^oC for ω=100 rad/s. The corresponding ω_1 in Eq.(18) are 0.02065 and 31.32, respectively. In other words, the corrected viscosity data are still located *below* the original data for ω>1, which is visible, even if very small, in Fig. 18, and should be located *above* the original data for ω<1, because $\omega_1>\omega$ in this region for this melt under these conditions of (T-$T_g(\omega)$) constant. In conclusion, the results of Figs. 18 and 19 are consistent with those of Figs. 16-17. The only difference is that, for Figs. 16 and 17, the amount of "Vinogradov shifting" of the viscosity-ω curve is partial, limited to ω>1. By "Vinogradov shifting" we refer to the famous scaling plot of Vinogradov who uses η^*/η^*_o and $\omega\eta^*_o$ for the vertical and horizontal variables to determine a mastercurve of all curves obtained at various temperatures [18]. The Vinogradov variable reducing technique is discussed in Part I of this series [1]. In our $T_g(\omega)$ correction technique, the effect of changing $T_g(\omega)$ because of frequency also results in a shift on both scales, to the left and upward, or to the right and downward, but the amount of Vinogradov shift is not constant and varies for each value of ω. This is what our correction amounts to.

In summary for this discussion, it is clear that if a melt has its T_α vary, either upward or downward, for whatever reason (see Figs 10 and 11 of Ref. 33, for instance), the analysis above shows that we should expect to see variation of the rheological behavior, in G' and G", at high and low ω. In simple terms, we will attribute these changes to an evolution of the free volume in the global system, which, in terms of the Grain Field Statistics [36] is looked at as a change of the number of "b" conformers becoming "F-conformers" (T_g decreases) or vice-versa. As we shall study in the next section, it is not just the amount of free volume of the local conformers which influences the mechanism of shear-thinning, as described above in terms of frequency of diffusion of a phase-wave, but also the production of trans-conformers (b or F types) resulting from a cooperative process governed by a stretch-relax mechanism characteristic of the existence of the elastic network.

D. The Cohesive Network Energy

Let us look again at Eq.(16), the Vogel-Fulcher description of the relationship between the Newtonian viscosity η_o and temperature T. This equation has been studied considerably in the literature and part I of this series reviewed its applicability over an extended temperature span, in particular to indicate the need for a change of the Vogel-Fulcher constants across the Boyer's $T_{l,l}$ relaxation [1]. In the previous section, we discussed the role played by T_2 which describes the temperature of collapse of the free volume and linearly relates to T_g. We now focus on the parameter Δ_o of Eq. (16) which an early paper by this author [19] associated with a Free Energy of activation (in the Eyring sense) of the state of the melt at rest (in fact, one would need to multiply Δ_o by the gas constant R, but in the following, R is equated to 1). Eq. (16) can be rewritten as:

(19)

$$\log \eta_o = \log \eta_G + \frac{(\Delta H_o - T\Delta S_o)}{T - T_2}$$

with

$$\log \eta_G = A + \frac{\Delta_o}{T_G - T_2}$$

where ΔH_o and ΔS_o are uniquely defined. Additionally $\Delta H_o = T_g \Delta S_o$

Let us now define ΔH_ω by the following equations:

(20)

$$\log \eta^*(\omega) = \log \eta_G + \frac{(\Delta H_\omega - T\Delta S_o)}{T - T_2}$$

which can be rewritten:

$$\Delta H_\omega = T\Delta S_o + (T - T_2).\log\left(\frac{\eta^*(\omega)}{\eta_G}\right)$$

or

$$\Delta H_\omega = \frac{T}{T_G}\Delta H_o + (T - T_2).\log\left(\frac{\eta^*(\omega)}{\eta_G}\right)$$

ΔH_ω is also uniquely defined given T and ω. Note that ΔH_ω is a decreasing function of ω since the second term of the equation giving ΔH_ω is negative and its absolute value increases with ω. We have found empirically [19] that ΔH_ω could be expressed as a function of κ_2 which is the elasticity of the network, defined in Eq. (5):

(21)

$$\Delta H_\omega = \kappa_2 \Delta_s + (1 - \kappa_2)\Delta H_o$$

A plot of $\Delta H_\omega - (1-\kappa_2)\Delta H_O$ vs κ_2 is shown in Fig. 20 for the PS grade of Fig. 17c.

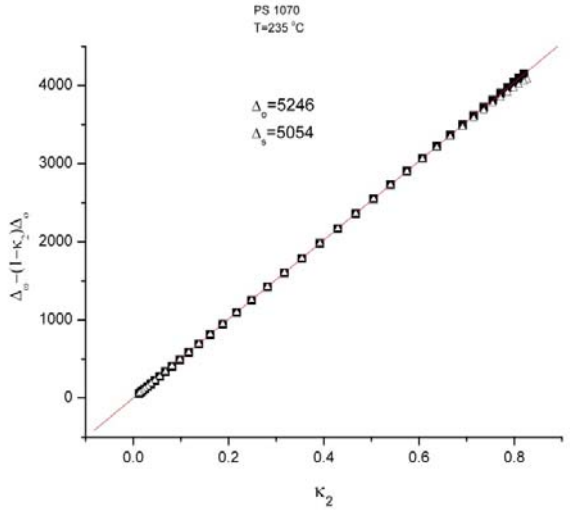

Fig. 20

Same PS grade as in Fig. 17c, but T=235 °C in this plot. The straight line is from Eq.(21) with the variables defined in Eq.(20). κ_2 is the network elasticity also equal to $[(G'/G^*)^2 - \kappa_1]$. See text.

For this polymer, the parameters of Eq. (19) are: log η^*_G= 14.446 , T_2=60.58 ^oC, ΔH_o=5246, ΔS_o=14.0, T_g=102 ^oC The parameter Δ_s is the slope of the straight line (passing through the origin) in Fig. 20, which equals 5054. Note in Fig. 20 the presence of two types of points, the black squares and the open triangles. The actual data are represented by the open triangles and the black squares are points calculated from the best linear fit passing through the origin, shortening the range for the fit to the lower κ_2 values (approximately up to 0.75). Once sees that the triangles are located slightly below the extrapolated line made up of the black squares for the very high κ_2 values. This is due to an entropic deformation of the elastic network at high stored elastic energy (see later). The difference between the black squares and the open triangles can be computed and increases with ω. As can be seen in Fig. 20, this difference is hardly visible when plotting the variables as (ΔH_ω -(1-κ_2)ΔH_o) *vs* κ_2 , but the correction becomes more apparent for higher strain γ, as shown later, or at lower temperature. The magnitude of the distortion of the elastic network at high stress is also a function of the chemical nature of the polymer.

Δ_S is smaller than ΔH_O by 3.66%, which seems like a small amount, but appears to be significantly reflecting the physics behind this type of analysis of the rheological data. Δ_s is the minimum value of ΔH_ω, found for κ_2=1. The maximum value of ΔH_ω is ΔH_o, found for κ_2=0, which corresponds to the Newtonian situation ($\omega \rightarrow 0$), and in such a case $\omega' = \omega'_o$. Eq. (21) suggests that as deformation proceeds, ΔH_ω is the moving average of ΔH_O and Δ_S in proportion to (1- κ_2), and κ_2, respectively i.e. in proportion to the amount of elasticity present in the network. One could tentatively say that there are two "states" the network "strands" could be in the activated state, with energy Δ_S, and the relaxed state, with energy ΔH_O, the number of activated strands being equal to κ_2 , for a given stress. By "activated", we do not refer to the Eyring description of rate processes, because each measurement of G'(ω,T) and G"(ω,T) is a steady state measurement and not a transient, but we refer to a mechanism of deformation producing a trans conformer from a cis or gauche conformer, i.e. a mechanism which modifies the conformational statistical distribution towards the most energetically stable and extended conformers, the trans-conformers (see Figs 12a and b). The reason Δ_S is smaller than ΔH_O, we

assume, is that the number of trans-conformers increases in the statistics for the activated state, Δ_S, compared to its equilibrium (κ_2=0) value, ΔH_o, In this sense, one can consider ΔH_o as the cohesive elastic energy representative of the interaction of the conformers at rest (κ_2=0) and Δ_S as its value at full activation of the elastic network (κ_2=1). The difference (ΔH_O-Δ_S) should be somewhat related to the energy difference between the trans and cis-gauche conformations.

In summary, not all the strands of the network of channels in Fig. 4 need to be activated *at once* when submitted to stress. In fact, it appears that while κ_2 of them are activated, (1-κ_2) are relaxed at the same moment. This conclusion is the same as what we found earlier, in Eq. 12. It matches an intermittent process of stretch-relax, the strands being activated for a fraction k of the time before relaxing and being counted as part of the relaxed strands (k is defined in Eq. 12). More will be said in the discussion.

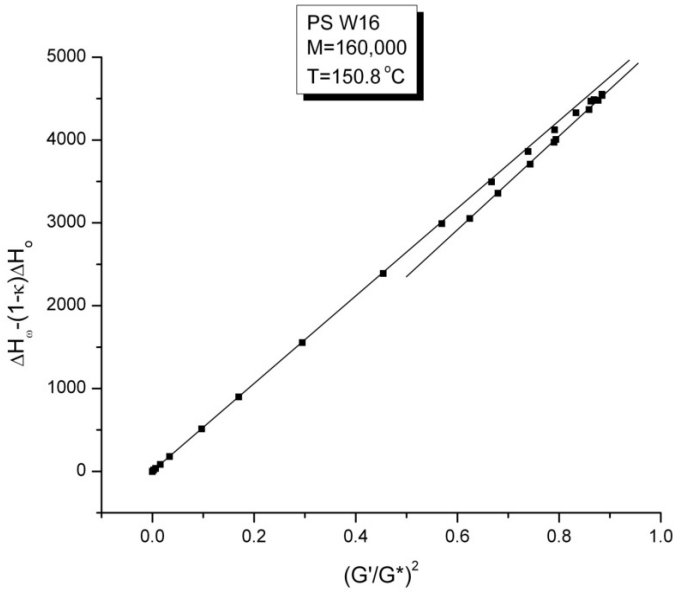

Fig. 21

Same type of plot as in Fig. 20 for PS (M=160,000) applied to an extended ω frequency range. Note that this is κ and not κ_2 implicated in the definition of the x and y axes; that the value of the maximum is function of M (see later); and that another straight line with a non-zero intercept and a larger slope, Δs, characterizes the high frequency response, passed the maximum of $\kappa=(G'/G^*)^2$.

Figure 21 is a plot similar to the one in Fig. 20, with some noticeable differences. The PS sample is here monodispersed with M=160,000. The x-variable is $\kappa=(G'/G^*)^2$ and not κ_2 like in Fig. 20, a difference which is also reflected in the y-axis variable. Furthermore, we observe a maximum on both axes, 4,500 for the y-axis, 0.9 for the x-axis, after which the curve turns back, and a different straight line passes through the points corresponding to a frequency beyond the maximum of κ. We have seen in Figs. 17b and c that $(G'/G^*)^2$ goes through a maximum as frequency increases in a frequency sweep test. What Fig. 21 reveals is that the slope of the straight line that characterizes the cohesive elastic energy of the fully activated network, Δ_S, is slightly different (smaller) for κ values below and above this maximum, and that the intercept no longer passes through the origin once the maximum of κ is reached. We know that an empirical rule attributes the beginning of the plateau modulus G_{oN} to the minimum of tan δ (the maximum of $\cos^2 \delta = \kappa$). We also saw (Fig. 17b) that correcting the dynamic data by $T_g(\omega)$ eliminated or postponed to higher frequency the occurrence of the maximum (see Fig. 17b). The question to answer is whether the onset of the rubbery plateau region corresponds to the elastic network starting to orient/yield? If it is the case, one could also consider the end of the rubbery plateau (at the transitional frequency) as the termination of a process equivalent to "the homogeneous cold drawing" of the elastic network. Also, if the network "orients" starting at the maximum of $(G'/G^*)^2$, could it be visualized in Fig. 4 as the preferential alignment of the free-volume found in excess in the phase-line regions (the light zones) with the shear direction? This view could be cartoon-sketched as the extension of the fisherman's net represented by the channels of the "disentangled" phase in Fig. 4. The distortion of the elastic network, shown in Fig. 20 to be initiated at high value of κ_2, just below the maximum of $(G'/G^*)^2$, is reshaping the free volume distribution in the melt. This is consistent with our approach in the previous section (Fig. 17c) where we suggested that the downturn of $(G'/G)^2$ was associated with a decrease of the free volume in the deformation direction, corresponding to an increase of $T_g(\omega)$. In this sense, T_α appears to be a property of the elastic entanglement network, and its increase with ω is attributed to the orientation of the network. This variation of the "entropy of the elastic network", at higher value of κ_2, modifies the relationship between ω' and stress in Eq. 13, which is at the origin of the complexity of non-linear effects (the κ_1-phase is induced to play a dynamic role in the deformation process). As shown in another section below, larger strain favors and amplifies the

orientation of the elastic disentanglement network, which makes non-linear effects dominate the response of the melt to deformation.

In summary, we suggest in our model that the shearing of a melt includes the following sequence of events: the stretching and relaxation of strands (i.e. sections) of the phase-line network, the total number of strands activated at one time being proportional to κ_2, the network elasticity; the increase of the trans-conformer population, modifying the isotropicity of the strands which are stretched; the increase of the b conformer population, corresponding to the influence of $T_g(\omega)$ on the free-volume, and a re-alignment (orientation) of the excess free volume after ω has reached a certain value corresponding to the onset of the rubbery plateau region. All these characteristics of the entanglement network deformation are strongly affected by temperature and strain, which the following sections focus on in detail.

E. Effect of Temperature

1. T ramp down experiments.

In a temperature ramp down experiment, the melt temperature is lowered at a fixed rate, here -1 ^{o}C/min, while the sample is continuously oscillated at a given frequency and strain amplitude, 5 rad/s and 2%, respectively, in Figs. 22a to c. Figure 22a shows the viscosity plotted against temperature and compares it to the Newtonian viscosity for the same polymer (the PS of Fig. 17c) calculated from Eq. 16. Fig. 22b displays the variation of the melt elasticity, $(G'/G^*)^2$, as the temperature cools down. The strain is low enough (2%) to maintain linear viscoelastic conditions during the ramp down. The temperature is varied between T=210 and 140 ^{o}C.

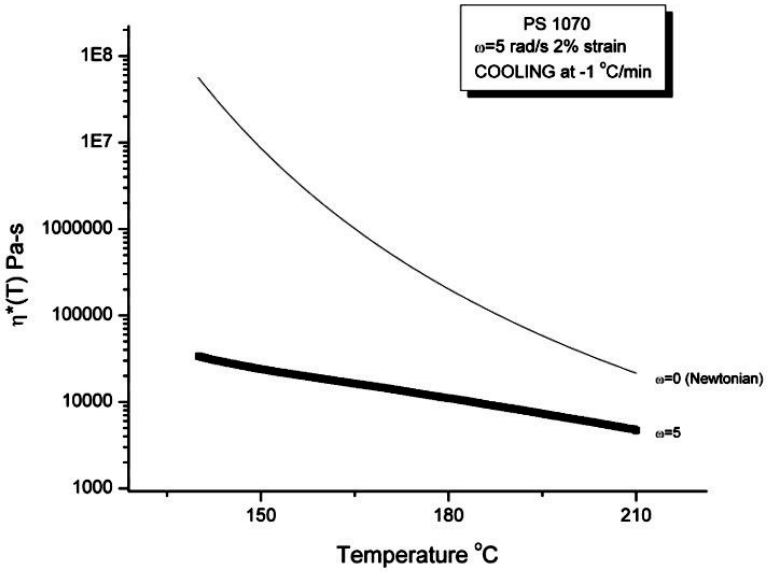

Fig. 22a

Dynamic viscosity (log scale) plotted against temperature during cooling at rate -1 °C/min. ω is 5 rad/s and γ = 2%. The upper curve corresponds to the Newtonian viscosity (ω→0) described by Eq. 16.

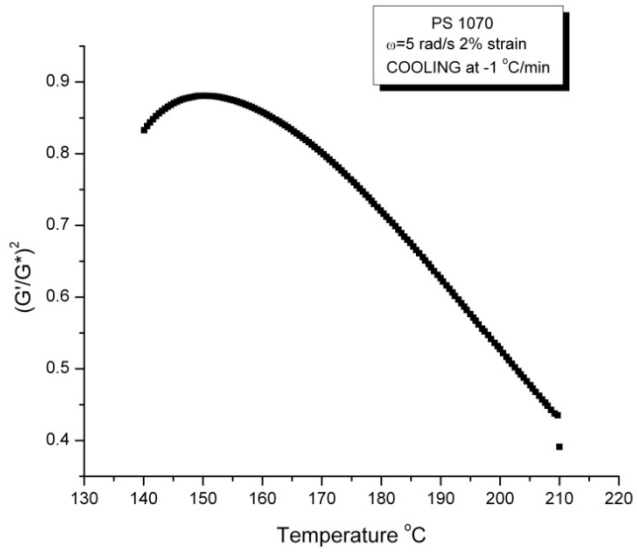

Fig. 22b

Melt elasticity, $(G'/G^*)^2$, plotted against temperature during T ramp down showing a maximum at T=150 °C for ω= 5 rad/s (γ=2%).

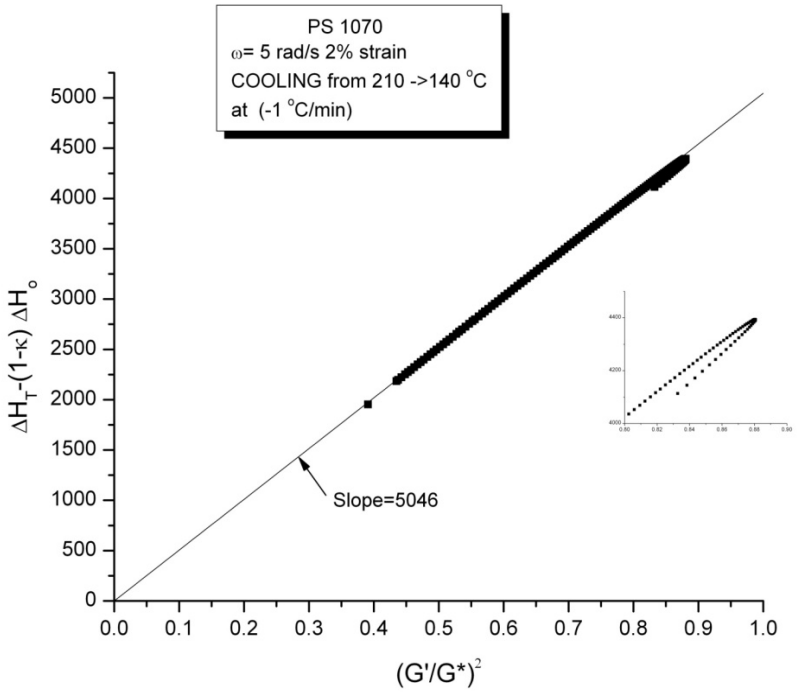

Fig. 22c

Determination of Δ_S (slope) from a T ramp down (same plot as in Figs 20,21).

In Fig. 22a, one clearly observes the phenomenon of shear-thinning by comparing, at each temperature, the difference between the Newtonian viscosity η^*_o and the $\eta^*(T)$ for the ω= 5 rad/s curve. The spread between the two curves, i.e. shear-thinning, increases as T gets closer to the T_g of the polymer. In this case of a constant ω during the temperature sweep, $T_g(\omega)$ remains constant, but $(T-T_g(\omega))$ decreases because of T. Fig. 22c is a test to determine if our analysis of shear-thinning as a function of frequency (Figs 20, 21) also applies to a temperature ramp down. The equivalent of Eq. (20) applied to temperature gives ΔH_T according to Eq. 22

(22)

$$\log \eta^*(T) = \log \eta_G + \frac{(\Delta H_T - T\Delta S_o)}{T - T_2}$$

which can be rewritten:

$$\Delta H_T = T\Delta S_o + (T - T_2).\log\left(\frac{\eta^*(T)}{\eta_G}\right)$$

Figure 22c is a plot of $[\Delta H_T - (1-\kappa)\,\Delta H_o]$ vs κ where $\kappa=(G'/G^*)^2$, the values of Fig. 22b. This plot is very similar to what we found in Fig. 20, with the same value for the slope Δ_s=5046. The

inset graph in Fig. 22c shows the detail around the maximum of κ, indicating a maximum of the variation of $[\Delta H_T - (1-\kappa)\,\Delta H_o]$ and of κ, as also observed during a frequency sweep (Fig. 21). The conclusion that shear-thinning produced by either an increase of frequency or a decrease of temperature is equivalent is not new, even expected and described by the Carreau-Yamada's equation, Eq. (2), when the fitting constants b_1 and b_2 are rendered temperature dependent. This is true in the linear viscoelastic regime. Yet, our emphasis is in demonstrating that shear-thinning is essentially a property of the elastic network and that this remains true whether we vary frequency or temperature. In the classical interpretations of viscoelasticity, the temperature dependence is based on a free volume explanation. The Vogel-Fulcher equation, or the equivalent WLF equation (both described and discussed in part I of this series [1]), are both based on free volume parameters. We emphasize, instead, the properties of the network and claim that shear-thinning is a consequence of the stressing of the phase-line network, sketched in Fig. 4. As explained in the previous sections, the stress to accommodate deformation in the terminal regime is the reflection of a property of the deformed network, $\omega'_{avg} / \omega'_o$ (see Eq. 14), which we also correlated with the proportion of activated strands of the network (Eq. (21). In our model, the free volume does not play the role assumed in the classical interpretation of the time temperature superposition principle, On the contrary, the decrease of free volume due to the increase of the numbers of b-conformers counteracts the effect of frequency and limits the decrease of viscosity by shear-thinning. Furthermore, the free volume splits up and is capable of structuring in our model, depending on which "phase" it belongs to (see Fig. 4). The orientation of the network results in the orientation of the free volume domains, which are no longer isotropic in the rubbery plateau region.

A word must be said about the use of κ_2 in Fig. 20, and of κ in Fig. 22. Does it make any difference to use one or the other to define Δ_S? In fact, it does. As already explained earlier (e.g. Fig. 11), the difference between the "melt elasticity" $\kappa = (G'/G^*)^2$, and the "network elasticity", $\kappa_2 = \kappa - \kappa_1$, is observed at low ω, and becomes quite significant at high strain % (see later). In the linear viscoelastic regime, which is what we have studied thus far, κ_1 is about 1 to 5 % of the value of κ. Let us see what this means for Eq. 21, which we can rewrite in terms of κ instead of κ_2:

(23)

$$\Delta H_\omega = (\kappa - \kappa_1)\,\Delta_s + (1 - (\kappa - \kappa_1))\,\Delta H_o$$
$$\Delta H_\omega = \kappa\Delta_s + (1 - \kappa)\,\Delta H_o + \kappa_1(\Delta H_o - \Delta_s)$$
and thus a plot of $(\Delta H_\omega - (1 - \kappa)\,\Delta H_o)$ *vs* κ
has $\kappa_1(\Delta H_o - \Delta_s)$ for Intercept.

Since, as already shown, $(\Delta H_o - \Delta_S)$ is about ΔH_o for PS in the linear regime, the intercept is approximately equal to 0.02% of the value of ΔH_ω, indeed, negligible. Yet, if we were to plot Fig. 21 on log-log scales, a visible deviation from linearity would be perceived at low value of κ, revealing the presence of κ_1. And, of course, when the value of either κ_1 or $(\Delta H_o - \Delta_S)$ or both become larger, the intercept becomes quite visible even on a linear scale, as demonstrated in Fig. 23

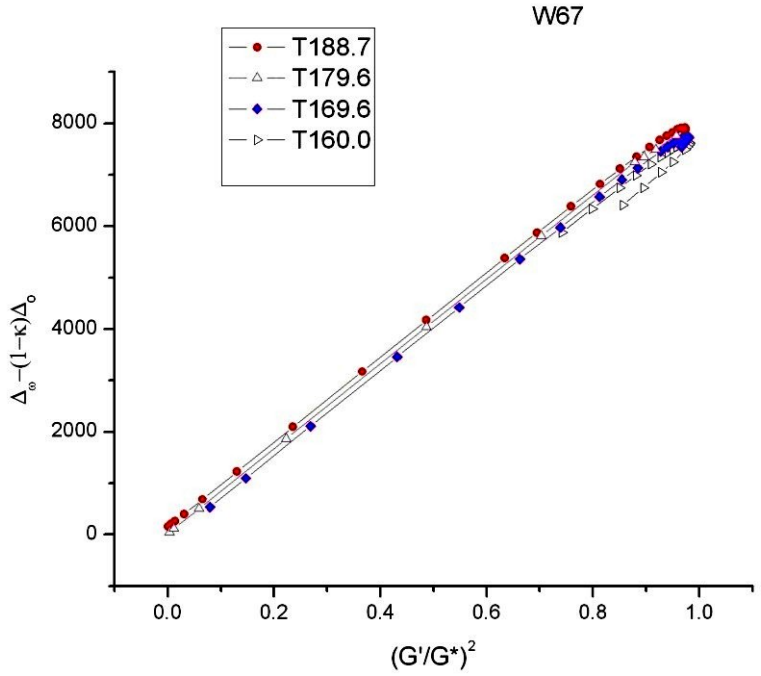

Fig. 23

PS (M=670,000) analyzed at different temperatures according to the procedure of Fig. 21 revealing the presence of the κ_1 term from the shift of the intercept. Also note the value of the maximum for this molecular weight, 7,700.

It appears in Fig. 23 that the straight lines defining Δ_s are parallel and shifted downwards as temperature decreases. The intercept becomes negative and its absolute value is growing as T decreases. This observation is consistent with our view of the co-existence of the κ_1 deformation mechanism at low ω values, on top of the elastic network deformation, due to κ_2.

2. Frequency sweeps at T constant.

In this section we define $\omega'(T)$ in Eq. (14) and determine its temperature variation. The procedure of analysis described in Figs. 3 and 7 can be repeated at each temperature using Eqs. 4-14 above to determine the fitting constants and calculate ω' at each □. We summarize in Fig. 24 results obtained for the PMMA melt of Figs 3-7 for T varying from 185 ^{o}C to 230 ^{o}C, and in Fig. 25 for a PC melt for T varying from 200 ^{o}C to 280 ^{o}C. Figures 24 and 25 are broken down in several graphs (a through g), of which the first 4, labeled a,b,c, and d, respectively, plot the same variables in order to assess both the similarities and the differences for these two amorphous polymers.

Figures 24a and b, and Figs. 25a and b provide the new presentation of the rheological results obtained at different temperatures. Essentially, the viscosity data (Figs. 24b and 25b) are characterized by the value of η^*_o and ω'_o and by their slope, which looks almost constant for PMMA (Fig. 24b), and decreases slightly with increasing temperature for PC (Fig. 25b). The variation with temperature (actually 1/T) of both log ω'_o and log η^*_o is plotted in Figs. 24c and d and Figs. 25c and d, respectively.

Comparing Figs. 24a and 25a, it appears that, for PMMA, the position of the curve $(G'/G^*)^2$ as a function of G*, is quasi-independent of temperature (over a span of 45 ^{o}), whereas it visibly decreases with increasing temperature for PC (Fig. 25a). In Figs. 24a and 25a, the magnitude of G* on the x-scale is also notably different for these 2 polymers, by a factor of 3 to 5, for the same $(G'/G^*)^2$. The T_g of the two polymers being about 40^{o} apart, we should compare, for instance, the T=230 ^{o}C PMMA melt with the T=270 ^{o}C PC melt: the elasticity of the two polymer melts at these two corresponding temperatures is totally different.

Let us further compare respective similar figures for PMMA and PC. The viscosity-ω' straight lines, on a log-log scale, look very similar for both polymers (Figs. 24b and 25b), but the fine details and magnitude of the variation differ significantly (Figs. 24c, 25c and 24d,25d, respectively). It is clear that the effect of increasing temperature is to shift the viscosity-ω' straight lines *downwards* and *to the right*, with a slight decrease of the slope, if need be. The temperature dependence of ω'_o and η^*_o seems to favor an activated process mechanism, as demonstrated by the Arrhenius behavior in Figs. 24c and 24d (for PMMA). The Arrhenius behavior is also clearly visible for PC in Figs. 25c and 25d, but <u>two</u> Arrhenius lines are needed that separate an apparent change of the network deformation mechanism in between[4]. The two-straight-line solution is better than a curved solution, as would be suggested by a WLF fitting function, because, for that later solution, the residuals for the fit are badly curved whereas they are random for the two-straight line alternative solution. The "transitional behavior" at around T=250 ^oC for the PC melt is further demonstrated by analyzing the temperature dependence of the slope and intercept, α_1 and α_o, of the straight lines of Fig. 25b, which is shown in Figs. 26a and b. It is clear in these Figures that a change of the fitting parameters is needed across a transition which coincides with the T_{LL} temperature of Boyer for PC [20]. This relaxation-transition in the upper melt temperature region is presently ignored by the majority of polymer scientists, although early [21, 22] and more recent [1] evidence for its manifestation are overwhelmingly pointing to its existence.

[4] Note that for PMMA there are not enough data points in Figs. 24c and d to eliminate the possibility that 2 Arrhenius lines should be defined instead of one. However, based on other results (not shown), there is only one Arrhenius line in that temperature span. A wider temperature span might show the need for two Arrhenius lines.

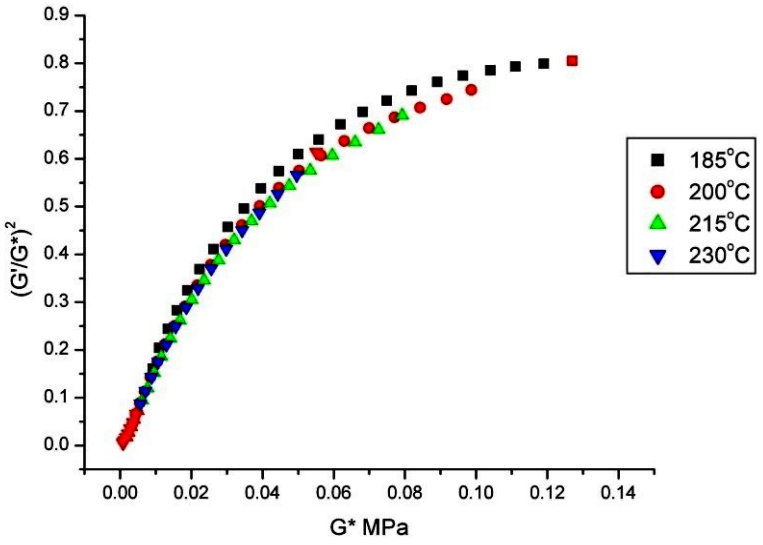

Fig 24a

$(G'/G^*)^2$ vs G* for PMMA 2% strain at various temperatures.

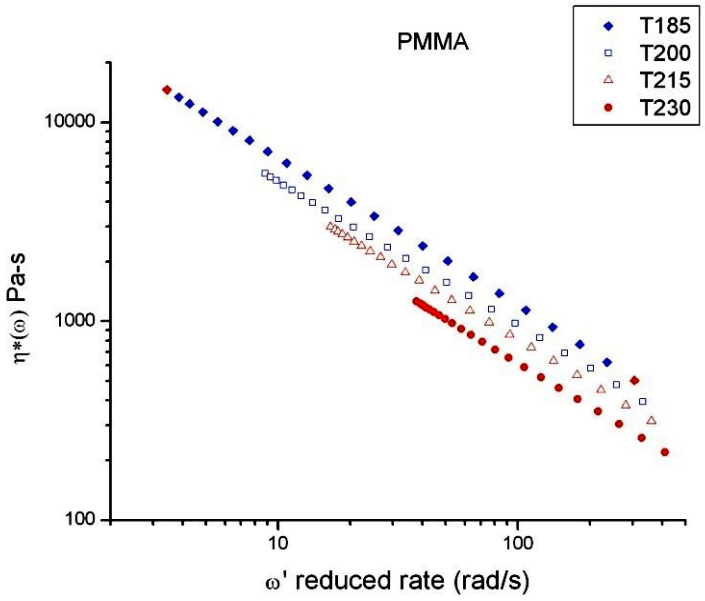

Fig 24b

log(η∗(ω)) vs log(ω') for PMMA 2% strain various temperatures.

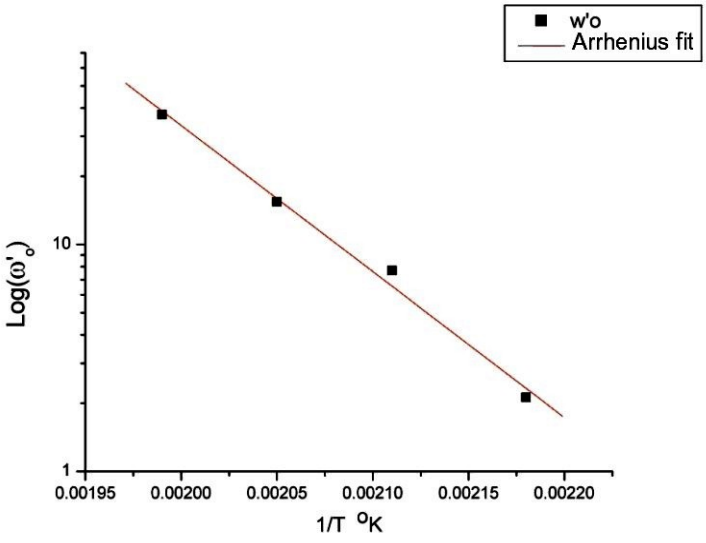

Fig 24c

log(ω'_o) vs 1/T for PMMA 2% strain.

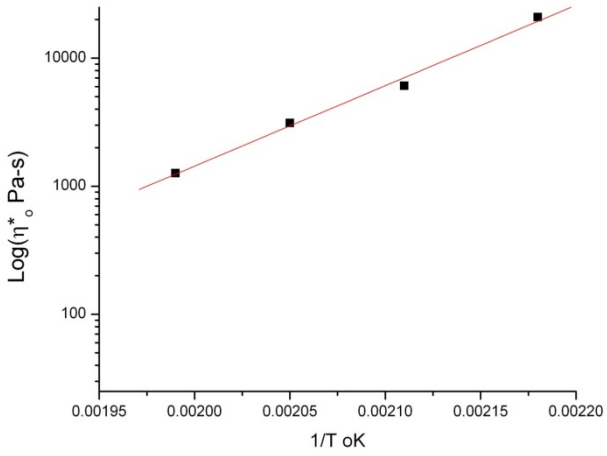

Fig 24d

log(η^*_o) vs 1/T for PMMA 2% strain

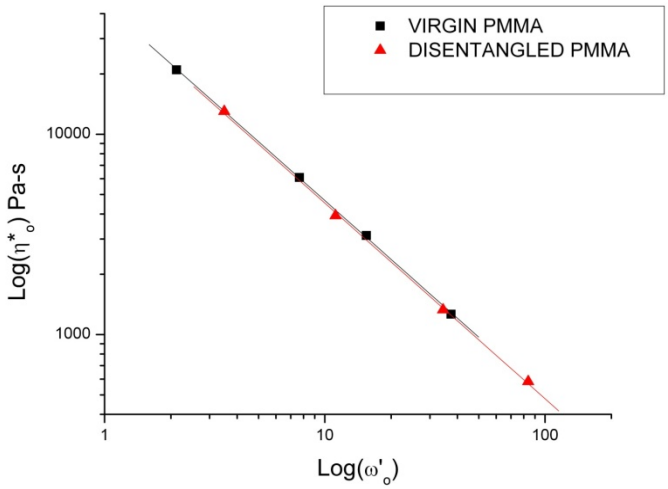

Fig. 24e

Plot of log $\eta^*_o(T)$ vs log $\omega'_o(T)$ for a Virgin PMMA and a "disentangled" PMMA. When the slope of such a plot is -1 $G^*_o=\eta^*_o\,\omega'_o$ is constant as T varies; this situation happens when the activation enthalpy for η^*_o and ω'_o is the same. This is the case here.

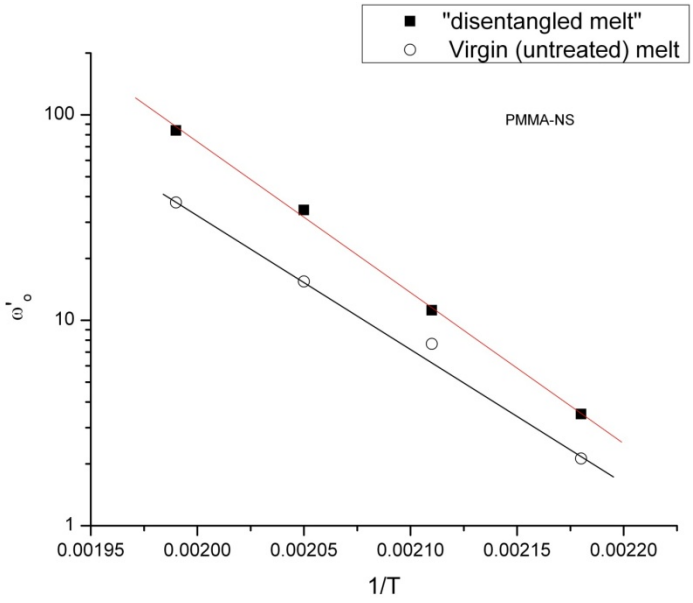

Fig. 24f

Same data as in Fig. 24e. Plot of log ω'_o vs $1/T$ (Arrhenius plot).

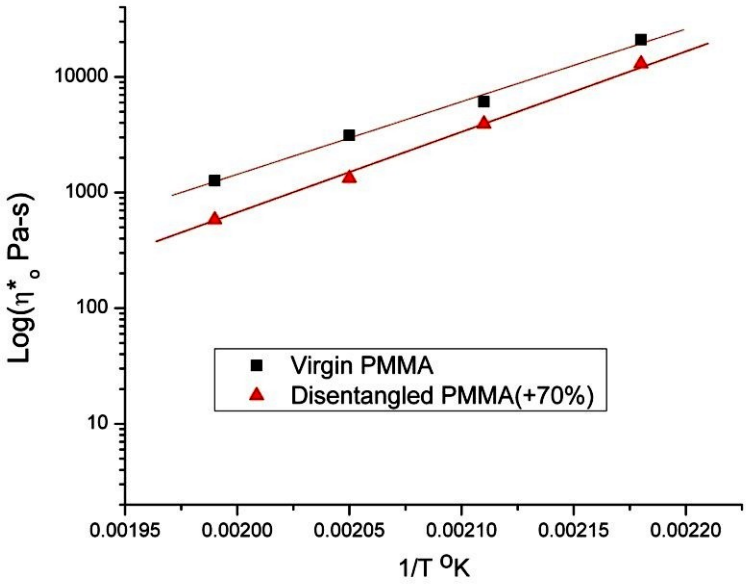

Fig. 24g

Same data as in Fig. 24e. Plot of log η^*_o vs 1/T (Arrhenius plot).

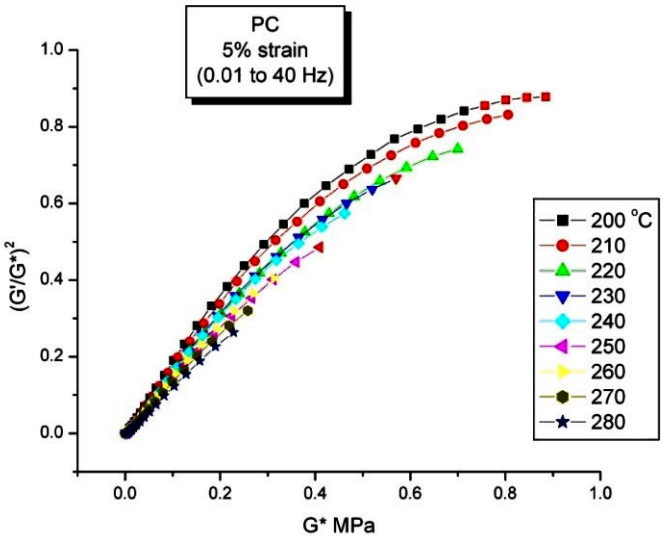

Fig 25a

(G'/G*)^2 vs G* for PC 5% strain various temperatures.

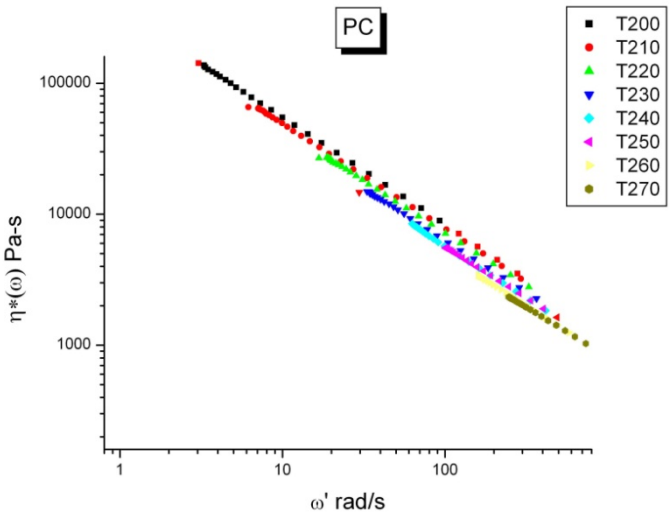

Fig 25b

log(η*(ω)) vs Log(ω') for PC 5% strain various temperatures

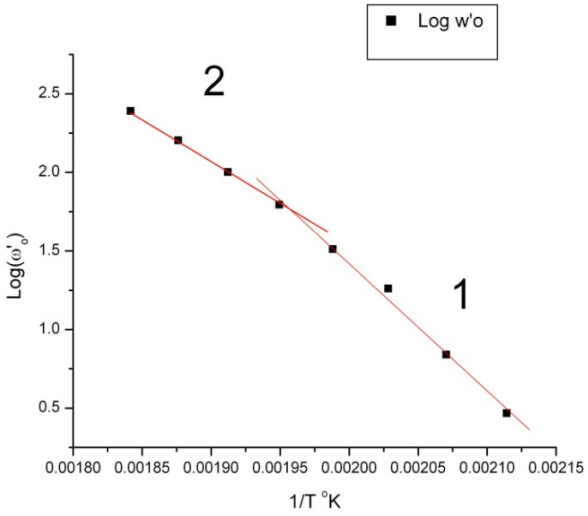

Fig 25c

log(ω'$_o$) vs 1/T for PC 5% strain. Two straight lines fit better than a continuous curve.

.

.

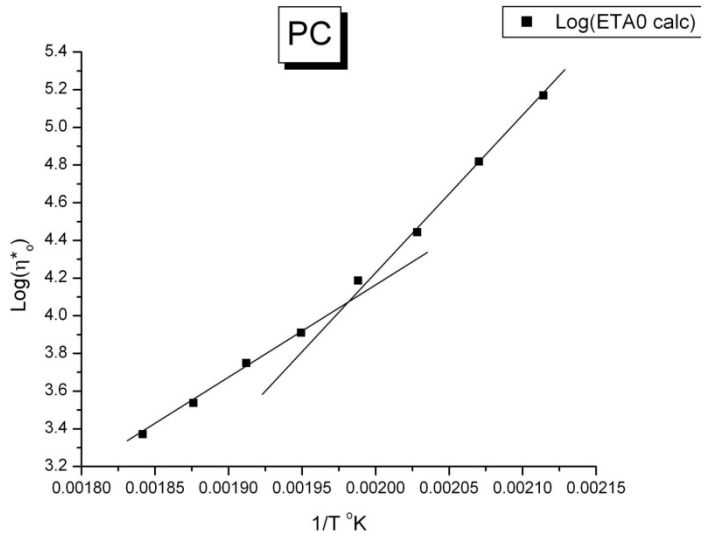

Fig 25d

Log (η*$_o$) vs 1/T for PC, 5% strain. Two straight lines fit better than a continuous curve.

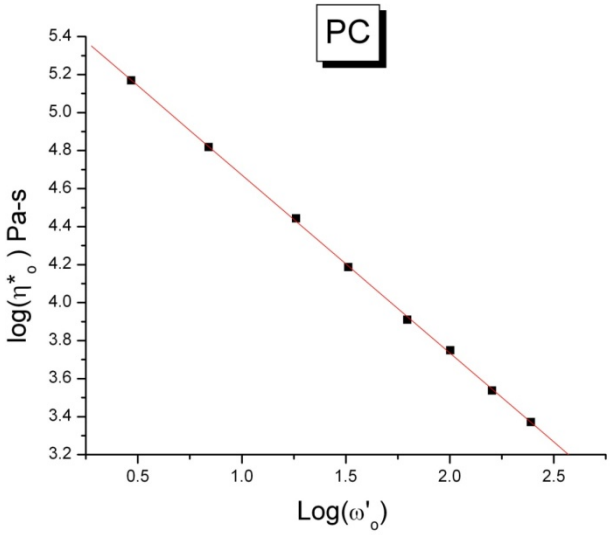

Fig 25e

log(η*$_o$) vs Log(ω'$_o$) for PC 5% strain various temperatures.Slope:-0.938

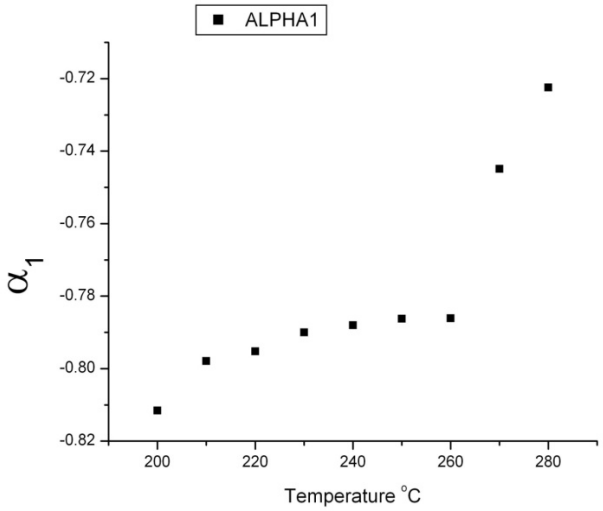

Fig 26a

Slope α_1 vs T for the straight lines of Fig 25b.

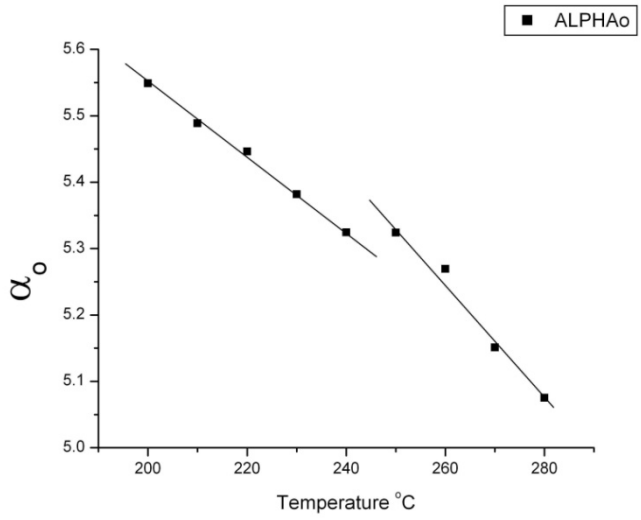

Fig 26b

Intercept α_o vs T for the straight lines of Fig 25b.

From the slope and intercept of the Arrhenius lines one can calculate the activation enthalpy and entropy, respectively, for the activated process(es) responsible for the changes of viscosity and ω'_o. For PMMA (Figs. 24c and d), the value of the slope and intercept of the straight lines in the

figures is as follows: in Fig. 24c, for ω'_o, intercept =14.4, slope -6,436.5; In Fig 24d, for η^*_o, intercept= -9.41, slope = 6,283.65; The magnitude of the slopes is *almost* the same (1% difference), but the intercepts are very different, by 5 orders of magnitude[5] A plot of log η^*_o (T) versus log ω'_o (T) is linear (Fig. 24e), since 1/T can be eliminated between the two Arrhenius equations of log η^*_o vs 1/T and log ω'_o vs 1/T. In Fig. 24e, we see the symbols for <u>two</u> melts, a Virgin PMMA (black squares), which corresponds to the melt of Figs. 24a to d, and a "disentangled melt" (triangles), described in part II of this series [2], which will also be discussed later in the section "effect of thermal-mechanical history". The same straight line goes through the untreated (virgin PMMA) and the disentangled melt, although the later has significantly different Arrhenius activation energy and frequency front factor for the description of log η^*_o (T) and log ω'_o (T). This is shown in Figs. 24f and g, and will be discussed later.

In Fig. 24e, a linear plot of log η^*_o vs log ω'_o for PMMA, the intercept is 4.64 and the slope -0.976. If we consider this value close enough to -1, the value of G^*_o (i.e. $\omega'_o\eta^*_o$) is, therefore, almost temperature independent and equal to $10^{4.64}$ = 44 KPa, This result would appear to confirm the fundamental role played by G^*_o to characterize the melt in the terminal region (note that the magnitude of G^*_o is ~1/3 smaller than G_{oN}, the plateau modulus, equal to 125 KPa for this PMMA grade, as determined from the value of G' at the maximum of $(G'/G^*)^2$.

Let us now compare results obtained for PMMA and for PC, in one hand Figs. 24f and g for PMMA (Virgin and "disentangled" melts), in the other hand Figs. 25c, d and e for PC. Figures 25c and d clearly evidence the change of the slope and of the intercept of the Arrhenius lines. Yet, like for PMMA in Figs. 24f and g, comparing the Virgin and disentangled melt results, the change in the flow mechanism for PC across T_{LL} appears to affect only a re-organization of the respective enthalpy and entropy of the interactions responsible for flow (in an Arrhenius or Eyring plot, the entropy is related to the frequency front factor [23]). This is demonstrated in Fig. 25e, which eliminates temperature as a variable, since it directly plots log η^*_o versus log ω'_o at each temperature: the transition "disappears", meaning there is no longer a break visible in the middle of the temperature range. This suggests, at least for this PC polymer

[5] the intercepts are given on a log scale.

melt, that the "transition" described as T_{LL} has its origin in changes occurring to the entanglement network that are very similar in nature to those triggered by disentanglement [1, 2].

We mentioned in part I of this series [1] that the viscosity of the melt below its T_{LL} temperature was lower than the value projected by extrapolation from the $T>_{TLL}$ data points, and called this phenomenon "Temperature induced shear-thinning".

In a sense, for a disentangled melt such as the disentangled PMMA of part II quoted in Figs. 24e-g, the viscosity situation is the same: the structure of the network of interactions has been (mechanically) modified to stabilize into a new melt which exhibits an increase of its MFI by 70% and behaves (temporarily) like a new grade of PMMA. We stated in the discussion of part II of this series [2] that the occurrence of the retention of the viscosity decrease benefits occurred when enthalpic and entropic forces coordinated resulting in a different entanglement network. Figs. 24 e-g and Figs. 25c-e are good examples of what we meant by that. The straight line in Fig. 24e or 25e is a signature of the presence of an entanglement network, independently of its properties such as its orientation or the influence of the thermal-mechanical history. In Figs. 25e the lack of break means that the slope and intercept of the Arrhenius lines on both sides of the transition are dependent upon one another. This happens because the entropy and enthalpy of activation defining the states of the network *compensate*.

Compensation of the enthalpy and entropy of relaxation modes in polymeric melts were found and analyzed by TSC/RMA spectroscopy [23] and were shown to reflect the state of interactive coupling between the conformers organizing their interaction as a network. It is quite interesting to find that a mechanical method of analysis of the melt (by dynamic viscosity measurement) yields the same type of conclusion. If, as we suggest, **two** types of dual-phases are present to describe the network, one representing the local interactions, and the other one responsible for the phase-line network, we need to determine the coupling laws between entropy and enthalpy (compensations) not only *within* each phase, but also *between* the phases. Also, notice in Fig. 25e that the slope is significantly different from -1 which implies that the Arrhenius slopes for ω'_o and η^*_o are different. G^*_o is no longer constant, and it appears that the fundamental description of the static network cannot be assigned to a single parameter.

In Fig. 24b we have a series of straight lines corresponding to frequency sweeps done at a given temperature. The points on the lines correspond to various frequency values. If we draw lines through the points taken on each isotherm having the same value of ω, we observe that these lines are straight and that their slope and intercept vary with the value of ω selected. The higher ω the steeper the straight line. In fact, the smallest slope magnitude (absolute value) for these lines corresponds to ω=0, which is nothing else than the straight line of log η^*_o versus Log ω'_o mentioned above. Without entering into details in this paper, let us say that it possible to determine, for each ω, cross-plots of log $\eta^*_\omega(T)$ vs 1/T and log ω'_ω (T) vs 1/T, that turn out to be linear (the correct procedure is actually to do the cross-plotting for each value of G*, not ω), allowing to calculate an entropy and enthalpy of activation for each ω. The mechanisms of shear-thinning and strain softening can advantageously be analyzed this way.

.

In Fig. 27a we show the ω' vs G* curves for the PMMA melt of Fig. 24 at 4 temperatures, T=185, 200, 215 and 230 ^oC. The curves are fitted by Eq. (11) to provide the temperature dependence of ω'_o (plotted in Fig. 24c), of G^*_1 (plotted in Fig. 27b) and of A_1. Figure 27c is a plot of A_1 vs ω'_o, showing that the two parameters are directly proportional to one another, with $k = \omega'_o/A_1 = 0.5918$ remaining constant in this range of temperature. Fig. 27b indicates that G^*_1 is temperature independent and equal to 28 kPa.

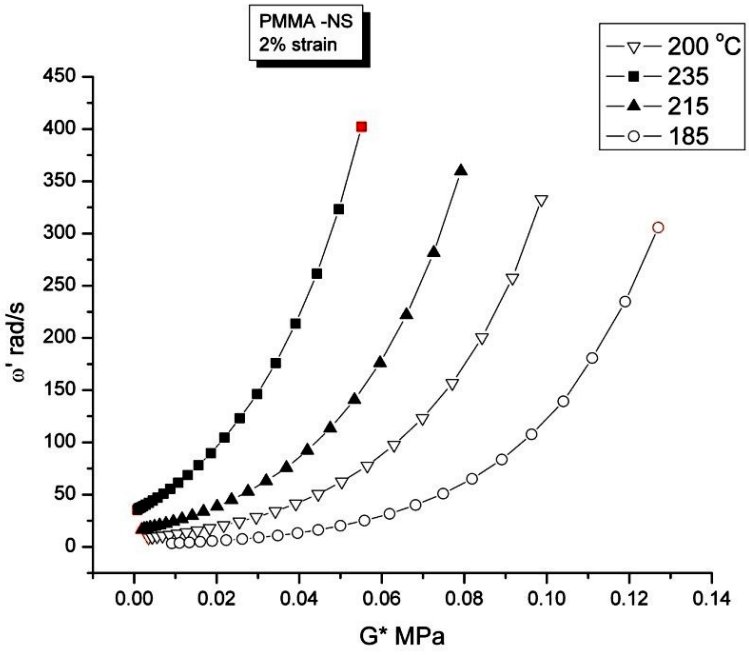

Fig. 27a Plot of ω' vs G* at 4 temperatures for PMMA (γ=2%).

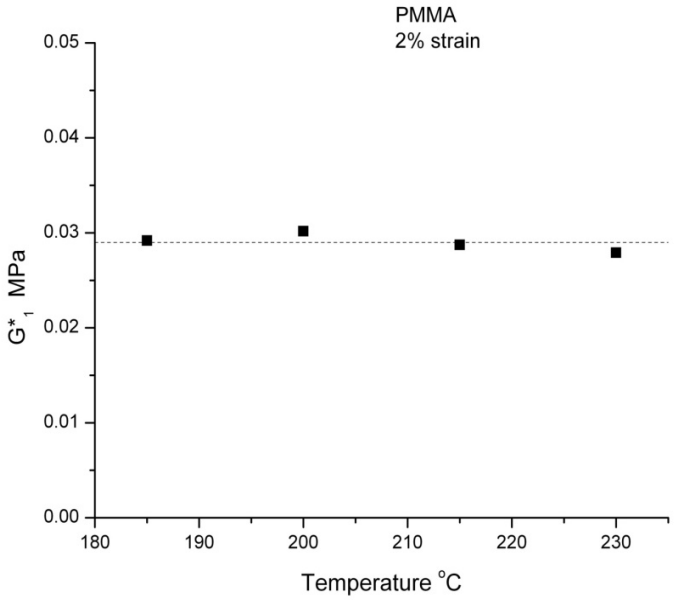

Fig. 27b For the data of Fig. 27a, invariance of G^*_1 determined by fitting with Eq. (11).

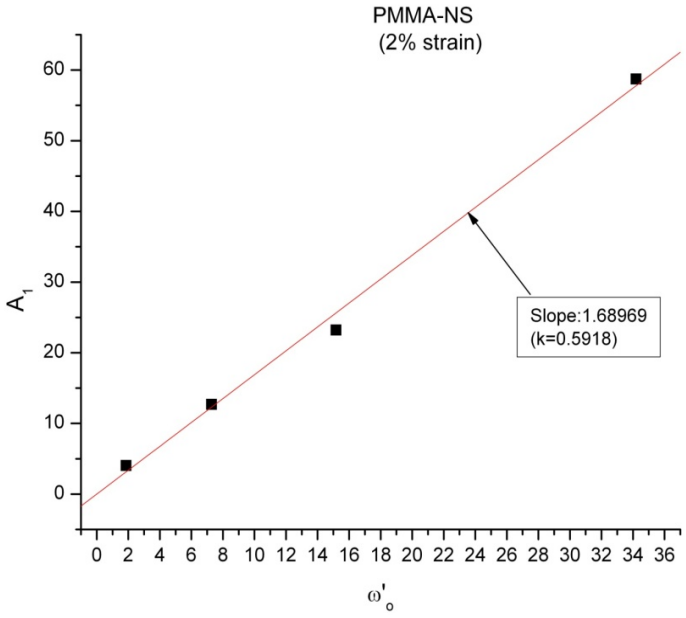

Fig. 27c
For the data of Fig. 27a, plot of A_1 *vs* ω'_o (determined from Eq. (11)) at various T to define the k factor**.**

In summary. In Eqs 11-14, the temperature dependence of ω' is totally determined by $\omega'_o(T)$. This confirms the validity of the Eyring model to describe the shear deformation behavior of the melt above T_g. We now ask, is this simple result universal, can it be used to describe linear visco-elastic data of other polymers?

3. Diversity of the temperature dependence depending on the polymer type.

The number of polymer melts we have tested is limited to about two dozen polymers, which, admittedly, is too small to conclude about the universality of our approach. In the following we show data and plots similar to those in Figs. 24-27 for data provided by other scientists, as well as data determined in our laboratory; the analysis presented above could be used to find the value of ω' at different ω and temperatures and the values of ω'_o, k and G_1, in addition to the Eyring parameters entering the description of $\omega'_o(T)$ and $\eta^*_o(T)$ in Eqs. 11-14.

This is despite a large variety of responses found for the melt elasticity, as illustrated by comparing Figs. 28a and b with Figs 29a and 30a, for instance.

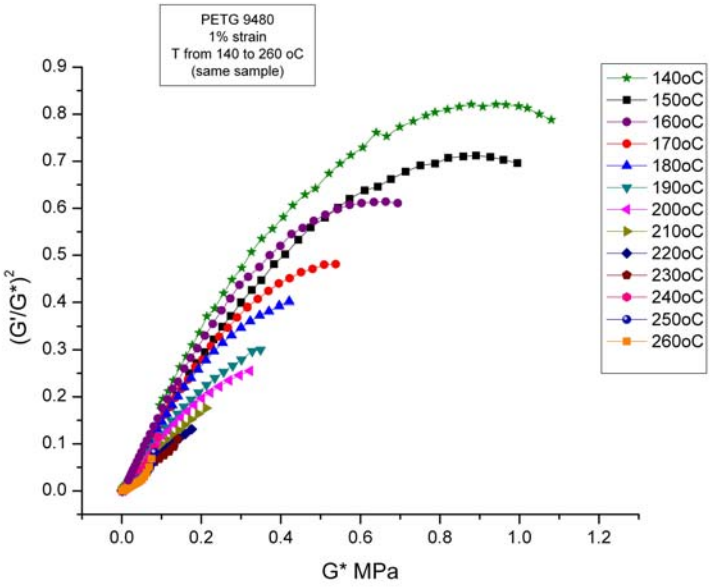

Fig. 28a

Melt elasticity $((G'/G^*)^2$ vs G* for PETG (grade 9480 from Eastman) at temperatures varying from 140 ^oC to 260 ^oC.

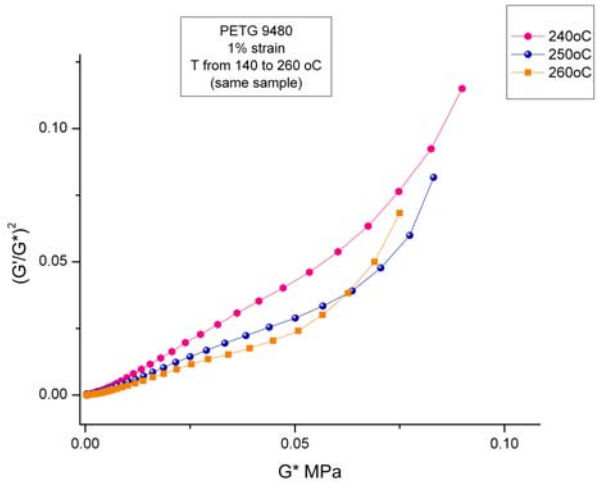

Fig. 28b

Detail of Fig. 28a focusing on the 3 highest temperatures.
Notice the upturn of the curvature for the last points (see text).

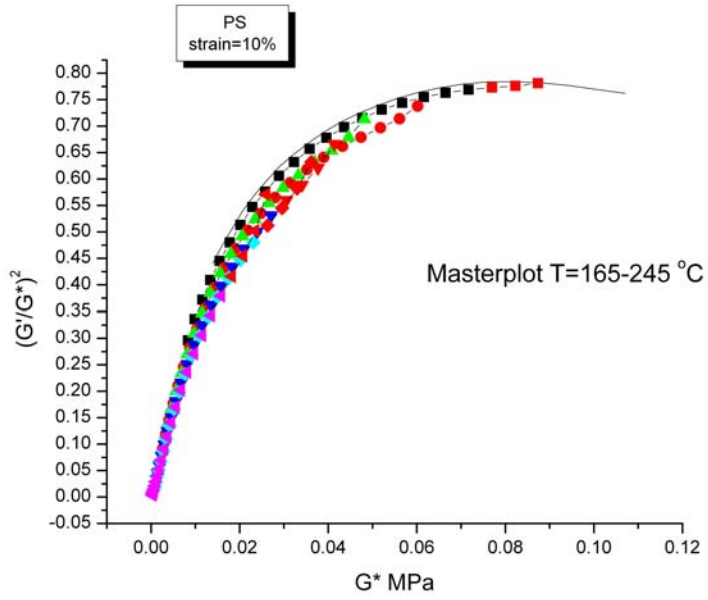

Fig. 29a

PS. Same data as in Fig. 1 but plotted against G* instead of log ω. To be compared with Figs 24a(PMMA), Fig. 25a (PC), Fig. 28a and Fig. 30a**.**

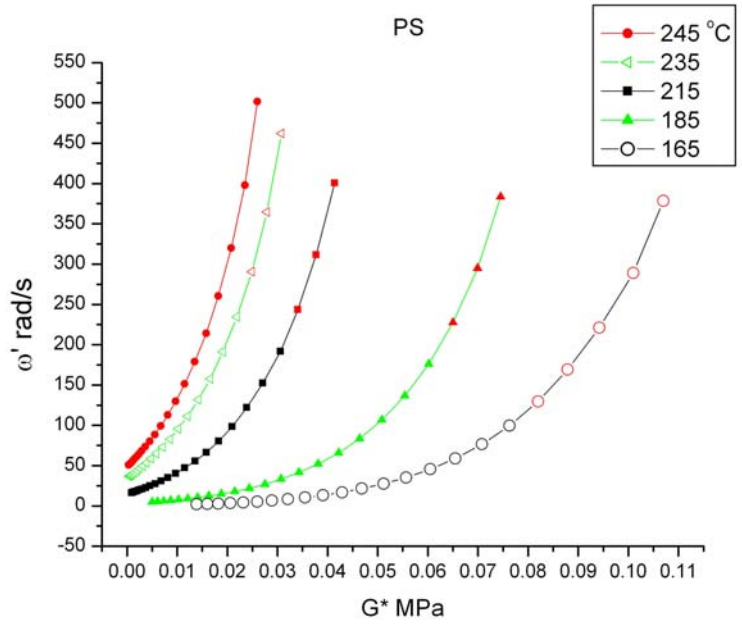

Fig. 29b

Variation of the network dynamic frequency ω' with G* at various temperatures for PS. Compare with Fig. 27a for PMMA. These curves can be fitted by Eqs. 11-14 to determine ω'_o (T), k, G^*_1

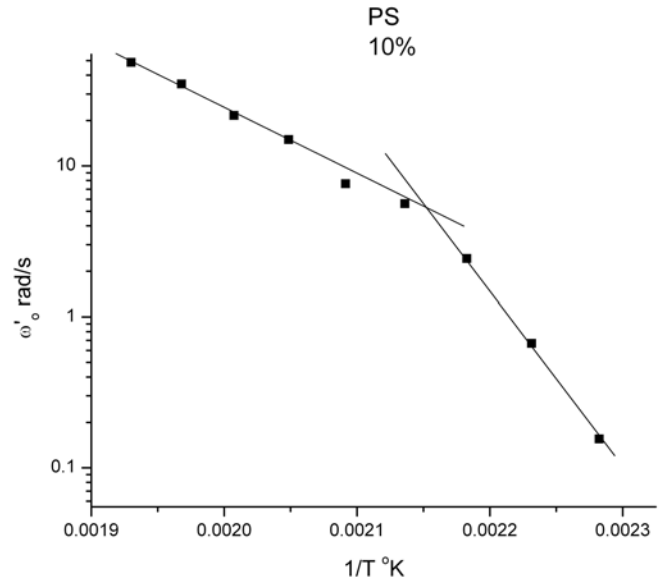

Fig. 29c

Temperature dependence of ω'_o for the PS of Fig. 1 showing 2 different Eyring mechanisms across a transition, as it is also observed for PC in Fig. 25c. Below T_{II}: Intercept=26.57192;Slope=-11993.617. Above T_{II}: Intercept=10.2257;Slope=-4420.72559

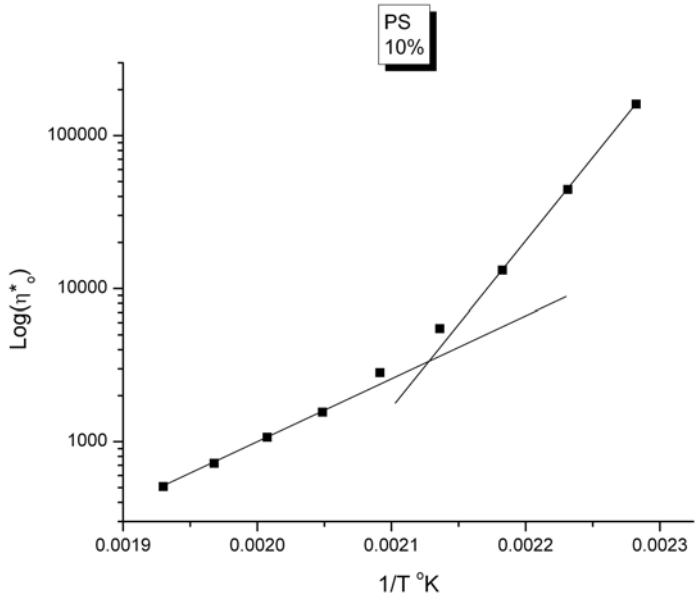

Fig. 29d

Temperature dependence of η^*_o for the PS of Fig. 1 showing 2 different Eyring mechanisms across a transition, as it is also observed for PC in Fig. 25d. Below T_{II}: Intercept=-19.69531; Slope=10,910.375. Above T_{II}: Intercept=-5.26479; Slope=4129.5466

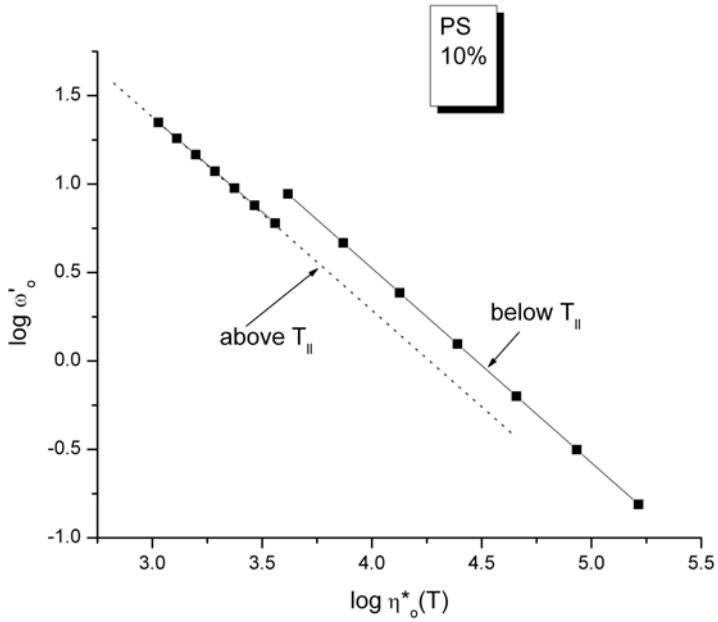

Fig. 29e

Plot of $\omega'_o(T)$ *vs* $\eta^*_o(T)$. For $T > T_{II}$: Intercept=4.58968; Slope=-1.0708. For $T < T_{II}$: Intercept=4.92115;Slope=-1.0993.

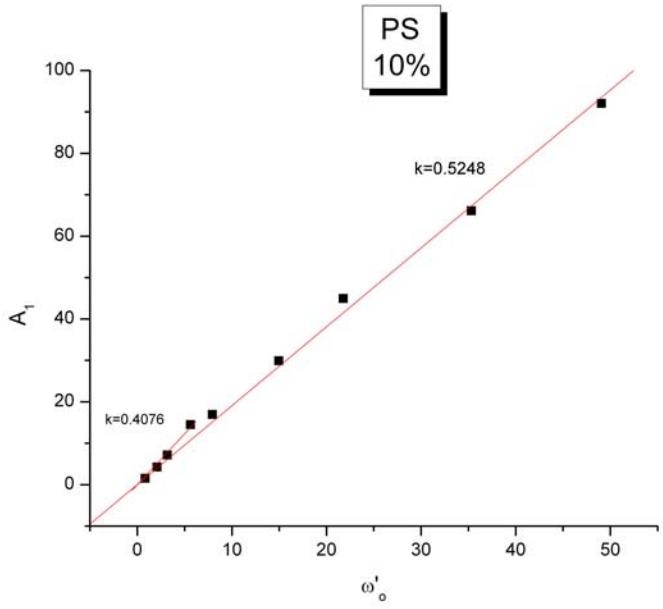

Fig. 29f

Determination of the melt k factor (ω'_o/A_1 of Eqs. 11-12) for the 2 temperature regimes observed in Figs. 29b and c. The 2 drawn straight lines pass through the origin; their slope determines k. if only one line was assumed to pass through all the points, k would be equal to 0.5171, but the first 4 points, corresponding to the lowest T, would appear to be systematically slightly below the line.

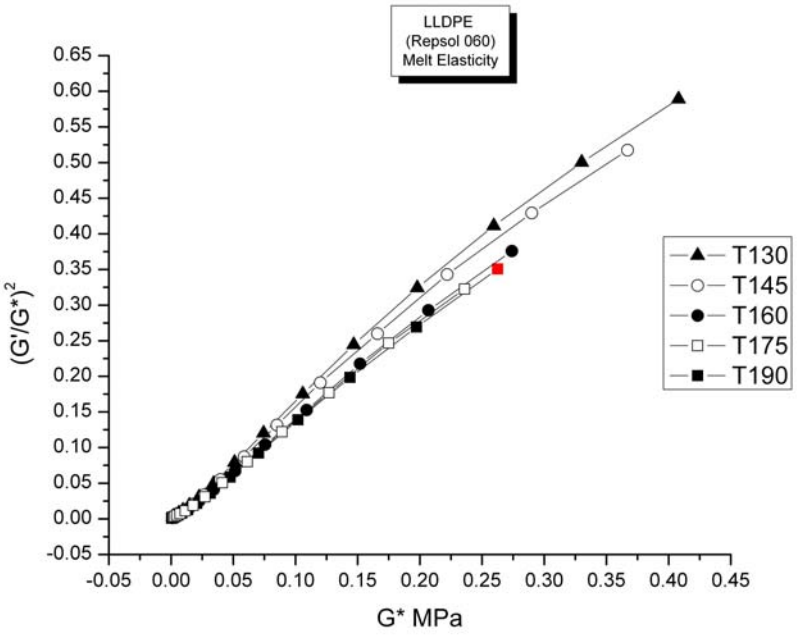

Fig. 30a

Melt Elasticity of a LLDPE (M_w=96,670, M_n=36,870, M_z=224,500)- Repsol 060- at temperatures varying from T=130 ^{o}C to 190 ^{o}C (Crystallization on cooling starts at T=105.15^{o}C, as determined by DSC).

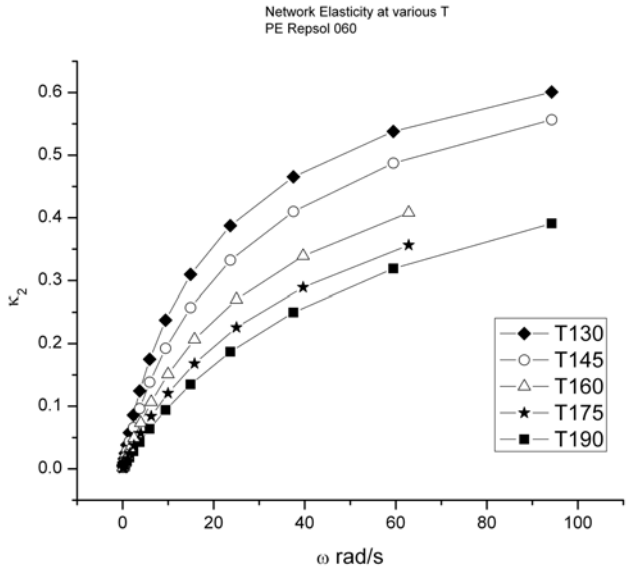

Fig. 30b

Network elasticity, χ_2, plotted against ω, at various temperatures. The values of χ_2 are extracted from the data of Fig. 30a according to the new analysis proposed in this paper (e.g. Fig.6).

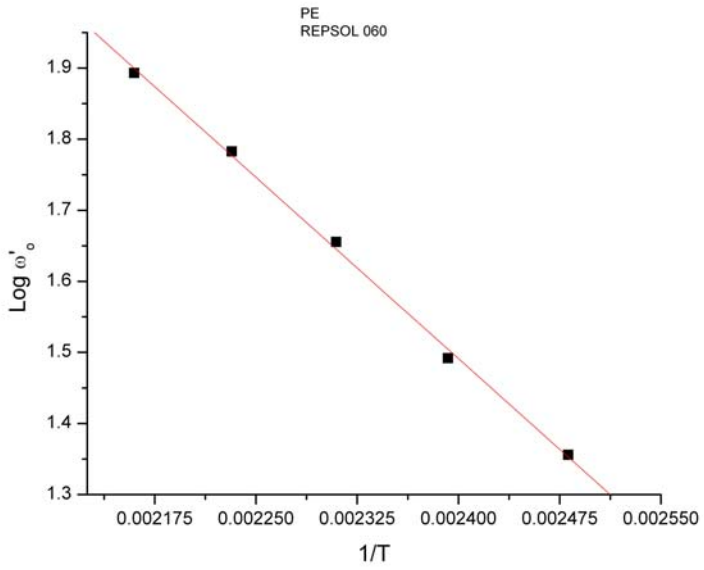

Fig. 30c

Temperature dependence of ω'_o of the LLDPE of Fig. 30a showing a single Arrhenius behavior in this temperature range. Intercept=5.5736; Slope=-1701.

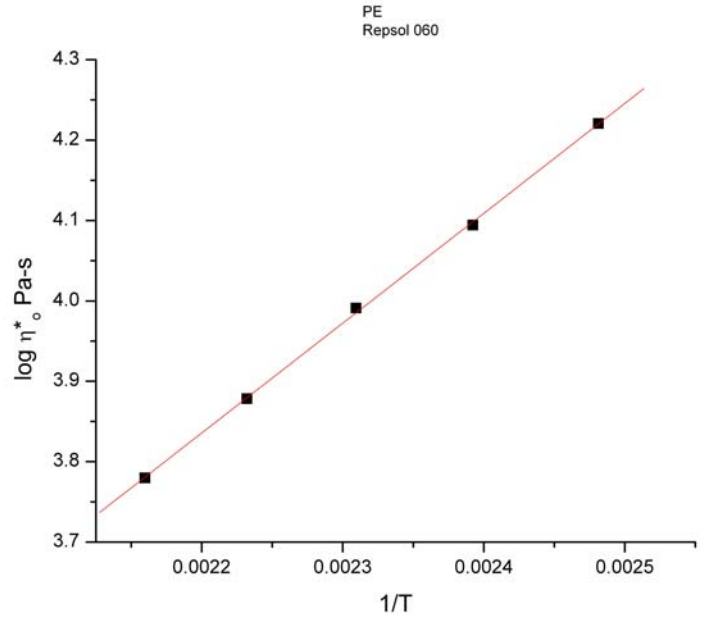

Fig. 30d

Temperature dependence of η^*_o of the LLDPE of Fig. 30a showing a single Arrhenius behavior in this temperature range. η^*_o is determined from Eq. 9. Intercept=0.82972;Slope=1366.3. The elimination of 1/T between the equations of $\eta^*_o(T)$ and $\omega'_o(T)$ gives a straight line for log ω'_o *vs* log η^*_o with intercept 6.6195 and slope 1.24817.

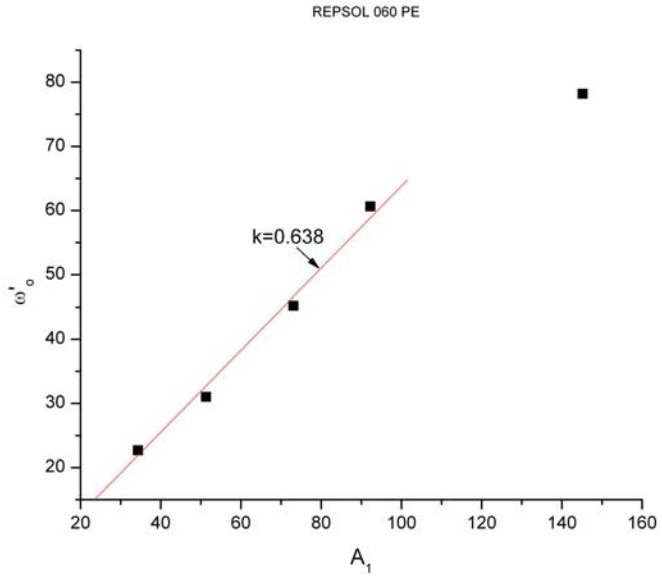

Fig. 30e

Determination of the melt k factor for LLDPE in this temperature range. k=0.638 from T=130 °C to 175 °C. The straight line in the figure goes through the origin**.**

The universal character of the results is shown in Figs. 28 through 30 applicable to 3 polymers, PETG (Figs 28a and b), PS (Figs 29 a through f), and LLDPE (Figs 30a through e). Some common features characterize all the $(G'/G^*)^2$ *vs* G* curves or the $(G'/G^*)^2$ *vs* log ω curves in the linear viscoelastic range:

- the melt elasticity, $(G'/G^*)^2$, increases with ω until a maximum value is reached (this corresponds to the minimum of tan δ). The cross-over point, found for $(G'/G^*)^2 = 0.5$, corresponds to an increase of ω and G* when T increases, and the values of ω and G* at the maximum of $(G'/G^*)^2$ also vary with T, similarly, but not identically, to the variation of ω_x and G^*_x with T.
- G*(ω) continues to increase with ω beyond the maximum of $(G'/G^*)^2$. It is important to make that point clear because, as we shall see in the next section, the effect of strain, γ, is quite different, leading to a different phenomenon than shear-thinning called "strain softening".

The coupling of the effect of ω and γ is unique to specific polymers, for instance it is quite different for PETG and PMMA, or PS and LLDPE, leading to a variety of response, rich in melt processing applications, specific to the chemical nature of the interactions in the polymer melts. The complexity of the coupled influence of frequency and strain on the viscoelastic behavior is shown even at low strain for certain polymers, such as PETG in Fig. 28b, or for the top curve (squares) of Fig. 2c. This is displayed by a visible upturn in the variation of $(G'/G^*)^2$ vs G^*, which might be explained as either a decrease of the increase of G^*, the early sign of strain softening, or, alternatively, by an increase of the variation of $(G'/G^*)^2$, essentially due to an increase of the cooperativity in the entanglement network. In the first scenario, which is explored in depth in the next section, strain softening is assumed to involve the increased participation of the κ_1 term in the deformation process by compensation, and κ_2 becomes less activated, eventually decreases as less strands of the phase-line network are required to participate. This solution is in clear contrast with the other alternative mechanism suggested which, on the contrary increases κ_2.

In our study of polymer melt rheology it is crucial to understand which mechanism of interactive motion results from the increase of ω or γ or $\omega\gamma$ (strain rate). (Refer to the discussion regarding Fig. 13). The importance of characterizing the various mechanisms of deformation associated with the coupling between strain softening and shear-thinning resulting, at higher stress, in melt yielding, is essential to determine which processing conditions result in sensitizing the melt to a durable orientation effect ("sustained orientation"). The involvement of the κ_1 term in the process of deformation is, we suggest, a required condition to enable the preservation of the viscosity reduction into pellets.

Other universal features of the rheological response characterize and describe shear-thinning: scaling viscosity by the Newtonian value, η^*_o, and ω' by ω'_o results in a single mastercurve for all temperatures (Eq. 15). Similarly, plots of (G^*/G^*_1) *vs* ω'/ω'_o revert to a single curve when T varies, which is due to the constancy of k with temperature in Eq. 15. The variation of ω'_o with T is best modeled with an Arrhenius relationship, even within temperature ranges where the behavior is traditionally described by a WLF fit. It appears that a pair of Arrhenius lines, instead of a continuous Vogel-Fulcher curve, applies much better to the temperature dependence of ω'_o.

This is clearly true for PMMA, for PS, for PC, and for many other classical amorphous melts submitted to our analysis, for which a WLF equation applies well to the description of the shift factors. The use of ω' instead of ω to shift the curves is the determining factor which reveals the two activated mechanisms of deformation across the T_{ll} transition, which, itself, becomes clearly defined, leaving very little ambiguity about its existence.

All the above conclusions apply to the deformation of the phase-line network, according to Eq. 15. In such a condition, the response of the material to the deformation is controlled by ω', i.e. by the network elasticity κ_2 (see Eq. 5).

We now study in the next section the effect of strain, which introduces a complexity due to the participation of the core phase, the κ_1 phase, in the cooperative bond re-organization process. As we shall see, dynamic rheological experiments conducted in the non-linear viscoelastic regime, i.e. at higher strain, can be analyzed by the same method proposed in the previous sections of this paper dealing with linear viscoelasticity.

F Effect of Strain %.

As a way to introduce the effect of strain on the viscoelastic behavior of a melt, let us first look at Fig. 31a which provides a set of frequency sweeps obtained at the same temperature but variable strain. Fig. 31a is a plot on log-log axes of complex viscosity, $\eta^*(\omega)$, vs ω, for the various strains (2% to 30%). The polymer is PMMA, the temperature is 230 ^oC. The strain is maintained constant at a given imposed value during the frequency sweep (Fig. 31b shows that this is true, except for a couple of ω values, for each strain).

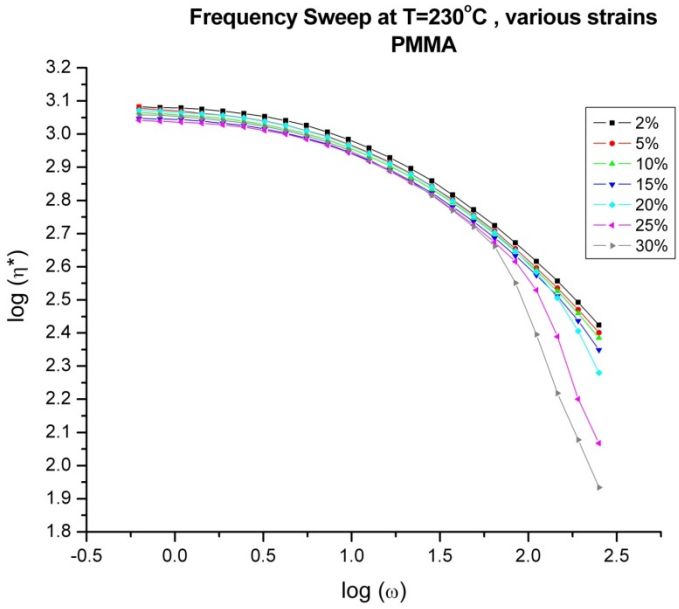

Fig. 31a

Plot of complex viscosity, $\eta^*(\omega)$, vs ω, for frequency sweeps done at various strains (2% to 30%). The polymer is PMMA, the temperature is 230 ^oC.

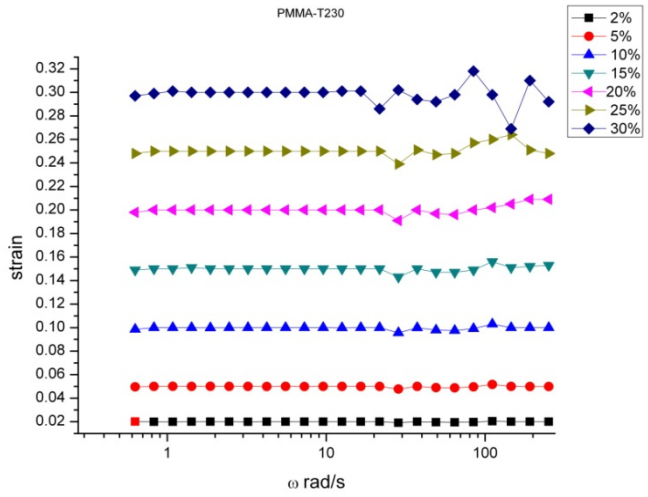

Fig. 31b

Plot of the strain vs ω for the frequency sweeps of Fig. 31a. The rheometer is stress controlled responding to a constant commanded strain.

The experimental procedure is as follows:

- molded disk is originally ~ 2 mm in thickness.
- the disk is dried at 60^{o}C for 17h in a vacuum oven. Test under N_2
- Frequency sweep from 0.1 to 40 Hz. Set amplitude to 2%.
- Start heating to 230^{o}C for 3 min,
- Make gap of 1.6 mm. Trim the rim to remove excess melt.
- Re-heat at 230 ^{o}C, wait for temperature to stabilize (approx. 2 min)
- Vary the frequency ω during the frequency sweep test in 23 steps.
- Change disk, perform same as above but increase amplitude to 5%.
- Repeat using 7 different disks changing amplitude for each disk (Fig. 31b).
- Repeat at a different temperature.

Fig. 31a clearly shows that strain affects the dynamic viscosity behavior, especially at higher ω values. By operating at higher strain, the decrease of viscosity with ω (shear-thinning) seems to be boosted, in other words the pseudo-plasticity of the melt appears to be very sensitive to strain (the pseudo-plasticity is the slope of the curves in Fig. 31a). We analyze this

phenomenon in details in Figs 31c to i. In these figures, the same data are looked at differently, by defining the plotting variables differently, or by changing what variable is plotted against what, using linear or logarithmic scale, etc. The reason for doing so is to emphasize, from the start of this analysis of non-linear viscoelasticity, that our well defined ideas coming from linear viscoelasticity, such as plotting dynamic data as in Fig. 31a, should be refined or revised.

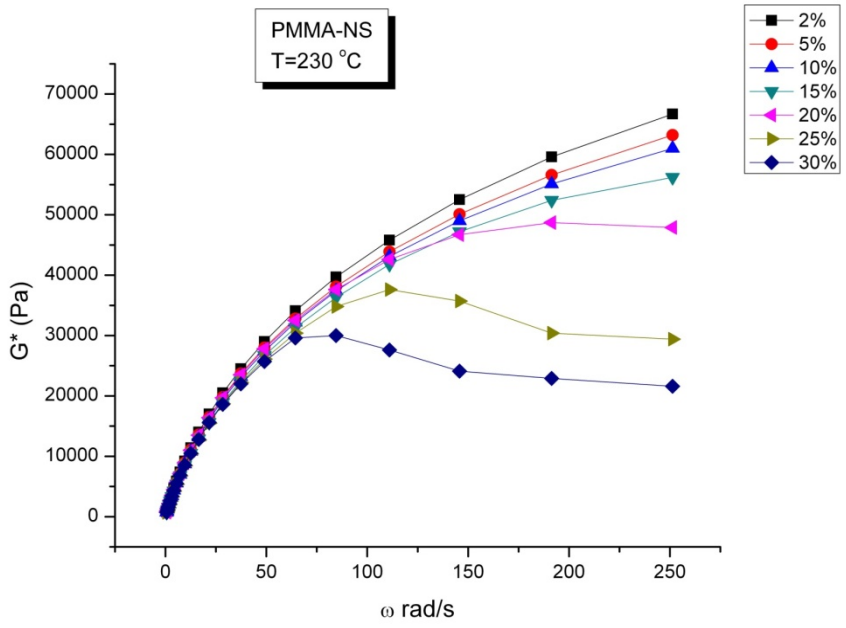

Fig. 31c

G* plotted vs ω, on linear scales for the data of Fig. 31a.

Fig. 31c is a re-plot of Fig. 31a showing the complex modulus, G*, plotted against the radial frequency, ω, on linear scales. The perspective is quite different, with an emphasis on the gradual effect of strain on the modulus, softening the modulus as strain increases, even as early as for the 5% strain (with respect to the 2% curve) and the appearance of a maximum at higher strain (20%, 25%,30% strain) beyond which G*(ω) remains approximately constant. This behavior is not typical of shear-thinning, which brings us to question our earlier qualification of the further decrease of viscosity at higher strain seen in Fig. 31a as "strain induced boosted shear-thinning". Fig. 31c supports the statement that strain softening might be (or become, at

high ω) a different mechanism of deformation than shear-thinning. Figure 31d is a plot of $(G'/G^*)^2$ vs ω for all the strains.

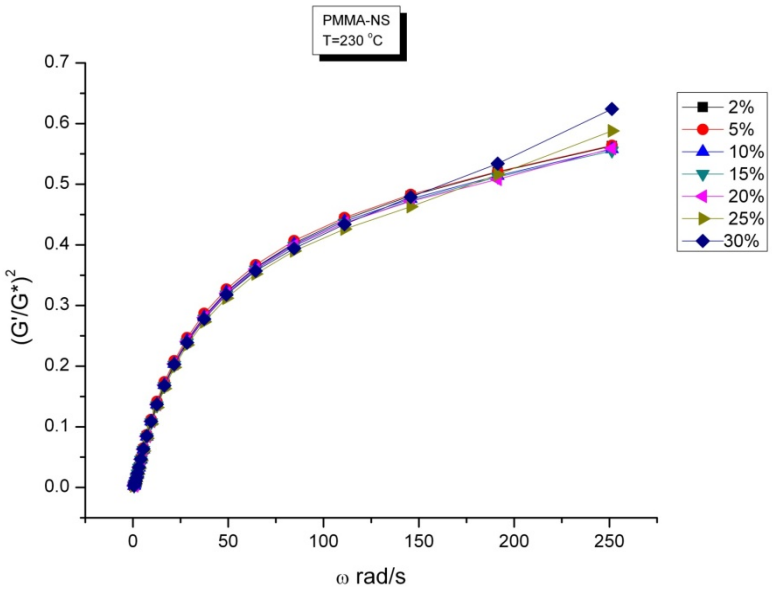

Fig. 31d

$(G'/G^*)^2$ vs ω for all strains for the data of Fig. 31a.

All curves seem to superpose onto the 2% curve, at least up to ω=100 rad/s, yet, beyond that, there seems to be a clear increase of the melt stored energy, visible by an upturn mostly observed for γ=25% and 30%. The mechanism of shear-thinning, by increasing the number of activated strands by ω, remains practically unaltered by strain, at first glance. It is worth noting, in passing, that any discounting of our results based on a possible melt fracture or surface artifact [24,25] would need to explain the continuous elasticity increase with ω observed in Fig. 31d. The reader is referred to the detailed discussion on this subject found in Part II of this series [2].

In Fig. 31e the stress is plotted against ω on linear scales.

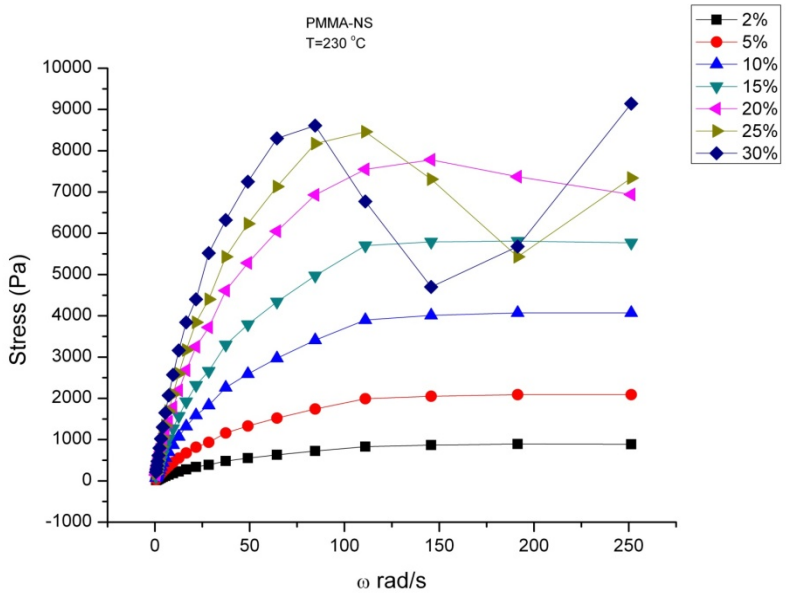

Fig. 31e

Stress (Pa) vs ω for the data of Fig. 31a.

This figure should be redundant with Fig. 31c in the linear range of viscoelasticity, since the modulus G*, the ratio of stress and strain, would normalize all the curves of Fig. 31e into a single curve in Fig. 31c. The fact that there are many curves in Fig. 31c, and not just one, makes us question whether modulus is the proper variable to follow when studying non-linearity induced by strain. This seems to be especially true for PMMA at this temperature when one sees that even at γ=5% or 10% , the effect of strain is quite visibly influencing the viscoelasticity of the melt (Fig. 31c). In Fig. 31d the effect of increasing ω is quite similar for γ= 2% to 15%: a plateau is reached after an initial increase of the value of the stress due to an increase of ω, and the value of the stress at the plateau increases with strain. For the 3 higher strains, 20-30%, the plateau value seems to have become unstable and the stress decreases, showing a minimum value before it starts to rise again at the highest frequencies (200-250 rad/s).

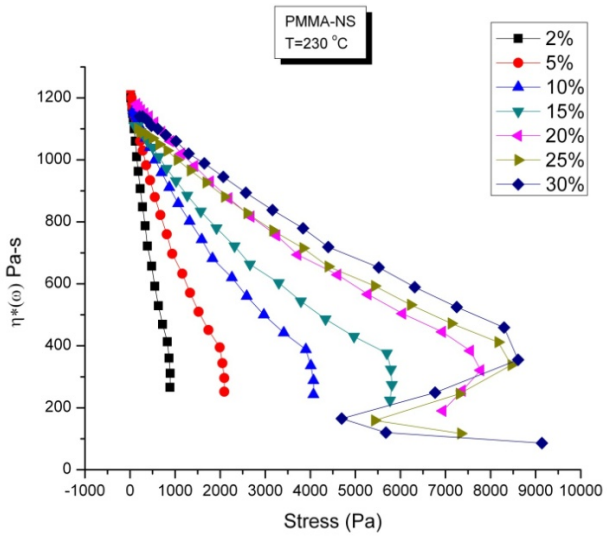

Fig. 31f

η*(ω) in Pa-s *vs* stress (Pa) for the data of Fig. 31a.

Figure 31f is another attempt to search for the correct variables to analyze the effect of strain on the rheological behavior; it is a plot of complex viscosity vs stress, using linear scales on both axes. This plot points to several interesting features unseen before (Figs 31a to e). It appears clear that the Newtonian viscosity is the same for all strains, approximately 1150 ± 50 Pa-s. Viscosity decays with stress, almost exponentially (actually 2 exponentials do a very good curvefitting job), the fastest drop of viscosity occurring for the lowest strain (2%). The mechanism leading to the exponential decay of viscosity is interrupted when viscosity reaches the same value, approximately 350 Pa-s, regardless of the strain, beyond which the stress either remains constant (γ<20%) or starts to decrease (γ=20%,25%,30%). Stress increases again, quite significantly, for both γ=25% and 30%, when the viscosity has decreased to 150 Pa-s. Fig. 31b, however, tells us that the strain was varying in this zone, the rheometer being unable to maintain it perfectly constant and equal to the commanded strain, and, for that reason, some caution in this range is justified.

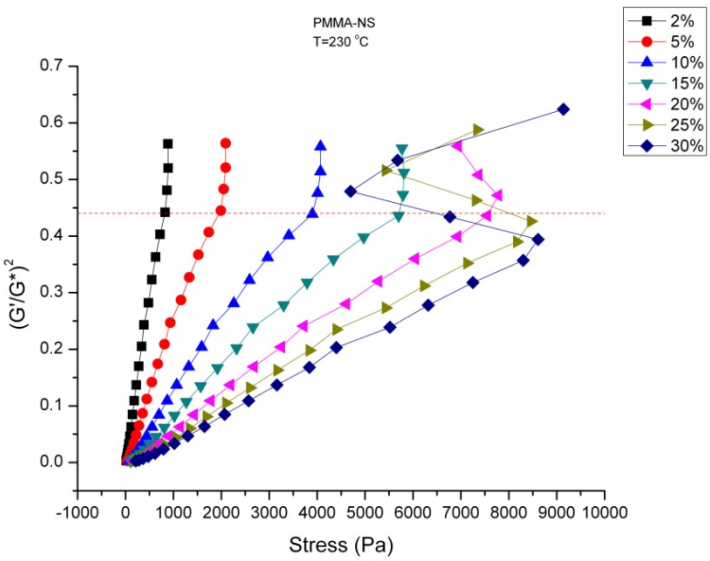

Fig. 31g

$(G'/G^*)^2$ vs stress for the data of Fig. 31a.

Fig. 31g is a plot of $(G'/G^*)^2$ against the stress for all strains. This plot is very similar, in many ways, to the previous figure, showing that the change from a shear-thinning mechanism occurs for the same value of $(G'/G^*)^2 = 0.44$ regardless of strain, the stress remaining constant beyond that, even as the stored elastic energy continues to rise. The analogy with yielding and "cold drawing" comes to mind. From what we have studied in an earlier section, we know that the mechanism of shear-thinning at low strain, described by the increase of ω' by the stress in Eq. (14), is disturbed at higher strain energy by the deformation of the elastic disentanglement network which induces a decrease of $(G'/G^*)^2$ (Fig. 21). This appears to still be true at higher strain, yet with an interesting difference: the stress "yields" before $(G'/G^*)^2$ does, the number of activated strands, when larger strain come into play. This may be a crucial observation that differentiates the role played by ω and γ in determining the stability of the entanglement network and its ability to deform plastically.

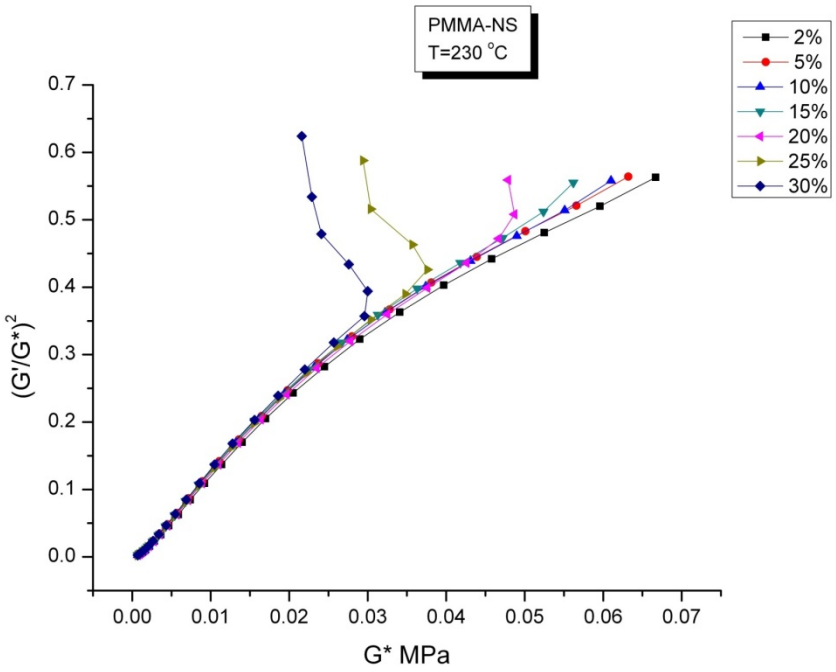

Fig. 31h

Masterplot of $(G'/G^*)^2$ vs G* for all strain using the data of Fig. 31a.

Fig. 31h shows that by plotting $(G'/G^*)^2$ vs G* at all strains we obtain confirmation that strain softening (observed as a decrease of the modulus with an increase of strain) corresponds to a departure from the basic shear-thinning behavior. As we shall see, the presence of two interlocked viscoelastic phases, as sketched in Fig. 4, which we saw explains shear-thinning by the variation of ω' with G*, is also responsible for the manifestation of strain softening, simply explained by the triggering of the participation of the core phase in the overall strain production mechanism, releasing the elastic network κ_2 at the expense of κ_1. An important aspect of the increased cooperation between the conformers, triggered by ω and strain, is shown in Fig. 31i, which shows the normal force plotted against stress, for all strains. In the linear viscoelastic regime (γ=2%), the frequency sweep does not generate much normal force, just a few grams. As strain increases, normal force increases like γ^2, even beyond the plateau reached by the stress.

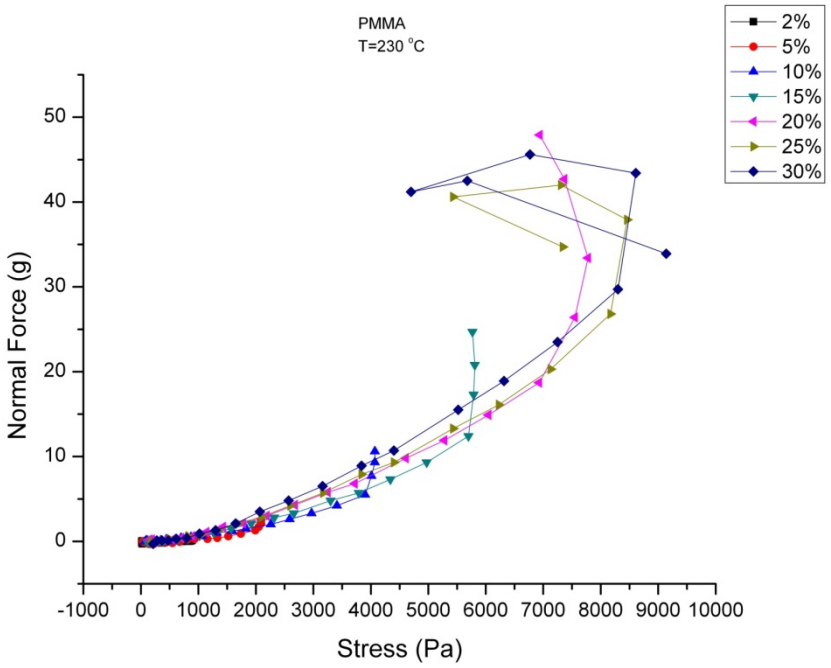

Fig. 31i

Normal force (in g) vs stress at all strains for the data of Fig. 31a.

The normal force can actually "yield" after the stress does, like $(G'/G^*)^2$, showing that it is a property reflecting the stability of the network of strands, unlike stress which is a more complex parameter. For instance, in Fig. 31i, the shear stress plateaus at 5,700 Pa for γ=15%, yet the normal force continues to increase from 12 g to 25 g without any sign of decrease. For γ=20%, the shear stress yields but not the normal force. For 25% and 30% the normal force yields just after the shear stress, i.e. for a higher ω. Once sees in Fig. 31i that the network cannot produce, under the specified conditions, more than approximately 40-45 grams of normal force, which corresponds to a stress of ~900 Pa, approximately 1/10 of the value of the shear stress at its maximum. These numbers can change a great deal, as temperature is varied. As strain increases to amplitudes much greater than 30% (not shown), which makes the core-phase response dominate the strain requirement, the normal stress produced by the network can grow by an order of magnitude before it "yields". The same thing is true if the melt temperature is lowered. Hence, the magnitude of the stresses is not what makes the entanglement network becomes unstable.

Figures 32a to c focus on the viscoelastic properties of the melt (G',G", G* etc.) at constant ω=251 rad/s, various strains. We simply follow the variation of the moduli G' and G" for the last point of the frequency sweeps in Fig. 31a.

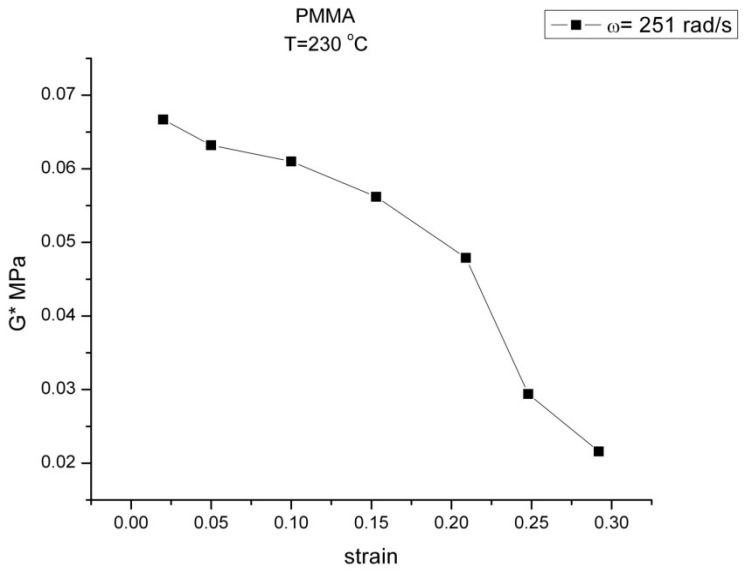

Fig. 32a

G* vs strain (2-30%) for ω=251 rad/s. Data taken from Fig. 31a.

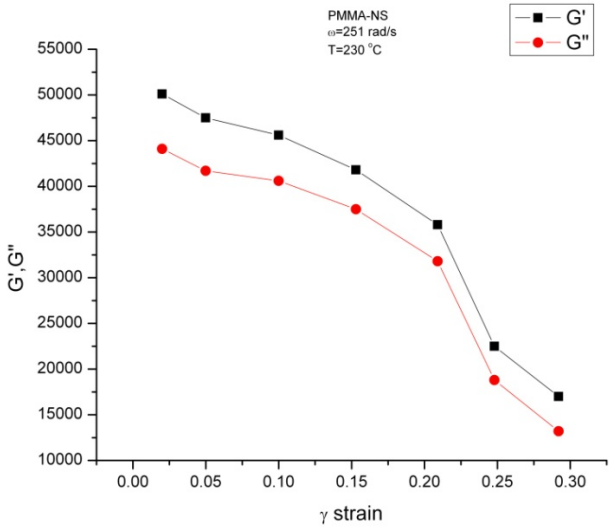

Fig. 32b

G' and G" vs strain (2-30%) for ω=251 rad/s. Data taken from Fig. 31a.

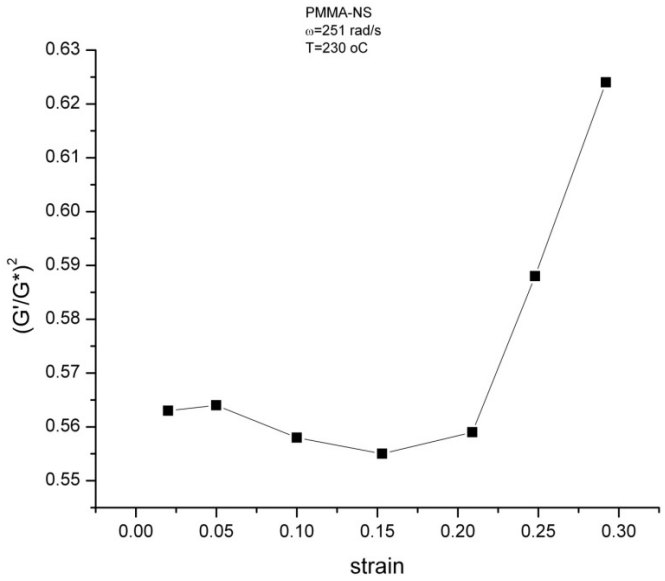

Fig. 32c

$(G'/G^*)^2$ vs strain (2-30%) for ω=251 rad/s. Data taken from Fig.31a.

The variation of G* vs strain is shown in Fig. 32a, G' and G" vs γ are plotted in Fig. 32b and Fig. 32c shows the variation of $(G'/G^*)^2$ as a function of the increasing strain. The first two plots clearly display the manifestations of strain softening, the modulus decreasing by more than a factor of 3 when strain increases from 5% to 30% (Fig. 32a). G' and G" decrease with strain identically (Fig. 32b), whereas the variation of $(G'/G^*)^2$ with strain (Fig. 32c) suggests a change of behavior after γ=20%. For the first 5 points (γ<25%), the value of $(G'/G^*)^2$ remains approximately constant during strain softening at this relatively high frequency (ω=251 rad/s). The resulting modulus decrease is more or less proportional to the strain increase (Fig. 32a and b), but, for the last two strains (25% and 30%), there is a further drop of modulus, as $(G'/G^*)^2$ sharply increases from 0.56 to 0.625. This behavior might seem contradictory: how can the melt become more elastic and, at the same time, become softer? As shown below, the explanation we suggest is that κ_1 takes over for κ_2 in the split of the melt elasticity (see Eq. 4), the core-phase contribution to the production of strain becoming the dominant mechanism. As already mentioned before and in Part II [2], the increase of the melt elasticity with strain (Fig. 32c), as strain softening occurs (Figs 32a and b) is not compatible with an explanation based on surface

artifacts or edge melt fracture [24,25]. Besides, the strain is too small in our experiments to trigger such experimental artifacts.

Figure 33 defines what we call “dynamic strain softening factors”, h’ and h”, which apply in this figure to 25% strain, the reference curve being 2%. h’ and h” are the respective ratio of G’(ω,25%) to G’(ω,2%) on one hand, and G”(ω,25%) to G”(ω,2%) on the other hand. In other words, the moduli at strain 25% are normalized by the values obtained under linear viscoelastic conditions, for each ω. The melt is PMMA at 230 ^{o}C. In the following figures, we study extensively this polymer, presenting results at various temperatures, either 215 ^{o}C, 225 ^{o}C or 230 ^{o}C. The general trend for h’(ω) and h”(ω) is to be lower than 1 and to decrease with ω in a “transition-like” fashion, the value of ω at the “transition” being here ~ 150 rad/s. The second observation is that h’ is systematically lower than h”, except perhaps at high ω values (for ω=250 in Fig. 33).

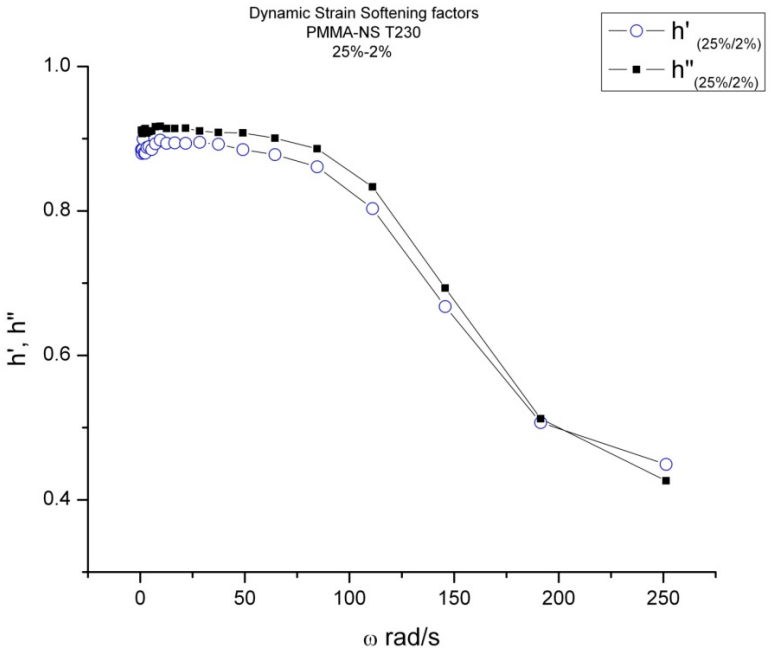

Fig. 33

Variation of the dynamic strain softening factors h’, h” versus ω for a strain of 25% with reference strain 2%.

It is also interesting to note that at low ω, h’ and h’ are equal to 0.9 and only slightly decrease until ω is approximately 100 rad/s, beyond which the decrease to 0.4 occurs steeply.

The strain softening factors are not the same for the elastic and loss moduli and vary with frequency. We study the influence of strain on the strain factor h* in Fig. 34. In this graph, the complex viscosity was chosen to determine the strain factor, instead of G' or G", so h* is the ratio of $\eta^*(\gamma\%,\omega)/\eta^*(2\%,\omega)$ with γ% varying between 5 and 30%. The main effect of increasing the strain, γ, is to lower the value of ω for the "transition" and the value of h* corresponding to what appears to be a plateau, i.e. the maximum softening value obtainable.

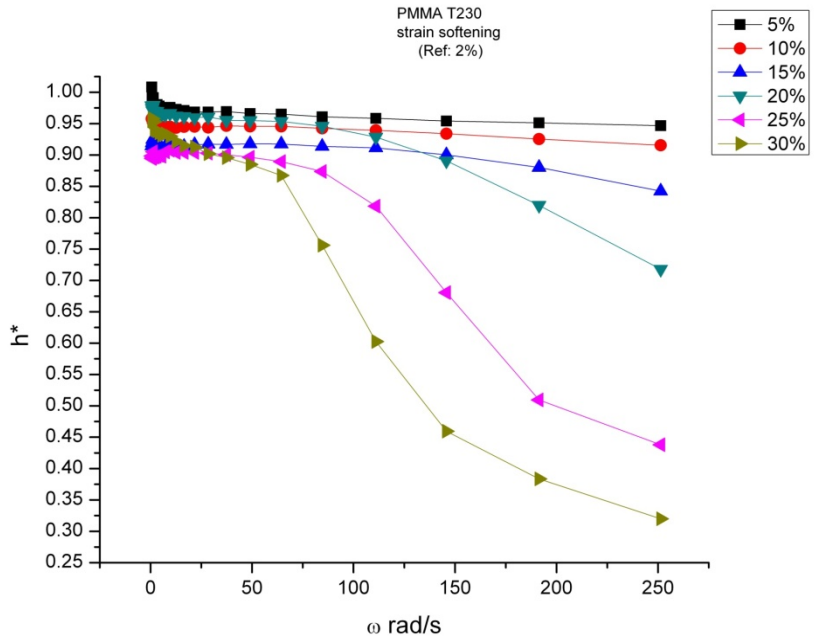

Fig. 34

Masterplot for PMMA of the strain softening factor h* vs ω at T=230 ^{o}C, all strains. h* is defined by the ratio of $\eta^*(\omega)$ at γ% and 2%.

In Fig. 34, one sees that h* remains constant for 5% and 10% strain, starts to curve down at ω~100 rad/s for γ=15% , and that this effect is amplified for the higher strains, the onset for the drop off of h* occurring at ω=25 rad/s for γ=30%. The maximum strain softening factor seems to be close to 0.4 for γ=25% and 0. 3 for γ=30%, showing that small values of strain are capable of producing very large strain softening factors, which translates to a very large reduction of viscosity beyond what is provided by shear-thinning. This is true for this PMMA melt but might be different for other polymers, as we shall mention later, for instance in the case of polypropylene. Another observation in Fig. 34 concerns the initial value of h* at low ω, which is not 1, except for the 5% curve, and which appears to slightly decrease with strain, e.g. it is 0.98

for 5%, 0.93 for 15%, and 0.90 for 25%. There is some scatter in the data (0.97 for 20%, for example), perhaps due to the fact that we change the sample for each frequency sweep done, yet it appears that strain may have a slight effect on the Newtonian viscosity value.

Figure 35 is another example of the variation of the dynamic strain softening factor with frequency. The polymer is Polystyrene at 235 ^{o}C studied under 100% strain for a frequency sweep between 0.1 and 6.28 rad/s. The reference frequency sweep curve was obtained for a strain of 5%.

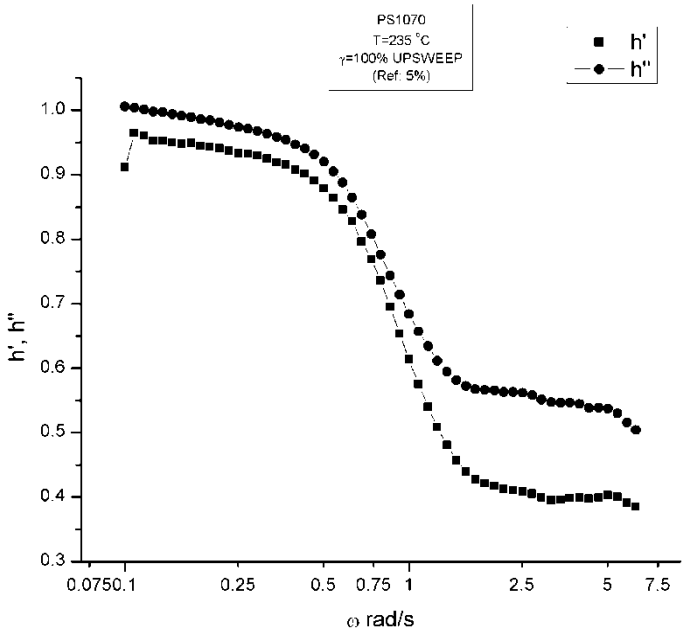

Fig. 35

Variation of the dynamic strain softening factors G'.G" with frequency for Polystyrene at 235 ^{o}C (Reference: 5% strain). The frequency sweeps the span 0.1 and 6.28 rad/s with γ=100%.

The same behavior as in Fig. 33 for PMMA is observed, with the "transition" observed for a very low ω~ 1 rad/s, due to the larger strain, and an amplified difference between h' and h", including in the plateau zone, 0.4 for h' (squares) and 0.55 for h"(dots). The last few points, from ω=5 to 6.28 rad/s, correspond to a further decrease of the moduli which may indicate another change of behavior after the plateau, which we associate with the stability of κ_1 , see later. Also note in Fig. 35 that h' does not cross h" at higher ω, unlike the behavior observed in Fig. 33. The significant difference between h' (ω) and h"(ω), triggered by the large strain amplitude, is a characteristics

of the cooperative and dissipative aspect of the elastic network which we now propose to address in terms of the parameters we defined to describe linear viscoelasticity: ω', k, G^*_1, Δ_s, Δ_o, κ_1 and κ_2. It is not clear to this author how the current understanding of strain softening [26-31] can reconcile with the dissipative character of strain softening, as clearly evidenced by Fig. 35.

In the following graphs, we report the results of analysis of the frequency sweep data obtained at various strains following the procedure described in the first part of this paper. Fig. 36a is a plot of Δ_ω vs $(G'/G^*)^2$ for the frequency sweeps done with 5%, 20%,30% and 40% strain. The melt is the same PMMA as in Fig. 34 but the temperature is 225 ^oC. The network cohesive energy, Δ_ω, is calculated from the viscosity following Eq. 20 (we have dropped the H from ΔH_ω to shorten the notation). The unit is here converted to calories.

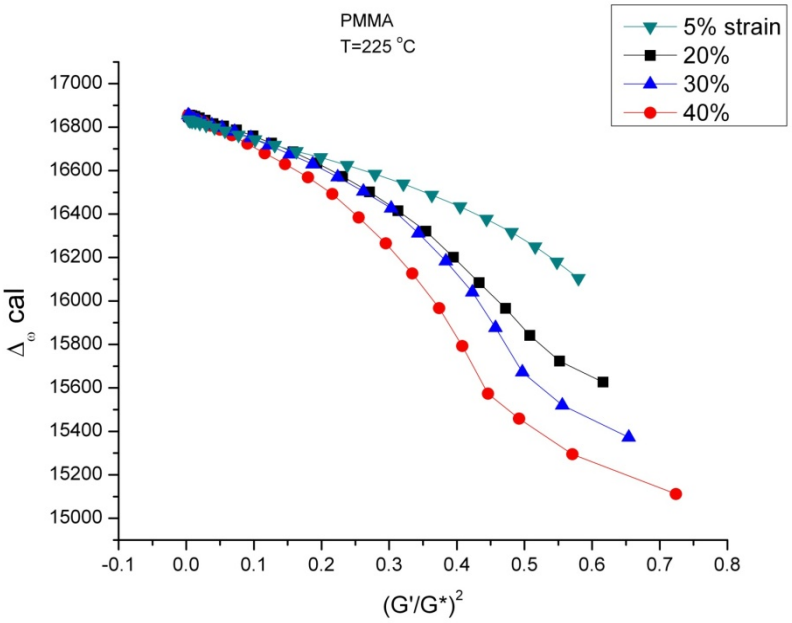

Fig.36a

Variation of the network cohesive energy, Δ_ω, with $(G'/G^*)^2$ for PMMA melt at T=225 ^oC, various strains.

One sees that the Newtonian value is approximately the same for all strains, equal to 16,864 cal. The same transition-like decrease observed in Fig. 34 for the strain softening factor h* is now observed for the variation of Δ_ω. In Fig. 36b, where the data are re-plotted as in Figs 21 and 23, in order to compute the slope Δ_s, it is observed that only the 5% curve is strictly linear

all the way up to the high ω values, the other data deviating somewhat beyond $\kappa=(G'/G^*)^2 \sim 0.3$, seemingly meaning that Δ_s would vary with κ at high strain, a typical non-linear effect explanation that we suggest is incorrect (see later).

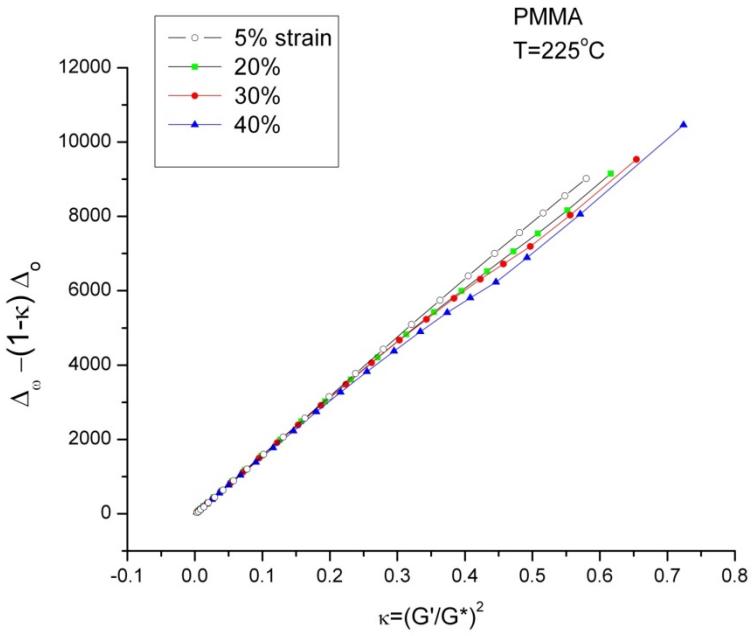

Fig. 36b.

Plot of the cohesive energy of the activated strands, $\Delta_o-(1-\kappa_2)\Delta_o$, *vs* the melt κ elasticity for γ=40%. Re-plotting the data of Fig. 36a according to Figs 21 and 23 to determine the value of Δ_S. Effect of the strain.

Figure 37a is a key figure to understand our new approach to non-linear viscoelasticity. It is a plot giving the split of $(G'/G^*)^2$ in terms of κ_1 and κ_2, as a function of ω, for γ= 40%. We have given an example of such an analysis in Fig. 6, for studying a PC melt in the linear range. The results are similar for a PMMA melt for γ=5% (not shown). In the linear range, the $\kappa_1=ELAS_1$ remains very small and the melt elasticity is controlled by the $\kappa_2=ELAS_2$ term. This is still the case in Fig. 37a, for γ=40%, but only in the low ω region (ω<12 rad/s). The κ_1 term (triangles) increases rapidly with ω, crosses the κ_2 curve (dots) and becomes the dominant process to store energy at high ω.

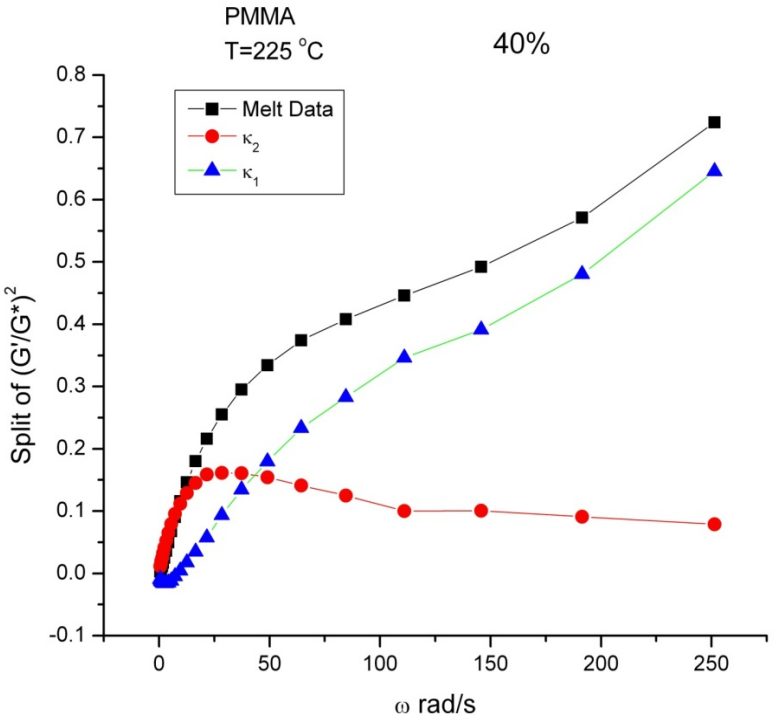

Fig. 37a.

Split of $(G'/G^*)^2$ vs ω into κ_1 and κ_2 for γ=40%. κ_1 and κ_2 are the core-phase and the phase-line elastic terms.

One sees, for instance, that for ω=251 rad/s more than 80% of the melt elasticity is produced by the κ_1 term. Now $G^*(\omega)$ is decreased because, according to Eq. 11, it is a function of ω', the phase-line network frequency, which increases as κ_2 decreases, pursuant to Eq. 5. In other words, strain softening is the consequence of the increased cooperativeness between the conformers, which leads to the activation of the conformers belonging to the core-phase to participate in the deformation process. Since there are more and more activated units to accommodate the strain deformation, there is less strain producing requirement on the κ_2 network, which starts to deactivate: this is perceived as the maximum for the κ_2 curve in Fig. 37a. Non-linear effects in polymer melts, triggered by strain, are therefore due to a phenomenon of compensation between the two dual phases, the core-phase and the entanglement phase, resulting in the activation of the core-phase.

Figure 37b analyzes the dynamic results at 40% in terms of melt cohesive energy.

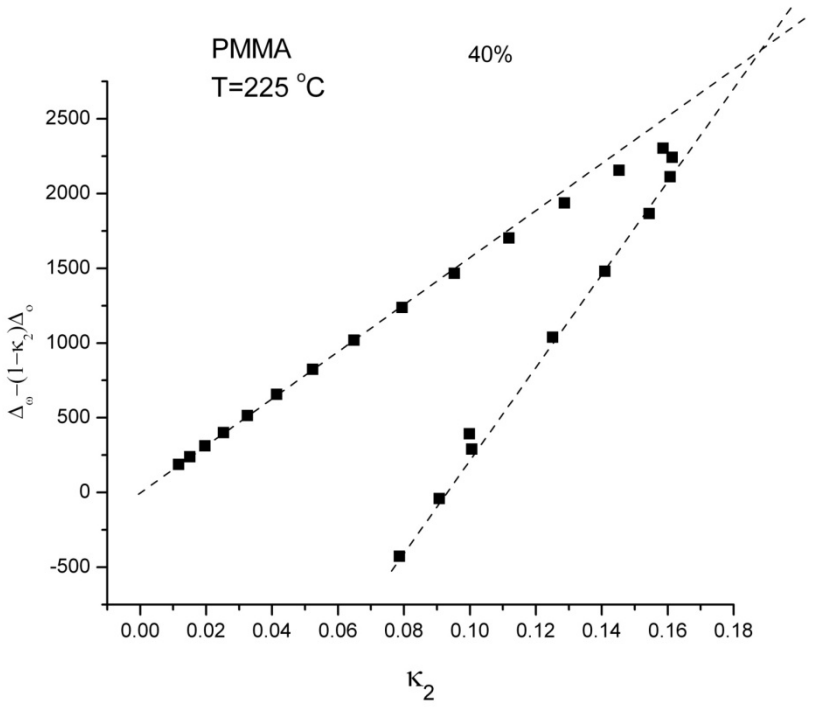

Fig. 37b

Plot of the cohesive energy of the activated strands, $\Delta_o-(1-\kappa_2)\Delta_o$, *vs* the network elasticity, κ_2 for γ=40%.

It is a plot of the cohesive energy of the activated strands, $\Delta_\omega-(1-\kappa_2)\Delta_o$, vs the network elasticity, κ_2. This figure is a re-plot of the 40% curve in Fig. 36b (the triangles), where κ_2 now replaces κ in the x and y-axes. The same procedure was discussed in the linear range, with respect to Fig. 20. Interestingly, Fig. 37b looks very much like Fig. 21, which shows the behavior of a melt (in the linear range) studied at a temperature such that $(G'/G^*)^2$ reaches its maximum value and beyond. Fig. 37c compares the situation for 5% and 40% using the same variables as in Fig. 37b. In Fig. 21, the melt past its maximum of κ is no longer in the terminal zone and is thereafter in the plateau region. This statement, in addition to Fig. 21, also applies to Fig. 37b, for the κ_2 phase, i.e. to the phase-lines network.

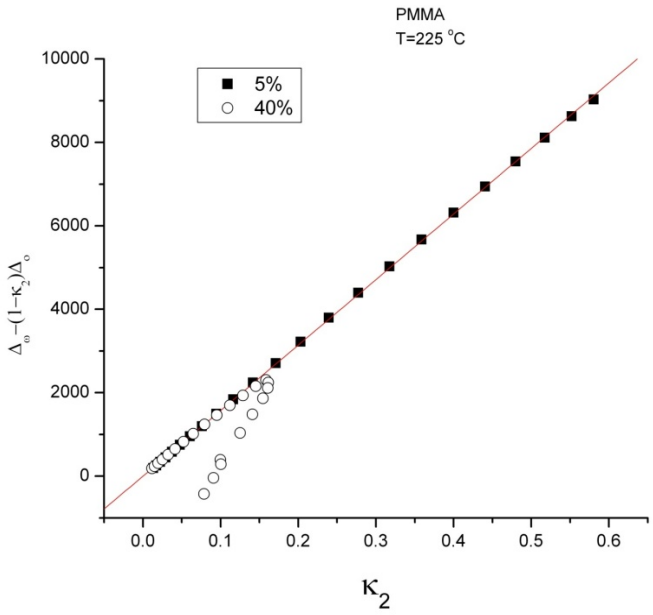

Fig. 37c

Comparison of the linear (5%) and non-linear (40%) strain effect using the same variables as in Fig. 37b and determination of Δ_s.

The only difference, it seems, between the 5% and the 40% curves in Fig. 37c is the very low value obtained for the maximum in the case of 40% strain. In the case of the 5% strain, the maximum is not even reached within the span studied at that temperature, What this means is that strain amplitude shortens the frequency range of the terminal zone of the κ_2 phase, making the plateau accessible for very low ω.

Figure 37d is the same type of plot as in Fig. 37b but applied to the κ_1 phase, which we call the core-phase. We use the same Δ_o to calculate the y-axis values, but κ_1 is now replacing κ_2 in the expressions on both axes. The straight line in Fig. 37d includes all points, up to the highest ω. and does not show any sign of maximum for either κ_1 or the number of activated strands for the core-phase, $\Delta_\omega-(1-\kappa_1)\Delta_o$. The mechanism of deformation in the core-phase appears to be similar to the one we described for the phase-lines (sequential stretch-relax), except that the κ_1 values remain below the expected maximum for κ_1, and thus the deformational behavior is expected to still be in the terminal region for that phase.

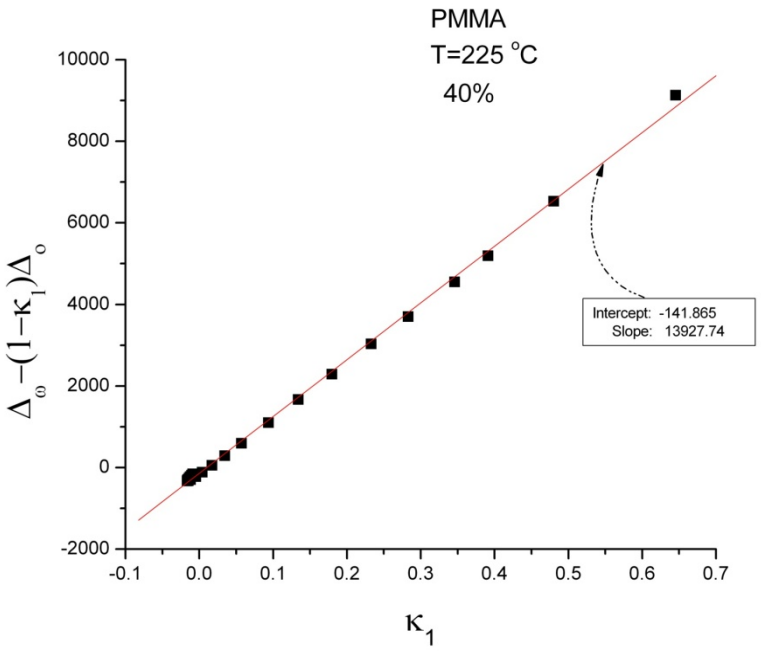

Fig. 37d

Plot of the number of activated strands for the core-phase, $\Delta_\omega-(1-\kappa_1)\Delta_o$ against κ_1. Same type of plot as in Fig. 37b but applied to the κ_1 phase, the core-phase.

All in all, one sees that the melt is deformed in an inhomogeneous way, viscoelastically speaking, since the κ_2 phase deforms in its plateau regime while the κ_1 phase is in the terminal zone. This is as if the melt had to maintain its cohesion despite of being sheared at different rates at different times. This is, perhaps, precisely the vision that emerges, that of a melt that is intermittently undergoing stretching and relaxation, with different frequencies and different sequential structures. In simple terms having some resonance from the musical world, if we correlate the viscoelastic state of a melt with the value of (T-Tα), we could say that the core and network phases synchronize a grand ensemble partition of the stored energy with two keyboards, one with the (T-Tα_1) scale and the other with the (T-Tα_2) scale, Tα_1 and Tα_2 being set by the value of the strain amplitude and the frequency. The result is that Δ_ω is coherently decreased proportionally to κ_1 and κ_2 and their relaxing states, (1-κ_1) and (1-κ_2). Are these sequential deformations identical for the two dual-phases; are the two viscoelastic relaxing states even identical? No, for both questions, as the answer is given by comparing Fig. 37c (the 5% κ_2-line) with Fig. 37d (the 40% κ_1-line). We assumed that Δ_o was the same for the two phases, but the

intercept of the straight line in Fig. 37d is -141.9, which is not zero. We can calculate a different Δ'_o for the core-phase, so that $\Delta_\omega-(1-\kappa_1)\Delta'_o$ vs κ_1 becomes a straight line going through the origin. This requires that the slope is also changed to Δ'_s. The solution is simply $\Delta'_o= (\Delta_o-141.9)=18542.2$ and $\Delta'_s= (13927.74-141.9)= 13,785.8$ for the data in Fig. 37d. The difference $(\Delta'_o-\Delta'_s)$ is equal to 2,937 cal which is 3.5 times greater than $(\Delta_o-\Delta_s) = 831$ cal for the κ_2 phase. The difference between these values is significant since it reflects the viscoelastic state difference between the two phases, i.e. it can be expressed as a function of $(T-T_\alpha)$ for each of the two dual phases. The details will be provided in a separate publication.

If Δ'_o is slightly different from Δ_o, it is likely that the Newtonian viscosity of each dual-phase is different, a conclusion that we expected to be true in view of the sweeping phase-line model sketched in Fig. 4, which would imply that the relaxing states reached upon activation are not the same for the κ_1-phase or the κ_2-phase. Note in Fig. 37c that the slope Δ_s for the lower branch of the line for 40% and the 5% line is the same. Strain is not changing the value of $(\Delta_o-\Delta_s)$ in each phase, it is changing the split of Δ_ω, the melt cohesive energy, between the κ_1 and the κ_2 components, and the value of κ_2 and of $(\Delta_\omega-(1-\kappa_2)\Delta_o$ for the reversal to occur. If we change the strain, all features remain the same in Fig. 37c, but the position of the reversal changes. We will see later that for the points located beyond the reversal, k=1 in Eq. 12. This means that there is full coherence between the activated strands (Eyring state) during their stretch-relaxation activation, whereas for $k<1$, i.e. for all the points below the maximum the activation of the phase-line strands is incoherent. For 40% strain, while activation coherence is achieved for the κ_2-phase for the highest ω, it is clear that it is not the case for the κ_1-phase, since none of the points are above the reversal maximum. The melt response, this cohesive orchestration of the activation mechanisms occurring simultaneously in dual-phases κ_1 and κ_2, continues to be asynchronous.

The crucial question is to determine the conditions, if they exist, that make both dual-phases synchronized at the same time. In that regard, the question of the stability of the network of interactions must be addressed, i.e. the question of the uniqueness of the solution or its time dependence. We need to understand if the instability of the entangled melt is triggered by what happens to κ_2, κ_1 or $\kappa=(\kappa_1+\kappa_2)$. The maximum of κ_2 does not indicate an instability of the melt, nor "yielding"; it indicates the decrease of the number of activated strands of the κ_2-network

because of the effective activation of the core-phase. Is the time dependency of G' (ω,γ) and G"(ω,γ) triggered by strain, reported and studied in Ref. [2], starting at the maximum of κ_2? Are these conditions adequate to produce "in-pellet disentanglement" [32a,32b]? It appears that the "transition" observed in Figs 33-35 and Fig. 36a corresponds to where κ_2 reaches its maximum, which occurs at a lower ω as strain increases. In other words strain softening is the result of the compensation between the straining of the two dual-phases, as already stated before. We saw earlier in the paper that shear-thinning was due to the increase of the network frequency ω' corresponding to the increase of the number of activated strands. The activation process is itself a dual process, a stretch then relax sequence, this is the first type of duality. This mechanism does not appear to occur in both dual-phases when the strain is in the linear range, at least for the polymers analyzed in this paper. Yet, as strain increases, so does the contribution from the core-phase: this is strain softening. As we saw illustrated for 40% strain, both dual phases then are actively responding to the strain deformation via a dual mechanism of stretch-relax (Figs 37b and d). These two mechanisms of deformation are dependent since the κ_1 and κ_2 phases compensate, this is a second type of duality. The duality of the stretch-relax mechanism and the duality of the compensation between the phases are crossed, as we call this, which constitutes the complexity of the physics of deformation of polymer melts. As we shall analyze in future presentations on this subject, the crossed duality is at the heart of the grain-field statistics which may also apply to other systems of particles in interaction. In the case of polymers, the "particles" are conformers. We mentioned at the beginning of this paper that conformers bonded intra-molecularly and inter-molecularly with each other define a grand ensemble statistics of interactive chains. We stipulated that the field of interactive coupling between the conformers was itself operating with crossed duality, unlike for a mean field which operates homogeneously. The difference is easily explained by analogy if one compares the mist of air and water molecules in a cloud or in rain, or in humid air and cold fog. The segregation of the molecules which can create visible dual-phases seems to generate a grain-like structure. The same phenomenon occurs with immiscible polymer blends. The fluctuation of free volume is locally responsible for the formation of small clusters of inter-bonded conformers embedded in a sea of inter-molecularly un-bonded conformers, yet still intra-molecularly bonded. The two intra- and inter- molecular bondings interact to create the collapse of the chain into a ball, the macro-coil, thus the result of a 1st duality, and the

interpenetration between macro-coils create another duality symbolized by phase-lines which diffuse by thermal motion with frequency ω'_o (Fig. 4); again a crossed duality.

Figures 38a and b show the effect of the strain, varying between 5% and 40%, on the curves $\kappa_2(\omega)$ and $\kappa_1(\omega)$, respectively.

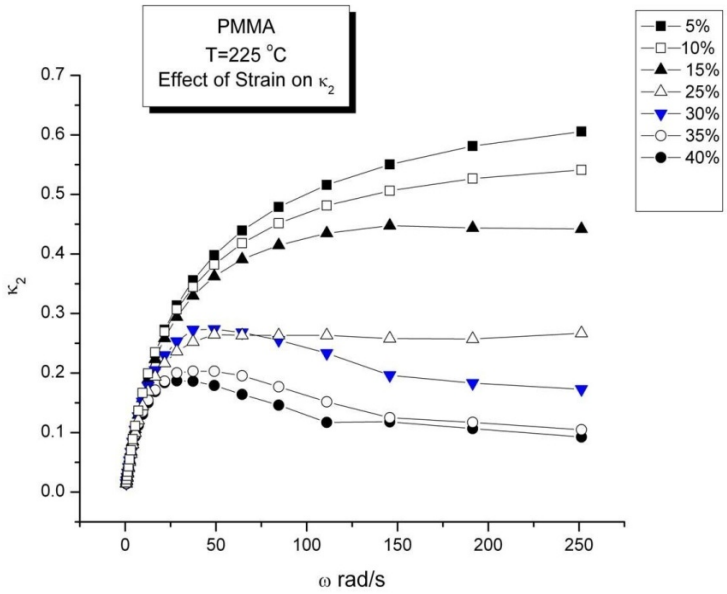

Fig. 38a

Masterplot of $\kappa_2(\omega)$ at various strains for PMMA at T= 225 °C continuously decreasing with strain as the cause of "non-linear behavior".

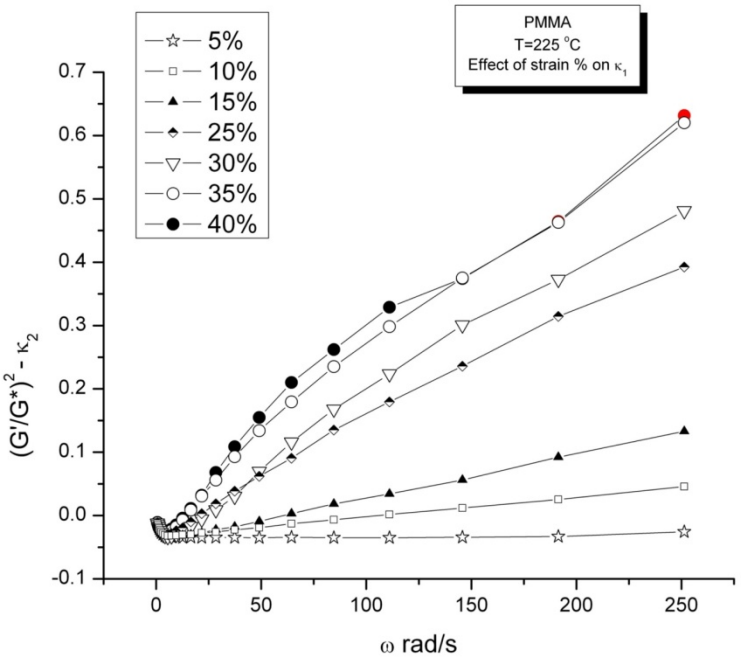

Fig. 38b

Masterplot of $\kappa_1(\omega)$ at various strains for PMMA at T= 225 °C continuously increasing with strain as deformation in the core-phase becomes increasingly activated.

This illustrates well the gradual compensation between κ_1 and κ_2 as strain increases. All of what we described for the 40% strain applies to the other strains, only the respective ω value when κ_2 reaches a maximum or the value of the maximum itself varies (Fig. 38a). One sees that for a value of the strain equal to 15%, and beyond, κ_2 never reaches 0.5, meaning there is no cross-over point for that dual-phase. Also, κ_2 reaches a maximum which holds on as a plateau at high ω, yet this plateau seems to decrease for strain larger than 20%, for which one needs to determine whether the decrease of κ_2 is due to increasing ω or to the time dependence of κ_2 , i.e to the instability of that dual-phase. In Fig. 38b, $\kappa_1 = [(G'/G^*)^2 - \kappa_2]$ is plotted against ω for the various strains. One observes for the 5% strain the typical negative κ_1 behavior reported at the beginning of this paper (Fig. 6) showing that this phase does not store up elastic energy as ω increases; the stretch-relax activation of the κ_2-phase drives the melt shear deformation, the κ_1-phase adapting passively by diffusion. One also observes in Fig. 38b that $\kappa_1(\omega)$ is almost linear for the 3 lowest strains above approximately ω=5, starting to curve downward from a linear behavior starting at 25% strain. The slope, κ_1/ω, increases rapidly with strain and appears to

reach a maximum for a strain between 35% and 40%. The last three upper points on the graph κ_1 vs ω in Fig. 38b are even identical for 35% and 40%.

In summary, the essential role of strain is to activate the κ_1-phase to participate *actively* (by shear-thinning) in the deformation process. Under linear viscoelastic conditions, the conformers in the κ_1 dual-phase do not deform (by conformational transformation), their motion is through diffusional reorganization, i.e. delocalization in the structure triggered by the stretch-relax deformation mechanism (shear-thinning) of the κ_2-phase conformers. When the κ_1-phase is activated as a result of an increase of the strain, for a given ω, strain softening occurs. Fig. 38b shows, in the case of PMMA, that strain softening can occur starting at strain as low as 10% and that it is very sensitive to the strain amplitude for that polymer melt.

We have also discussed in this section the synchronization or asynchronization of the stretch-relax mechanism occurring in both of the dual-phases (in an interactive way). This relates to how k varies with strain and strain rate and saturates to the value of 1. Fig. 39 is a plot of ω' vs G* comparing the 5% and 40% strain.

In Fig. 39 we plot ω' versus G* for the two strains, 5% and 40%, for the same data shown in Figs. 36-38. Equation 12 can be used to fit the 5% curve over the full range of data points, to determine ω'_o, G^*_1 and k. For the 40% curve, we need to restrict the applicability of Eq. 12 to the low ω range (< 3 rad/s) to avoid a value of k greater than 1, which would not make sense physically. The only choice of k we can use for the regression is k=1.

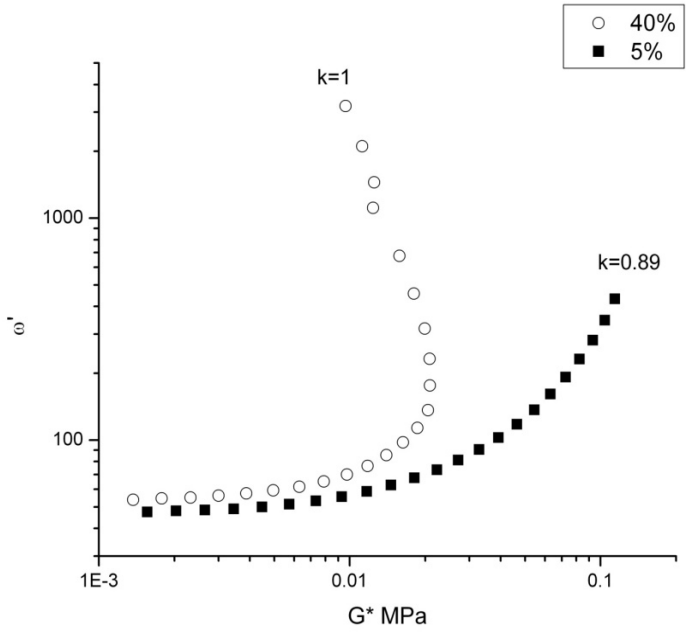

Fig. 39

Plot of ω' versus G* for the two strains 5% and 40% for the same data shown in Figs 36-38. The k values shown are according to Eq. 14.

For this restricted range, with k=1, we found that ω'_o remained the same as for the 5% strain and G^*_1 was found to be smaller. Note that k=0.89 for 5%, which is very high, meaning that the melt is very cooperative even at low strain. This high value of the interactive coupling constant k is a characteristics of PMMA melts, compare to other polymer melts at the same ($T-T_g$). This results not only in higher melt elasticity (Fig. 10), but in a coherent shear-thinning process for the κ_2-network phase, which conditions the participation of the κ_1-phase in the deformation process, thus favors strain softening. For 40% strain, which is still a relatively small strain, k=1 from the very first ω value onward, which illustrates well the high interactivity of the conformers in the network. Note that it is conceivable that for lower ω than used experimentally k=0.89 then increases to 1, which is the state of the system when we start the experiment. In Fig. 37b, the first 10 points, starting at $\kappa_2 \sim 0.01$, are aligned and the slope is Δ_s, the same as for 5% (Fig. 37c). This illustrates the fact that a dual-phase can be undergoing a stretch-relax process (shear-thinning) incoherently (k<1) or coherently (k=1), which refers to whether all activated systems are activated synchronously (k=1) or not. The formula which applies to an incoherent stretch-relax

deformation mechanism is Eq. 14 (also Eq. 12), whereas it is Eq. 13 that is used when k=1. As previously stated, this situation corresponds to validating the use of the Eyring activated process to describe deformation of the melt. Yet, we mentioned that for the 40% case in Fig. 39, we could only curve fit the lower ω range (the first 10 points) with the Eyring equation, Eq. 13. This is because this equation only considers the deformation occurring in the κ_2-phase, which ignores the stress requirement to deform the κ_1-phase (Fig. 38b). Obviously, the situation becomes a little bit more complicated and we leave the solution to future publication. Yet, to show one simple way to get the κ_1-phase deformation involved, we present Fig. 40 which applies to the data of Fig. 39, for 40%, assuming k=1. In this figure, we plot $\{G^*_1 \, Ln(\omega'/A_1) - G^*\}$ vs κ_1 and find that the data align on a straight line passing through the origin, at least within a good approximation (r^2=0.998). The slope of the straight line is 0.256, with the dimension of a stress. In other words, the Eyring formula continues to apply outside the curvefitting range for its applicability (the first 10 points) provided G* is substituted by (G*+0.256 κ_1). This describes strain softening analytically.

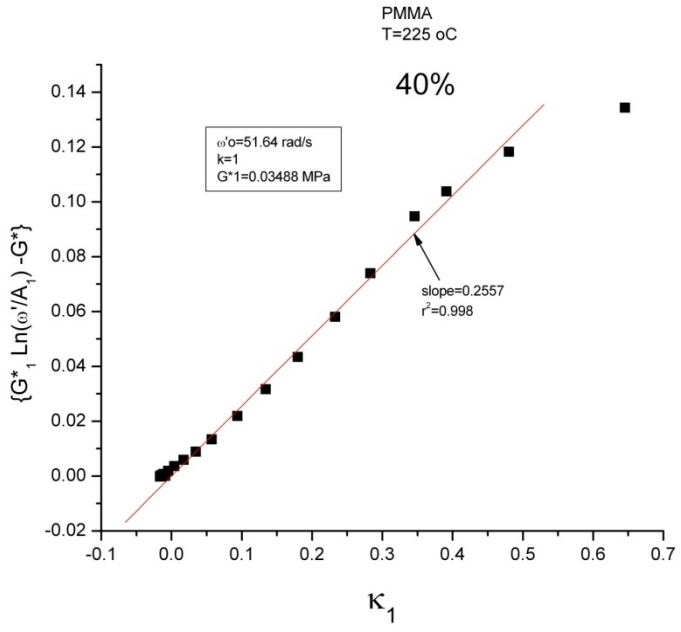

Fig. 40

Attempt to determine for γ=40% the influence of κ_1 on the potential energy barrier defining the variation of ω' with stress when k=1 (Eyring state, Eq. 13).

The implication of Fig. 40 is that another modulus, generated by and increasing with the stretch-relax mechanism occurring in the κ_1-phase needs to be added to the measured modulus to evaluate the amount of plasticization of the activation energy that determines ω'. As just said, except for another example shown with respect to Fig. 42c, we leave the merit of such an approach to another future publication.

In Fig. 41 we compare, on a log-log plot, the decrease of the viscosity with the increase of ω' for the two strains 5% and 40%.

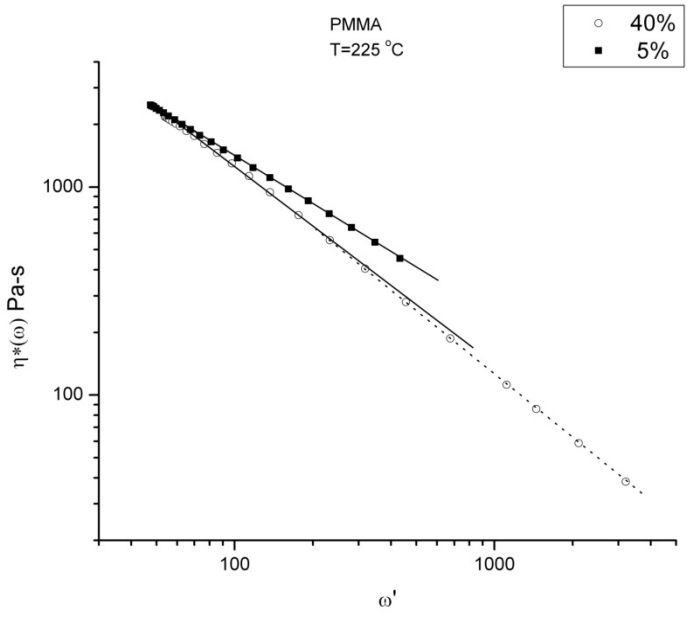

Fig. 41

Comparison of η*(ω) vs ω' (log-log) for 5% and 40% strain. The 40% curve breaks down into 2 straight lines. See text.

The top straight-line (squares) applies to the 5% strain. One sees that the difference between the 5% and 40% strain is two fold: first, at low ω, the straight line passing through the 40% data is steeper than the 5% line. Shear-thinning is boosted by working under higher strain. Second, for all the points for which κ_2 has passed over the maximum in Fig. 37b (the points of the lower branch), corresponding to the highest ω´ values, another straight line passes through them in Fig. 41. Its slope is even steeper than the one found at low ω´. The same phenomenon is visible for other non-linear conditions, for instance in Fig. 42a, for T=215 °C and 20% strain.

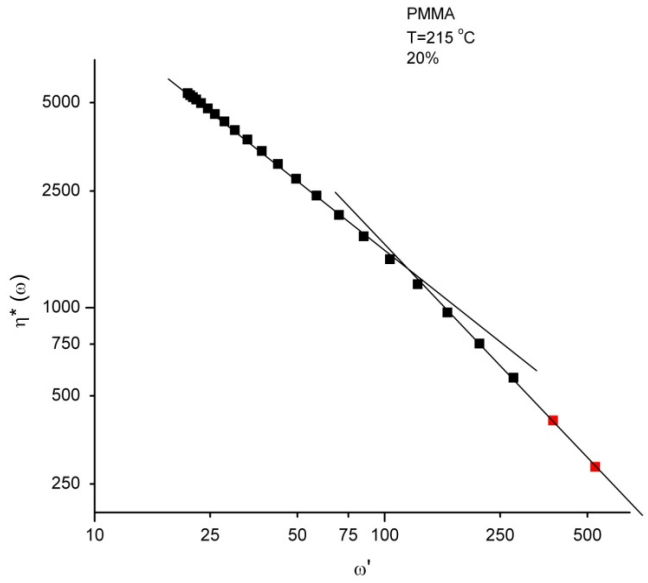

Fig. 42a
η∗(ω) vs ω' (log-log) for T=215 °C, 20% strain.

It is always difficult to validate the existence of a transitional change from the appearance of a break in the application of a curvefitting equation. After all, the linearity of η∗(ω) and ω' on a log-log plot, is purely empirical, and perhaps a better equation would apply extending its range to a larger ω' span. Yet, if we look now at Fig. 42b, which provides the split of $(G'/G^*)^2$ vs ω for the data of Fig. 42a, we observe that κ_2 reaches a maximum and that the last 5 or 6 points are already strongly influenced by the growth of κ_1.

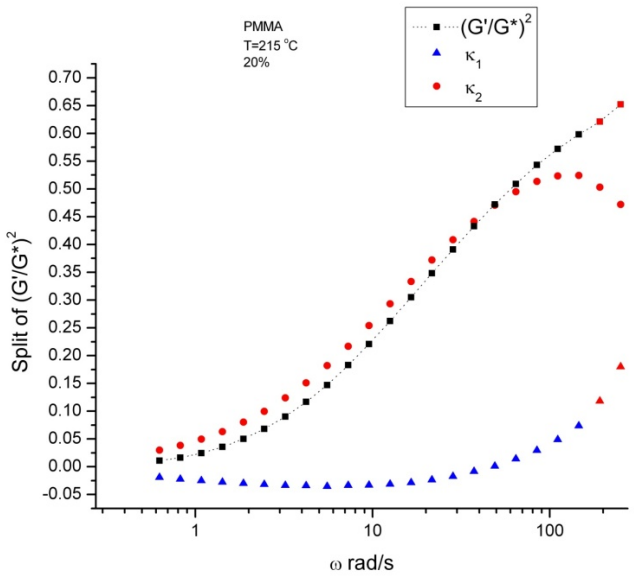

Fig. 42b
Split of $(G'/G^*)^2$ vs ω into $\kappa_1(\omega)$ and $\kappa_2(\omega)$ for the data of Fig. 42a.

This parallels the situation found for the last 10-12 points in Fig. 37b. The increase of the pseudo-plasticity observed in the ω' plane is, therefore, due to the compensation between the κ_2 and κ_1 dual-phases, as already explained for the 40% strain. At low ω, below the maximum of κ_2, the boosted shear-thinning is due to the effect of the strain on the interactive coupling constant, increasing its value to 1. The coherence between the activated strands optimizes shear-thinning, which explains the lower value of h* in Fig. 34 in the low ω range as strain increases, and, likewise, the steeper slope of Δω vs κ at the beginning of the curves in Fig. 36a.

Figure 42c is the equivalent to Fig. 40 for the T=215 ^oC temperature, 20% case. The line is, indeed, straight for all values of κ_1, which seems to validate our previous approach, yet the intercept is not zero, and the slope is quite different from 0.256, the value found in Fig. 40; it is 2.5, which adds an additional level of complexity.

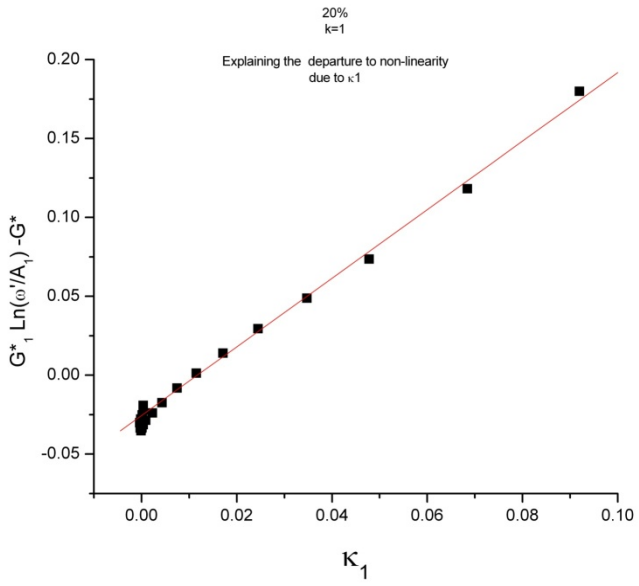

Fig. 42c
Same plot as in Fig. 40 applied to the data of Fig. 42a (γ=20%, T=215 ^{o}C).

We believe that, in view of Fig. 37d, which suggests that the κ_1-phase deforms, when it has been solicited to do so, by a similar stretch-relax mechanism as the κ_2-phase, it appears more appropriate to define and find for that phase the equivalent of ω' (which would be equal to ω/κ_1) and thus of ω'_o, k, and G^*_1. The Dual-Phase character of the rheological parameters and of the formula to find them will be fully developed in part IV of this series.

In Figs. 43a to c, we show an example of a polypropylene melt with a very low interactive coupling constant, k=0.1775, and a decrease of its total stored melt elasticity with strain. Fig. 43a is the graph of $(G'/G^*)^2$ vs ω at various strain, which should be compared with the same plot for PMMA, in Fig. 31d.

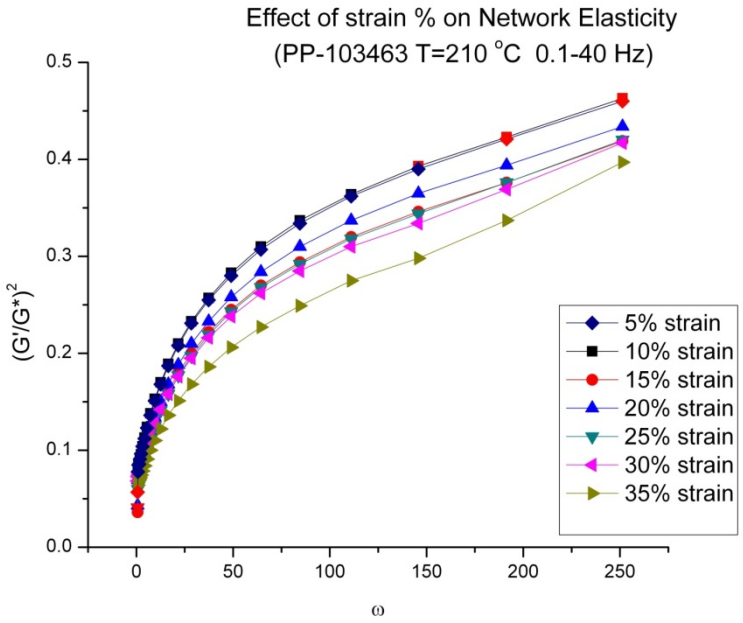

Fig. 43a

Masterplot of $(G'/G^*)^2$ vs ω for PP at 210 °C for 5% to 35% strain.Compare with Fig. 31d for PMMA.

The important difference between these two plots is the observation that, for PP, strain decreases the total value of the energy stored in the melt, whereas, for PMMA, the total value of $(G'/G^*)^2$ either remain constant with strain or increases. Notice in Fig. 43a that the melt, at this temperature of 210 °C, is below its cross-over (i.e. $(G'/G^*)^2=0.5$) for all frequencies, even at the low strain 5%. This is a sign that the melt is not showing a strong elastic behavior, even when its temperature is lowered by 20 ° or so (not shown).

Fig. 43b is a test of Eq. 12 for the 10% strain showing a very good correlation.

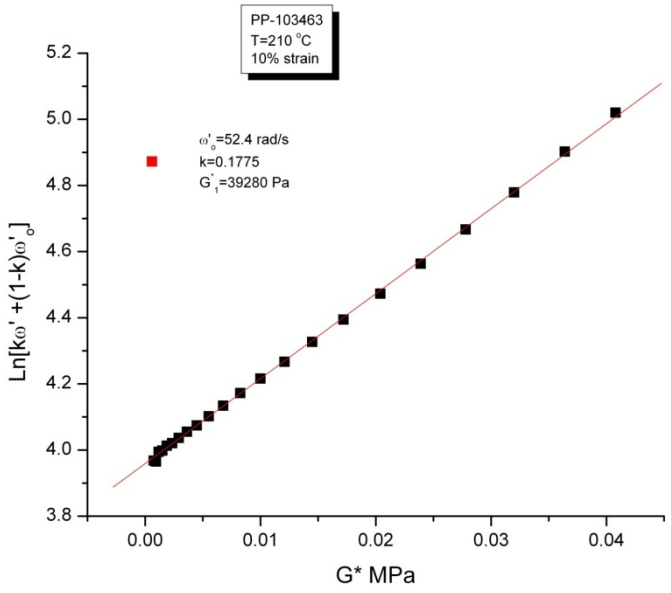

Fig. 43b

Determination of ω'_o, k and G^*_1 by plotting the variables of Eq. 12 for the data of Fig. 43a Strain=10%.

The interactive coupling (blinking) constant k is 0.1775, which should be compared with the value found for the PMMA melt interactivity at 225 ^oC, k=0.89 for 5% strain. The PP melt of Fig. 43a is showing a very small amount of stretch during shear-thinning, the deformation being dominated by ω'_o, i.e. by the phase-line sweeping mechanism controlled by diffusion.

In order to see if the κ_1-phase is solicited at all, we study in Fig. 43c the split of $(G'/G^*)^2$ at various frequencies ω.

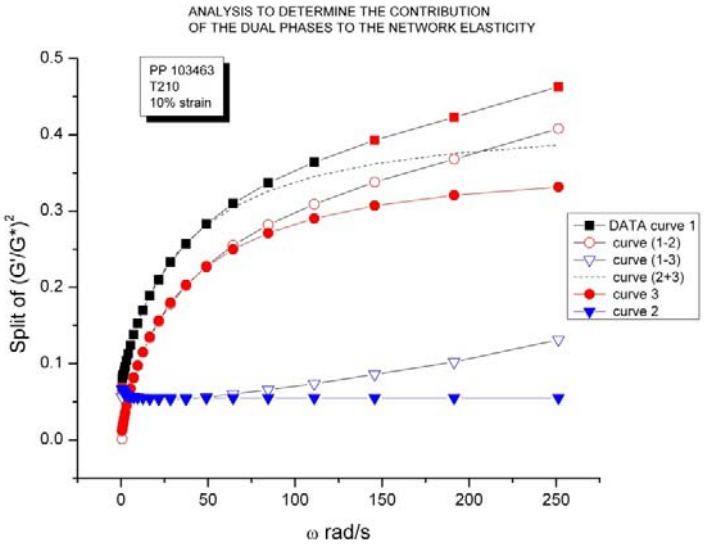

Fig. 43c
Split of $(G'/G^*)^2$ vs ω into κ_1 and κ_2 for the PP data of Fig 43a. See text.

This figure should be compared with Fig. 13, previously discussed, which was used to consider the dilemma of the non-linearity brought in by the synergy of ω and γ, whether it was caused by the stretching of the κ_2 -phase network or by the involvement of the κ_1-phase in the strain production. Figure 13 is a plot similar to Fig. 43c which applies to the same melt at the same temperature, but the strain is 25% in Fig. 13 and only 10% in Fig. 43c. Additionally, Fig. 13 provides a split of the stored elasticity against G*, whereas it is plotted against ω in Fig. 43c. So, the results apply to slightly different strain conditions, but this is not relevant to the point we want to address. We have described at the beginning of the paper how to extract from the fitting of $(G'/G^*)^2$ vs G* the κ_1 term corresponding to curve 4 in Fig. 13 and curve 2 in Fig. 43c. The positive value found for κ_1 for certain polyolefines have already been commented on above, and, noticeably, we find that this is true for this PP melt, whether in Fig. 13 or Fig. 43c. Similarly, the variation of κ_2 given by Eqs. 5 and 7 is given by curve 3 in both figures. The dilemma explained earlier with regard to Fig. 13 can be re-stated for Fig. 43c by comparing curve (2+3) with curve 1 (the data). The curve fit is good all the way except for the highest frequencies (ω >70) where a clear difference is observed. The dilemma can be stated by considering either curve (1-2), the open dots, as the true variation of κ_2 with ω (and curve 2 remains as it is), or curve (1-3), the open triangles, as the true variation of κ_1 with ω, curve 3 remaining the same. In the former

alternative, one needs to modify the κ_2 formula to account for an upturn at high ω (this can easily be achieved by modulating the formula given in Eqs. 5 and 7 by an exponential function of ω). For the latter alternative the κ_1 term starts to grow, as explained for the PMMA melt, triggering a strain softening effect. It is this last solution that we favor, the essential reason being that we found, empirically, that all the curves 3 of κ_2 vs G* are the same regardless of strain (not shown), an invariant that appears to be a basic result underlying the contribution of the Dual-Phases to the network elasticity. This result is also true for the PMMA melt analyzed above. In other words, strain softening is not due to a boosted elasticity of the network of entanglements but to the deformation in the κ_1 phase via a mechanism of compensation. Note that in the case of Fig. 43c, although κ_1 starts to raise (open triangles), its value at ω=250 is only 0.1, showing that very little shear-thinning is occurring in that phase under those conditions. Nevertheless, strain softening has started for that PP melt, yet the stretch-relax mechanism is dominated by the relaxation step, and the system is highly incoherent. These are not favorable conditions for inducing "melt disentanglement" [2, 32a, 32b].

In Fig. 44, we see the split of $(G'/G^*)^2$ vs ω for a PS melt which has been submitted to a certain thermo-mechanical history prior to performing the frequency sweep done at 217.5 ^oC, with a strain of 30%. The frequency increases during the test, an option usually designated "an upsweep".

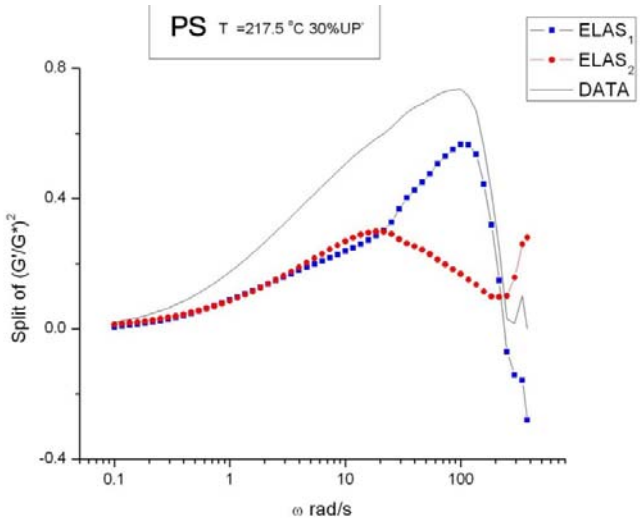

Fig. 44
Split of $(G'/G^*)^2$ vs ω into κ_1 and κ_2 for PS melt at T=217.5 ^oC and γ=30%

In the legend box, $ELAS_1$ and $ELAS_2$ designate κ_1 and κ_2. The $(G'/G^*)^2$ curve is also shown in the figure ("DATA"). One sees for this pre-sheared melt that both κ_1 and κ_2 rise simultaneously with ω, that κ_2 reaches a maximum at ω~20 rad/s while κ_1 continues to rise, yet that κ_1 itself reaches a maximum at ω=100 rad/s before rapidly decreasing. The maxima for κ_2 and κ_1 are 0.3 and 0.6, respectively. It is interesting to see the large impact of a pre-shearing treatment of the melt (a condition called "shear-refinement") on the modification of the rheology of the Dual-Phases; an untreated PS melt behaves very closely to what we have analyzed for PMMA (see Figs. 37a and 42b). The new method of analysis of viscoelastic data presented in this paper appears quite powerful to determine what happens to shear-thinning or strain softening as a result of a given shear-refinement treatment. In Fig. 44, from ω=0.1 to 20 rad/s the two dual-phases are in the terminal zone, both shear-thinning incoherently. Between ω=20 and 100 rad/s, the κ_2-phase (phase-line network) is shear-thinning coherently in the rubbery plateau, but the κ_1-phase is still incoherent. For ω between 100 and 200 rad/s, both dual-phases are stretching coherently, a condition that may have consequences on the long term stability of the deformed state obtained. This type of experiment and analysis with the Dual-Phase model, we suggest, must be systematically accomplished to understand the impact of thermo-mechanical treatments, such as "Rheo-Fluidification", also called "disentanglement" [32a, 32b], on the long term stability of new states for the entanglement network.

In Fig. 45a we study the variation of the activated strands coherence factor, k, as a function of ω for the Polystyrene melt of Fig. 17c analyzed at T = 150° C and 2% strain. The reason for lowering the temperature is to make apparent the maximum of the melt elasticity, $\kappa=(G'/G^*)^2$, within the range of frequencies studied. For ω = 0.01 to ~7 rad/s, the value of k is constant at 0.5. This range corresponds, in Fig. 17c, to the left of the maximum of $(G'/G^*)^2$, the value of k starting to deviate at exactly the value of ω for the maximum.

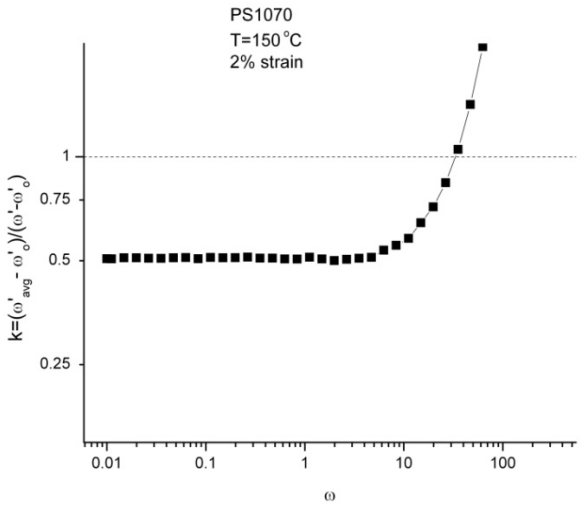

Fig. 45a

Plot of the activated strand coherence factor, k, vs ω for PS at T=150 °C, 2% strain. Same data as in Fig. 17c.

When ω is greater than 7, k quickly rises with ω and becomes 1 for ω ~ 37 rad/s. The meaning of Fig. 45a is that k only remains constant over a restricted range of frequencies, up to the maximum of the melt elastic stored energy. The points located above the horizontal line k = 1 cannot physically be larger than 1 so that, in fact, they remain equal to 1 once k has reached this value. Equation 15 controlled the mechanism of deformation while k was constant and remained valid in the regime where k increased to 1, yet is now in default for the points above the k=1 line. We assume ,**first,** that Eq. 13 remains valid but now applies to a modulus, $G^{*(2)}$, that defines deformation in the κ_2-phase; **second,** that there is another complementary modulus, $G^{*(1)}$ generated by the stretching of the κ_1-phase; **third,** finally, that we have $G^*=G^{*(1)} + G^{*(2)}$, i.e. the sum of the two *phase-moduli* is equal to G*, the measured modulus. These assumptions will be studied in detail in other future publications, in particular in part IV of this series. What is important to say, here, is that we assume, in our understanding of the concept of the dual-phase submitted to a deformation, that the elasticity of the network and the stress to accommodate the strain requirement go hand in hand, and both split. Our assumptions amount to splitting G* into two components, the way it was shown in this paper for the splitting of the melt elasticity. Figure 45b shows the split of G* for the melt of Fig. 45a. $G^{*(2)}$ is calculated from the values of ω', assuming k=1 beyond ω=37 rad/s. $G^{*(1)}= G^*-G^{*(2)}$.

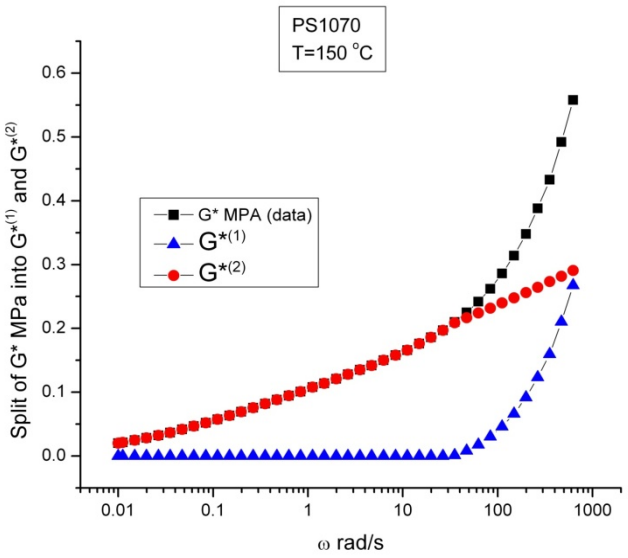

Fig. 45b
Split of G* vs ω into $G^{*(1)}$ and $G^{*(2)}$ for the data of Fig. 17c and 45a.

One sees that the upturn of G* after the maximum of $(G'/G^*)^2$ is due to the growth of the $G^{*(1)}$ term (the triangles) which had remained practically non-existent up to that point. For Fig. 17c we mentioned earlier that the inflection perceived in the shape of the $\eta^*(\omega)$–ω curve (on a log-log scale basis), resulting in a slow down of shear-thinning, was due to the effect of ω on the magnitude of (T-Tg(ω)), which we associated with a decrease of free volume. Figure 45b says that this is due mainly to the growth of the stress by the activation of the deformation process in the κ_1-phase. These two propositions reconcile if it is understood that the free volume in the core-phase is smaller than the free volume in the κ_2-phase. Note in Fig. 45b that $G^{*(2)}$ is practically equal to G* in the terminal range up to k=1, where the split of G* into $G^{*(1)}$ and $G^{*(2)}$ becomes visible. The value of G* at that level is 0.21 MPa, the value usually quoted for the shear modulus of Polystyrene for the rubbery plateau.

Figure 45c plots the elasticity stored in the κ_2-phase as a function of the modulus, $G^{*(2)}$, developed in that phase.

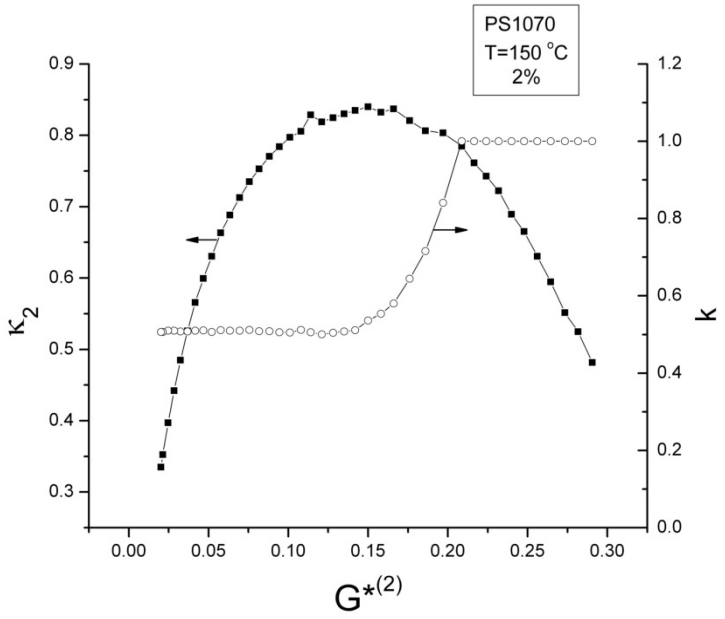

Fig. 45c

Network elasticity, κ_2, vs $G^{*(2)}$ for phase $-\kappa_2$, and, plotted simultaneously, variation of the activated strand coherence factor,k, for the data of Fig. 45a.

On the same plot, but using a different y-axis (on the right hand side), we show the variation of the activated strands coherence factor, k. It is clear that the onset of coherence (k=1) occurs beyond the maximum of κ_2. This observation appears to also be true at other temperatures, as illustrated in Fig. 47d. The classical determination of the plateau modulus is empirically done at the minimum of tan δ, which corresponds to the maximum of $(G'/G^*)^2$, In our view, this is not quite correct since it yields a lower value of G^o_N than what we find, for k=1. We show in Fig. 45d that, for all temperatures between 150 °C and 185 °C, G* ~0.2 MPa for k=1 (corresponding to ω=37 rad/s).

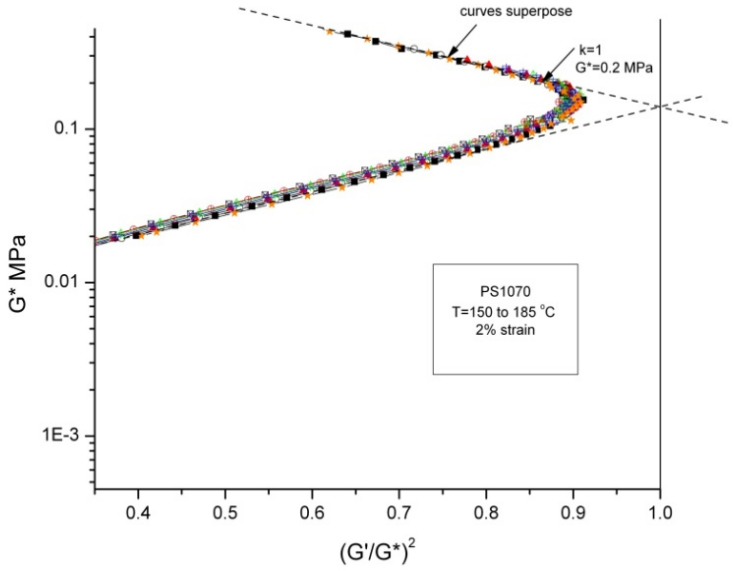

Fig. 45d
Masterplot for PS for T between 150-185 °C of the G* vs $(G'/G^*)^2$ obtained for γ=2%.

In addition, it appears that coherence makes the curves superpose whereas incoherence (k<1 corresponding to ω<37 rad/s) presents some significant scatter. We need to confirm this last observation to validate its generality at other temperatures, in particular below the T_{LL} temperature of the melt. Yet, in Fig. 45d the curves located beyond the maximum superpose starting at k = 1. It appears very significant that the range of applicability of the equation describing the function between ω' and G* in Eq. 13 is governed by the activated strands coherence factor, k. When shear thinning occurs incoherently, which is visible in Fig. 45a as the flat portion where k is constant, then the curves in Fig. 45b do not superpose, yet as soon as k = 1 they do. Thus we ask, does deformation in the rubbery plateau region correspond to a coherent stretch-relax mechanism of deformation?

Another question which rises from this study at lower temperature and low strain (2%) is whether the transition incoherence → coherence of the stretch-relax mechanism initiates the same interplay between κ_1 and κ_2 which we described as the cross-dual phase interaction for the effect of higher strain (Figs.37a to d). In Figs. 45b and c the increase of $G^{*(1)}$ at k=1 is not associated with an increase of κ_1 (not shown) If κ_1 does not increase when $G^{*(1)}$ increases, this means that the deformation in the κ_1-phase is not occurring by shear-thinning; on the contrary it occurs by the involvement of a more viscous melt in the overall process of deformation. The κ_1-

phase is now deformed, but this occurs by diffusion, and the lower free volume in the κ_1-phase makes it harder. In other words, at low strain lower temperature, the decrease of κ_2 beyond the maximum in Fig. 45c is not compensated by an increase of κ_1, which is what we observed at higher strain, higher temperature. At lower strain and lower temperature we suggest that the decrease of the number of activated strands in the κ_2-phase is being compensated with an increase of the involvement of the κ_1-phase conformers proceeding by diffusion, not by the stretch-relax mechanism, at least not until a minimum of $(G'/G^*)^2$ is reached at even higher ω. The origin of the decrease of the number of activated strands of the κ_2-phase is the entropic deformation of the network trickled down by the increase of $G^{*(1)}$ at κ_1 constant.

In summary, what appears to be happening at low strain, low temperature, high ω (see Fig. 17c), is quite different from the cross- dual shear-thinning occurring in both phases at higher temperatures under larger strain (Figs 37a to d). An important question that needs to be elucidated regards how strain affects the respective roles played by κ_1, κ_2 and $G^{*(1)}$, $G^{*(2)}$ in the plateau region. Figures 45e and f compare G* vs ω and $(G'/G^*)^2$ vs ω, respectively, for a strain of 5% and 40%.

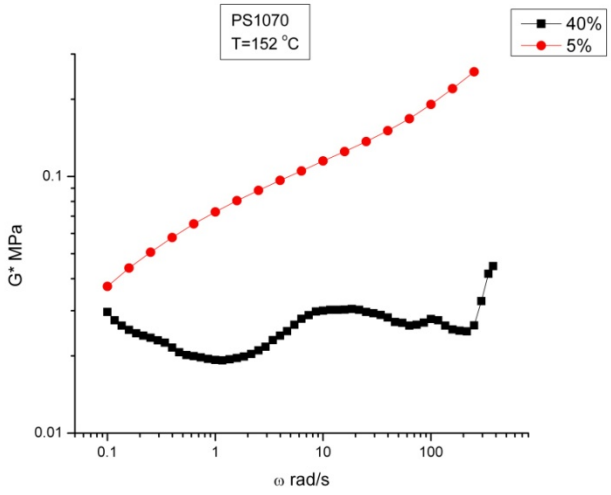

Fig. 45e
Comparison for PS of the 5% and 40% G*(ω) curves obtained at T=150 °C. See text.

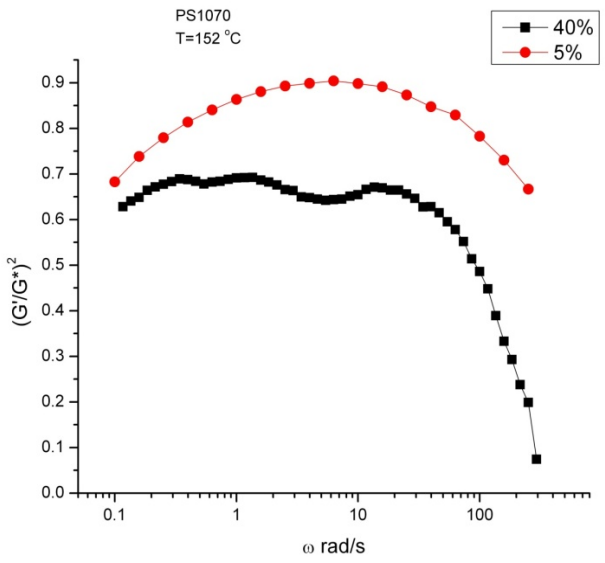

Fig. 45f
Comparison of $(G'/G^*)^2$ vs ω for the data of Fig. 45e.

The 5% case has already been discussed when addressing Figs. 17c and 45b (note the log-log scale used in Fig. 45e). One sees for γ=40% (squares) in Fig. 45e a significant decrease of the modulus relative to 5% across the frequency sweep range, and that the corresponding values of $(G'/G^*)^2$ in Fig. 45f are also lower for all values of ω than for γ=5%. The decrease of the modulus is a clear sign that strain softening is operating, even at the lowest ω =0.1 rad/s (see Fig. 34). Therefore, the involvement of the κ_1-phase in the strain production is activated from the onset of the frequency sweep. Notice that $(G'/G^*)^2$ drops very steeply at higher frequency after staying more or less constant until ω has reached approximately 35 rad/s. The near constant value of $(G'/G^*)^2$ is maintained by the compensation between κ_1 and κ_2, balancing their variation with opposite signs (κ_2 decreases, κ_1 increases), followed by a sharp decrease of κ_1 after it has passed its maximum (see Fig. 44 for an example of a drop off of κ_1). In Fig. 45e, the complex modulus G* (ω) first decreases from 0.03 to 0.02 MPa, followed by a reversal of the modulus that returns it to its initial value and then it stays constant between ω = 100 to 200 rad/s while, in that same small range, $(G'/G^*)^2$ in Fig. 45f drops off sharply. This behavior is the result of a complex interplay between the dual-phases. Contrary to what we concluded for γ=5%, the deformation at 40% involves a cross-dual stretch-relax mechanism which is strongly interactive.

Details are beyond the scope of this thesis. We see, however, that the same analytical tools that we have used to study the high temperature region can be used to determine the deformation of the dual-phases at lower temperature, higher strain. There is, of course, a lot to be said regarding the mechanisms of deformation as we continue to increase ω or get closer to T_g, but the analytical method presented here is still applicable in these other regimes.

G. The melt behavior at low frequency.

We have described in some detail, above, the activation of the stretch-relax mechanism by the increase of the elastic strain energy resulting from an increase of ω, and have suggested that when both of the dual-phases are activated by such a deformation process strain softening occurs. We now turn our attention to the deformation process occurring at low ω, for instance as described in Fig. 6, to understand the interplay of κ_1 and κ_2 in this regime of low elastic energy. This low ω range extends out from the Newtonian region and was already revealed in Fig. 5 without expanding on its meaning. We see in Fig. 5 that the squares apply to the variation of the complex viscosity with ω_R (simply defined as the ratio of ω and $(G'/G^*)^2$). Unlike ω', which is defined from κ_2 and increases continuously with ω, ω_R first decreases at low ω, reaches a minimum, then turns around and increases with ω. This is true for the linear viscoelastic range (Fig. 5) but remains true even for larger strain, as shown in Fig. 46a.

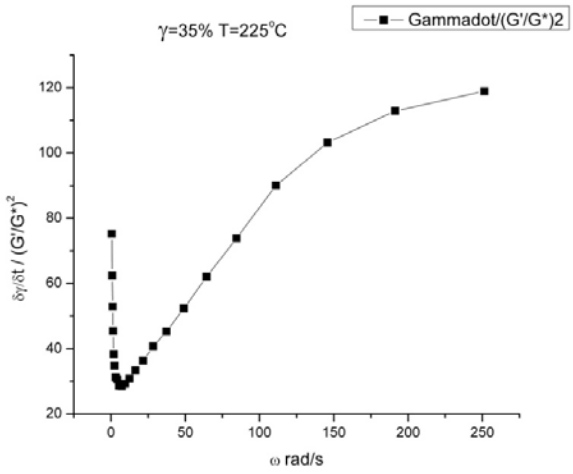

Fig. 46a
R strain rate vs ω for PMMA at T=225 °C, γ=35%.

In this figure, ω_R is multiplied by the strain (here 35%) so, actually, the y-axis is the strain rate, $\omega\gamma$, divided by $(G'/G^*)^2$. which we call R. One sees, at low ω, that R decreases, reaches a minimum and then increases. Figure 46b compares the melt viscosity *versus* R for γ=5% and 40% showing that the effect of the strain essentially affects the stretch-relax mechanism represented by the non-horizontal linear sections; the low ω region seems to be the same for 5% and 40%, simply shifted horizontally. The amount of horizontal shift is due to the use of the strain in the definition of the x-variable on a log scale.

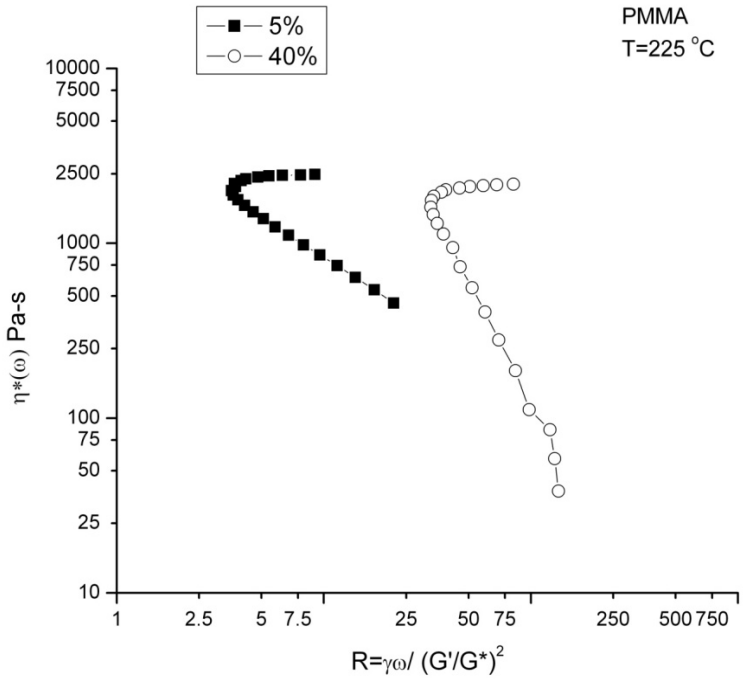

Fig. 46b
Comparison of $\eta*(\omega)$ vs R (log-log) for 5% and 40% strain.

Let us study in the following figures some of the characteristics of the melt behavior when R decreases to determine whether our description of the mechanism of deformation (the stretch-relax mechanism) still applies or is altered in any way by the lack of melt elasticity. In Fig. 46c we plot, for γ=5%, the value of Δ_s against R (which we wrote as the derivative of the strain divided by $(G'/G^*)^2$).

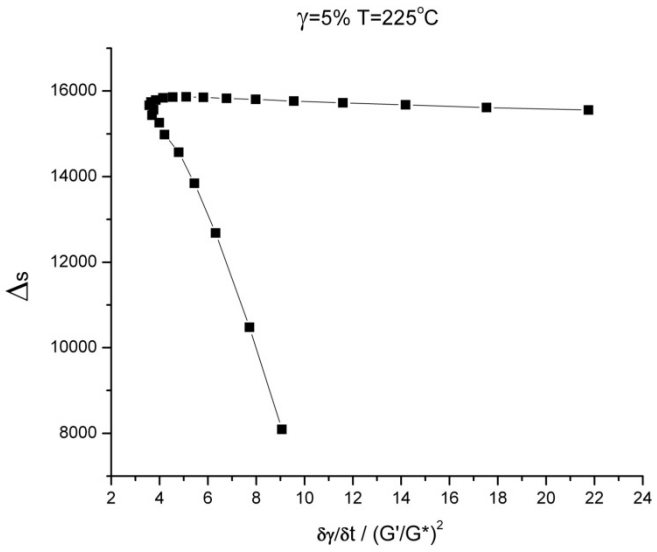

Fig. 46c

Variation of Δs vs R for PMMA, T=225 °C, 5% strain showing that Δs is not constant at low ω (first 9 values) when R decreases.

It is clear that Δ_s remains constant only after the minimum of R has been reached. As R decreases, at low ω, Δ_s *appears* to rapidly increase, here from 8,000 to 16,000. Fig. 46d applies to γ=10% and plots the normal force (in g) versus R. The normal force remains quasi zero as R decreases and only starts to increase at the change of the sign of the variation of the R strain rate.

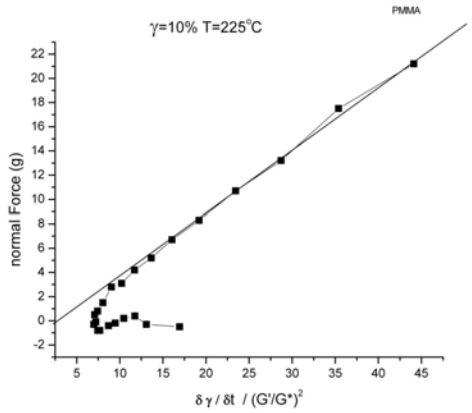

Fig. 46d

Normal Force vs R for PMMA, γ=10%, showing that the normal force remains equal to zero as long as R decreases.

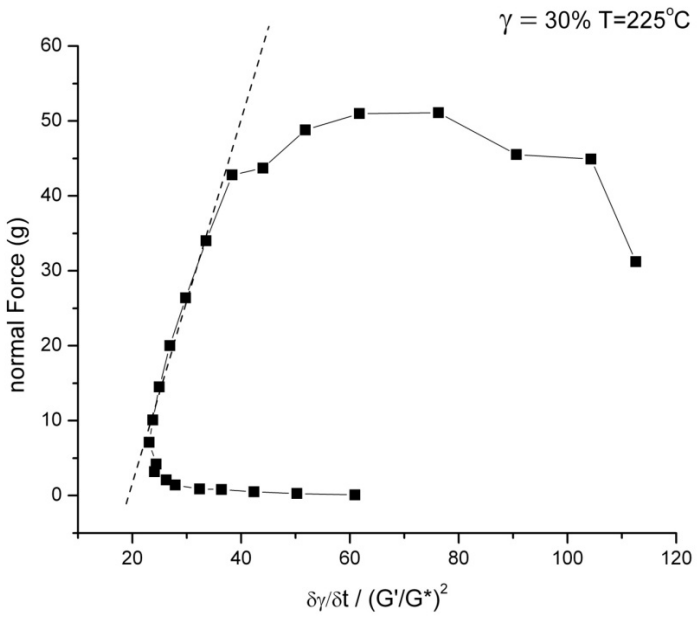

Fig. 46e
Same plot as in Fig. 46d but for γ=30%.

This observation is confirmed in Fig. 46e for a larger strain, γ=30%. In fact, the same observations that Δ_s is not constant at low ω and that the normal force is almost zero in that range are valid at all temperatures, for all strains, and appear to be a characteristic of the melt behavior for all polymers as one approaches true linear viscoelastic conditions.

One may wonder the meaning of R and why this variable was not at the center of our analysis earlier, perhaps even questioning why we are not claiming a change of the melt mechanism of deformation below the minimum of R. Eqs. 6 and 7 provide an answer to this question. Clearly, the decrease or increase of R is due to the relative value of $\delta\kappa_1$ and $\delta\kappa_2$ and their sign in the calculation of δR in the differentiation of Eq. 7. κ_1 is defined by Eq. 6, which can easily be differentiated, and κ_2 is determined after the value of κ_1 is subtracted from $(G'/G^*)^2$ in Eq. 7. It is remarkable that when κ_1 decreases at low ω, such as shown in Fig.6 (triangles), there is no or little normal force (Fig. 46e), yet that as soon as κ_1 has reached its plateau value, which occurs at the minimum of R, the normal force starts to rise.

What this means is that there is a compensation effect occurring between κ_1 and κ_2 that explains the properties of the melt in the linear viscoelastic regime, the normal force created by the deformation in the κ_1-phase pulling on the melt (negative force), whereas the increase of κ_2 applies a positive (pushing) normal force. The zero normal force observed in this low ω range is actually due to a compensation and is predictable from the math describing the interplay between the variation of κ_1 and κ_2. One certainly does not need to evoke a change of the deformation mechanism to explain this observation. We mentioned earlier in the paper that in this low ω regime the κ_1-phase deforms in a way that dissipates elastic energy forcing the phase-line network to store a little more elastic energy by compensation (dots in Fig. 6). In other words, in this quasi-linear viscoelastic region, the network of tie-lines compensates for the deformation mechanism occurring in the κ_1-phase that makes κ_1 vary fast at low G* values. As already pointed out, the fast variation of κ_1 with G* at low ω described by Eq. 6 depends on the initial state of the conformers in the κ_1-phase, which is influenced by thermo-mechanical history. Therefore, the linear viscoelastic range seems to be quite appropriate and very sensitive for studying the state of the melt after a pre-shearing history, or to compare the effect of topology (molecular weight, branching, etc.) which influences the proportion of the dual-phases. Furthermore, and this is a rather unexpected conclusion, the study of the melt in the linear viscoelastic range seems to shine light on the phenomenon of compensation between both of the dual-phases, a phenomenon that we introduced to understand non-linear viscoelastic effects, such as the influence of strain. The mechanisms of compensation might differ in the linear and in the non-linear regimes, but, in essence, shear-thinning, strain softening and linear viscoelastic deformation all derive from specific interplay of compensation between the dual-phases. We suggested viewing the melt at ω–> 0 as a 3D thermal diffusion wave of the phase-line network sweeping the whole melt to homogenize the free volume difference between the κ_1 and κ_2 phases. The phase-line wave fluctuates with frequency ω'_o. As κ_2 increases, ω' increases; this is the main attribute of shear-thinning. One may ask, what makes κ_1 compensate?

Let us go back to the calculation of Δ_s from Eq. 21. We saw earlier (Fig. 46c) that, at low ω, Δ_s rapidly increases before it holds constant. If one applied Eq. 21 assuming Δ_s constant, even in the range of κ_2 values where R decreases, one would find a higher value for the cohesive energy Δ_ω than the value corresponding to the data. The difference, times the absolute

temperature is the entropic deformation of the elastic network, which is the reason for κ_1 to become negative. In other words, the compensation by κ_1 at low ω, which occurs by a modification of the statistical conformation of the conformers of the core-phase, results in the deformation of the phase-line network, so Δ_s remains constant. This happens along with an increase of ω'caused by the increase of ω and κ_2. The entropic deformation of the entanglement network is only visible in this compensating range where κ_1 varies, at low ω, yet will also be triggered by non-linear effects occurring at high ω and large strain, as κ_1 varies as a consequence of a new compensation between the deformed dual-phases. This is shown in Figs. 47a and b for the PMMA melt of Figs. 42a to c.

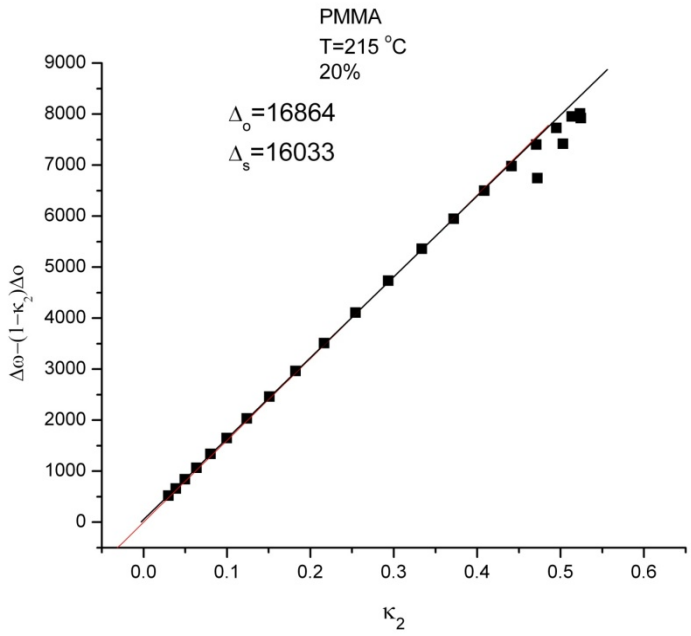

Fig. 47a

Determination of Δ_s from a plot of the cohesive energy of the activated strands vs κ_2 for PMMA T=215 °C, 20%.

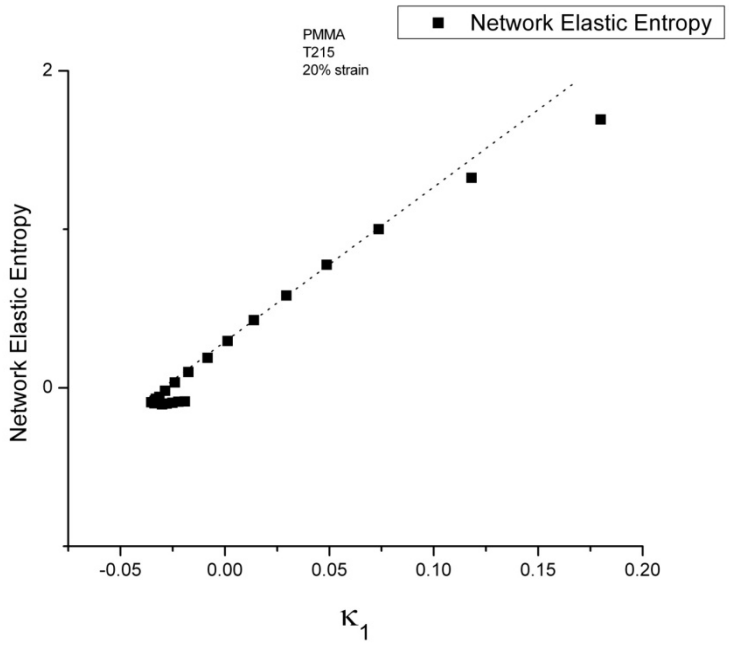

Fig. 47b

Variation of the Network Elastic Entropy as a function of κ_1 for PMMA T=215 ^{o}C, 20%.

Figure 47a is a graph to determine the value of Δ_s from the slope of a plot of the total cohesive energy of the activated strands vs the network elasticity κ_2. One sees a clear deviation from the straight line for the points corresponding to the highest ω values. The reversal of κ_2 is also visible. One may deduce that Δ_s decreases in this region. We suggest, however, that this is not the case, i.e. Δ_s remains constant, yet that the elastic network of phase-lines deforms, dragged by the increase of κ_1 already explained with regard to Fig. 42b. We determine the variation of the elastic network cohesive energy by the difference between the value obtained from the straight line in Fig. 47a, therefore at Δ_s constant, and the experimental value, shown as the black squares in Fig. 47a. We multiply this difference by the absolute temperature to define the "network elastic entropy", and plot it in Fig. 47b against the value of κ_1. One sees that the network elastic entropy remains zero up until κ_1 starts to grow positively, as determined by Fig. 42b. Figure 47b suggests a coupling between the start up of the deformation process in the κ_1-phase and the orientation of the tie-lines in the κ_2-phase network. Interestingly, the coupling involves an activated stressed network that interacts by compensation with a local mechanism of diffusion and conformational transformations: global vs local, entropic vs enthalpic, to greatly simplify.

SUMMARY AND CONCLUSIONS

In this paper we propose a new understanding of the rheology of polymeric melts using dynamic frequency sweeps to define the concepts. We introduce the Cross-Dual-Phase model which we claim can serve as the basis to describe the state of conformer interactions when long chain macromolecules entangle. Our objective is to understand melt deformation in terms of the conformers which are statistically described by the Cross-Dual-Phase model and derive the properties of the melt (modulus, viscosity) within that context. The inter- and intra- molecular bonding between conformers couple up to form a statistics which no longer focuses on the properties of single macromolecules embedded in a mean field of neighboring interactions that restricts their motions. In our statistical description of the state of the conformers, our system is composed of all the conformers belonging to all the macromolecules and we need to determine whether the conformers are cis, gauche or trans ("c,g,t") and also whether there are of the "b" type or "F" type depending on their degree of inter-molecular interactive coupling (the F-conformers are free from inter-molecular bonding).

The dual-phase statistics, [b/F $\leftrightarrow$ (c,g,t)], which governs the population of the isomeric states of the conformers, explains the collapse of the macromolecules into a coil and the split into two dual-phases, "the Cross-Dual-Phases", when the chain length of the macromolecules reaches a critical value. This split of the statistics into two co-existing and interactive populations ("phases"), i.e. $[b/F \leftrightarrow (c,g,t)]_1$ and $[b/F \leftrightarrow (c,g,t)]_2$, is responsible, we suggest, for what is usually described as the entanglement network characteristics of polymers. The state of the conformers in the two dual-phases, i.e how many of them are -trans, cis, gauche- and, also, of the type b or F, are different.

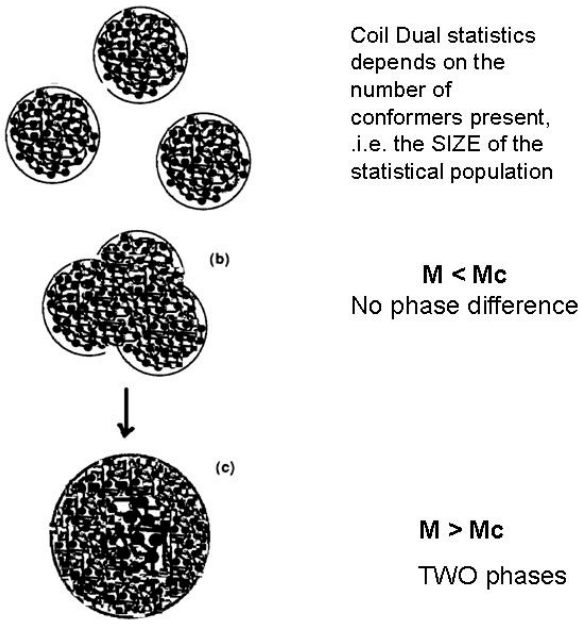

Fig. 48

Interpenetration of a set of 3 "macro-coil" systems. The equations of the Grain-Field-Statistics [35] are applied to solve this problem and result in an interesting result regarding the homogeneity of the [b/F ↔ (c,g,t)] solution. When the number of conformers per macro-coil is smaller than a certain critical value, M_c, the interpenetration does not result in any distinction between the conformers of the intersection and the conformers from the original sets. The statistics [b/F ↔ (c,g,t)] is modified by the interpenetration, but is everywhere identical. This is not the case for M>Mc, where a split of the statistics into 2 different groups occurs, creating two dual-phases $[b/F \leftrightarrow (c,g,t)]_1$ and $[b/F \leftrightarrow (c,g,t)]_2$. This is the heart of the new understanding of polymer entanglement and polymer physics.

Figure 48 gives a sketch of the split into two dual-phases, as already introduced in Chapter 1 and earlier publications [33, 34]. The black balls represent the b-conformers, the white regions between black balls the F-conformers, the change of size of the balls and of the white regions represents, in our cartoon picture, a different solution for the b/F and (c,g,t) variables in that region, which co-exists as a new dual-phase with the dual-phase of the smaller black balls and smaller white regions. One sees that the interpenetration of macro-coils does not split into two dual-phases when the chain length in the macro-coil is less than a certain value M_c. When the chain length, however, reaches above that critical system size, the solution is no longer homogeneous and there is a split of the statistics into two different groups, $[b/F \leftrightarrow (c,g,t)]_1$ and $[b/F \leftrightarrow (c,g,t)]_2$, of dual-phases. The word **Cross**-Dual-Phase intends to convey the idea that the

two dual-phases are coupled and dependent, one of the dual-phases defining **a channel network** which we have called the phase-line network (or entanglement network) in this paper, delimitating cells of **core-phase,** the other dual-phase. In other words the Grain Field Statistics does not define 4 phases but two dual-phases, like two types of crystallographic structures co-existing interactively or two types of clouds floating in the sky. Melt cohesion implies a fluctuation of the channel/core phase contours, which is constantly in motion, like froth in an agitated sea near the shore (Fig. 4). Perhaps an easy way to visualize the concept is to consider that the two dual-phases have a shifted T_g (say 3 to 10 ^oC difference), for instance because of a small difference in free volume, represented by the F-conformers.

In this chapter we provide basic answers to the fundamental questions which arise when one analyzes viscometry results arising from melt deformation in a dynamic rheometer; shear-thinning and strain softening. The drive for the dual-phase deformation process is the increase of the population of the **extended** conformers (e.g. trans) in the direction of the strain imposition and this can be achieved by two mechanisms:

1. Stress modification of the conformer potential energy to favor trans conformers. We call this sequence "stretching"
2. When there is more than one system, **transport** of conformers **by diffusion** in the direction of deformation (assuming the trans are the more abundant conformers because more stable). We call this sequence "relaxing".

Fig. 49 gives a sketch of a cross dual-phase being deformed in a stretch-relax sequence.

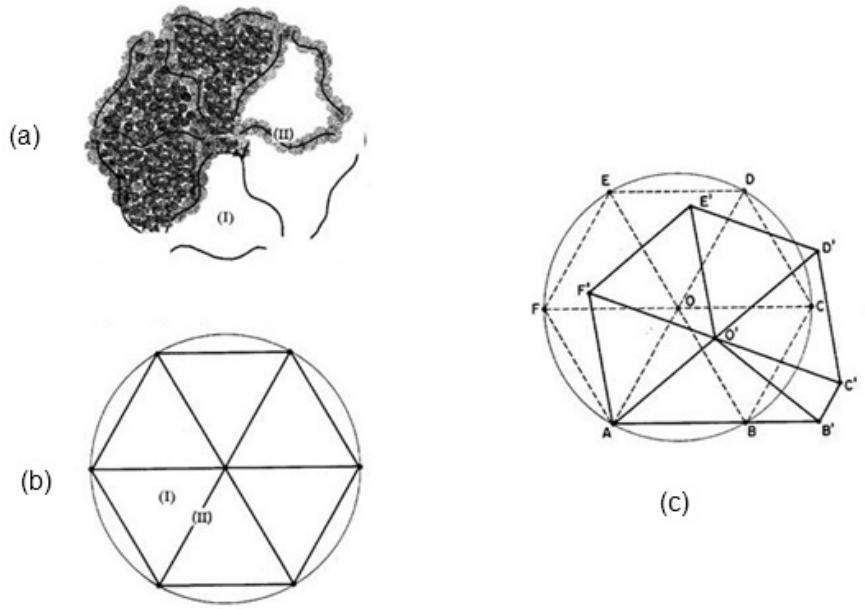

Fig. 49

(a) Sketch of a network of phase-lines strands (II) bordering 6 core-phase cells (I); (b) geometric representation of (a); schematic representation in (c) of the deformation process involving the stretching of a phase-line strand (AB→AB′) during time t_l (Fig. 50a) followed by its relaxation and the simultaneous re-organization of the cooperative set of type I core-phase conformers by rotation/diffusion (B→B′, C→C′, D→D′, E→E′, F→F′, etc.)

The two dual-phases play a distinct but complementary role which is determined by their initial visco-elastic state and by the deformation requirement, i.e. the rate of deformation and the magnitude of the strain, at the corresponding temperature. The channel network formed by the "softer" dual-phase (the one with the lower T_g, thus the higher free volume content) is mechanically activated **first**, manifested by the shear-thinning response to an increase of strain rate or frequency. Shear-thinning at low strain and low frequency (lower than the frequency for the maximum of $(G'/G^*)^2$) involves the stretch-relax mechanism of deformation of an increasing number of activated network strands as frequency increases. There are two ways to increase the number of activated strands, either increase the frequency of activation for any given strand, or increase the number of strands activated simultaneously. We show formulas in this paper that provide a way to distinguish between the collective aspect of shear-thinning (Eqs. 20, 21) and the dynamic response of the activated process (Eq. 14). Both play a significant role which varies with temperature and strain. We study in this paper both variables in depth.

The temperature dependence section makes us return to the existence of the T_{LL} transition [1,2, 20], which is evidenced in many figures (Figs. 25c and d, Figs 26a and b, Figs. 29c , d and e). We suggest that the transition T_{LL} corresponds to the temperature below which the role played by the dynamic response of the stretch-relax process (k in Eq. 12) becomes dominant, whereas k is constant above T_{LL}, shear-thinning being described by the increase of the number of simultaneously activated strands. According to this explanation, shear-thinning becomes more efficient below T_{LL} because both mechanisms that lower viscosity (Eqs. 12 and 20) reinforce each other: the increase of k in Eq. 12 increases ω', thus decreases viscosity, and the decrease of ΔH_ω in Eq. 21, by the increase of the number of activated strands, κ_2, also results in the lowering of viscosity in Eq. 20. In our model, the recognition of the existence and manifestation of T_{LL} is important because it reveals the competition between the singularity of the stretch-relax activation dynamism of a single strand and the collective response of several strands activated simultaneously, as a function of the elastic strain energy, κ_2, of the channel phase ($\omega'=\omega/\kappa_2$). The sequential aspect of the deformation process that characterizes shear-thinning is the result of a minimization of the free energy for the stretch-relax activation. The stress required to modify the potential energy barrier of the isomeric conformation statistics increases with the strain production, i.e. with the excess number of trans-conformers with respect to the equilibrium value. This is schematically shown in Figs. 50a which plots the stress/kT vs time as the kinetic length %, defined in Fig. 12b increases (k here is the Boltzmann´s constant). Fig. 50b provides the variation of the conformational population as stress originates from a forced re-organization to produce the extended conformations.

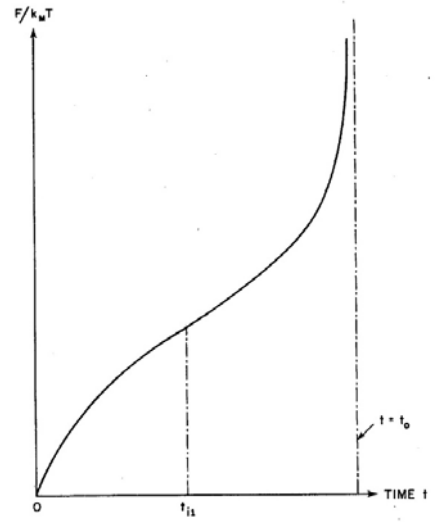

Fig. 50a Stress/kT vs time for the "stretching" of a system of conformers [b/F ↔ (c,g,t)] by isomeric conformational rotation. The strain produced by the system depends on how many flexed conformers are turned into extended ones. The maximum strain possible is 40%. See Fig. 12b. Stress is required to keep the conformational state out of equilibrium.

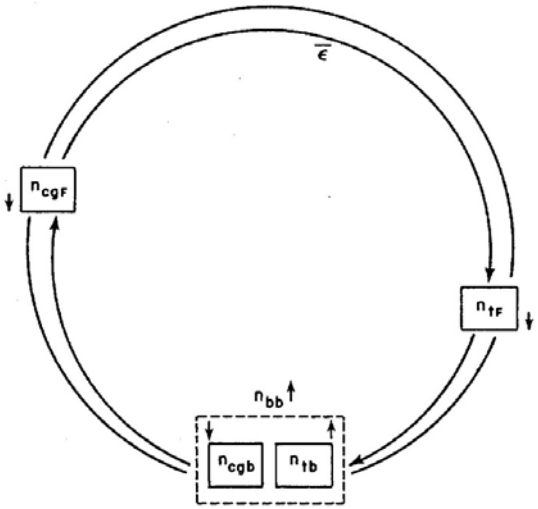

Fig. 50b In this representation of the state of the conformers during stretching, we specify, at each t, how many conformers of the systems are b type (n_{bb}), F type ($n_{cgf}+n_{tf}$), cis-gauche ($n_{cgf}+n_{cgb}$)or trans ($n_{tf}+n_{tb}$). The arrow besides the boxes provides the changes occurring to populations (down arrow for a decrease, up arrow for an increase). The symbol ε symbolizes that a change between the cgF (flexed) and tF (extended) conformer populations generates strain as shown in Fig. 12b. When the system starts to relax at time t_I (its strain rate becomes 0), all values are modified with a kinetics very similar to thermal diffusion.

One sees in Fig. 50a that the stress to produce the conformational changes to produce strain ε has the overall shape of a Langevin's function, with an infinite value for the stress corresponding to a strain approximately equal to 40% (Fig. 12b). The minimization of the free energy imposes that the stretched system start to relax (at constant strain) when the stress reaches the inflection point of the Langevin function (t_{I1} in Fig. 50a). The temperature dependence of t_{I1} [34-36] explains the time-temperature equivalence observed in visco-elastic experiments. At any moment of the stretch-relax mechanism, the increase of the trans-conformers by conformational rotation only lasts t_{I1} seconds, followed by a local re-organization and transport of the bonds by diffusion during the relaxing sequence. The stretch sequence corresponds to an elastic solid-like deformation mechanism, and the diffusional relaxation is a dissipative process, very similar to what occurs by thermal diffusion. The stretch-relax sequencing of a strand occurs with frequency ω', meaning that it repeats itself with period 1/ω', of which t_{I1} seconds are devoted to elastic stretching and $(1/\omega' - t_{I1})$ to relaxation-diffusion. Under thermal diffusion conditions, there is no elastic deformation, thus $t_{I1}=0$. The frequency ω'_o describes the thermal diffusion of the phase-wave at the corresponding temperature and can serve as a normalizing frequency to describe shear-thinning (Eq. 12). As strain is applied, ω' and t_{I1} are both functions of the rate of deformation, with 1/ω' and t_{I1} decreasing. One easily understands that the timing of the ω' sequencing and that of the t_{I1} sequencing play a role in the visco-elastic response to deformation (as evidence by the change of behavior at T_{LL}). To simplify, let's say that the parameter k, which we have defined in Eq. 12, translates the coherence between the two sequencing, one related to the activation of multi-strands, the other one related to the stretch-relax sequencing within the activation process itself. The coherence (or synchronization) between "inter-strands activation" and the "intra-strand activation" is a characteristic of shear-thinning which, we suggest, is an important aspect of the melt deformation process.

We have determined that the maximum of stored elastic energy, $(G'/G^*)^2_{max}$, , which corresponds to the frequency at which the phase angle δ is minimum, is correlated to the entanglement network topology (the channel structure in Fig. 4) which itself is a strong function of the chain length, thus of the average molecular weight and its distribution. This, we assume, is due to the inability of "closed-loops dual-phase regions" to bear stress through the cooperative

activation of the network of strands, reducing the total number of strands that can be activated. A dual-phase closed loop is schematically shown in Fig. 51.

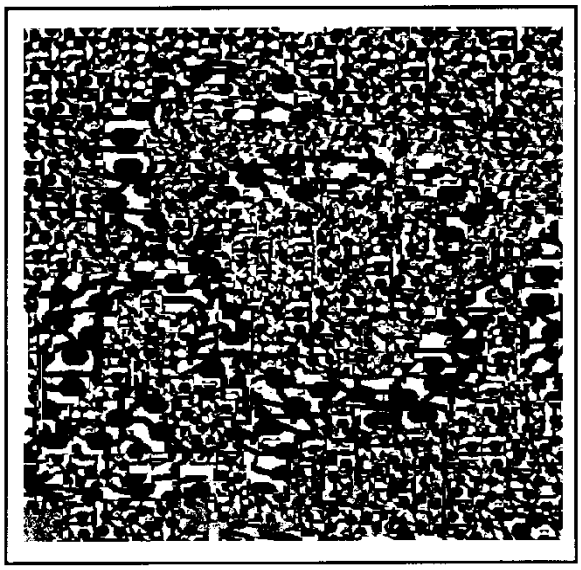

Fig. 51
Sketch of a closed-loop (inactive) dual-phase strand (the larger scale black balls and white interface). This part of the Cross-Dual-Phase is isolated from the network of phase-lines and does not participate in the stretch-relax cooperative deformation mechanism.

At low strain, in the linear visco-elastic range, the terminal region extends out to the maximum of $(G'/G^*)^2$, and the mechanism of deformation is essentially that of the entanglement phase network, the κ_2-phase, characterized by the sequential activation of the phase-line strands (the large black balls and interface), without the need to modify the structure of the network. Shear-thinning, under such circumstances, proceeds by the increase of the number of activated strands as ω increases, without recourse to a change of the timing of the stretch-relax sub-sequencing (k remains constant in Eqs. 12 to 15). In the rubbery plateau regime, which starts just beyond the maximum of $(G'/G^*)^2$, k has become 1, signaling the coherence and synchronization of all the activated strands cooperatively responding to the deformation. The coherence implies a more efficient coordination between the stretch-relax strain producing sequences, which releases the demand for the number of cooperative strands, $(G'/G^*)^2$ decreases, compensated by the increased involvement of the core-phase during the relaxing sequence of activation (Figs 45a

and b). This decrease of the number of activated strands is compensated by an increase of the involvement of the κ_1-phase in the deformation process and results in the flattening of the modulus increase with ω, perceived as a plateau region. During that plateau regime of deformation, the entanglement κ_2-phase network orients in the direction required by the strain, which influences how ω' varies with ω and stress. When all the strands are oriented (schematically represented in Fig. 52), this is the end of the rubbery plateau region, and the beginning of the transition regime. The entanglement network is fully oriented and $(G'/G^*)^2$ has reached its minimum value.

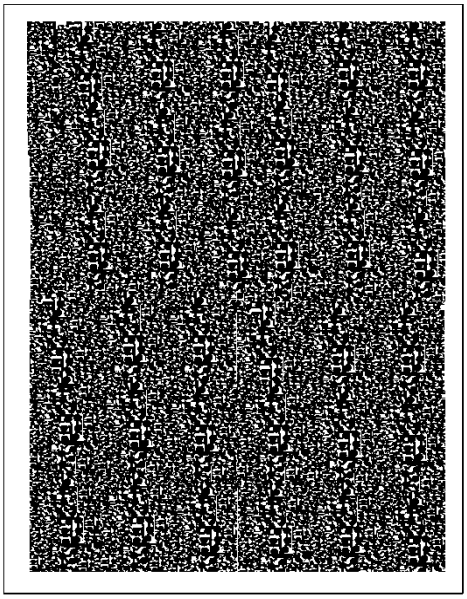

Fig. 52
Sketch of a fully oriented Cross-Dual-Phase. This is assumed to be the state of the network at the end of the rubbery plateau region, beginning of the T_α transition.

The strain energy which was stored in the κ_2-phase is now used to maintain the trans-conformers of the κ_1-phase out of equilibrium. There is, in the plateau regime, a gradual compensation of the phase-line network entropy, resulting from its orientation, and of the κ_1-network enthalpy. The corresponding frequency when the elastic network entropy is at its maximum is the frequency of the T_α at that temperature. When temperatrure varies, so does the frequency of the minimum of $(G'/G^*)^2$, thus T_α is function of ω. The behavior of the melt at T_α

and between $T_\alpha(\omega)$ and T_g permits to determine the characteristics of the potential energy giving rise to the isomeric conformational stretch process.

We studied in this paper the frequency dependence of the moduli G'(ω) and G"(ω) at constant (T-$T_\alpha(\omega)$), i.e at constant free volume, and compared the results with those obtained at constant T. The idea behind this approach stems from the coupling between the b/F statistics, which controls the local amount of free volume, and the (c,g,t) statistics which is disturbed by stress in the stretch-relax mechanism of deformation that describes shear-thinning. Coupling between the inter- and intra- molecular forces is at the center of the dual-phase kinetics [35], and, therefore, it should be possible to separate out the effect of free volume from the effect of the isomeric conformational changes by operating at constant free volume. Note that in the currently accepted models of viscoelasticity, viscosity is the product of a function that varies with temperature only with a function that varies with molecular weight, i.e. the effect of free volume is considered separate from the effect of topology, a conclusion that we discussed and disputed in part I of this series [1]. In our analysis of rheological data at constant free volume, we find that the classical Maxwell rules establishing the proportionality between G' and ω^2 and G" and ω in the terminal regime do not hold. This is shown in Figs 53a and b, as explained in the captions.

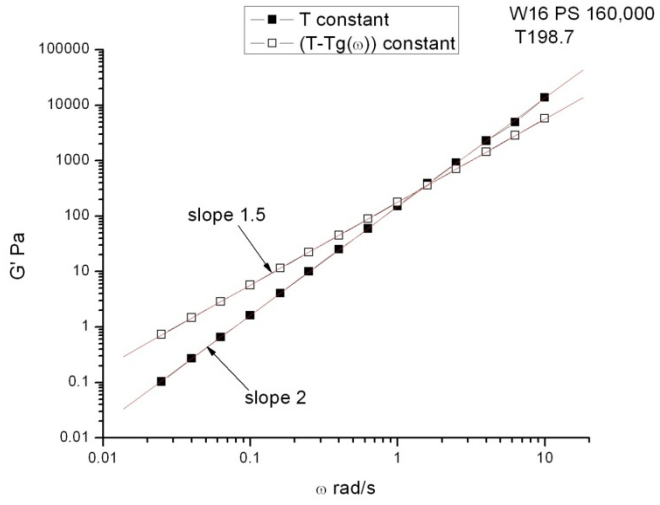

Fig. 53a

Plot (log-log) of G'(ω) vs ω during frequency sweep presented at either constant temperature T and at (T-Tg(ω)) constant. The slope at low ω is equal to 2 and 1.5, respectively. Data of Marin [13] on PS.

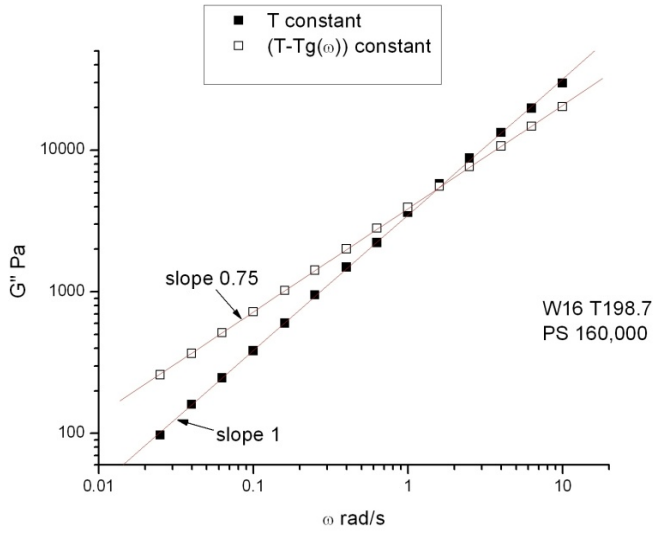

Fig. 53b

Plot (log-log) of G'(ω) vs ω during frequency sweep presented at either constant temperature T and at (T-Tg(ω)) constant. The slope at low ω is equal to 1 and 0.75, respectively. Data of Marin [13] on PS.

We found that free volume played an important role in the mechanism of shear-thinning, yet that it was not to simply shift horizontally the rheological parameters as it is stipulated by the time-temperature superposition principle. On the contrary, we suggested that the shifting of the curves located below or beyond the maximum of $(G'/G^*)^2$ did not occur with the same shift factor, explaining the corruption of the results (for instance to determine η^*_o) when extrapolations were made from Carreau's fits performed on wide ω ranges extending across the frequency for the maximum of $(G'/G^*)^2$. We demonstrated that the increase of frequency played two roles as far as viscosity was concerned: it produced shear-thinning, by the stretch-relax mechanism mentioned above, and it also increased viscosity by reduction of free volume, as $(T-T_g(\omega))$ was reduced, due to the difference of the shift factor as ω increases. The increase of viscosity is visible at low temperature (Fig. 17c), being responsible for the so-called second Newtonian plateau observed at high strain rate or frequency. Finally, we showed that operating at constant free volume substantially increased the value of the terminal time obtained at the maximum of G'/ω (Fig. 19), as well as the value of the Newtonian viscosity which increased by several decades (Fig. 18).

We provide in this conclusion a last result regarding the molecular weight dependence of the viscosity at constant free volume, in order to compare with the classical behavior found at constant temperature, the Newtonian viscosity varying like $M^{3.4}$, as it is well known [29]. Our interest is to determine whether the famous 3.4 exponent that characterizes the melt viscosity dependence on molecular weight (for entangled polymers) would be different when the rheological data are determined at constant free volume; in particular, whether de Gennes had been right in the first place, predicting the exponent to be equal to 3.0 in his famous early work [29].

Our result is shown in Fig. 54. It relates to all monodispersed PS samples studied by Marin [13], re-analyzed at constant $(T-T_g(\omega,M))$.

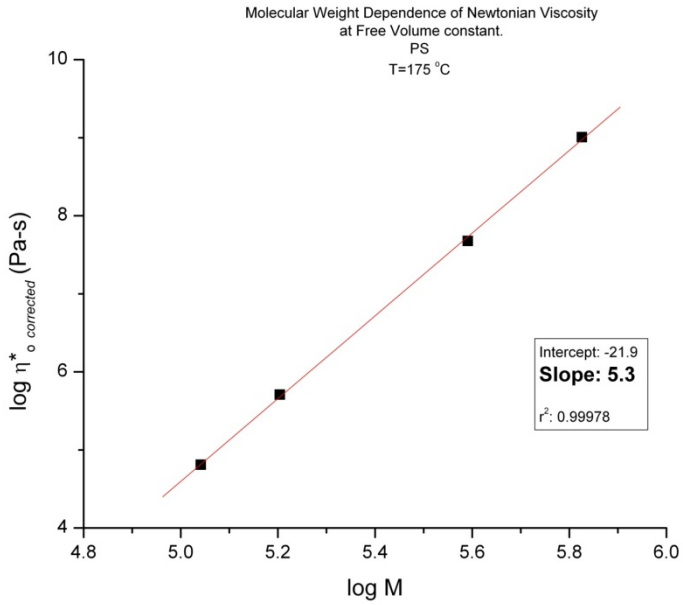

Fig. 54

Plot (log-log) of Newtonian viscosity vs M for a series of monodispersed PS . Data of Marin [13]. The original data are corrected to keep (T-Tg(ω)) constant and a WLF-Carreau fit is done to determine the Newtonian viscosity for each PS. The points shown on this curve are calculated at the same temperature. The slope is 5.3.

The exponent is not 3.0, nor 3.4, it is 5.3. Besides, in the Vogel-Fulcher's expression of the temperature dependence of the friction factor (Eq. 16), the famous T_2 - for which viscosity becomes infinity- is raised from 55 °C to 123 °C, when the free volume is accounted for [35, 36]. These results show how important it is to correctly describe the effect of the free volume on

molecular mobility when analyzing dynamic rheological data. The mythical constants, 3.4 for the viscosity exponent, $T_2=T_g-52.5$ for the WLF equation, are the results of cooperative contributions from free volume and conformer rotations. The influence of free volume is not separable the way it is traditionally presented: in our analysis, free volume influences both the T and M factors in the viscosity expression.

Interestingly, the temperature of 123 ^oC found for T_2 is 23 ^oC above the T_g of Polystyrene, determined by DSC, for instance. And this temperature is precisely the temperature of compensation for this polymer for all the relaxation modes occuring below T_g. Refer to Fig. 13 of Ref. 23, or Fig. 26 of Ref. 33, for instance. One knows that the coupling between the molecular motions below T_g, resulting in compensation, occurs in a very restricted free volume environment, compared to what is assumed to occur above T_g. It is, therefore, somewhat satisfying to find that the T_2 obtained after removing the effect of free volume is the same as the compensation temperature found from a study of motions in the solid state. It is also remarkable to see how the free volume is intrinsically coupled with the effect of molecular chain length above T_g: mobility is much more reduced (by a factor 100) than what one thought was only due to molecular weight alone. The influence of molecular weight is described by the exponent 5.3, an extraordinary large number. It is only because the free volume is interactively coupled with the configurational effect that we observe the 3.4 exponent. As said before, viscosity does not separate into a term that varies with T only and a term that is function of M only. This formulation is only a convenient approximate representation.

We also study in this article the effect of strain on the visco-elastic behavior, i.e. describe the non-linear visco-elasticity in terms of the Cross Dual-Phase model. The effect of strain is, expectedly, perceived at several levels, at the level of shear-thinning of the κ_2-phase, but also, most importantly, by the trickling down of the involvement of the κ_1-core phase in the strain production process. This compensation of the role played by the two dual-phases is the dominant reason for strain softening to occur (the decrease of the modulus as strain increases, the effect being amplified at higher frequencies). Usually, strain softening is experimentally observed and studied in step-up relaxation experiments, where the melt is suddenly shear-strained to a certain value of strain in a very short time. A high frequency response torque gauge measures the

amount of force needed to achieve the commanded strain, from which stress and viscosity are derived. By changing the value of strain during the initial step up, one can determine if the torque is proportional to strain, and when it is not, in the "non-linear region", one can define the strain softening or hardening factor, h, the ratio of the non-linear modulus to the linear modulus found at low strain. For strain softening melts h <1 since it is observed that the modulus, stress divided by strain, decreases with increasing strain magnitude.

In Chapter 4 (also in Ref. [2]) and in a long section of this Chapter (Figs. 31a-44) we presented and analyzed dynamic frequency sweep experiments conducted at various strains indicating that strain softening was the result of an increase of the strain amplitude observed, along with shear-thinning at higher frequencies. Shear-thinning corresponds to the decrease of viscosity as shear rate (or frequency) increases. When shear-thinning is observed, the modulus increases with shear rate. For modulus, strain-softening corresponds to a decrease of modulus as strain increases. Yet, when strain-softening is observed, the stress increases with strain. The analogy between the two propositions above makes us conclude that, in strain-softening, strain and modulus play the same role played by strain rate and viscosity in shear-thinning, respectively. What changes between shear-thinning and strain softening is the identity of the cooperative systems involved in the compensation process. For shear-thinning, we saw that deformation proceeds from the competition between the simultaneous activation of several strands of the entanglement network and the stretch relax timing sequence defining the activation of each strand. For strain softening, the two dual-phases are mechanically activated by coupled and interactive shear-thinning mechanisms that operate by compensation of their individual stress and the elastic strain energy. The visco-elastic state of each of the κ_1 and κ_2 dual-phases is different at each stage of deformation, a situation that eventually will lead to yielding or even melt decohesion and fracture, as the strain demands continue to increase.

We found that the compensation (interplay) between the two dual-phases originates from the invariant of the $\kappa_2(\omega)$ vs $G^*(\omega)$ as strain varies, which permits to determine the shear-thinning parameters characteristic of the specific stretch-relax mechanisms occurring in each dual-phase $(\omega'_o, k, G^*_1, \Delta s)_{i=1,2}$. The decrease of G' and G" with increased strain is essentially due to the transfer of strain production to the core-phase (κ_1-phase), which is de facto taking the burden from the stressed κ_2-phase, releasing it from operating in solo mode, and this for a relatively lower stress cost.

We summarize our cross dual-phase understanding of strain deformation by the following formula:

(24)

$$[b/F \leftrightarrow (c,g,t)]_1 \leftrightarrows [b/F \leftrightarrow (c,g,t)]_2$$

The dual headed arrow inside the brackets relates to the dual aspect of the conformers, covalently bonded to adjacent conformers, and either inter-molecularly bonded or free to rotate. This duality defines a local statistics that interactively couples free volume and conformational distribution along the chain. The split of the statistics into two groups, here symbolized by the the two brackets, 1 and 2, only occurs for chains above a critical length (Fig. 48). This is inherent to the Grain-Field-Statistics [35]. What we have shown in this paper is that at low strain, the driving phase is phase 1, with shear-thinning fully understood from the changes occurring to phase 1's statistics. In that situation, phase 2 statistics "drags along", re-organized by diffusion. The increase of ω' with stress may be perceived as an increase of the sweeping wave motion across the melt volume, probably resulting in the resizing of the core-phase defined between the phase-line boundaries (Figs. 4 and 49). In other words, the core-phase remains passive in the linear viscoelastic regime, which explains why the classical theories of linear viscoelasticity, based on a triggered relaxation mechanism (spring+piston), have been quite successful describing it.

Perhaps the power of our two dual-phase approach becomes more apparent when the second dual-phase "wakes up", incited to do so by the increased demands either in terms of increased strain rate or increased strain. This is where the core-phase comes to "rescue phase 1", so to speak (which we call "compensation"), and releases it from extreme variations which would cause de-cohesion or failure. The compensation mechanism can take several aspects because of the ability of the dual-phase themselves to respond, individually or collectively, by a stretch-relax strain producing mechanism which modulates the involvement of the inter-phases coupling. When strain softening is in full mode, though, as clearly evidenced, for instance, for the PMMA melt of Figs 37a to c, both cross dual-phases are activated by shear-thinning (Fig. 37d), and therefore both dual-phases are active and interactively producing strain. We saw, in that particular example, that the viscoelastic states of the two dual-phases were different, one

being in the rubbery plateau region, the other in the terminal region. Obviously, the question of visco-elastic cohesion comes to mind, with perhaps the possibility to tackle with the Cross-Dual-Phase model the difficult problems associated with internal yielding, shear banding, de-cohesion and fracture. It is clear that cohesion requires a certain harmony between the statistical changes occurring **within** the dual-phases (intra) and i**nter** dual-phases. The analytical tools developed in this paper appear to be applicable to determine the criteria for which the strain rate and strain reach critical conditions.

What about disentanglement? How would this concept be defined in terms of the Cross Dual-Phase model? A simple answer would indicate that disentanglement has occurred if the amount of the two-dual phases has changed. Another point of view would be more general and include the network (phase-lines) topological changes in the definition of disentanglement. We have now much more information regarding shear-thinning and strain softening and their interdependence to be able to answer a few fundamental questions. The time dependence of G', G" and $\eta*(\omega)$ triggered by an increase of strain (say Figs. 3a and b of Ref. 2) is not necessarily producing any disentanglement, if the definition excludes network topological changes. In fact, in most conditions permitted in a lab rheometer, there is rarely disentanglement at all, yet the time dependence is not an artifact, it is due to the dynamic aspect of the compensation between the two dual-phases (Eq. 24). This is the reason we symbolize this compensation by a double-arrow in Eq. (24), since this is how chemists describe the dynamic character of reaction kinetics. If, however, the orientation of the network of phase-lines is considered as disentanglement (see Fig. 52), then disentanglement starts at the maximum of $(G'/G^*)^2$. Yet, we can assert that this type of "disentanglement", especially at low strain, will not produce any viscosity drop that can be preserved in a pellet that will show up on reheating [2, 32a, 32b]. So, how would we create an effective disentanglement which would retain viscosity reduction in a pellet until at least it is re-heated? We will let the reader figure out; the basis for the answer is exposed in this paper.

In summary, one sees that the new analytical tools presented in this paper to analyze rheological data are particularly tuned to address non-linear viscoelastic issues raised by the increase of strain rate and strain. That being said, our presentation of the basic model can only be considered as an introduction to the subject, which is vast, rich and diversified. In particular, the

questions regarding secondary effects such as chain breakage and branching under high stresses have not been addressed. Our objective was how to understand polymer melt flow from the perspective of our model of the Cross-Dual-Phase. More than 10 years ago, this model was used [33, 34] to describe interactive motions and transitions in polymers observed by Brilloin scattering and low frequency Raman spectroscopic methods (Boson peaks), as well as by thermally induced depolarization current analysis. The challenge ever since had been to apply the Cross-Dual-Phase model to viscoelastic flow data.

Before closing, we want to assert and show with a couple of examples that our model describes linear viscoelasticity at least as well as the currently accepted models of reptation [29] and their ramifications [27,30]. This is presented in Figs. 55a to c.

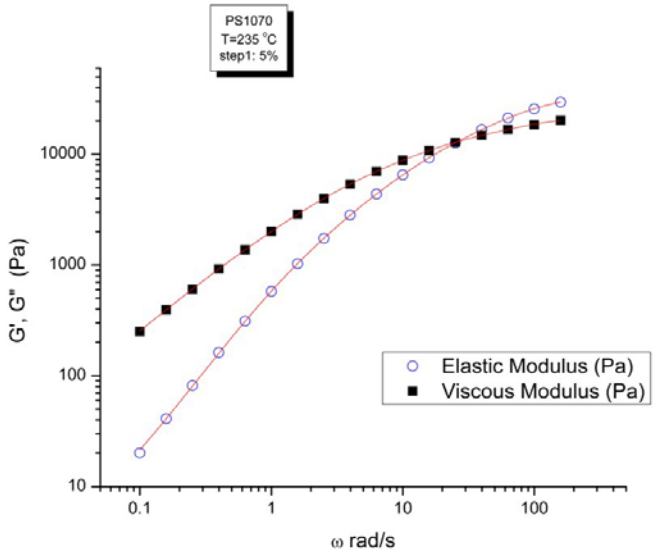

Fig. 55a

Fit of G'(ω) and G"(ω) with equations derived from the cross dual-phase model. The strain is 5%. This is the domain of linear viscoelasticity for this PS melt studied in the terminal region. The lines going through the data are calculated from fits by Eqs 5, 7, and 12.

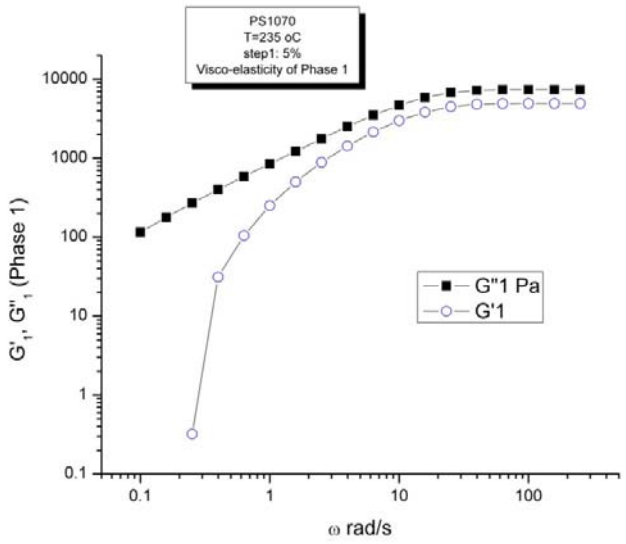

Fig.55b

Split of G'(ω) and G"(ω) into two components. The solution is derived from the split of $(G'/G)^2$ into $\kappa_1+\kappa_2$, and of G* into $G^{*(1)}+G^{*(2)}$. This plot gives the result of the split for the phase-line phase (called here phase-1). The moduli apply to a soft melt for which there is no cross-over, a behavior also found for unentangled polymer melts (M<Me).

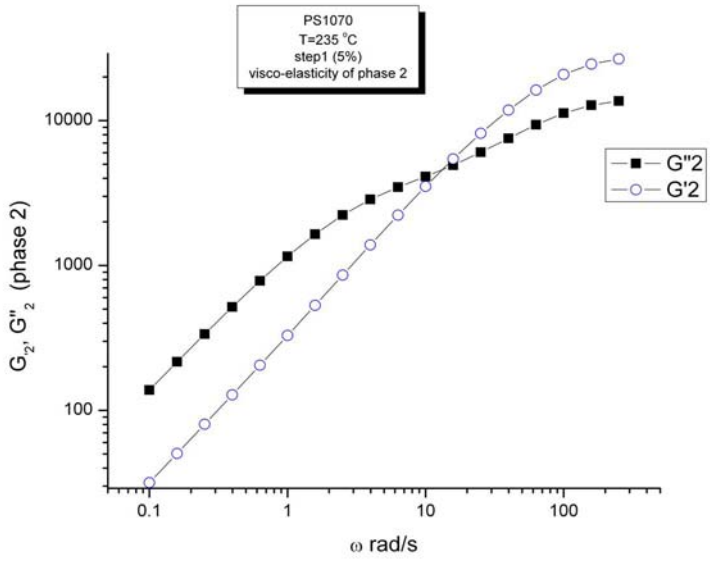

Fig.55c

Split of G'(ω) and G"(ω) into two components. The solution is derived from the split of $(G'/G)^2$ into $\kappa_1+\kappa_2$, and of G* into $G^{*(1)}+G^{*(2)}$. This plot gives the result of the split for the core- phase (called here phase-2). The moduli are larger, there is a cross-over, a behavior also found for entangled polymer melts (M>Me).

One clearly sees that the solution obtained for G'(ω) and G"(ω) in the linear viscoelastic range describes very well the data. There is yet another advantage using the dual-phase model to characterize the linear or non linear viscoelastic regime. This is briefly demonstrated in Fig. 56.

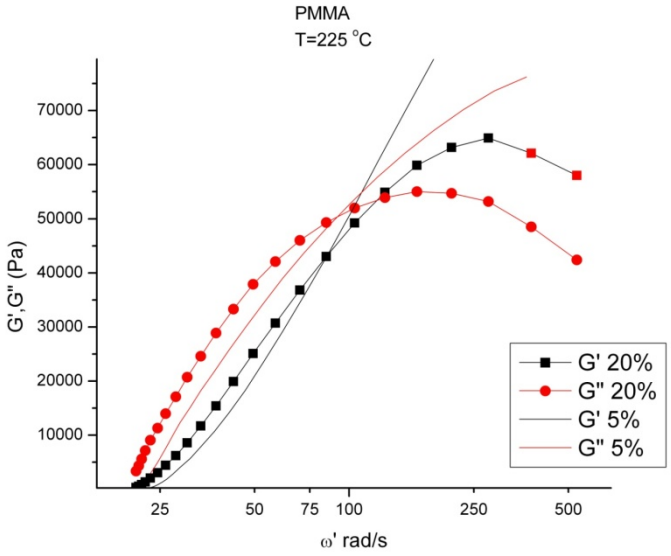

Fig. 56
Rheology in the ω' domain. Instead of using ω to plot and analyze the data, it may be advantageous to express all rheological variables (moduli, viscosity) as a function of ω', which is the frequency of the network under stress.

If ω' is the true frequency characteristics of the response of the elastic network, the rheology should be transposed into that plane and we should compare data against ω' and not ω. This is what we offered when expressing viscosity as a function of ω' (Eq. 8), or establishing the relationship between G* and ω' (Eq. 14). If results (G',G") are presented vs ω' (and not ω), or better ω'/ω'_o, it appears that a different perspective emerges, as illustrated in Fig. 56. For instance, the 20% strain moduli are located above the 5% value for a given ω' until the κ_1 –phase participation comes into play which results in a lowering of the 2% strain moduli. It is interesting to note that in the ω' plane there is apparently strain hardening of the 20% strain moduli G' and G" at low ω' values since the curves for 20% are located above those for 5%. As we said, the new cross dual-phase analysis opens up new perspectives and challenges, even in the linear viscoelastic range.

In conclusion, this paper is the first presentation of a new analysis of polymer flow within the framework of the Cross-Dual-Phase model of polymer interactive coupling. This new understanding of visco-elasticity and flow opens up new perspectives and challenges which may very well drive new applications in polymer processing, mixing and other practical applications.

In our opinion, the prime importance of describing correctly the deformation of a polymer melt goes far beyond the objective to successfully formulate visco-elasticity or rubber elasticity in linear or non-linear conditions, and consists of establishing "the dynamic structure of entropy", i.e. the physics of interlocking scales, how to integrate mathematically the results of interactions occurring at a certain scale into new parameters which define another scale. In other words, understanding network entanglements in polymer melts might offer one important step into the understanding of the mechanism of scale change under conditions different than critical conditions (phase transitions).

REFERENCES (CHAPTER 5)

[1] J.P. Ibar, "*The Great Myths of Polymer Melt Rheology, Part I: Comparison of Experiment and Current Theory*", J. Macromol. Sci., Phys.,B 48,1163 (2009).

[2] J.P. Ibar, "*The Great Myths of Rheology,Part II: Transient and Steady-State Melt Deformation: The Question of Melt Entanglement Stability*", J. Macromol. Sci.Phys., B 49, 1148 (2010)

[3a] L. Noirez, H. Mendil-Jakani and P. Baroni, "*Identification of finite shear-elasticity at low thickness in the liquid state of molecular and polymeric glass-formers*", Phil. Mag., ISSN 1478–6435 print/ISSN 1478–6443 online, 2010
DOI: 10.1080/14786435.2010.536176

[3b] L. Noirez, P. Baroni and H. Mendil-Jakani, "*The missing parameter in rheology: hidden solid-like correlations in viscous liquids,polymer melts and glass formers*" Polym Int 2009; 58: 962–968.

[4] A. C. Lunn: "*The Molecular Basis of Homogeneous Deformation in Glassy Polycarbonate,*" MIT Doctoral Thesis, Department of Mechanical Engineering (1972), pp. 18, 19, 20.

[5a] A.J. Kovacs, "*Glass Transition in Amorphous Polymers: a Phenomenological Study*", Fortschr. Hochpolym.-Forsch., 3, 394 (1963).

[5b] A.J. Kovacs, J.J. Aklonis, J.M. Hutchinson, A.R. Ramos, "*Isobaric volume and enthalpy recovery of glasses. II. A transparent multiparameter theory*", J. Polym. Sci., Polym. Phys. Ed., 17, 1097 (1979).

[6] L C E Struik, "*Physical Aging in Amorphous Glassy Polymers*", p.78 in Annals of the New York Academy of Sciences, M. Goldstein and R. Simha Editors, ANYAA9, 279 1-246, 1979

[7] C.T. Moynihan, and C.A. Angell, « *Bond Lattice or Excitation Model Analysis of the Configurational Entropy of Molecular Liquids*.". J. Non-Cryst. Solids, 274, 131-8 (2000)

[8] Jürn W. P. Schmelzer and Ivan Gutzow « *The Prigogine-Defay ratio revisited*" , J. Chem. Phys. 125, 184511 (2006);

[9] C.T. Moynihan et al, « *Structural Relaxation in Vitreous Materials* », p.15 in Annals of the New York Academy of Sciences, M. Goldstein and R. Simha Editors, ANYAA9, 279 1-246, 1979

[10] J.H. Gibbs and E.A. diMarzio, "*Nature of the Glass Transition and the Glassy State"*, J. Chem.. Phys., **28,** 373 (1958).

[11] J-C Majeste, Doctoral Thesis, Universite de Pau et Pays de l'Adour (UPPA), France (1998).

[12] R.F. Boyer,"*Encyclopedia of Polymer Science and Technology", Vol.* 13, p.285-286 Figs 5 and 6, Wiley, New York (1970).

[13] G. Marin, Doctoral Thesis, Universite de Pau et Pays de l'Adour (UPPA), France (1977). Also G. Marin and W.W. Graessley, Rheol. Acta, 16, 527 (1977).

[14] W.W. Graessley, Advances in Polymer Science, Vol. 16, "*The Entanglement Concept in Polymer Rheology*", p. 55, Springer (1974).

[15] P.E. Rouse Jr, "*A Theory of the Linear Viscoelastic Properties of Dilute Solutions*", J. Chem. Phys., 21,1272 (1953).

[16] A. Kovacs, "*The Isothermal Volume Contraction of Amorphous Polymers*", J. Polym. Sci.,30,131 (1958).

[17] C.A. Hieber and H.H. Chiang, "*Some Correlations Involving the Shear Viscosity of Polystyrene Melts*", Rheologica Acta, 28, 231 (1989).

[18] G.V. Vinogradov ,"*Investigation of Polymer Melts with a Constant Pressure Capillary Viscometer"*, Akad. Nauk.154, 1421 (1964).

[19 J.P. Ibar, ANTEC SPE Proceedings., paper 224 (1999), "*A New Formulation and Interpretation of Shear-Thinning of Polymeric Melts. Effect of Temperature, Strain Rate and Frequency*".

[20]] R.F. Boyer's: "*Computational Modeling of Polymers*", J. Bicerano, Ed., Marcel Dekker, New York, pp 1-52 (1992).

[21] R.F. Boyer, "*The High Temperature (T>Tg) Amorphous Transition in Atactic Polystyrene*",J. Polym. Sci. [C] 14, 267 (1966).

[22] H.Hocker, G.J. Blake, and P.J. Flory, Trans. Faraday Soc.,

[23] J.P. Ibar, "*Application of Compensation Phenomena to the Thermal Analysis Characterization of Polymers: Introducing the Degree of Disorder (DOD) Number*.", Polym. Eng. Sci, 31(20), 1487 (1991)

[24} C. Friedrich, K. Mattes, D. Schulze, paper presented at MACROIUPAC 2004, Paris, France "*Non-Linear Viscoelastic Properties of Polymer Melts as Analysed by LAOS-FT Experiments").*

[25] K.M. Mattes, R. Vogt, C. Friedrich, "*Analysis of the edge fracture process in oscillation for Polystyrene melts"*, Rheol. Acta, 47, 929(2008)

[26] R.G. Larson, "Non-Linear Viscoelasticity", Chapter 4 in, "*Rheology Principles, Measurements, and Applications*", C. W. Macosko Editor, John Wiley, New York, (1994)..

[27] M.H. Wagner, P. Rubio, and H. Bastian, "The molecular stress function model for polydisperse polymer melts with dissipative convective constraint release" J. Rheol., 45, 1387 (2001).

[28] R.S. Rivlin and K.N. Sawyers, "Nonlinear Continuum Mechanics of Viscoelastic Fluids", Ann. Rev. Fluid. Mech., 3,117-146 (1971).

[29] P.G. de Gennes, "Scaling Concepts in Polymer Physics", Cornell University Press, Ithaca, New York (1979); M. Doi and S.F. Edwards, "*The Theory of Polymer Dynamics*", Clarendon Press, Oxford (1986).

[30] G.J. Marrucci, J.Non. Newt. Fluid Mech., "*Dynamics of Entanglements: a nonlinear model consistent with the Cox-Merz rule*", 62, 279 (1996); G. Marrucci and G. Iannruberto, "*Interchain pressure effect in extensional flows of entangled polymer melts*", Macromolecules, 36, 3934 (2004).

[31] S-Q Wang et al., « *Nonquiescent Relaxation in Entangled Polymer Liquids after Step Shear* », Phys. Rev. Lett., 97, 187801 (2006).

[32a] J.P. Ibar. "*Processing Polymer Melts under Rheo-Fluidification Flow Conditions: Part I Boosting Shear-Thinning by Adding Low Frequency non-linear Vibration to Induce Strain Softening*", submitted to J. Macromol.Sci.Phys. (2012)

[32b] J.P. Ibar, "*Processing Polymer Melts under Rheo-Fluidification Flow Conditions: Part 2. Simple Flow Simulation*", submitted to J. Macromol. Sci. Phys. (2012).

[33] J.P. Ibar, "*Do We Need a New Theory in Polymer Physics?"* J. Macromol. Sci.-Rev. Macromol. Chem. Phys., C37, 389 (1997).

[34] J. P. Ibar, "*The $T_{\square}$, T_g and T_{LL} "Transitions": Are these the Manifestation of a Unique Relaxation Process?"* in Order in the Amorphous "State" of Polymers; Keinath, S. E.,Miller R. L., Rieke, J. R. Eds.; Plenum Press: New York, 371 (1987).

[35] J.P. Ibar “Grain-Field Statistics of Conformers in Interactions”, book in preparation (2012).

[36] J.P. Ibar, ¨*Stability of the Entanglement Network of Polymers*¨, HDR-Professorship Dissertation-Science Physique, Universite de Pau et Pays de l´Adour (2010).

[37] L.A. Utracki, ¨*Pressure Dependence of Newtonian Viscosity*¨, Polym. Eng. Sci., 23(8), 446 (1983).

Chapter 6

THE ELASTIC DISSIPATIVE STATE OF POLYMERIC MELTS. SOLID-LIKE BEHAVIOR IN THE MOLTEN STATE.

A Introduction

It is commonly admitted in rheology that for a given set of pressure, temperature and strain rate of shear deformation, the melt viscosity is known and calculable by formulas with tabulated parameters. The problem with that statement is that it is simply NOT TRUE**,** as clearly evidenced in Chapter 4, for instance, for which a Rheo-Fluidification treatment can destabilize the state of entanglement of a melt "at will" resulting in many subsequent viscosity-frequency sweep responses at the same T, same P.

This is due to the "elastic dissipative" nature of polymer melts. The correct statement could read like this: for a given set of pressure, temperature and strain rate, one cannot define a unique viscosity!!!

The previous Chapters of this thesis have qualified this answer further:

- the viscosity is function of the stability of the state of interactions between the macromolecules , itself function of the thermal-mechanical history of the melt.
- the viscosity can remain apparently stable for long times (say 200,000 to 1 million times longer than its longest relaxation time at the corresponding T,P), yet applying even a small amount of shear energy can destabilize the melt which, upon release of that energy will remain apparently stable at that new viscosity .

Some examples:

Figure 1: In this Figure a PC melt (Makrolon 2608) is studied under N_2 in a dynamic rheometer, submitted to a time sweep at constant frequency of 1 Hz and a small strain amplitude of 1%. T=300 ^{o}C. The sample was vacuum dried before the test. Its initial measured viscosity is 450 Pa-s. This viscosity is in the Newtonian range, at this high T, low ω and low strain**. It is stable for 17 minutes.** After about 17 min the complex viscosity starts to increase and after approximately 2 hours its magnitude has almost doubled: from 450 Pa-s it has reached 825 Pa-s. Note, the viscosity increases, not decreases, which eliminates all kinds of explanations based on the chemical degradation of the molecular weight.

Now for the possibility that an increase of molecular weight would be responsible for this increase of viscosity, we checked the M_w by GPC and nothing had changed (within the accuracy of this method). Other possible explanations (migration of small M_w fractions, esterification) are discussed in a paper published recently [1]:

"**Investigation of the Dynamic Rheological Properties of a Polycarbonate Melt Presenting Solid-Like Characteristics and a Departure from Pure Liquid Newtonian Behavior at Long Relaxation Times"**, J. P. Ibar, Z. Zhang, Z. M. Li, and A. Santamaria, J. Macromol. Sci., Part B: Phys., 54 (6): 649-710, 2015.

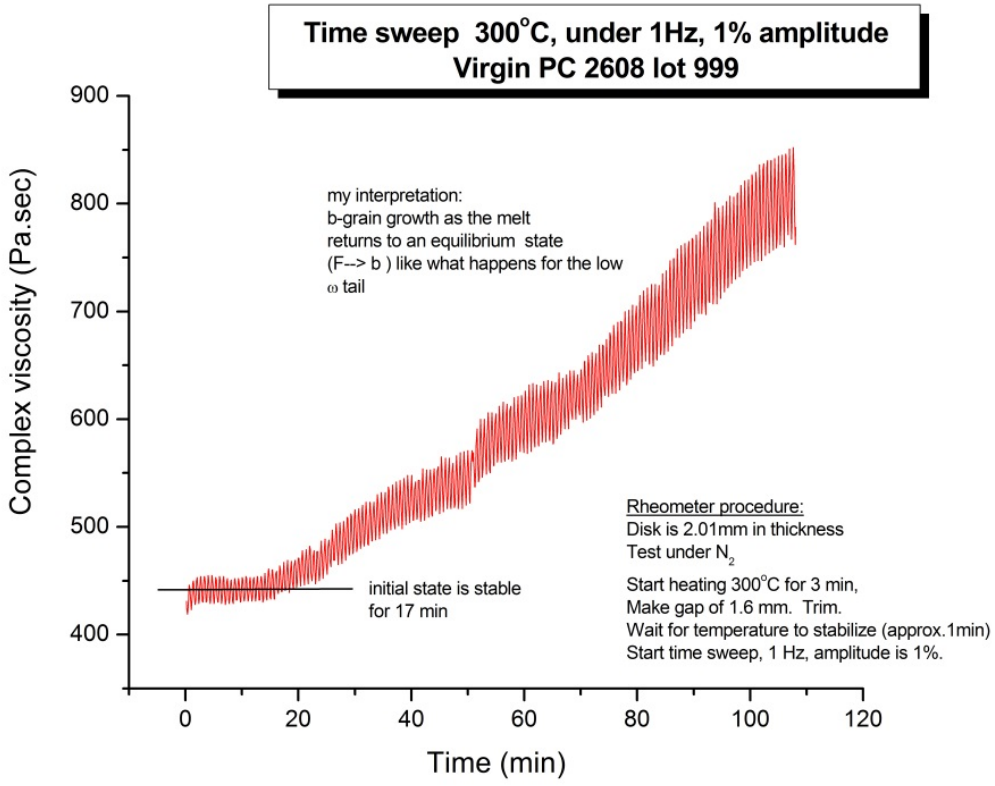

Fig. 1

Complex Viscosity of PC in the Newtonian region (T=300 °C, 1 Hz, 1% strain) plotted against time (time sweep). The small fluctuation of the viscosity signal is due to a small T sinusoidal fluctuation which was added to understand some features of the elastic dissipative state: this feature should be ignored here and its meaning will be explored in a different publication). Note that the Newtonian viscosity of the melt is stable for 17min only.

However, as explored in the paper [1], none of these possible explanations survive all the other experimental tests designed to understand the meaning of the viscosity changes.

Let us consider another example:

Figure 2 (taken from Ref.1 (its Fig.1)).

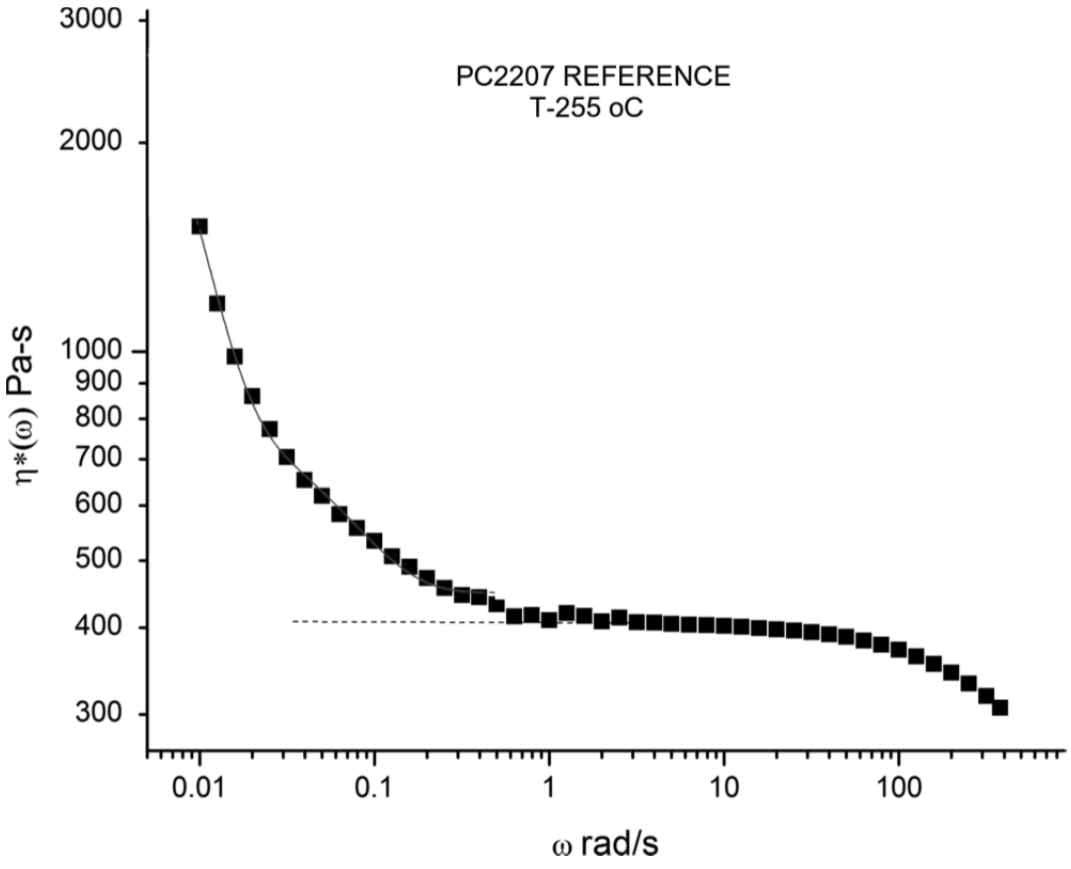

Fig. 2

Dynamic Viscosity vs. ω for Makrolon 2207 at T = 255 ^{o}C. The strain is 5%, the gap is sub-millimetric.

The viscosity decreases as ω increases according to two mechanisms. The low ω viscosity tail (ω < 0.6 rad/s) corresponds to solid-like characteristics of the melt. Then we observe the classical Newtonian viscosity plateau (0.6 < ω< 3.0), also depicted with the dotted line, and finally, for ω > 3 rad/s. the shear-thinning mechanism observed can be fitted with the classical formula by Carreau, for instance.

This shear-thinning behavior at larger ω is a classic, emerging from the Newtonian state, which is well established for ω values below ω ~ 3 rad/s. "Normally", for a stable Newtonian

state, the value of the Newtonian viscosity at that temperature of 255 ^{o}C would correspond to the points on the dashed line at low frequencies, down to 0.01 rad/s. What is unusual is the departure of the viscosity at low ω, which we call "the low ω tail". For instance if we run a downsweep experiment (ω varies from high to low), we observe that the Newtonian value starts to rise at each new measurement along the way, as frequency decreases. The final viscosity at the end of the frequency downsweep is about 3 times the value of the Newtonian viscosity.

Effect of strain% (not shown): we increased the strain from 5% to 35% and observed that the lower viscosity tail decreases in magnitude to become almost flat (non-existent).

Two observations; two conclusions:

-1st: the time lapsed to do the measurements from ω=1 rad/s down to ω=0.01 rad/s is very long: 6113 sec, i.e. 102 min (out of a total time of 105 min for the overall test): this means that the melt is annealed for 102 min while it is in the Newtonian state, a situation very similar to what is presented in Fig. 1 and with the same results (an increase of the Newtonian viscosity).

-2nd: the test was immediately followed by a frequency upsweep using the same parameters (10 points per decade, same T). We also run the frequency upsweep first, followed by the downsweep: same results: the reversibility of the results obtained for upsweeps and downsweeps eliminates all explanations based on artifacts due to the type of instrument used, chain segregation, chain growth and mutation by polycondensation and chain degradation.

B Noirez et al. solid-like results.

The increase of viscosity at vanishing frequency ω seen in Fig. 2 has the same solid-like appearance as that mentioned by Noirez et al.[2] for very narrow gaps for PBD and polybutylacrylate. This is shown in Fig. 3. This is a plot of $\eta^*(\omega)$ vs ω for the polybutylacrylate M=47,500 data used by Noirez et al [2]. The gap is 25 μ and the temperature 25 ^{o}C , i.e. 89 ^{o} above the T_g of this polymer (Note: the data of Noirez et al. were kindly provided by these authors to permit this new analysis of their Fig. 4). The curve shown corresponds to a frequency sweep done at 30% strain, in the linear visco-elastic region. Noirez et al. also varied the strain, from 0.2% to 200% to show that increasing strain decreases the magnitude of the low viscosity tail: see Fig. 4 below (note: the original data by Noirez et al. include lower strain % values, down to 0.2%, not shown because they show some scatter).

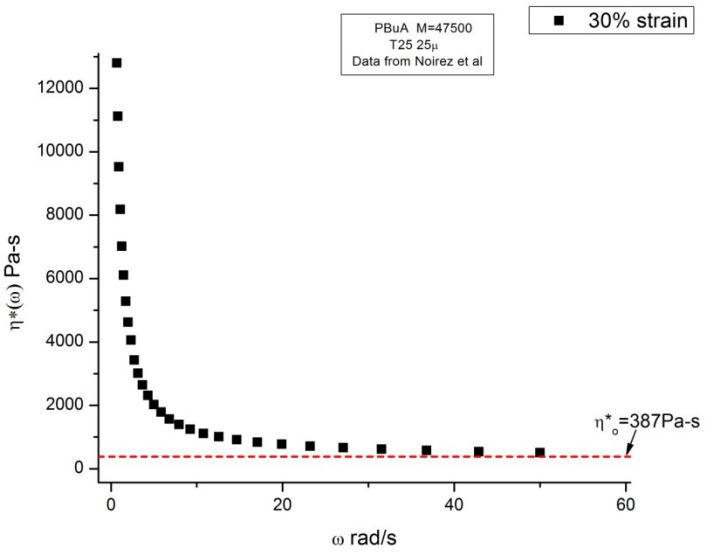

Fig. 3

This plot is made from data of G'(ω) and G"(ω) provided by Noirez regarding their Fig.4 in Ref. 2.

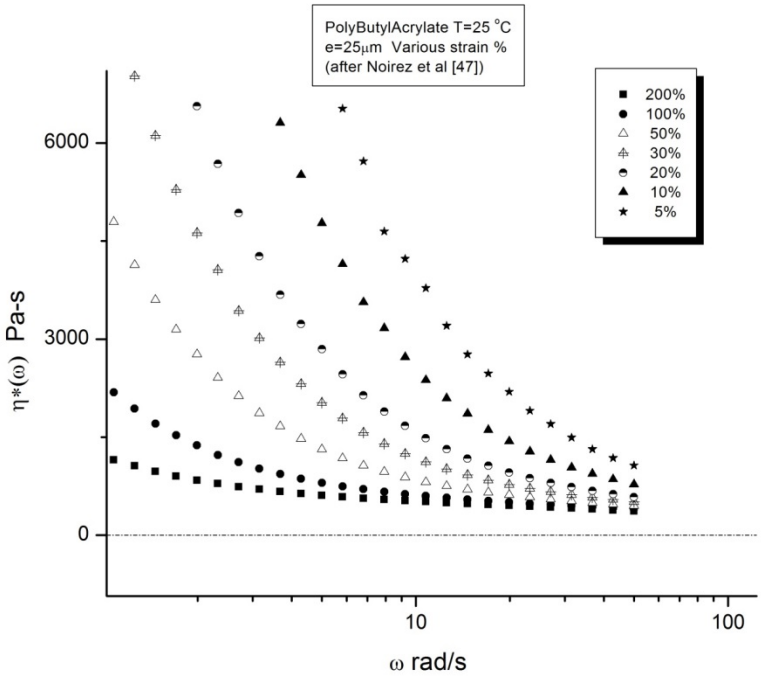

Fig. 4

Same Polybutylacrylate as in Fig. 3 (same T=25 °C, same 25μ gap). Strain varies from 5% to 200%

The axes are linear in Figs. 3 and 4, suggesting an hyperbolic variation of $\eta^*(\omega)$, converging towards the Newtonian viscosity η^*_o (dashed line). It is clear that increasing strain reduces the amplitude of the viscosity tail observed, an experimental fact also observed for Makrolon 2207, as mentioned above. The most obvious correspondence between the solid-like data of Noirez et al. (PBuA) and the results of Fig. 2 on PC is best demonstrated by using a log-log plot for the 200% strain data (bottom curve of Fig. 4):

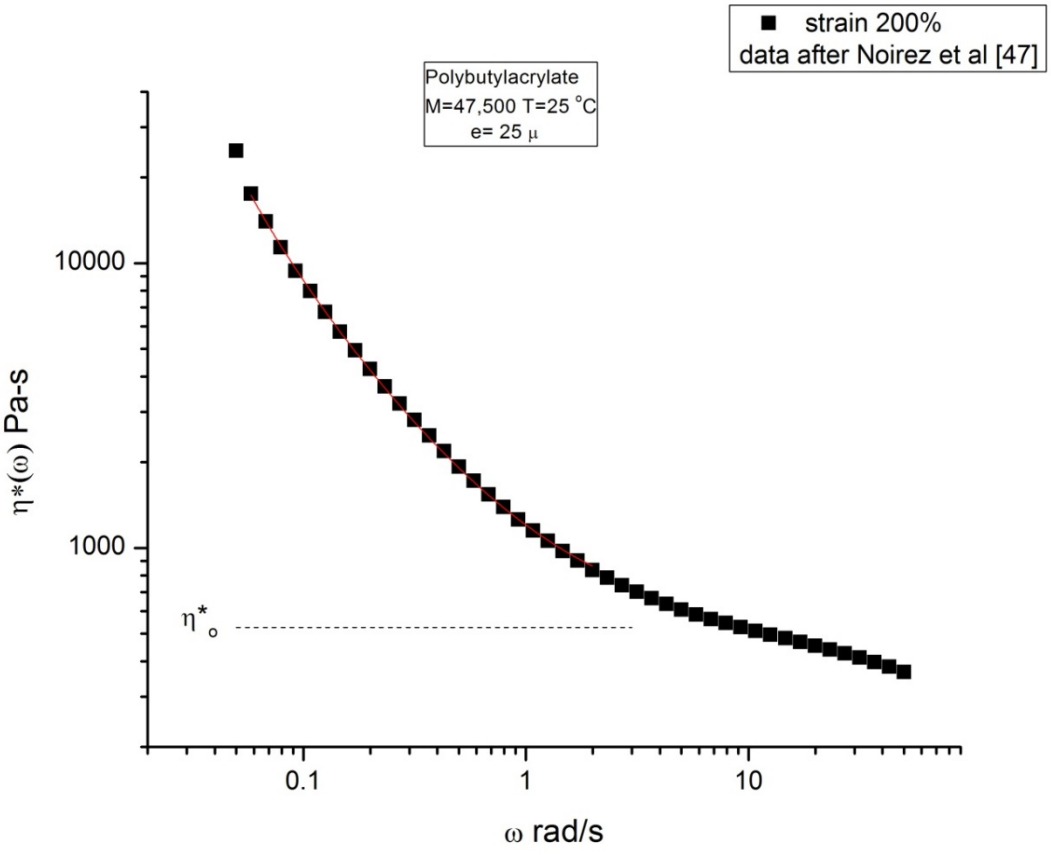

Fig. 5

Same curve as the bottom one in Fig. 4 (γ=200%) with a log scale for the y-axis. Compare with Fig.2.

In this plot, we observe the same features as in Fig. 2: the low ω tail below ω~1 and the change of curvature to initiate the classical shear-thinning at ω>3 rad/s. Clearly, one could curvefit the 10 data points located beyond ω~10 by a Carreau's equation leading to the dashed line for the Newtonian viscosity.

To understand what phenomenon creates this instability of the liquid Newtonian state, it is interesting to consider how $(G'/G^*)^2$ varies with ω. Fig. 6 is such a plot for the data of Fig. 5, i.e for the 200% strain. Fig. 7 is the same plot for all the strains corresponding to Fig. 4.

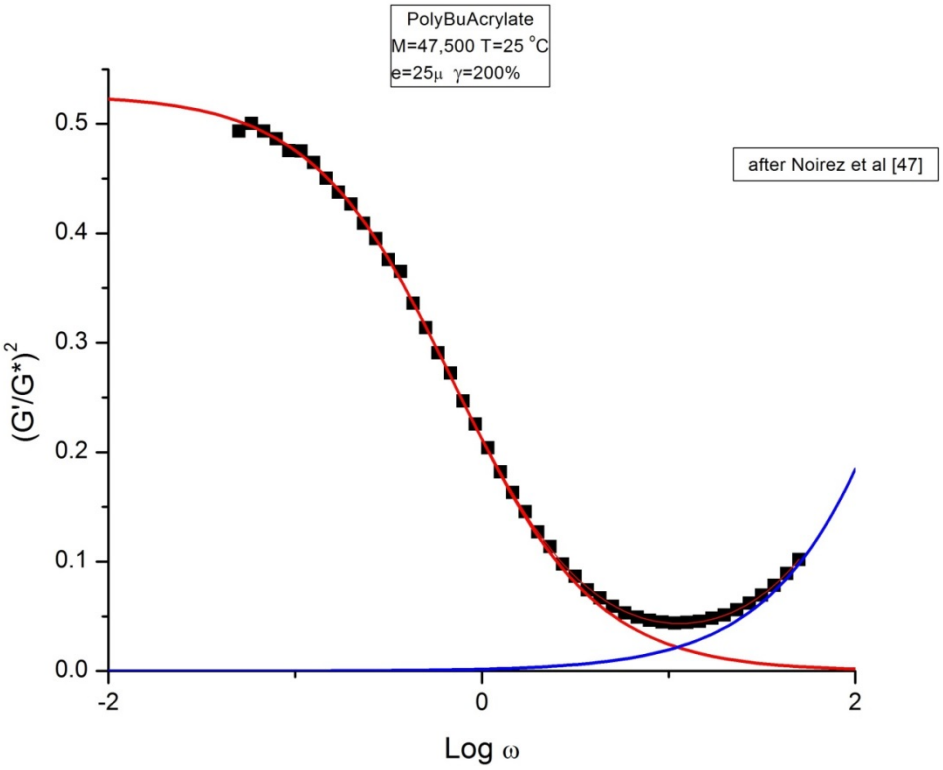

Fig. 6

This plot of $\chi=(G'/G^*)^2$ vs log ω for the data of Fig. 5 permits to deconvolute the two components of $\chi=\chi_1+\chi_2$ corresponding to the red and blue curves, respectively. The strain is 200% here.

This Figure shows that the stored elasticity in the melt is at its maximum at low ω (thus the solid-like character of the melt), that it decreases as ω increases (the red curve), reaches a minimum and then increases (the blue curve). The overall variation of $\chi=(G'/G^*)^2$ can be fitted by the sum of two functions, χ_1 and χ_2, drawn as the red and the blue line, respectively, in Fig. 6:

$\chi=\chi_1+\chi_2$ with $\chi_1=p_1\,(1-\tanh(p_2\,\mathrm{Log}\omega+p_3))$ and $\chi_2=0.5\,(1+\tanh(p_5\,\mathrm{Log}\omega+p_6))$

with $p_1, p_2, \ldots, p_6$ fitting parameters.

It really does not matter (for the present discussion) how the expressions of $\chi_1(\omega)$ and $\chi_2(\omega)$ look like, what is important is that χ_1 decreases sigmoidally from a maximum which decreases as strain increases (see Fig. 7), and that χ_2 increases sigmoidally itself (although we only observe the lower portion of the sigmoid as the blue curve).

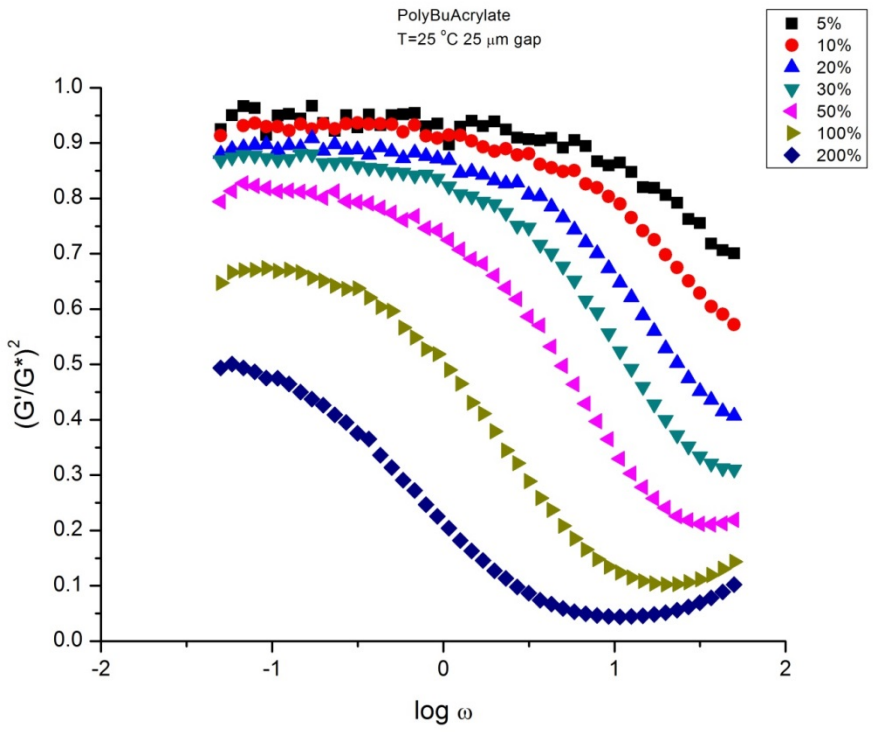

Fig. 7

Same as in Fig.6 at different strains between 5 and 200%

The increase of χ_2 with log ω is a characteristic of the **blinking mechanism** describing shear-thinning in the Dual-Phase model of polymers rheology, which other models fit with the Carreau's equation. This corresponds to the high ω end viscosity decline in Figs. 2 and 5. It is a network property. The deformation occurs by a sequential stretch/relax mechanism involving parts of the network channel characterizing the Cross-Dual-Phases (the entanglement phase-line).

The variation of χ_1 has a different origin. It has two characteristics: it is a function of the b-grain population of the melt due to the [b/F <-->(c,g,t)] statistics, but it is also the Newtonian

state for the blinking mechanism, corresponding to the relaxed stage of the stretch/relax sequence. The population of b-grains (the b-conformers) determines the degree of "glassy-like" character of the melt. By "glassy" I don't mean to qualify the kinetics, which, in a melt, are orders of magnitude faster than in a glass, I relate to the population of b-grains that dominates to a very large extent in a glass (95% or more). Graph 7 shows that the low frequencies and low strains induce the highest elasticity in the melt, the highest value of χ_1, $\chi_{1max}=2\ p_1= 0.975$ (extrapolated to $\omega=0$ and strain=0), hence the highest concentrations of b-grains. But the thermal/mechanical stability of these b-grains is totally different below T_g and in a melt at T_g+89 ^oC.

For the PBuA sample of Noirez et al. which are re-analyzed here, the magnitude of χ_1 and the separation of χ_1 and χ_2 are remarkable; it is due to the small gap used (25 μ) and we offer an explanation why below. At larger gaps, say > 1mm, or at large strain, χ_1 does not take on such large values, as will be explained below, yet the effect of the shear deformation on the b/F structuring, although low, is still measurable even for classical 2mm thick samples but one needs to look for it and extract it from the value of χ (see Chapter 5 and Ref. 6).

The effect of strain on the fitting parameters describing $\chi_1(\omega)$, $\chi_2(\omega)$ can be quantified to tell us what are the favorable conditions to observe such solid-state behavior in the melt, and what to expect for χ_1 when the gap is not micrometric.

$$\chi = \chi_1 + \chi_2$$

Expression of χ_1

$$\chi_1 = p_1(1 - \tanh(p_2 \log\omega + p_3))$$

$$p_1 = -0.08606 + \frac{1.7854}{\gamma + 3.1215} \text{ where } \gamma \text{ is the strain}$$

$$p_3 = 1.7126 - \frac{4.979}{\gamma + 1.2765}$$

$$-\frac{p_3}{p_2} = -0.47897 + 2.12925\, e^{-\frac{\gamma}{1.07057}} + 1.03877\, e^{-\frac{\gamma}{0.09887}}$$

note that $(-p_3/p_2)$ is the log ω value of the sigmoidal inflection point.

Expression of χ_2

$$\chi_2 = p_4(1 + \tanh(p_5 \log\omega + p_6))$$

with $p_4 = 0.5$

$$p_5 = 1.0 + \frac{0.22623}{\gamma - 0.039}$$

$$p_6 = -2.892 - \frac{0.39266}{\gamma - 0.039}$$

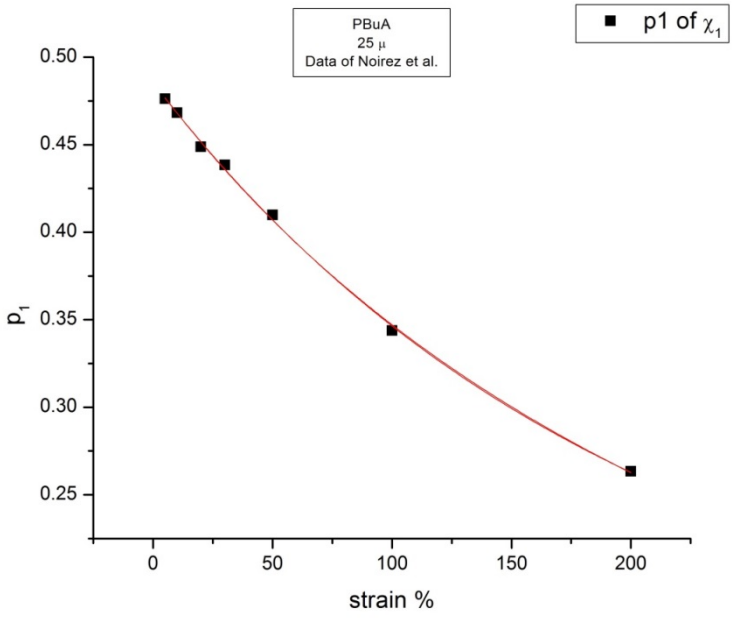

Fig. 8

The maximum value of χ_1, corresponding to $\omega=0$, is equal to $2p_1$ which is shown to decrease with γ

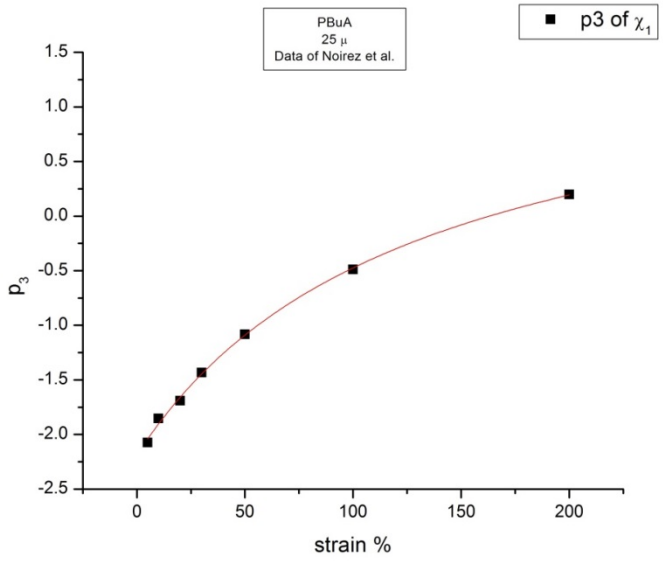

Fig. 9

P_3 is a fitting parameter of $\chi_1(\omega)$ which varies with strain as shown

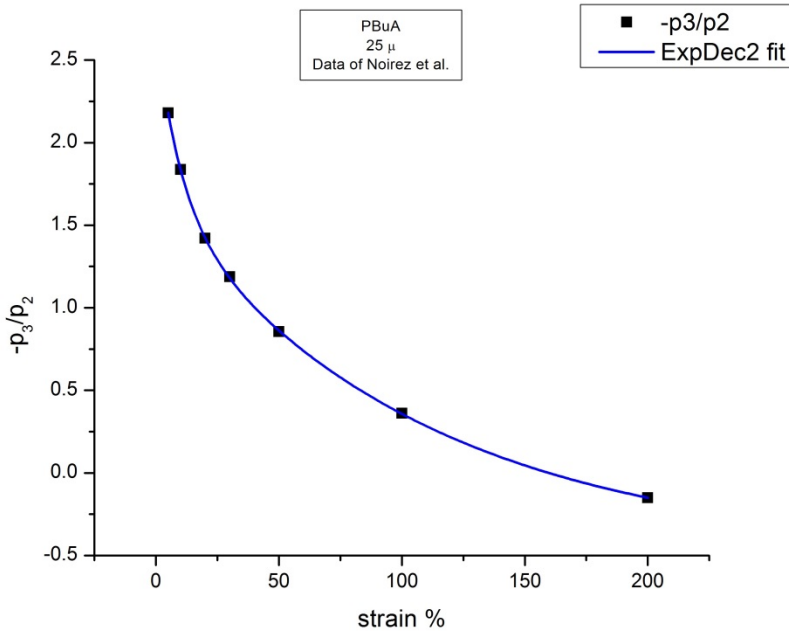

Fig. 10

This graph shows that the log ω for the inflection point of the sigmoid of $\chi_1(\omega)$, i.e. (-p3/p2), decreases with strain. At high strain, $\chi_1(\omega)$ drops to 0 for very low ω values. This is why the melt looks liquid-like.

Figures 8 -10 show how p_1, p_3 and $(-p_3/p_2)$ vary with strain: one can use very simple fitting functions to express these variations quantitatively. For instance the variation of p_1 in the expression of χ_1, extrapolated to large strains, tells us that p_1 non only becomes very small but also negative (-0.086). We observed such negative values for χ_1 for the melts we studied in Chapter 5 and Ref. 6 for which classical gaps and classical surface for the plates were used. But, as we already pointed out, this is the same phenomenon: the proof of the existence of the b/F duality.

Shear deformation decreases χ_1 because the entropy defined by the fluctuations of the phase-line channel is compensating for the thermal agitation of the b/F conformers, creating a fluctuating standing wave propagating constantly through the medium to homogenize (average out) the differences between the phases. This is the equivalent of an elastic wave, which I call 'phase-wave', sweeping through the entire network of conformers in interactions. In the dual-phase model, this 'sweeping' mode of deformation of a melt is not simply due to thermal energy (kT) but also to the mechanical energy input. This is the mode of deformation at low $\omega\gamma$, occurring for a melt 'at rest', i.e. in Newtonian conditions. ω'_o is the frequency for the sweeping wave. Figures 2-6 show that ω'_o is not simply function of T, but also depends on $\omega\gamma$, external parameters: this is a very different view than pure thermodynamic equilibrium!

As the glassification of the melt occurs (F-->b), **favored by anything which permits the conformers to reach the b-conformer state**- which is of less energy thus more stable- the b-grain population increases, the diffusional sweeping phase-wave requires more energy to diffuse through the melt since there are more b-grains to carry through, which means, in rheological terms, that viscosity increases as the concentration of b-grains increases (also equivalent to a decrease of free volume).

This is a well-known result, that the Newtonian viscosity can be described in terms of free volume (Doolittle, Ferry). In other words, the momentum of the sweeping phase-wave, its density times its speed of propagation, is expected to vary with the local density of the melt, i.e. with the amount of b-grains/free volume, and this is the reason we observe the increase of

viscosity in Graph 1 (for a melt initially out of equilibrium), or the instability of the Newtonian state as ω decreases in Figs. 2 and 3.

One can express the variation of the free volume in Fig. 3 by making the T_2 of the Vogel-Fulcher's formulation of the Newtonian viscosity VARIABLE with ω:

$$\log \eta_o = A + \frac{\Delta_o}{T - T_2}$$

In simple terms, the decrease of χ_1, due to b--> F, is equivalent to an increase of free-volume, which can be interpreted as the lowering of T_2 in the Vogel-Fulcher's equation of the Newtonian viscosity, or an increase of ω'_o, the phase-wave sweeping frequency. As soon as blinking starts to operate and χ_2 controls the viscosity variations, T_2 remains constant.
Of course, one could also express the free volume variation due to the b/F structuring in terms of T_g instead of T_2. This is expressed by the WLF equation:

$$\log \eta_o = A + \frac{B}{T - T_2}$$

$$\log \eta_o = \log \eta_{o_g} - \frac{C_{1g}(T - T_g)}{(C_{2g} + (T - T_g))}$$

$$T_2 = T_g - C_{2g}$$

($C_{2g} \sim 50\ ^oC$ according to the WLF equation)

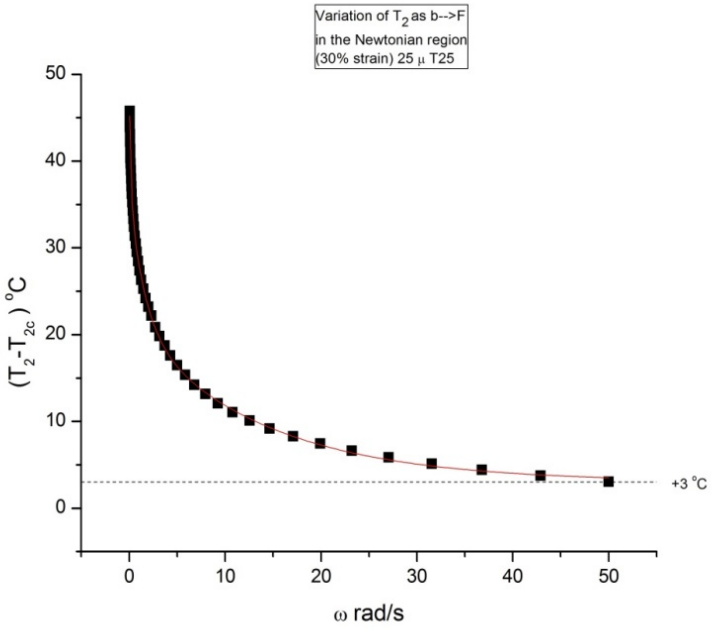

Fig. 11

$T_2(\square)$ is the value which makes $\eta^*(\omega)= \eta^*_o$ calculated by the Vogel-Fulcher. T_{2c} is the classical value. As ω increases, b-->F, and the system returns to its T_{2c} value which remains constant during blinking.

By "melt glassification" we mean the increase of the b-grain population that makes the melt more glassy-like, a melt for which the fluctuation of local density favors the clusters of b-conformers, either increases their number or their size, and this translates into an increase of T_g and log η_{og} , not just superficially, at the interface between the plates and the melt, but in the bulk.

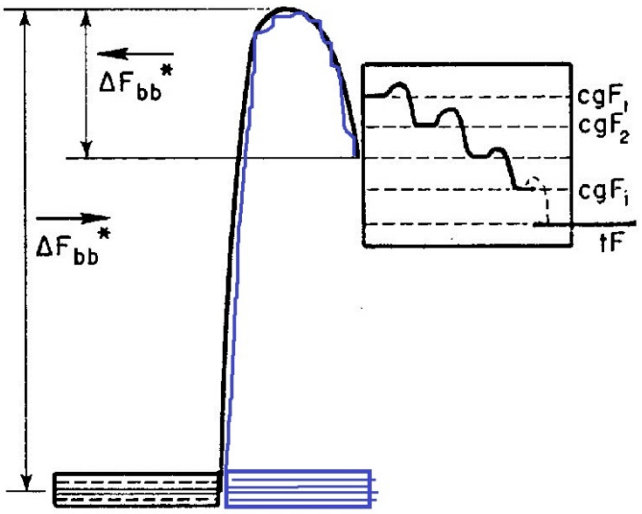

Cross-Dual-Phase
amorphous polymer
(entangled)

Fig. 12

The lower level is the b-conformer level, the same for all b-conformers regardless of their cis-gauche-trans conformation and whether they belong to the Cross-Dual-Phase e or c (the blue and black colors). The F-levels are differentiable according to the conformer's rotational isomeric energies. What differentiates the e and c states is their population statistics (in the F and b levels) which we symbolize by $[b/F \leftarrow>(c,g,t)]_e \leftrightarrow [b/F \leftarrow>(c,g,t)]_c$. The fact that this overall statistics remains stable is due to the elastic dissipative nature of the interactions. The elastic dissipative phase-wave propagates through the melt to homogenize in time the population statistics differences. For an un-entangled melt, the blue lines in the graph are not existent. For a melt which can crystallize, the tF level of the F-state can stabilize into another level, st-t, which is more stable than the b-level, and which gives rise to nuclei.

C Why narrowing the gap makes χ_1 increase (the melt is more "glassy-like")?

Noirez et al. report [2] that working at thinner gaps favors the appearance of the solid-like character (increases χ_1 in Fig. 7), and that, conversely, increasing the gap makes the melt go back to its classical behavior of a pure liquid (in the Newtonian regime). This observation made many

scientists believe that Noirez et al. only observed surface effects [3,4], probably due to capillary forces, in any case nothing which could justify the claim by these authors that the bulk of the melt exhibited solid-like characteristics [2].

As already said, the phenomenon of b-grain glassification in the molten state is a property of the bulk, but it is expected to be influenced by anything which favors the creation of b-conformers, such as the influence of melt confinement which is known to affect the T_g near the surface. But is this the reason for the Newtonian viscosity increase seen in Figs. 2-5?

No, not according to the dual-phase view of the Newtonian state as a standing sweeping elastic wave propagating through the medium to keep it homogeneous.

Strain is defined as the product of a geometrical factor (R/e) and of the angle of oscillation, θ. If the gap e decreases, the strain increases, so to keep in line with the type of strain which produces linear visco-elasticity, one can work at lower oscillation amplitude, which decreases the velocity of deformation, thus of the momentum of the standing elastic dissipative wave. The need to homogenize the melt requires an increase of the density to balance the loss of velocity, and this is the reason for the increase of b-grains. The increase of strain at constant gap is done by increasing θ, which increases the momentum of the elastic dissipative phase-wave and, to compensate, the b-grain population now starts to melt out.

In other words, we suggest that the gap effect is the same as the strain effect or the increase of ω effect (which also decreases χ_1), and this is actually what we observe.

These observations are actual illustrations of what an elastic dissipative melt is like (Fig. 12).

D Is there a surface effect in the experiments reported by Noirez et al [2]?

We suggest that **there is one**, and it is observed for the 3 lowest ω values in Fig. 7. What is seen for these 3 points is a reversal of the b-grain formation ($\chi_1 \searrow$) as ω decreases, as if the stored elasticity now declined (and-although more difficult to assess- as if the viscosity had

started to nose down). But this makes sense. Noirez told me that she used special *low* surface energy materials for the plates so that the melt could perfectly wet the surface: this situation creates the opposite of a high surface energy surface which raises T_g (with respect to the bulk T_g value).

The paper that studies the effect of the surface energy of surfaces and the thickness on the T_g of ultrathin polymer films is by David S. Fryer et al. [5]. This is what their Abstract says:

> The glass transition temperatures (*T*g's) of ultrathin films (thickness 80-18 nm) of polystyrene (PS) and poly(methyl methacrylate) (PMMA) were measured on surfaces with interfacial energies (γSL) ranging from 0.50 to 6.48 mJ/m2. The surfaces consisted of self-assembled films of octadecyltrichlorosilane (OTS) that were exposed to X-rays in the presence of air. Exposure to X-ray radiation systematically modified the OTS by incorporating oxygen-containing groups on the surface. The interfacial energy for PS and PMMA on the OTS surface was quantified as a function of X-ray dose using the Fowkes-van Oss-Chaudhury-Good model of surface tension. The *T*g values of the films were characterized by three complementary techniques: local thermal analysis, ellipsometry, and X-ray reflectivity. Within the resolution of the techniques, the results were in agreement. At low values of γSL, the *T*g values of PS and PMMA films were below the respective bulk values of the polymers. At high values of γSL, the *T*g values of PS and PMMA films were higher than the bulk values and increased monotonically with increasing γSL. The deviation of the *T*g values of the films compared to the bulk values increased with decreasing film thickness. For a specific film thickness of PS and PMMA, the difference between the *T*g of the film and *T*g of the bulk polymer ($\Delta Tg = (Tg_{film} - Tg_{bulk})$ scaled linearly with γSL irrespective of the chemistry of the polymer.

According to this study, although it concerns ultrathin samples, the melt surface interface could play a role on the T_g of the layers located just below the surface, which the Dual-Phase model would explain in terms of an increase or decrease of the b/F population, with respect to the bulk value. The paper gives examples of a rise or a decrease of T_g by ±30 ^oC, a substantial amount, indeed, the thinner the sample the more the ΔT_g varies. So, it is possible that the surface effect plays a small role in the samples by Noirez, with a decrease of T_g effect for the first 3 ω, as we suggested, which could explain the systematic drop of χ_1 observed for almost all strains in Fig. 7 for the first 3 ω.

Even if the above explanation can be validated, the surface energy effect would remain very small on thicker samples, since 25μ is a thick sample compared to the 18-80 nanometer thickness of the films studied by these authors. This is why, perhaps, it can only be perceived at

the lowest ω values for which the sweeping wave has its lowest momentum, being over-ridden by the opposite effect (b-->F) at higher ω. In summary, the solid-like character observed is not a surface effect, it is an elastic dissipative effect in the bulk.

E. The question of the nature of the elasticity in the solid-like melt.

On this important issue the Dual-Phase explanation [1] differs from that of Noirez et al.[2].
These authors suggest that the melt solid-like elasticity is that of the rubbery plateau elasticity. We propose a different interpretation.

Take the extrapolation in Fig. 11 of (T_2-T_{2c}) vs ω for ω=0: it is 50 ^oC, i.e. the value of C_{2g} in the WLF equation. This means that $T_2=T_g$, hence that the viscosity is infinity at T_g. I conclude that the **extrapolated elastic state of the melt at ω=0 is that of the glass, not the rubbery state**.

There is another reason why we affirm that the melt solid-like elasticity is fundamentally not related to the modulus of the rubbery plateau: rubber elasticity is characterized by the entropic deformation of the entanglement network, which is controlled by χ_2, unlike the increase of the elastic energy at low ω (Fig. 7) which is controlled by χ_1. χ_2 verifies the linearity of a MXPLOT, χ_1 does not. This is shown in Fig. 13 below applied to the 200% strain data for which χ_2 is not negligible.

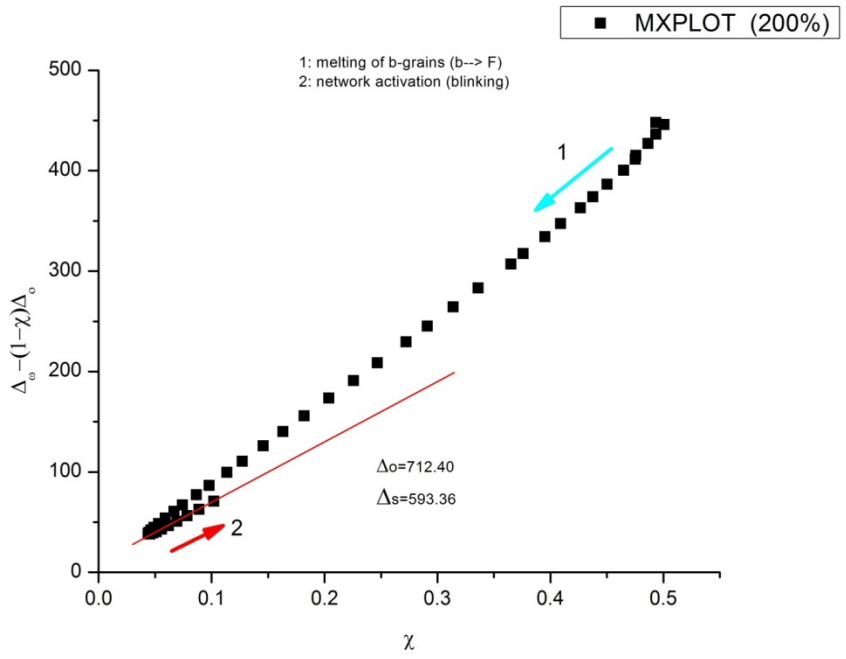

Fig. 13

This plot arises in Chapter 5 from the blinking mechanism of deformation which splits the cohesive energy Δ_ω between its stretched and its relaxing components, giving an explanation of shear-thinning.

An MXPLOT (Chapter 5) establishes a relationship between the stretched strands, $\Delta_s\,\chi$, and the relaxing strands, $(1-\chi)\Delta_o$, for a blinking mechanism of deformation, by studying the variation of the cohesive energy of interactions under shear, Δ_ω against the number of activated strands for a given (ω,T), χ. One can find Δ_ω from the variation of $\eta*(\omega)$. See Chapter 5 of the thesis. $(\Delta_o-\Delta_s)$ relates to the average isomeric state of the F-conformers; it is positive for a stretched system because the trans conformation, tF, is more stable than the cis and gauche conformations, cg_1, cg_i (Fig. 12), and because the stretching stage of blinking involves an increase of the trans conformers in the direction of flow. This is, indeed, observed for line 2 in Fig. 13 (the red arrow) for which we determine Δ_o= 712.40 and Δ_s=593.36 (thus $(\Delta_o-\Delta_s)$=119 >0), but it is not true for the upper line in Fig. 13 (the cyan arrow) with a slope higher than Δ_o and Δ_s. χ decreases in region 1, at low ω, because χ_1 decreases towards 0, whereas χ increases in region 2, for the highest ω values, because χ_2 increases in this region (see Fig. 6). We conclude that region 1 corresponds to the b/F structuring within the sweeping elastic dissipative wave

characteristic of the Newtonian state, and that region 2 corresponds to the stretch/relax mechanism of the blinking process, characteristics of the classical shear-thinning.

It is shown in Chapter 5 that as ω continues to increase in region 2, χ_2 increases at first then decreases, which we associate with the orientation of the Cross-Dual-Phase network for an entangled ($M>M_e$) melt. This network entropy effect may be coupled with a change of the b/F structure which modifies χ_1, but it is a compensating effect and has nothing to do with the low ω instability of the sweeping (diffusion) wave.

F. Conclusion

The solid-like character of polymeric melts is due to the elastic dissipative nature of the interactions which favors the b-state (Fig. 12). The Grain-Field Statistics applied to all the conformers belonging to all the macromolecules provides the population of the $[b/F\leftarrow\text{-->}(c,g,t)]_e$ and $[b/F\leftarrow\text{-->}(c,g,t)]_c$. When the mechanical energy input produced by the deformation is very low, which is the condition set by working with a thin gap in linear viscoelastic mode, b-grain glassification of the Newtonian melt produces the increase of the viscosity and of the elasticity observed. This is predicted by the Cross-Dual-Phase model of polymer interactions which validates the experimental findings of Noirez et al.[2]

In several of the previous Chapters of this thesis I insisted on the problems encountered in polymer physics by using such provocative titles as: “the great myths of rheology”, “trouble with polymer physics” etc. But in this Chapter, I focused on teaching a different view, a different rheology to explain classical and unclassical experimental facts. This illustrates the new polymer physics, the emergence of a new understanding of the interactions.

It is expected that an extensive investigation of this “elastic dissipative” character of the interactions will permit to explain in a different way than the classical interpretations the properties of polymeric glasses, melts and rubbers.

G. References (Chapter 6)

[1] J. P. Ibar, Z. Zhang, Z. M. Li, and A. Santamaria, J. Macromol. Sci., Part B: Phys., 54 (6): 649-710, 2015. *"Investigation of the Dynamic Rheological Properties of a Polycarbonate Melt Presenting Solid-Like Characteristics and a Departure from Pure Liquid Newtonian Behavior at Long Relaxation Times***"**.

[2] L. Noirez; H. Mendil-Jakani; P. Baroni; Phil. Mag. 2011, 91, 1977. '*Identification of finite shear-elasticity in the liquid state of molecular and polymeric glass-formers*'.

[3] G.B. McKenna, Eur. Phys. J. E (2006) DOI: 10.1140/epje/e2006-00001-0 *« Commentary on rheology of polymers in narrow gaps"***.**

[4] D. Vlassopoulos, Eur. Phys. J. E (2006) DOI: 10.1140/epje/e2006-00008-5 « *Commentary on the observations of solid-like rheological response in unentangled polymer melts by H. Mendil, P. Baroni, L. Noirez, D. Collin, P. Martinoty"*

[5] David S. Fryer, Richard D. Peters, Eui Jun Kim, Jeanne E. Tomaszewski, Juan J. de Pablo, Paul F. Nealey, Chris C. White and Wen-li Wu, *Macromolecules* 2001, *34,* 5627-5634 **"***Dependence of the Glass Transition Temperature of Polymer Films on Interfacial Energy and Thickness"***.**

[6] J.P. Ibar, J. Macromol. Sci., Part B, Phys. 52:222-308, 2013) "*The Great Myths of Polymer Rheology. Part III: Elasticity of the network of entanglement*".

Chapter 7

SHEAR-THINNING OF POLYMERIC MELTS: THE FAILURE OF THE REPTATION MODEL.

Small angle neutron scattering (SANS) studies on polymer melts under steady-state flow provide in-situ information at a molecular scale on how the flow field is transmitted to the melt. Such experiments, called "Rheo-SANS", are difficult to set up and require special equipment but their results are fundamental to test experimentally the accepted claim by the reptation model [1, 2-8] that the shear-thinning of entangled polymer chains is due to significant orientation of the segments between entanglements under the shear flow. We quote below two significant Rheo-SANS studies, one by Watanabe et al. in Japan, published in 2007 [9], and the other one by Noirez et al. in France, published in 2009 [10].

Both studies concluded that the chains remain largely undeformed under steady-state shear flow conditions for which extensive shear-thinning was present. These results represent a formidable challenge to the reptation model of melt deformation [2-8].

A *Rheo-SANS results of Watanabe et al. (2007).*

In order to examine the chain conformation changes under shear flow for a well characterized monodispersed entangled polymer and the orientation distribution along the chain backbone, Watanabe et al. examined the Rheo-SANS behavior for an entangled polybutadiene sample dissolved in a deuterated oligomeric butadiene at the volume fraction of 0.28. The rheometer was a Couette apparatus, allowing high flow shear rates at constant temperature [9]. The shear rate, normalized by the reptation time, was between 24 and 29 sec^{-1} and at these shear rates the viscosity of the systems was significantly smaller than the zero-shear viscosity (by a factor of ~ 40). Despite this intense shear-thinning, Watanabe et al. observed that "*the I(q) data just moderately deviate from the Debye function (describing the data at equilibrium)... These SANS data allow us to examine the current molecular picture for the entangled chains under fast shear flow. This picture assumes that successive entanglement segments are not orientationally correlated and behave as independent stress sustaining units even under fast flow... Thus, the above assumption fails for the entangled chains under fast flow.*"

In other words, at a shear rate that reduced the Newtonian viscosity by a factor 40, i.e. under strong non-Newtonian conditions, the chain rms end to end distance hardly varied from its value under static (equilibrium) conditions.

B *Rheo-SANS of Noirez et al (2009).*

Noirez et al., apparently unaware of the results by Watanabe et al. [11] yet using a similar Quartz Couette rheometer set up, reported on in-situ observations of polymer melts under steady-state shear flow using neutron scattering [10]. The amorphous melts studied by these authors were an entangled polybutadiene (T_g=-110 ^oC, M_w =29 M_e) characterised by a reptation time τ_d =7 10^{-3} s (ω_x=143 rad/s) and a low molecular weight (unentangled) polybutylacrylate (Tg=-64 ^oC, $M_w \sim M_e$), characterised by τ_d=10^{-3} s (ω_x=1,000 rad/s). Both melts were monodisperse and sheared at room temperature (i.e., far above their respective T_g). The melts were sheared with a range of strain rates spanning the zone from far below the reptation time to far above it (from 0.011 s^{-1} to 1000 s^{-1}) to determine the variation of the chain dimensions across the reptation time; the admitted theories claim these times include the onset of shear-thinning and of chain orientation/disentanglement [2, 4, 12, 13]. Figure 1 of Noirez et al. clearly demonstrated that the two components, azimuthal and longitudinal, of the radius of gyration (R_v and R_z) remained constant at 80 Å as the shear rate varied from the Newtonian range to a highly shear-thinned melt, and, besides, that no change of the radius of gyration occurred as the melt crossed τ_d. The authors concluded "*that the chains remain largely undeformed under steady-state shear flow... These observations are of prime importance; they reveal that the flow mechanism and its viscoelastic signature reflect a collective effect and not properties of individual chains.*"

In summary, both Watanabe et al. and Noirez et al. concluded that the macromolecular dimensions remain unchanged as the melt is sheared in the non-Newtonian region, conflicting with the currently accepted understanding of shear-thinning. The failure of the existing models to interpret such a fundamental aspect of polymer rheology cannot remain unchallenged [14-20].

C. Discussion and Conclusions

Classical visco-elasticity theory considers the rheological deformation of polymer melts as resulting from the behavior of singular chains embedded in a sea of interactions with other chains. In the existing theories of macromolecular physics, the emphasis is put on determining the shape of the individual macromolecules, often called their chain conformation. The presence of neighboring and interpenetrating macromolecules is perceived as a disturbance to the ideal conformation of the chain. In the traditional texts, the field of interaction responsible for the disturbance is homogeneous. One can, therefore, describe the behavior of the melt by describing what happens to a single chain after it has been established how to incorporate the effect of the interactions between the chains.

Thermodynamically speaking, "molecular dynamics" deals with the physics of systems that are single chains. This is the case for the popular reptation model introduced by de Gennes [2, 3] and fine tuned by Doi and Edwards [4], Marrucci [5, 6], Wagner [7], McLeish [18] and many others. Macromolecules are able to rearrange their multiple chain conformations with the change of the thermal or mechanical energy input. In the case of shear deformation, the Newtonian viscosity is classically considered to describe the internal friction between the bonds of interacting macromolecules which assume a stable thermodynamics state, the equilibrium state at a given temperature and pressure. The non-Newtonian behavior, shear-thinning, is due to a modification by the flow of the dimensions of the macromolecules, i.e. of their conformation, which can be calculated from the effect of the shear rate on the rms end to end distance of the macromolecule and the amount of slippage (disentanglement) occurring. Theoretical models predict that for a shear rate strong enough to overpower the ability of the chain to relax, -and this happens at the reptation time-, shear-thinning starts to be observed, corresponding to an increase of the rms end to end distance (chain orientation). In the classical formula that describe the non-Newtonian dependence of viscosity with shear rate, the amount of shear-thinning is only a function of two parameters (in addition to the strain rate, of course): the Newtonian viscosity and the value of the reptation time. But these two parameters can be correlated to each other and to the dimensions and interactions between the chains, which simplifies the description of the flow deformation process to the description of the dependence of the reptation time with temperature, pressure, and chain length (the

interactions between the macromolecules, defined by "their entanglement", is already incorporated in the definition of the reptation time).

In summary, the effect of strain rate, temperature, molecular weight, according to the accepted reptation model, could all be related to a simple explanation: the deformation and relaxation of single macromolecular chains confined to move within the boundaries of a tube, the entanglement tube, whose lifetime was the reptation time. The whole process would continuously be happening, from very low strain rate to high shear-thinning producing strain rate. Additionally, the reptation model provided a new understanding of "entanglement" by quantifying the dimensions of the tube and correlating it to the reptation time. The interactions between the macromolecules could be described topologically, the tube serving as the new topological description of the environment of the bonds.

This was the beauty of the reptation model of de Gennes [2], which succeeded in scaling the effect of all variables into the description of a single parameter, the reptation time. However, this extraordinary tour de force had to be refined over the years to account for a better description of reality, in particular the molecular weight dependence of the reptation time which did not follow the predicted M^3 variation [3].

Yet, despite all of its elegance, apparent success and sophistication, we suggest that the reptation model is not correctly describing the reality of the interactions between the macromolecules (Rheo-SANS experiments of Watanebe et al. [9] and Noirez et al. [10]) and should be abandoned. The reason for this radical proposition is that the dynamics of the interactions defining the melt properties should not be defined by thermodynamic systems which are the single macromolecules. We have also proposed to re-consider the concept of entanglement, the corner stone of polymer physics.

We have briefly exposed in Chapter 1 (the preamble), a different model of understanding of the coupling between the conformers of polymer macromolecular chains, creating a novel statistics (the “Grain-Field-Statistics”) that does not singularize individual chains embedded in a sea of mean field interactions. Conformers belong to two types of sets: they belong to a

macromolecule, which links them via covalent forces, and they belong to the grand ensemble of conformers which are linked by **inter-intra** molecular forces, van der Waals, dipole-dipole, and electrostatic interactions, which affect and define the viscous medium. That duality is intrinsic to polymers. Instead of considering the evolution of a single chain as the system, it is considered that the system to study is the global set of chains of conformers with a re-definition of their conformational statistics to account for the coupling of their inter and intra molecular interactions (see Fig. 8). The dual-phase statistics, [b/F ↔ (c,g,t)], which governs the population of the isomeric states of the conformers, explains the collapse of the macromolecules into a coil and the split into two dual-phases, "the Cross-Dual-Phases", when the chain length of the macromolecules reaches a critical value, M_e. This split of the statistics into two co-existing and interactive populations ("phases"), i.e. $[b/F \leftrightarrow (c,g,t)]_1$ and $[b/F \leftrightarrow (c,g,t)]_2$, is responsible, we suggest, for what is usually described as the entanglement network characteristics of polymers. The state of the conformers in the two dual-phases, i.e., how many of them are -trans, cis, or gauche- and, also, of the type b or F, are different.

In the Dual-Split model, the free volume plays a dynamic role in the deformation process; it is not constant at a given temperature, as described in the classical WLF approach, but is an integral part of the interactive tissue which describes the interactions between conformers. It is coupled with the formation and melting of b-grains, a local glassification of the state of the conformers, which, as already said, is symbolized by [b/F <--> (c, g, t)] where b and F stand for "bonded" and "free", and c, g, t designate the conformational state of the conformers: cis, gauche, and trans. In fact, we have shown [15, 21] that the equations of rheology must be revised when working at constant free volume instead of constant temperature, as is usually the case. The classical assumption of separating the free volume dependence from the molecular weight dependence of the terminal time and the Newtonian viscosity is in default when working at constant free volume, and the classical exponent of 3.4 for the molecular weight dependence of η^*_o becomes 5.2, showing the intrinsic involvement of free volume with the macro-coil length, contrary to classical views [15, 21].

The dissipative stability of a Cross-Dual-Phase melt is predicted by the Grain-Field statistics [36], for which the fluctuation of free volume plays a role as important as the average

free volume in determining the changes in the conformation statistics of the conformers. The model also predicts the influence of stress on the statistical population in each of the cross-dual-phases, giving rise to shear-thinning effects, strain softening effects and, ultimately, to the orientation and to the instability of the network of channels, i.e. the "entanglement network".

These new concepts provide new grounds to study the properties of polymeric melts; the objectives for the research reported in this chapter was precisely driven by such concepts. For instance, in the new understanding of the visco-elastic behavior, two types of shear-thinning are expected due to a fundamental difference of deformation between the “phase-line sweep deformation” mechanism (occurring at low ω with frequency ω'_o) and the “blinking network activation” mechanism which characterizes the stretch/relax deformation of the entanglement network channels. Shear-thinning due to blinking occurs with frequency $\omega' > \omega'_o$ which is also a measure of the amount of activation of the entanglement network. Shear-thinning of the sweeping phase lines occurs by way of the b/F transitions in the cross-dual-phases. It is influenced by the thermal-mechanical history and thus by any previous treatment involving blinking steps. We have shown in previous publications [15, 16] that the rheological parameters of a melt can not be solely characterized by its viscosity response, nor by G'(ω) and G"(ω) which are themselves profoundly modified by any previous treatment in the non-linear visco-elastic region [17]: the melt could be brought out of equilibrium with respect to its entanglement state. Furthermore, new stable entanglement states could be generated and, as a consequence, the rheology of the melt could be significantly modified.

In chapter 6 we have shown the existence of two types of shear-thinning behavior for a polycarbonate grade that does not present any characteristics different than those of a traditional homopolymer melt. The lower ω increase of viscosity at vanishing frequency (region 1) has the same solid-like appearance as that mentioned by Noirez et al. for very narrow gaps for PBD and polubutylacrylate [22], and we suggest that it is due to the decrease of ω'_o, the sweeping wave frequency, to compensate for an increase of b-grains at low ω. This local b-grain glassification of the melt occurs at temperatures far above T_g, and slows down the diffusion of the elastic sweeping wave which is continuously sweeping across the melt in order to homogeneize it

(temporal averaging). Thus it reveals its presence. The modulations of ω'_o, also present in region 2, in the plateau region of region 3 (domain of the blinking mechanism) reveal the instability of the network phase with respect to its free volume content, which suggests that the "intra-Dual-Phase" compensation dominates for polycarbonate, a result that is not necessarily the same for other polymers (PMMA in Ref. 15; also Figs. 12 and 13). In region 3 we observed the classical shear-thinning characteristics which could be described by the classical empirical equations. We discussed in the previous chapter (and its Ref. 1) several possible explanations for the low ω viscosity tail observed for PC2207: artifacts due to the type of instrument used, chain segregation, chain growth and mutation by polycondensation and chain degradation, but none of these possibilities appear to stand in view of the reversibilty of the results.

We concluded that this observed drift of ω'_o with ω and time, explaining the instability of the Newtonian state, revealed the fundamental dual-phase like nature of the melt; it revealed that its visco-elastic properties, say η^*_o, should be understood, not by the properties of the macromolecules, but by the properties of the dual-phases, its sweeping diffusion nature, its channeling nature, and shear-thinning by the description of its stress bearing activation mechanisms.

The understanding of entanglement is radically different in the reptation model and in the model we propose. For instance, for the Cross-Dual-Phase model of entanglements, there is no disentanglement during shear-thinning, nor does shear-thinning occur by inducing a change of the rms end to end distance of the macromolecules. These projections are backed by the Rheo-SANS experimental evidence discussed in Refs. 43 and 44. Also, in the model we introduced in chapter 5 and in several papers [23, 14-16], strain softening is correlated to the stability of the entanglement network via either intra-Dual-Phase free volume compensation, [b/F <--> (c,g,t)], or inter-Dual-Phase compensation, $[b/F <--> (c,g,t)]_1 \leftrightarrow [b/F <--> (c,g,t)]_2$,and, for melt processing, the understanding of which mode of entanglement stability dominates has profound consequences: such as a reduction of the melt viscosity by "dual-phase disentanglement" leading to a better processability, easier compounding and the possibility to retain in pellets the viscosity reduction benefits induced during melt processing.

In summary, the new statistics provides a new understanding of entanglements as a double dual-phase system (Figs. 8-11 of Chapter 1), describes viscoelasticity and flow properties in a quantitative and original way [15] and suggests that the entanglement network can become unstable under conditions of non-linear viscoelastic deformation [16, 17]. Furthermore, the various stages of the deformation behavior of a melt as a function of frequency or temperature, i.e. the terminal zone, the rubbery plateau and the transition to the glassy state, can easily be expressed qualitatively and quantitatively with the new definition of the entanglement network. Finally, as shown in this chapter, the solid-like character of the melt at vanishing frequency appears to be a result of the dual-phase nature of the conformers interactions.

REFERENCES (CHAPTER 7)

[1] Vlachopoulos, J., Strutt, D., "The role of rheology in polymer extrusion". In New Technology for Extrusion Conference. Milan, Italy. 2003, Nov (pp. 20-21).

[2] de Gennes, P. G., "Scaling concepts in polymer physics", Cornell University Press, 1979.

[3] de Gennes,P. G., "Reptation of a Polymer Chain in the Presence of Fixed Obstacles**",** J. Chem. Phys., 1971, 55, 572–579.

[4] Edwards, S. F., Doi, M., "The theory of polymer dynamics", Clarendon, Oxford, 1986.

[5] Marrucci, G., "Dynamics of Entanglements: A nonlinear model consistent with the Cox-Merz rule". J. Non-Newton. Fluid Mech., 1996, 62, 279-289.

[6] Marrucci, G., Ianniruberto, G., "Interchain pressure effect in extensional flows of entangled polymer melts", Macromolecules, 2004, 37, 3934-3942.

[7] Wagner, M. H., Rubio, P., Bastian, H., "The molecular stress function model for polydisperse polymer melts with dissipative convective constraint release", J. Rheol., 2001, 45, 1387-1412.

[8] McLeish, T. C. B., Larson, R. G., "Molecular constitutive equations for a class of branched polymers: The pom-pom polymer", J. Rheol.,1998, 42, 81-110.

[9] Watanabe, H., Kanaya, T., Takahashi, Y. "Rheo-SANS behavior of Entangled Polymer *Chains with Local Label Under Fast Shear Flow*",2007, Activity Report on Neutron Scattering Research: Experimental Reports 14,Report Number: 146.

[10] Noirez, L., Mendil-Jakani, H., Baroni, P., "New light on old wisdoms on molten polymers: Conformation, slippage and shear banding in sheared entangled and unentangled melts", Macromol. Rapid Commun., 2009, 30, 1709-1714.

[11] L. Noirez, private communication.

[12] Williams, M. L., Landel, R. F., Ferry, J. D., "The temperature dependence of relaxation mechanisms in amorphous polymers and other glass-forming liquids." J. Am. Chem. Soc., 1955, 77, 3701-3707.

[13] Graessley, W. W., The entanglement concept in polymer rheology, Advances in Polymer Science,

Volume 16, Springer-Verlag, Berlin, Heidelberg, New York,1974.

[14] Ibar, J. P. The Great Myths of Polymer Melt Rheology, Part I: Comparison of Experiment and Current Theory. J. Macromol. Sci., Part B, Phys., 2009, 48, 1143-1189.

[15] Ibar, J. P. The Great Myths of Rheology Part III: Elasticity of the Network of Entanglements. J. Macromol. Sci., Part B, Phys., 2013, 52, 223-309.

[16] Ibar, J. P., "The Great Myths of Rheology, Part II: Transient and Steady-State Melt Deformation: The Question of Melt Entanglement Stability", J. Macromol. Sci., Part B, Phys., 2010, 49, 1148-1258.

[17] Ibar, J. P., "Processing Polymer Melts under Rheo-Fluidification Flow Conditions, Part 1: Boosting Shear-Thinning by Adding Low Frequency Nonlinear Vibration to Induce Strain Softening", J. Macromol. Sci., Part B, Phys. 2013, 52, 407-441.

[18] Ibar, J. P., "Processing Polymer Melts under Rheo-Fluidification Flow Conditions, Part 2: Simple Flow Simulations", J. Macromol. Sci., Part B, Phys., 2013, 52, 442-461.

[19] Ibar, J. P., "Stability of the Entanglement Network of Polymers". HDR Dissertation-Science Physique, Universite de Pau et Pays de l´Adour, 2010.

[20] Ibar, J. P., "Grain-Field Statistics Applied to Polymer Physics: the Network of Entanglements", book in preparation (2016).

[21] Ibar, J. P., "Rheology of Polymers at constant Free Volume: Revisiting the Classical Concepts and Equations", ICR 2012-XVIth International Congress on Rheology, Lisbon, 2012

[22] Noirez, L., Mendil-Jakani, H., Baroni, P., "Identification of finite shear-elasticity in the liquid state of molecular and polymeric glass-formers", Phil. Mag., 2011, 91, 1977-1986.

[23] Ibar, J. P., "Do we need a new theory in polymer physics?", J. Macromol. Sci., Part C: Polym. Rev., 1997, 37, 389-458.

Chapter 8

THESIS CONCLUSIONS

ENTANGLEMENTS: A NEW INTERPRETATION AND ITS PERSPECTIVES IN SCIENCE AND TECHNOLOGY.

The plastics industry is the source of 4% of worldwide energy consumption and Europe takes a share of approximately 20% of the total production of plastic materials. The industry's main problem relates to the high viscosity of molten plastics which in turn leads to high energy consumption during processing. Large resources are invested all over the world every year to improve processability of existing and new resins.

The driving force behind this research is a new comprehension of flow of polymer melts and of its application to process them at higher throughputs, with less degradation and at a lower energy cost, to obtain better and cheaper finished products. The key to make this happen is a better understanding of entanglements, its relationship to viscosity, and the development of entanglement manipulation technology to obtain a significant reduction of the viscosity of the melt (by "disentanglement"). This thesis is the introduction to a new model of polymer chains interactions and entanglement applied to the understanding of polymer rheology and, in particular, "the disentanglement technology", i.e. the development of engineering processing solutions that substantially decrease the viscosity of melts, permits to process them at lower temperatures, under low pressure, without or with much less degradation and with improved dispersion when additives are compounded. By implementing the "disentanglement technology" into the standard and established industrial procedures, the temperature needed to process polymers can be reduced by 50-100 °C which will impact significantly the reduction of energy consumption in the European Union and worldwide. My prime objective in writing this thesis was to expose the experimental reasons which lead me to a different model to explain the source of molecular motions and flow in polymers. The new model provides another simple, sounded and quantitative explanation of the rheological response of polymer melts including those experiments which the classical approach fails to describe. This new understanding of polymer interactions and entanglement expresses a paradigm shift in polymer physics which leads to a roaster of new innovative applications.

My research ahead is divided into two interwoven general tasks: a theoretical one and a practical one, both needing the collaboration of research partners (High Education Universities and European Institutes, as well as industrial partners), whose participation is needed as complementary experts in the field of rheology, processing and characterization/synthesis.

- (a) On the theoretical side, my objective is to set up an educational program, which I call “New School Polymer Physics”, which will compare the teaching of the classical school with respect to visco-elasticity and rheology with that of the new theory of flow of polymer melts based on my new understanding of interactions and entanglements (the Dual-Phase model).

- (b) On the application side, this educational program will include research objectives starting with the teaching of the know-how of equipment design and melt manipulation software to reduce viscosity by “disentanglement”. Case study applications of the “disentanglement technology” in specific industrial areas will be covered such as extrusion to lower energy requirement by 40%, increase of permeability in films for the food industry, improved dispersion of nanoparticles in polymer melts, processing under much lower pressure and at lower temperature at identical throughput, increase of productivity and cost reduction for injection molding, extrusion and compounding lines, extrusion for the pharmaceutical industry, the biomaterial fabrication for the medical industry, and the 3D printing industry. These applications are of immediate interest to the targeted group of universities and research Institutes which are willing to work with me to participate in the New School Polymer Physics initiative (European ERASMUS+ project, Marie-Curie ITN-ETN). These willing participants are innovators and experts in these fields and users of those applications. For instance, the high temperatures necessary for processing plastics (in extrusion or injection molding) prevents the pharmaceutical industry to incorporate temperature sensitive active pharmaceutical ingredients into pharmaceutical grade polymers, which is a very innovative approach that has attracted significant interest in pharmaceutical technology. The new understanding of flow in entangled polymers explains how to “disentangle” melts, reduce their viscosity drastically and process them at low temperature to make it feasible.

In this thesis I exposed in the preamble (Chapter 1) the basic principles behind this new model of polymer physics which considers the compensation between the local and collective

interactions of conformers, statistical units belonging to the macromolecules defined by their conformational potential. In this thesis presentation, the “Grain-Field-Statistics”, a statistical model of dissipative dynamic systems in interactions is qualitatively applied to conformers to formulate a different understanding of entanglements and their relative stability. I have shown in many chapters of this thesis how to express the non-linear visco-elastic effects such as shear-thinning, strain softening and normal stress in terms of the conformers statistics parameters describing melt deformation (Dual-Phase "sweeping" and "blinking").

I revealed (in Chapter 2) that new types of experiments (Rheo-Fluidification) resulted in the possibility to obtain non-equilibrium entanglement states for polymeric melts which could be preserved in a pellet formed after the treatment, a property which I coined "sustained-orientation". This new state of polymer matter appears to challenge the current established models of polymer physics, because oriented melts could remain oriented for hours at temperatures T_g+100 ^oC, yet could slowly recover in time their initial un-oriented equilibrium state. This esoteric behavior can be understood within the framework of the concepts that explain entanglements from the view point of the Grain-Field statistics (entropic-enthalpic compensation).

I explained in Chapters 3 and 6 that many unresolved issues plague our understanding of rheology when its interpretation is based on molecular dynamics models which fundamentally consider the singular macromolecule as the basic statistical unit.

I described how the new physics can lead to the preparation of new exciting materials and new material properties for polymers, such as the ability to flow polymer melts at the same throughput rate, yet at temperatures much lower than normally practiced, i.e 50-100 ^oC below their recommended extrusion temperature, still without any increase of pressure (Chapter 4).

Chapter 5 provides the analytical tools to determine quantitatively the parameters of the Dual-Phase model: the frequency of the elastic dissipative wave and its variation with frequency and strain.

Chapter 6 shows that one can observe the two mechanisms of deformation of a sheared melt (the sweeping mode and the blinking mode) and how the solid-like character of a melt emerges from the local dual-phase interactions between the conformers (b-glassification).

Chapter 7 suggests that Rheo-SANS experiments conducted by two independent groups in Japan and France challenge the current interpretation of shear-thinning by the reptation school, a real problem which we claim should be considered seriously and cured to avoid the abandon of the reptation model until this is satisfactorily explained.

As an example of the potential innovative application of these new concepts, I want to introduce now the idea of storing mechanical energy into the bonds of polymers, transforming them into “Plastic-Fuel-Battery energy storage materials”. Using Rheo-Fluidification melt deformation in a special new way, I propose that the sustained-orientation property I obtained in preserving into a pellet the viscosity reduction of the treated melt be adapted to the problem of the storage of energy in a molded plastic part. The principle is to use enthalpic-entropic compensations to obtain "sustained-orientation" in compression mode to "charge up" plastic melts into novel out of equilibrium entanglement states which are yet sustained upon cooling. The "charged" plastic melts are then cooled and transformed into powder form or small pellets. This powder is the new "plastic fuel" capable of releasing the stored mechanical energy by mere thermal heating activation, via solar energy for instance. This technology, if validated, could be applied to recycled plastics, giving them a new life. Early experimental evidence done on a LLDPE of 200,000 molecular weight (MI=0.5) suggested that this was, indeed, happening. The cooled and solidified Rheo-fluidified melt could produce 10,000 PSI of pressure on re-heating when its temperature raised 30 ^{o}C above its T_g (37 ^{o}C).

What I call the "Pink-Flow" Technology describes the second generation of machinery, process and new materials produced pursuant to this new understanding of the parameters to control the "entanglement stability" of polymer melts. In other words, Pink-Flow makes use of the Grain-Field-Statistics to create thermal-mechanical-chemical histories during processing capable of stabilizing entanglements into quasi-stable non-equilibrium states exhibiting quite exciting novel properties. As said above, one of these applications may be the ability to store in the conformational organization of the bonds of “the entanglement elastic network” of recycled

plastics, a mechanical energy generated by an electrical drive powering a special Rheofluidizer/ extruder. The electrical energy would then be stored as non-equilibrium entangled states in plastic powder form. To repeat what I suggested above, this could be achieved when a certain compensation between the enthalpic and entropic forces which make up the entanglement network reach sustained orientation conditions. The release of the stored energy would be triggered by simple heating, perhaps generated or solely produced by solar energy. This “Pink-Flow” process could not only give a new value to plastics after their original usage, but also provide means to store electrical energy into plastic fuel powder or pellets.

Why the name "Pink-Flow"?

Obviously, the similarity with the famous rock band of the 70's announces the esoteric character of the results, and the diversity of response of a treated melt, unlike anything one would expect from a well behaved polymer. The wording seems to be appropriate to the behavior. Additionally, the first generation of processors I invented and described in patents and papers was called "EZ-Flow", although , retrospectively, I should have called it "Not-so EZ-Flow", because, as it turned out, mastering the technology remained empirical and the cost of the equipment and of finding the proper processing windows remained relatively high (nevertheless the technology is currently being used in the industry).

Future work: Axes of Fundamental Research Proposed at The New School Polymer Physics.

- Rheology of melts under shear and elongational ***vibratory flow***. Applications to processing and applications to improve the properties of molded products.

- Determination of PVT equation of state *under vibration*. Influence of cooling rate on PVT equation. Influence of pressure, cooling rate, frequency and amplitude of vibration on the viscoelastic characteristics of polymer melts, including viscosity and melt elasticity. Refer to the following review :” *Control of Polymer Properties by Melt Vibration Technology: A Review.*”, Polym. Eng. & Sci., Vol.38, No1,1 (1998).

- Continuation of the work presented in this thesis: new experimental set up and theoretical work to understand the ***stability of entanglements*** and their modulation of the rubbery and rubbery flow regions (terminal and rubbery plateau zones). Effect of coupling pure shear and shear oscillation in the non-linear visco-elastic region, on the spectrum of relaxation times and the reptation time, and in particular on the memory function of the melt. Determination and modification of the constitutive equations to be implemented in flow simulation software to integrate non-linear visco-elastic effects produced under vibration conditions.

- Theoretical work on ENTANGLEMENT and ENTROPY in polymers. Set up of new experiments and theoretical calculations using the Dual Split statistical model to demonstrate the interactive coupling nature of Entropic and Enthalpic forces in polymer melt deformation. An article, published in 1997, sets up the question: "*Do we need a new Theory in Polymer Physics?*", J. Macromol. Sci. Reviews in Macromol. Chem. & Phys, C37(3),389-458(1997). This thesis is supporting a positive answer to this query.

- Some recent results I have presented on disentanglement and re-entanglement of melts (chapters 2-6) seems to indicate that there is, indeed, the need to modify or complement our present understanding of melt deformation and polymer physics. I have only initiated such an approach and part of the theoretical work proposed would concentrate to consolidate this model, improve it and apply it to the understanding of various problems of polymer science and engineering. I include in Appendix A the preface of my new book on the Grain-Field Statistics which explains the deformation of open dissipative systems and its application to conformers in interactions.

- What about crystallization? This thesis did not present the intensive work I did on the influence of entanglement stability on crystallization which lead to a Polymat lecture on February 8th 2013 ("*The influence of the Entanglement State on the Crystallization of PET: Grain-Glassification versus Crystallization"*). This is, obviously, an important research topic which will require a lot of attention. I can only say that the concept of crystallization emerges naturally from the treatment of conformers in interaction. When conformers with the same stable conformation create the equivalent of a b-grain, it becomes the nucleus for crystallization

growth. I call it the st-t (stabilized-trans) conformation state, the most stable state achievable. For certain polymers, that state is preponderant and easily accessible, and they are semi-crystalline polymers. Thus I treat crystallization as another conformation state that allows to pump or release trans conformers from/into the global system statistics. This is why I suggested that crystallization competes with the b-conformational state. The only difference is that in the b-state conformers have all kinds of cis, gauche trans conformation, whereas they have only one when they assume the st-t state, thus the later is more stable.

- As already mentioned, I intend to teach a graduate level course to discuss polymer properties either with the traditional approach ("the singular chain entropy" approach of de Gennes and Doi-Edwards), versus the new theory of Grain-Field-Statistics of conformers in interactions, the global interactive coupling approach which I introduce. **Topics**: control of rheology of melts prior to and during processing; Shear-refinement; effect of coupling shear and vibration on relaxation times spectrum and reptation time, influence on the slip-stick process at the wall.

- Modelization of flow under non-linear viscoelastic conditions. Modelization by computer of a meshed network of interactive open dissipative systems driven by the Dual-Split Statistics equations. This research could be an attempt to complement the traditional *thermomechanical approach* presently in vigor in simulation software with a new approach based on coupling kinetics of conformers in global interaction.

- The primary ***practical goal*** of my proposed teaching and research is to provide a science base for molding processes under vibration so that mold, screw and die design and process control can be done rationally based on scientific laws rather than only on experiences. Research results are expected to have real impact on industrial practices. This same goal without vibration is not new, but, the adjunction of vibration to the molding process requires a total rethinking in terms of its impact on the flow pattern, the slip at the wall, viscous heating and shear-thinning, i.e. on the pressure-temperature requirements.

- Yet the ***ultimate goal*** of the New School Polymer Physics is to be able to correlate the physical state and the properties of material molded to its molecular and processing parameters, i.e. to be able to tailor at will performance of product to its chemical structure. This goal requires perhaps to understand viscoelastic flow of polymers in molecular terms and not, as now done successfully, in thermomechanical terms. As an illustration of this, consider flow induced crystallization which occurs in blow molding of bottles. The problem requires to define flow at the molecular level and to correlate orientation of the conformers in one direction with the ability to form crystallites and crystals. The kinetics of crystallization in non-isothermal conditions, in the complex context of a variable pressure in the mold cavity (and perhaps even of an added vibration), is responsible for the generation of the small nuclei which determine final stiffness and gas permeability. Experimental work and simulation should be able to tackle this challenging problem.

- Fundamental research should also contribute to the basic understanding of the physics of the technology of polymer processing in general and address the challenge of using computers to model the manufacturing process itself, as well as the mechanical behavior of the objects made out of the new melts involved.

- An important aspect of the program will be the involvement of researchers and Professors from the industry and from other universities, in particular from the US (MIT and University of Connecticut), from Germany (SKZ Institute and the University of Wurzburg), from England (University of Greenwich and University of Cambridge), from Portugal (New University of Lisbon), from France (University of Montpellier2, Laue Langevin Institute) and from China (Sichuan University at Chengdu).

- The research program of the New School Polymer Physics, if implemented at the University of the Basque Country, i.e. supported within an academic environment of high expertise in polymer physics and chemistry, should be able to generate a large number of papers, books, seminars that will position the research done by its professors and students in an international context. I am currently writing two books on this subject and have recorded approximately 110 hours of video presentations.

- As the economy becomes more global, one of the important reasons for success is the advancement of technology and technology transfer when a new technology is developed. Research on melt entanglement stability should be a major source of new ideas and fundamental knowledge based on which many novel technologies could be developed. While government is often the major source of funding to support university research, the practically of the application of the research could ease the collaboration between University, Government and Industry.

Jean Pierre Ibar

August 8th 2016

APPENDIX A

PRESENTATION OF THE GRAIN-FIELD STATISTICS SIMULATION IN A NEW COMING BOOK"GRAIN-FIELD STATISTICS APPLIED TO POLYMERS"

A primary motivation for my research is the interpretation of non-classical phenomena observed during the relaxation of high molecular weight liquids, highly viscous liquids and polymeric materials. The chemical structure of macromolecules is well understood nowadays, and their syntheses are well monitored. This, I believe, is not fully true of their thermal and mechanical properties, i.e. of polymer physics in general. The whole subject of visco elasticity, rubber elasticity, viscosity and glass formation has been the concern of extensive research for the last 30 years. For the most part, a consensus exists that our understanding of the linear-viscoelastic range (at low deformation) is pretty good. Yet, problems and questions of polymer physics are still not fully answered, especially in the domain of non-linear visco-elasticity. In this book, I try to define the principles of a new statistical theory which I call the "Grain-Field-Statistics", and apply it to the understanding of the coupling between conformers, which are basic bond-units defined along the chain of macromolecules. The network of interactions between the conformers is a single Dual-Phase system when the chain length is below a critical molecular weight, but is a two Dual-phase network called "the Crossed Dual-Phase Network" when the chain length is above the critical molecular weight.

The current established understanding of polymer physics is based on the description of the properties of a single chain embedded in a sea of average interaction from the other chains that disturbs its properties, for instance its ability to deform to adapt to a stress field. The statistics is treated from a pure macromolecular perspective, like in the case of rubber extensibility: how is the strain extending the rms end to end distance characteristic of the equilibrium coil shape assumed by the chain?

In the type of research I propose in this book, I look at polymer physics from a different angle, in particular I consider the statistics of a system consisting of a set of interactive conformers belonging to all the chains put together at once. The system is no longer a single macromolecule made up of covalently interactive conformers, although this situation is also studied. The system is the global set of conformers belonging to all macromolecules. I no longer

attribute to a mean field the influence generated by the other molecules on the configurational properties of a single chain (defining its entropy and enthalpy), I attribute a “grain-structure” to the field that describes the result of interactive coupling, i.e. I consider the existence of an inhomogeneous density of state due to local fluctuations of the interactions. The evolution with time of the state of interaction between the conformers, when the system is submitted to a mechanical force or to a temperature variation describes the change of the physical properties. This new statistics leads to the elaboration of a different understanding of visco-elasticity, rubber elasticity, and of the concept of entanglement of the macromolecules.

In order to tackle polymer physics from this new angle I need first to introduce a statistical model which can describe this concept of local grain structure of the interactions between conformers. This statistical model is called the Grain Field Statistics (GFS) which I apply to the description of the evolution of the interactions between conformers belonging to a system.

In reality, the Grain Field Statistics is generated by a potential which is not fixed and constant, as would be the case for a mean field potential, it is a sinusoidal wave function with a mean value and with a periodic fluctuation across the mean, characterized by its frequency, its amplitude and its phase. The mean value is normally independent of the fluctuation function, except at phase transitions, and varies to minimize the collective dissipative function of the system in interactions when the system is submitted to constraints that perturb the conformers statistics. This definition of the potential is not an ad hoc assumption, it is the result of studying the minimization of the dissipative energy through various simulations. I will need to explain in details how I ended up with such an assumption. In fact, it can be shown that fluctuating the potential instead of keeping it constant results in minimizing the dissipative function of a system where the b and F conformers fluctuate as if there were grains of b-conformers in a sea of F-conformers, in other words as if the b and F conformers co-existed as a fluctuating dual-phase. This will become clearer when I will present the results of coupling the dual-phase kinetic equations to describe the statistics under thermal equilibrium.

I have at my disposal a software program which I conceived some time ago (the code was written by Paul Denning, a mathematician educated at Imperial College in London and Aston University -now deceased- to whom this book is dedicated) that solves many of the

various sets of equations corresponding to the various assumptions I made about interactive coupling. The various chapters of the book present the results of the simulations and their meaning in terms of polymer physics and flow.

STATISTICS SIMULATIONS PRESENTED IN THE VARIOUS CHAPTERS

Chapter 0: Introduction to the parameters of the Statistics

Define conformers variables: Δ_m, υ_m , Δ_{eo}

Chapter I: Closed Dissipative Systems

1. Cooling and effect of cooling rate.
2. Heating at constant rate. Hysteresis effects.
3. Isothermal return kinetics to equilibrium (annealing)
4. Internal constraint in a System (forcing Dissipative Energy).

Chapter II: Open Dissipative Systems

1. Definition of Open and Crossed-Systems.
2. Effect of Total System population B_o
3. Effect of Temperature, Energy Barrier.
4. Cohesive waves and Crossed Systems:
5. Effect of Fluctuation amplitude and Frequency.
6. Structure of Dissipative Systems.
7. Energetic Structure as a function of Temperature.
8. Kinetic Structure as a function of Temperature.

Chapter III: Interactive Coupling between Dissipative Systems

1. Energetic Kinetic Network.
2. Crossed-System of order 2.
3. Multi-order Crossed-Systems.
4. Definition of Equilibrium Conditions: Cohesive waves at Equilibrium.
5. Minimization of Cohesive and Dissipative Energy.
6. Network of Self Dissipative Cohesive Systems:”entanglements”

Chapter IV: Non Equilibrium States

1. Effect of Cooling, heating, annealing on population statistics.
2. Effect of forcing a change of Δ_e on the statistics (mechanical force)

Chapter V: Mechanical constraint

"Deformation" (Mechanical Perturbation) of a Self Dissipative System.

1. Definition of Kinetic Length, Kinetic Stretch Rate of a System.
2. Definition of Stress and Strain and influence on Dual Split Kinetics
3. Stress-Strain curves for a deformed Self -Dissipative System.
4. Relaxation of a Self-Dissipative System.
5. Effect of Temperature.
6. Effect of Kinetic Stretch Rate.
7. Coupling between Relaxing and Deformed Systems
8. "Visco-Elasticity" of a Network of Self-Dissipative Systems.
9. Relaxation of a Network of Self-Dissipative Systems.